Towards the penside detection of triclabendazole efficacy against *Fasciola hepatica* parasites of livestock

Thesis submitted in candidature for the degree of Doctor of Philosophy at Aberystwyth University

By Clare Florence Collett

July 2019

Word Count of thesis: DECLARATION	79,152
This work has not previously been accepted in substance for any degree and is not concurrently submitted in candidature for any degree.	
Candidate name	Clare Florence Collett
Signature:	
Date	31.03.2020

STATEMENT 1

This thesis is the result of my own investigations, except where otherwise stated. Where *__correction services__ have been used, the extent and nature of the correction is clearly marked in a footnote(s).

Other sources are acknowledged by footnotes giving explicit references. A bibliography is appended.

Signature:	
Date	31.03.2020

[*this refers to the extent to which the text has been corrected by others]

STATEMENT 2

I hereby give consent for my thesis, if accepted, to be available for photocopying and for inter-library loan, and for the title and summary to be made available to outside organisations.

Signature:	
Date	31.03.2020

NB: *Candidates on whose behalf a bar on access (hard copy) has been approved by the University should use the following version of Statement 2:*

I hereby give consent for my thesis, if accepted, to be available for photocopying and for inter-library loans after expiry of a bar on access approved by Aberystwyth University.

Signature:	
Date	

Candidate's Surname/Family Name	Collett
Candidate's Forenames (in full)	Clare Florence
Candidate for the Degree of	PhD
Academic year the work submitted for examination	2019

Summary:

Fasciolosis is an increasing global concern to animal welfare, agricultural productivity, public health and food security. The incidences of *Fasciola hepatica* is set to increase with predicted climatic trends, and independent emergences of anthelmintic resistant parasite populations are threatening the sustainability of flukicides worldwide, which is highly concerning in the continuing absence of a commercial vaccine. Inappropriate anthelmintic applications, particularly for triclabendazole (TCBZ) as the drug of choice, will only continue to increase the risk and occurrence of treatment failure and the subsequent spread of anthelmintic-resistant parasites. The development of new biomarker candidates for future penside diagnostic application will lead to an easy and useful test for the farmer, veterinarian and researcher in pursuing the goal of monitoring infection, drug efficacy and ultimately parasite elimination. In this thesis, proteomic and immunologic methods were utilised to dissect *in vitro*-derived adult *F. hepatica* procathepsins within adult excretory/secretory products, and a new polyclonal antibody was produced which was confirmed to be specific to native and recombinant fluke-derived procathepsin antigens. Additionally, a mixed wild type parasite population was compared *in vitro* with a newly identified TCBZ-resistant liver fluke strain isolated in Kilmarnock (Scotland, United Kingdom), finding potential phenotypic and proteomic indicators of *in vivo* TCBZ challenge and resistance. A panel of biomarkers previously associated with TCBZ-sulphoxide challenge were also bioinformatically characterised and tested *in vitro* as prospective diagnostic candidates, indicating the potential utility of these and procathepsins. In summary, this thesis has elucidated new findings and produced several new biomarkers of potential significant value for future *F. hepatica* control in livestock.

KESS Funding Statement:

Knowledge Economy Skills Scholarships (KESS 2) is a pan-Wales higher level skills initiative led by Bangor University on behalf of the HE sector in Wales. It is part funded by the Welsh Government's European Social Fund (ESF) convergence programme for West Wales and the Valleys.

i. Abstract

Fasciolosis is an increasing global concern to animal welfare, agricultural productivity, public health and food security. Environmental changes are contributing to *Fasciola hepatica* expansion, which are set to worsen by predicted climatic trends. Independent emergences of anthelmintic resistant parasite populations worldwide are also threatening the sustainability of the few available flukicides, whilst exacerbating the economic impacts of fasciolosis on food production. Inappropriate flukicide applications, particularly for triclabendazole (TCBZ) as the drug of choice, will only continue to increase the risk and incidences of treatment failure and spread of anthelmintic-resistant parasite populations, which is particularly devastating to TCBZ-mediated parasite control in the continuing absence of a commercial vaccine. With these current prognoses, tools for to identify anthelmintic efficacy require improvement to sustain flukicidal activities and effective infection management. Furthermore, the development of new biomarker candidates for future penside application will lead to an easy and useful test for the farmer, veterinarian and researcher in pursuing the goal of monitoring infection, drug efficacy and ultimately parasite elimination.

In this thesis, a representative profile of adult stage *F. hepatica* procathepsin L zymogens is dissected. Proteomic and immunologic methods identified the presence of zymogens within *in vitro* cultured adult excretory/secretory products, and a new polyclonal antibody raised to a recombinant mutant procathepsin L1A antigen was utilised to identify prominent immunodominance of the inhibitor (pro-) peptides in intact native procathepsins. Additionally, key phenotypic and proteomic characteristics were identified between a mixed wild type population and compared with a new confirmed TCBZ-resistant liver fluke strain isolated in Kilmarnock (Scotland, United Kingdom), providing knowledge towards the study of proteins potentially involved in the TCBZ resistance phenotype. In addition, following on from previous findings, a panel of biomarkers associated with TCBZ-sulphoxide (TCBZ-SO) challenge were bioinformatically characterised, cloned and recombinantly expressed, where possible, for use in pilot diagnostic tests. Hereon, the potential diagnostic utility of several candidates was found, including the procathepsin L1A antigen and counterpart polyclonal antibodies. In summary, this thesis has elucidated new findings about cathepsin protease antigens and has made progress towards the analysis and production of several new biomarkers, which are of potential significant value for future *F. hepatica* control in livestock.

ii. Acknowledgments

Firstly, I would like to thank the European Social Fund, KESS2 and Hybu Cig Cymru for funding this PhD project and my supervisors Professor Peter Brophy and Doctor Russell Morphew for their encyclopaedic suggestions and reassuring guidance throughout my PhD.

I extend particular thanks to the technical staff who have assisted throughout my time in IBERS in everything from abattoir trips to ordering consumables, as well as the general running of lab equipment and hardware – so, many thanks to Rob, Colin, Julie, Mike, and Graham in particular. I am very grateful to Helen as well for her time and effort spent running my mass spec samples and tolerating my questions and requests. Also, thanks to Professors Jo Hamilton and Karl Hoffmann for respectively providing immeasurable immunology knowledge and extensive lab equipment, which were both invaluable for my work. Further thanks to Professor Luis Mur and Doctor Justin Pachebat for sharing their specialised facilities and imaging suites, from which I got a lot of good use.

For a great portion of my PhD work I relied on the generosity of Ridgeway Research and Randall Parker Foods Ltd to acquire animal and fluke samples, for which I am very grateful.

I would also like to thank my fellow PhD/postdoctoral pals during my time in Aber, for day-to-day support, company, reciprocal comic relief and convincing arguments to stop endless lab hours and to just leave some tasks til the next day. In fact, everyone in the veterinary parasitology and schistosome research groups, my office neighbours and multiple IBERS research groups were a great and helpful bunch of people and friends to have had during these challenging three years – Aliyah & co, Chelsea, Claire, Dave, John, Flavia, Alex H & fam, Niall, Kathy & Toby, Fiona, Nathan, Rebekah, Cat, Kat, Alex F, Ilze, Tom, Ben, Holly and Adam. Also, thanks to the lacrosse club 2016–2019 for good laughs and fun games, welcoming me and teaching me a sport I quickly learnt to love, I am very grateful for the friends I made through this team.

Lastly, I have the utmost appreciation and gratitude for my family (Colletts, Forsters and Sarres), my partner Barney and his family, and my close friends for their unwavering support, encouragement and for tolerating my prolonged infrequent free-time and PhD frustrations.

iii. Abbreviations

1-DE	1-dimensional electrophoresis
2-DE	2-dimensional electrophoresis
3-D	3-dimensional
γ-GT	Gamma-glutamyl transferase
µg	Microgram
µL	Microlitre
µm	Micrometre
µM	Micromolar
Ω	Ohm·centimetres
A_{xxx}	Absorbance (xxx nm)
aa	Amino acid
Ab	Antibody
ABP	Actin-binding protein
ABZ	Albendazole
ACT	Actin
ADP	Adenosine-5'-diphosphate
Ag	Antigen
ANOVA	Analysis of variance
ATP	Adenosine-5'-triphosphate
B12	Cobalamin
BCIP	5-bromo-4-chloro-3-indolyl phosphate
BMA	Beta-D-mannose
bp	Base pairs
BSA	Bovine serum albumin
BZ	Benzimidazole
C-O	Cut-off
C-RT	Coproantigen reduction test
CA	Calcium
cDNA	Complementary deoxyribonucleic acid
Ce	*Caenorhabditis elegans*
CeACT-1	*Caenorhabditis elegans* actin-1
CeCRT-1	*Caenorhabditis elegans* calreticulin-1
CeDJR-1.1	*Caenorhabditis elegans* DJ-1
CeENO-1	*Caenorhabditis elegans* enolase-1
CFA	Complete Freunds' adjuvant
CHAPS	3-((3-cholamidopropyl) dimethylammonio)-1-propanesulfonate
CL	Cathepsin L
CL1	Cathepsin L1
CLO	Closantel
cm	Centimetre
CNX	Calnexin
COB	Co-methylcobalamin
COWS	Control of Worms Sustainably
CRT	Calreticulin
Da	Dalton

DALY	Disability-adjusted life year
DEPC	Diethyl pyrocarbonate
Dm	*Drosophila melanogaster*
DmDJ-1β	*Drosophila melanogaster* DJ-1β
DMEM	Dulbecco's modified eagle medium
DMSO	Dimethyl sulfoxide
DNA	Deoxyribonucleic acid
DTT	Dithiotreitol
EASS	Extracellular actin scavenger system
Ec	*Equus callabus*
EcGEL	*Equus callabus* gelsolin
ECM	Extracellular matrix
EDTA	Ethylenediaminetetraacetic acid
EHA	Egg hatch assay
ELISA	Enzyme-linked immunosorbent assay
EM	Electron microscopy
ENO	Enolase
EQ	Equilibration (buffer)
ES	Excretory/secretory (products)
ESI-QUAD TOF	Electrospray ionisation quadrupole time-of-flight
EV	Extracellular vesicle
F-actin	Filamentous actin
FABP	Fatty acid binding protein
FDR	False discovery rate
FEC	Faecal egg count
FEC-RT	Faecal egg count reduction test
FhΔCRT	*Fasciola hepatica* mutant calreticulin
FhΔpCL1	*Fasciola hepatica* mutant procathepsin L1
FhACT	*Fasciola hepatica* actin
FhCL1	*Fasciola hepatica* cathepsin L1
FhCL2	*Fasciola hepatica* cathepsin L2
FhCRT	*Fasciola hepatica* calreticulin
FhDJ-1	*Fasciola hepatica* DJ-1
FhENO	*Fasciola hepatica* enolase
FhGAPDH	*Fasciola hepatica* glyceraldehyde-3-phosphate dehydrogenase
FhGEL	*Fasciola hepatica* gelsolin
FhpCL1	*Fasciola hepatica* procathepsin L1
FhTPI	*Fasciola hepatica* triose phosphate isomerase
FT	Flow-through
FMN	Flavin mononucleotide
G-actin	Globular actin
GAL	Beta-D-galactose
GAPDH	Glyceraldehyde-3-phosphate dehydrogenase
GEL	Gelsolin
GLDH	Glutamate dehydrogenase
GLMM	Generalised linear mixed model
GST	Glutathione-*S*-transferase

HCC	Hybu Cig Cymru
HEPES	4-(2-hydroxyethyl)-1-piperazineethanesulfonic acid
HIS	Histidine
Hs	*Homo sapiens*
HsACT-1	*Homo sapiens* actin-1
HsCRT	*Homo sapiens* calreticulin
HsDJ-1	*Homo sapiens* DJ-1
HsENO-1	*Homo sapiens* enolase-1
HsENO-2	*Homo sapiens* enolase-2
HsGAPDH	*Homo sapiens* glyceraldehyde-3-phosphate dehydrogenase (hepatic)
HsGAPDS	*Homo sapiens* glyceraldehyde-3-phosphate dehydrogenase (spermatogonian)
HsGEL	*Homo sapiens* gelsolin
HSP	Heat shock protein
HsPARK7	*Homo sapiens* Parkinsonism gene 7
IAA	Iodoacetamide
IB	Inclusion body
ID	Identity
IFA	Incomplete Freunds' adjuvant
Ig	Immunoglobulin
IgG	Immunoglobulin G
IMAC	Immobilised metal ion affinity chromatography
IPTG	Isopropyl β-D-1-thiogalactopyranoside
ITS2	Internal transcribed spacer 2
K-Fh	Kilmarnock *Fasciola hepatica*
kDa	Kilodalton
L	Lethal
LAMP	Loop-mediated isothermal amplification
LB	Luria Broth
LC-MS/MS	Liquid chromatography-tandem mass spectrometry
M	Molar
MΩ	Megohm·centimetres
mA	Milliamp
MG	Magnesium
mg	Milligram
mL	Millilitre
MLG	Multilocus genotype
mM	Millimolar
MmCRT	*Mus musculus* calreticulin
M_r	Relative molecular mass
mRNA	Messenger ribose nucleic acid
MW	Molecular weight
MWCO	Molecular weight cut-off
MWU	Mann Whitney U (test)
NAD(P)	Nicotinamide adenine dinucleotide (phosphate)
NAG	N-acetyl-D-glucosamine
NBP	Nicotinamide 8-bromo-adenine dinucleotide phosphate

NBD	N6-benzyl-nicotinamide-adenine-dinucleotide
NBT	Nitro blue tetrazolium
NCBI	National Centre for Biotechnology Information
NCM	Nitrocellulose membrane
NdeI	*Neisseria denitrificans* I
NDP	Dihydro-nicotinamide-adenine-dinucleotide phosphate
NEJ	Newly-excysted juvenile
ng	Nanogram
NGA	N-acetyl-D-galactosamine
nL	Nanolitre
nm	Nanometre
NotI	*Nocardia otitidis-caviarum* I
OcCRT	*Oryctolagus cuniculus*
OD	Optical density
ORF	Open reading frame
PAGE	Polyacrylamide gel electrophoresis
PBS	Phosphate buffered saline
PBS-T	Phosphate buffered saline Tween® 20
Pc	Polyclonal
PDB	Protein database
PCR	Polymerase chain reaction
PFA	Paraformaldehyde
pGEL	Plasma gelsolin
pI	Isoelectric point
PIM	Percentage identity matrix
pK_a	Acid dissociation constant
PMSF	Phenylmethylsulfonyl fluoride
PT	Post-treatment
PVDF	Polyvinyl difluoride
rFhΔCRT	Recombinant *Fasciola hepatica* mutant calreticulin
rFhACT	Recombinant *Fasciola hepatica* actin
rFhCL1	Recombinant *Fasciola hepatica* cathepsin L1
rFhCRT	Recombinant *Fasciola hepatica* calreticulin
rFhDJ-1	Recombinant *Fasciola hepatica* DJ-1
rFhENO	Recombinant *Fasciola hepatica* enolase
rFhGAPDH	Recombinant *Fasciola hepatica* glyceraldehyde-3-phosphate dehydrogenase
rFhGEL	Recombinant *Fasciola hepatica* gelsolin
rFhΔpCL1	Recombinant *Fasciola hepatica* mutant procathepsin L
rFhpCL1	Recombinant *Fasciola hepatica* procathepsin L
RFX	Rafoxanide
RNA	Ribonucleic acid
ROS	Reactive oxygen species
RPM	Revolutions per minute
RT	Reduction test
SAM	S-adenosylmethionine
SEC	Size exclusion chromatography

Sc	*Saccharomyces cerevisiae*
ScENO-1	*Saccharomyces cerevisiae* enolase-1
SD	Standard deviation
SDS	Sodium dodecyl sulfate
SDS PAGE	Sodium dodecyl sulfate polyacrylamide gel electrophoresis
Sj	*Schistosoma japonicum*
SL	Sub-lethal
Sm	*Schistosoma mansoni*
SmACT-1	*Schistosoma mansoni* actin-1
SmENO	*Schistosoma mansoni* enolase
SmGADPH	*Schistosoma mansoni* glyceraldehyde-3-phosphate dehydrogenase
SmGEL	*Schistosoma mansoni* gelsolin
SNP	Single nucleotide polymorphism
TbbENO	*Trypanosoma brucei brucei* enolase
TBS	Tris buffered saline
TBS-T	Tris buffered saline Tween® 20
TCA	Trichloroacetic acid
TCBZ	Triclabendazole
TCBZ-S	Triclabendazole-susceptible
TCBZ-SO	Triclabendazole sulfoxide
TCBZ-SO_2	Triclabendazole sulfone
TCBZ-R	Triclabendazole-resistant
TEM	Transmission electron microscopy
Th(1/2)	T helper cells type 1/2
TPI	Triose phosphate isomerase
w/v	Weight by volume
WHO	World Health Organisation
wpi	Week post-infection
WT-Fh	Wild type *Fasciola hepatica*
UK	United Kingdom
UV	Ultraviolet
v/v	Volume by volume
X-gal	5-bromo-4-chloro-3-indolyl-β-D-galactopyranoside
ZN	Zinc

Contents

1 Chapter 1: General introduction

1.1 Parasitism

1.1.1 Classification

Early observers of symbiotic relationships defined parasites as a collection of organisms that interact (De Bary, 1879). These highly diverse and loosely defined interspecific associations are now characterised by more informative phenotypes. To this end, mutual, commensal and parasitic distinctions have been proposed in order to better reflect the complex and varied dynamics of these biological relationships (Ewald, 1987; Leung and Poulin, 2008; Martin and Schwab, 2012). The Crofton classification remains the most favoured for parasitic interactions and was developed following quantitative assessments of these interspecific symbioses (Crofton, 1971). Crofton described four major principles to define a parasite having:

1. Physiological dependence on its host;
2. Population expansion and dispersal within the host population;
3. The capability of killing hosts in high numbers;
4. A higher fecundity than its host.

Evolutionary studies have shown independent development of parasitism by free-living organisms in phylogenetically-separate ancient taxa, and the subsequent convergence of lineages that share biological characteristics into strategically defined groups (Huyse *et al.*, 2005; Poulin, 2011; Poulin and Randhawa, 2015). Archaic and extant parasitic relationships are responsible for the evolution and continuing dynamic changes throughout biological domains. Indeed, the competitive nature and inevitable consequences of failure in a parasitic relationship necessitate an arms race between infecting and host species to adapt, often at the molecular level, to modulate infection dynamics for mutual survival (Poulin and Randhawa, 2015). This has led to a huge range of parasitic organisms that are currently responsible for global health, agricultural and economic problems.

1.1.2 Helminths

Helminths are a highly diverse group of multicellular invertebrate metazoans, which are distantly related to each other from a common ancestor and classified by their parasitic associations with their hosts (Castro, 1996; Gunn and Pitt, 2012a). There are many inter-taxonomic differences between helminths, including major genetic and physiological factors between taxonomic groups, which give rise to diverse infection dynamics (GIGA Community

of Scientists, 2014; Moreau and Chauvin, 2010; Robinson and Dalton, 2009). Helminths are separated into acoelomate Platyhelminthes and pseudocoelomate Nematoda with respect to the absence of a digestive tract (Platyhelminth, Class: Cestoda), the presence of a blind-ended gut (Platyhelminth, Class: Trematoda) or a pseudo-digestive tract (Nematoda). Most helminths lay eggs to propagate; Platyhelminthes live either as hermaphrodites or are dioecious, whereas many Nematoda species are dioecious (Castro, 1996; Gunn and Pitt, 2012a). These differences reflect the niches these helminths strive to acquire during parasitism, whereby some Platyhelminthes can reproduce via parthenogenic clonal expansion if necessary in an intermediate host, and also capture nutrients via their tegument, completely (cestodes) or partially alongside their blind-ended digestive tract (trematodes), from the environment of their definite host (Dalton *et al.*, 2004; Halton, 1967, 1997).

Multiple immune evasion mechanisms have been characterised in helminths, which have developed to avoid host defences against infection. This is the key strategy to successful parasitism as it that ensures sexual maturity for egg or live young reproduction, promotes unimpaired biological development, re-infection and transmission (Benesh *et al.*, 2014; Poulin and Randhawa, 2015). Parasite control relies on the understanding of such factors influencing infection dynamics and transmission strategies, which are loosely classified by the promotion of population (R) or host (K) stability, investing to some degree towards future parasite populations or infection longevity, respectively (Poulin and Randhawa, 2015; Sorrell *et al.*, 2009). Different helminth species can be identified with characteristics of R- and K-strategists, whereby fecundity and embryonic development are coupled on a spectrum of possible ratios, giving rise to under or highly developed young with consequently varied infective abilities (Kohagne, 2013; Poulin and Randhawa, 2015). The Trematoda class of Platyhelminthes include the Digenean sub-class, a group of helminths which utilise a free-living stage and subsequently undergo expansive asexual reproduction in a molluscan host (Castro, 1996). Therefore, many parasitic digenetic trematodes are a great cause for concern due to the multiple biological and environmental parameters which impact parasite transmission *ex vivo*, leading to seasonal influxes of infection risk and disease incidence (Hotez *et al.*, 2008; Huyse *et al.*, 2005; Morand *et al.*, 2006).

1.1.3 Parasites of major current global concern

Multiple parasites are currently of global public health concern and economic impact due to the infections of human, livestock and companion animal populations, including by uni- and multi-cellular organisms of distinct and long-standing biological taxa (Araújo and Ferreira, 2000; Bouchet *et al.*, 2003). Parasites of global medical and veterinary importance are noted for their gross impact on economic productivity by increasing disability-adjusted life years (DALYs), particularly by tropical human and zoonotic malarial (Sachs and Malaney, 2002), schistosomal (King, 2010), trypanosomal (Fèvre *et al.*, 2008; Lee *et al.*, 2013) and filarial nematode (Coffeng *et al.*, 2013; Ottesen, 2000) parasites. However, foodborne parasites and parasites of food production animals cause global economic deficits through their impact on agricultural productivity (Charlier *et al.*, 2014a; Perry and Randolph, 1999), as well as increased DALYs through transmission to humans (Keiser, 2009; Roberts *et al.*, 1994; Torgerson *et al.*, 2015).

Helminth parasites account for significant global economic impacts through their reductions in herd/flock growth rates, meat and milk yields, which is further hindered by the current limitations in integrated parasite management strategies (Charlier *et al.*, 2014a; Perry and Randolph, 1999). Of the endemic helminth parasites of British livestock, *Fasciola hepatica* continues to be of major concern due to mortality risks to sheep and long-term underlying influences on cattle meat and milk productivity (Bennett and Ijpelaar, 2005; Boray, 1997; Howell *et al.*, 2015).

1.2 *Fasciolidae* (Trematoda: Digenea)

Fasciolidae is a family of digenean flatworms responsible for globally important zoonoses of humans and livestock (Castro, 1996; Lotfy *et al.*, 2008; Mas-Coma *et al.*, 2005). Of the liver-infecting species of major medical and veterinary importance, *Fasciola hepatica*, *Fasciola gigantica* and *Fascioloides magna* liver flukes cause similar diseases due to their mode of infestation and host liver infection (Malcicka, 2015; Mas-Coma *et al.*, 2005). However, despite closely similar disease profiles these fluke species vary in their biology, global distribution and molluscan intermediate hosts (Lotfy *et al.*, 2008).

Fasciolosis can refer to disease caused by any single or mixed species infection by *Fasciolidae spp.*, depending on the geographic location and the intensity of livestock

agricultural activity, both of which aggravate transmission through the provision of definitive hosts on land appropriate for intermediate molluscan hosts and free-living parasites (Lotfy *et al.*, 2008; Mas-Coma *et al.*, 1999). *Fasciola hepatica*, the common liver fluke, is found worldwide as it is transmissible in temperate climates and has also been shown highly capable to adapt under environmental selection pressures expected from global warming (Figure 1.2A) (Fox *et al.*, 2011; Kenyon *et al.*, 2009b; Mas-Coma *et al.*, 1999; Short *et al.*, 2017; van Dijk *et al.*, 2010). Conversely, *F. gigantica* is larger as adults than respective *F. hepatica* flukes and occurs in tropical regions of the Middle East, Asia and Africa, with even more sporadic and focal prevalence patterns in areas with intensive agriculture (Figure 1.2B) (Lotfy *et al.*, 2008; Mas-Coma *et al.*, 1999). The least common liver fluke is *F. magna*, also known as the giant liver fluke, which is native to North America but also found in Europe (Figure 1.2C) (Lotfy *et al.*, 2008; Malcicka, 2015).

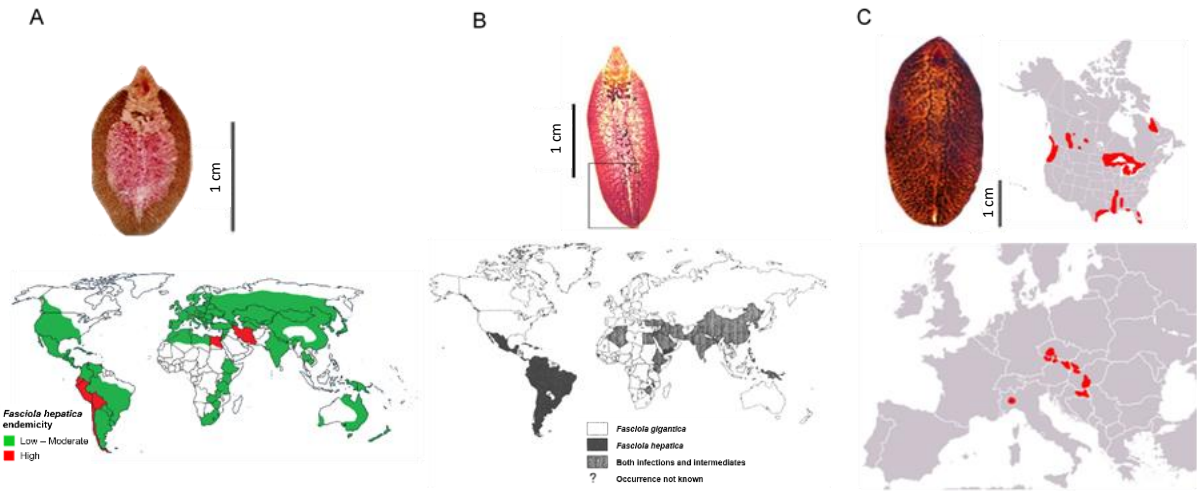

Figure 1.2. Morphology and biogeography of the digenean *Fasciolidae spp.* of liver fluke parasites. (A) *Fasciola hepatica* (image acquired from Wellcome Images) has a global distribution with the highest prevalence in temperate climates (map adapted from Martins dos Santos, (2012)). (B) *Fasciola gigantica* (image acquired 07/03/2018: www.medicine.cmu.ac.th/dept/parasite), but more common in tropical countries (image acquired 30/06/2016: www.infectionlandscapes.org/2012/07/liver-flukes-part-2-fascioliasis). (C) *Fascioloides magna* has a limited distribution in areas of North America and Europe (images acquired from Malcicka (2015)).

1.2.1 *Fasciolidae* biogeography and global parasitological importance

The biogeography of *Fasciolidae spp.* has revealed the relative geographic isolation of *Fascioloides magna* compared to the two *Fasciola spp.*, whereby *F. magna*-infected wild fauna are reported in regions of North America, Canada and some western European

countries, but remain difficult to estimate and risk spreading disease into domesticated cattle herds (Bazsalovicsová *et al.*, 2015; Lotfy *et al.*, 2008; Malcicka, 2015). However, *Fasciola hepatica* and *F. gigantica* are both globally important zoonotic agents of what has long been classified as a neglected tropical disease, with the greatest threat to public health in regions of high endemicity including in South America, northern Africa, China, Korea and several western, northern and southern countries of Asia (Hotez *et al.*, 2008; Lotfy *et al.*, 2008; Mas-Coma *et al.*, 1999). Despite associations with inhabited temperate (*F. hepatica*) or tropical (*F. gigantica*) regions, contributions of climatic, environmental and biological factors eliciting *Fasciola spp.* transmission and overlap have also led to multiple putative intermediate identifications of unique morphology (Afshan *et al.*, 2014; Ashrafi *et al.*, 2015, 2006; Hussein and Khalifa, 2010; Periago *et al.*, 2008, 2006; Valero *et al.*, 2018). Thus, the importance of *Fasciola* parasites and the considerable threat they pose to animal and human health continues to grow (Mas-Coma *et al.*, 2005, 1999; Mas-Coma and Bargues, 1997; Tolan, 2011).

1.2.2 The life cycle of *Fasciola hepatica*

The lifecycle of *Fasciola hepatica* is complex (Figure 1.2.2). Maintaining the lifecycle outside of the definitive host is dependent on several climatic factors and the availability of intermediate host species (Castro, 1996; Gunn and Pitt, 2012b; Moazeni and Ahmadi, 2016). Following egg passage with vertebrate faeces, egg embryonation and miracidial development before hatching requires a temperature of no less than 10°C and will only occur in moist soil that is at or beyond its water retention capacity (Ollerenshaw, 1959; Ross and McKay, 1929). The consensus for minimum hatching temperature is also 10°C, as found by Ross and McKay (1929), though other studies have indicated the variability of hatching rates depending on variable temperature and light stimuli, including 6–8 weeks at 16°C or 2–3 weeks at 25°C (Jepps, 1933), and higher hatching rates below 20°C (Gold and Goldberg, 1976) and with light exposure (Gold and Goldberg, 1976; Shaw and Simms, 1930). Additional geographic factors thereby play an important role in certain regions, due to the effects of latitude and altitude on temperature, rainfall, evapotranspiration and solar radiation, which influence the environment accommodating eggs, larval stages and intermediate snail host populations (Mas-Coma *et al.*, 2001; Morley and Lewis, 2015). Egg viability after considerable periods of refrigeration (4°C) has been recorded, including six months with partial development (Ross

and McKay, 1929) and two and a half years with no observed development (Krull, 1934), but still leading to viable parasite liberation and life cycle continuation. Though eggs do not develop over winter conditions (Thomas, 1883) and are desiccated after dry periods (Walton, 1918), eggs can lie dormant and subsequently hatch when conditions become favourable, though hatch rates are reduced following temperature fluctuations (Claxton *et al.*, 1999).

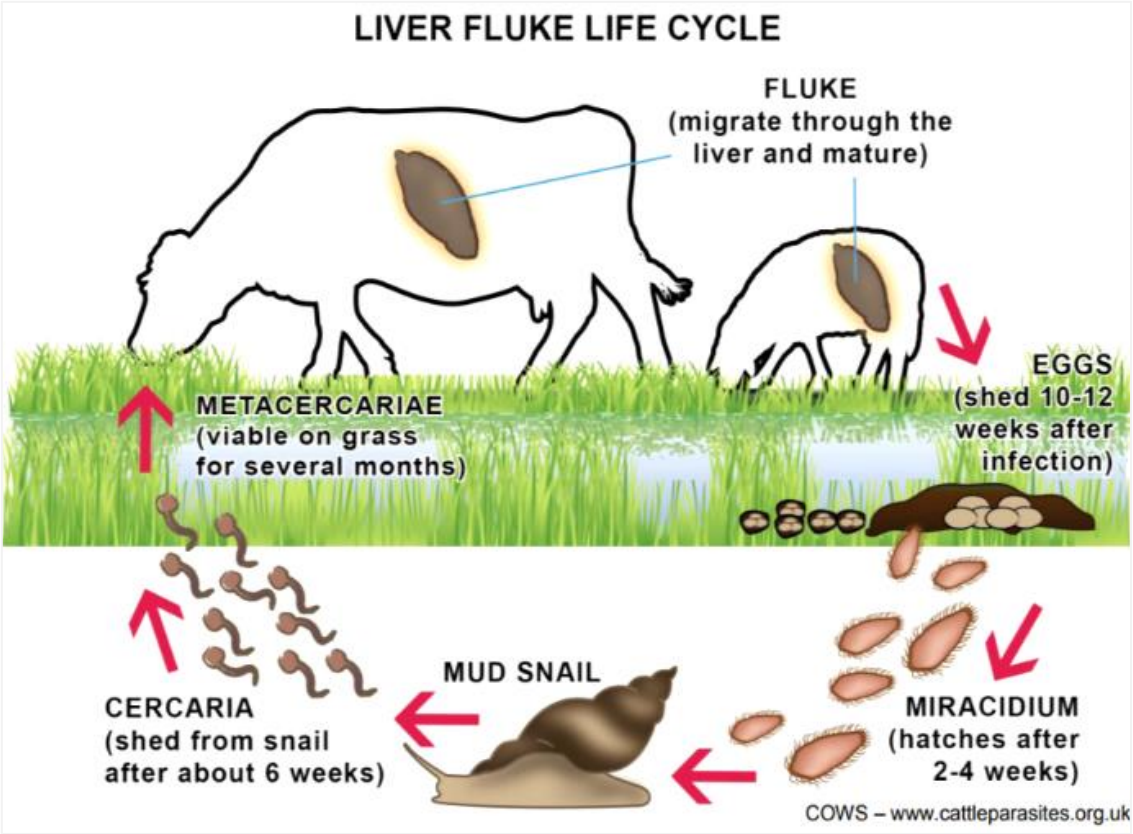

Figure 1.2.2. The life cycle of *Fasciola spp.* of liver flukes. Image acquired from the Control of Worms Sustainably (COWS) Technical Manual (December, 2013).

After hatching, ciliated miracidia must seek Lymnaeid mud snail hosts within 8–24 hours, after which energy stores are depleted and free-living miracidia die (Shaw and Simms, 1930). During snail invasion the miracidium creates a firm attachment, then contracts and relaxes its body, gradually shedding its ciliated epithelial cells as it mechanically bores through the host epithelial barriers (Wilson *et al.*, 1971). The muscular movements are also thought to force chemical secretions from the apical gland and accessory gland cells of the miracidium, which further facilitates cytolysis and snail tissue dissolution (Wilson *et al.*, 1971). Once fully penetrated into the snail, the miracidium is now surrounded by a new body wall within which it develops into the immature sporocyst stage by two and a half hours post-attachment

(Wilson *et al.*, 1971). By 24 hours following snail infection, miracidial cells are reorganised to form an inactive sporocyst of germ cells, which is fully developed after one week post-infection (wpi) (Rondelaud *et al.*, 2009; Wilson *et al.*, 1971).

Following sporocyst maturation, the next parasite stage and first mother redia emerges within two wpi and goes on to produce daughter rediae after three wpi. Rediae, predominantly the first mother redia, contribute to clonal amplifications of many 100s of cercariae, the third larval stage, by eight wpi from monomiracidial snail infections (Rondelaud *et al.*, 2009). Several generations of rediae are produced in the snail, though direct nutrient competition with the host (Kendall, 1949) and air and soil temperatures exceeding 20°C has shown to reduce redial production (Nice and Wilson, 1974; Smith and Wilson, 1980). Mature cercariae begin to emerge from snails as early as 4 wpi (Lee *et al.*, 1995), with most shedding after six wpi, which only occurs in the presence of water and when temperatures exceed 9°C (Kendall and McCullough, 1951; Wilson and Draskau, 1976). Consequently to these requirements, cercarial production from rediae and their maturation can be disrupted due to adverse environmental and biotic conditions, especially if the most productive first mother redia dies (Rondelaud *et al.*, 2009). However, the impact of snail starvation and abiotic fluctuations do not inhibit cercarial production but only act to reduce and delay it subsequently. As such, host starvation can briefly increase cercariae numbers (Wilson and Draskau, 1976) before significantly reducing the rates of cercarial production (Kendall and Ollerenshaw, 1963). Additionally, desiccation (Rondelaud, 1994) and temperatures reaching below 10°C (Claxton *et al.*, 1999; Kendall and Ollerenshaw, 1963; Wilson and Draskau, 1976) can also decrease cercarial production within the snail compared to unstressed snails. Due to climatic influences on snail population dynamics, the highest snail abundance is associated with wet weather and mild temperatures, and the peak number of snails in the field, and thereby transmission potential, is therefore seasonal when these environmental conditions occur (Relf *et al.*, 2011). However, snails that do not die from food shortages, environmental causes or due to the damaging ordeal of infection, particularly by larval migrations (Lee *et al.*, 1995; Pike and Erasmus, 1967; Thomas, 1883; Wilson and Draskau, 1976), go on to recover and can thus continue as hosts for the rest of their lives, leading to significant contamination potential.

Once liberated from the snail host, cercariae use their muscular tail to swim towards suitable vegetation shortly after leaving the snail to encyst, typically preferring slightly

submerged surfaces, artificial surfaces or grass blades (Dreyfuss *et al.*, 2004). Encystment occurs via mechanical processes of attachment, tail removal and swift cellular reorganisation (Pike and Erasmus, 1967). After approximately two hours, the cercaria is unrecognisable as a newly formed cyst with four distinct concentric layers, including a hardened granular shell that protects the metacercarial inner cyst (Dixon, 1965; Pike and Erasmus, 1967). Livestock pastures or silage and hay from arable land fertilised with infected animal slurry are high risk for encysted forms, though snails can assist in widening this distribution (Rapsch *et al.*, 2008). Metacercarial infectivity reduces over time, though mild temperatures and moisture are ideal to sustain viability, whereby the longest period before viability falls below 10% is close to one year post-encystment (Valero and Mas-Coma, 2000), though this could potentially be even longer (Mas-Coma *et al.*, 2018). Factors negatively impacting metacercariae viability and its duration include desiccation, high temperatures and sunlight (Boray, 1969; Boray and Enigk, 1964; Hodasi, 1972), though cold temperatures can also accelerate viability reductions (Boray, 1969). Even within detrimental environments, up to 50% of overwintering metacercariae can remain infective (Ollerenshaw, 1971), and hay can remain as sources of infection following long-term storage of eight (Marek, 1927) or even 17 (Rajcevic, 1929) months, particularly if poorly stored in damp conditions (Enigk and Hildebrand, 1964). Additionally, a recent review has highlighted the unknown extent of ensilaged grass impacting metacercariae infectivity (John *et al.*, 2019), though previous studies suggest viability is reduced following the high temperatures and fermentation conditions of this process (Enigk *et al.*, 1964; Wikerhauser and Brglez, 1961).

When ingested, metacercariae excyst at the mammalian host duodenum following biochemical cues that are experimentally reproducible, initiated by the high temperature (39°C), high carbon dioxide concentration and redox environment (Dawes and Hughes, 1970; Moazeni and Ahmadi, 2016; Wikerhauser, 1960). Newly-excysted juveniles (NEJ) pierce the intestinal wall and enter the abdominal cavity (Dawes, 1963), at which point their migration towards the bile duct may cross the liver parenchyma (Dawes, 1962a, 1962b, 1961) or directly invade the bile duct to avoid growth limitations of the former pathway (Moazeni and Ahmadi, 2016). The growth rate and maximum fluke length depends on host species, but egg-laying determines classification of an adult *in vivo* or *in vitro* (Dawes, 1962a; McCusker *et al.*, 2016); specific fluke characteristics at weekly time points post-infection are summarised in Table 1.4.2.1. Adults inhabit the biliary system for the remainder of the host's life, unless treated,

producing over 20,000 eggs per day that re-enter the gastrointestinal tract at the hepatopancreatic duct (ampulla of Vater), for subsequent release with faecal matter that restarts the lifecycle (Moazeni and Ahmadi, 2016; Walker *et al.*, 2006). Since livestock are optimal hosts for perpetuating parasite populations, heavy burdens or undiagnosed infections leads to considerable pasture contamination.

1.2.3 Transmission of *Fasciola hepatica*

1.2.3.1 Ecological factors of pond snail distribution

Common sites for snail habitation and consequential metacercarial encystment are those subject to temporary or prolonged poaching of pastures, including damage to the grass and underlying soil layers due to wet weather and livestock footfalls, during the summer and especially autumn periods, with conducive conditions dictated by soil quality, vegetation density, altitude and temperature (Kendall, 1970; Mas-Coma *et al.*, 2009; Selemetas *et al.*, 2015). Snail abundance, health and activities, which are influenced by habitat availability, are also critical for parasite development and subsequent distribution (Caron *et al.*, 2008; Novobilský *et al.*, 2014; Rondelaud *et al.*, 2013). As such, cysts are frequently found in grasses and aquaculture crops adjacent to natural pools and water courses, as well as artificial irrigation systems (Keiser and Utzinger, 2005; Mas-Coma *et al.*, 2005; Roberts and Copeman, 2006). This arrangement is ideal to seek a significant host range, particularly by grazing ruminants and humans consuming contaminated crops (Esteban *et al.*, 2002; Mas-Coma *et al.*, 2005, 1999).

1.2.3.2 Lymnaeidae as intermediate hosts of Fasciola spp.

Lymnaeidae phylogenetics are instrumental for the identification of important intermediate host species, which has been improved with species' genetic identifiers on top of supporting geographic location and morphology evidence (Bargues *et al.*, 2003; Correa *et al.*, 2011, 2010). Consequently to incorrect snail identification, this has led to false estimations of species' importance and their responsibility for the geographic spread of fasciolosis (Mas-Coma, 2005; Mas-Coma *et al.*, 2005; Rondelaud *et al.*, 2014). *Galba* and *Radix* genera dominate as intermediate hosts for *Fasciola hepatica* and *F. gigantica* respectively, where primary snail species is greatly influenced by geographic cross-overs of snail and parasite

(Bargues *et al.*, 2003; Sanabria *et al.*, 2012). Although artificial conditions have led to parasite adaptation to non-primary snail species, there have been a number of reports where natural conditions have fostered unusual Lymnaeid-*Fasciola* interactions (Dreyfuss *et al.*, 2012; Jones *et al.*, 2015; Novobilský *et al.*, 2013; Rondelaud *et al.*, 2014). In light of explicit snail genetic identifiers, a further range of snail species have been identified with at least 25 and 9 frequent or accidental interactions with *F. hepatica* and *F. gigantica* respectively (Jones *et al.*, 2015; Novobilský *et al.*, 2013). As such, it is probable that there is a greater abundance of susceptible snail hosts than originally thought, which are providing a previously unprecedented contribution to disease expansion beyond any one snail species' capacity (Boray, 1978; Kendall, 1970; Rapsch *et al.*, 2008; Rondelaud *et al.*, 2014).

1.2.4 Fasciolosis epidemiology

1.2.4.1 High-risk areas for Fasciola hepatica *transmission*

Meteorological factors including temperatures, rainfall, altitude and vegetation coverage are together significant in influencing snail abundance as well as the viability of free-living parasites (Fox *et al.*, 2011; Mas-Coma *et al.*, 2009). Prolonged wet, mild conditions in areas with widespread vegetation coverage and low altitudes are high-risk for epidemic outbreaks, and thus many geographic regions worldwide have existing or a reported increase in zoonotic disease incidence, including western Europe, northern Africa, Asia, Central and South America and parts of Oceania (Fürst *et al.*, 2012; Mas-Coma *et al.*, 2005; World Health Organization, 1995). Furthermore, the nature of *Fasciola hepatica* transmission exposes ruminant livestock as vulnerable disease reservoirs in focal populations, causing great concern to global veterinary and public health (Cabada and White, 2012; Mas-Coma *et al.*, 2005, 1999; Mas-Coma and Bargues, 1997; Selemetas *et al.*, 2015; Skuce and Zadoks, 2013).

Endemicity is further influenced by imports of infected animals and human cases, increased vegetation availability for metacercariae, and lapses in hygiene and sanitation; causing increasingly frequent parasite exposure to a younger demographic (Chand *et al.*, 2009; Esteban *et al.*, 2002, 1999; Keiser and Utzinger, 2005; Mas-Coma *et al.*, 1999). Although infections arise from ingesting contaminated vegetation, the general public has additional contact with NEJs, adults and eggs in infected meat. Moreover, there is especially high risk if parasites and viable eggs are absconded through suboptimal slaughterhouse hygiene standards and meat inspections (Nyindo and Lukambagire, 2015). There have been several

studies conducted in areas of Africa, Asia, Europe and Oceania that have measured rising numbers of liver fluke in abattoirs in recent years, indicating the ongoing prevalence and persisting threats of *F. hepatica* (Charlier *et al.*, 2014b; MacGillivray *et al.*, 2013; Skuce and Zadoks, 2013; Swai and Ulicky, 2009). Bringing together all risk factors, human populations generally display hypoendemic infection statuses with foci of increased incidence in farming communities. As such, human fasciolosis was previously estimated to infect 2.4 million people (Rim *et al.*, 1994). However the risk of acquiring the disease has been increasing since the 1970s (Mas-Coma and Bargues, 1997), and so more recent estimations for the global burden of fasciolosis is between 35–72 million with a further 180 million people at risk (Nyindo and Lukambagire, 2015).

1.2.4.2 Impacts of Fasciola hepatica *livestock infections on food security*

Economic losses as a result of fasciolosis in the agricultural industry amount to an estimated US$3 billion globally (Boray, 1997; FAO, 1994) and £40 million in the United Kingdom (UK) alone (Bennett and Ijpelaar, 2005). The damage of migrating juveniles *in vivo* causes direct economic losses through this acute disease stage in ovines, caprines and young bovine stock (Charlier *et al.*, 2014b; Gunn and Pitt, 2012a; Taylor, 2012). However, considerably more economic potential is lost in chronic bovine infections, whereby indirect cumulative costs are accrued by the reduction of meat and milk productivity (Cawdery *et al.*, 1977; Kaplan, 2001; McIlroy *et al.*, 1990; Morgan *et al.*, 2013; Ross, 1970; Torgerson and Claxton, 1999). Specifically, livestock performance impacts resulting from fasciolosis have been reported for the last few decades by a large number studies from several countries (Table 1.2.4.2.). As determined from these reports, the most financial losses arise from bovine fasciolosis including chronic and subclinical infections, with many studies reporting significant quantifiable reductions in milk yield leading to major production losses, and multiple economic factors resulting from reduced fertility (Table 1.2.4.2.). Less costly are losses due to reduced weight gain leading to poor growth rates and losses in meat yield and carcass price. However, it has been demonstrated that repeated anthelmintic treatment can lead to a recovery in weight, lactation, peak milk production and pregnancy rates (Charlier *et al.*, 2012; Loyacano *et al.*, 2002).

Table 1.2.4.2. Quantitative and qualitative impacts of fasciolosis on livestock performance.

Fasciolosis impacts				Effect of flukicide application			Reference
Body weight‡	**Meat yields**	**Milk yields**	**Fertility**	**Body weight‡**	**Milk yields**	**Fertility**	
-8.9%		-10%	Delayed puberty Increased inter-calving interval (+13 days) Additional services (0.630–0.868; +38%) Increased service period (+13 days) Reduced birth weight				a
-0.07 kg·herd^{-1}·day^{-1}		-0.5 kg·cow^{-1}·day^{-1}	Increased inter-calving interval (+20 days) Additional service (+0.5)				b
				+5.80%		+13% (pregnancy rate)	c
		-0.7 kg·cow^{-1}·day^{-1} (-3%)	Increased inter-calving interval (+4.7 days)				d
	-3.4 kg·herd^{-1} (-0.702%, warm carcass weight)						e
		-1.5 kg·cow^{-1}·day^{-1} (-5.15% herd level) -2.0 kg·cow^{-1}·day^{-1} (-6.80%, animal level)					f
					Higher peak production +9% (lactation persistence)		g
	-0.5% (cold carcass weight) -0.3%, (carcass price)						h

‡ refers to growth rates

a. Schweizer *et al.*, 2005 (*average figures from original studies published: 1970–1996; see review for full list)
b. Bennett *et al.*, 1999
c. Loyacano *et al.*, 2002
d. Charlier *et al.*, 2007
e. Charlier *et al.*, 2009
f. Mezo *et al.*, 2011
g. Charlier *et al.*, 2012
h. Sanchez-Vazquez and Lewis, 2013

The human population is predicted to exceed 9.8 billion by 2050 (United Nations, accessed 09/03/2018: UN population prospects 2017, www.bit.ly/33xFwmU). This will increase demands for food security and agricultural intensification, which will consequentially lead to the spread of zoonoses between livestock and human populations (Fitzpatrick, 2013; Foresight and Farming, 2011; Jones *et al.*, 2013). *Fasciola hepatica* will consequently be one of many infectious disease agents to threaten the future of food security and safety (Jones *et al.*, 2013).

1.2.4.3 Climate change impacts on fasciolosis

Predicting outbreaks of fasciolosis has been improved by the Ollerenshaw index, which uses meteorological data (1.2.4.1) to calculate disease risk in a given geographic location with accuracy (Ollerenshaw, 1966; Ollerenshaw and Rowlands, 1959). This is useful to assess the impacts of environmental trends such as climate change, which are expected to directly influence parasite incidence and disease prevalence patterns (Charlier *et al.*, 2016; Fox *et al.*, 2011; Mas-Coma *et al.*, 2009; van Dijk *et al.*, 2010). There is now a consensus that climate change will impact temperature and rainfall in temperate countries, leading to wetter, warmer and shorter winters, and warmer summers. Between 1961–2004 climatic changes were monitored in Scotland (Barnett *et al.*, 2006), and average rainfall measures in spring, autumn and winter all increased, with close to 20% higher annual rainfall compared to previous years. In the same study, temperature records also demonstrated an incremental rise by 1°C in mean monthly temperatures, and one prediction saw a further 4°C increase expected by 2080 (Barnett *et al.*, 2006). With these changes introduces further shifts to ecosystems through increased moisture, shortened frosts and prolonged herbage growing seasons in spring and autumn, all of which are contingent factors for snail and *Fasciola hepatica* survival (Kenyon *et al.*, 2009b). Thus, climatic projections have translated to an augmentation in fasciolosis risk in endemic areas, with the increase in wet and mild conditions all year round expected to expand the geographic range and seasonality of outbreaks (Fox *et al.*, 2011; Kenyon *et al.*, 2009b; Mas-Coma *et al.*, 2009; Morgan *et al.*, 2013; Pritchard *et al.*, 2005; Rapsch *et al.*, 2008; Selemetas and Waal, 2015; Silva *et al.*, 2016; van Dijk *et al.*, 2010).

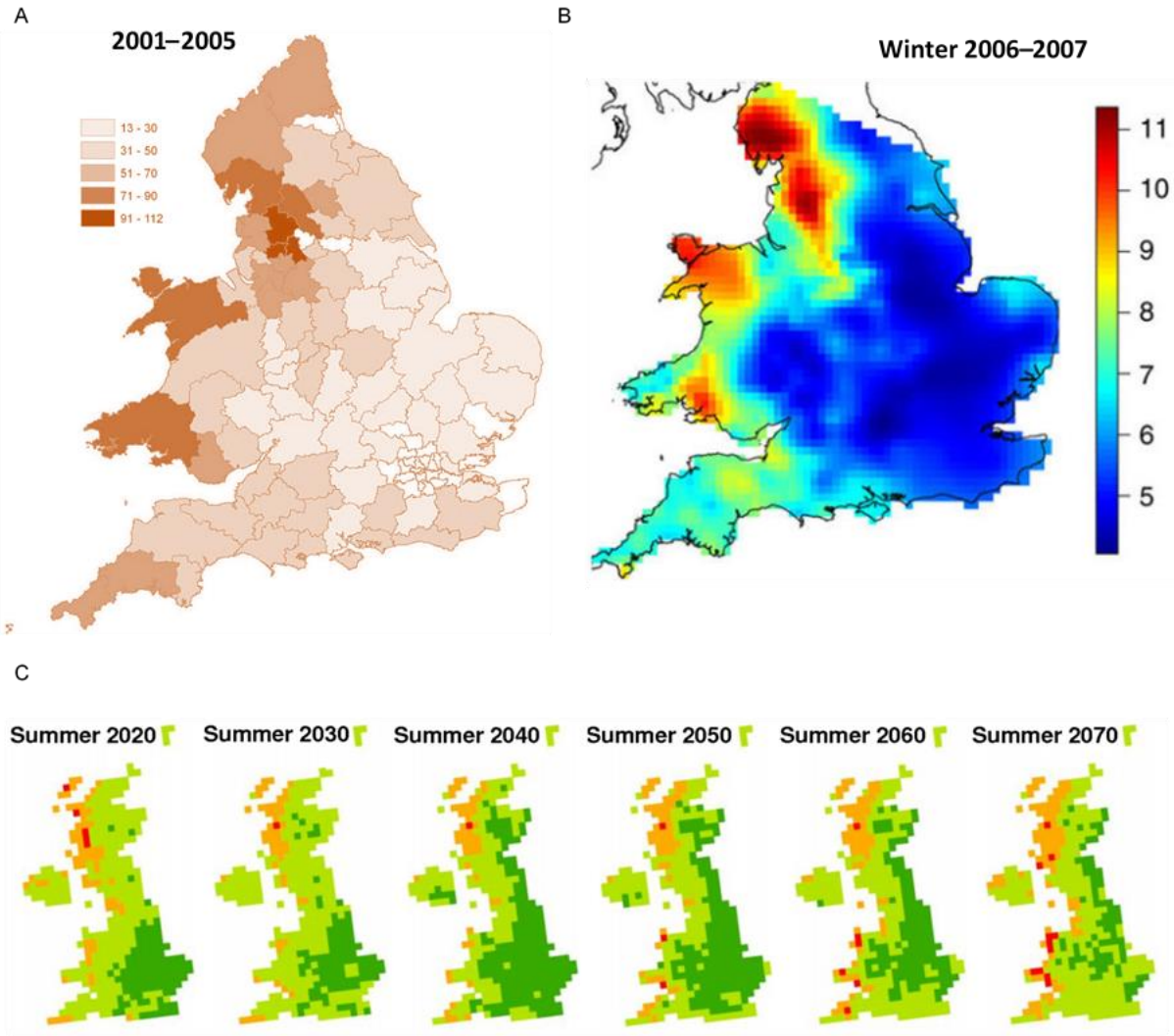

Figure 0. Predicted *Fasciola hepatica* infection prevalence in the Great Britain. (A) The mean prevalence of *F. hepatica* in 2006 was predicted using bulk milk tank enzyme-linked immunosorbent assay (ELISA) data and climatic datasets within the Ollerenshaw index from the preceding years 2001–2005 for England and Wales postcode areas (McCann *et al.*, 2010) (scale: predicted percent positivity values), supported by (B) observational data from bulk milk tank ELISA data collected between November 2006 and January 2007 (Claridge *et al.*, 2012) (scale: smoothed square-root-transformed percent positivity values). (C) The predicted risk of *F. hepatica* infection was calculated using climatic and environmental risk factors outlined in the Ollerenshaw index (Fox *et al.*, 2011) (scale: little or no disease, **dark green**; occasional losses, **light green**; disease prevalent, **orange**; serious epidemic, **red**). Images acquired from authors as specified.

Fasciola hepatica management under climate change influences will be challenging due to the increase in unfavourable conditions and continued agricultural intensification in high-risk areas, simultaneously promoting parasite transmission (Jones *et al.*, 2013; Morgan *et al.*, 2013; van Dijk *et al.*, 2010). Bulk observational datasets for *F. hepatica* prevalence and projected meteorological data have been used to map past and future prevalence models in

the UK (Figure 1.2.4.3) (Claridge *et al.*, 2012; Fox *et al.*, 2011; McCann *et al.*, 2010). The predicted climate changes and impacts on parasite incidence risk show fluctuations in certain areas over some time periods. However, these previous findings indicate a steady increase towards epidemic levels in Western areas in the coming decades, indicating the substantial growing threat of fasciolosis beyond its current and previous distribution.

1.2.5 Biology of *Fasciola hepatica* infection

1.2.5.1 Hepatic fasciolosis

Fasciolosis disease dynamics are influenced by several factors associated with host and infective parasite, whereby the metacercarial dose and host species, size and health, including infection resistance, can impact the severity of infection and its overall symptomaticity (Aksoy *et al.*, 2005; Boray, 1969; Boyce *et al.*, 1987). Ovine and caprine ruminants may die as a result of *Fasciola hepatica* infection (Kistner and Koller, 1975), or could suffer severe acute and sub-acute disease if infected with up to 1000 metacercariae owing to NEJ-associated damages, whereas a lower dose of 100 metacercariae instead leads to low-level chronic disease that is not necessarily accompanied by acute-like symptoms (Vercruysse *et al.*, 2001). Conversely to smaller ruminants, bovines tolerate heavy infections and are thereby prone to subclinical chronic disease and long-term associated health problems (Vercruysse *et al.*, 2001).

The varied infection characteristics between ruminants are testament to the diverse innate host biological factors which influence parasite establishment (Boray, 1969; Boyce *et al.*, 1987). Parasite numbers can also influence infections through the relative degree of crowding, whereby high numbers of infective parasites will negatively influence pre-patency length, reducing juvenile growth rates and subsequent egg output per adult (Valero *et al.*, 2006). This effect could be interpreted as a mechanism of controlling intra-host competition, thereby negatively regulating pathogen burden and preventing the host being overwhelmed (Roberts, 2000). Resultantly, there is a wide range of possible infection phenotypes by *F. hepatica* from asymptomaticity to mild, severe or fatal disease.

1.2.6 Fasciolosis symptomaticity

During the pre-patent infection, juveniles are very destructive through blood feeding and enzyme-assisted migration through abdominal and parenchymal tissues (Behm and

Sangster, 1999; Moazeni and Ahmadi, 2016). This physiological damage thus coincides with an increased risk of opportunistic infections (Behm and Sangster, 1999; Boray and Love, 2007; Moreau and Chauvin, 2010). In sufficient numbers, NEJs invariably cause some form of clinical disease, manifestations of which include mild or severe weight loss, lethargy, anaemia, haemorrhaging, jaundice and oedemas as direct and indirect results of tissue damage, blood loss and immunocompromisation (Behm and Sangster, 1999; Boray and Love, 2007; Chiodini *et al.*, 2003). Fatalities are indicative of fasciolosis in sheep in particular (Behm and Sangster, 1999), but on-farm diagnosis often requires support from environmental risk assessments and infection history before confirming the placement of other symptoms (MacGillivray *et al.*, 2013).

Figure 1.2.6. Clinical and post-mortem signs of *Fasciola hepatica* infection in livestock. (A) Fibrotic liver tissues and biliary tract (sliced sections of infected liver) and (B) granulomas as a result of liver fluke infection. (C) Pale eyelids caused by anaemia in an infected sheep. (D) Bottle jaw caused by secondary bacterial infection in an infected calf. Images C–D acquired from Boray and Love, (2017).

The chronic infection phase onwards from 12 weeks post-infection (wpi) involves biliary infestation by mature flukes, leading to the fibrosis and granulomatosis of liver tissues (Figure 1.2.6A–B). Hereon also, disease pathologies arise from the long-term blood loss and immunological modulation by these mature stage parasites (Behm and Sangster, 1999; Moazeni and Ahmadi, 2016). Sufficient numbers can eventually lead to clinical signs, including diarrhoea, loss of condition, emaciation, susceptibility to metabolic and bacterial diseases and severe ventral and intermandibular oedemas (Figure 1.2.6C–D) (Behm and Sangster, 1999). Despite this, subclinical infections with adult fluke are associated with impacts on broad level herd performance, especially in beef and dairy farms, through the reduction in fertility and milk yields (Charlier *et al.*, 2014b; Howell *et al.*, 2015).

1.2.7 Molecular components of pathogenesis: excretory/secretory (ES) products

1.2.7.1 ES production

Fasciola hepatica excretory/secretory (ES) products include a wide range of proteinaceous and vesicular components, the molecular phenotype of which responds to the external environment and stresses experienced by the fluke (Haçariz *et al.*, 2015; Morphew *et al.*, 2007, 2013; Young *et al.*, 2010). ES proteomes also vary according to infection stage, whereby the abundance of virulence factors is measurably increased post-excystment, proposed to function towards host blood feeding, migration, or immune evasion (Cancela *et al.*, 2010; Cuesta-Astroz *et al.*, 2017; Cwiklinski *et al.*, 2015c, 2015b; Robinson *et al.*, 2009).

The continuous uptake and digestion of host blood is followed by the frequent regurgitations of digest products with ES, which flukes expel from their blind-ended gut at approximately three hour intervals (Brady *et al.*, 1999; Wilson *et al.*, 2011). Further to fluke vomitus, the glycocalyx spontaneously changes at a high turnover rate, releasing tegumental protein and extracellular vesicle (EV) secretions into the ES mixture, whereby tegumental antigenic rejuvenation deflects direct immunological attacks (Dalton *et al.*, 2004; Hamilton *et al.*, 2009; Hanna, 1980; Wilson *et al.*, 2011). Influxes of ES into the host liver extracellular matrix also causes physiological damage when parasite enzymes remain active and degrade host tissues (Dalton *et al.*, 2003; Jefferies *et al.*, 2001). The ES products and individual proteins have therefore drawn particular research interest to identify biomarkers of infection, in

addition to components of the immunogenic and drug metabolism phenotypes (Brophy *et al.*, 2012; Chemale *et al.*, 2010; Halferty *et al.*, 2008; Morphew *et al.*, 2014; Toner *et al.*, 2010a).

1.2.7.2 Immunomodulation

Tissue- and non-tissue-dwelling helminths modulate host immunity to promote longevity and infection chronicity, inducing Th1- or Th2-mediated immune phenotypes respectively (Dalton *et al.*, 2013; Moreau and Chauvin, 2010; Mulcahy *et al.*, 2005). As predominantly tissue-dwelling parasites, *Fasciola hepatica* uses excretory/secretory (ES) proteins and extracellular vesicles (EVs) with immunomodulatory functions to boost and modulate the Th2 host response and thus prevent a Th1 dynamic (Beckham *et al.*, 2009; Carmona *et al.*, 1993; Coakley *et al.*, 2017; Dixit *et al.*, 2008; Dowling *et al.*, 2010; Haçariz *et al.*, 2015; Montaner *et al.*, 2014; Rodríguez *et al.*, 2015). The exposure and molecular activities of ES products promote Th2 and regulatory immunity, which intensifies with increasing parasite numbers and sets up an optimal immunological environment to downregulate pro-inflammatory Th1 immunity and promote Th2-driven tissue repair (Dalton *et al.*, 2013; Mulcahy *et al.*, 2005; Zafra *et al.*, 2013a, 2013b). Consequently, fluke activities in the predominating Th2 environment lead to extensive tissue damage by fibrosis, calcifications and perforations (Berasaín *et al.*, 1997a; Brady *et al.*, 1999; Dalton *et al.*, 2003; McGonigle *et al.*, 2008) and destabilise the protective immunity driven by immunoglobulins (Berasaín *et al.*, 2000; Smith *et al.*, 1993a) and effector cells (Carmona *et al.*, 1993; Escamilla *et al.*, 2017; Hamilton *et al.*, 2009; Vukman *et al.*, 2013). Thus, liver fluke infection can acutely and cumulatively increase the risk of host immunological susceptibility to opportunistic Th1-targeted pathogens, including bacteria (Boray, 1969; Boray and Love, 2007; Dixit *et al.*, 2008).

1.2.7.3 Virulence-associated factors

Fasciola hepatica ES products contain a pathogenic mixture of virulence-associated proteins, including enzymes such as the well-characterised cathepsin proteases, glutathione transferases (GSTs) and fatty acid binding proteins (FABPs), that assist in host invasion, parasite nutrition and/or detoxifying effects to nullify host immune defences. Cathepsin proteases, divided into two major subgroups B and L, are coherently excreted by juvenile and adult flukes respectively (McVeigh *et al.*, 2012) and responsible for much of the

aforementioned physiological disruption and immune-associated pathologies (1.2.7.1–1.2.7.2) (Beckham *et al.*, 2009; Collins *et al.*, 2004; Cwiklinski *et al.*, 2015b; Garcia-Campos *et al.*, 2016; Morphew *et al.*, 2011; Robinson *et al.*, 2008b; Stack *et al.*, 2007) via collagenolytic (Berasaín *et al.*, 1997a; Corvo *et al.*, 2009) and fibrinolytic (Dowd *et al.*, 1995; Mebius *et al.*, 2018) mechanisms. Fatty acid binding proteins (FABP) are also associated with interference of the host immune system and associated tilt towards the Th2 response (Figueroa-Santiago and Espino, 2014; Smooker *et al.*, 2001), acting beyond the important role of FABP to sequester host fatty acids (Morphew *et al.*, 2016). Tissue invasion is further influenced by the glycosidase enzymes, including *β*-galactosidase, *β*-glucosidase and *β*-N-acteylhexosaminidase, which cleave host glycans and glycoproteins and are thus particularly utilised by juveniles at the host duodenum where mucin glycoproteins are enriched (Irwin *et al.*, 2004). Enolase is multifunctional in pathogenic entities, including in *F. hepatica* (Bernal *et al.*, 2004; Morphew *et al.*, 2014), cancer (Liu and Shih, 2007; Song *et al.*, 2014) and other microorganisms, particularly unicellular, intracellular-invading pathogens (Figueiredo *et al.*, 2015; Funk *et al.*, 2016; Ghosh and Jacobs-Lorena, 2011). Enolase is an essential component of glycolysis and gluconeogenesis but "moonlights" as a virulence factor via its host plasminogen-binding properties, permitting uninhibited plasmin-mediated tissue degradation (Bernal *et al.*, 2004; Ponting *et al.*, 1992).

1.2.7.4 Parasite defence strategies: factors for detoxification and xenobiotic metabolism

Beyond direct invasion strategies, *Fasciola hepatica* has retained xenobiotic detoxification capabilities including peroxiredoxin and thioredoxin antioxidants (Donnelly *et al.*, 2005; McGonigle *et al.*, 1998; Salazar-Calderon *et al.*, 2000; Sekiya *et al.*, 2006), FABPs (Esteves and Ehrlich, 2006; Figueroa-Santiago and Espino, 2014) and glutathione transferases (GST) (Brophy *et al.*, 1995; Cervi *et al.*, 1999; Chemale *et al.*, 2006; Creaney *et al.*, 1995; Fernández *et al.*, 2015; LaCourse *et al.*, 2012). Moreover, detoxification pathways are employed by many parasites to reduce their own internal physiological damages, for example via reactive oxygen species' (ROS) assault on their membranes by host cytotoxic effector cells (Brophy *et al.*, 2012, 1995; Callahan *et al.*, 1988). The heat shock protein (HSP) family are a large group of highly conserved proteins which are ubiquitous in life, and associated with the

environmental stress response (Spiess *et al.*, 1999). HSPs are also thought to be important immunomodulatory proteins of infectious microorganisms through proposed roles in immunogenicity and anti-inflammatory virulence, which it is thought to conduct in place of its chaperoning and housekeeping activities under stressful conditions (Bellmann *et al.*, 1996; Bernal *et al.*, 2006; Higón *et al.*, 2008; Silva *et al.*, 1998; Spiess *et al.*, 1999; Srivastava, 2002). HSP70 is both spatially- and temporally-regulated in *F. hepatica*, with expression identified at the tegument (Morphew *et al.*, 2013) and its abundance is measurably higher during acute as opposed to chronic infection (Smith *et al.*, 2008), which supports its possible role in immunomodulation during early infection when acute inflammatory responses are aberrant.

The characterisation of ES, tegument and cytosol-derived proteins as possible targets for vaccine, chemotherapy and diagnosis have only partially been conducted (Dalton *et al.*, 1996; Mendes *et al.*, 2010; Morrison *et al.*, 1996; Piacenza *et al.*, 1999; Sexton *et al.*, 1990; Wijffels *et al.*, 1994). Cathepsin L (CL) proteases have taken the lead as targets for vaccines, short-term chemotherapy, and diagnostics for liver fluke (Carnevale *et al.*, 2001; Golden *et al.*, 2010; Mezo *et al.*, 2007, 2004; Mulcahy and Dalton, 2001), and currently is the target for commercially released diagnostic test kits and other prominent test designs for *F. hepatica* (Bio-X Diagnostics, Belgium). Further investigations of the neglected targets might be of equal significance and, depending on their native properties and expression pattern, provide novel descriptive indicators of infection, virulence and drug resistance status (Chemale *et al.*, 2010; Farahnak *et al.*, 2012; Harmsen *et al.*, 2004; Hodgkinson *et al.*, 2013; Morphew *et al.*, 2014; Stitt *et al.*, 1995).

1.3 Fasciolosis control strategies

1.3.1 Helminthic vaccines

1.3.1.1 Concepts and problems of helminth vaccine commercialisation

Vaccination is generally termed ‘the Holy Grail’ for parasitic worm control, but the problematic protection rates observed in field trials has limited their commercial viability for agricultural application thus far, having led to only minimal or moderate protection (Dalton and Mulcahy, 2001; Hein and Harrison, 2005; Waller, 1999). In order to produce significant immunity, formulations of attenuated whole or partial organisms aim to utilise a complete antigenic mixture to induce natural immunity; whereas an isolate or mixture of immunogens

are conversely used to trigger target-specific immunity (Dalton and Mulcahy, 2001; Hein and Harrison, 2005; Smith and Zarlenga, 2006). Such vaccine designs are often limited by their subsequent incomplete protection, whereby partial or non-specific immunity drawn by unnatural parasite exposure may cause inadequate targeting or killing of future infecting parasites and thus lead to inconsistent trial results, which are further influenced in universal applicability by animal age, adjuvant compatibility, and the complexity of natural immunological events during infections (Dalton and Mulcahy, 2001; Hein and Harrison, 2005; Maqbool *et al.*, 2016; Smith and Zarlenga, 2006). Parasite stage specificity is of additional importance to ensure the greatest protection. However, vaccine candidate progression requires advanced immunological understanding as well as clear clinical, therapeutic and economic benefits to encourage industry interest, including the reduction in anthelmintic administration (Hein and Harrison, 2005; Molina-Hernández *et al.*, 2015; Smith and Zarlenga, 2006).

Select few helminth vaccines have reached commercialisation for use with livestock, but no commercial vaccines have been successful for *Fasciola hepatica* (Dalton and Mulcahy, 2001). One of the earliest and notably successful commercial helminth vaccines was Dictol, which was developed in the 1960s using attenuated larvae for *Dictyocaulus viviparous*. The sub-unit vaccine Barbervax® was however a more recent and commercially successful product, effective against susceptible or drug-resistant *Haemonchus contortus* nematodes, which was trialled in Australia, Europe, Central and South America, and Africa, but only registered for use in Australia since late 2014 (Besier *et al.*, 2013; Smith, 2014). Subsequent candidates for other nematodes of farmed and companion animals have since been developed with varied success (Hein and Harrison, 2005; Maqbool *et al.*, 2016; Smith and Zarlenga, 2006), and particularly high protection has also been observed in vaccine trials for zoonotic cestodiases, including *Echinococcus granulosus*, and Taeniid *spp.* (Bethony *et al.*, 2011; Dalton and Mulcahy, 2001; Herd *et al.*, 1975; Lightowlers *et al.*, 2000; Pathak and Gaur, 1990; Rickard and Williams, 1982; Smith and Zarlenga, 2006). Specifically, several notable recombinant candidates for echinococcosis and taeniasis have achieved above 92% protection (Bethony *et al.*, 2011; Lightowlers *et al.*, 2000), which is an outstanding feat in the midst of otherwise immunologically complex dynamics of helminthic infections that impede vaccination attempts (Hein and Harrison, 2005; Lightowlers *et al.*, 2003). Thus, despite

extensive research studies, trials and success with other parasites however, trematodes continue to escape vaccine attempts (Knox *et al.*, 2001; Taylor, 1980).

1.3.1.2 Vaccine developments for fasciolosis

Some nematodiases and cestodiases can be managed, in principle, by vaccines, either recombinant or native antigens, through their short-term prophylactic effects and thereby reducing the clinical impacts of infection on productivity. However, there has been limited success in developing a protective vaccine for fasciolosis (Hillyer, 2005; Molina-Hernández *et al.*, 2015). For example, cathepsin L (CL) classes (Golden *et al.*, 2010; Hillyer, 2005; Jayaraj *et al.*, 2009; Tort *et al.*, 1999; Wijffels *et al.*, 1994; Zafra *et al.*, 2013a) and glutathione transferases (GSTs) (LaCourse *et al.*, 2012; Morrison *et al.*, 1996; Sexton *et al.*, 1990; Smooker *et al.*, 1999; Zafra *et al.*, 2013c, 2013b) have been major vaccine candidates in *Fasciola hepatica* because of their well understood importance in establishment of both NEJs and adult flukes (Beckham *et al.*, 2009; Cancela *et al.*, 2008; Corvo *et al.*, 2009; Cwiklinski *et al.*, 2015b, 2015a; LaCourse *et al.*, 2012; Line *et al.*, 2019; Robinson *et al.*, 2011; Zafra *et al.*, 2013c, 2013b). Unfortunately, previous vaccine trials with *Fasciola hepatica* GST, including native and recombinant forms, have reported varied protection rates, with non-significant reduction in worm burden in goats following recombinant GST (LaCourse *et al.*, 2012; Zafra *et al.*, 2013c, 2013b) and reductions in worm number by 57% in sheep (Sexton *et al.*, 1990) and 49-69% (adjuvant dependent) in cattle (Morrison *et al.*, 1996) following native GST vaccination compared to unvaccinated control infections. CL proteases have also shown varied protection between 42.5-72.4% in cattle (Dalton *et al.*, 1996; Golden *et al.*, 2010) and 43.0-78.0% in sheep (Piacenza *et al.*, 1999). These data were dependent on the formulation of different CL proteases and pairing with other parasite-specific proteins including the immunogenic adult-associated leucine aminopeptidase (LAP) (Marcilla *et al.*, 2008; Piacenza *et al.*, 1999) and the juvenile-specific haemoglobin (Dalton *et al.*, 1996). However, in one trial, the protection of sheep has been shown to improve in the absence of CL proteases, for example with LAP leading to 89% reduction in worm burden compared to unvaccinated controls (Piacenza *et al.*, 1999), suggesting the difficulty of exploiting immunomodulatory proteins such as CL proteases as vaccines. In spite of this, where these studies found reduced pathology as a

result of vaccination, their application may not be sufficient for prophylaxis, but instead realistically only provide short-term chemotherapeutic options.

Numerous other candidates with roles in virulence and immunity have been tested in livestock and disease models, including the use of protein antigens (Dalton *et al.*, 2013; Hillyer, 2005; Jayaraj *et al.*, 2009; LaCourse *et al.*, 2012; Smith and Zarlenga, 2006; Zafra *et al.*, 2013b, 2013a, 2013c) or DNA (Espino *et al.*, 2010; Kofta *et al.*, 2000; Smooker *et al.*, 2001, 1999). These studies found moderate to complete protection against heavy worm burdens and reductions in liver damage through the stimulation of Th2 immunity and humoral immune memory without the negative effects of the localised immunomodulatory properties of *F. hepatica* ES products. Despite the lack of protection against infection, the reduced impacts of disease shown by previous fluke vaccine candidates has continued motivation of research into the molecular footprints of flukes for future vaccination progression, and the hitherto partial immunity and commonly inconsistent properties of vaccines have not discouraged endorsements for a fasciolosis vaccine (Hillyer, 2005; Molina-Hernández *et al.*, 2015). The immediate problem in the absence of a vaccine is emerging global drug resistance in *F. hepatica* (and other parasitic helminths) (Brennan *et al.*, 2007; Fernández *et al.*, 2015; Gaasenbeek *et al.*, 2001; James *et al.*, 2009; Kelley *et al.*, 2016; Sanabria *et al.*, 2013). At the time of writing this thesis, it can only be reported that a new target and vaccination strategy needs to be discovered to support fasciolosis disease control in the future (Dalton and Mulcahy, 2001; Golden *et al.*, 2010; Hein and Harrison, 2005; Smith and Zarlenga, 2006).

1.3.2 Chemotherapy and integrated management of fasciolosis

It is unrealistic to control and prevent exposure to infectious *Fasciola hepatica* and other helminths through pasture and herd management alone (Morgan *et al.*, 2013). However, the most successful approach would be the incorporation of pasture-based managements with strategic chemotherapy (Barger, 1999; Maqbool *et al.*, 2016). Integrated parasite management can be difficult to implement in some regions due to the complexity of the liver fluke life cycle compared to gastrointestinal nematodes, requiring reduced grazing allowance, increased pasture rotation, reduced herd size and livestock mixing to help reduce exposure (Maqbool *et al.*, 2016; Vercruysse and Claerebout, 2001; Waller, 1999). Additionally,

the involvement of intermediate snail hosts and their role in parasite propagation further complicates pasture-based control strategies.

Focal wet areas and water-courses influence the distribution of free-living parasites and snail hosts, which is increasing the utility of geographic information systems to map epidemiological locations for suitable snail habitats in high-risk regions (Aleixo *et al.*, 2015; Dutra *et al.*, 2010; Hendrickx *et al.*, 2004; McCann *et al.*, 2010). Though challenging, further measures to interrupt transmission can use this information to target snail populations through improving water flow and drainage systems to avoid suitable habitat accumulation or through the application of molluscicides during high-risk periods (Maqbool *et al.*, 2016).However, additional avoidance of grazing in high risk areas is not always possible to attain.

Natural antagonistic and facilitative relationships between trematode rediae has been observed (Hourdin *et al.*, 1992), though presents difficulty in its application, and additionally relies on the artificial production and distribution of competing trematodes (Berg, 1973; Roberts and Suhardono, 1996). Determining snail infectivity has also been attempted in hopes of promoting infection-resistant snails and identifying potential susceptible hosts (Boray, 1978; Gutiérrez *et al.*, 2003; Rondelaud *et al.*, 2015, 2014), though wider, negative ecosystem changes could coincide. However, more successful biological controls of *Lymnaeid* hosts using molluscicidal plants and extracts (Medina and Ritchie, 1980; Medina and Woodbury, 1979; Meléndez and Capriles, 2002; Sunita *et al.*, 2013; Sunita and Singh, 2011), competing or predatory snails (Berg, 1973; Roberts and Suhardono, 1996; Rondelaud *et al.*, 2002), predatory fly larvae (Lindsay *et al.*, 2009; Mc Donnell *et al.*, 2014; Rondelaud *et al.*, 2002) and water birds have also been considered as favourable alternatives to chemical molluscicides, particularly in the short-term. Despite these approaches for fasciolosis and other snail-borne diseases, target snail exposure and specificity are ongoing concerns, whilst environmental application to the point of successful transmission interruption may be difficult to fully achieve. Consequently, these measures are commonly neither appropriate or cost-effective for many farmers, with further detrimental impacts to water sources and without the assurance of prophylaxis, which undermines their suitability for some areas affected by fasciolosis (Roberts and Copeman, 2006).

1.3.2.1 Flukicides for hepatic fasciolosis management

Realistic fasciolosis management currently relies heavily on anthelmintic applications several times per year, rather than farm-level implementation of other less efficient control measures towards integrated parasite management discussed previously (Maqbool *et al.*, 2016; Morgan *et al.*, 2013). Several benzimidazoles (BZs) are effective flukicides, especially albendazole (ABZ) and triclabendazole (TCBZ) for their respective efficacy against adults aged over 12 weeks (Johns and Dickeson, 1979) and all flukes aged over two weeks (Boray *et al.*, 1983; McKellar and Scott, 1990). TCBZ formulations were first created in the 1980s (Boray *et al.*, 1983) to utilise its broad-spectrum activities in agricultural applications against parasitic *Fasciolidae spp.* (Fairweather, 2005). However, several effective alternative flukicides to benzene-imidazole BZs have since been developed, including halogenated salicylanilides such as closantel (CLO) and rafoxanide (RFX). These have alleviated some pressure of treatment options, especially for chronic bovine infections (Fairweather and Boray, 1999; Swan, 1999), and provide room to sustain efficacious treatment options for severe and acute infections in ovines and other less common livestock hosts (Ortiz *et al.*, 2014). Resultantly, veterinary as well as medical fasciolosis cases are primarily treated with TCBZ and other BZ derivatives to utilise their consistent and broad activities, whereby TCBZ is effective against infections by *Fasciola hepatica*, *F. gigantica* (Santra *et al.*, 1999; Sanyal and Gupta, 1996) and *Fascioloides magna* (Foreyt, 1989). With relatively low costs and few comparable substitutes, TCBZ has justifiably continued as the mainstay treatment alongside ABZ where appropriate (Boray *et al.*, 1983), which is causing fears of emerging parasite drug resistance from unrelenting and intensive exposure (Fairweather and Boray, 1999).

Multiple economically important parasitic helminths contribute to ongoing impacts on herd efficiency and productivity (Maqbool *et al.*, 2016; Morgan *et al.*, 2013). Strategic selection and staggered administration of anthelmintic formulations is therefore essential, especially since outbreaks of parasitic helminths often arise in similar spring and autumnal seasonal patterns and cause disease via concurrent and recurring infections (Barger, 1999; Maqbool *et al.*, 2016). There is difficulty in maintaining single broad-spectrum anthelmintics due to the risks of encouraging resistance, though some BZs including ABZ and salicylanilides including CLO conserve known flukicidal, anti-nematodal and anti-cestodal activities (Fairweather and Boray, 1999; Swan, 1999). Mixed anthelmintic and antiparasitic formulations can avoid some problems by treating concurrent infections, either additively or

synergistically, sometimes with the added benefit of discouraging resistance when concerning different drug targets between species (Borgsteede *et al.*, 2008; Fairweather, 2005; Martínez-Valladares *et al.*, 2014; Swan, 1999; Wolstenholme *et al.*, 2006).

1.3.2.2 Anthelmintic and flukicide sustainability

Challenges of chemical-based management is the lack of sustainability, and there is a pressing need to reduce our dependence on anthelmintics but continue to alleviate parasite densities and subsequent pasture contamination to reduce disease prevalence, especially for *Fasciola hepatica* (Boray *et al.*, 1983). Efficient and appropriate treatment timing, dosage and application is respectively required for maximal therapeutic potential, lethality without permitting resistance, and targeted treatment within herds (Maqbool *et al.*, 2016; Morgan *et al.*, 2013). Despite these measures however, problems in upholding drug shelf life is compromised by over-exposure of active helminth infections to anthelmintics, which is motivated by inappropriate applications in livestock suffering clinical disease. This risks the selection of drug resistant parasite populations and inspires the need for future strategies to conserve our most efficacious flukicides in lack of newer developments (Skuce and Zadoks, 2013). However, there is also a valid argument towards sustaining drug efficacy and shelf life through the deliberate maintenance of drug-susceptible parasites, particularly nematodes, in refugia (Kenyon *et al.*, 2009a; Le Jambre, 2006; Maqbool *et al.*, 2016; Morgan *et al.*, 2013; Waller, 1999). These factors indicate the current difficulties of fasciolosis management that still hinges on TCBZ since this drug's first applications, being the most effective chemotherapeutic agent for successful management and sole drug that can ensure animal recovery from acute disease (Boray *et al.*, 1983).

1.4 Drug resistance emergence

Drug-induced changes to liver flukes by TCBZ are measurable in both NEJ and adult *Fasciola hepatica*. Damages are observed at the fluke tegument (Halferty *et al.*, 2009, 2008) and to adult reproduction through interruptions to spermatogenesis and egg viability (Alvarez *et al.*, 2009; Hanna, 2015). These findings explain the efficacy of TCBZ during both the acute and chronic disease phases, which may be based on the higher turnover and cellular activities of areas involving microtubules and specifically β-tubulin, a proposed binding target of TCBZ

(Fairweather, 2005; Fairweather and Boray, 1999). Thus, owing to the importance of these structures in fluke survival, the incidence of resistance may be directly due to molecular changes to parasite microtubule components. In fact, this is supported by shared single nucleotide polymorphisms (SNPs) that have been demonstrated in tubulin gene sequences leading to amino acid substitutions at key BZ binding sites in BZ-resistant helminths (Brennan *et al.*, 2007). Non-target protein level factors of liver fluke that are associated with TCBZ, including drug binding, diffusion and uptake, and these provide additional candidates for driving resistance mechanisms. Resistance via molecular alterations to existing drug chaperones are suspected to involve the GST phase II detoxification system (Fernández *et al.*, 2015) and the phase III P-glycoprotein transporter (Wilkinson *et al.*, 2012), though the roles are still disputed between different parasite isolates (Kotze *et al.*, 2014). For example, there is evidence to suggest the lack of phase III P-glycoprotein involvement in TCBZ resistance in Latin America (Solana *et al.*, 2018) and Australia (Elliott and Spithill, 2014). Besides SNPs and amino acid modifications that parasites may acquire for resistance phenotypes, more intrepid changes resulting from transcriptomic and epigenetic variations between flukes of different drug efficacy responses may equally contribute (Cancela *et al.*, 2010; Cwiklinski *et al.*, 2015b, 2015a; Kelley *et al.*, 2016), as has been observed in other parasitic organisms (Berg *et al.*, 2013; Kotze *et al.*, 2014).

1.4.1.1 Tracking the spread of TCBZ resistance

TCBZ resistance in *Fasciola hepatica* was first reported in Australian livestock in the 1990s (Overend and Bowen, 1995). Since then there have been 30 isolated incidents of TCBZ resistance in livestock worldwide (Figure 1.4.1.1) (Kelley *et al.*, 2016), emerging in existing endemic regions within the UK (Daniel *et al.*, 2012; Gordon *et al.*, 2012; Hanna *et al.*, 2015; Kamaludeen *et al.*, 2019; Mitchell *et al.*, 1998, 2006), Europe (Alvarez-Sanchez *et al.*, 2006; Moll *et al.*, 2000; Mooney *et al.*, 2009) and South America (Olaechea *et al.*, 2011; Ortiz *et al.*, 2013). Initial attempts to manage TCBZ-resistant parasites exploited alternative treatment options with known efficacy even against TCBZ-resistant *F. hepatica* (Coles *et al.*, 2000). This strategy was also constructive in testing the flukes' fidelity to resistance in absence of TCBZ. However, in the tested European liver fluke populations the lack of TCBZ exposure did not cause relapse to susceptibility (Borgsteede *et al.*, 2005), which reflects previous results of

resistant nematodes when tested with this approach (Waller, 1999). Consequently, TCBZ resistance characteristics may not be reversible once developed, and further evidence of this unrelenting problem has since been confirmed in Australian liver fluke field isolates, many years since the first emergence of TCBZ resistance (Brockwell *et al.*, 2014).

The necessity to control liver fluke outbreaks whilst suppressing the risks of flukicide resistance has led to the utilisation of multiple drugs with varied efficacy against parasite stages (Fairweather and Boray, 1999; Swan, 1999), as described above. Subsequently, this has resulted in different populations of drug-resistant liver fluke arising, including TCBZ but subsequently also towards ABZ (Mitchell *et al.*, 2006) and CLO (Novobilský and Höglund, 2015), two major options for liver fluke management. Thus, there are presently concerns for the potential expansion of multidrug-resistant *F. hepatica*. This is worsened due to recurring reports of drug-resistant populations, increasing annual disease incidence rates (Mitchell, 2002), and added impacts of climate change that predict increased endemicity in the near future (Fox *et al.*, 2011).

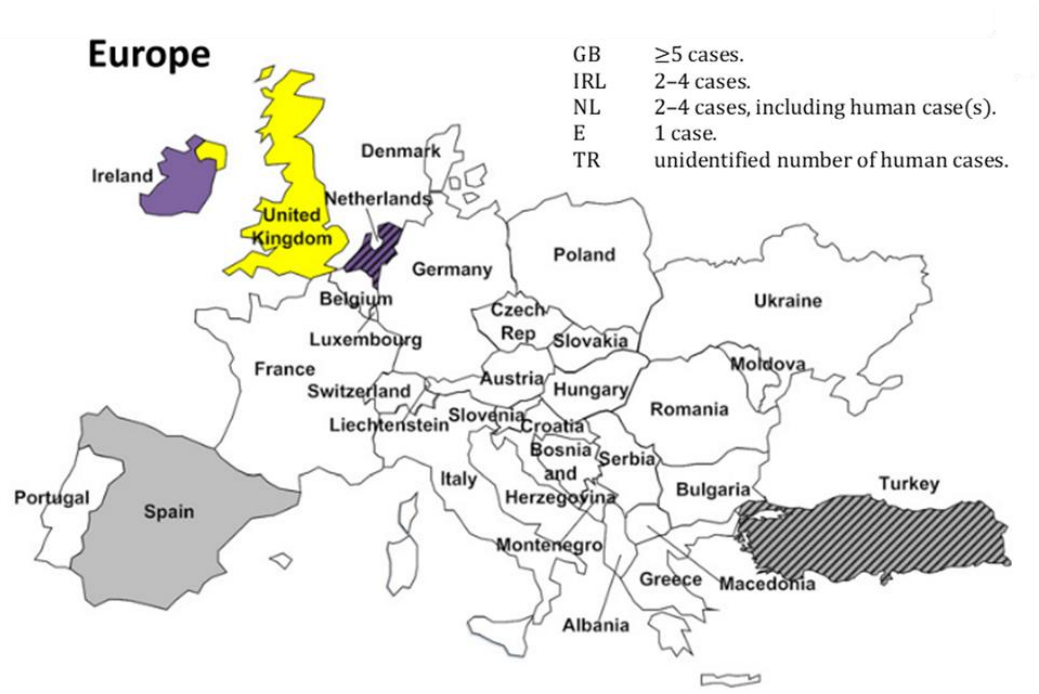

Figure 1.4.1.1. Summary of European TCBZ resistance by 2016. Published reports of *Fasciola hepatica* isolates with confirmed TCBZ resistance in five countries, with the highest number of cases of drug resistance in livestock in the UK. Image acquired from Kelley *et al.* (2016).

Abbreviations: GB, Great Britain; IRL, Ireland; NL, Netherlands; E, Spain; TR, Turkey.

1.4.2 Current options for fasciolosis diagnosis

1.4.2.1 Diagnostic timescale for Fasciola hepatica

Tools to detect helminth infection are essential for parasite control, especially in light of the major threat of anthelmintic resistance and the continued absence of effective vaccine or novel drug developments (Charlier *et al.*, 2014b; Roeber *et al.*, 2013). Sensitive and specific diagnosis at the herd-level is also important during integrated management practices, facilitating the identification of infected from uninfected individuals and treatment success (Sargison, 2012; Vercruysse and Claerebout, 2001). A range of highly sensitive and specific laboratory-based diagnostic tests have been developed for the detection of *Fasciola hepatica*, including commercial kits by Bio-X, IDEXX, Pourquier and Svanovir® and non-commercial equivalents (Carnevale *et al.*, 2001; Charlier *et al.*, 2008; Cornelissen *et al.*, 1999; Flanagan *et al.*, 2011a; Kuerpick *et al.*, 2013; Mezo *et al.*, 2007; Molloy *et al.*, 2005; Salimi-Bejestani *et al.*, 2005), whereby coproantigen detection kits are capable of immunodiagnosis from 3–4 wpi due to juvenile and adult cathepsin antigen secretions (Corvo *et al.*, 2009; Dixit *et al.*, 2008; McGinty *et al.*, 1993). However, during non-seasonal periods, clinical signs can remain unnoticed during subacute or chronic biliary infections and, if conducted during this time, test results further depend on parasite numbers and test timing post-infection or -treatment that negatively influences antigen circulation (Almazán *et al.*, 2001; Espino and Finlay, 1994; Marcilla *et al.*, 2008; Paz-Silva *et al.*, 2003; Rodríguez-Pérez and Hillyer, 1995) and recovery from faeces (Gordon *et al.*, 2012; Kajugu *et al.*, 2015; Martínez-Sernández *et al.*, 2016; Mezo *et al.*, 2004; Ubeira *et al.*, 2009). Infection stages including the relative fluke size and age, diagnostic method and TCBZ efficacy testing between 0–17 wpi (experimental and natural) with *F. hepatica* are summarised in Table 1.4.2.1. Though it has been possible to culture and maintain juveniles *in vitro* for 6 months to a nominal *in vivo* size of 7 mm (Table 1.4.2.1) (McCusker *et al.*, 2016), the development of sexual organs and egg production still requires the conditions of *in vivo* culture for parasite maturation. Consequently, studies of experimental model and ruminant animal infections have been valuable in establishing the timeline of parasite development for indicators of flukes at different infection time points (Table 1.4.2.1), including the migrations and maturation of juveniles, and egg formation of adults.

Table 1.4.2.1. Timeline of experimental liver fluke infection dynamics, diagnosis and drug efficacy determination. Abbreviations: Ab, antibody; ELISA, enzyme-linked immunosorbent assay; γ-GT, gamma glutamyl transferase; GLDH, glutamate dehydrogenase; ITS2, internal transcribed spacer 2; PCR, polymerase chain reaction.

Parasite stage	Metacercariae	Newly-excysted juvenile	Juveniles flukes		Maturing flukes, including immature and mature forms				Adult flukes									
Parasite length (mm), host-dependent	0.257 mm, hour 0-1, *in vitro*[a]; 0.14 x 0.15 mm, hour 2-3, mouse[b,c]	0.17-0.51 mm, day 1-7, mouse[b,c]	2.19 mm, day 13, mouse[b]; 1.00 mm, day 14, sheep[f]	3.32 mm, day 21, mouse[b]; 2.50 mm, day 21, sheep[f]	4.40-5.12 mm, day 28, mouse[b,d]; 4.00 mm, day 28, sheep[f]	5.00-10.60 mm, day 36-37, mouse[b-e]; 4.80 mm, day 35, sheep[f]	7.00-10.40 mm, day 43-45, mouse[d,e]; 7.00 mm, day 42, sheep[f]	7.50-13.00 mm, day 48-49, mouse[e]; 4.6 mm, day 49, sheep[g]	10.00-13.10 mm, day 53-56, mouse[d,e]; 9.50-13.50 mm, day 49, sheep[f,g]	12.2 mm, day 63, mouse[d]	10.50-20.90 mm, day 69-71, mouse[d,e]; 12.00 mm, day 70, sheep[f]	n/a	14.40 mm, day 81, mouse[d]; 18.00 mm, day 84, sheep[f]	n/a	n/a	16.00 mm, day 108, mouse[e]; 22.80-25.90 mm, day 105, sheep[f,g]	n/a	14.00 mm, day 119-120, mouse[d,e]
Parasite location *in vivo*	Duodenum, alimentary canal	Abdominal cavity; liver parenchyma	Liver parenchyma; earliest recorded entry to bile duct in mice (day 24)[b]		Liver parenchyma; earliest recorded entry to bile duct in sheep (day 28)[d]			Liver parenchyma; earliest recorded entry to bile duct in cattle (day 49)[e]	Biliary system									
Week (day) post-infection	0 (0)	1 (7)	2 (14)	3 (21)	4 (28)	5 (35)	6 (42)	7 (49)	8 (56)	9 (63)	10 (70)	11 (77)	12 (84)	13 (91)	14 (98)	15 (105)	16 (112)	17 (119)
Diagnostic tests currently available	n/a	n/a	Stool, nested PCR, sheep[h]; stool, PCR, sheep[i]	Stool, PCR, sheep[h]; serum Ab, ELISA, sheep[h]; serum Ab, ELISA, cattle[1][j]	Stool, ELISA, cattle[k]; serum Ab, ELISA, cattle[1,2][j][2][j]	Serum Ab, ELISA, cattle[3][l]	Stool, ELISA, day 43, sheep[1][m]; serum GLDH titre, sheep[n]	Stool, ELISA, day 47, 50, sheep[1], [2][o]	Serum γ-GT titre, sheep[j]; stool, ELISA, day 53, sheep[3][o]; stool, FEC, day 59, sheep[1][o]	Stool, FEC, sheep[h,k][1][m]; stool, ELISA, day 60[2][m], day 62[4][o], sheep	Stool, FEC, sheep[h,k][3][o]; serum γ-GT titre, sheep[n]	Stool, FEC, day 75[4][o], day 77[2][m,o], sheep; serum Ab, cattle[3][j]	n/a	n/a	n/a	n/a	n/a	n/a
Triclabendazole efficacy tests currently available	n/a	n/a	n/a	n/a	n/a	n/a	n/a	n/a	n/a	Serum γ-GT and GLDH titres, sheep[j]	n/a	n/a	n/a	Stool, FEC-RT, day 91 [2,4] day 94[3], sheep[o]	Stool, C-RT[2][m][2,4][o], day 101[3][o], FEC-RT[3][o], sheep	n/a	Post-mortem-RT, fluke recovery*, sheep[k]	n/a

A. (Hussein *et al.*, 2010).
B. (Dawes, 1962a).
C. (Dawes, 1961).
D. (Dawes, 1962b).
E. (Lagrange and Gutmann, 1961).
F. (Dow *et al.*, 1968).
G. (Kistner and Koller, 1975).
H. (Martínez-Pérez *et al.*, 2012), PCR: CoxI; Nested PCR: CoxI and rRNA; ELISA: Bio-X K201.
I. (Robles-Pérez *et al.*, 2013), PCR: ITS2.
J. (Kuerpick *et al.*, 2013), [1] Pourquier ELISA; [2] ES ELISA; [3] rFhCL1.
K. (Gaasenbeek *et al.*, 2001), post-mortem-RT: >95% fluke burden reduction*.
L. (Cornelissen *et al.*, 1999), [1] native ES-ELISA; [2] synthetic, mature CL1-peptide7-ELISA; [3] native CL1-ELISA.
M. (Flanagan *et al.*, 2011a), ELISA: Bio-X K201. [1] Sligo (TCBZ-R); [2] Cullompton (TCBZ-S).
N. (Raadsma *et al.*, 2007).
O. (Flanagan *et al.*, 2011b), ELISA: Bio-X K201. RT: >95% reduction test. [1] Oberon (suspected TCBZ-R); [2] Cullompton (TCBZ-S); [3] Fairhurst (TCBZ-S); [4] Leon (TCBZ-S).

Infection patency and adult fluke numbers determine measurable faecal egg counts (FEC), the most widely used test that benefits from high specificity (Cornelissen *et al.*, 2001; El-Bahi *et al.*, 1992; Gordon *et al.*, 2012; Palmer *et al.*, 2014; Valero *et al.*, 2012), despite the timing differences observed between different host infections (Table 1.4.2.1). Due to the often intrahepatic biliary habitation of chronically infecting flukes, FECs are influenced by fluctuations of eggs that are transmitted to faeces leading to unrepresentative and inconsistent FEC data, and invasive alternatives for direct egg or antigen detection from the bile duct (Braun *et al.*, 1995; El-Bahi *et al.*, 1992). Coproantigen detection is consequently considered a more sensitive and specific faecal-based test that is applied as early as 4 wpi (Almazán *et al.*, 2001; Brockwell *et al.*, 2013; Gaasenbeek *et al.*, 2001; Kajugu *et al.*, 2015; Mezo *et al.*, 2004; Valero *et al.*, 2012). No antigenic determinants currently qualify as informants of parasite maturity or drug susceptibility, though FEC and coproantigen reduction testing (FEC-RT, C-RT) have been established as the primary method to monitor treatment success two weeks post-treatment (Daniel *et al.*, 2012; Flanagan *et al.*, 2011a, 2011b; Gordon *et al.*, 2012).

There are no commercial diagnostic kits to define the larval infection stage of *F. hepatica*, although infection-associated host markers are also utilised to monitor infection presence and progress. Host plasma enzymes are a sensitive reflection of infection stage as the flukes begin to migrate through tissues and cause damage to the liver (glutamate dehydrogenase, GLDH) from 6 wpi and bile ducts (gamma glutamyl transferase, γ-GGT) from 8 wpi (Dalton *et al.*, 1996; Golden *et al.*, 2010; Raadsma *et al.*, 2007). Similarly to the nature of circulating and copro-antigens being a direct reflection of fluke presence, DNA-based diagnoses can be developed as molecular targets are elucidated, and are detectable from host samples after only 2 wpi by PCR (verses *F. hepatica* internal transcribed spacer 2, ITS2; Robles-Pérez *et al.*, 2013), nested PCR (verses *F. hepatica* CoxI and rRNA; Martínez-Pérez *et al.*, 2012) or loop-mediated isothermal amplification (LAMP) (Ai *et al.*, 2010a, 2010b; Cabada and White, 2012). Despite the reputably high specificity and sensitivity of immunologic tests that detect infection after 3 wpi (Table 1.4.2.1), indirect methods of anti-*F. hepatica* serum detection is limited by the interference of previous fluke exposure that has been successfully treated (Brockwell *et al.*, 2013; El Bahy *et al.*, 1994; Reichel *et al.*, 2005). Despite the complexity of ELISA kits, peptide, recombinant protein, ES, Bio-X K 201 (anti-CL monoclonal antibody-based) and Pourqier (F2 antigen-based), remain major tools for field and research diagnoses

(Brockwell *et al.*, 2013; Cornelissen *et al.*, 2001, 1999; Kuerpick *et al.*, 2013, 2012; Novobilský *et al.*, 2012; Palmer *et al.*, 2014). However, progression to improve current methods via the diagnosis of infection stage and anthelmintic efficacy are priorities for a new line of candidate tests that are required to adapt to the current threats of climate change impacts and flukicide resistance.

1.4.2.2 Current utilisation of fasciolosis diagnostics

DNA-based molecular diagnostics such as PCR can identify, distinguish and quantify the prevalence of *Fasciola spp.*-specific DNA sequences with very high specificity and sensitivity from only two wpi (Ai *et al.*, 2010a, 2010b; Martínez-Pérez *et al.*, 2012; Robles-Pérez *et al.*, 2013; Rokni *et al.*, 2010; Shahzad *et al.*, 2012). LAMP is an especially important step forward towards the development of field-based tests, due to its thermal stability and point-of-care medical applications for a wide range of diseases (Ai *et al.*, 2010b; Mori and Notomi, 2009; Ndao, 2009). However, though LAMP can maintain PCR-level sensitivity and specificity, crude DNA extraction for sample preparation remains difficult and prevents routine application of LAMP for penside, non-laboratory-based diagnoses of *F. hepatica* and other livestock helminths (Deng *et al.*, 2019; Mugambi *et al.*, 2015). Despite the improvement to diagnostic timing brought through immunologic and molecular advancements, the reliability, specificity and moderate sensitivity of FEC means it maintains a primary position in fasciolosis diagnostics. However, there continues to be a gap in the liver fluke market to introduce a simplistic and field-appropriate molecular or serological test to inform farmers and veterinarians of infections for subsequent treatment selection, and these tests have long been developed for other neglected parasitic diseases (Ashton *et al.*, 2011; Campbell and Landry, 2013; Nabity *et al.*, 2012; Ndao, 2009; Tsang *et al.*, 1989). To this end, desirable features for enhanced application within current fasciolosis control regimes would be a field-appropriate platform that can discriminate parasite stage, virulence or drug response for appropriate interventions.

Currently, commercial laboratory-based tests, as well as non-commercial 'academically' produced kits of similar design, remain disadvantaged for application in fasciolosis control. Specifically, as an ELISA format, they require expertise, are lengthy, expensive to conduct and unable to quantify infection relative to fluke burden, and the

interpretation of results remains unavoidably complicated, especially with the consideration of kit-specific drawbacks of variable sensitivity and/or specificity (Charlier *et al.*, 2014b; Palmer *et al.*, 2014). However, some molecular-based tests can be condensed into less complex and/or economically-demanding formats, such as LAMP (Ai *et al.*, 2010b), dot ELISAs (Arjmand *et al.*, 2014; Meshgi *et al.*, 2018; Shaheen *et al.*, 1989), lateral flow tests (Martínez-Sernández *et al.*, 2011; Walsh *et al.*, 2018) and agglutination tests (Intapan *et al.*, 2004; Levieux *et al.*, 1992). Thus, as indicated above, there is a window of technical and commercial opportunity to develop penside tests for fasciolosis (Martínez-Sernández *et al.*, 2011; Shaheen *et al.*, 1989; Walsh *et al.*, 2018).

1.4.2.3 Evaluating flukicide efficacy

Academic literature continues to report that the trends in fasciolosis management indicate current interventions will not be realistic or efficacious for long-term and cost-effective control. In reality, with the absence of a vaccine and new anthelmintics, slowing the rate of drug resistance to current drugs remains a cornerstone to attempting to sustain control of helminth parasites (Maqbool *et al.*, 2016; Molina-Hernández *et al.*, 2015; Waller, 1999). Unfortunately, the current options to measure drug efficacy are simply adaptations of existing diagnostic methods, which record numeric (FEC) or relative (antigen ELISA) quantitative reductions in parasite factors before and after treatments in order to establish the present treatment efficacy and advise future treatment plans (Fairweather, 2011c; Flanagan *et al.*, 2011b, 2011a; Hanna *et al.*, 2015; Jones *et al.*, 2013; Novobilský *et al.*, 2012; Sargison, 2012). Though the measurement of host damage or parasite abundance are additionally useful to assess treatment efficacy against disease, the rising rates of reported drug resistance reduce the usefulness of these reduction tests, since they instigate chemotherapeutic exposure in order to demonstrate efficacy statuses. Furthermore, problems remain in the classification of 'true' drug resistance or treatment failure, influenced by the parasite or incorrect drug administration, respectively (Fairweather, 2011b, 2011c). This knowledge also supports the growing requirement to develop more reliable and bespoke diagnostics for monitoring treatment success.

1.5 PhD proposal

New functional genomics investigations continue to identify molecules of the immunomodulatory and drug-associated subproteomes of *Fasciola hepatica* that are of potential interest for prospective molecular studies, diagnostics and vaccine developments (Cwiklinski *et al.*, 2015a; Cwiklinski *et al.*, 2018; Jefferies *et al.*, 2001; Morphew *et al.*, 2007; Robinson *et al.*, 2009). For example, the discovery of TCBZ susceptibility- and survival-associated biomarkers (Morphew *et al.*, 2014) identified diagnostically-significant candidates that warranted immediate further investigation. Immunologic tests have been at the forefront of fasciolosis diagnostics due to the expanding profile of the fluke's somatic and ES proteomes offering new biomarker candidates (Dalton *et al.*, 2013; Montaner *et al.*, 2014; Morphew *et al.*, 2013; Vukman *et al.*, 2013). The 'omics technologies have also delivered new vaccine candidates via reverse vaccinology strategies (Molina-Hernández *et al.*, 2015). Thus, expanding the options available in fasciolosis control strategies via new polyomics approaches will hopefully improve farm management of liver fluke.

This thesis aims to investigate a panel of molecular candidates towards the development of a novel diagnostic approach to monitor *F. hepatica* infection and drug susceptibility. Thus, the thesis structure following this introduction includes a common methodology section (Chapter 2: General Materials and Methods) and collective discussion (Chapter 7: General Discussion) and conclusion (Chapter 8: Final Conclusions and Recommendations), which are separated by four experimental chapters with specific objectives, each exploring molecular targets of putative diagnostic interest:

1. Chapter 3: Identifying and characterising immunogenic subcomponents of cathepsin L zymogens;
2. Chapter 4: Delineating phenotypic and proteomic differences between representative wild type *F. hepatica* parasites and a TCBZ-resistant isolate strain via *in vitro* anthelmintic challenges;
3. Chapter 5: Discovering the biology underpinning TCBZ-SO-associated *F. hepatica* protein biomarker candidates via a bioinformatic pipeline in order to support decisions on recombinant expression and purification;
4. Chapter 6: Designing and validating novel diagnostic tools from selected candidates via the production of recombinant and synthetic antigens and polyclonal antibodies.

2 Chapter 2: General materials and methods

2.1 Introduction to Chapter 2: General materials and methods

In order to avoid duplication and prevent repetition for the passing reader, the following methodology (2 Chapter 2: General materials and methods) was compiled to comprise all techniques that were utilised within two or more of the experimental chapters, whether wet- or dry-lab in description. However, further methods that were not commonly used and specific to individual experimental chapters can be found in the relevant methodology sections of each chapter: sections 3.3; 4.3; 4.3; 6.3.

2.2 *Fasciola hepatica in vitro* culture

2.2.1 Fluke collection and incubation for ES antigen production

The methodology for maintaining liver fluke *in vitro* culture was adapted from Morphew *et al.* (2014). Briefly, live adult *Fasciola hepatica* were collected at a local abattoir on a normal working day of the production line from freshly slaughtered sheep livers with natural infections. Flukes were washed in 1X PBS (pH 7.4, Sigma-Aldrich, UK) at 37°C, which was refreshed every 15 minutes for 1 hour. Adults were grouped into DMEM (pH 7.4, Gibco™) supplemented with HEPES [15 mM], glucose [61 mM], calcium acetate [2.2 mM], magnesium sulphate [2.7 mM], serotonin [1 µM] and gentamycin [5 $\mu g \cdot \mu L^{-1}$] at 37°C. Flukes were cultured for 4 h (including transport to proteomics laboratory) to establish a biological baseline and for adjustment to *in vitro* culture conditions. Next, the flukes were transferred to fresh media for a further 4 h or other specified culture period with 10 size-matched replicates and 3 mL per fluke.

2.2.2 Treatment for induction of death-associated ES products

Following the primary culture incubation, a selection of fluke replicate groups were terminated in ethanol with 1% (w/v) ethyl 4-aminobenzoate based on the procedure described by Morphew *et al.* (2007). Flukes were submerged for up to 15 seconds then subsequently washed in 1X PBS and transferred to fresh DMEM medium for a third incubation for 5 h.

2.2.3 Fluke and ES sample storage

Flukes were removed from cultures and individually stored for subsequent proteomic analysis by immediate snap-freezing in liquid nitrogen or immediate fixing for electron microscopic analysis. Media containing ES products was stored at -80°C until required.

2.3 Protein handling and preparation

2.3.1 Somatic protein preparation

Flukes were thawed on ice and ground using 1 g tissue per mL in ice cold homogenisation buffer (1 M potassium phosphate (pH 7.4), 1% Triton-X, EDTA-free protease inhibitor cocktail) and centrifuged at 21,000 x *g* for 30 minutes to separate lipids and insoluble protein from solubilised proteins.

2.3.2 ES product preparation

Crude ES was spun at up to 300 x *g* at 4°C for 10 minutes followed by 700 x *g* at 4°C 30 minutes to remove eggs, fluke tissue and liver particulates.

2.3.3 Protein precipitation

To remove *in vitro* liquid culture supplements and biomolecules from ES fractions and to remove unwanted salts or organic compounds, proteins were precipitated by 1:1 mixing with 20% (w/v) trichloroacetic acid (TCA; Fisher Sci, UK) in ice cold 100% (v/v) acetone (Fisher Sci, UK) and incubating for an hour at -20°C. Samples were repeatedly subjected to centrifugation at 21,000 x *g* for 20 minutes and washing in fresh ice cold 100% (v/v) acetone. Samples were stored directly at -20°C or resuspended in distilled water (18.2 MΩ) or suitable buffer for downstream applications.

Clarified media were precipitated using the TCA-acetone method as follows. Briefly, proteins were precipitated by 1:1 mixing with ice cold 20% (w/v) TCA in acetone for an hour at -20°C and with centrifugation at 21,000 x *g* for 20 minutes at 4°C, with two further ice-cold acetone washes. Protein pellets were stored at -20°C until required.

For 2-DE analyses, precipitated proteins were resuspended in protein buffer A (8 M urea, 2% w/v CHAPS, 33 mM dithiotreitol (DTT), and 0.5% v/v carrier ampholytes (Biolyte 3-10, Bio-Rad, UK)).

2.3.4 Protein sample concentration analysis

Protein concentration was calculated using the Bradford assay, using BSA as a standard, as previously described (Bradford, 1976) at A_{595} using a Varian Cary 50 Bio UV-V Spectrophotometer (Agilent Technologies, UK). For small sample volumes and/or where sample purity was also of interest, protein samples were analysed at A_{280} against the equivalent resuspension buffer using a NanoDrop® ND-1000. Protein samples were stored at -20 or -80°C until required.

2.4 Proteomic analyses

2.4.1 Sodium dodecyl sulfate polyacrylamide gel electrophoresis (SDS-PAGE)

2.4.1.1 *1-D SDS-PAGE*

Protein samples were mixed thoroughly in buffer B ([4X] 277.8 mM tris-HCl, pH 6.8: 44.4% (v/v) glycerol: 4% (w/v) SDS; 0.02% bromophenol blue). β-mercaptoethanol [1:10 dilution] or DTT [50 mM] were added to buffers prior to use and samples were denatured at 95°C for 10 minutes in order to disrupt disulphide bridges. Polyacrylamide (30% acrylamide/bis 29:1 solution, Bio-Rad) gels made in-house using the Bio-Rad Mini-PROTEAN® Tetra hand cast system with short 7 cm front and back plates with integrated 0.75 mm or 1.0 mm spacers for use with 10- or 15-well combs (Bio-Rad, UK). Electrophoresis was conducted at ambient temperature using the Protean Mini Tetra System (Bio-Rad, UK) in [1X] TGS buffer and proteins were separated at 75 V through the stacking gel (4.5% acrylamide; 0.5 M tris, pH 6.8; 0.4% (w/v) SDS), followed by 150 V through the resolving gel (12.5% acrylamide; 1.5 M tris, pH 8.5; 0.4% (w/v) SDS) as required. Gels were fixed (10% (v/v) acetic acid; 40% (v/v) ethanol) and stained with Coomassie blue (PhastGel Blue R, Amersham Biosciences, UK) with 10% (v/v) acetic acid and 30% (v/v) methanol or Coomassie blue solution (QC Colloidal Coomassie, Bio-Rad) then destained in 1% (v/v) acetic acid as required.

SDS-PAGE gels were imaged using a GS-800 densitometer (Bio-Rad, UK) or a Typhoon FLA9500 (GE Health Life Sciences, UK) and images were prepared using Quantity One 1-D Analysis Software V.4.6.9 (Bio-Rad, UK) or ImageQuant TL V.8.1 (GE Health Life Sciences, UK) where required. For low concentration proteins, polyacrylamide gels were stained with silver nitrate (0.1% solution, Fisher Scientific, UK), then destained and reimaged as described.

2.4.1.2 *2-D SDS-PAGE*

7 cm linear pH 3-10 IPG strips (Bio-Rad, UK) were rehydrated overnight at ambient temperature with proteins resuspended in 125 µL of rehydration buffer containing 25 µg of the protein sample. Hydrated strips were isoelectrically focussed at 10,000-11,000 Vh using a Protean Mini IEF Cell (Bio-Rad, UK) to separate protein samples in the first dimension then equilibrated in 2-DE equilibration buffer (50 mM tris-HCl; 6 M urea; 30% (w/v) glycerol; 2% (w/v) SDS) with DTT [10 $mg \cdot mL^{-1}$] for 15 minutes then IAA [25 $mg \cdot mL^{-1}$] for a further 15 minutes. 7 cm polyacrylamide gels were prepared as described (2.4.1) and prepared strips were fixed in molten overlay agarose (0.5% (w/v) agarose; 0.125 M tris (pH 6.8); [100 $mg \cdot mL^{-1}$] bromophenol blue) and electrophoresed, stained and imaged as described (2.4.1.1).

2.4.2 Western hybridisation

2.4.2.1 *Primary antibodies*

Polyclonal (Pc) antibodies (Ab) were raised to a recombinant procathepsin L Leu12Pro mutant (rFhΔpCL1) in two laboratory rabbits (Lampire Biological Laboratories, USA). Immunisations with approximately 0.3 mg antigen (Ag) mixed with an equal volume of complete or incomplete Freunds' adjuvant (CFA/IFA) were given at day one (Ag-CFA), 21 (Ag-IFA) and 42 (Ag-IFA), with the first two via the popliteal lymph node following Evan's blue introduction, and the final booster by intradermal injection. Blood samples were harvested at day zero (pre-immunisation bleed) and after 30 (test bleed) and 50 (production bleed) days, followed by a final collection after 61 days (terminal bleed). All blood samples were then prepared for separation and isolation of whole sera.

Whole sheep sera were isolated from blood collected at weekly intervals from experimental infections with TCBZ-susceptible (TCBZ-S) or -resistant (TCBZ-R) *F. hepatica* isolates as specified per protocol (Ridgeway Research Ltd., UK). Pooled sera for the comparison of serum responses between 0–17 weeks post infection (wpi) and following clinically-administered TCBZ treatment (10 $mg \cdot kg^{-1}$) at week 12 were pooled from three sheep individually infected with one of three TCBZ-S strains: Aberystwyth; Italian; Miskin (TCBZ-S, excluding week 17: Italian and Miskin); or TCBZ-R strains: Kilmarnock; Penrith; Stornoway.

2.4.2.2 *Secondary antibodies*

Anti-rabbit (A3687, produced in goat), -sheep (A5187, produced in donkey) and -bovine (A0705, produced in rabbit) raised against whole IgG molecules conjugated to alkaline phosphatase were used according to the manufacturer's instructions (Sigma-Aldrich, UK), detailed below in full.

2.4.2.3 *General protocol for immunoblotting (western hybridisation)*

Nitrocellulose membrane (NCM) with 0.45 µm pores was used for all western hybridisations (Amersham Biosciences, UK) unless otherwise stated. NCMs were first wetted with distilled water (UV-sterilised; 18.2 MΩ) and then membrane, gel blot papers and Scotch-Brite pads were allowed to equilibrate in Bjerrum buffer (25 mM (w/v) tris, pH 8.3; 192 mM (w/v) glycine; 20% (v/v) methanol).

SDS-PAGE-separated proteins were transferred onto NCM at 40 V for two hours or at 20 V for 16 hours using a Trans-blot Cell (Bio-Rad, UK). Protein transfer was confirmed by temporary staining with Amido Black (0.1% (w/v) Amido Black; 10% (v/v) acetic acid; 25% (v/v) isopropanol) for up to 1 min and washing with 10% (v/v) acetic acid and 25% (v/v) isopropanol for imaging (Figure 2.4.2.3). Staining was removed via washes with TBS-T (TBS: 100 mM tris, pH 7.5; 154 mM sodium chloride; TBS-T: TBS; 1% (v/v) Tween® 20) and membranes were blocked for at least 16 h at 4°C in TBS-T with 5% (w/v) skimmed milk powder.

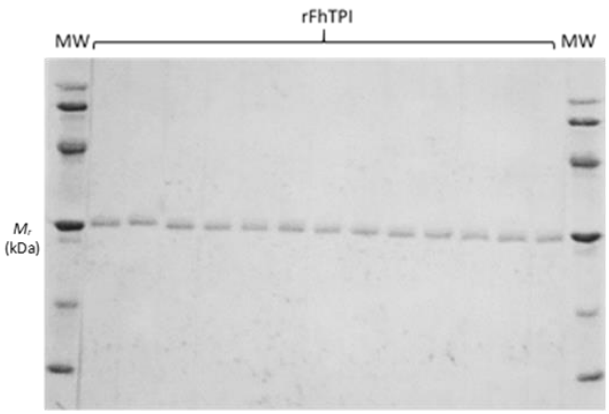

Figure 2.4.2.3. Transfer confirmation via NCM Amido Black staining. NCMs were submerged in 0.1% (w/v) Amido Black to confirm protein transfer from SDS-PAGE gels. An exemplar NCM transfer of recombinant purified *F. hepatica* triose phosphate isomerase (rFhTPI, AGJ83762.1; GenBank v204: www.ncbi.nlm.nih.gov/protein/AGJ83762.1) is shown. Abbreviations: MW, Amersham Low Molecular Weight SDS Calibration Kit (M_r).

Blocked membranes were washed in fresh TBS-T and subsequently incubated with primary antibody at a precalculated dilution in TBS-T with 1% (w/v) skimmed milk powder for 1 h. Membranes were washed with TBS to remove unbound antibodies and subsequently

incubated with secondary antibodies with an alkaline phosphatase (ALP) conjugate diluted to 1:30,000 in TBS-T as recommended (Sigma-Aldrich, UK). Antigen-antibody binding was confirmed by membrane development in 5-bromo-4-chloro-3-indolyl-phosphate (BCIP; Sigma-Aldrich, UK) and nitro blue tetrazolium (NBT; Thermo Scientific, UK) dissolved in working ALP substrate buffer solution (100 mM tris-HCl, pH 9.5; 100 mM NaCl; 5 mM $MgCl_2$) as required until reactions were stopped with distilled water (UV-sterilised; 18.2 MΩ).

Where required, all antibodies were stripped from membranes by incubating NCM in stripping solution (200 mM glycine; 3.5 mM SDS; 1% Tween® 20; pH 2.2) for a maximum of 10 minutes. The stripping solution was then removed from membranes in two TBS washes followed by two TBS-T washes for 5 minutes each before resuming the original protocol.

2.4.3 Liquid chromatography-tandem mass spectrometry (LC-MS/MS)

1-DE gel slices and 2-DE gel spots were aseptically excised and individually prepared for liquid chromatography and tandem mass spectrometry. Firstly, 1-DE and 2-DE gel pieces were destained (25 mM (w/v) ammonium bicarbonate; 50% (v/v) acetonitrile; both Fisher Scientific, UK) and dehydrated (100% (v/v) acetonitrile). 1-DE samples were additionally resuspended in denaturating washes with DTT [10 mM] and iodoacetamide (IAA) [55 mM] and re-dehydrated. Proteins were digested overnight with sequencing grade modified trypsin [10 ng·µL^{-1}] (Promega, UK) in 50 mM (w/v) ammonium bicarbonate, washed in ultrapure water and resuspended in 50% (v/v) acetronitrile with 5% formic acid (v/v) before drying and final resuspension in 0.1% formic acid (v/v).

Tryptically-digested peptides (1–10 µL injection volume) were analysed following separation using an electrospray ionization quadrupole time-of-flight machine (ESI-QUAD-TOF, Agilent 6550 iFunnel Q-TOF, Agilent Technologies, UK) coupled to a HPLC Prot-ID Chip (Agilent Technologies, UK), with all parameters set as detailed by Davis *et al.* (2019).

Where required, peptide samples (10 µL injection volume) were separated using an Orbitrap Fusion Tribrid mass spectrometer (referred to hereon as an electrospray ionisation (ESI) -TRAP; Thermo Scientific, UK) coupled to an UltiMate 3000 liquid chromatography tower (Dionex, Thermo Scientific, UK) and Zorbax Eclipse Plus reverse phase C18 column maintained at 30°C (2.1 mm x 50 mm, particle size 1.8 µm; Agilent Technologies, UK). Mobile phases for gradient elution were maintained at a flow rate of 0.1 mL/min, using ultra-pure water (18.2

MΩ) with 0.1% formic acid (mass spectrometry grade; Fluka, UK) (eluent 1), and 95:5 acetonitrile (Optima, Fisher Scientific, UK): ultrapure water with 0.1% formic acid (eluent 2). The initial condition was 3% eluent 2 with a linear increase to 40% over 9 minutes, increasing to 100% eluent 2 in a further 2 minutes then held for 1 minute at 100% eluent 1 before equilibration at initial conditions for a further 1.5 minutes. Ions were generated using a heated ESI (H-ESI) source with a voltage of 3500 in positive mode, sheath gas at 25°C, aux gas at 5°C, a vaporiser temperature of 75°C and an ion transfer temperature of 275°C. Standard peptide analysis parameters were used comprising a data dependent MS^2 experiment, whereby parent ions were detected in profile mode in the 375–1500 m/z range in the Orbitrap at a resolution of 120,000 and a maximum injection time of 50 milliseconds in positive mode. MS^2 data were then collected in data-dependent mode including charge states of 2–7, and dynamic exclusion of masses for 20 seconds after initial selection for MS^2. Ions were formed by fragmentation by collision induced dissociation with a collision energy of 35%, and resulting ions were detected in the ion trap in centroid mode.

Data files were submitted to MASCOT (www.matrixscience.com) against the relevant genome and/or proteome databases as specified per sample in each experimental chapter: including the National Center for Biotechnology Information NR database (GenBank v204, Benson *et al.*, 2015: www.ncbi.nlm.nih.gov) or an additional preliminary search against the WormBaseParaSite *F. hepatica* genome drafts (WBPS, parasite.wormbase.org: PRJEB6687 WBPS v10, 2014; PRJNA179522 WBPS v10–14, 2014–2018). Search parameters were selected as follows for trypsin digestion with up to one missed cleavage, peptide charges of 2.0–4.0+, ±1.2 Da peptide tolerance (monoisotopic, $_{13}C = 0$), ±0.6 Da MS/MS tolerance, and permitting modifications including carbamidomethyl groups (fixed) and oxidation (variable). Options were selected where required and specified per sample for greater inclusion of potential hits (error tolerance) or to assess the reliability of resultant hits (decoy).

3 Chapter 3: Investigating the procathepsin L subproteomes of *in vitro* cultured live and dead *Fasciola hepatica* parasites

3.1 Abstract

Of the proteomic components of *Fasciola hepatica* ES products, cathepsin L (CL) proteases of multiple proteomic classifications (clades 1–5) have become leading molecular biochemical and diagnostic targets, drawing in great and unparalleled research interest. In contrast, CL zymogens comprising the inactive protease region intact with N-terminal signal and inhibitor peptides (prepro-CL), or following signal cleavage (pro-CL), have demonstrable antigenic potential but are understudied precursors to the well-known enzyme. To explore this knowledge-gap, immunogenicity of prepro- and pro-CL zymogens was investigated to assess their potential utility for the diagnosis of *F. hepatica* infection.

Following *in vitro* culture of adult *F. hepatica*, native CL zymogens were recovered from SDS-PAGE-separated excretory/secretory (ES) products. This discovery also demonstrated an association between CL zymogen abundance and fluke viability and fitness, further indicating the stringent regulation of these zymogens, which may also act to reduce pre-/pro-CL antigen exposure in the ES products of this parasite. Subsequently, three recombinantly-produced pro-CL1 zymogens (rFhpCL1) were bioinformatically dissected to determine antigenic properties, including predicted pan-CL family clade epitopes. Upon identification of multiple antigenic regions and peptides of interest, anti-rFhpCL1 polyclonal antibodies were produced and CL zymogen specificity was then shown. Furthermore, immunogenicity was demonstrably conserved between rFhpCL1 zymogens and multiple native CL zymogen clades, and there was no observable reactivity toward respective enzyme derivatives.

Consequently to the findings of this chapter, new information has been determined concerning the antigenicity of zymogen-specific epitopes. In addition, new tools with preliminary evidence of diagnostic utility have been produced and are ready for pilot testing with experimentally-infected samples toward novel diagnostics of fasciolosis.

3.2 Introduction

3.2.1 Molecular profiles of *Fasciola hepatica* cathepsin-like proteases

Fasciola hepatica-derived cysteine proteinases belong to a large superfamily of ubiquitous papain-like enzymes (McGrath, 1999; Stack *et al.*, 2007; Turk *et al.*, 2012), and were first identified as nutrition-enhancing enzymes with cathepsin-like activity, resembling mammalian cathepsin C (Halton, 1967) and CL proteases (Dalton *et al.*, 2003, 2004; Dalton

and Heffernan, 1989; Dowd *et al.*, 1994; Robinson *et al.*, 2008a; Smith *et al.*, 1993b). CL proteases have since been confirmed as a major contributor to cathepsin-like enzyme activity of adult *F. hepatica* secretions (Dowd *et al.*, 1994; Smith *et al.*, 1993b).

Many helminths of medical and veterinary importance express cysteine proteases, utilised as virulence enhancers including towards invasion of the host and parasite nutrition (Caffrey *et al.*, 2018; Robinson *et al.*, 2008a). However, amongst parasitic helminths, *F. hepatica* has the largest family of cathepsin L cysteine proteases, with 17 different CL members in 5 clades, as well as three isotypes of juvenile-specific cathepsin B (CB) proteases (Cwiklinski *et al.*, 2015b; Robinson *et al.*, 2008b; Wilson *et al.*, 1998). CL1, 2 and 5 clades are secreted by adults and CB, CL3 and CL4 clades are secreted by juveniles (Meemon and Sobhon, 2015; Wilson *et al.*, 1998). This developmental regulation facilitates the timely secretion into appropriate host environments of enzymes possessing particular substrate specificities that are ranging, but overlapping in nature (Caffrey *et al.*, 2018; Meemon and Sobhon, 2015; Robinson *et al.*, 2008a). CL and CB proteases are consequently temporally-regulated and with specialist roles during *in vivo* infection, where CB is essential for juvenile tissue penetration (McGonigle *et al.*, 2008; Meemon and Sobhon, 2015), CL1 can cleave TLR3 (Donnelly *et al.*, 2010), CL1 and CL2 proteases can cleave host IgG (Berasaín *et al.*, 2000; Carmona *et al.*, 1993; Smith *et al.*, 1993a), CL1–3, particularly CL2 and CL3, can degrade collagen (Berasaín *et al.*, 1997b; Corvo *et al.*, 2013; Robinson *et al.*, 2011), whilst CL1, CL2 (Berasaín *et al.*, 1997b) and CL5 (Norbury *et al.*, 2011) have demonstrated further digestive capabilities of host laminin and fibrin. Juvenile liver fluke secrete CL3, CL4 and CB in order to actively assist abdominal tissue penetration before initialising hepatic invasion and immune evasion via CL1–5 secretions, interrupting important signal transduction and cytotoxic cell stimulation (Caffrey *et al.*, 2018; Carmona *et al.*, 1993; Dalton *et al.*, 2003; McGonigle *et al.*, 2008; Robinson *et al.*, 2008a; Smith *et al.*, 1993a). Furthermore, as a prominent component of the adult and juvenile *F. hepatica* secretomes (excretory/secretory (ES) products), changes to the abundance of cathepsin proteases relative to each other and to other proteinaceous components have been informative of parasite age, and stressors in the immediate environment including host immune pressures, flukicide exposure and fluke death (Chemale *et al.*, 2010; Morphew *et al.*, 2007, 2014). Thus, this orchestrated stage-specificity and overlapping cathepsin protease release consequently allows *F. hepatica* the freedom to best link these enzymes according to the host environments, potentially driving the parasite's

ability to infect a range of vertebrate hosts (Moreau and Chauvin, 2010; Robinson *et al.*, 2008a; Vercruysse and Claerebout, 2001).

3.2.2 Activation and functional secretion of *Fasciola hepatica* cathepsin proteases

All mammalian cysteine proteases localise to the lysosome, where the organelle's low luminal pH triggers autocatalysis (McGrath, 1999; Turk *et al.*, 2001). Nascent proteases are first guided by the short-length signal "pre" peptide that is subsequently cleaved at pre-determined signal peptidase cleavage sites (site 1-Ala-Xaa-Ala-site 2) (Perlman and Halvorson, 1983) in the endosomal system. The pro-form is then guided further by an inhibitor "pro" peptide, which assists further post-translational processing and regulates enzyme activation (Beckham *et al.*, 2006; Coulombe *et al.*, 1996; Dalton *et al.*, 2004; Lowther *et al.*, 2009; McGrath, 1999; Roche *et al.*, 1999; Turk *et al.*, 2012, 2001). In parasitic helminths *F. hepatica* is an exemplar of cathepsin molecular processing (Figure 3.2.2), whereby preprocathepsin cysteine protease zymogens are packaged into specialised lysosome-like secretory vesicles at the gastrodermis ready for export into the gut (Collins *et al.*, 2004; Smith *et al.*, 1993b). Vesicles of inactive proteolytic enzymes are then delivered into the acidic gastrointestinal (GI) lumen (Collins *et al.*, 2004), leading to autocatalytic activation via inhibitor (pro-) peptide removal, which is also replicable *in vitro* (Dalton *et al.*, 2004; Lowther *et al.*, 2009; Stack *et al.*, 2007). Once active, the mature cathepsin proteases optimally digests host haemoglobin (Hb) and albumin for gastrodermal peptide absorption within the small acidic pH range representative of the GI lumen, including FhCL1 at pH ≤4.5 (Lowther *et al.*, 2009) and FhCL5 at ≤5.5 (Norbury *et al.*, 2011), though FhCL1 and FhCL2 have been shown to exhibit stable activity in wide-ranging pH conditions for prolonged periods (pH 4.0–8.5, 37°C, ≤24 hours) (Dowd *et al.*, 2000). Since *F. hepatica* has a blind-ended gut, the contents are regurgitated at regular intervals of approximately 3 hours, expelling digesta alongside cysteine proteases into the external environment at the parasite-host interface (Brady *et al.*, 1999; Collins *et al.*, 2004). Thus, host Hb and degraded tissue are presumably digested internally at the coinciding peak of cysteine protease activity and abundance (Brady *et al.*, 1999; Collins *et al.*, 2004), likely facilitated by the low pH dissociating the Hb tetramer and catalysed by coinciding erythrocyte-derived glutathione (Lowther *et al.*, 2009). Following vomitus expulsion and consequential enzyme influx at physiologically-relevant pH, cysteine protease activities

become an external biochemical tool for the parasite, being subsequently utilised for host interstitial tissue digestion and immune evasion (Berasaín *et al.*, 2000, 1997b; Brady *et al.*, 1999; Dalton *et al.*, 2003; Lowther *et al.*, 2009).

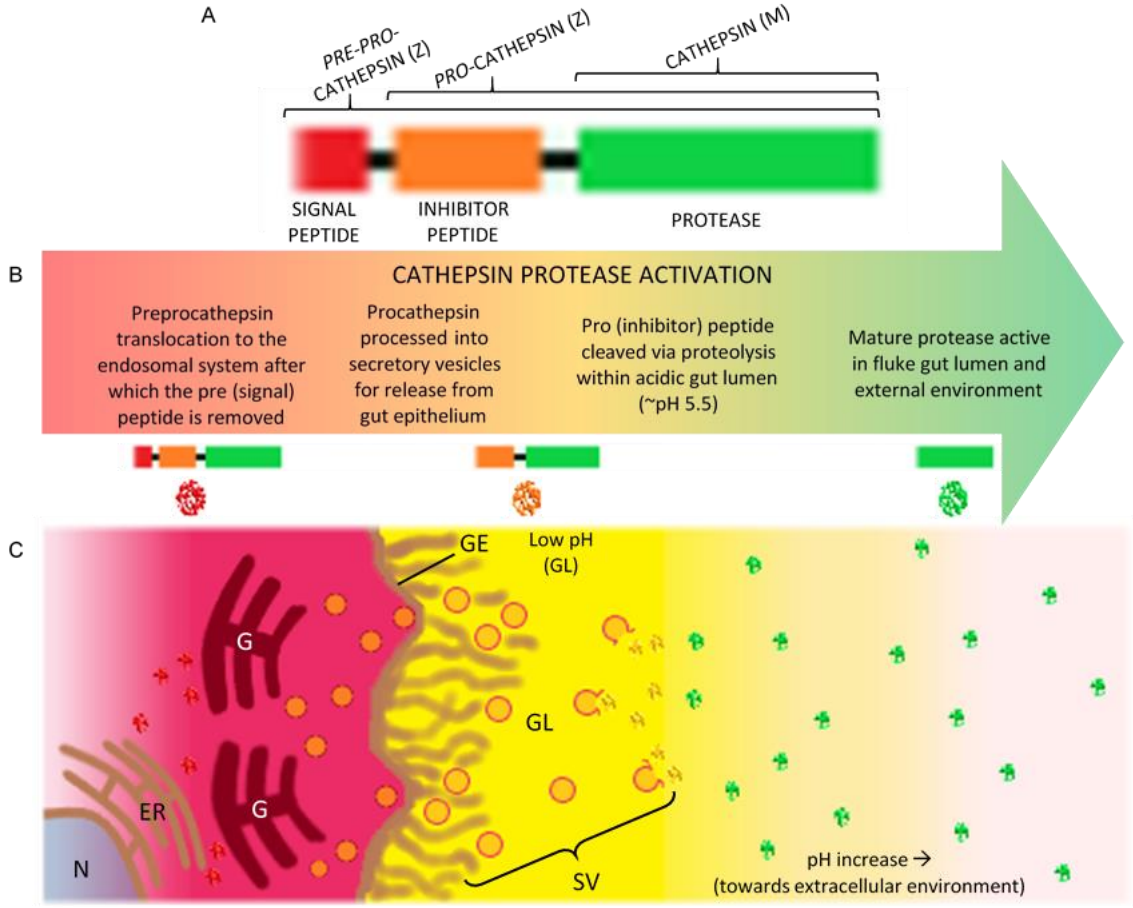

Figure 3.2.2 Diagrammatic representation of *Fasciola hepatica* cathepsin activation and secretion *in situ*. Cathepsin proteins are comprised of (A) Z, zymogen preprocathepsin (including signal and inhibitor peptides), procathepsin (including inhibitor peptide) and M, mature cathepsin protease regions. (B–C) Protease activation occurs via a multi-tiered process, involving intracellular and extracellular transport leading to the cleavage of the signal peptide, procathepsin transport into the fluke gut lumen and pH-induced inhibitor peptide cleavage, and expulsion of mature cathepsin proteases with excretory/secretory (ES) products. Graphic adapted from Collins *et al.* (2004).

Abbreviations: N, nucleus; ER, endoplasmic reticulum; G, golgi apparatus; GE, gut epithelium; GL, gut lumen; SV, secretory vesicles.

3.2.3 Diagnostic roles of *Fasciola hepatica* cathepsin L subunits

The commercial MM3-based BIO K201 and K211 Bio-X ELISA laboratory-based kits have improved fasciolosis diagnostics via CL protease-based contributions (Mezo *et al.*, 2007, 2004). Since their release, these serum and coproantigen kits have been assessed for supporting the monitoring of parasite drug sensitivity and treatment success (Charlier *et al.*, 2008; Flanagan *et al.*, 2011a). However, the application of these tests remains problematic with respect to determining low burden or asymptomatic infections, with serum titres being a potential source of confusion between seasons and post-treatment, and with further modifications required to improve test accuracy, including between different host species (Almazán *et al.*, 2001; Charlier *et al.*, 2008; Novobilský *et al.*, 2012; Palmer *et al.*, 2014). The MM3 antibodies (mouse splenic monoclonal IgG) were originally produced following the isolation of a 13–25 kDa antigen fraction of *F. hepatica* ES products (Mezo *et al.*, 2004). This ES subproteome of *Fasciola hepatica* is mainly constituted by cathepsin L proteases (Jefferies *et al.*, 2001; Morphew *et al.*, 2007) and MM3 immunoreactivity has also confirmed predominant recognition of native CL1- and CL2-specific epitopes (Muiño *et al.*, 2011), as well as the detection of recombinant refolded CL1 (Martínez-Sernández *et al.*, 2011). There is however no evidence to suggest MM3 can bind to non-mature pre- or procathepsin regions, and antigen conformation has demonstrated it can significantly influence the recognition and lack thereof by MM3 and other antibodies raised against folded (native) or unfolded (linear) CL antigens (Muiño *et al.*, 2011).

The antigenic propensity of CL zymogens, specifically the signal and inhibitor sequences, are yet to be considered as diagnostic candidates for *F. hepatica*, especially due to the abundance and established immunoreactivity of CL protease epitopes with host serum and MM3. However, studies have noted signal sequences in general to be multifaceted both prior to and after cleavage from the parent protein, with prospective and growing applications in diagnostics, vaccines and molecular biology techniques (Kovjazin *et al.*, 2011; Martoglio and Dobberstein, 1998; Owji *et al.*, 2018). Certain constituent residues of signal peptides have been observed to facilitate and directly stimulate immunogenicity, including compositions with hydrophobic amino acids (Cys, Leu, Val) (Kolaskar and Tongaonkar, 1990; Martoglio and Dobberstein, 1998) and unconventional D-amino acids (van Regenmortel and Muller, 1998). Indeed, it has been found in some cases that signal sequences contain the highest frequency

of immunogenic epitopes of a given antigen (Kovjazin *et al.*, 2011) and may have an unprecedented contribution to overall antigenicity (El Hage *et al.*, 2008), including as a decoy epitope (Thaa *et al.*, 2013). Furthermore, the innate properties and function can further assist in major histocompatibility complex I presentation through the guidance of signal peptide-fused antigen for intracellular translocation (Hombach *et al.*, 1995; Sojikul *et al.*, 2003). The generation of peptide-length sequences for *in vitro* diagnostics and vaccines for fasciolosis have demonstrated the capacity of serum recognition (Cornelissen *et al.*, 1999; Intapan *et al.*, 2005; Meshgi *et al.*, 2018) and protection (Garza-Cuartero *et al.*, 2018), respectively, though this is influenced by epitope predictions and *in situ* availability. The propeptide has also demonstrated immunodominance in CL zymogen-mediated protection (inhibitor–protease) (Harmsen *et al.*, 2004), though the diagnostic utility of the CL signal- and inhibitor-specific peptides, either cleaved or from intact CL zymogens (signal–inhibitor–protease) are yet to be investigated. Thus, cathepsin zymogens and specifically signal and inhibitor peptides pose as potentially valuable diagnostic candidates.

3.2.4 Chapter 3 aims

Cathepsins have long been a major target of fasciolosis diagnostics and vaccine strategies owing to the overabundance of mature cathepsin proteases in *Fasciola hepatica* excretory/secretory (ES) products, their dominating contribution to ES proteolytic activity and the subproteomic changes following TCBZ exposure (Carnevale *et al.*, 2001; Dalton *et al.*, 2013; Mezo *et al.*, 2004; Molina-Hernández *et al.*, 2015; Morphew *et al.*, 2014; Toet *et al.*, 2014). The substantial biochemical stability of *F. hepatica* cathepsin L (CL) cysteine proteases compared to mammalian orthologues has promoted their durability as molecular therapy and diagnostic candidates (Cordova *et al.*, 2001; Dowd *et al.*, 2000; Norbury *et al.*, 2011). However, the relative abundances and antigenicity of CL zymogens are understudied in comparison to its activated forms (Carnevale *et al.*, 2001; Reszka *et al.*, 2005), likely due to the lower levels of prepro- and procathepsins which precluded further reductionist biochemical focus onto these immature zymogens (Collins *et al.*, 2004). Consequently, there is a distinct knowledge gap concerning the immunogenicity and diagnostic capabilities of *F. hepatica* CL zymogens, prompting a detailed analysis of the subproteomic profiles of secreted cathepsin zymogens. Thus, the specific objectives of this chapter were to:

1) Determine and identify the proteomic profile and changing abundance of prepro- and procathepsin L zymogens in the ES products of *in vitro*-cultured live untreated and dead (by non-specific flukicide) adult flukes;
2) Confirm, via gel-based proteomics and mass spectrometry, the precise accession and sequence identities of three recombinant procathepsin L zymogens for prospective *in silico* and *in vitro* antigenicity studies;
3) Using the sequences of the three aforementioned recombinant pro-CL1 and native ES products-derived procathepsin L zymogens:
    a) Identify representative antigenic peptides based on conserved immunogenic sequences, confirmed using *in vitro* tandem mass spectrometry liquid chromatography and bioinformatics predictions, and;
    b) With the above findings, investigate the contribution of antigenic epitopes of procathepsin L zymogens using anti-rFhΔpCL1 polyclonal antibodies, and determine their abundance in *F. hepatica* ES products.

3.3 Materials and methods

3.3.1 Native procathepsin L zymogens

Adult *F. hepatica* were cultured as described in the General materials and methods (2.1), whereby size-matched flukes were selected for direct *in vitro* culture or termination in ethyl 4-aminobenzoate (1% (w/v) in ethanol) prior to *in vitro* culture. Whole excretory/secretory products were prepared using TCA precipitation and analysed using SDS PAGE and liquid chromatography tandem mass spectrometry (LC-MS/MS) as previously described (2.3–2.4; 2.4.3), with searches conducted against the GenBank database (v204).

3.3.2 Recombinant procathepsin L zymogens

Two procathepsin L1 proteins were recombinantly expressed (*Pichia pastoris* GSII5 yeast cells), purified and provided as gifts by Professor Dalton (Queen's University, Belfast), including a wild type (rFhpCL1^{WT}) and a C-terminal pro-segment Leu-Pro mutant (rFhΔpCL1: Leu12Pro at pro-peptide C-terminus, at position 95 within the complete protein sequence *in situ*) (Stack *et al.*, 2008) designed to prevent autocatalytic pro-peptide cleavage (Roche *et al.*, 1999). A second procathepsin L recombinantly expressed (*Escherichia coli* M15 [pREP4] bacterial cells) under denaturing conditions, purified and refolded (rFhpCL1), was kindly provided by Doctor Martínez-Sernández (Universidad de Santiago de Compostela, Spain) (Muiño *et al.*, 2011).

3.3.2.1 *rFhpCL1^{WT} activation*

rFhpCL1^{WT} was activated as described by Collins *et al.* (2004) and Stack *et al.* (2008), using activation buffer (0.1 M sodium citrate, pH 5.0; 2 mM DTT; 2.5 mM EDTA) and incubating at 37°C for 0, 30, 60, 90 and 120 minutes. Reactions were stopped at each time point using ice prior to preparation for SDS PAGE.

3.3.3 Procathepsin L-based peptide design

LC-MS/MS-identified protein sequences from whole ES and recombinant procathepsin L hits were aligned using Clustal O (Madeira *et al.*, 2019: www.ebi.ac.uk/tools/msa/clustalo) and analysed by Molecular Evolutionary Genetics Analysis version 7 (MEGA v7, Kumar *et al.*, 2016) using 1000-replicate bootstrapped, neighbour-joining phylogenetic trees, with level 1

gamma distribution and Poisson corrections. Sequence alignments for the comparison of residue conservation between multiple sequences were produced using the ExPASy BoxShade tool (v3.21; K. Hofmann and M. Baron, Swiss Institute of Bioinformatics: embnet.vital-it.ch/software/BOX_form.html). Further assessments of residue conservation were conducted using the Scorecons Server under default settings (Thornton Group, European Bioinformatics Institute: www.ebi.ac.uk/thornton-srv/databases/cgi-bin/valdar/scorecons_server.pl) to identify and evaluate residue diversity of a given sequence alignment. Peptide properties, including secondary structures, were assessed using ExPASy (Gasteiger *et al.*, 2003: www.expasy.org) and JPred4 (Drozdetskiy *et al.*, 2015: www.compbio.dundee.ac.uk/jpred) prediction tools. Antibody and B cell epitopes of individual sequences were predicted using the Kolaskar and Tongaonkar method (Kolaskar and Tongaonkar, 1990) with tools by the Immunomedicine Group (Universidad Complutense Madrid: imed.med.ucm.es/Tools/antigenic.pl). 3-D structural overlay assessments for the comparison of predicted native antigen epitope and peptide exposure were conducted using the Vector Alignment Search Tool (VAST; Charette *et al.*, 2006; Gibrat *et al.*, 1996: www.ncbi.nlm.nih.gov/Structure/VAST/vastsearch.html) and "see in 3D" version 4.3.1 (Cn3D v4.3.1; Wang *et al.*, 2000). Paired sequence alignments were converted to pdb files for this purpose using the iPBA webserver (Gelly *et al.*, 2011; Dynamics of Structures and Interactions of Biological Macromolecules Group, Université Paris: www.dsimb.inserm.fr/dsimb_tools).

3.3.4 Anti-procathepsin L1 polyclonal antibodies

Polyclonal antibodies (PAb) were raised to rFhΔpCL1 in two laboratory rabbits (Lampire Biological Laboratories, USA) and used in western hybridisation as previously described (2.4.2).

3.4 Results

3.4.1 Comparison of live and dead *in vitro*-cultured *Fasciola hepatica* ES CL zymogens

Whole ES products were isolated from *in vitro* cultured live and dead (ethyl 4-aminobenzoate-terminated) adult flukes in order to identify and compare the CL zymogen subproteome of live- and dead-cultured *Fasciola hepatica*. Three biological replicates (General materials and methods: 2.1) were pooled for analysis by duplicate 2-D SDS PAGE (Figure 3.4.1; for replicate sample gel images see Supplementary materials: Figure S1). Representative proteomes indicated differing abundances of several protein spots, in-keeping with previous findings (Morphew *et al.*, 2007), including the change in abundance of proteins corresponding to previously-identified fatty acid binding protein and enolase isoforms. 2-DE demonstrated different abundances of these proteins between the live and dead groups, which could be associated with pro-active regulation by live flukes (Figure 3.4.1A) verses passive, unregulated release by dead flukes (Figure 3.4.1B).

Further to previous protein identifications in adult ES products (Morphew *et al.*, 2007; Morphew *et al.*, 2011), proteins comprising the 2-DE gel region pertaining to CL zymogens, i.e. within the 30–38 kDa and 5.2–7.8 pI (Figure 3.4.1, boxed), were investigated by direct excision and LC-MS/MS analysis via ESI-QUAD-TOF and ESI-TRAP, and searched against the GenBank database (v204; Table 3.4.1). Four and eight protein hits were consistent between duplicate gel sections for live and dead adult fluke ES products using each method, respectively, whereby three and four CL hits were respectively identified (Table 3.4.1). Interestingly, both samples also contained proteins identified as *Nicotiana tabacum* actin (Q05214.1, www.ncbi.nlm.nih.gov/protein/Q05214.1; 90.16% amino acid sequence ID with cytoplasmic *F. hepatica* actin (THD22051.1: www.ncbi.nlm.nih.gov/protein/THD22051.1)) or *Opisthorchis viverrini* actin-like proteins (XP_009173845.1: www.ncbi.nlm.nih.gov/protein/XP_009173845.1; XP_009173846.1: www.ncbi.nlm.nih.gov/protein/XP_009173846.1; XP_009178086.1: www.ncbi.nlm.nih.gov/protein/XP_009178086.1; 99.73%, 99.73% and 100% amino acid sequence ID with cytoplasmic *F. hepatica* actin (THD22051.1), respectively). Furthermore, only the dead sample contained *F. hepatica* enolase (CAK47550.1: www.ncbi.nlm.nih.gov/protein/CAK47550.1), which is contrary to previous discoveries of this

glycolytic enzyme in non-terminated live (Morphew *et al.*, 2007) or TCBZ-SO-treated (Chemale *et al.*, 2010; Morphew *et al.*, 2014) adult flukes. Overall the dead sample had a more diverse protein population within the analysed region, as well as indicating the majority of proteins present as CL zymogens (Table 3.4.1: emPAI scores). In addition and as based on the present sequence coverage information (Table 3.4.1: average percentage coverage; collective residue coverage), CL zymogen residues specific to the pro-peptide were detected in both live and dead samples (Table 3.4.1: residues 16–105 of 326; 1–59 of 280; 1–18 of 239). Furthermore and according to previous classification of cathepsin clades (Morphew *et al.*, 2011), zymogens identified in the dead sample were members of the CL1 (CL1A, AAP49831.1: www.ncbi.nlm.nih.gov/protein/AAP49831.1), CL2 (ABQ95351.1: www.ncbi.nlm.nih.gov/protein/ABQ95351.1) and CL5 (AAF76330.1: www.ncbi.nlm.nih.gov/protein/AAF76330.1) clades and not just CL1 (CL1A, AAB41670.2: www.ncbi.nlm.nih.gov/protein/AAB41670.2; CL1D, ACJ12893.1: www.ncbi.nlm.nih.gov/protein/ACJ12893.1) as in the live sample. These findings of small clade diversity in the live sample is in-keeping with the CL1 clade as the previously most abundant, based on mature cathepsin proteases detected from *in vitro*-cultured adult *F. hepatica* ES products (Morphew *et al.*, 2011), but also provide evidence for changes to this phenotype upon fluke death (Morphew *et al.*, 2007).

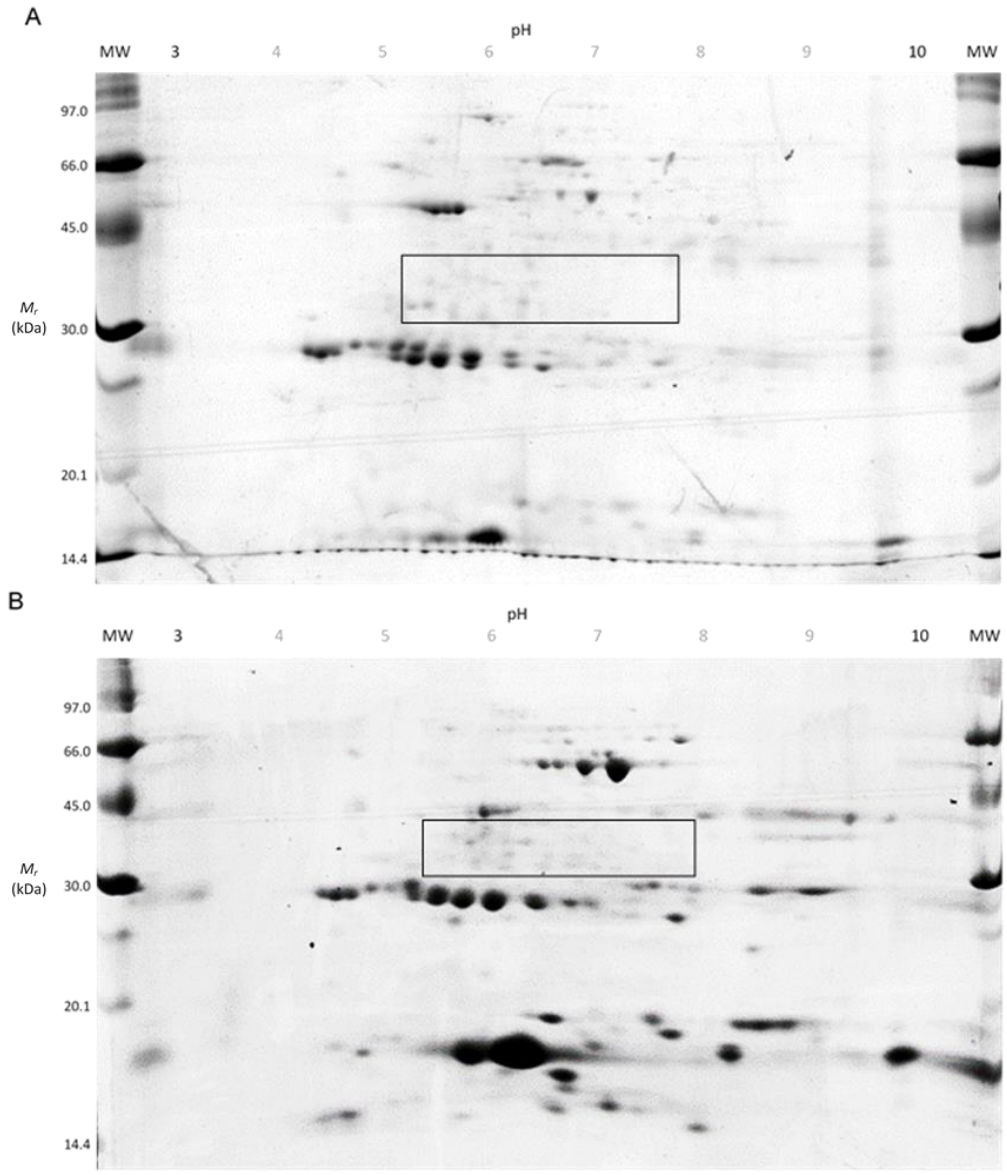

Figure 3.4.1. Representative 2-D SDS PAGE of excretory/secretory (ES) products from *in vitro* cultured live and dead adult *Fasciola hepatica*, and pre-selection of CL zymogens for identification within live and dead subproteomes. 25 µg ES products of live untreated (A) and dead (ethyl 4-aminobenzoate-treated) (B) liver flukes were separated by 2-DE (7 cm IEF 3–10; 12.5% SDS PAGE). The boxed area covering the region of 30–38 kDa and 5.2–7.8 pI and representing the area expected to consist of CL zymogens (including prepro- and procathepsins), were investigated via excision and LC-MS/MS (Table 3.4.1).

Abbreviations: MW, Amersham Low Molecular Weight SDS Calibration Kit (M_r).

Table 3.4.1. LC-MS/MS identification of 2-DE-separated *Fasciola hepatica* CL zymogen subproteomes. The presence and identity CL zymogens in 2-DE-separated (Figure 3.4.1) whole ES from untreated live and ethyl 4-aminobenzoate-terminated dead adult flukes was investigated by LC-MS/MS. CL protein hits are shown following identification against the GenBank database (v204) using an in-house MASCOT (Matrix Science) server, with consistent hits between duplicate trypsin-digested 2-DE gel sections analysed by ESI-QUAD-TOF or ESI-TRAP, and calculated average values for MASCOT scores, alongside unique (non-duplicate) peptide matches, percentage coverage of peptides over the hit sequence, detected residues, and relative abundance calculated according to Exponentially Modified Protein Abundance Index (emPAI) values. Reported are significant hits identified with a score of 67 or greater ($P < 0.05$), including protein family groupings in **bold**. Superscripts refer to consistent proteins identified as top hits from samples analysed by ESI-QUAD-TOF (a) or ESI-TRAP (b).

ID	MS/MS ion search						Highest scoring GenBank hit			
	GenBank hit	MASCOT score (Av)	Peptides matched (non-duplicate)	Sequence coverage		Exponentially modified protein abundance index (emPAI)	Protein (length, aa)	Organism	Accession	E-value
				Average percentage coverage (%)	Collective residue coverage (aa)					
Live	**gi|116488416[a]**	**116.5±58.5**	**4.0±0.0**	**19.5±1.5**	**57–81, 91–106, 116–124, 186–205, 231–253, 289–298, 308–324**	**0.365±0.155**	**Secreted cathepsin L 1 (1–326)**	***F. hepatica***	**AAB41670.2**	**0.0**
	gi|157862759[b]	**101.0±54.0**	**2.0±0.0**	**11.5±0.5**	**12–35, 70–78, 140–152, 185–207**	**0.280±0.070**	**Cathepsin L, partial (1–280)**	***F. gigantica***	**ABV90502.1**	**0.0**
	gi|461465	99.5±7.5	7.0±0.0	30.0±4.0	-	0.245±0.165	Actin	*Nicotiana tabacum*	Q05214.1	0.0
	gi|211909240[b]	67.5±20.5	3.0±0.0	14.5±1.5	58–81, 116–124, 186–198, 231–253, 289–298, 308–324	0.200±0.010	Cathepsin L1D (1–326)	*F. hepatica*	ACJ12893.1	0.0
Dead	**gi|31558997**	**459.5±261.5**	**10.5±0.5**	**52.5±6.5**	**42–81, 84–147, 186–205, 215–298**	**2.360±1.830**	**Cathepsin L (1–326)**	***F. hepatica***	**AAP49831.1**	**0.0**
	gi|41152540	**384.5±286.5**	**8.0±1.0**	**52.5±6.5**	**4–60, 99–118, 128–166, 202–211, 221–237**	**3.930±3.510**	**Cathepsin L protein (1–239)**	***F. hepatica***	**AAR99519.1**	**9E-180**
	gi|148575301	**237.0±152.0**	**10.5±0.5**	**51.0±2.0**	**50–81, 84–97, 106–115, 151–209, 215–302, 308–324**	**1.020±0.840**	**Secreted cathepsin L2 (1–326)**	***F. hepatica***	**ABQ95351.1**	**0.0**
	gi|190350155	153.5±62.5	10.5±0.5	33.0±7.0	-	0.335±0.025	Enolase	*F. hepatica*	CAK47550.1	0.0

	gi|684403575	135.5±37.5	14.0±1.0	51.5±7.5	-	0.440±0.020	Hypothetical protein T265_09499	*Opisthorchis viverrini*	XP_009173845.1	0.0
	gi|684403578	135.5±37.5	14.0±1.0	46.0±7.0	-	0.440±0.020	Hypothetical protein T265_09500	*O. viverrini*	XP_009173846.1	0.0
	gi|684415044	135.5±37.5	7.5±0.5	54.0±11.0	-	0.440±0.020	Hypothetical protein T265_09500	*O. viverrini*	XP_009178086.1	3E-128
	gi|8547325	**126.0±70**	**10.5±0.5**	**33.5±0.5**	**42–81, 84–102, 116–124, 151–165, 186–198, 206–214, 254–266, 289–302**	**0.475±0.295**	**Cathepsin L (1–326)**	***F. hepatica***	**AAF76330.1**	**0.0**

3.4.2 *In vitro* investigations of recombinant procathepsin L1 proteins

Three recombinant procathepsin L (signal–inhibitor–mature) zymogens were characterised *in vitro*. Following confirmation of protein identity and sequence, sequence conservation and antigenicity was compared with native-derived equivalents using *in silico* bioinformatic phylogenetic tools and predictions, followed by *in vitro* immunological methods.

3.4.2.1 *Recombinant mutant procathepsin L1 (rFhΔpCL1)*

A recombinant Eukaryote-expressed inactive mutant (Leu-Pro C-terminal prosegment substitution; L95P *in situ*) procathepsin L (rFhΔpCL1) (Stack *et al.*, 2007) was kindly gifted by Professor Dalton (Queen's College Belfast, UK). 1-D 12.5% SDS PAGE indicated rFhΔpCL1 resolved at approximately 37 kDa (Figure 3.4.2.1A), which was the predicted size of the complete procathepsin L zymogen, including signal and inhibitor peptides (36.90 kDa). A second band of relatively lower abundance was also observed at approximately 70–80 kDa, which may be a homodimer since this is the expected molecular weight (73.80 kDa) (Figure 3.4.2.1A).

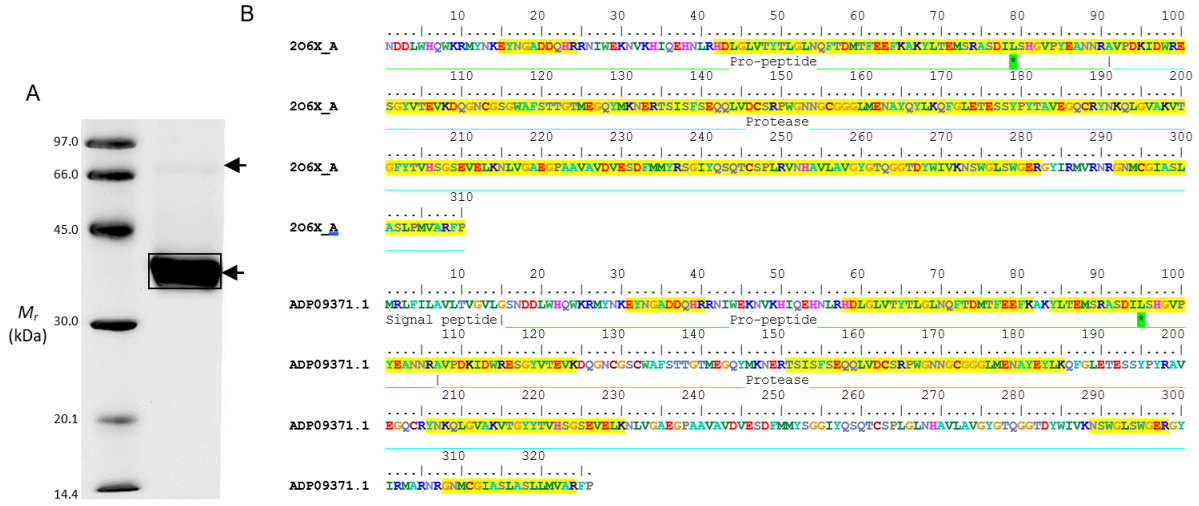

Figure 3.4.2.1. 1-DE and LC-MS/MS analysis of a recombinant mutant *Fasciola hepatica* procathepsin L1 (rFhΔpCL1). (A) 2 µg rFhΔpCL1 was analysed by 12.5% SDS PAGE. The 37 kDa fragment (boxed) was prepared and submitted in duplicate for LC-MS-MS analysis, confirming two consistent hits for procathepsin L1 chain A (2O6X_A: www.ncbi.nlm.nih.gov/protein/2O6X_A) and cathepsin L-like proteinase (ADP09371.1: www.ncbi.nlm.nih.gov/protein/ADP09371.1). Sequences were analysed (B), confirming rFhΔpCL1 sequence coverage (highlighted) of the pro-peptide (16–105 aa) and protease (106–326 aa) regions. The pro-peptide C-terminal mutant residue is shown (*: Leu12Pro (Stack *et al.*, 2007); L95P *in situ*), however LC-MS/MS did not detect this amino acid substitution.

The 37 kDa fragment of rFhΔpCL1 was prepared for duplicate analysis by LC-MS/MS to confirm protein identification (Figure 3.4.2.1A, boxed; Table 3.4.2). Data indicated two high-scoring and consistent *Fasciola hepatica* protein results for rFhΔpCL1, including the highest scoring hit: procathepsin L1 chain A (2O6X_A: www.ncbi.nlm.nih.gov/protein/2O6X_A; Stack *et al.*, 2008); and cathepsin L-like proteinase (ADP09371.1: www.ncbi.nlm.nih.gov/protein/ADP09371.1) (Table 3.4.2). The protein sequence coverage by peptides of rFhΔpCL1 is shown (Figure 3.4.2.1B), indicating the abundant presence of peptides matching to the pro-peptide and protease regions of 2O6X_A (73.0% average sequence coverage) and ADP09371.1 (39.0% average sequence coverage). A sequence alignment between these two sequences was conducted (not shown), identifying 10 residue differences within the protease region (2O6X_A vs ADP09371.1: Gly116Cys; Gln166Glu; Thr182Arg; Phe202Tyr; Arg237Ser; Ser238Gly; Arg250Gly; Val251Leu; Val288Ala; Pro304Leu) and confirming the absence of the signal peptide sequence (1–15 aa) from 2O6X_A (Figure 3.4.2.1B). To obtain a single sequence match for rFhΔpCL1, the closest GenBank (v204) sequence pertaining to 2O6X_A and ADP09371.1 was investigated by submitting protein sequences to BLAST, which identified a secreted cathepsin L1 (AAB41670.2) with 99.0% and 97.0% identity, respectively (data not shown). The cathepsin L clade identity of AAB41670.2 was investigated using the summary report by Morphew *et al.* (2011), indicating rFhΔpCL1 putatively belongs within the cathepsin L1A clade.

3.4.2.2 *Recombinant wild type procathepsin L1 (rFhpCL1^{WT})*

The non-mutant wild type Eukaryote-expressed recombinant of the procathepsin L1 (rFhpCL1^{WT}) was kindly gifted by Professor Dalton (Queen's University Belfast, UK). rFhpCL1^{WT} was incubated in activation buffer (3.3.2.1) and time-course samples were analysed as described by (Stack *et al.*, 2008). 1-D 12.5% SDS PAGE indicated increased procathepsin L autocatalysis and generation of the mature enzyme and other lower molecular weight derivatives (Figure 3.4.3A). The procathepsin L zymogen predicted for the complete protein sequence (36.90 kDa) and a second distinct zymogen of approximately 35 kDa was observed (Figure 3.4.2.2A), which may indicate signal peptide removal (predicted: 34.75 kDa). Both zymogen fragments were most abundant in the PBS (no activation buffer, no 37°C incubation) and 0-minute (resuspended in activation buffer, no 37°C incubation) samples, decreasing in concentration after 30 minutes incubation with increasing concentrations of zymogen

intermediates (30-34 kDa), enzyme (24.25 kDa) and fragmentation derivatives (<24 kDa) (Figure 3.4.2.2A).

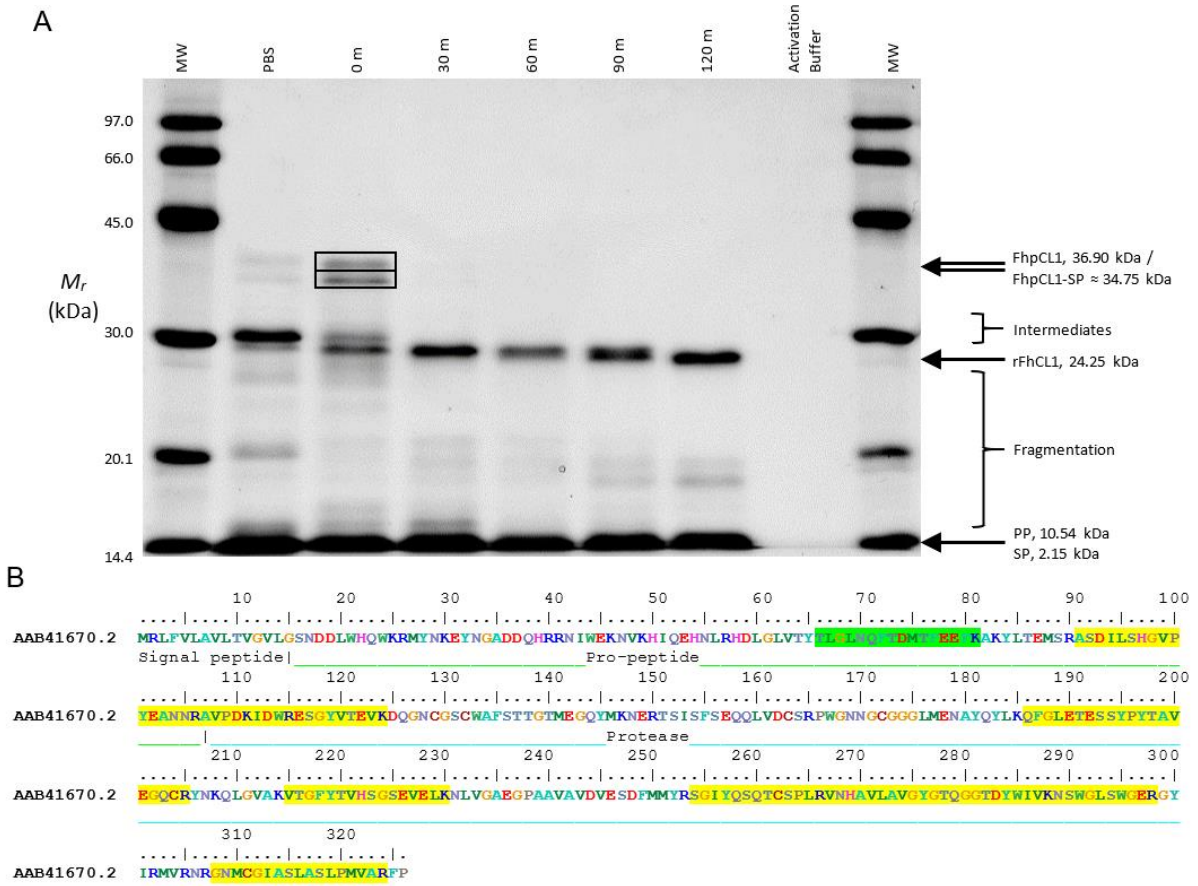

Figure 3.4.2.2. *In vitro* activation, 1-DE and LC-MS/MS analysis of wild type recombinant procathepsin L1 (rFhpCL1^{WT}). 5 µg protein was loaded per lane following the induced autocatalysis of rFhpCL1^{WT} and analysed by 12.5% SDS PAGE (A). The protein's exposure to activation buffer demonstrate increased protein processing into intermediate and fragment products (0 m, resuspended in activation buffer) compared to negative rFhpCL1^{WT} (PBS only). Incubation at 37°C led to increasing concentrations proteins of lower molecular weight (30-120 m). The two largest fragments of approximately 35 and 37 kDa (boxed) were prepared and submitted in duplicate for LC-MS-MS analysis, confirming one consistent top hit for secreted cathepsin L1 (AAB41670.2: www.ncbi.nlm.nih.gov/protein/AAB41670.2). Sequences were analysed (A) and highlighted residues indicate positively matched peptides following LC-MS/MS analysis of rFhpCL1 proteins resolved at 37 kDa and 35 kDa, whereby yellow indicates both sample matches and green indicates only 35 kDa matches.

Abbreviations: MW, Amersham Low Molecular Weight SDS Calibration Kit (M_r); SP, signal peptide; PP, pro-peptide.

The 37 and 35 kDa fragments of rFhpCL1^{WT} were prepared for duplicate analysis by LC-MS/MS (Figure 3.4.2.2A, boxed; Table 3.4.2). Data indicated the cathepsin L-like proteinase (AAB41670.2) was the highest scoring and consistent *F. hepatica* protein result for rFhpCL1^{WT} (Table 3.4.2). The protein sequence coverage by peptides of rFhpCL1^{WT} is shown (Figure 3.4.2.2B), indicating the abundant presence of peptides matching to the pro-peptide and protease regions (39% average sequence coverage). Thus, rFhpCL1^{WT} was putatively assigned to the cathepsin L1A clade as for rFhΔpCL1 due to the greatest sequence similarity to AAB41670.2 (Morphew *et al.*, 2011).

3.4.2.3 *Recombinant procathepsin L1 (rFhpCL1)*

The recombinant Prokaryote-expressed procathepsin L1 (rFhpCL1) was kindly gifted by Doctor Martínez-Sernández (Universidad de Santiago de Compostela, Spain). This recombinant protein was purified under denaturing conditions and refolded to regain its native conformation. However, the rFhpCL1 product appeared to fragment upon denaturing conditions for SDS PAGE and, contrary to induced maturation of rFhpCL1^{WT}, may autonomously undergo autocatalytic processing and/or degradation. Specifically, 1-DE indicated the abundance of six fragments, including the mature enzyme and subunits of lower molecular weight, with those of the highest abundance resolving at approximately 25 kDa (assumed to be rFhCL1, 24.25 kDa) and 14≤18 kDa, respectively (Figure 3.4.2.3A). The intact zymogen (rFhpCL1), an intermediate and a further fragment were also present in lower abundance, resolving at approximately 36.61 kDa (fragment sample 1), 32 kDa (fragment sample 2) and 18 kDa (fragment 4), respectively (Figure 3.4.2.3A).

All six resolved fragments of rFhpCL1 at approximately 37, 32, 28, 24, 18 and 14 kDa were prepared for duplicate analysis by LC-MS/MS (Figure 3.4.2.3A, boxed, samples 1–6; Table 3.4.2). Data indicated the cathepsin L protein CatL1-MM3p, partial (CCA61803.1: www.ncbi.nlm.nih.gov/protein/CCA61803.1) was the highest scoring and consistent *F. hepatica* protein result for rFhpCL1 (Table 3.4.2), followed by the cathepsin L-like proteinase (ADP09371.1) in samples 3 and 6, and the cathepsin L (BAB86959.1: www.ncbi.nlm.nih.gov/protein/BAB86959.1) in sample 6. The protein sequence coverage by peptides of each rFhpCL1 fraction is shown (Figure 3.4.2.3B), indicating the abundant presence of peptides matching to the pro-peptide (16–105 aa) and protease (106–326 aa)

regions of CCA61803.1 (44.8% average sequence coverage, all fragment samples) and ADP09371.1 (42.2% average sequence coverage, fragment samples 3 and 6), and the protease region of BAB86959.1 (28.0% average sequence coverage, fragment sample 6). Since CCA61803.1 and ADP09371.1 FhCL1 isoforms are absent from the report by Morphew *et al.* (2011), the closest GenBank (v204) CL sequence was identified (AAR99518.1: www.ncbi.nlm.nih.gov/protein/AAR99518.1) with 96% and 95% sequence identity, respectively (data not shown). Consequently rFhpCL1 was putatively assigned to the CL1A clade as identified in this study (Morphew *et al.*, 2011).

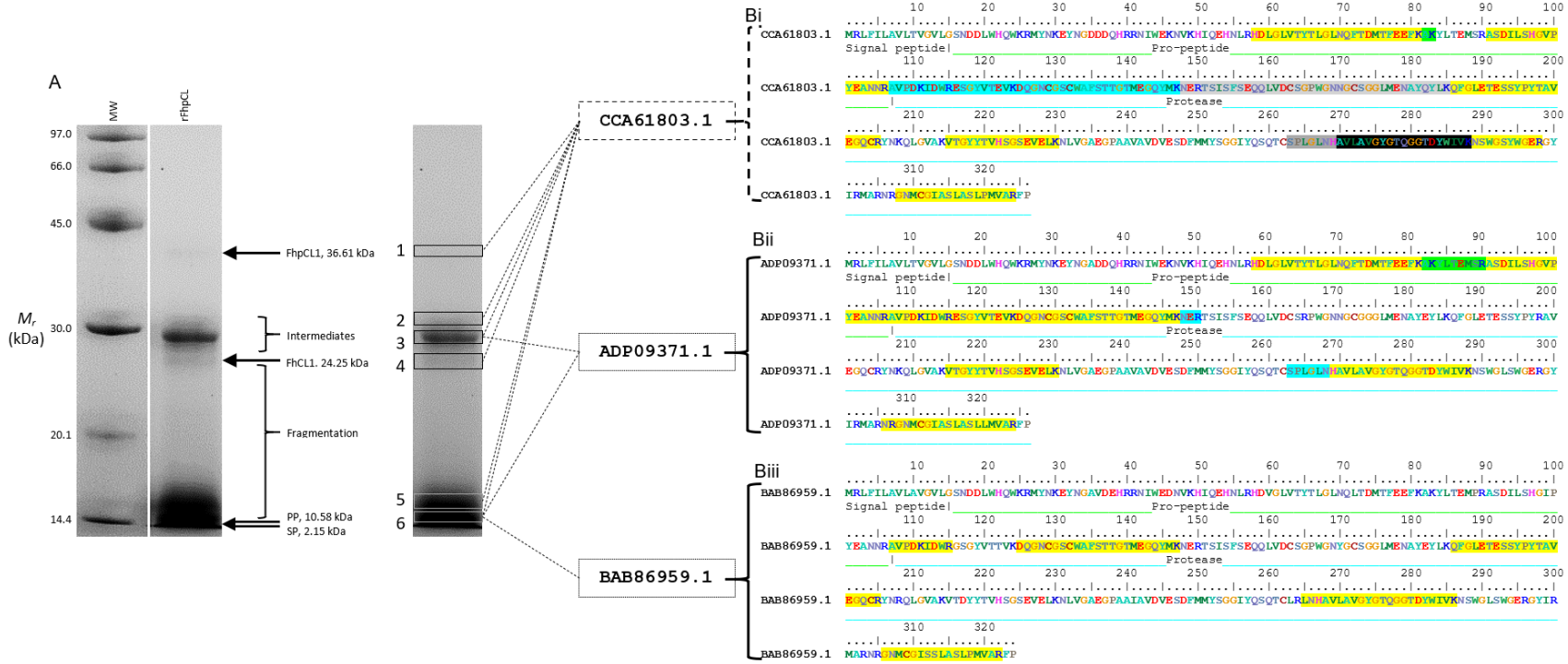

Figure 3.4.2.3. 1-DE and LC-MS/MS analysis of a recombinant procathepsin L1 (rFhpCL1). (A) 20 µg rFhpCL1 in PBS was analysed by 12.5% SDS PAGE. Six protein fragments (numbered: 1–6) between 10-37 kDa were prepared and submitted for duplicate LC-MS-MS analysis (Table 3.4.2), confirming one consistent hit for cathepsin protein CatL1-MM3p, partial (CCA61803.1: www.ncbi.nlm.nih.gov/protein/CCA61803.1) across all fragment sizes, cathepsin L-like proteinase (ADP09371.1: www.ncbi.nlm.nih.gov/protein/ADP09371.1) across fragments 3 and 6 only, and cathepsin L (BAB86959.1: www.ncbi.nlm.nih.gov/protein/BAB86959.1) in fragment 6 only. Sequences were analysed (Bi-iii) and highlighted residues indicate positively matched peptides following LC-MS/MS analysis, whereby sequences highlighted in yellow indicates matches by all samples. Further highlight colours indicate matching by one or more samples. CatL1-MM3p (Bi) had variable coverage depending on fragment samples, highlighted in green (fragments 1, 5 and 6), turquoise (fragments 2, 3, 4, 5 and 6), light grey (fragment 4), dark grey (fragment 3) and black (fragments 3 and 6). Cathepsin L-like proteinase (Bii) had some coverage variation, highlighted in turquoise (fragment 3) and green (fragment 6).

Abbreviations: MW, Amersham Low Molecular Weight SDS Calibration Kit (M_r).

Table 3.4.2. LC-MS/MS identification of 1-DE-separated recombinant *Fasciola hepatica* procathepsin L proteins. The recombinant mutant (rFhΔpCL1) and wild type (rFhpCL1^{WT}) procathepsin L (Belfast) and a second recombinant procathepsin L (Spain) were analysed by duplicate 12.5% SDS PAGE and bands of interest were selected for investigation using LC-MS/MS. Proteins were identified against the GenBank database (v204) using an in-house MASCOT (Matrix Science) server, including reliable error tolerance and reporting significant hits consistent between duplicates with an average score of 67 or greater ($P < 0.05$). Top hits are shown, and hits based on peptide samesets, subsets and intersections are shown in the Supplementary materials: Table S1.

Recombinant procathepsin L sample	Approximate molecular weight (sample number)	MS/MS ion search				Highest scoring GenBank hit			
		GenBank hit	MASCOT score (Av)	Peptides matched (non-duplicate)	Sequence coverage (%)	Protein	Organism	Accession	E-value
rFhΔpCL1	37	gi|163310848	1677.0±1078.0	71.5±37.5	73.0±10.0	Chain A, Crystal Structure Of Procathepsin L1	*F. hepatica*	2O6X_A	0.0
		gi|310751866	441.5±281.5	30.5±17.5	39.0±8.0	Cathepsin L-like proteinase	*F. hepatica*	ADP09371.1	0.0
rFhpCL1^{WT}	37	gi|116488416	132.5±56.5	17.0±4.0	38.5±1.5	Secreted cathepsin L 1	*F. hepatica*	AAB41670.2	0.0
	35	gi|116488416	117.0±51.0	13.5±3.5	41.0±4.0	Secreted cathepsin L 1	*F. hepatica*	AAB41670.2	0.0
rFhpCL1	37 (**1**)	gi|379991182	87.0±13.0	10.5±3.5	30.0±4.0	Cathepsin protein CatL1-MM3p, partial	*F. hepatica*	CCA61803.1	0.0
	32 (**2**)	gi|379991182	101.0±29.0	14.0±4.0	36.5±7.5	Cathepsin protein CatL1-MM3p, partial	*F. hepatica*	CCA61803.1	0.0
	28 (**3**)	gi|379991182	479.0±21.0	40.5±0.5	62.5±0.5	Cathepsin protein CatL1-MM3p, partial	*F. hepatica*	CCA61803.1	0.0
		gi|310751866	245.0±20.0	24.0±1.0	42.5±0.5	Cathepsin L-like proteinase	*F. hepatica*	ADP09371.1	0.0
	24 (**4**)	gi|379991182	148.0±24.0	18.5±4.5	45.0±1.0	Cathepsin protein CatL1-MM3p, partial	*F. hepatica*	CCA61803.1	0.0
	18 (**5**)	gi|379991182	270.5±32.5	20.5±1.5	44.0±0.0	Cathepsin protein CatL1-MM3p, partial	*F. hepatica*	CCA61803.1	0.0
	≤14 (**6**)	gi|379991182	462.0±16.0	40.5±3.5	51.0±0.0	Cathepsin protein CatL1-MM3p, partial	*F. hepatica*	CCA61803.1	0.0
		gi|310751866	203.0±35.0	27.0±0.0	42.0±0.0	Cathepsin L-like proteinase	*F. hepatica*	ADP09371.1	0.0
		gi|19909509	123.5±18.5	16.0±2.0	28.0±0.0	Cathepsin L	*F. gigantica*	BAB86959.1	0.0

3.4.3 *In silico* and *in vitro* determination of CL zymogen antigenicity

3.4.3.1 Fasciola hepatica *CL zymogen B cell epitope predictions and* in vivo *findings*

Short-length peptides were designed for prospective synthesis and diagnostic testing using *in silico* antigenic predictions for CL zymogens, including proteins previously identified in native and recombinant fractions (3.4.1–3.4.2). Sequences were selected if complete, i.e. including signal peptide–inhibitor peptide–mature protease sequences (1–326), with the exception of the model partial procathepsin L1 sequence, 2O6X_A which is missing the signal peptide (1–16 N-terminal residues).

CL zymogen epitopes were assessed, finding similar antigen epitope predictions between the nine sequences tested. On average there were 12.56 antigenic peptide determinants per sequence, with the fewest (n = 11) present in 2O6X_A (CL1A, NB: signal sequence absent) and ABQ95351.1 (CL2), and the most (n = 14) present in ACJ12893.1 (CL1D) and AAF76330.1 (CL5) (for all prediction plots and antigenic determinant sequences see Supplementary materials: Figure S2). An exemplar of these data are shown for the cathepsin L proteinase (ADP09371.1, CL1A) (Figure 3.4.3.1), whereby 13 peptides (7–28-mer) presented scores exceeding the overall protein antigenic propensity, and the highest-scoring antigenic determinants in particular were present within all regions including the N-terminal (4–15), mid-sequence (152–163) and C-terminal (208–235; 283–289; 311–321) (Figure 3.4.3.1). Thus, antigenic predictions suggested all three CL protein domains contain peptide sequences with potential antigenic propensity, including candidate sequences with highly conserved sequences (Supplementary materials: Figure S2).

In order to select a short-list of peptides for further study, *in silico* immunogenicity predictions, and experimental data from *in vivo* serum testing were used (Table 3.4.3.1). Peptide candidates from analogous *in silico* epitope predictions are shown as based on heterologous cathepsin L sequences, including a purified native CL1 protease sequence, collated by Cornelissen *et al.* (1999) alongside current antigenic sequence determinants for ADP09371.1 (Table 3.4.3.1). 19 peptide candidates in total are presented in accordance with their sequence position, whereby eight additional peptides were identified by Cornelissen *et al.* (1999) (Table 3.4.3.1). Included are heterogeneous sequences from different sequence sources, such as peptides 2, 3, 4, 7 and 8, as well as lengthened homo- and hetero-geneous versions of antigenic sequences predicted for ADP09371.1 and other aforementioned

cathepsins, including peptides 1 (partially overlapped by peptide 2), 9 and 10 (fully and partially overlapped by peptide 8, respectively) (Table 3.4.3.1).

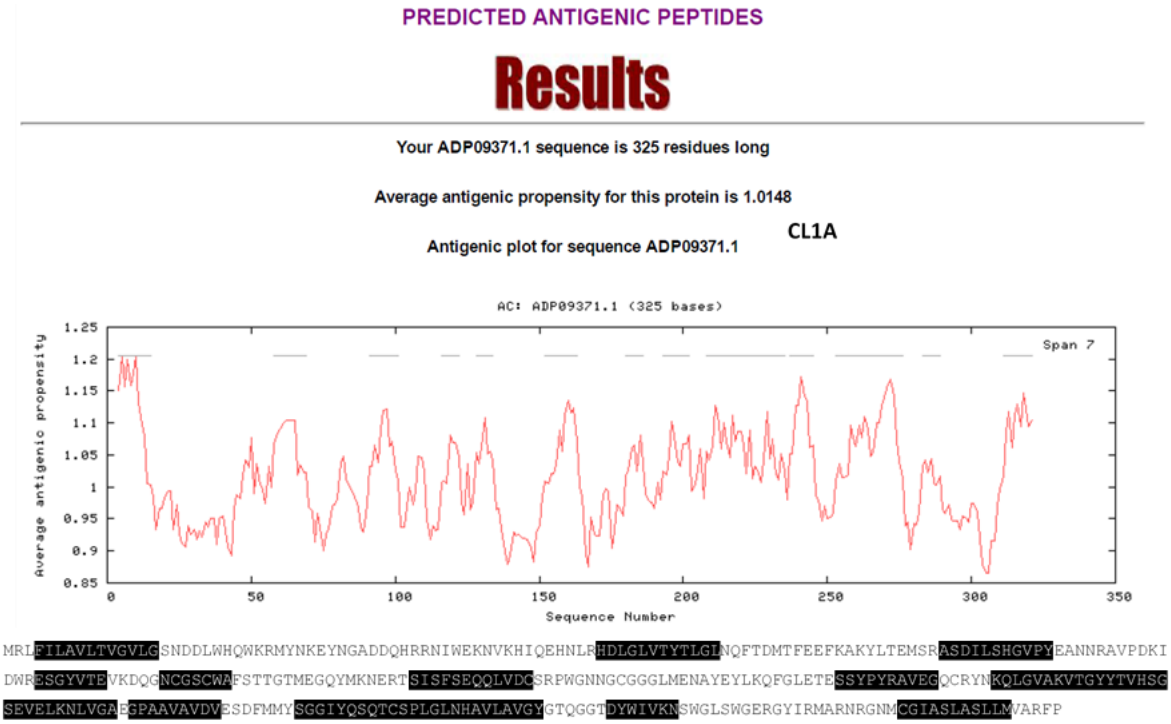

Figure 3.4.3.1. Antigenic peptide predictions for *Fasciola hepatica* cathepsin L proteinase (ADP09371.1). 13 antigenic determinants were predicted in the selected CL amino acid sequence, ranging between residues 1–321 of between 7- and 28-mer in residue length. Antigenicity plots for other *F. hepatica* cathepsin L sequences identified in native and recombinant samples are available in the Supplementary materials: Figure S2 (Appendix).

Of the sequences tested by Cornelissen *et al.* (1999, 2001) demonstrating immunogenicity *in vivo*, two of interest were peptides 7 and 8 (Table 3.4.3.1), which due to 13 overlapping residues mid-sequence had only 7-mer unique sequences up- and down-stream, respectively. Furthermore, *in silico* predictions also indicated residues within this region (Cys_{103}–Cys_{129}) with antigenic propensity, providing the basis for the primary peptide candidate of the procathepsin L protease region in the first instance. Thus, without *in vivo* immunogenicity evidence to support the predicted antigenic propensity of signal- and inhibitor-derived peptides, candidates were selected based on predictions alongside sequence conservation (Table 3.4.3.1; for a detailed comparative sequence alignment with antigenic peptide predictions see Supplementary materials: Figure S2). Owing to the inherent signal peptide length, the peptide Met_1–Gly_{15}≤Leu_{20} was chosen, since all full-length sequences tested here demonstrated high conservation of this region (>70%, Figure S2).

Conversely, and due to the length of the inhibitor peptide and limitations of the current study for one target peptide per region, 15-mer sequences within the Trp_{21}–Asn_{40} region and predicting several antigenic residues (peptides 2–4, Table 3.4.3.1) were further studied. Therefore, with respect to the above considerations and to also accommodate prospective syntheses, peptide frames were shifted and final peptide sequences were established: Lys_6–Lys_{20} (N'-LAVLTVGVLGSNDDL-C'); Arg_{26}–Arg_{40} (N'-RMYNKEYNGADDQHR-C'), and Arg_{115}–Cys_{129} (N'-RESGYVTEVKDQGNC-C').

Table 3.4.3.1. Antigenic peptide determinants of procathepsin L sequences based on *in silico* prediction tools and *in vivo* testing. Peptides with predicted antigenicity by B cell epitope recognition are shown for a representative cathepsin L proteinase sequence (ADP09371.1)[1,2,3] and based on previous predictions and *in vivo* findings for a cathepsin L1A sequence[4,5] (Cornelissen *et al.*, 2001, 1999). Bolded sequences indicate significant immunoreactivity of peptides by infected calf sera (Cornelissen *et al.*, 1999) and early field diagnosis (Cornelissen *et al.*, 2001).

Peptide	CL protein aa region[1,2,4] (mer)	Predicted antigenic sequence[3]; tested *in vivo*[4,5]
1	4–15 (12)[A,2]	FILAVLTVGVLG[3]
2	13–32 (20)[A-B,2] 15–33 (20)[A-B,4]	LGSNDDLWHQWKRMYNKEYN CGSNDDLWHQWKRMYNKEYN[4]
3	14–33 (20)[A-B,2] 18–34 (20)[B,4]	GSNDDLWHQWKRMYNKEYNG CSNDVSHWEWKRMYNKEYNG[4]
4	24-42 (19)[B,2] 25-42 (19)[B,4]	WKRMYNKEYNGADDQHRRN CKRMYNKGYNGADDQHRRN[4]
5	58–69 (12)[B,2]	HDLGLVTYTLGL[3]
6	91–101 (11)[B,2]	ASDILSHGVPY[3]
7	103–122 (20)[B-C,2] 103–122 (20)[B-C,4] 104–122 (20)[B-C,4]	ANNRAVPDKIDWRESGYVTE **CNNRAVPDKIDWRESGYVTE**[4] CNNRDVPASIDWREYGYVTE[4]
8	110–129 (20)[C,2,4]	**DKIDWRESGYVTEVKDQGNC**[4,5] ASIDWREYGYVTEVKDQGNC[4]
9	116–122 (7)[C,2]	ESGYVTE[3]
10	128–134 (7)[C,2]	NCGSCWA[3]
11	152–163 (12)[C,2]	SISFSEQQLVDC[3]
12	180–186 (7)[C,2]	AYEYLKQ[3]
13	193–202 (10)[C,2]	SSYPYRAVEG[3]
14	208–235 (28)[C,2]	KQLGVAKVTGYYTVHSGSEVELKNLVGA[3]
15	237–245 (8)[C,2]	GPAAVAVDV[3]
16	253–276 (24)[C,2]	SGGIYQSQTCSPLGLNHAVLAVGY[3]
17	283–289 (7)[C,2]	DYWIVKN[3]
18	296–311 (16)[C,2,4]	GERGYIRMARNRGNMC[4]
19	311–321 (10)[C,2]	CGIASLASLLM[3]

1 Signal peptide: 1–15 (A); Inhibitor peptide: 16–107 (B); Protease: 108–TER (C).
2 Based on ADP09371.1 as protein with least phylogenetic distance from CL clades measured (Figure 3.4.3.2).
3 Immunomedicine Group antigenicity tool (Kolaskar and Tongaonkar, 1990; Universidad Complutense de Madrid: imed.med.ucm.es/Tools/antigenic).
4 As reported for heterologous sequences of CL(1) (Cornelissen *et al.*, 1999);
5 Cornelissen *et al.*, (2001).

3.4.3.2 In silico *sequence conservation and mapping of CL zymogen antigenic epitopes*

Amino acid conservation between 15-mer peptides in nine procathepsin Ls proteins were analysed by *in silico* sequence phylogeny (Figure 3.4.3.2.1). Findings indicated high sequence conservation of designed peptides (Figure 3.4.3.2.1A; 66.67–100% ID, Figure 3.4.3.2.1B; 0.42044 units of evolutionary distance, Figure 3.4.3.2.1C), which was reflected by whole sequence percentage identities (75<97% ID, data not shown) and the known clustering of CL clades (Morphew *et al.*, 2011). Residue conservation scores for each peptide were also calculated using the Scorecons Server (Thornton Group, European Bioinformatics Institute: www.ebi.ac.uk/thornton-srv/databases/cgi-bin/valdar/scorecons_server.pl), that identified residues within the prospective positions had low diversity scores of 39.90% (6–20, excluding 2O6X_A), 35.10% (26–40) and 43.30% (115–129), a positive indicator of high residue conservation (Scorecons data summarised in supplementary materials: Table S2). Biochemical properties of designed peptides were predicted using Jpred4 (Jnet: Drozdetskiy *et al.*, 2015) based on constituent residues (Table 3.4.3.2). Molecular, structural and functional characteristics identified in the signal peptide agree with the known signal peptide insolubility (Collins *et al.*, 2004), based on solvent inaccessibility, and further suggest *in situ* exposure and solubility of the majority of pro- and mature peptide residues, supporting their suitability for prospective synthesis and testing.

3-D structural predictions were compared using Cn3D overlays of procathepsin L1A structures to identify *in situ* positioning and potential exposure of candidate peptide epitopes (Figure 3.4.3.2.2). Structures of 2O6X_A, AAB41670.2, ADP09371.1, and CCA61803.1 were analysed by pairwise overlay 3-D structural alignments (Figure 3.4.3.2.2A–F), illustrating the high fidelity of tertiary structures, with the exception of the 2O6X_A His_{81}–Pro_{93} loop, which consistently adopted an isomeric fold (Figure 3.4.3.2.2A–B,D*) despite 100% CL1A sequence identity at this and up-/down-stream flanking sequences (Figure 3.4.3.2.1). The only other discrepancy was shown at the N-terminal (Met_1–Ser_{16}) between AAB41670.2, ADP09371.1 and CCA61803.1 (Figure 3.4.3.2.2C,E–F,H–I**), whereby the orientation of a loosely-coiled helix was angled at varying degrees towards the main protein structure. A relatively extreme change was found in all pairs containing AAB41670.2, caused by an additional intra-helical loop at the C-terminus and the consequential perpendicular positioning of N-terminal residues in closer proximity to the 24-mer Asp_{37}–Asp_{60} α-helix (Figure 3.4.3.2.2A,C,E), which is likely influenced by the Ile5Val residue substitution in this sequence (Figure 3.4.3.2.1A).

A

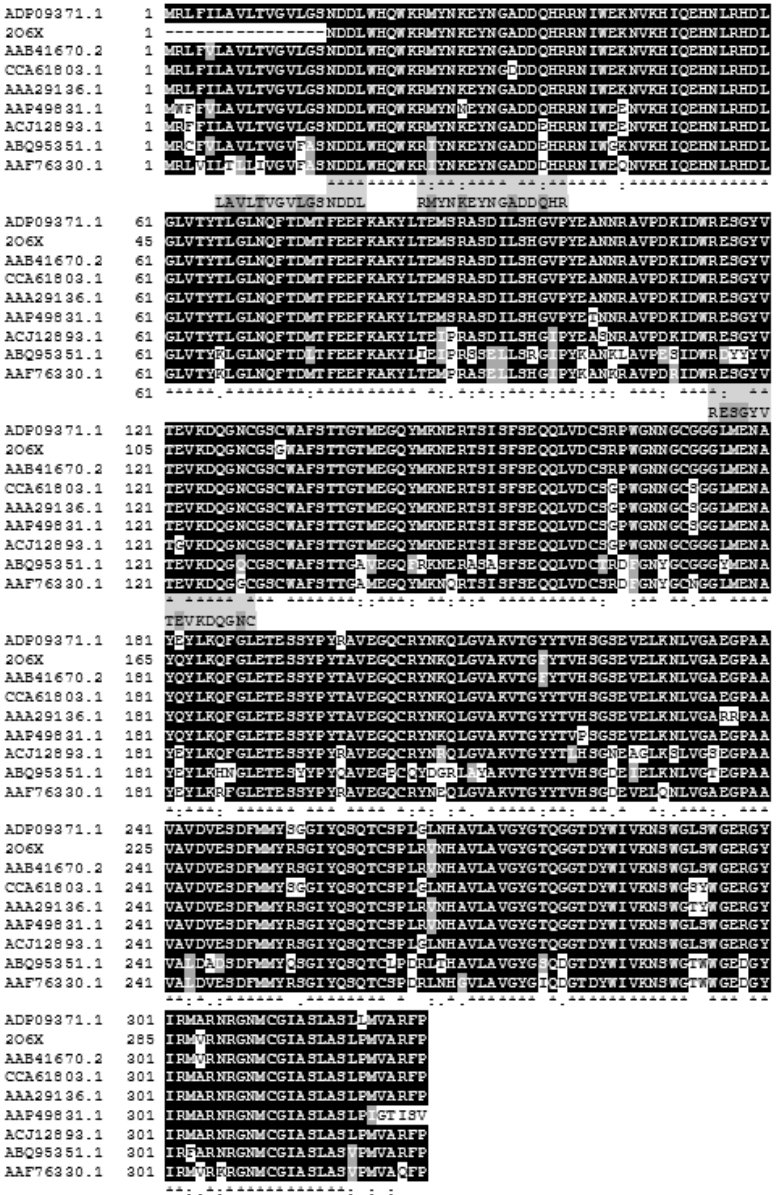

B

Percentage identity matrix

Signal peptide design: LAVLTVGVLGSNDDL

		1	2	3	4	5	6	7	8	9
1	ADP09371.1	100.00								
2	2O6X	100.00	100.00							
3	AAB41670.2	100.00	100.00	100.00						
4	CCA61803.1	100.00	100.00	100.00	100.00					
5	AAA29136.1	100.00	100.00	100.00	100.00	100.00				
6	AAP49831.1	100.00	100.00	100.00	100.00	100.00	100.00			
7	ACJ12893.1	100.00	100.00	100.00	100.00	100.00	100.00	100.00		
8	ABQ95351.1	86.67	100.00	86.67	86.67	86.67	86.67	86.67	100.00	
9	AAF76330.1	66.67	100.00	66.67	66.67	66.67	66.67	66.67	80.00	100.00

Inhibitor peptide design: RMYNKEYNGADDQHR

		1	2	3	4	5	6	7	8	9
1	ADP09371.1	100.00								
2	2O6X	100.00	100.00							
3	AAB41670.2	100.00	100.00	100.00						
4	CCA61803.1	93.33	93.33	93.33	100.00					
5	AAA29136.1	100.00	100.00	100.00	93.33	100.00				
6	AAP49831.1	93.33	93.33	93.33	86.67	93.33	100.00			
7	ACJ12893.1	93.33	93.33	93.33	86.67	93.33	86.67	100.00		
8	ABQ95351.1	86.67	86.67	86.67	80.00	86.67	80.00	93.33	100.00	
9	AAF76330.1	86.67	86.67	86.67	80.00	86.67	80.00	86.67	93.33	100.00

Protease peptide design: RESGYVTEVKDQGNC

		1	2	3	4	5	6	7	8	9
1	ADP09371.1	100.00								
2	2O6X	100.00	100.00							
3	AAB41670.2	100.00	100.00	100.00						
4	CCA61803.1	100.00	100.00	100.00	100.00					
5	AAA29136.1	100.00	100.00	100.00	100.00	100.00				
6	AAP49831.1	100.00	100.00	100.00	100.00	100.00	100.00			
7	ACJ12893.1	93.33	93.33	93.33	93.33	93.33	93.33	100.00		
8	ABQ95351.1	73.33	73.33	73.33	73.33	73.33	73.33	66.67	100.00	
9	AAF76330.1	93.33	93.33	93.33	93.33	93.33	93.33	86.67	73.33	100.00

C

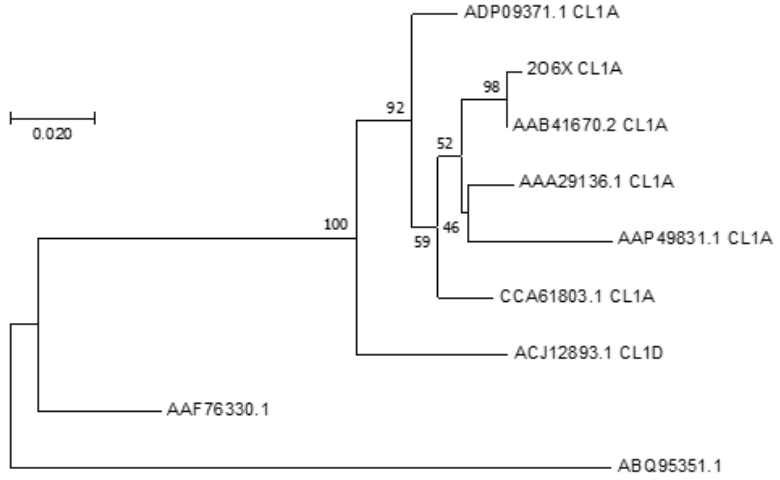

Figure 3.4.3.2.1. Investigation of immunogenic peptide conservation and phylogenetic analysis of procathepsin Ls identified from native and recombinant proteins. Procathepsin L sequences identified from native *Fasciola hepatica* ES products (3.4.1) and recombinant procathepsin L1 proteins (3.4.2) were aligned (A) to assess the conservation of sequences at putative immunogenic peptides at three protein regions (6–20; 26–40; 115–129). (B) No peptide was fully conserved between all sequences, with average conservation of 91.29–91.67%, though the signal peptide had the highest average percentage conservation and all CL1A sequences were the most conserved, with between 86.67-100.00% identity between all peptide designs. Putative candidate immunogenic peptide sequences for signal (Lys_{6}–Lys_{20}), inhibitor (Arg_{26}–Arg_{40}), and protease (Arg_{115}–Cys_{129}) peptide designs had a minimum of 66.67%, 80.00% and 66.67% conservation, respectively, though all CL1A sequences shared 100.00% identity between signal and protease peptide designs, and >90% sequence identity in the inhibitor peptide design. (C) A neighbour-joining phylogenetic tree was produced, which demonstrated a high degree of sequence clustering due to sequence similarities (total tree distance = 0.42044), notably for proteins belonging to the CL1 clade and with closest distances between CL1A sequences.

Table 3.4.3.2. Predicted biochemical and biophysical properties of procathepsin L-derived peptides. Candidate peptide sequences were analysed using the Jpred4 (Jnet) server (Drozdetskiy *et al.*, 2015), with sequence-based structural predictions by Jnetpred and Jnet hidden Markov models* and differential predictions for solvent accessibility during prospective residue interactions. Secondary structure predictions denoted are for residues forming an alpha helix (α), beta sheet (β) or undetermined structure (–); solvent accessibility (+) or inaccessibility (–); and confidence scores of X out of 10.

Properties	Signal peptide	Inhibitor peptide	Protease
Mass (Av. g·mol^{-1})	1485.679	1896.995	1684.782
Amino acid sequence	L A V L T V G V L G S N D D L	R M Y N K E Y N G D D D Q H R	R E S G Y V T E V K D Q G N C
Secondary structure*	α α α β β β β β__ _ _ _ _ _ _ _	α α α _ _ _ _ _ _ _ _ _ _ _ _ _	_ _ _ _ _ β β β β β _ _ _ _ _
Solvent accessibility	+ + _ _ _ _ _ _ _ _ _ + + + + +	+ + _ + + + _ + + + + + + + + +	+ + + + _ _ _ + _ + + + + + +
Confidence score (X/10)	8 7 5 3 2 6 8 7 5 4 8 9 9 9 9	5 4 0 4 6 7 7 7 7 7 7 7 8 8 9	7 7 7 7 3 5 8 8 8 5 3 7 8 9 9

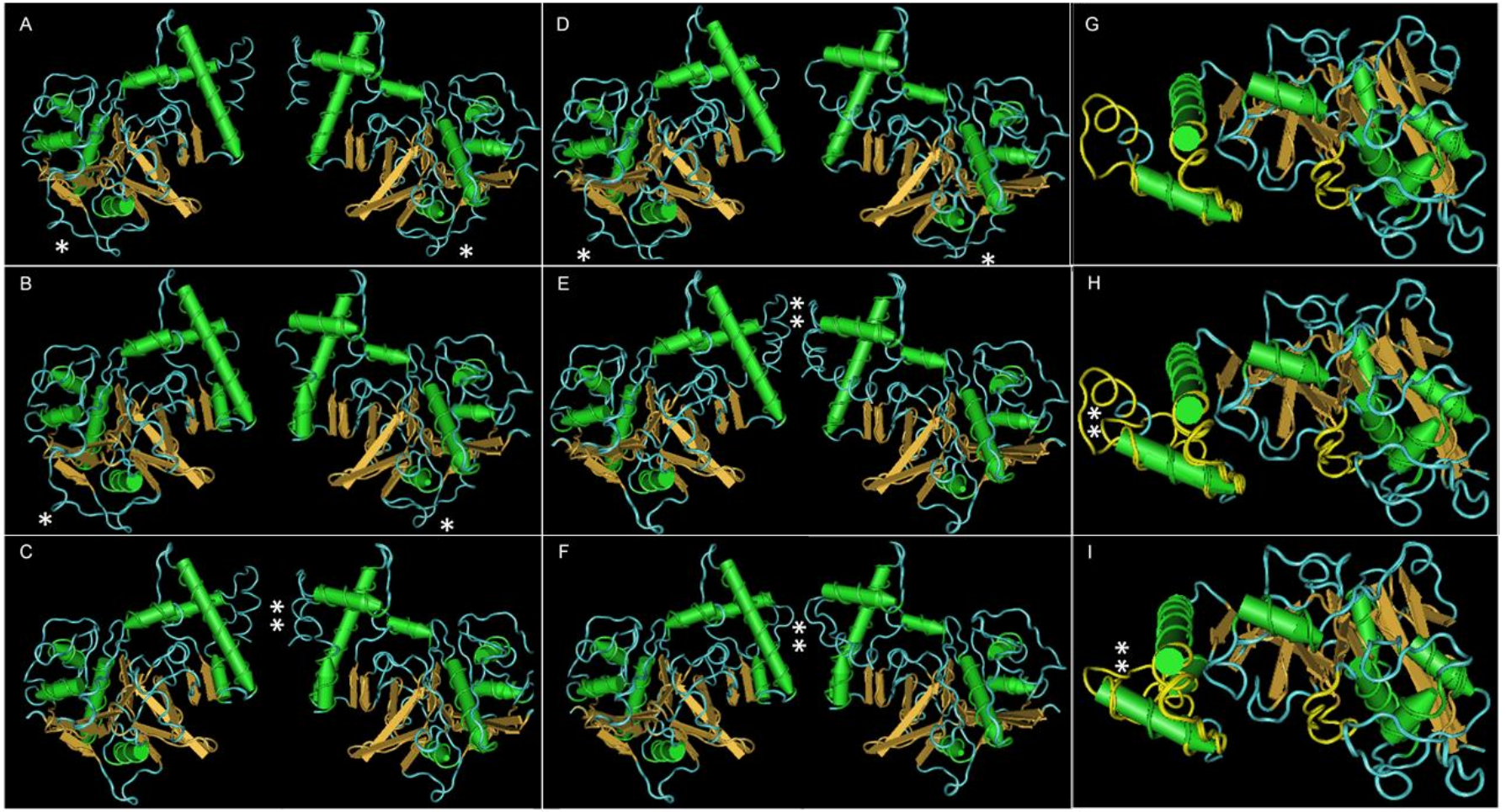

Figure 3.4.3.2.2. 3-D structural exploration and comparison of the exposure and accessibility of procathepsin L-derived peptide candidates *in situ*. Pairs of procathepsin L1A sequences were prepared for 3-D structural overlays using Cn3D v.4.3.1, comparing predicted structures of 2O6X_A, AAB41670.2, ADP09371.1, and CCA61803.1: (A) 2O6X_A vs AAB41670.2; (B) 2O6X_A vs CCA61803.1; (C) AAB41670.2 vs CCA61803.1; (D) 2O6X_A vs ADP09371.1; (E) AAB41670.2 vs ADP09371.1; (F) ADP09371.1 vs CCA61803.1. Positioning of peptide candidates were confirmed at peripheral epitopes, represented by 3-D overlays with 2O6X_A vs AAB41670.2 (G), AAB41670.2 vs ADP09371.1 (H), and ADP09371.1 vs CCA61803.1 (I). Asterisks indicate non-overlapping 3-D structures found in 2O6X_A (*) and AAB41670.2, ADP09371.1, and CCA61803.1 (**).

3.4.3.3 *Testing the specificity of polyclonal anti-rFhΔpCL1*

Antigenic epitope conservation of recombinant and native CL zymogens was tested using anti-rFhΔpCL1 polyclonal antibodies (anti-rFhΔpCL1 IgG), which were raised in two laboratory rabbits (Lampire Biological Laboratories, USA). Optimum anti-rFhΔpCL1 titres for immunological (western hybridisation) assays were determined by probing the pre- and post-immunisation sera of each rabbit (1:500–1:30,000-diluted) against 1 µg rFhΔpCL1 antigen separated by 12.5% SDS PAGE and transferred onto NCM (Figure 3.4.3.3A–B).

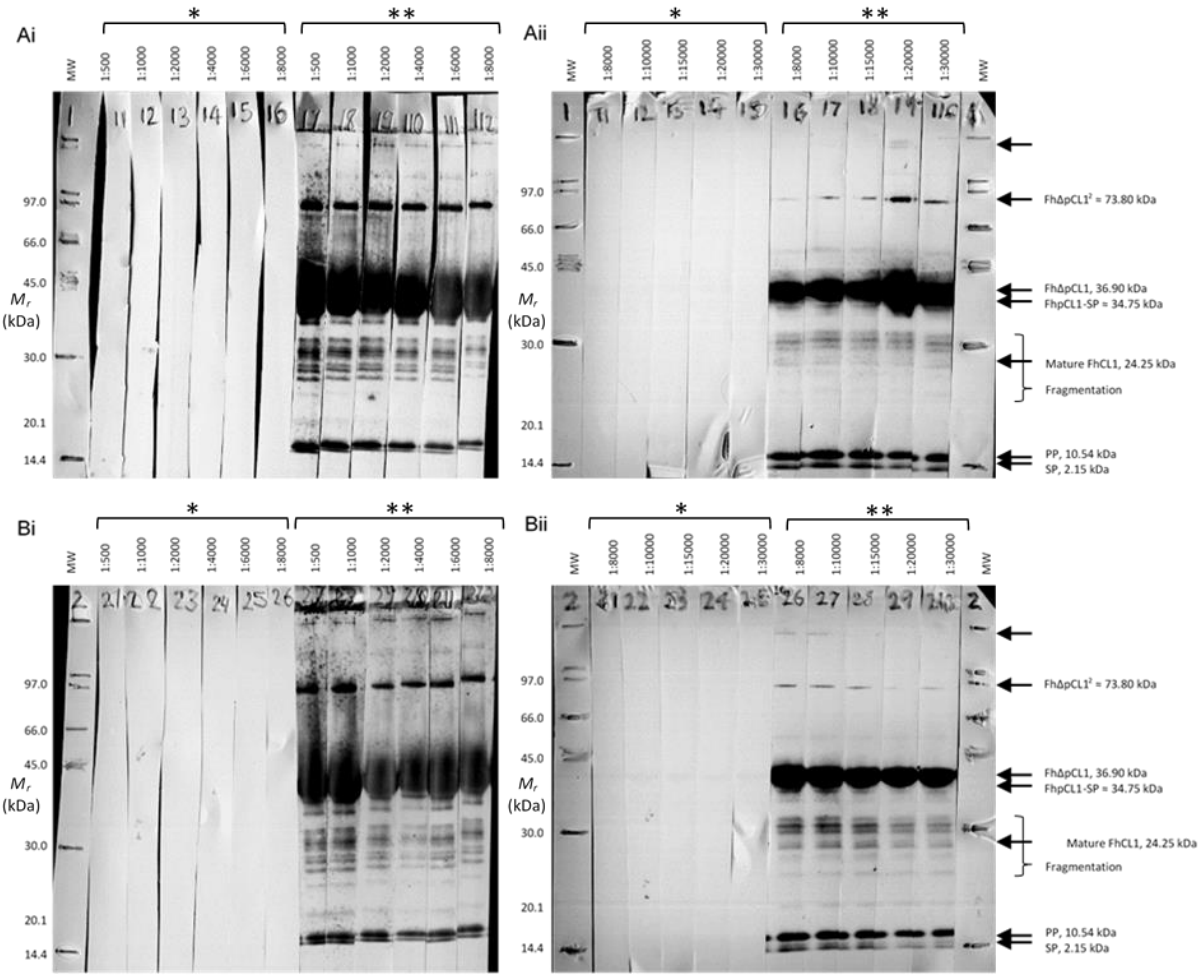

Figure 3.4.3.3. Anti-rFhΔpCL1 optimisation using western hybridisation against recombinant mutant *Fasciola hepatica* procathepsin L1 (rFhΔpCL1). 1 µg rFhΔpCL1 was probed with (*) pre- and (**) post-immunisation serum from two rabbits (A-B) at dilutions between 1:500 and 1:8,000 (A–Bi) and 1:8,000 and 1:30,000 (A–Bii). Antibody-antigen binding was detected using alkaline phosphatase-conjugated anti-rabbit IgG raised in goat. Abbreviations: MW, Amersham Low Molecular Weight SDS Calibration Kit (M_r).

Western hybridisation indicated anti-rFhΔpCL1 antibodies were present post-immunisation, not pre-immunisation, and were highly reactive to the intact 37 kDa antigen

as well as other bands separating at approximately 75 kDa, 35 kDa, 15 kDa and ≤14 kDa (Figure 3.4.3.3, annotated with appropriate sizes of zymogen, dimers and putative fragments). Intriguingly, these additional bands are not visible in Coomassie-stained acrylamide gel separation of rFhΔpCL1 (Figure 3.4.2.1) or following transfer to NCM and Amido black staining (data not shown), suggesting low abundance but sustained immunogenicity of these proteins and the high sensitivity of anti-rFhΔpCL1 PAbs.

Anti-rFhΔpCL1 dilutions between 1:500 and 1:8,000 with 6 minutes in AP substrate solution contributed to blot over-development (Figure 3.4.3.3A–Bi). However, this was improved following further dilutions between 1:8,000 and 1:30,000 with 10 minutes' incubation in AP substrate solution (Figure 3.4.3.3A–Bii). The optimal dilution was determined to be at and beyond 1:30,000, i.e. the lowest dilution to be tested and maintain highly sensitive detection of the 37 kDa zymogen and other proteins of lower abundance.

3.4.3.4 *Anti-rFhΔpCL1 immunoreactivity and specificity within the FhCL1A clade*

3.4.3.4.1 Recombinant FhpCL1 antigens

The experimentally formed protein fractions following autocatalytic conversion of rFhpCL1^{WT} (3.4.2.2) and rFhpCL1 (3.4.2.3) were investigated for anti-rFhΔpCL1 recognition by 1-DE and western hybridisation (Figure 3.4.3.4.1). Antibodies bound almost exclusively to the rFhpCL1^{WT} fractions containing the zymogen-specific pro-peptide (pp) and signal peptide (sp) if present, and also to a minor extent to intermediary and protease proteins (Figure 3.4.3.4.1A). Conversely, a greater proportion of rFhpCL1 protein fragments of ranging molecular weights were demonstrated to possess anti-rFhΔpCL1 epitopes based on several western hybridisations (Figure 3.4.3.4.1B). At the lowest overall protein concentration loaded, the most antigenic components of the rFhpCL1 sample were demonstrated to be proenzyme (pCL), intermediates (I), and peptide-sized fractions (pp±sp) (Figure 3.4.3.4.1B), similarly to rFhpCL1^{WT} (see: Figure 3.4.3.4.1A, 0 m) and rFhΔpCL1 (see: Figure 3.4.3.4.1A-Bii, 1:30,000). However, immunoreactivity by potential protease-sized bands (CL1) and additional proteins resulting from possible fragmentation (F) was also shown (Figure 3.4.3.4.1B), suggesting that suspected immunogenic zymogen peptides are present in the immunoreactive fragments, or that more epitopes of rFhpCL1 are exposed and/or antigenic than in rFh(Δ)pCL1A(^{WT}).

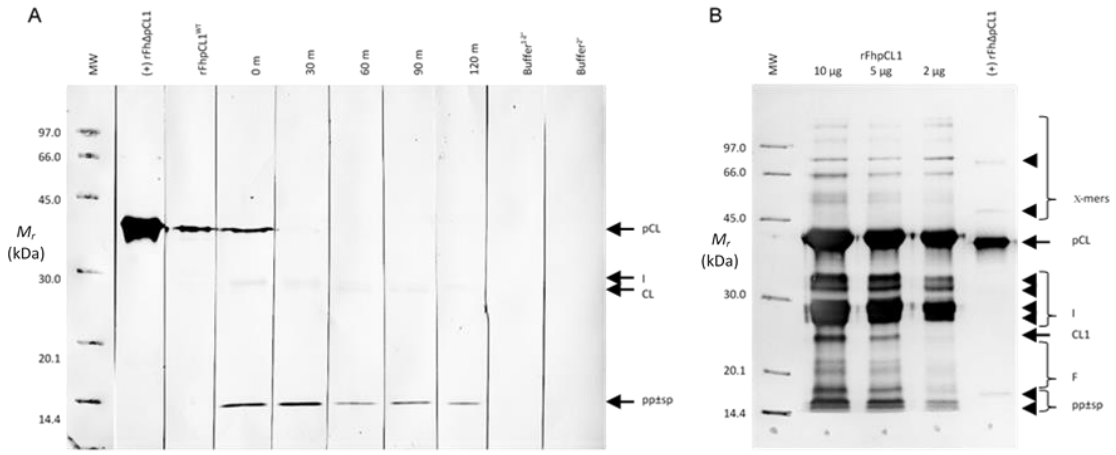

Figure 3.4.3.4.1. Anti-rFhΔpCL1 recognition within the FhCL1A clade using western hybridisation. (A) 0.5 µg recombinant mutant *Fasciola hepatica* procathepsin L1 (rFhΔpCL1, +, positive control: 2O6X/ADP09371.1) and 2 µg of protein from each fraction of rFhpCL1 activation (AAB41670.2; 3.4.2.2) was probed with anti-rFhΔpCL1 serum diluted to 1:15,000, identifying predominant immunoreactivity at bands corresponding to the proenzyme (pCL), which was replaced by low molecular weight peptide-sized fragments upon zymogen activation (pp±sp), with minor and decreasing reactivity at intermediate (I) and suspected protease (CL) bands over the time course. (B) 0.05 µg rFhΔpCL1 (+) and 10, 5 and 2 µg rFhpCL1 (3.4.2.3) was probed with anti-rFhΔpCL1 serum diluted to 1:10,000, identifying antibody recognition of several bands in the protein fraction, predominantly corresponding to the proenzyme (pCL), intermediates (I) and peptide-sized fragments (pp±sp).
Abbreviations: MW, Amersham Low Molecular Weight SDS Calibration Kit (M_r).

3.4.3.4.2 Native adult FhCL zymogens and proteases

Representative ES products from *in vitro* cultured live and dead (ethyl 4-aminobenzoate-terminated) adult flukes (3.4.1) were probed with anti-rFhΔpCL1 to determine the abundance and immunoreactivity of native cathepsin L zymogens and proteases (Figure 3.4.3.4.2). Western hybridisation of 2-DE-separated ES demonstrated antibody recognition of an array of cathepsin zymogens secreted by live flukes (Figure 3.4.3.4.2A), with an increase in both immunoreactive isoforms and protein spot abundance by dead flukes (Figure 3.4.3.4.2B). Minor immunoreactivity of protein spots of possible cathepsin proteases was also demonstrable at the 1:5,000 antibody dilution, which was reflected in relative reactivity between live and dead samples (Figure 3.4.3.4.2). Together with LC-MS/MS analyses of proteomic samples within the zymogen region (see: Figure 3.4.1, boxed; Figure 3.4.3.4.2, pCL), anti-rFhΔpCL1 recognition shown here can be putatively concluded to resolve from antibody binding to multiple procathepsin L isoforms, including those of the CL1A clade but possibly also other CL clades.

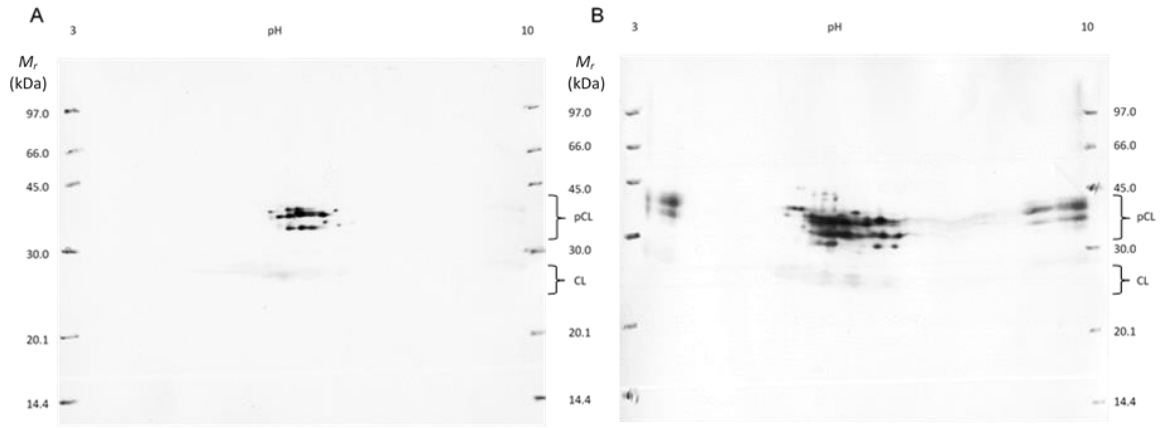

Figure 3.4.3.4.2. Anti-rFhΔpCL1 recognition of native *Fasciola hepatica* cathepsin zymogens and proteases using western hybridisation. 25 µg 2-DE-separated excretory/secretory (ES) products isolated from *in vitro* cultured live (A) and dead (B) (ethyl 4-aminobenzoate-terminated) adult *F. hepatica* were probed with anti-rFhΔpCL1 diluted to 1:5,000. Data suggest highest immunoreactivity in protein spots separating at the same position as CL proenzymes (pCL) and minor antigenicity of potential proteases (CL) in these native samples. Abbreviations: MW, Amersham Low Molecular Weight SDS Calibration Kit (M_r).

3.5 Discussion

This chapter has explored the cathepsin L (CL) zymogen subproteomes of *Fasciola hepatica*. Specifically, both prepro- and procathepsins were recovered for the first time from native ES products (Chapter 3; 3.2.4: objective 1). CL zymogen antigenicity was also investigated via a combined *in silico* and *in vitro* methodology pipeline that formally identified native and recombinant procathepsin (FhpCL) zymogens (Chapter 3; 3.2.4: objectives 1 and 2), which provided sequences for the predictions of *in silico* antigenic epitope sequences (Chapter 3; 3.2.4: objective 3a). In addition, project-raised anti-rFhΔpCL1 polyclonal antibodies were utilised to detect native and recombinant FhpCL zymogens and thus determine the conservation of putative immunogenic epitopes (Chapter 3; 3.2.4: objective 3a). The present strategy thus uncovered the immunodominance of the signal peptide of preprocathepsin zymogens and their presence in ES products. An increase in zymogen abundance and cathepsin clade representation within *in vitro*-cultured dead compared to live parasites was also indicated. Furthermore, predicted immunogenicity is in-keeping with previous findings (Cornelissen *et al.*, 2001, 1999) but identified the signal peptide as a major epitope of antigenic interest, which also demonstrated immunodominance over other zymogen epitopes and immunoreactivity with anti-preprocathepsin L IgG.

CL proteases are the most dominant component of the ES products of juvenile and adult flukes (Dalton *et al.*, 2003; Jefferies *et al.*, 2001; Morphew *et al.*, 2007), likely owing to their multifaceted roles for Hb digestion, pathogenesis and immune evasion (Berasaín *et al.*, 2000; Cancela *et al.*, 2008; Corvo *et al.*, 2009; Dalton *et al.*, 2013, 2003; Figueroa-Santiago and Espino, 2017; Lowther *et al.*, 2009; McGonigle *et al.*, 2008; Meemon and Sobhon, 2015; Robinson *et al.*, 2011; Tort *et al.*, 1999). CL zymogen recovery in adult *F. hepatica* ES products has not previously been described, though LC-MS/MS has been proven here to be sufficiently sensitive for their detection in whole 2-DE-separated ES protein, and find evidence for their differential abundance between live and dead flukes (3.4.1). There is further evidence supporting the sustained abundance of different cathepsin classes and CL clades in *F. hepatica* ES products between adults and juveniles (Cancela *et al.*, 2008; Garcia-Campos *et al.*, 2016; McGonigle *et al.*, 2008; Morphew *et al.*, 2011; Robinson *et al.*, 2009; Wilson *et al.*, 1998), as well as dead (Morphew *et al.*, 2007) and TCBZ-treated adults (Faridi *et al.*, 2014; Morphew *et al.*, 2007). Changes to zymogen abundance are yet to be determined within juveniles or

following flukicide exposure, though the comparison of ES from live and dead *in vitro*-cultured adult flukes provides insight into the biological regulation of this important protein in this parasite. With increased prepro- and procathepsin abundance in dead fluke ES, this confirms the termination of normal actively-regulated aspects of excretory/secretory processing, since preprocathepsin zymogens are sequestered within gastrodermal vesicles and pro-peptide- and pH-mediated protease regulation is maintained and accompanied by nominally three-hourly vomitus expulsion (Berasaín *et al.*, 1997b; Collins *et al.*, 2004; Dalton *et al.*, 2003; Smith *et al.*, 1993b). Consequently, the reduction or elimination of ES release due to the termination of actively-regulated digesta expulsion in dead flukes may be the direct cause for increased CL zymogen abundance, resulting from the passive egress of gut contents post-obit (Morphew *et al.*, 2007). Thus, one could interpret intact zymogen CL abundance as a potential indicator of fluke viability and fitness, whereby live-associated activities of ES regulation reduces the opportunity for zymogen appearance, which is supplanted by passive release in equivalent dead parasites.

Surprisingly, prepro- and procathepsin zymogens have received little attention despite extensive genome-, transcriptome- and proteome-based analyses that have characterised many molecular candidates from *F. hepatica* of diagnostic, anthelmintic and vaccine interest (Cancela *et al.*, 2008, 2010; Cwiklinski *et al.*, 2015b; Hodgkinson *et al.*, 2013). Moreover, mature protease counterparts have conversely been promoted to the frontline of fasciolosis diagnostics and vaccines (Martínez-Sernández *et al.*, 2016; Mezo *et al.*, 2004). Consequently, there is limited understanding of the immunogenic potential of the inhibitor (Cornelissen *et al.*, 1999; Harmsen *et al.*, 2004) and signal regions of *F. hepatica* cathepsins until this thesis. Using newly synthesised polyclonal IgG classes raised against an intact preprocathepsin L ((anti-)rFhΔpCL1), the immunodominance of the zymogen CL epitopes has been confirmed. The antigenicity of signal and inhibitor components is likely responsible for this observed reactivity, since intermediates resolving within 32–38 kDa by 1-D and 2-D SDS PAGE contributed most of this activity (Figures 3.4.3.4.1–3.4.3.4.2). Furthermore, mature proteases did not elicit analogous recognition to zymogen peptide-associated fractions, including by native or recombinant wild type proteases. However, recognition was provoked by a second recombinant protease derivative at the highest concentrations tested (Figure 3.4.3.4.1B), possibly due to an overabundance of protein leading to non-specific antibody-antigen binding, or else an increased proportion of denatured protein carryover from previous steps

of purification, thereby exposing an adequate abundance of additional antigenic regions in this unfolded state. Nevertheless, zymogen-specific antigenic sequences appeared highly conserved, both bioinformatically (3.4.3.2; Figure S2) and *in vitro* (3.4.3.2–3.4.3.4), though separation, recovery and/or immunoreactivity of the cleaved native signal peptide could not be identified, which would have helped in elucidating its antigenic contribution.

Interestingly, there have been no prior reports identifying the presence or immunogenicity of intact CL zymogens in *in vitro F. hepatica* ES products. However, it has previously been shown that CL1- and CL3-derived synthetic propeptides are capable of eliciting immunoprotection (Harmsen *et al.*, 2004), which also presents synthesis as an effective approach to study pre- and pro-CL peptides and raise peptide-specific monoclonal antibodies. Despite the present findings, the *F. hepatica* ES anti-rFhΔpCL1 recognition profile does not limit immunorecognition to signal-, inhibitor- or mature-specific CL zymogen peptides, and so may also involve transient conformational epitopes when the prepro- and pro-enzymes adopt these molecular weights. Indeed propeptide-specific epitopes may contribute to preproCL immunogenicity, whereby conformational changes to this peptide are inducible upon low pH exposure that functions to contribute to autocatalytic activation (Collins *et al.*, 2004; Jerala *et al.*, 2002; Ménard *et al.*, 1998; Rozman *et al.*, 1999; Vernet *et al.*, 1995). Until legitimate identification of signal- or inhibitor-specific antigenicities can be differentiated, it could be hypothesised that the release of the cleaved peptides may be tactically- and temporally-released as antigenic decoys for immune evasion, as has been suggested for the former peptide class in other disease models (El Hage *et al.*, 2008; Kovjazin *et al.*, 2011; Thaa *et al.*, 2013). In contrast to this theoretical endpoint, the apparent absence of anti-signal peptide antibody recognition in current *in vitro* profiles potentially provides further avenues of study, i.e. to investigate the *in situ* molecular characteristics and fate(s) of CL zymogen signal peptides. Thus, this chapter has provided new insight into the lesser-known antigenic properties of signal and inhibitor peptides, which demonstrate extensive zymogen-specific immunoreactivity *in situ*, including against several CL clades.

3.6 Conclusions

Fasciola hepatica cathepsin proteases have provided a wide scope for research prospects, with extensive evidence supporting their utility as diagnostic, vaccine and drug

targets. Recently, CL proteases have been identified as potential indicators of fluke fitness phenotype (Morphew *et al.*, 2014). The potential of zymogen CLs within these molecular fields has not been fully realised, though this work has resolved the presence of CL zymogens in ES products, and potential host exposure *in vivo*. CL zymogens have also demonstrated their indication as phenotypic determinants of fluke viability, based on the increase in abundance following fluke death *in vitro*. Natural host immunity against cathepsins is predominantly associated with the mature protease region, which has thus precluded any anticipated involvement of the prepro- peptide regions, and has been shown to possess significant, conserved antigenic properties. The diagnostic utility of short-length antigenic peptides with predicted and established reactivity with *F. hepatica*-infected host serum has shown success for CL-based designs (Cornelissen *et al.*, 2001; Meshgi *et al.*, 2018), and though demonstrably immunogenic, CL signal-based peptide design is a novel enterprise. Overall therefore, the findings presented here have exemplified the value of CL zymogens as a diagnostic tool, which are an asset that has been previously overlooked.

4 Chapter 4: *In vitro* phenotypic and proteomic assessments of wild type *Fasciola hepatica* and a newly isolated TCBZ-resistant field strain following TCBZ exposure

4.1 Abstract

At present, the mechanisms of action of triclabendazole (TCBZ; TCBZ-sulfoxide/sulfone (SO/SO_2)) and TCBZ resistance in *Fasciola hepatica* are unknown, though microscopic and molecular approaches have previously helped to distinguish differences between TCBZ-susceptible (TCBZ-S) and TCBZ-resistant (TCBZ-R) phenotypes. However, such findings are typically derived via exposure with the potent TCBZ-SO drug rather than both parent (TCBZ) and derivatives (TCBZ-SO/-SO_2), despite the bioavailability and flukicide activity of all components post-TCBZ treatment. In order to investigate macroscopic and molecular biomarkers associated with anthelmintic challenge, work here set out to explore the impacts of non-specific flukicide and representative TCBZ treatment.

Flukes used for this study were *in vitro*-cultured adults of mixed field strains with unknown TCBZ-susceptibility from the UK (wild type, WT-Fh), and a confirmed TCBZ-R isolate originating from infections in Kilmarnock, Scotland (K-Fh). Macroscopic changes following non-specific flukicide in the WT-Fh group were documented, indicating severe damage to the tegument infrastructure and impacting the secreted extracellular vesicle (EV) profile. When comparing WT-Fh and K-Fh following sub-lethal TCBZ, TCBZ-SO and TCBZ-SO_2 treatment, collective data indicated anthelmintic challenge led to specific stark differences in viability scores between fluke groups, as well as differences between the collective TCBZ-exposed excretory/secretory proteomes.

As per the findings of this chapter, microscopic and proteomic indicators of fluke viability were identified, offering new targets of potentially significant diagnostic importance and value in the determination of flukicide efficacy and susceptibility status.

4.2 Introduction

In order to introduce and provide a comprehensive overview of triclabendazole (TCBZ) for this chapter: primary sections will first outline the pharmacodynamics and flukicide mechanisms behind its preferred application (4.2.1); with progression into more detailed mechanisms of drug action and resistance pathways (4.2.2); host and parasite TCBZ metabolism (4.2.3); a current overview of TCBZ-susceptible and -resistant (TCBZ-S/-R) strains recovered from livestock (4.2.4); and putative diagnostic roles of extracellular vesicles (EVs) in TCBZ-S/-R phenotypes (4.2.5).

4.2.1 Triclabendazole (TCBZ): the flukicide of choice

Anthelmintic activities by TCBZ and its two activated sulphoxidised (-SO) and sulphonated (-SO_2) metabolites have been well-documented since the first *in vivo* assessments (Boray *et al.*, 1983). *In vitro*-cultured adult *Fasciola hepatica* become immobilised after 30 hours of exposure to a lethal dose of TCBZ [100 µg·mL^{-1}] and after 18 hours with a lethal dose of TCBZ-SO [100 µg·mL^{-1}], suggesting the sulphoxised metabolite has almost double the flukicidal potency of its parent drug (Fairweather *et al.*, 1984). Comparisons between sub-lethal doses [15 µg·mL^{-1}] of TCBZ and its metabolites for 24 hours has further revealed the negative effects of drug exposure, leading to ultrastructural damages at the tegument and gastrodermis tissues, with increasing severity caused by TCBZ<TCBZ-SO<TCBZ-SO_2 (Halferty *et al.*, 2009). Similar disruptions have been reported *ex vivo* (Toner *et al.*, 2010b) and have also been observed in the closely-related species, *F. gigantica*, from 48 hours after *in vivo* TCBZ treatment (Shareef *et al.*, 2014), suggesting anthelmintic molecular mechanisms are similar across *Fasciola spp*. Interestingly, there is no evidence for direct ovicidal activity, based on *in vitro* egg exposure to any one TCBZ or metabolite compounds in either TCBZ-susceptible (TCBZ-S) or TCBZ-resistant (TCBZ-R) *F. hepatica* strains (Alvarez *et al.*, 2009). However, *in vivo* TCBZ treatment leads to disruptions to reproductive tissues, vitellogenesis and spermatogenesis (Hanna *et al.*, 2010; Savage *et al.*, 2014; Stitt *et al.*, 1991; Stitt and Fairweather, 1996; Toner *et al.*, 2011b), impaired egg production after two days post-treatment (PT) (Toner *et al.*, 2011a) and a complete inhibition in egg production after 24 hours PT (Hanna *et al.*, 2012).

4.2.2 Molecular mechanisms of TCBZ activity and resistance

The molecular mechanisms leading to these pathologies are not fully understood, but similarly to albendazole (ABZ) and its sulphoxide (ABZ-SO) and sulphone (ABZ-SO_2) derivative (Fetterer, 1986), TCBZ and its more active TCBZ-SO metabolite are thought to interact with microtubules, and specifically β-tubulin (Bennett and Köhler, 1987; Fetterer, 1986; McConville *et al.*, 2006; Robinson *et al.*, 2002), subsequently interrupting correct spindle formation in TCBZ-S flukes, whereby similar effects are induced by tubulin inhibitors (Stitt *et al.*, 1991; Stitt and Fairweather, 1993a, 1993b, 1992). Disruptions to this structurally-integral protein could be critical in triggering apoptosis in the mitotically- and meiotically-dividing cells

in these tissues following exposure to these anthelmintics (Hanna *et al.*, 2013). This is supported by instances of resistance to benzimidazoles (BZ), a group of compounds from which ABZ and TCBZ are derived, which are due to parasite tubulin mutations at certain amino acid residues that prevent normal BZ antagonism (Brennan *et al.*, 2007; Kwa *et al.*, 1994). *Fasciola hepatica* adults have been identified with diverse tubulin proteins, with five alpha- and six beta-tubulin isotypes (Ryan *et al.*, 2008), which may differ in TCBZ-binding capacity and consequently have the potential to contribute to resistance via key point mutations. However, it has been shown that TCBZ-R is not solely dependent on tubulin mutations, as ABZ is equally effective against TCBZ-R as it is in TCBZ-S strains (Mottier *et al.*, 2006b). Furthermore, these authors demonstrated recovery of susceptibility in TCBZ-R *F. hepatica* following co-ivermectin anthelmintic exposure, which is known to target nematode p-glycoprotein ATP-binding cassette drug transporters (Xu *et al.*, 1998) and thus the *F. hepatica* p-glycoprotein has previously been identified a molecular candidate of potential interest for TCBZ-R isolates (Ceballos *et al.*, 2010; Mottier *et al.*, 2006b; Wilkinson *et al.*, 2012). This putative involvement of drug efflux mechanisms is supported by ultrastructural comparisons between TCBZ-R and TCBZ-S isolates, whereby TCBZ exposure causes minimal tissue disruption in resistant flukes (Hanna *et al.*, 2010), which is reversible by P-glycoprotein inhibition (Savage *et al.*, 2014). Thus, TCBZ-treated TCBZ-R isolates demonstrate treatment is ineffectual in disrupting egg production and hatching compared to TCBZ-S isolates, providing another technical indicator of TCBZ susceptibility (Arafa *et al.*, 2015; Fairweather *et al.*, 2012; Hanna *et al.*, 2015).

4.2.3 TCBZ metabolism: insights from *in vivo* and *in vitro* studies

At the penside, anthelmintic regimens are adjusted for an intraruminal dose at 10 $mg \cdot kg^{-1}$ (Boray *et al.*, 1983; Smeal and Hall, 1983), which leads to the rapid generation of the sulphoxide and sulphone derivatives (Mottier *et al.*, 2004b) that peak in plasma circulation from approximately 18 (TCBZ-SO) and 36 (TCBZ-SO_2) hours PT (Hennessy *et al.*, 1987). TCBZ bioconversion occurs in hepatocyte microsomes, leading to high levels of recovery from liver tissues, bile and fluke tissues *ex vivo* (Moreno *et al.*, 2014), locations which are ideal for liver and bile stage parasite exposure. The conjugation of metabolites to plasma proteins further prolongs their pharmacological availability, whereby of an intraruminal TCBZ dose, 35.8%

becomes plasma-conjugated metabolites (TCBZ-SO majority) compared to only 9.7% becoming freely available in bile (Hennessy *et al.*, 1987). Fluke uptake of TCBZ/-SO/-SO_2 occurs via trans-tegumental molecular mechanisms thought to involve diffusion (Mottier *et al.*, 2004a). Oral uptake is important for fluke nutrition via blood ingestion (Halton, 1997). However, TCBZ/-SO/-SO_2 ingestion has been found nonessential for anthelmintic mechanisms, based on the limited differences observed between the gut tissues of treated flukes with ligatured or non-ligatured suckers (Toner *et al.*, 2010c, 2009). Additionally, histological damages following TCBZ exposure at the tegument syncytium is severe in comparison at the gastrodermis (Toner *et al.*, 2010b), supporting the long-standing hypothesis of tegumental microtubule-directed anthelmintic activities (Fairweather, 2009, 2005; Stitt and Fairweather, 1993a, 1993b), especially in light of the reduction to such damages in TCBZ-resistant fluke (Robinson *et al.*, 2002). Furthermore, passive trans-tegumental diffusion inevitably leads to tegumental and muscle damages despite sucker ligation (Toner *et al.*, 2010c, 2009) and can also continue after fluke death (Mottier *et al.*, 2006a). Following TCBZ treatment *in vivo*, TCBZ and both sulphoxide and sulphone metabolites are all recoverable from fluke tissues *ex vivo* (Moreno *et al.*, 2014; Mottier *et al.*, 2004b, 2004a). In addition to direct TCBZ and metabolite uptake, flukes can also metabolise TCBZ, as the sulphoxidised derivative has also been traced in fluke tissues after one hour post-exposure of the parent drug (Mottier *et al.*, 2004b). This suggests *in vivo* TCBZ treatment may lead to the exposure and uptake of all three bioactive drugs by flukes, which can lead to flukicidal mechanisms both directly and indirectly following TCBZ bioconversion after drug exposure.

4.2.4 *Fasciola hepatica* isolates of defined TCBZ susceptibility and resistance

Fluke isolates of defined TCBZ susceptibility and resistance continue to be the paradigm for comparative phenotypic studies, particularly the well-studied Cullompton and Sligo isolates, respectively (Coles and Stafford, 2001; Fairweather, 2011c; Flanagan *et al.*, 2011b). More TCBZ-R strains have also been verified via *in vivo* faecal egg count and coproantigen reduction tests (FECRT, CRT) and in comparison to TCBZ-S strains to confirm their statuses for further study, including TCBZ-S Fairhurst, Sunny Corner and Leon isolates, and TCBZ-R Oberon and Dutch isolates (Fairweather, 2011c; Flanagan *et al.*, 2011b; Gaasenbeek *et al.*, 2001).

There have been more recent resistance outbreaks and isolations of these strains in the UK (Ridgeway Research Ltd., personal communication), though there has been no further investigations of established TCBZ-R isolates beyond preliminary identifications of drug efficacy (Fairweather, 2011c). In order to fully understand resistance emergence, we must therefore take steps to identify and distinguish the molecular phenotypes of TCBZ-S and TCBZ-R flukes through genomic, transcriptomic and proteomic study (Hodgkinson *et al.*, 2013; Kotze *et al.*, 2014; Morphew *et al.*, 2014). Furthermore, we must consider comparisons of isolated strains with a representative and mixed population sample from geographically separated origins (wild type: natural infections with presumed TCBZ-S or -R response status), in order to nullify the bias of genetically restricted, *in vitro*-maintained strains of confirmed drug response status.

4.2.5 Roles of *Fasciola hepatica* extracellular vesicles (EV) during infection and TCBZ exposure

Extracellular vesicle (EV) is an umbrella term for the wide array of vesicular bodies that originate from endosomal and plasma membranes. Functions were once thought to selectively remove cellular protein, lipid and RNA species, but have since been identified as the important carriage of cargo into the extracellular compartment for intercellular communication (Raposo and Stoorvogel, 2013; van Niel *et al.*, 2018). *Fasciola hepatica* is one of many helminths and pathogens of medical and veterinary importance whose EVs are thought to communicate in this way towards pathogenesis in the host (Coakley *et al.*, 2015; Cwiklinski *et al.*, 2015c). EV release has been identified at gut and tegumental tissues of *F. hepatica* and in other helminths, via characteristic mechanisms of budding and blebbing from vesicular networks (Coakley *et al.*, 2017; Cwiklinski *et al.*, 2015c; Marcilla *et al.*, 2012; Montaner *et al.*, 2014; Twu and Johnson, 2014). The qualitative characteristics of EVs are of additional note, particularly in parasite-host reactions and the response to host and chemotherapeutic pressures, since EVs are a reflection of the genetic or proteomic footprint and the biological status of the parent cells (Akers *et al.*, 2013). EVs may therefore echo the molecular activities at the *F. hepatica* gut and/or tegument at any given time, whether actively secreting biomarkers and virulence factors towards immune or drug evasion, or during flukicide success where vesiculation of apoptotic bodies are a by-product of apoptotic

cell death (Akers *et al.*, 2013). The production of EVs occurs through a variety of bioactive pathways (van Niel *et al.*, 2018), suggesting the respectively high and low abundances of apoptotic bodies and EVs offer a biological indication of cell viability during programmed death. Furthermore, cellular energy conservation under stressful conditions has been described in some instances to promote exosome degradation (Papandreou and Tavernarakis, 2017), arguing that quantitative changes in EV release and recovery could indicate parent cell viability. Together with proteinaceous species of the *F. hepatica* excretory/secretory (ES) products (Jefferies *et al.*, 2001; Morphew *et al.*, 2007, 2014), EVs contribute to the prolific and ranging ES profile of this trematode, providing communicative, immunomodulatory and metabolic molecular arms during parasite-host interactions (Cameron *et al.*, 2017; Cwiklinski *et al.*, 2015c; Hamilton *et al.*, 2009; Marcilla *et al.*, 2012). However, there are preliminary signs that environmental stresses, including anthelmintic exposure, can influence the abundance and complexity of EV populations (Davis, 2019, personal communication), supporting the potential role of EVs or their contents as a measurable marker of the outcome of anthelmintic challenge.

4.2.6 Chapter 4 aims

Previous *in vitro* studies investigating anthelmintic responses in liver fluke have revealed the molecular dynamics and phenotypes but based on separate treatments by TCBZ or its two major metabolites, with particular focus on the effects of the sulphoxidised form (Chemale *et al.*, 2010; Morphew *et al.*, 2014; Robinson *et al.*, 2002; Stitt *et al.*, 1995). Such attention to TCBZ-SO in particular is possibly founded on the more abundant and potent tendencies of this metabolite *in vivo*. However, this disconnected or reductionist approach does not measure the overall complexity of the fluke response in the host environment to all bioactive compounds. Following anthelmintic administration, flukes are known to uptake all three anthelmintic forms (Mottier *et al.*, 2004b) and changes in the levels of metabolite recovery from flukes are highly reflective of host circulating plasma-conjugate levels, which peak by 24 hours PT (Moreno *et al.*, 2014). Thus, it must be presumed that the actual *in vivo* molecular profiles are inclusive of all drug exposures and resultant phenotypes, and thus studying the molecular dynamics of all compounds together, albeit *in vitro*, is highly relevant and reflective of the response to TCBZ dosing of animals. As described above, the involvement

of newly described EVs as indicators of fluke viability, in terms of anthelmintic susceptibility, is also of current interest. Consequently, this chapter aimed to:

1) Identify and compare differences in EV release between live control and dead (via non-specific flukicide) flukes;
2) Measure the biological phenotypes of natural wild type flukes and a newly identified TCBZ-R (Kilmarnock) isolate based on *in vitro* fluke fitness/viability using an *in vitro* evaluation score system and statistical tests;
3) Identify and compare differences between the molecular phenotypes of EV-depleted ES proteomes from drug-exposed (TCBZ, TCBZ-SO and TCBZ-SO_2) *in vitro* cultures between the wild type mixed strain and the TCBZ-R Kilmarnock isolate via gel-based proteomics and mass spectrometry.

4.3 Materials and methods

4.3.1 Liver fluke culturing

4.3.1.1 Wild type Fasciola hepatica *(WT-Fh) isolates*

Live adult *Fasciola hepatica* from natural infections were collected at a local abattoir as described in the General materials and methods (2.2.1). Flukes were removed from the livers from multiple flocks delivered to a local abattoir from nationwide provenances, and thus the mixed field strains (wild type mixed TCBZ-susceptibility: WT-Fh) were expected to have mixed drug susceptibility status that is representative of wild type flukes with an assumed exposure to anthelmintics and undetermined TCBZ susceptibility status.

Ten flukes from live WT-Fh fluke culture were terminated using ethyl 4-aminobenzoate (1% (w/v) in ethanol) in order to assess the contribution of EVs to the molecular phenotype of flukes under flukicide exposure. These flukes were briefly submerged and subsequently washed with PBS and incubated in fresh supplemented DMEM for the collection of dead-associated ES products, as described in the General materials and methods (2.2.2). ES products from both live and dead cultures of ten flukes were subsequently prepared for EV isolation (4.3.1.4) before preparation for transmission electron microscopy (TEM) (4.3.2.1). For TEM analysis of tegument sections for the comparison between live and dead fluke phenotypes, five WT-Fh were used after collection from *in vitro culture* and following either PBS washing only (live group) or ethyl 4-aminobenzoate (1% (w/v) in ethanol) exposure and PBS washing (dead group). Flukes were subsequently prepared for TEM according to the method described in section 4.3.2.2.

4.3.1.2 TCBZ-resistant Kilmarnock Fasciola hepatica (K-Fh) *isolates*

Flukes of known TCBZ resistance status were identified and isolated from a sheep flock in Kilmarnock, Scotland by staff at Ridgeway Research Ltd. (www.ridgewayresearch.co.uk/parasite-catalogue/Fasciola-hepatica) following TCBZ treatment failure and subsequent recovery of adults and viable eggs at slaughter. Infections with this Kilmarnock isolate (TCBZ-R: K-Fh) were maintained in two experimental sheep infections, with TCBZ administration of veterinary practitioner-recommended dosing at 12 weeks post-infection (wpi) and termination at 16 wpi for live adult K-Fh *Fasciola hepatica* collection.

4.3.1.3 TCBZ-associated ES product collection: in vitro *maintenance*

Methodology for *in vitro Fasciola hepatica* maintenance and TCBZ-associated *F. hepatica* ES product collection was revised from Morphew *et al.* (2014). Briefly, initial *F. hepatica* collection, washing and culturing was conducted as described in the General materials and methods (2.2.1), including separate cultures for WT-Fh (4.3.1.1) and K-Fh (4.3.1.2) strains. Thereafter, three replicates of 10 adult (sized matched) *F. hepatica* were taken from the baseline culture media and placed into fresh culture media supplemented with either TCBZ (Sigma-Aldrich, UK), TCBZ-SO (Sigma-Aldrich, UK) or TCBZ-SO_2 (Sigma-Aldrich, UK) at 15 $\mu g \cdot mL^{-1}$ (sub-lethal dose) in DMSO (final concentration 0.1% (v/v)). For control samples, DMSO (final concentration 0.1% (v/v)) only was added to *F. hepatica* cultures. All cultures were then incubated at 37 °C for 5 hours.

The viability scores of each replicate fluke group were based on relative motility observations (Table 4.3.1.3), adapted from the scoring system developed by Doctor Neil Mackintosh (2011) and adapted from Chang and Flores (2015). All individuals were measured and scored to ensure flukes in all treatment groups and in each strain were evenly matched in physiological status, with a score of at least 4 after collection from livers (0 h) and at least 3 after pre-incubation washing (0–1 h) and before drug exposures (5–10 h). After 10 hours' *in vitro* culture, flukes were removed from culture media and immediately snap frozen in liquid nitrogen. Culture media and *F. hepatica* were stored at -80°C until required.

Table 4.3.1.3. *Fasciola hepatica* viability scoring system and their descriptors, based on the viability assay developed in IBERS by Doctor Neil Mackintosh (2011) and adapted from Chang and Flores (2015). Viability scores were defined according to relative motility observations scored between 0–5.

Viability Score	Description
5	High motility
4	Mobile, with <2 second pauses
3	Mobile, with >2 second pauses
2	Minimal motility, long pauses
1	Immobile
0	A second score of 1

4.3.1.4 Extracellular vesicle (EV) separation

EVs were isolated from the ES-enriched WT-Fh strain culture media as follows according to the recommendation and method by Davis *et al.* (2019). EVs were concentrated from clarified culture samples (2.3.2; 4.3.1.3–4.3.1.4) using 30 kDa MWCO Amicon Ultra-15 Centrifugal Filter Units (Merck Millipore, UK) as instructed by the manufacturer. Briefly, samples were applied and centrifuged at 4000 x *g* for 20 minutes at 4°C or until approximately 300-500 µl of sample was retained, containing the EVs and the >30 kDa ES proteomic fraction. Filtration flow through, containing the <30 kDa ES proteomic fraction was stored at -80°C until required. The >30 kDa sample was depleted of EVs by passing through qEVoriginal size-exclusion chromatography (SEC) columns (IZON science, UK) according to the manufacturer's protocol with minor adaptations as follows for the collection of EVs. Briefly, the column was rinsed with 10 mL of filtered (0.22 µm, Star Labs, UK) 1X PBS (Sigma-Aldrich, UK), and then the sample of ≤500 µL was added and allowed to drain, followed by 2 mL washes of PBS as recommended. The first 2.5 ml of flow through immediately after sample application was discarded, and the next 2.5 ml of flow through, containing EVs, was collected and stored at -80°C. When required for the collection of all vesicles for subsequent analyses, the entire 5 mL of sample flow through following sample application was collected. Following EV separation, the column was washed with PBS, then the next 10 mL of flow through, containing proteins, was collected to be combined with the respective <30 kDa ES sample fraction for subsequent preparation for 2-DE proteomics.

4.3.2 Transmission electron microscopy (TEM)

4.3.2.1 Preparation of WT-Fh extracellular (EV) samples

Extracellular vesicle (EV) samples purified by SEC, including first and second SEC EV fraction collections (EV_1-EV_2), from live and dead fluke cultures were further concentrated using 3 kDa MWCO Amicon Ultra-0.5 Centrifugal Filter Units (Merck Millipore, UK) as instructed by the manufacturer. Briefly, samples were applied and centrifuged at 14000 x *g* for 30 minutes at 4°C or until approximately 50 µl was retained, then PBS (0.22 µm-filtered) was added for sample collection in 150 µL then 50 µL volumes to ensure maximal EV recovery in an approximate volume of 250 µL from filter tubes using centrifugations at 1000 x *g* for 2 minutes. Samples were stored at -80°C until required.

EVs were prepared for transmission electron microscopy (TEM) visualization as previously described (Davis *et al.*, 2019) and briefly summarised as follows. Thawed EV samples were fixed onto formvar-carbon coated EM grids using 2% (w/v) paraformaldehyde (PFA) in PBS (0.22 µm-filtered), placing the grid onto 10 µL of EV-PFA solution on Parafilm® and incubating grids (Formvar-carbon coat facing down onto droplet) at room temperature (approximately 20–25°C) for 20 minutes. Grids were then washed using PBS for one minute then fixed with 1% glutaraldehyde in PBS at room temperature for five minutes before washing eight times at room temperature for two minutes each with distilled water (UV-sterilised; 15 MΩ). Grids were then probed with uranyl-oxalate 4% (w/v, 0.22 µm-filtered) to provide contrast to EV material using 50 µL/grid at room temperature for five minutes and embedded using 50 µL/grid with 2% (w/v) methyl cellulose and uranyl acetate (w/v, pH 4, 0.22 µm-filtered) in distilled water at room temperature for up to 10 minutes on ice before removing the liquid and air-drying the grids. Prepared grids were stored with the Formvar-carbon face-up in a dry place until required. EM grids were analysed with help by Mr John Tomes using a JEOL JEM1010 transmission electron microscope (JEOL Ltd, Japan) and images were taken using a Kodak Megaplus (Figure 4.3.2.1).

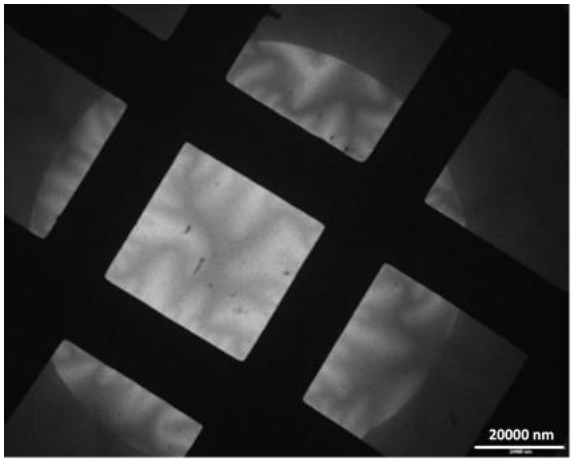

Figure 4.3.2.1. Low magnification transmission electron microscopy (TEM) of prepared Formvar-carbon-coated EM grids. Light-coloured grids with thin methyl cellulose were selected for optimal contrast of extracellular vesicles (EVs).

4.3.2.2 Preparation of whole fluke samples

Five size-matched flukes were taken directly from *in vitro* culture, representing the biological baseline, and a further five flukes of the treatment group were taken and then individually terminated prior to transmission electron microscopy (TEM) analysis using ethyl 4-aminobenzoate (1% (w/v) in ethanol) as described (4.3.1.1).

TEM images of live and dead flukes were subsequently prepared by Mr Alan Cookson at the Aberystwyth University Advanced Microscopy and Bio-imaging laboratory as follows based on the protocol described by Evans *et al.* (2012). Intact adult flukes of approximately 2 cm in length when fully extended were selected and individually fixed using 2.5% glutaraldehyde in sodium cacodylate buffer (0.1 M sodium cacodylate (Agar Scientific, UK), pH 7.2) at 4°C overnight. Samples were then washed twice in wash buffer and then placed in 1% osmium tetroxide (Agar Scientific, UK) solution dissolved in sodium cacodylate buffer for at least one hour, before washing twice in fresh sodium cacodylate buffer. Samples were drained and placed in an ultra-pure water bath and then dehydrated in an aqueous ethanol series (30%, 50%, 70%, 95% & 100%) for at least an hour in each mixture. Specimens were embedded in resin by infiltration, using mixtures of 2:1, 1:1 and 1:2 of ethanol and LR White (hard grade) resin (London Resin Company Ltd, UK) before being transferred to suitable gelatine or polyethylene moulds and polymerised at 60°C overnight. 1–2µm thick sections were taken to assess the correct orientation of the samples and subsequently dried onto plain glass slides and viewed after staining with Azur II and Methylene Blue (both Sigma-Aldrich, UK) for 2 minutes. A suitable area was chosen for TEM examination, specifically lateral tegument sections on the periphery of prepared specimens (Figure 4.3.2.2*). Ultra-thin 60-80 nm sections were cut on a Reichert-Jung Ultracut E Ultramicrotome with a Diatome Ultra 45° diamond knife and collected on Gilder GS2X0.5 3.05 mm diameter nickel slot grids (Gilder Grids, UK) float-coated with Butvar B98 polymer (Agar Scientific, UK) films. All TEM sections were double stained with uranyl acetate (Agar Scientific, UK) and Reynold's lead citrate (TAAB Laboratories Equipment Ltd, UK) and observed using a JEOL JEM1010 transmission electron microscope (JEOL Ltd, Japan) at 80 kV. The resulting images were photographed using Carestream 4489 electron microscope film (Agar Scientific, UK) developed in Kodak D-19 developer for 4 min at 20 °C, fixed, washed and dried according to the manufacturer's instructions. The resulting negatives were scanned with an Epson Perfection V800 film scanner and converted to positive images.

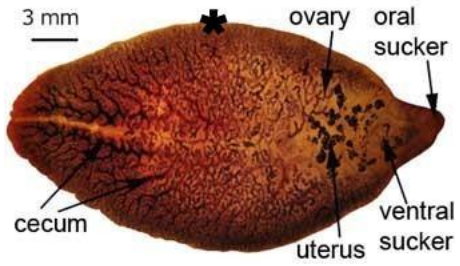

Figure 4.3.2.2. Light micrograph of whole adult *Fasciola hepatica*. Tissues selected for transmission electron microscopy (TEM) analyses are indicated (*). Image by Mr Alan Cookson.

4.3.3 Sample preparation and 2-DE proteomics

Excretory/secretory (ES) products depleted of extracellular vesicles (EVs) were recombined by mixing the <30 kDa MWCO Amicon flow through samples with the >30 kDa qEVoriginal-filtered protein fractions. Pooled samples were precipitated and resuspended in buffer A and quantified in readiness for 2-DE (General materials and methods: 2.3.3–2.3.4).

2-DE was conducted as previously described in the General materials and methods (2.4.1.2) with adjustments for the 17 cm IPG strips and 20 cm^2 SDS PAGE gels as follows. 17 cm linear pH 3-10 IPG strips (Bio-Rad, UK) were passively rehydrated overnight at ambient temperature with EV-depleted ES resuspended in 300 µL of buffer A, whereby the entire protein products available (40≤100 µg) from each treatment group (WT-Fh, K-Fh; DMSO control, TCBZ, TCBZ-SO, TCBZ-SO_2) were used *per* gel conducted in duplicate. All IPG strips were isoelectrically focussed overnight for 60,000–70,000 V-h using the Protean IEF Cell (Bio-Rad, UK) to separate protein samples in the first dimension. IPG strips were then equilibrated in buffer B with DTT [10 $\mu g \cdot mL^{-1}$] for 15 minutes then buffer B with IAA [25 $\mu g \cdot mL^{-1}$] for a further 15 minutes. Proteins were separated in the second dimension on the Protean II system (Bio-Rad, UK) using 12.5% polyacrylamide gels (General materials and methods: 2.4.1). Electrophoresis conditions were fixed at 20 mA and 30 mA per gel through the stacking and resolving gels, respectively. Gels were fixed, stained, destained and imaged using a GS-800 calibrated densitometer (Bio-Rad, UK) (General materials and methods: 2.4.1).

4.3.4 *In silico* protein spot mapping

Images of 2-DE gels were analysed using Progenesis PG220 v.2006, including duplicate gels of three biological replicates per treatment (TCBZ, TCBZ-SO, TCBZ-SO_2) for wild type mixed (WT-Fh) and TCBZ-R Kilmarnock (K-Fh) liver fluke isolates. Analysis was performed using manual spot selection, non-spot background subtraction and manual matching between gels of each group. Normalised spot volumes were calculated using the Progenesis 'total spot volume multiplied by total area' method and were used to analyse the relative protein abundance change between comparisons of up and/or down regulation of spots, similarly to previous studies (Chemale *et al.*, 2010; Morphew *et al.*, 2014), with significance set to ±1-fold change.

4.3.5 Statistical analyses

Viability score data were analysed using generalised linear mixed modelling (GLMM) to assess the effect of treatments, strains and time points on viability score outcomes, using R studio V1.1.463 (R Studio Inc.). The analysis included data from the latter two time points (3–4), after treatment had been administered. Viability score data across all time points were also analysed using non-parametric tests in SPSS® v.24 (IBM®).

Statistical evaluations of protein abundance were conducted using SPSS® v.24. Firstly, an independent samples T test was used to test for evidence of a difference between WT-Fh and K-Fh, based on the logarithmically-transformed protein concentration. Subsequently to test for evidence of a difference within fluke groups, the Kruskal Wallace test was used, analysing protein concentration by treatment in each group, WT-Fh and K-Fh. Lastly, to identify differences in protein spot abundances between WT-Fh and K-Fh, normalised protein spot volume data computed by Progenesis (4.3.4) were used to test the effect of strain on protein abundance, which was determined using an analysis of variance (ANOVA, significance threshold set to 0.05).

4.4 Results

4.4.1 Transmission electron microscopy (TEM) investigation of extracellular vesicle (EV) abundance between live and dead wild type *Fasciola hepatica* excretory/secretory (ES) products

Changes to the extracellular vesicle (EV) population of adult wild type *Fasciola hepatica* were investigated using transmission electron microscopy (TEM). Excretory/secretory (ES) products of 10 *in vitro* cultured flukes (live) and 10 flukes exposed to ethyl 4-aminobenzoate (dead) were separated using qEV original SEC columns in order to remove proteinaceous ES products whilst isolating and concentrating EVs. Two SEC fractions ($EV_{1\text{-}2}$: first and second 2.5 mL SEC fraction) from each fluke treatment group were collected separately to compare the abundance of predominantly larger (EV_1, Ø>500 nm: apoptotic bodies) or smaller (EV_2, Ø<500 nm: exosomes and microvesicles) EVs fractionated in each sample. Both groups demonstrated the presence of vesicular bodies, though the live $EV_{1–2}$ samples had a higher abundance of microvesicles compared to dead $EV_{1\text{-}2}$ samples (Figure 4.4.1A–D). Both live and dead EV_1 fractions demonstrated the presence of large vesicles with apoptotic body-like characteristics, of approximately ~1000 nm Ø and containing varied contents including some discernible internal exosome-like vesicles (Figure 4.4.1Ai, Ci) and possible organelle derivatives (Figure 4.4.1Cii). The presence of small-size vesicles in EV_1 samples was also consistent between samples (Figure 4.4.1A, C), indicating that small vesicles were incompletely separated by the qEV original SEC columns, or were otherwise associated by previous or sustained contact with/internalisation by larger vesicles that allowed them to pass into the first fraction. There was a very high abundance of small-sized vesicles ranging below 500 nm in the live EV_2 sample (Figure 4.4.1B), including from possibly different origins due to their variably stained appearance, indicating changes to EV surface or contents. Conversely, the dead EV_2 sample contained fewer EV-like vesicles overall (Figure 4.4.1D), which were also predominantly of similar appearance in the context of internal and external staining, with multiple which were highly characteristic of exosomes (dark, <100 nm), and others similar in appearance to larger-sized microvesicles (light and dark, 50<500* nm, dictated by SEC fractionation). For further images of EVs observed within these samples, see Supplementary materials: Figures S3–S4.

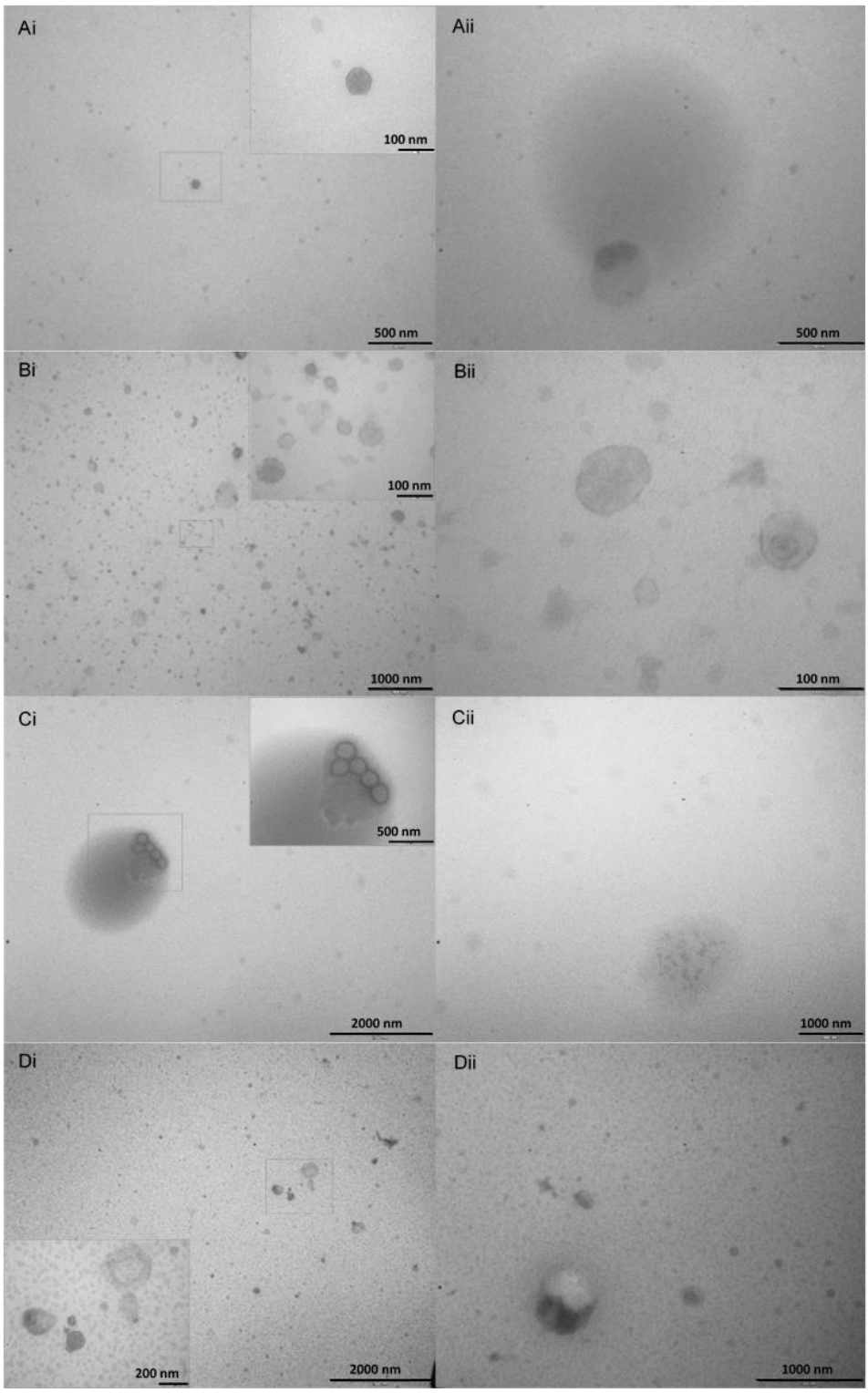

Figure 4.4.1. Transmission electron microscopy (TEM) visualisation of *in vitro*-cultured live and dead adult wild type *Fasciola hepatica* excretory/secretory (ES) product-derived extracellular vesicles (EVs) isolated using size-exclusion chromatography. EVs derived from 10 adult *F. hepatica* from natural infections were analysed by TEM following *in vitro* culture (A-B) or following exposure to ethyl 4-aminobenzoate (C-D). EVs were purified via qEVoriginal SEC columns, including the collection of large-sized vesicles (first fraction, EV_1: i) and small-sized vesicles (second fraction, EV_2: ii) as described (4.3.1.4–4.3.2.1). NB: (Di–ii) background staining artefact leading to speckled appearance, not to be mistaken for EVs/exosomes.

4.4.2 Transmission electron microscopy (TEM) visualisation of the live and dead wild type *Fasciola hepatica* tegument

Changes to the tegumental syncytium of adult *Fasciola hepatica* were investigated using TEM. Five flukes each from *in vitro* culture (live) and five flukes exposed to ethyl 4-aminobenzoate and washed in PBS (dead) were selected and prepared for TEM imaging (Figure 4.4.2). Ultrastructural differences at the tegument of flukes in the live fluke group demonstrated evidence of a highly-organised network of syncytial tissues, including processes of vacuolation for EV export and direct EV membrane budding, leading to the production and completed release of microvesicles (<500 nm) and exosomes (<100 nm) into the external media (Figure 4.4.2A–C).

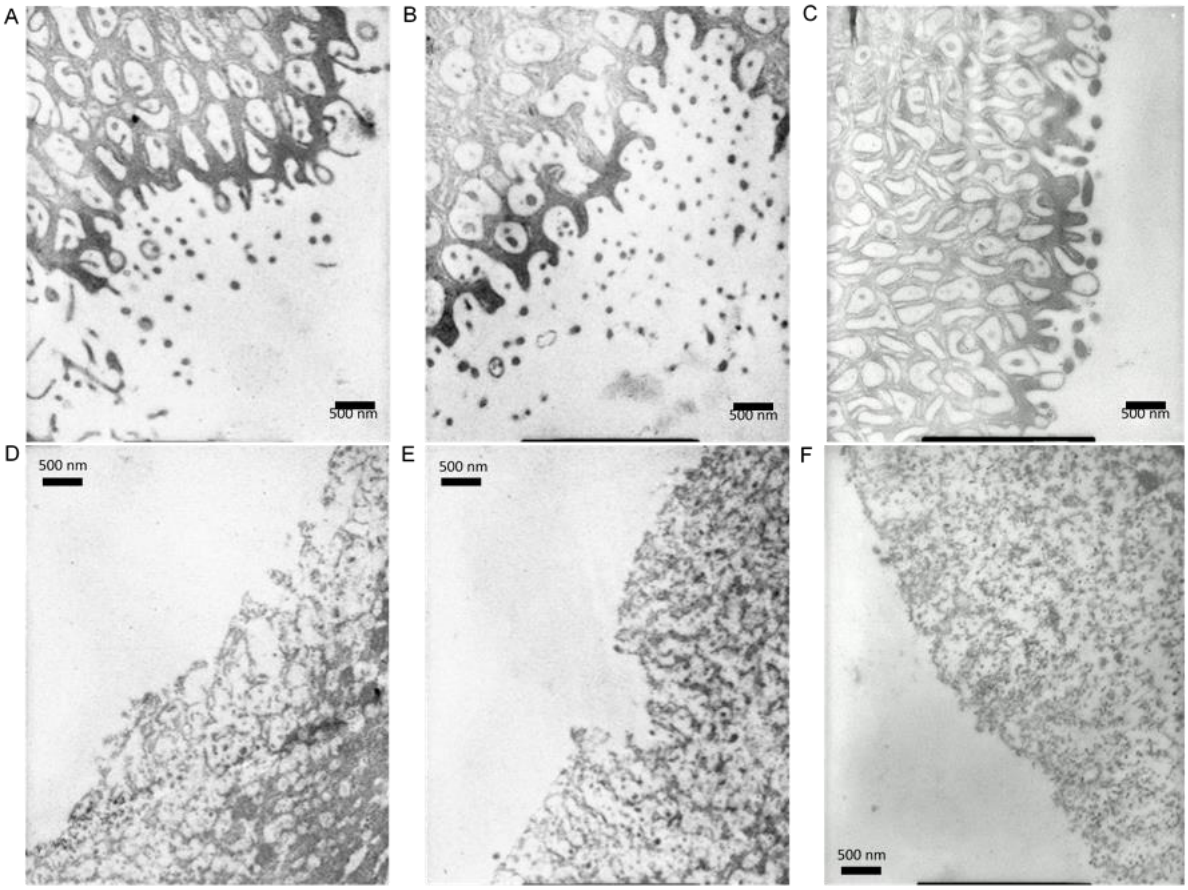

Figure 4.4.2. Representative transmission electron microscopy (TEM) visualisation of the *Fasciola hepatica* tegument after *in vitro* culture (A–C) and after exposure to ethyl 4-aminobenzoate (D–F). Ten size-matched adult *F. hepatica* were analysed by TEM following *in vitro* culture: five flukes were directly selected (live) (A–C) and five were selected following exposure to ethyl 4-aminobenzoate (dead) (D–F). Tegument disruption, including loss of syncytial network structure, and the loss of tegumental extracellular vesicle (EV) production were observable in the dead group.

Conversely to findings in live flukes, the dead fluke group indicated disruption of untreated characteristics, with partial or complete dissociation of the strict syncytial networks and a major reduction or ceased capacity for EV secretion, leading to possible passive release of small membrane and fractions and pre-formed exosome-like vesicles (Figure 4.4.2D–F). Thus, based on differential ultrastructural tegument (Figure 4.4.2) and purified EV (Figure 4.4.1) characteristics between live and dead fluke groups, the tegumental infrastructure and EV population are potential indicators of *F. hepatica* viability, since the treatment led to extensive changes to the tegumental capacity for EV release (Figure 4.4.2; for further images see Supplementary materials: Figures S5–S6) and consequential reduction in EV abundance from ES products.

4.4.3 *In vitro* viability assay of triclabendazole/-sulphoxide/-sulphone (TCBZ/-SO/-SO_2)-treated wild type (WT-Fh) and Kilmarnock (TCBZ-R, K-Fh) *Fasciola hepatica*

All WT-Fh and K-Fh flukes were assessed for biological viability and physiological integrity at the end of each time point using the viability scoring system (Table 4.3.1.3). Fluke scores were all 5.0 at the start of the experiment and not influenced by PBS (0–1 h) but declined following DMEM acclimatisation culturing (1–5 h) before drug treatment, reducing the average viability from 5.0 to 3.0 for wild type and 3.5 for Kilmarnock strains (Figure 4.4.3). After the drug treatments (5–10 h) Kilmarnock flukes (K-Fh) scored an average of 4.0 (TCBZ-SO) or 4.5 (DMSO; TCBZ; TCBZ-SO_2), whereas abattoir (WT-Fh) flukes scored an average of 2.0 for all treatments.

Generalised linear mixed modelling (GLMM) was conducted to investigate the effect of treatment, strain and time point (3 and 4) (fixed effects) on viability score. There was no evidence for a difference in viability scores between all treatment groups and the control (all $P>0.1$). However, there was evidence of a difference in fluke viability scores between strains ($P < 0.00001$) and time points ($P < 0.00001$, Figure 4.4.3**). The Mann Whitney U test was used to assess the difference in viability score between all time points within strains, conducted pairwise, finding there to be significant differences between every time point, excluding the first two ($P < 0.001$, Figure 4.4.3*).

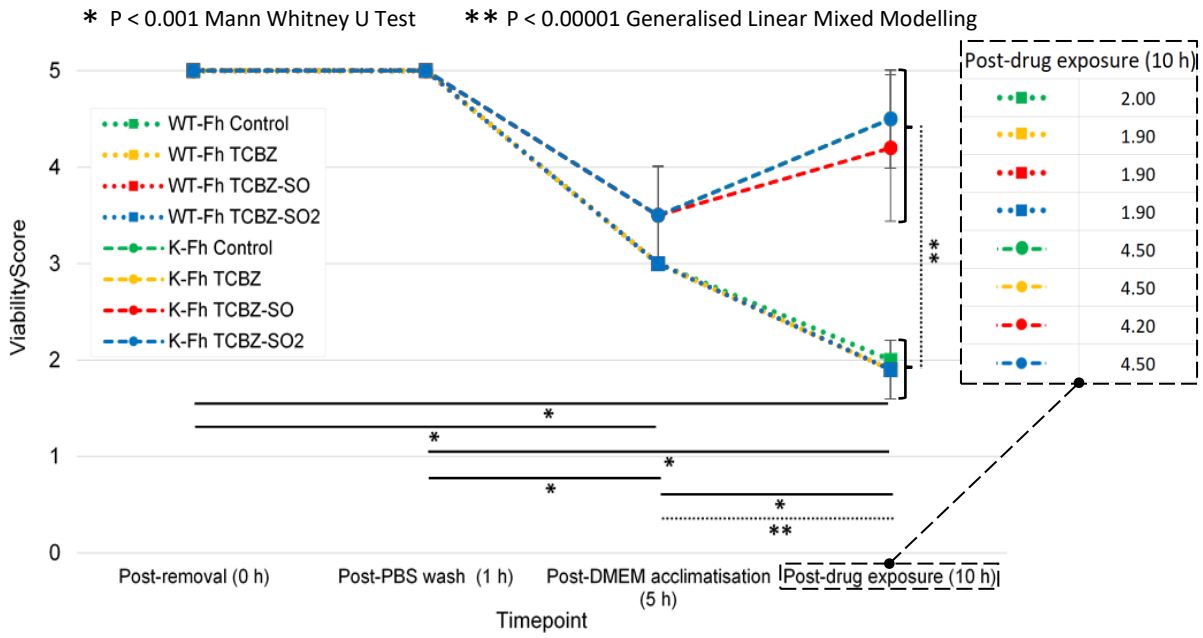

Figure 4.4.3. Graphic representation for the average viability scores of wild type (WT-Fh) and Kilmarnock (K-Fh) *Fasciola hepatica* taken at all experimental timepoints. Viability scores (0–5) were taken for triplicates of ten flukes in each treatment (DMSO; TCBZ; TCBZ-SO; TCBZ-SO_2) and strain (wild type, WT-Fh; Kilmarnock, K-Fh). Error bars represent standard deviation across the three replicates of ten flukes per treatment. Asterisks indicate evidence for a difference in the viability score outcome calculated by generalised linear mixed modelling (GLMM) to be associated with strain between post-DMEM acclimatisation and post-drug exposure (**P < 0.00001, GLMM: ⋯); and calculated by a Mann Whitney U (MWU) test to be associated with the time points indicated (*P < 0.001, MWU: —).

4.4.4 *In vitro* proteomics

Whole excretory/secretory (ES) products pooled from triplicate treatment groups *per* strain (WT-Fh and K-Fh) were prepared for *in vitro* proteomics as described, using SEC to remove EVs and TCA purification to concentrate non-EV-associated proteins. Resuspended ES samples were analysed by the Bradford assay to calculate concentrations (µg/µL) and whole protein content (µg protein/replicate sample) (Figure 4.4.4.1).

Independent samples parametric and non-parametric tests were conducted to investigate the effect of strains and treatments on protein concentrations following the addition of equal buffer A to each identically prepared sample. There was no evidence for a difference in protein concentration between strains based on an independent samples T Test using logarithmically transformed concentration values (all P>0.1). Protein concentrations

within each strain and between all treatments was subsequently investigated using the non-parametric Kruskal-Wallis test, finding no difference in protein concentration between treatments in the wild type (WT-Fh) strain. However there was evidence of a difference in protein concentration between treatment groups, including the untreated control group, in the Kilmarnock (K-Fh) strain (P = 0.012, Figure 4.4.4.1*).

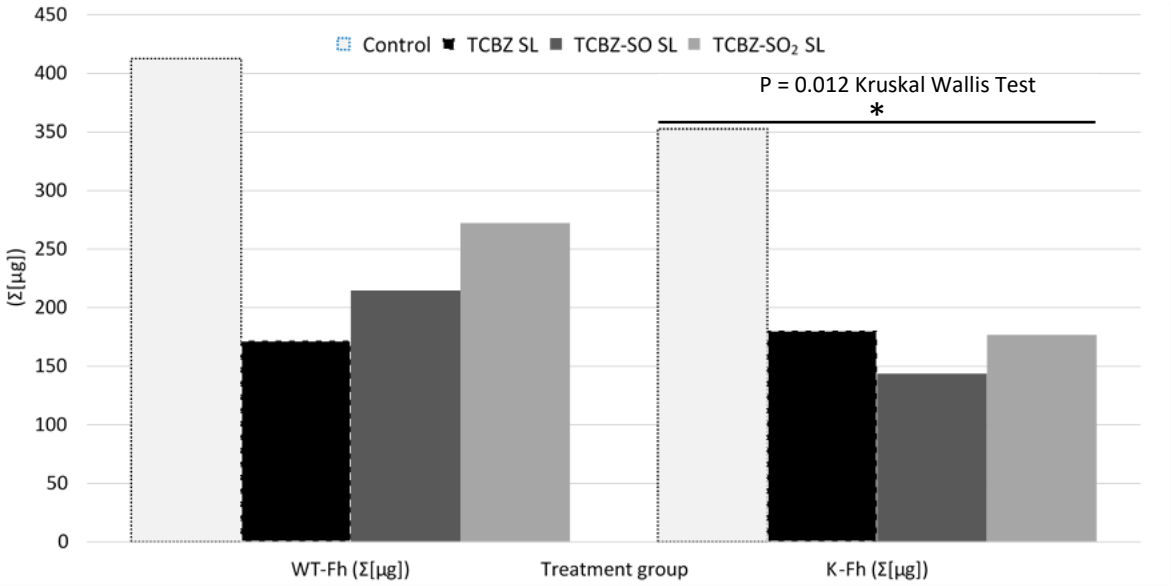

Figure 4.4.4.1. Comparison of non-EV protein ES production between anthelmintic-treated and untreated control wild type (WT-Fh) and Kilmarnock (K-Fh) *Fasciola hepatica*. Triplicate EV-depleted ES products were pooled from three replicate samples in each treatment group (untreated control; TCBZ; TCBZ-SO; TCBZ-SO_2) and analysed using the Bradford assay to determine whole protein content. Asterisks indicate evidence for a significant difference in protein concentration (n=3 readings) between the K-Fh treatment groups, including the untreated control group, calculated using the Kruskal-Wallis test (* P = 0.012).

All available protein material pooled from triplicate EV-depleted ES samples for each treatment (40–100 µg) was analysed by duplicate 2-DE and protein spots were mapped using Progenesis PG220 v.2006 (Figure 4.4.4.2; for all individual gel images, see Supplementary materials: Figures S7–S8). All protein spots in all gels were identified by manual spot selection and normalised spot volumes were calculated for all spots that were matched between all gels of each strain including all treatments (WT-Fh: Figure 4.4.4.2A; K-Fh: Figure 4.4.4.2B). The resultant gels are hereon referred to as reference gels.

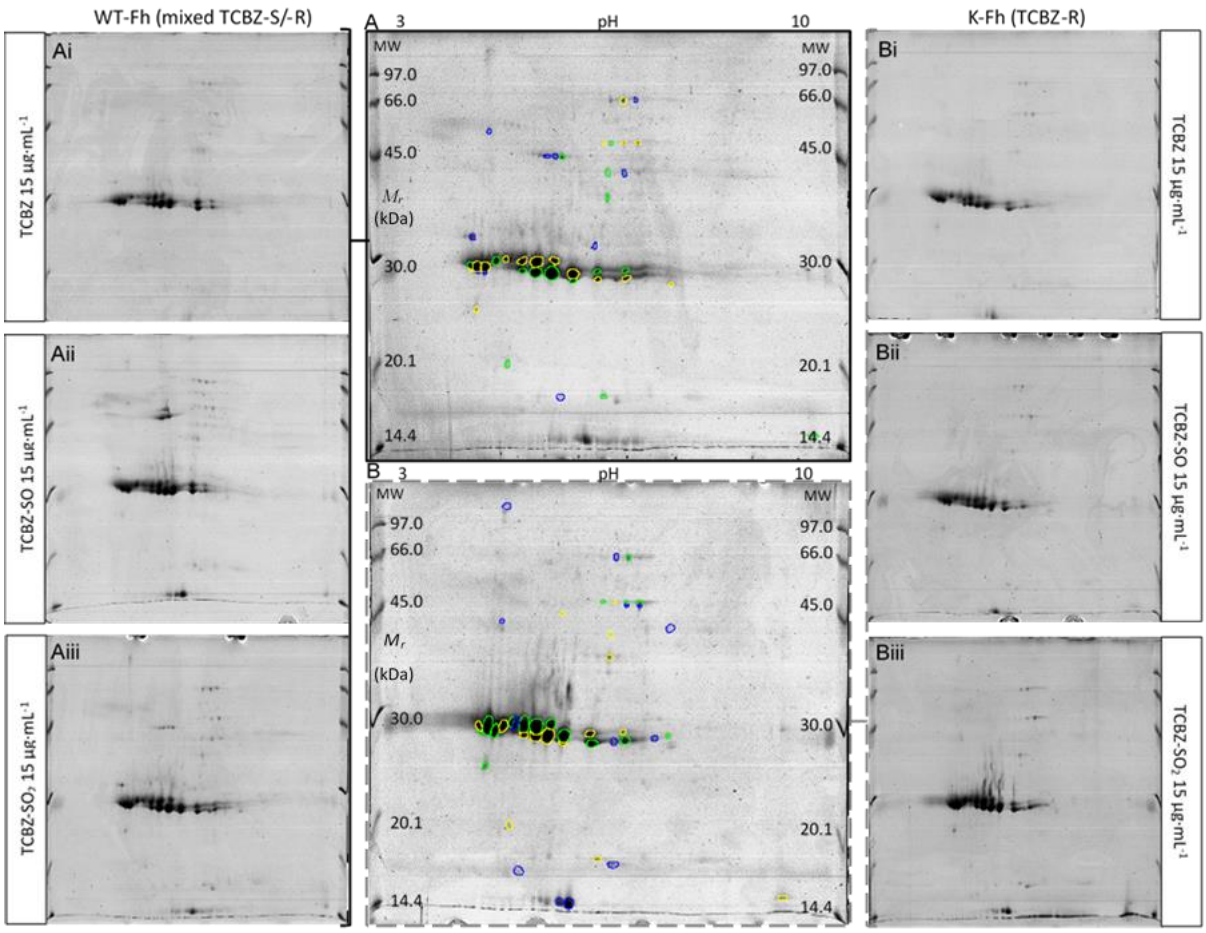

Figure 4.4.4.2. Representative 2-DE analysis of EV-depleted ES products from TCBZ, TCBZ-SO and TCBZ-SO$_2$ anthelmintic-challenged WT-Fh (undetermined TCBZ susceptibility) and K-Fh (TCBZ-R) *Fasciola hepatica*. Total EV-depleted ES protein material was pooled from triplicate *in vitro* cultures supplemented with sub-lethal [15 µg·mL^{-1}] TCBZ, TCBZ-SO or TCBZ-SO$_2$ for duplicate 2-DE analysis (40–85 µg/gel: 17 cm linear IEF 3–10; SDS PAGE). Representative reference gels are shown for WT-Fh (A) and K-Fh (B), whereby 41 and 44 spots present and matched following collation between duplicates (one gel per treatment group shown, i–iii) and across all treatments (excluding DMSO control), respectively.

Abbreviations: MW, Amersham Low Molecular Weight SDS Calibration Kit (M_r).

Using Progenesis, an ANOVA was conducted to compare the effect of strain on protein abundance, specifically testing for differences between normalised spot volumes present and matched between strain-specific reference gels (produced by collating spots present in all treatment-specific gels per strain). There was evidence of a difference in the abundance of 31 protein spots (±1.3≤-fold change) between WT-Fh and K-Fh strains, for which seven were considered significant ($P < 0.05$) (Figure 4.4.4.3A; Table 4.4.4). 23 protein spots were additionally unmatched between strain-specific reference gels, including 10 in WT-Fh (Figure 4.4.4.3B) and 13 in K-Fh (Figure 4.4.4.3C), suggesting these are produced in greater

abundance and/or irrespective of TCBZ/-SO/-SO_2-specificity in the respective strains following anthelmintic exposure.

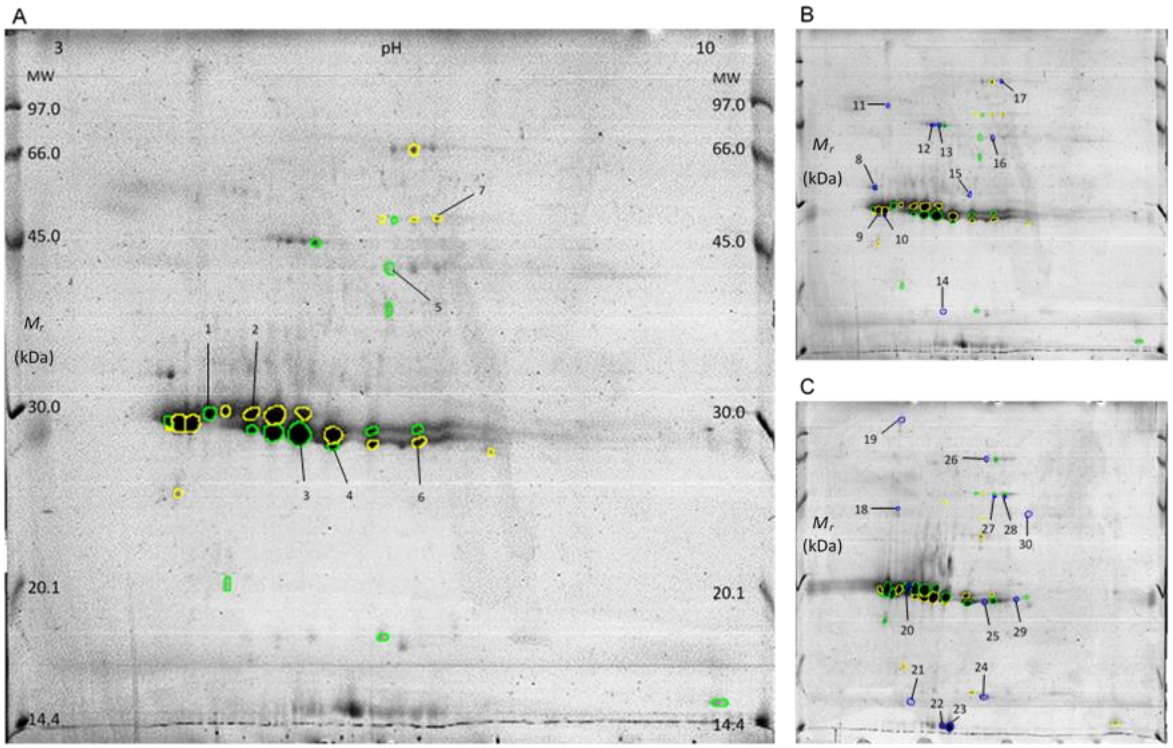

Figure 4.4.4.3. Analysis of proteomic profiles and protein abundances between TCBZ, TCBZ-SO and TCBZ-SO_2-challenged WT-Fh (undetermined TCBZ susceptibility) and K-Fh (TCBZ-R) *Fasciola hepatica* strains. (A) Significant differences in the abundance of seven proteins ($P < 0.05$; ±1-fold, range: 1.35–2.46-fold) were calculated between WT-Fh and K-Fh strains based on normalised spot volumes of strain-specific reference gels, which were collated from gel spots present and matched between all treatment-specific gels per strain (sub-lethal [15 µg·mL^{-1}] TCBZ, TCBZ-SO, TCBZ-SO_2). Green- and yellow-coloured spots respectively indicate ≥1-fold higher or lower abundance of specific proteins in WT-Fh compared to K-Fh. A further 23 protein spots were also unmatched between strain-specific reference gels, with (B) 10 identified from all WT-Fh gels and (C) 13 identified from all K-Fh gels.

Abbreviations: MW, Amersham Low Molecular Weight SDS Calibration Kit (M_r).

Duplicate 2-DE-separated proteins spots of interest were analysed by LC-MS/MS (ESI-TRAP), including from gels of TCBZ-, TCBZ-SO- or TCBZ-SO_2-exposed flukes from the WT-Fh- or K-Fh-specific strains where relevant, with selection dictated by protein abundance to facilitate LC-MS/MS detection as follows. Replicate spots numbered 1–7 were acquired from a gel of each strain (replicate 1: WT-Fh; replicate 2: K-Fh), spots 8–17 were acquired from WT-Fh gels, and spots 18–30 were acquired from K-Fh gels, as summarised in Table 4.4.4 (left

column: A, WT-Fh TCBZ; B, K-Fh, TCBZ; C, WT-Fh TCBZ-SO; D, K-Fh TCBZ-SO; E, WT-Fh TCBZ-SO_2; F, K-Fh TCBZ-SO_2). LC-MS/MS-identified protein hits were calculated between both replicates and selected when exceeding the MASCOT significance threshold score (≥66, $P < 0.05$) (Table 4.4.4).

10 spots were unidentified by LC-MS/MS using the data inclusion criteria (Table 4.4.4: 5, 9, 11, 12, 17, 18, 24, 26, 30), caused either by low protein abundance, low peptide recovery, or sequences being unmatched against those present in the GenBank (v204) database. However, data from individual replicate submissions notwithstanding the threshold score permitted hypothetical dissection for putative identification. Though the overall score was sub-threshold, spot nine was consistently identified as for spot eight (cathepsin L/L1), suggesting modifications and/or isoform separation (Figure 4.4.4.3B). Neither spot 11 nor 12 had consistent replicate identification, though each had above-threshold hits including serpin, and gelsolin and actin, respectively. Similarly, spots 17 and 18 were identified in one replicate as a thioredoxin-glutathione reductase and serpin, respectively, and spot 24 was consistently identified as a superoxide dismutase across both LC-MS/MS replicates, though below the threshold score. Interestingly, spot 5 replicates identified different proteins, including enolase (replicate 1: WT-Fh TCBZ-SO_2) or cathepsin L (replicate 2: K-Fh TCBZ-SO_2), presenting possibly uneven 2-DE separation, prominence of an enolase isoform in WT-Fh or CL zymogens in K-Fh. However, based on the physical evidence from 2-DE, the putative CL zymogen identity of spot 5 fits closer to the expectant molecular weight for this protein.

LC-MS/MS data indicated highly similar protein profiles between the two strains across all treatments, including enolase (spots 7, 16, 27, 28), gelsolin (spots 14, 21) and CLs (spots 1, 2, 3, 4, 6, 8, 10, 20) with specific identifications of clades CL1 (spots 2, 3, 4, 6, 8, 25, 29) and CL2 (spots 1, 10, 20). Predicted molecular weights and isoelectric points for protein hits matched to those calculated by Progenesis, supporting these identities, though referral to 2-DE molecular weight separation suggested dubiety of 14, 16 and 21 spots being intact protein forms of the matched hits (Figure 4.4.4.3B–C). Strain distinctions were also present, including actin (spot 13) and a cathepsin B (CB)-like protein (spot 15) in WT-Fh, and FABP type 15 (spot 22) and 2 (spot 23) in K-Fh (Figure 4.4.4.3; Table 4.4.4), suggesting these proteins are most consistently abundant within each strain following TCBZ, TCBZ-SO and TCBZ-SO_2 exposure.

Table 4.4.4. Proteomic characterisation and liquid chromatography tandem mass spectrometric identification of protein hits of interest from 2-DE-separated ES protein (non-EV) products of drug-treated wild type (WT-Fh) and Kilmarnock (K-Fh) *Fasciola hepatica* and untreated controls. Protein spots of interest and their biochemical properties including molecular weight and isoelectric point were identified using Progenesis, including significant changes in abundance determined by ANOVA (Figure 4.4.4.2). In-gel isolated proteins were identified by LC-MS/MS by ESI-TRAP analysis of duplicate trypsin-digested protein spots against the GenBank database (v204) using an in-house MASCOT (Matrix Science) server, reporting significant hits identified with an average score of 66 or greater ($P < 0.05$). Replicate and gel IDs refer to the replicate number (n=2) and the origin of each protein spot: A, WT-Fh TCBZ; B, K-Fh TCBZ; C, WT-Fh TCBZ-SO; D, K-Fh TCBZ-SO; E, WT-Fh TCBZ-SO_2; F, K-Fh TCBZ-SO_2.

Proteomics (Progenesis)				**LC-MS/MS Ions search**							
Spot number (Replicate and gel ID)	**All rows: Phenotype Rows 1–8: X-fold change Significance**	**Molecular weight (kDa)**	**Isoelectric point (pI)**	**GenBank hit**	**MASCOT score (Av)**	**Peptides matched (non-duplicated)**	**Sequence coverage (%)**	**Protein**	**Organism**	**Accession**	**E-value**
1	**WT-Fh < K-Fh**	25.018	5.062	gi|157862755	546.0±472.0	6.0±1.0	41.0±12.0	Secreted cathepsin L2	*F. gigantica*	ABV90500.1	0.0
(1E, 2B)	**2.33-fold**			gi|452260	463.5±201.5	8.5±0.5	57.0±2.0	Cathepsin L-like proteinase	*F. hepatica*	CAA80447.1	4E-123
	P = 0.040			gi|20136379	177.0±109.0	8.0±2.0	40.0±13.0	Cathepsin L, partial	*F. hepatica*	AAM11647.1	0.0
				gi|452254	76.5±20.5	4.0±0.0	24.0±0.0	Cathepsin L-like proteinase	*F. hepatica*	CAA80444.1	4E-123
2	**WT-Fh > K-Fh**	24.845	5.273	gi|41152540	1012.0±208.0	38.5±2.5	73.5±0.5	Cathepsin L protein	*F. hepatica*	AAR99519.1	9E-180
(1E, 2F)	**2.04-fold**			gi|41152538	982.5±300.5	44.0±3.0	64.5±0.5	Cathepsin L protein	*F. hepatica*	AAR99518.1	0.0
	P = 0.042			gi|20136379	895.0±219.0	31.5±0.5	58.0±0.0	Cathepsin L, partial	*F. hepatica*	AAM11647.1	0.0
				gi|116488416	460.5±66.5	40.5±1.5	57.0±0.0	Secreted cathepsin L 1	*F. hepatica*	AAB41670.2	0.0
				gi|310751866	315.0±49.0	27.5±0.5	44.0±0.0	Cathepsin L-like proteinase	*F. hepatica*	ADP09371.1	0.0
				gi|452254	222.5±127.5	9.0±3.0	51.5±13.5	Cathepsin L-like protease	*F. hepatica*	CAA80444.1	4E-123
				gi|10798511	272.5±61.5	37.0±4.0	66.5±0.5	Cathepsin L1	*F. hepatica*	CAC12806.1	0.0
				gi|211909240	187.5±11.5	29.0±3.0	54.5±5.5	Cathepsin L1D	*F. hepatica*	ACJ12893.1	0.0
				gi|211909242	187.5±11.5	29.0±3.0	54.5±5.5	Cathepsin L1D	*F. hepatica*	ACJ12894.1	0.0
				gi|157862755	91.5±16.5	10.5±1.5	24.5±7.5	Cathepsin L, partial	*F. gigantica*	ABV90500.1	0.0
3	**WT-Fh < K-Fh**	23.954	5.739	gi|41152540	2269.0±4.0	44.0±3.0	81.0±7.0	Cathepsin L protein	*F. hepatica*	AAR99519.1	9E-180
(1E, 2F)	**1.42-fold**			gi|116488416	1496.5±41.5	42.5±2.5	57.0±0.0	Secreted cathepsin L 1	*F. hepatica*	AAB41670.2	0.0

	P = 0.002			gi|41152538	1284.5±12.5	41.5±2.5	64.5±0.5	Cathepsin L protein	*F. hepatica*	AAR99518.1	0.0
				gi|211909240	1152.5±15.5	44.0±1.0	63.5±0.5	Cathepsin L1D	*F. hepatica*	ACJ12893.1	0.0
				gi|211909242	1152.5±15.5	44.0±1.0	63.5±0.5	Cathepsin L1D	*F. hepatica*	ACJ12894.1	0.0
				gi|157862759	1079.5±3.5	32.5±0.5	48.5±1.5	Cathepsin L, partial	*F. gigantica*	ABV90502.1	0.0
				gi|10798511	690.0±47.0	42.0±1.0	62.5±0.5	Cathepsin L-like protease	*F. hepatica*	CAC12806.1	0.0
				gi|19909509	224.5±18.5	20.0±1.0	28.0±0.0	Cathepsin L-like protease	*F. gigantica*	BAB86959.1	0.0
				gi|108735858	78.0±3.0	11.0±0.0	39.0±0.0	Cathepsin L-like protease	*F. hepatica*	ABG00260.1	5E-167
4	**WT-Fh < K-Fh**	25.548	5.998	gi|211909240	925.5±469.5	38.5±4.5	60.0±1.0	Cathepsin L1D	*F. hepatica*	ACJ12893.1	0.0
(1A, 2F)	**1.35-fold**			gi|211909242	925.5±469.5	38.5±4.5	60.0±1.0	Cathepsin L1D	*F. hepatica*	ACJ12894.1	0.0
	P = 0.018			gi|41152540	553.0±17.0	35.5±2.5	69.0±0.0	Cathepsin L protein	*F. hepatica*	AAR99519.1	9E-180
				gi|116488416	351.0±20.0	31.0±4.0	51.0±6.0	Secreted cathepsin L 1	*F. hepatica*	AAB41670.2	0.0
				gi|10798511	247.0±40.0	31.5±1.5	60.0±0.0	Cathepsin L1	*F. hepatica*	CAC12806.1	0.0
5	**WT-Fh < K-Fh**	40.698	6.571	-	-	-	-	-	-	-	-
(1E, 2F)	**2.46-fold**										
	P = 0.015										
6	**WT-Fh > K-Fh**	23.820	6.816	gi|211909240	727.0±207.0	38.0±1.0	61.0±0.0	Cathepsin L1D	*F. hepatica*	ACJ12893.1	0.0
(1E, 2F)	**1.42-fold**			gi|211909242	727.0±207.0	38.0±1.0	61.0±0.0	Cathepsin L1D	*F. hepatica*	ACJ12894.1	0.0
	P = 0.026			gi|41152540	191.0±13.0	31.5±2.5	69.0±0.0	Cathepsin L protein	*F. hepatica*	AAR99519.1	9E-180
				gi|310751866	184.0±13.0	20.0±0.0	37.0±4.0	Cathepsin L-like proteinase	*F. hepatica*	ADP09371.1	0.0
				gi|166235906	88.0±1.0	8.0±1.0	28.0±0.0	Thioredoxin peroxidase	*F. gigantica*	ABY85785.1	2E-163
				gi|255683591	88.0±1.0	8.0±1.0	28.0±0.0	Thioredoxin peroxidase 1	*F. gigantica*	ACU27401.1	2E-163
				gi|259090533	88.0±1.0	8.0±1.0	29.5±1.5	Peroxiredoxin	*F. gigantica*	ACV91889.1	1E-141
7	**WT-Fh > K-Fh**	50.848	6.975	gi|190350155	411±283	37.0±23.0	52.5±22.5	Enolase	*F. hepatica*	CAK47550.1	0.0
(1C, 2F)	**1.73-fold**										
	P = 0.002										
8	**WT-Fh**	27.519	4.516	gi|10798511	109.0±32.0	10.5±0.5	12.0±4.0	Cathepsin L1	*F. hepatica*	CAC12806.1	0.0
(1E, 2E)				gi|148284737	93.0±22.0	3.0±1.0	31.5±1.5	Cathepsin L	*F. hepatica*	ABN50361.2	0.0
9	**WT-Fh**	24.015	4.605	-	-	-	-	-	-	-	-
(1A, 2A)											
10	**WT-Fh**	23.956	4.723	gi|452258	271.0±143.0	19.5±1.5	42.0±0.0	Cathepsin L-like protease	*F. hepatica*	CAA80446.1	0.0

(1A, 2A)				gi|148575301 gi|148283737	271.0±143.0 107.5±31.5	19.5±1.5 9.0±1.0	42.0±0.0 30.0±0.0	Secreted cathepsin L2 Cathepsin L	*F. hepatica* *F. hepatica*	ABQ95351.1 ABN50361.2	0.0 0.0
11 (1C, 2C)	**WT-Fh**	55.229	4.767	-	-	-	-	-	-	-	-
12 (1E, 2E)	**WT-Fh**	45.567	5.663	-	-	-	-	-	-	-	-
13 (1E, 2E)	**WT-Fh**	45.611	5.779	gi|226467798 gi|461465	94.0±16.0 89.5±11.5	16.0±1.0 10.5±4.5	32.5±1.5 15.0±1.0	Actin 5C RecName: Full-Actin	*S. japonicum* *Nicotiana tabacum*	CAX69775.1 Q05214.1	0.0 0.0
14 (1E, 2E)	**WT-Fh**	18.951	5.868	gi|353231888	83.5±4.5	1.0±0.0	3.0±0.0	Putative gelsolin, partial	*S. mansoni*	XP_018651848.1	0.0
15 (1E, 2E)	**WT-Fh**	26.887	6.384	gi|452268	102.5±12.5	3.0±0.0	33.0±0.0	Cathepsin B-like protease	*F. hepatica*	CAA80451.1	3E-66
16 (1E, 2E)	**WT-Fh**	40.657	6.791	gi|190350155	363.5±28.5	39.0±2.0	58.0±9.0	Enolase	*F. hepatica*	CAK47550.1	0.0
17 (1E, 2E)	**WT-Fh**	73.815	6.952	-	-	-	-	-	-	-	-
18 (1B, 2F)	**K-Fh**	41.214	4.943	-	-	-	-	-	-	-	-
19 (1B, 2F)	**K-Fh**	113.844	4.932	-	-	-	-	-	-	-	-
20 (1B, 2F)	**K-Fh**	24.695	5.193	gi|41152538 gi|8547325 gi|20136379 gi|148283737 gi|452254 gi|108735840 gi|157862755	343.5±70.5 357.5±22.5 294.5±63.5 176.0±87.0 154±46.0 124.0±10.0 91.0±18.0	31.5±4.5 30.5±3.5 21.5±5.5 39.0±28.0 10.0±2.0 14.0±2.0 12.5±0.5	64.5±0.5 47.0±6.0 58.0±0.0 36.0±2.0 58.0±7.0 35.0±4.0 27.0±0.0	Cathepsin L protein Cathepsin L Cathepsin L, partial Cathepsin L Cathepsin L-like protease Cathepsin L2 Cathepsin L, partial	*F. hepatica* *F. hepatica* *F. hepatica* *F. hepatica* *F. hepatica* *F. hepatica* *F. gigantica*	AAR99518.1 AAF76330.1 AAM11647.1 ABN50361.2 CAA80444.1 ABG00259.1 ABV90502.1	0.0 0.0 0.0 0.0 4E-123 7E-167 0.0
21 (1F, 2F)	**K-Fh**	18.858	5.317	gi|353231888	67.5±5.5	1.0±0.0	3.0±0.0	Putative gelsolin, partial	*S. mansoni*	XP_018651848.1	0.0

22 (1F, 2F)	**K-Fh**	18.542	5.917	gi|47115698	234.5±43.5	23.5±1.5	73.0±3.0	RecName: Full=Fatty acid-binding protein Fh15	*F. hepatica*	Q7M4G0.3	2E-76
23 (1F, 2F)	**K-Fh**	18.529	6.074	gi|124012088	669.0±58.0	29.0±1.0	87.5±3.5	RecName: Full=Fatty acid-binding protein type 2	*F. hepatica*	Q7M4G1.2	6E-72
				gi|47115698	99.5±17.5	8.0±2.0	55.5±14.5	RecName: Full=Fatty acid-binding protein Fh15	*F. hepatica*	Q7M4G0.3	2E-76
24 (1F, 2F)	**K-Fh**	19.025	6.640	-	-	-	-	-	-	-	-
25 (1F, 2F)	**K-Fh**	23.479	6.623	gi|211909240	203.5±80.5	24.5±2.5	40.0±0.0	Cathepsin L1D	*F. hepatica*	ACJ12893.1	0.0
				gi|211909242	203.5±80.5	24.5±2.5	40.0±0.0	Cathepsin L1D	*F. hepatica*	ACJ12894.1	0.0
				gi|166235906	82.5±12.5	5.0±0.0	27.5±0.5	Thioredoxin peroxidase	*F. gigantica*	ABY85785.1	2E-163
				gi|255683591	82.5±12.5	5.0±0.0	24.5±0.5	Thioredoxin peroxidase 1	*F. gigantica*	ACU27401.1	2E-163
				gi|259090533	82.5±12.5	5.0±0.0	24.5±0.5	Peroxiredoxin	*F. gigantica*	ACV91889.1	1E-141
26 (1B, 2F)	**K-Fh**	72.422	6.583	-	-	-	-	-	-	-	-
27 (1F, 2F)	**K-Fh**	48.334	6.751	gi|190350155	107.0±4.0	15.5±4.5	36.5±11.5	Enolase	*F. hepatica*	CAK47550.1	0.0
28 (1F, 2F)	**K-Fh**	48.187	6.971	gi|190350155	270.0±73.0	25.5±7.5	48.5±8.5	Enolase	*F. hepatica*	CAK47550.1	0.0
29 (1F, 2F)	**K-Fh**	23.744	7.257	gi|211909240	185.5±26.5	16.0±1.0	35.0±1.0	Cathepsin L1D	*F. hepatica*	ACJ12893.1	0.0
				gi|211909242	185.5±26.5	16.0±1.0	35.0±1.0	Cathepsin L1D	*F. hepatica*	ACJ12894.1	0.0
30 (1F, 2F)	**K-Fh**	41.256	7.442	-	-	-	-	-	-	-	-

4.5 Discussion

4.5.1 Routes in the establishment of TCBZ resistance

There have been multiple experimentally confirmed TCBZ resistance cases globally, including in the UK (Kelley *et al.*, 2016; Mitchell *et al.*, 1998; Moll *et al.*, 2000) since the first report of TCBZ resistance in the mid-1990s (Overend and Bowen, 1995). Environmental and genetic factors contribute to these incidences, since the potential for liver fluke spread is positively influenced by global and domestic livestock imports, which can genetically diversify fluke infrapopulations (Beesley *et al.*, 2017; Vilas *et al.*, 2012; Walker *et al.*, 2011, 2007). Additionally, with suboptimal anthelmintic applications leading to prolonged exposure and sub-lethal TCBZ dosing, this can consequently pressure flukes to adopt recessive homozygous virulence traits, attained via high rates of gene flow and maintained by potential parthenogenesis events and clonal amplification during transmission (Beesley *et al.*, 2017; Hodgkinson *et al.*, 2013). Thus, geographic separation may cause isolated strains to become more genetically diverse from one another and lead to the employ of one or more molecular mechanisms towards the TCBZ-R phenotype. Subsequently, comparative genetic and proteomic assessments would be highly informative to elucidate the molecular differences between TCBZ-susceptible and TCBZ-resistant fluke that may lead to the identification of resistance-conferring markers. In this thesis, an experimentally identified TCBZ-R strain (K-Fh: Ridgeway Research Ltd., provenance in Kilmarnock, UK) of known TCBZ exposure and resistance status was studied alongside flukes acquired from natural infection and considered to be a group of wild type (WT-Fh: Randall Parker Foods, provenance untraced from nationwide suppliers, UK) flukes with unknown previous TCBZ exposure.

4.5.2 Molecular determinants of viability and TCBZ exposure

The macroscopic assessment of fluke viability was here used as a broad indicator of *in vitro* fitness and drug-induced deterioration (Figure 4.4.3). Excretory/secretory (ES) profiles, including proteomic and molecular fractions, have previously provided further specific molecular differences between live and dead flukes (3.4.1; Morphew *et al.*, 2007), as well as TCBZ-SO-specific proteomic changes between wild type and known TCBZ-S/-R strains (4.4.4; Chemale *et al.*, 2010; Morphew *et al.*, 2014). *Fasciola hepatica* extracellular vesicles (EVs) have since been well-characterised in the context of parasite-host molecular signalling

pathways (Cwiklinski *et al.*, 2015c; Davis *et al.*, 2019). However, the purification and identification of large EV populations, especially apoptotic bodies, has only now been explored to compare differences in their abundance between live and dead flukes (Figure 4.4.1). As a major producer of EVs, the infrastructure and subsequent secretion capabilities from the tegument was of interest and found to be drastically reduced upon non-specific fluke death (Figure 4.4.2). Such histological and functional disruption corresponded with previous findings relating to trans-tegumental anthelmintic uptake (Toner *et al.*, 2010c, 2009), suggesting the current procedure could accelerate the negative influences of TCBZ, TCBZ-SO and TCBZ-SO_2. By their very nature as a mechanistic biproduct of programmed cell death (Montaner *et al.*, 2014), apoptotic body recovery from liver fluke ES products may be indicators of early tegumental damage and ongoing gastrointestinal shedding and restructuring, which could complement other molecular phenotypes of fluke fitness and death *in vitro*. Thus, the present TEM analyses present distinctions in the tegumental tissues and EV populations between live and dead flukes. Furthermore, the findings support the hypothesis that outer surfaces likely succumb first to the influence of xenobiotics, which may lead to an immediate halt in tegument produced EVs and augmented gastrodermal apoptotic body release.

Under the assumption of TCBZ-induced ultrastructural damages as previously reported (Toner *et al.*, 2010c, 2009), viability assessments were used here for identification of macroscopic and outward indicators of fluke fitness (Figure 4.4.3). Using MWU tests between each treatment and time point per strain, there was evidence to suggest that the K-Fh TCBZ-R isolate had enhanced overall fitness under *in vitro* culture conditions ($P < 0.001$). A GLMM further confirmed significant evidence for a difference between the strains following anthelmintic challenge ($P < 0.00001$). These outcomes suggest flukes of the WT-Fh group had reduced *in vitro* stamina compared to those of the K-Fh strain, particularly upon all drug exposures, though fitness could not directly be associated with TCBZ-R traits.

4.5.3 Dissecting TCBZ-associated proteomic profiles between WT-Fh and K-Fh flukes

In order to identify molecular targets specifically associated with anthelmintic exposure, whether efficacy determinants or biomarkers, the two strains of *Fasciola hepatica*

were studied here to elucidate proteomic changes as a consequence of TCBZ exposure. Additionally, the influence of all drug forms was investigated (TCBZ, TCBZ-SO and TCBZ-SO_2) as an *in vivo* representation of concurrent anthelmintic exposure. 2-DE analyses revealed thirty protein spots had differential abundances between WT-Fh and K-Fh strains across all treatments (sub-lethal [15 $\mu g \cdot mL^{-1}$]: TCBZ, TCBZ-SO, TCBZ-SO_2). Specifically, seven proteins demonstrated a significant ($P < 0.05$) change in abundance between strains (spots 1–7), and a further 10 (spots 8–17) and 13 (spots 18–30) proteins were identified as unique to the WT-Fh and K-Fh groups consistently abundant across all anthelmintic challenges, respectively.

When considering the assumptions of the differential TCBZ susceptibilities of each strain, protein profiles indicated no substantial differences in the overall molecular phenotype (Table 4.4.4; Figure 4.4.4.3; WT-Fh spots 8–17 and K-Fh spots 18–30), but rather demonstrated strain-associated changes in the abundance of proteins and specific protein spots (including putative isoforms) that were consistent between both strains across all drug exposures (Table 4.4.4; Figure 4.4.4.3; spots 1–7). Enolase has previously been identified to increase in abundance upon anthelmintic challenge in TCBZ-S *F. hepatica* ES and cytosolic fractions (Table 4.4.4; Figure 4.4.4.3; Chemale *et al.*, 2010; Morphew *et al.*, 2014), supporting the hypothesis of TCBZ-induced stimulation of metabolic enzyme activity. Conversely, a range of protein spots identified as CL proteases were found to change in abundance in the ES proteome following TCBZ-SO exposure (Table 4.4.4; Figure 4.4.4.3; Morphew *et al.*, 2014), but no difference was found between cytosolic extracts of TCBZ-S and TCBZ-R flukes (Chemale *et al.*, 2010). Here, despite identifications of enolase and CLs with changing abundance, enolase, CLs and further spots were also identified with apparent strain specificity, including gelsolin and thioredoxin peroxidase, suggesting possible isoforms or post-translational protein modifications causing these different allocations.

Actin 5C (spot 13) and cathepsin B (CB, spot 15) were exclusively matched to the WT-Fh group, and FABP 15 (spot 22 and 23) and FABP Fh2 (spot 23) were identified only in K-Fh-specific profiles, suggesting strain-specific differences following sub-lethal anthelmintic challenge, similarly to previous findings (Chemale *et al.*, 2010; Morphew *et al.*, 2014). Actin localises within the tegumental bodies, spines and musculature of the tegument and gastrodermis of fluke (Stitt *et al.*, 1992b) and so changes to its cytosolic abundance (Chemale *et al.*, 2010) and secretion patterns (Morphew *et al.*, 2014) have formerly been associated with TCBZ-SO-induced changes to muscular and presumably also generalised cytoskeletal

dynamics. Possible disruption of actin filaments through TCBZ-interactions with their tubulin partners (Stitt *et al.*, 1991; Stitt and Fairweather, 1996) could account for such cellular and histological dissociation, which also fits with the assumed TCBZ-S status of the WT-Fh group. Conversely, the identification of a CB-like was a surprising discovery (Cancela *et al.*, 2008; Wilson *et al.*, 1998), a clade which has not previously been identified in adult *F. hepatica* ES products and moreover expressed by juveniles up to 5 weeks post-excystment (Beckham *et al.*, 2009; Cancela *et al.*, 2008; Law *et al.*, 2003; Wilson *et al.*, 1998). However, the short sequence coverage of LC-MS/MS-identifiable peptides against the partial CB-like protein sequence (106 amino acids) suggests this may be a loose classification, supported by the coinciding but low MASCOT-scoring CL hits calculated in replicate two only (data not shown). Furthermore, cathepsin peptide recovery at this 2-DE-separated protein spot is suggestive of low-level zymogen/intermediate protein release, possibly related to TCBZ-induced gastrodermal degradation (Figure 4.4.4.3; Table 4.4.4). The discovery of two distinct FABPs is in-keeping with previous postulations of their multifaceted roles in *Fasciola spp.* (Chemale *et al.*, 2010; Morphew *et al.*, 2016; Pankao *et al.*, 2006) whereby nutrient acquisition and/or xenobiotic metabolism could also be enacted to support K-Fh flukes following TCBZ/-SX exposure. The discoveries of this chapter have provided yet more evidence of the dynamic changes to the molecular secretome, as well as new TCBZ- and TCBZ efficacy-associated targets of future interest and investigation.

4.6 Conclusions

Through the study of TCBZ-R and mixed-susceptibility parasites, this chapter has identified distinct molecular biological phenotypes pertaining to fluke fitness and anthelmintic susceptibility. Rudimentary differences were demonstrable between live and dead extracellular vesicle (EV) profiles (Chapter 4; 4.2.6: objective 1), from which further investigation found evidence of severe histological deterioration at the tegument leading to reduced capacity for EV production at this surface. Comparisons of TCBZ-challenged fluke found macroscopic viability scores of a TCBZ-R *Fasciola hepatica* strain were significantly higher compared to a naturally acquired TCBZ-S/-R group, both during normal pressures of *in vitro* culture and following sub-lethal TCBZ/-SO/-SO_2 [15 $\mu g \cdot mL^{-1}$] challenge (Chapter 4; 4.2.6: objective 2). Finally, proteomic differences were broadly apparent between the two

anthelmintic-treated strains, that upon LC-MS/MS identification confirmed several targets of interest related to TCBZ exposure and efficacy status (Chapter 4; 4.2.6: objective 3), some of which supports previous findings (Chemale *et al.*, 2010; Morphew *et al.*, 2014). Consequently, the experimental exploration of live, dead and a drug-resistant strain of *F. hepatica* has led to the elucidation of several molecular differences that may provide useful information and biomarkers of anthelmintic exposure, efficacy status and fitness.

5 Chapter 5: Investigating TCBZ-SO-associated diagnostic biomarkers of the *Fasciola hepatica* proteome

4.1 Abstract

As it stands, triclabendazole-resistant (TCBZ-R) populations of *Fasciola hepatica* are independently emerging worldwide and reportedly distinguished in resistance mechanisms. In ongoing efforts to identify biomarker fingerprints of TCBZ-susceptible (TCBZ-S) and TCBZ-R molecular phenotypes, several candidates of interest have been identified with potentially significant diagnostic utility in defining treatment efficacy status. To this end, seven proteins of interest were bioinformatically dissected and prepared for *in vitro* recombinant expression for prospective diagnostic testing.

Following previous identifications of *F. hepatica* biomarkers related to *in vitro* TCBZ, TCBZ-SO and TCBZ-SO_2 challenge, proteins candidates selected for study in this chapter were: actin (FhACT), calreticulin (FhCRT), enolase (FhENO), DJ-1 deglycase (FhDJ-1), gelsolin (FhGEL), glyceraldehyde-3-phosphate dehydrogenase (FhGAPDH), and triose phosphate isomerase (FhTPI). A range of dry lab techniques were employed to bioinformatically predict and assess the biochemical properties of all targets, providing an informative background prior to wet lab methods. Subsequently, *in vitro* recombinant protein expression and purification was attempted, which was successfully executed for FhCRT, FhGEL and FhTPI, enabling more detailed proteomic evaluation.

Subsequently to the methodology pipeline developed in this chapter, seven *F. hepatica* biomarkers associated with TCBZ anthelmintic exposure were comprehensively examined *in silico*, and blueprints for their *in vitro* production have been established. FhCRT, FhGEL and FhTPI demonstrated the greatest ease of production and could be purified with high yields. Thus, these three candidates were suitable for subsequent detailed proteomics in addition to prospective further testing within the remit of this thesis.

4.2 Introduction

4.2.1 Current understanding of *Fasciola hepatica* TCBZ resistance

An understanding of parasite population dynamics is increasingly recognised as a prerequisite for assessing the threat of drug resistance (Beesley *et al.*, 2017; Gilleard and Beech, 2007; Huyse *et al.*, 2005; Silvestre and Humbert, 2002; Vilas *et al.*, 2012; Walker *et al.*, 2011, 2007). To this end, *Fasciola hepatica* genotypes are naturally aggregated due to miracidial clonal expansion and their geographic restriction (Beesley *et al.*, 2015; Vilas *et al.*,

2012). The subsequent population dynamic can lead to high frequencies of adult self-fertilisation or more rarely parthenogenic events (by gynogenic/aspermic individuals) in definitive hosts (Fletcher *et al.*, 2004), and consequently also the maintenance of recessive drug resistance traits (Beesley *et al.*, 2017, 2015; Hodgkinson *et al.*, 2013; Vilas *et al.*, 2012). Thus, *F. hepatica* infrapopulations can maintain high genetic diversity despite common gene flow restrictions and potential genotype aggregation during transmission (Beesley *et al.*, 2017; Hodgkinson *et al.*, 2013; Vilas *et al.*, 2012). However, global and domestic movements and management practices of ruminants by humans are also highly attributable to the high level of gene flow and genetic diversity, whereby both clonal and multilocus genotypes (MLG) are well represented in geographically separated locations (Beesley *et al.*, 2017; Robles-Pérez *et al.*, 2015; Vilas *et al.*, 2012; Walker *et al.*, 2011, 2007).

In the absence of fully understanding the mechanisms of how parasitic worms become resistant to drugs, anthelmintic resistance can simply be quantitatively estimated by tracking drug-induced downstream changes, either at the molecular level via parasite protein turnover or at the morphological level by egg count reductions (Coles *et al.*, 2006; Gilleard, 2013; Walker *et al.*, 2011). For example, mechanisms exploited by *F. hepatica* to become TCBZ resistant remain undefined since the mode of action or metabolic route of TCBZ in liver fluke are still unknown (Hodgkinson *et al.*, 2013; Kelley *et al.*, 2016). Moreover, many routes towards anthelmintic resistance mechanisms within parasitic helminths have been proposed (Matouskova *et al.*, 2016; Ubeda *et al.*, 2008; Wilkinson *et al.*, 2012; Wolstenholme *et al.*, 2006). Examples include, single nucleotide polymorphisms (SNPs) leading to altered specificities of drug targets and transporters, and transcriptional upregulation of xenobiotic-metabolising enzymes and efflux transporters to enhance drug removal via coupled transportation or uncoupled excretion, respectively (Brophy *et al.*, 2012; James *et al.*, 2009; Matouskova *et al.*, 2016; Wolstenholme *et al.*, 2006).

Thus, the high genetic diversity of flukes at the animal, farm and regional level combined with high gene flow rates increases the potential for horizontal transfer of resistance alleles (Beesley *et al.*, 2017; Vilas *et al.*, 2012; Walker *et al.*, 2011, 2007), and thus the chance of resistance-associated alleles passing several generations, and more so if improved fitness is also associated with this phenotype (Walker *et al.*, 2006). Consequently to uncover multifactorial resistant phenotypes, genome-wide and global proteomic approaches are suited in identifying more drug- and mechanism-specific markers of

resistance than searching via reductionist biology approaches for orthologous drug targets in other species (Cwiklinski *et al.*, 2015a; Gilleard, 2013; Hodgkinson *et al.*, 2013; Morphew *et al.*, 2014).

4.2.2 Biomarkers of TCBZ exposure and resistance

The specific molecular mechanisms of the novel benzimidazole (BZ) TCBZ remain to be fully uncovered. The other BZ anthelmintics are widely known to bind and inhibit a range of helminth tubulins, thus similarly to colchicine and tubulozole as broad-acting tubulin inhibitors (Fetterer, 1986; Stitt and Fairweather, 1993a). In contrast, TCBZ does interact with tubulin, however, only Fasciolidae tubulins (Bennett and Köhler, 1987). TCBZ-Fasciolidae tubulin interactions subsequently lead to interruptions or discontinuations of microtubule-driven processes, and so particularly effect tissues dividing with a high turnover (Fetterer, 1986; Lacey, 1988; Stitt *et al.*, 1992a; Stitt and Fairweather, 1996, 1993b, 1993a). To this end, disruptions to cell division of critically important vitelline and spermatogonial cells are also directly responsible for the subsequent halt in egg production and impacts on egg viability (Alvarez *et al.*, 2009; Stitt and Fairweather, 1996, 1992). In addition, TCBZ-induced tegumental damage reduces the capacity for cell repair following regular activities of stress-induced blebbing, sloughing and vesicle secretion (Halferty *et al.*, 2009, 2008; Stitt *et al.*, 1995; Stitt and Fairweather, 1993b, 1993a; Toner *et al.*, 2010a). These TCBZ-associated cellular physiology impacts are well-documented in TCBZ susceptible flukes, requiring *in vivo* recommended doses plus a significant period of *in vitro* exposure to TCBZ flukicide (Vercruysse and Claerebout, 2001; Wolstenholme *et al.*, 2006). In infected ruminants, quantitative reductions (>95%) of measurable fluke cathepsin L-based protein turnover is the current best and only molecular laboratory indicator available to measure anthelmintic resistance (Daniel *et al.*, 2012; Flanagan *et al.*, 2011a, 2011b; Novobilský *et al.*, 2012). There are as yet no definitive molecular assays to measure TCBZ treatment failure as opposed to resistance failure. Therefore, a knowledge gap remains in our understanding of TCBZ-associated molecular biomarkers of *Fasciola hepatica*, as well as the role of such biomarkers during anthelmintic metabolism and/or evasion that may yet have an effective role in parasite management through effective drug efficacy diagnoses.

4.2.3 Chapter 5 aims

Genomic and transcriptomic approaches are efficient and high throughput in identifying molecular determinants and markers of interest, including anthelmintic- and resistance-associated biomarkers (Hodgkinson *et al.*, 2013; Kotze *et al.*, 2014; Nahum *et al.*, 2012). Conversely, proteomics using standardised *in vitro* formats can discover and measure functionally relevant protein candidates that are potentially important in parasite-host interactions, immune evasion and/or anthelmintic exposure (Brophy *et al.*, 2012; Morphew *et al.*, 2007, 2013, 2014; Robinson *et al.*, 2009). To this end, seven previously discovered TCBZ-associated protein biomarkers were characterised in this thesis. These biomarkers were identified through respective changes in their abundances following proteomic screening of *Fasciola hepatica in vitro* ES products in direct response to TCBZ-SO metabolite challenge at the terminating lethal (L) concentration [50 $\mu g \cdot mL^{-1}$] or the non-terminating sub-lethal (SL) concentration [15 $\mu g \cdot mL^{-1}$] of this flukicide (Morphew *et al.*, 2014). In brief, protein allocation as biomarkers of sub-lethal TCBZ survival (resulting in detrimental effects only) or as lethal TCBZ termination (resulting in flukicide) was dependent on their presence and regulation during SL and L *in vitro* TCBZ-SO challenge (Morphew *et al.*, 2014). L-associated biomarkers were categorised as markers of drug-terminating susceptible flukes, including actin (FhACT), deglycase DJ-1 (FhDJ-1), gelsolin (FhGEL), and triose phosphate isomerase (FhTPI). Conversely, proteins with demonstrably active regulation post-treatment, whether with temporal, down- or up-regulated expression and especially SL association, were deemed as non-terminating fluke biomarkers, including calreticulin (FhCRT), enolase (FhENO) and glyceraldehyde-3-phosphate dehydrogenase (FhGAPDH). Therefore, the specific objectives of this chapter were to:

1) Utilise bioinformatic approaches to evaluate the Morphew *et al.* biomarkers for roles in cellular, physiological and TCBZ-SO anthelmintic interaction;
2) Generate and clone genetic constructs of target candidates for recombinant expression, purification and integrity confirmation via mass spectrometry.

4.3 Methods

4.3.1 Cloning *Fasciola hepatica* biomarkers

4.3.1.1 In silico *methods*

4.3.1.1.1 Target sequence selection, acquisition and analysis

TCBZ-SO response biomarkers were selected for study following their proposal by Morphew *et al.* (2014). Protein hits of *Fasciola hepatica* and other organisms were accessed using the National Center for Biotechnology Information (GenBank v204 (Benson *et al.*, 2015): www.ncbi.nlm.nih.gov) identifiers provided by Morphew *et al.* (2014) and aligned using BLASTP to the highest scoring *F. hepatica* gene sequences delivered by the Liverpool University genome project (PRJEB6687, WBPS v10, 2014). However, where no polymerase chain reaction (PCR) amplicons were observed, other sequence sources were used when successful, including UniProt and SwissProt (GenBank v204), and the Washington University genome project (PRJNA179522, WBPS v10–14, 2014–2018)). Consequently, target sequences are representative of *F. hepatica* wild type acquired from the cDNA of parasites from natural infections in UK sheep flocks collected from freshly slaughtered livers (Randall Parker Foods Ltd., Wales).

4.3.1.1.2 Bioinformatic predictions

DNA and amino acid sequences were analysed following PCR amplification, cloning and sequencing (4.3.1.2) using BioEdit (v7.0.5.3) (Hall, 1999). Subsequently, representative sequences were used as templates for genetic and proteomic assessments to reflect wild type isotypes. Consequences of any residue substitutions were predicted using PROVEAN Protein (Choi, 2012; Choi *et al.*, 2012: provean.jcvi.org) and MutPred2 (Li *et al.*, 2009: mutpred2.mutdb.org) tools.

Protein characteristics including domains, localisation, and structural, functional and antigenic epitopes, were predicted using ExPASy tools (Gasteiger *et al.*, 2003: www.expasy.org), CBS (DTU health tech bioinformatics, formerly the Center for Biological Sequence Analysis: www.cbs.dtu.dk/biotools), InterPro (Jones *et al.*, 2014: www.ebi.ac.uk/interpro), CATH/Gene3D (CATH-Plus v4.2, Dawson *et al.*, 2017: www.cathdb.info), SUPERFAMILY (v1.75, Gough *et al.*, 2001: supfam.org), PROSITE (Sigrist *et al.*, 2013: prosite.expasy.org), Motif Scan (Pagni *et al.*, 2007: myhits.isb-sib.ch/cgi-

bin/motif_scan), SignalP (Nielsen, 2017: www.cbs.dtu.dk/services/SignalP), and the Immunomedicine Group (Kolaskar and Tongaonkar, 1990; Universidad Complutense Madrid: imed.med.ucm.es/Tools/antigenic.pl). Hypothetical multi-dimensional structures were modelled to homologous templates, with the confidence of each sequence match scored as a percentage (0–100%), using Phyre2 (Kelley *et al.*, 2015: www.sbg.bio.ic.ac.uk/phyre2) and SWISS-MODEL (Arnold *et al.*, 2006; Benkert *et al.*, 2011; Guex *et al.*, 2009: swissmodel.expasy.org), and ligand binding properties were predicted using 3DLigandSite (Wass, Kelley and Sternberg, 2010: www.sbg.bio.ic.ac.uk/3dligandsite).

For phylogenetic analyses, sequences were processed using the Molecular Evolutionary Genetics Analysis (MEGA, v7; Kumar *et al.*, 2016). Alignments were used to generate 1000-replicate bootstrapped, neighbour-joining phylogenetic trees with level 1 gamma distribution and Poisson corrections (Felsenstein, 1985; Kumar *et al.*, 2016; Saitou and Nei, 1987; Zuckerkandl and Pauling, 1965). The percentage of replicate trees in which taxa clustered within the bootstrap test were labelled at each branch, and units of the evolutionary distance were presented as the number of amino acid substitutions per site.

4.3.1.1.3 PCR primer designs

Primers (Eurofins, Germany; Sigma-Aldrich, UK) were designed for full-length gene amplification or truncated to avoid downstream *in vitro* bacterial host cell toxicity and unfavourable proteomic properties (Table 4.3.1.1.3). Melting temperatures and complementarity were pre-determined using Primer3 (Kõressaar *et al.*, 2018; Koressaar and Remm, 2007; Untergasser *et al.*, 2012: primer3.ut.ee) and the Multiple Primer Analyzer (Breslauer *et al.*, 1986: Thermofisher Scientific bit.ly/2RAzEHt).

Table 4.3.1.1.3. Primer designs for *F. hepatica* gene amplification. Full-length and truncated gene sequences were targeted as specified, including start and stop codons (bolded) for initial cloning. Restriction enzyme-binding sequences for NdeI and NotI (underlined) were added in addition (NdeI: 5'-CAT**ATG**-3') and in place of (NotI 5'-GCGGCCGC-3') the start and stop codons, respectively, for subsequent subcloning progression.

Target name and source	Cloning	Subcloning
Actin BN1106_s101B000531.mRNA-1, PRJEB6687, WormBaseParaSite	For 5'-**ATG**GCTGAAGAGGACGTTGC-3' Rev 5'-**CTA**GAAGCATTTGCGATGAA-3'	For 5'-CAT**ATG**GCTGAAGAGGACGTTGCT-3' Rev 5'-GCGGCCGCGAAGCATTTGCGATGAAC-3'
Calreticulin BN1106_s2673B000071.mRNA-1, PRJEB6687, WormBaseParaSite	For 5'-**ATG**GTTGGTACGTGGTACTTC-3' Rev 5'-**TTA**CAACTCCTCATGATCGGC-3'	For 5'-CAT**ATG**GTTGGTACGTGGTACTTC-3' Rev 5'-GCGGCCGCGCCGATCATGAGGAGTTG-3'

Truncated Calreticulin BN1106_s2673B000071.mRNA-1, PRJEB6687, WormBaseParaSite		For 5'-CAT**ATG**GAAGTTTACTTGGAAGAAAA-3' Rev 5'-GCGGCCGCGCCGATCATGAGGAGTTG-3'
DJ-1 Deglycase BN1106_s1971B000297.mRNA-1, PRJEB6687, WormBaseParaSite	For 5'-**ATG**GCAGTGTCAGCACTT-3' Rev 5'-**TCA**ACGAACAAGCATTTT-3'	For 5'-CAT**ATG**GCAGTGTCAGCACTT-3' Rev 5'-GCGGCCGCACGAACAAGCATTTT-3'
Enolase U10297.1, GenBank	For 5'-**ATG**GCAATAAAAGCGATC-3' Rev 5'-**TTA**TGGTCGGCGGAAGTTCT-3'	For 5'-CAT**ATG**GCAATAAAAGCGATCCA-3' Rev 5'-GCGGCCGCTGGTCGGCGGAAGTT-3'
Gelsolin D915_01476, PRJNA179522, WormBaseParaSite	For 5'-**ATG**GCTGGTCTGACGAA-3' Rev 5'-**TTA**GTCCCAAATTTTCTCCATC-3'	For 5'-CAT**ATG**GCTGGTCTGACGAAGC-3' Rev 5'-GCGGCCGCGTCCCAAATTTTCTCCAT-3'
Glyceraldehyde-3-phosphate dehydrogenase KF700239.1, GenBank	For 5'-**ATG**TCCAAACCCAAAGTG-3' 5'-**TCA**CAAATGGTCAATAGTAT-3'	For 5'-CAT**ATG**TCCAAACCCAAAGTG-3' Rev 5'-GCGGCCGCCAAATGGTCAATAGTAT-3'

4.3.1.2 In vitro *genetic recombination*

4.3.1.2.1 PCR conditions

50-250 ng cDNA template was used for PCR amplification and adjusted as required. For colony PCRs, 5 µL of bacterial colony samples resuspended in 10 µL nuclease-free DEPC-treated water (Ambion, Invitrogen, UK) was used per reaction, and the remainder was used for subculturing (4.3.1.2.4). PCRs were conducted using MyTaq™ Red for diagnostic reactions and MyFi™ for high fidelity, according to the manufacturer's instructions (Bioline, UK). All PCRs were conducted using a Techne TC-4000 thermocycler (Bibby Scientific, UK) and conditions were designed per target (Table 4.3.1.2.1), with adjustments to annealing temperatures and extension time as required. DNA concentration and purification quality was determined using a NanoDrop® ND-1000 (Thermo Scientific, UK).

Table 4.3.1.2.1. PCR experimental design for *F. hepatica* gene amplification. Reaction conditions for DNA target amplification was setup according to each gene cloning or subcloning primer pair, with the only adjustments to the annealing temperature ([a]) or extension time ([b]) to suit primer-target binding and amplicon sequence extension, respectively.

Stage	Time	Temperature	Process	
1	1 min	95°C	Initial denaturation (including bacterial colony lysis)	
2	30 sec	95°C	Denaturation	35 cycles
	30 sec	49–65°C [a]	Annealing	
	30–45 sec [b]	72°C	Extension	
3	5–7 mins [b]	72°C	Final extension	

A. Annealing temperatures were calculated according to the melting temperatures of any primer pairs used concurrently.

B. Extension times were adjusted per target, with 30 s per 500 bp and 5 s per additional 500 bp.

4.3.1.2.2 DNA gel electrophoresis

1% agarose (molecular biology grade, Melford, UK) gels were hand cast, using tris-acetate buffered EDTA (TAE) (Thermo Scientific, UK) and with GelRed™ (Biotium, UK) or Sybr™ Safe (Invitrogen™, UK) intercalating agents. Where required, DNA loading buffer (Bioline, UK) was used prior to sample loading and HyperLadder™ 1kb (Bioline, UK) or FastLadder (NEB,

UK) molecular markers were used as recommended by the manufacturers. Gels were electrophoresed in TAE at 50–125 V as dictated by target sizes, whereby PCR products of 1.0-1.5 kilobase pairs (kbp) were typically conducted at 110 V for 5–10 minutes followed by 100 V for 45–60 minutes and larger fragments of 3.0+ kbp at 100 V for 10–20 minutes and 50–75 V for 60–75 minutes.

Electrophoresed DNA gels were imaged using the U:Genius^3 (Syngene) or Typhoon™ FLA 9500 (GE Healthcare, UK) systems. Where required, fragments of interest were aseptically extracted and purified using the ISOLATE II PCR and Gel Kit (Bioline, UK) as per the manufacturer's instructions with only minor adjustments to increase the post-ethanol centrifugation to three minutes and eluting (with re-eluting) using nuclease-free DEPC-treated water. Where required, DNA samples were further purified and concentrated using the MSB® Spin PCRapace kit (Thistle Scientific, UK).

4.3.1.2.3 Biomarker gene-pGEM-T® Easy ligations

MyFi™ PCR amplicons with 3' adenine overhangs were ligated into the linear cloning vector, pGEM-T® Easy (Promega, UK), as directed or with approximately 3:1 insert:vector quantities (specifically calculated as described below: 4.3.1.2.6.2; Figure 4.3.1.2.6.2). Ligations were conducted overnight at 4°C using T4 ligase as recommended (Promega, UK; Thermo Scientific, UK).

4.3.1.2.4 Biochemical *Escherichia coli* transformation

Chemically-competent bronze efficiency α-select *Escherichia coli* (Bioline, UK) were transformed with 1–5 ng cloning vector DNAs in 1–3 µL suspension per 25 µL cells or 2.5–5 µL suspension per 50 µL cells using the heat-shocking method as advised alongside the positive control plasmid pUC19 (Bioline, UK). Specifically, cells were incubated with pre-chilled DNA samples on ice for 30 minutes before heating for 15–30 s at 42°C and incubation on ice for a further 2 minutes. Cells were grown at 37°C for 1–1.5 hours in 450 or 900 µL SOC medium (Sigma-Aldrich, UK) for 25 or 50 µL starting cell volumes, respectively. 50–150 µL cells were then grown on LB agar plates (Melford, UK) pre-treated with ampicillin [100 $\mu g \cdot mL^{-1}$], IPTG [1 mM] (both Thermo Scientific, UK) and X-gal [100 $mg \cdot mL^{-1}$] (Melford, UK) for plasmid selection and screening. Plate cultures were incubated at 37°C overnight (14–18 hours) or room

temperature for up to 72 h and stored at 4°C for longer term as required (<3 months). Subcultures were setup using picked colonies or following colony PCR (4.3.1.2.1) in ampicillin-treated [100 µg·mL^{-1}] LB Broth (Miller, UK; Sigma-Aldrich, UK; Thermo Scientific, UK) overnight at 37°C and 180–200 rpm.

Plasmid DNA was extracted using the ISOLATE II Plasmid Mini Kit (Bioline, UK) with protocol modifications as follows. 1.5 mL liquid media fractions were pelleted and treated individually with 20% of the recommended buffer volumes before combining and continuing as recommended until elution in nuclease-free DEPC-treated water.

4.3.1.2.5 Bacterial transformant storage

Liquid cultures were stored at 4°C for short periods (<1 week) or prepared for long-term storage as glycerol stocks by mixing equal volumes of cell cultures with autoclaved 50% glycerol (Thermo Scientific, UK) in distilled water (UV-sterilised; 15 MΩ) in cryostable tubes. Subcultures of glycerol stocks were setup taking a scrape of cryostocks into fresh LB broth with appropriate antibiotic supplementation.

4.3.1.2.6 Generation of biomarker expression vectors

4.3.1.2.6.1 Restriction endonuclease digestions

Cloned target sequences were isolated from pGEM-T® Easy via double restriction digestions using NdeI (CA/TATG) and NotI (GC/GGCCGC) endonucleases followed by gel excision (4.3.1.2.2). Reaction volumes of 10 µL (diagnostic) or 20 µL (subcloning) were used with a minimum of 1 Weiss unit (U) each of NdeI and NotI per 100 ng DNA and with buffer D or buffer O as per the manufacturers' guidelines (Thermo Scientific, UK; Promega, UK). Reactions were incubated at 37°C for 2–4 hours and deactivated at 65°C for 20 minutes. For diagnostic digestions, 250 ng–1 µg plasmid DNA was used, whereas subcloning used 1–3 µg insert (X-pGEM®-T Easy) and parent expression vector (pET-23a(+)/-28b(+) (Merck, UK)).

4.3.1.2.6.2 Biomarker gene-expression vector subcloning

Ligations were attempted as previously described (4.3.1.2.3) within the range of 1:1–10:1 insert:vector ratios in accordance with the standardised ligation reaction equation (Figure 4.3.1.2.6.2). 10–100 ng gel-purified NdeI-NotI-linearised Novagen® pET-23a(+)/-

28b(+) vectors (Merck, UK) were ligated with gel-purified NdeI-NotI-digested insert DNA for cloning in *E. coli* as before (4.3.1.2.3–4.3.1.2.4), except without IPTG and X-gal and with 50 $\mu g \cdot mL^{-1}$ kanamycin (Sigma-Alrich, UK) antibiotic selection for pET-28b(+)-based construct transformants.

$$\text{Insert X [ng]} = \frac{\text{Y ng [vector]} \times \text{X kilobase pairs [insert]}}{\text{Y kilobase pairs [vector]}} \times \frac{\text{insert}}{\text{vector}} \text{ [ratio]}$$

Figure 4.3.1.2.6.2. Equation for the calculation of optimal insert-vector ligation conditions in subcloning.

4.3.1.2.7 Recombinant DNA sequence confirmation

Constructs were confirmed via PCR (4.3.1.2.1), restriction endonuclease digestions (4.3.1.2.6.1) and Sanger DNA sequencing (n≥3) using M13 (pGEM®-T Easy: M13-forward 5'-GTAAAACGACGGCCAG-3', M13-reverse 5'-CAGGAAACAGCTATGAC-3') or T7 (pET: T7-forward 5'-TAATACGACTCACTATAGGG-3', T7-reverse 5'-CCGCTGAGCAATAACTAGC-3') universal primers. The *FhTPI-pET-46 Ek/LIC* construct was generated by Zinsser *et al.* (2013b) and kindly provided by Professor David Timson (Queen's University Belfast, UK), and thus only DNA sequencing confirmation was performed. DNA sequencing results were analysed and aligned to *in silico* genome-derived sequences using the BioEdit Sequence Alignment Editor (Hall, 1999). Confirmed constructs, including correct sequence and vector landmarks (Table 4.3.1.2.7) were subsequently selected for recombinant expression.

Table 4.3.1.2.7. Insert-expression vector construct characteristics.

Target name	Insert	Expression vector	HIS tag location (terminus)
Actin	*FhACT*	pET-28b(+)	C
Calreticulin	*FhCRT*	pET-23a(+)	C
Truncated calreticulin	*FhΔCRT*	pET-28b(+)	C
Deglycase DJ-1	*FhDJ-1*	pET-28b(+)	C
Enolase	*FhENO*	pET-28b(+)	C
Gelsolin	*FhGEL*	pET-28b(+)	C
Glyceraldehyde-3-phosphate dehydrogenase	*FhGAPDH*	pET-28b(+)	C
Triose phosphate isomerase	*FhTPI*	pET-46Ek/LIC	N

4.3.1.2.8 Expression cell lines

Chemically-competent BL21(DE3) (Bioline, UK), One Shot® BL21(DE3) Star™ (Thermo Scientific, UK) or BL21(DE3)pLysS (Promega, UK) cells were transformed with prepared constructs according to the manufacturers' guidelines with adjustments as follows. Briefly, 5–10 ng or 2.5–5 ng DNA per 50 µL or 25 µL cell volume, respectively, was used and

transformants were cultured with appropriate antibiotic supplementation as previously described (4.3.1.2.4–4.3.1.2.6).

4.3.2 Recombinant expression

4.3.2.1 Setup of pET-BL21 expression systems

For expression, BL21(DE3) transformants were diluted into fresh antibiotic-supplemented LB Broth and grown at 37°C with 140–180 rpm. Cultures were induced with IPTG upon reaching mid-log phase (A_{600} = 0.6–1.0), which was measured by a Varian Cary 50 Bio UV-V Spectrophotometer (Agilent Technologies, UK) or a NanoDrop® ND-1000 (Thermo Scientific, UK), and temperatures were adjusted as specified (Table 4.3.2.1). Aliquots taken hourly until upto 4 hours post-induction and the remainding culture at the end of incubation were subsequently prepared for protein isolation (4.3.3).

Table 4.3.2.1. Expression conditions for *Fasciola hepatica* target biomarkers. Pilot conditions included a range of IPTG induction concentrations and where necessary, several temperatures were tested. Further conditions were attempted for troubleshooting, and optimal recommended parameters are shown in **bold**. The outcome of purification of recombinant proteins (4.3.4), where conducted, is also shown.

Target name	Construct	Cell line	Pilot conditions				Conditions of troubleshooting attempts and **optimised recommendations**				Recombinant protein purification outcome
			Culture dilution	IPTG [mM]	Temperature (°C)	Duration (hours)	Culture dilution	IPTG [mM]	Temperature (°C)	Duration (hours)	
Actin	*FhACT*-pET-28b(+)	BL21(DE3)pLysS	1:70	0.05 0.1 0.5 1.0	37	5	-	-	-	-	Attempted
Calreticulin	*FhCRT*-pET-23a(+)	BL21(DE3)	1:40	0.0 0.6 1.0	28, 32	5	1:40	1.0	18 28 37	16 5 5	Attempted
Truncated calreticulin	*FhΔCRT*-pET-28b(+)	BL21(DE3)pLysS	1:40	0.1 0.5	37	5	**1:40**	**0.5**	**37**	**3–5**	Successful
Deglycase DJ-1	*FhDJ-1*-pET-28b(+)	BL21(DE3)pLysS	1:70	0.05 0.1 0.5 1.0	18	24	**1:40**	**0.05**	**37**	**5**	Attempted, partial success
Enolase	*FhENO*-pET-28b(+)	BL21(DE3)pLysS	1:40	0.1 0.5	37		1:40	0.1	37	5	Attempted
Gelsolin	*FhGEL*-pET-28b(+)	BL21(DE3)pLysS	1:40	0.0 0.5 1.0	37	5	**1:40**	**0.5**	**37**	**5**	Successful
Glyceraldehyde-3-phosphate dehydrogenase	*FhGAPDH*-pET-28b(+)	BL21(DE3)pLysS	1:40	0.05 0.1 0.5 1.0	30	5	1:40	0.1	18	24	Attempted
Triose phosphate isomerase	*FhTPI*-pET-46 Ek/LIC	One Shot® BL21(DE3) Star™	1:40	0.0 1.0 2.0	37	3	**1:40**	**1.0**	**37**	**5**	Successful

4.3.3 Recombinant protein processing

4.3.3.1 Protein isolation

Cells were pelleted at 10,000 x *g* for 10 minutes at 4°C and resuspended in lysis buffer (0.1 M sodium phosphate, pH 7.4; 0.4 M sodium chloride; 5 mM magnesium chloride). Resuspensions were stored at -80°C until needed or directly lysed by subjecting cells to three cycles of freeze-thawing in liquid nitrogen and a water bath heated to 42°C, followed by three cycles of 15 s sonication and 15 s wet ice incubations.

Lysate and inclusion body (IB) fractions were separated by centrifugation at 11,000 x *g* for 10 minutes at 4°C and soluble sample filtration through 0.22 µm polyethersulfone membranes (Merck Millipore, Germany). IB-expressed target proteins were instead subjected to centrifugation at 21,000 x *g* and pellets were washed by resuspending in fresh lysis buffer and collected following re-centrifugation at 11,000 x *g*. Samples were stored at -80°C for long-term or -20°C for short-term periods until required. For analysis by SDS PAGE, samples were directly taken, including for IBs where 5 µL volume of insoluble IB fractions were loaded per lane after mixing pellets in 20 µL distilled water (UV-sterilised; 18.2 MΩ).

4.3.3.2 IB protein extraction and solubilisation

For rFhCRT and rFhGAPDH IBs, protein extraction and solubilisation was based on the protocol by Allahyari *et al.* (2015). Briefly, IB pellets separated from the soluble fraction (4.3.3.1) were washed in pre-chilled IB lysis buffer (30 mM tris-Cl, pH 8.0; 300 mM sodium chloride; 1 mM PMSF (for FhGAPDH only); 1 mM EDTA) followed by pre-chilled IB lysis buffer containing 1.0% Triton X-100 (v/v) and 1 M urea (w/v) (Thermo Scientific, UK), with centrifugation after each step for 20 minutes at 4°C at 8,800 x *g* for rFhCRT and 4,000 x *g* for rFhGAPDH. Pellets were then solubilised in IB denaturation buffer (30 mM tris-Cl, pH 9.0; 500 mM sodium chloride; 1 mM PMSF; 8 M urea; 1 mM DTT; 5 mM imidazole) at room temperature for 2 hours followed by centrifugation as before to isolate the supernatant containing solublised IB proteins. All wash steps and fractions were collected and stored as before (4.3.3.1).

4.3.4 Recombinant protein purification

4.3.4.1 Immobilised metal ion affinity chromatography (IMAC)

Filter-sterilised soluble lysates containing polyhistidine-tagged recombinant proteins were purified using immobilised metal ion affinity chromatography (IMAC) in accordance with manufacturers' guidelines unless otherwise specified where required. Columns were loaded with HIS-Select Nickel and Cobalt (Sigma-Alrich, UK) or Nickel-Nitrilotriacetic acid (Ni-NTA) cartridges (Web Scientific, UK) were used alongside the ÄKTAprime plus v2.01 liquid chromatography system (GE Healthcare Life Sciences, UK) and analysed with PrimeView™ v1.00.

Sodium phosphate buffers were prepared for all IMAC procedures, adjusted to pH 6.0 for rFhCRT/rFhΔCRT or pH 8.0 for all other targets (6.8% di-hydrogen monosodium phosphate; 93.2% disodium monophosphate (Thermo Scientific, UK)) with sodium chloride (0.3 M (Thermo Scientific, UK)) and imidazole (Acros Organics, UK) for equilibration (EQ, 20 mM), wash (10 mM) or elution (50–500 mM) buffers. Elution buffers were applied stepwise with increasing imidazole concentrations and a denaturation buffer (EQ with 8 M (w/v) urea (Thermo Scientific, UK)) was used following all IMAC elutions.

4.3.4.2 Standardisation of polyhistidine-tagged recombinant protein purification

IMAC procedures were conducted as described (4.3.4.1) at 4°C or ambient (18–21°C) temperatures and resins were prepared by washing with at least 10 bed volumes of distilled water (UV-sterilised; 18.2 MΩ) followed by 5-10 bed volumes of EQ buffer at 5 mL per minute. Samples were acclimatised to the operating temperature and supplemented with imidazole to a final concentration of 10 mM and approximately 100 mg target protein per 1 mL resin was applied and re-applied at a flow rate of 1–2 mL per minute for one–two hours or up to a maximum of four hours as recommended by the manufacturers. Wash buffer was subsequently applied at a flow rate of 5–10 mL per minute until optical density (A_{280}) readings of the flow-through was equal to or less than that of the wash buffer. 1–10 mL elution buffer was then applied with increasing imidazole concentration, followed by a final purge using sodium phosphate buffer with 8 M urea and 50 mM imidazole. All flow-through and elution samples containing protein fractions were collected and stored on ice prior to 4°C storage overnight or -20°C storage for longer than 24 hours prior to further processing.

4.3.4.3 IMAC under denaturing conditions and on-column refolding

IB-isolated recombinant denatured proteins (4.3.3.2) were purified using IMAC under denaturing conditions (8 M urea) followed by on-column refolding and protein elution under native conditions, based on the protocol by Barbosa *et al.* (2006) with minor adjustments as follows. All buffers were made and used as previously described (4.3.4.1–4.3.4.2), except with the addition of 0, 4, or 8 M urea (w/v) and 1 mM DTT (w/v) in EQ buffers used in decreasing order of urea concentration to enable protein refolding prior to protocol continuation under native conditions as before.

4.3.4.4 Concentration and buffer exchange of IMAC eluents

4.3.4.4.1 Filtration

Amicon® Ultra 10K or 30K-Centrifugal Filters (Merck, UK) were used in the first instance to concentrate IMAC-purified recombinant samples according to the molecular mass each protein target. Centrifugal filters were used as recommended by manufacturer as follows. All steps were conducted at 4°C excluding the optional sodium hydroxide wash, and following centrifugation distilled water (18.2 MΩ) was used to wash/resuspend samples, which were collected and stored at -20°C for short-term or -80°C for long-term periods until required.

4.3.4.4.2 Centrifugal vacuum

For samples resuspended in water and with low protein concentration sample volumes were reduced and concentration increased as required using a HETO Holton MAXI dry plus centrifugal vacuum, operated between 30–40°C and at 1,700 RPM.

4.3.5 Proteomic analyses and identification

4.3.5.1 SDS PAGE and mass spectrometry

Protein concentrations were determined (2.3.4) and 1-D (1-DE) and 2-D (2-DE) SDS PAGE was conducted (2.4.1) as previously described. 1-DE- and 2-DE-separated proteins were prepared for liquid chromatography tandem mass spectrometry (LC-MS/MS) using an ESI-QUAD TOF system as described in the General materials and methods (2.4.3) with further specifications. Hits were identified against the *Fasciola hepatica* genome (PRJEB6687, WBPS

v10) using an in-house MASCOT (Matrix Science) server and further identified against GenBank (v204). Where required, a decoy search was performed to report the false discovery rate of reverse protein sequences above identity or homology thresholds.

4.3.5.2 Western hybridisation

SDS PAGE-separated proteins were directly transferred to nitrocellulose membrane (NCM) and analysed as previously described (2.4.2).

4.3.5.2.1 HisProbe™-HRP

HisProbe™ (Thermo Scientific, UK) was diluted to 1:5,000 in TBS with 1% (w/v) milk and 1% (v/v) Tween® 20 and incubated at room temperature for an hour, after which membranes were washed with TBS twice for 15 minutes each and directly detected using the chemiluminescent peroxidase substrate-3 working solution (Sigma-Aldrich, UK) as recommended by the manufacturer. Blots were imaged using a UVP BioSpectrum Imaging System (UVP, USA) with 5 minutes' exposure.

4.3.5.2.2 Anti-HIS-AP

A second unconjugated anti-histidine tag antibody produced in rabbit (SAB1306082, Sigma-Aldrich, UK) was used for subsequent western hybridisations between 1:1,000–1:2,000 as previously described (4.3.5.2.1). Membranes were subsequently incubated with secondary goat anti-rabbit-alkaline phosphatase conjugate (A3687, Sigma-Alrich, UK) diluted to 1:30,000 in TBS for an hour at room temperature, then washed with fresh TBS prior to detection using the nitro-blue tetrazolium (NBT)/5-bromo-4-chloro-3-indolyl-phosphate 4-toluidine (NBT/BCIP) system as required (100 mM tris, pH 9.5; 100 mM sodium chloride; 5 mM magnesium chloride; 0.4 mM NBT (Thermo Scientific, UK); 0.45 mM BCIP salt (Melford, UK)) and imaging using a GS-800 Calibrated Imaging Densitometer (Bio-Rad, UK).

4.4 Results

4.4.1 *In silico* analyses

4.4.1.1 Sequence selection for TCBZ-SO-associated biomarkers

Molecular candidates for measuring TCBZ efficacy in *Fasciola hepatica* were selected from a previous study by Morphew *et al.* (2014), that identified target proteins in SL TCBZ-SO-associated survival or L TCBZ-SO-associated termination phenotypes. In this thesis, seven of these shortlisted candidates were selected for characterisation and recombinant expression for prospective assessments of diagnostic potential, including actin (ACT), calreticulin (CRT), deglycase DJ-1 (DJ-1), enolase (ENO), gelsolin (GEL), glyceraldehyde-3-phosphate dehydrogenase (GAPDH), and triose phosphate isomerase (TPI). Specific protein hits presented by Morphew *et al.* (2014), where present, were searched against GenBank or WormBase ParaSite databases as described (2.4.3) to identify the highest scoring *F. hepatica* orthologues, and successful PCRs finalised hit selections (Table 4.4.1.1).

Table 4.4.1.1. Biomarkers of interest identified by Morphew *et al.*, (2014) and pre-selected as diagnostic candidates for *Fasciola hepatica*.

Biomarker	Drug response phenotype	Top hit accession (Genbank)	*F. hepatica* orthologue selected (identifier)	Percentage identity to original hit (E value)	Sequence length (bp)/(aa)
Actin	Termination	XP_002575979	BN1106_s101B000531.mRNA-1	96.8% (0.0)	1131 / 376
Calreticulin	Survival	Unassigned	BN1106_s2673B000071.mRNA-1	n/a	1269 / 422
DJ-1	Termination	AAW26651	BN1106_s1971B000297.mRNA-1	63.2% (9.4E-73)	552 / 183
Enolase	Survival	AAA57450	AAA57450.1	n/a	1449 / 431
Gelsolin	Termination	XP_002572334	D915_01476	62.6% (1.4E-44)	1095 / 364
Glyceraldehyde-3-phosphate dehydrogenase	Survival	AAG23287	AIE44418.1	75.5% (2.0E-107)	1017 / 338
Triose phosphate isomerase	Termination	ABS19444	AGJ83762.1	68.0% (1.0E-117)	1014 / 253

4.4.1.2 Actin (FhACT)

4.4.1.2.1 FhACT family association and structural assessments

FhACT (PRJEB6687, WBPS v10: BN1106_s101B000531.mRNA-1; scaffold 101: 37,533–38,663; one exon) was predicted with actin protein family association using WormBase ParaSite with cross-referencing from InterPro. FhACT was matched to the actin superfamily (IPR004000) by PANTHER (1–376), Pfam (4–376), and SMART (6–376). Actin signatures were also identified by PRINTS (27–36, 50–61, 62–84, 116–121, 141–160, 237–253), predicting

conservation of FhACT with the 1ATN model DNASE I complex. Further family-specific actin and actin-like protein domains and signatures were matched by Gene3D (9–138, 139–180, 274–339, 340–372: actin-related protein; 181–273: actin chain A, domain 4), Superfamily (5–154, 147–376: actin-like ATPase domain), and PROSITE (54–64, 357–365: actin, conserved domain IPR004001; 105–117: actin/actin-like, conserved domain IPR020902). NCBI also assigned nucleotide binding capabilities to N-terminal (9–182) FhACT residues, based on sequence conservation with nucleotide binding domains of sugar kinase, heat shock protein 70 and actin superfamilies (12D, 13N, 14G, 15S, 17M, 19K, 138Q, 155D, 156S, 157G, 158D).

Further FhACT actin-related protein functions were identified through gene ontology (GO) terms, including involvement in the cell cycle (GO:0007049), endocytosis (GO:0006897), exocytosis (GO:0006887), intracellular protein transport (GO:0006886), actin cytoskeleton organization (GO:0030036) and leukocyte migration (GO:0050900) biological processes. Localisation into cellular components was also predicted, including the molecular function as a structural constituent of cytoskeleton (GO:0005200), as well as direct associations with intracellular (GO:0005622), adherens junction (GO:0005912), bicellular tight junction (GO:0005923) and focal adhesion (GO:0005925) cellular pathways.

The hypothetical 3-D structure of FhACT was produced using Phyre2 (Figure 4.4.1.2.1A) as based on a multi-template analysis against the two highest scoring model templates, which aligned 96% of FhACT residues (3–373) with 100% confidence (Figure 4.4.1.2.1B). These models were *Oryctolagus cuniculus* skeletal muscle actin (92% ID; 1O1F, PDB: www.rcsb.org/structure/1O1F) and *Komagataella phaffii* actin-1 (84% ID; 4PL7, PDB: www.rcsb.org/structure/4PL7), whereas the third highest-scoring model was the *Sus scrofa* actin-related motor protein dynactin (54% ID; 5AFU, www.rcsb.org/structure/5AFU).

FhACT consists of 10 arrays of alpha-helices interrupted by eight short-length beta-pleated sheets, including two larger sheets at the N-terminus and mid-N terminal regions (Figure 4.4.1.2.1A). Phyre2 structural modelling predicted the tertiary structure of FhACT to be highly similar to other Eukaryotic actin monomers (Dominguez and Holmes, 2011; Pollard, 2016; Sheterline *et al.*, 1999), with a highly-folded, flat structure comprised of four subdomains with inter-domain grooves, a central cleft, and both amino and carboxyl termini folded into subdomain one (Figure 4.4.1.2.1A). Major loops are formed with structural and functional significance, including the β-hairpin (H-, Asp_{11}–Cys_{17}), sensor (S-, Pro_{70}–Asp_{78}), and

DNase I-binding (D-, Arg_{39}–Asp_{51}) loops (Dominguez and Holmes, 2011; Graceffa and Dominguez, 2003; Kudryashov *et al.*, 2010).

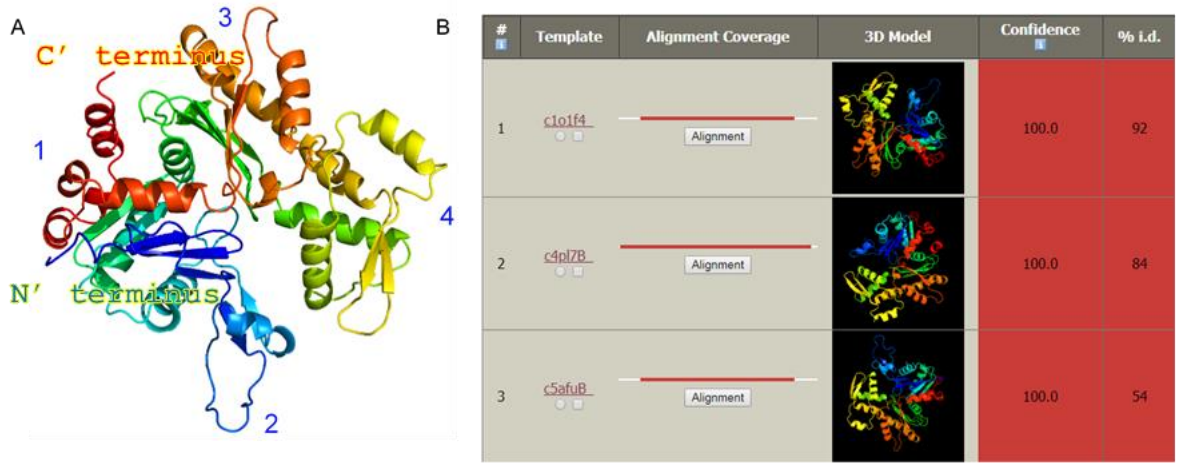

Figure 4.4.1.2.1. 3-D prediction and model templates for FhACT using Phyre2. The 3-D protein structure was predicted for FhACT, showing four (1–4) major subdomains in its tertiary structure (A). This prediction was based on FhACT sequence modelling with the two highest-scoring templates of three high scoring models shown (B), including two muscle-associated actins (PDB: 1O1F, 4PL7) and one dynactin (PDB: 5AFU) model templates.

As documented in model actins, FhACT demonstrates a major central cleft between subdomains 3 and 4 (pointed end) and a larger target-binding groove between subdomains 1 and 3 (barbed end) (Figure 4.4.1.2.1A), the angular positioning of which is critical for filament extension (Dominguez and Holmes, 2011; Pollard, 2016). This quaternary structure also involves interactions of multiple exposed residues, at the domain and inter-domain level (Dominguez, 2004; Dominguez and Holmes, 2011; Pollard, 2016). Notably the domain 1 hydrophobic pocket, the 1–3 inter-domain hydrophobic cleft residues (HsACT-1; P60709, UniProt, www.uniprot.org/uniprot/P60709; Tyr_{143}, Ala_{144}, Gly_{146}, Thr_{148}, Gly_{168}, Ile_{341}, Ile_{345}-Leu_{346}, Thr_{351}, Met_{355}) and outlying residues of domain 3 (Met_{283}, Ile_{287}, Asp_{288}; Pro_{322}, Met_{325}) and 4 (Pro_{243}–Gly_{245}) are important for longitudinal polymer stability (Dominguez and Holmes, 2011), as well as key sites for actin-binding proteins (Dominguez, 2004).

4.4.1.2.2 FhACT sequence conservation and functionality

Sequence, structural and functional conservation of FhACT with model proteins was investigated through phylogenetic analysis against *Schistosoma mansoni*, *Caenorhabditis elegans*, *Homo sapiens* and *Oryctolagus cuniculus* ACTs (Figure 4.4.1.2.2.1). Data here support

extensive literature and phylogenetic analyses suggesting high ACT sequence conservation (Dominguez and Holmes, 2011; Pollard, 2016), particularly between the trematode genera examples tested here (Figure 4.4.1.2.2.1B: 91.76–99.20; B–C: FhACT-SmACT-1/putative ≥96.81–97.07%, 0.028–0.0034 units of evolutionary distance). FhACT demonstrates only minor residue variation at the N-terminal compared with mammalian and nematode ACTs (Figure 4.4.1.2.2.1A). Residues of functional and structural importance (Dominguez, 2004; Dominguez and Holmes, 2011; Graceffa and Dominguez, 2003), including those important for polymerisation (Kudryashov *et al.*, 2010; Mundia *et al.*, 2012), were also conserved (Figure 4.4.1.2.2.1A).

Conserved active sites and ligand binding activities of FhACT were investigated using 3DLigandSite based on the final model calculated by Phyre2, with 96% residues modelled at >90% confidence (Figure 4.4.1.2.2.2). 21 residues between Gly^{14} and Trp^{357} of FhACT were predicted to have ligand binding properties with significant structural alignment scores (42.9≤43.0 average MAMMOTH score). Heterogens included calcium and magnesium metal ions, and adenosine-5'-diphosphate (ADP) and adenosine-5'-triphosphate (ATP) non-metallic ligands (Figure 4.4.1.2.2.2). These findings are in-keeping with previous evidence for these divalent cations binding to G-actin for monomer activation and F-actin for filament elongation (Cooper *et al.*, 1983) by stimulating ATP and ADP binding for filament polymerisation and depolymerisation, respectively (Dominguez and Holmes, 2011; Pollard, 2016).

It has been found that the filamentous state of actin enhances its ATPase activity and the exposure of each monomer's target-binding cleft, permitting interactions between longitudinal filaments and multiple actin-binding proteins through the conformational changes induced by ATP hydrolysis (Dominguez, 2004; Dominguez and Holmes, 2011; Pollard, 2016). Furthermore, Cooper *et al.*, (1983) demonstrated the kinetic differences between cation concentration for actin treadmilling, whereby the polymerisation rate is faster in the presence of magnesium compared to calcium, which could explain the respective binding availabilities of five or 19 metal ions by FhACT (Figure 4.4.1.2.2.2).

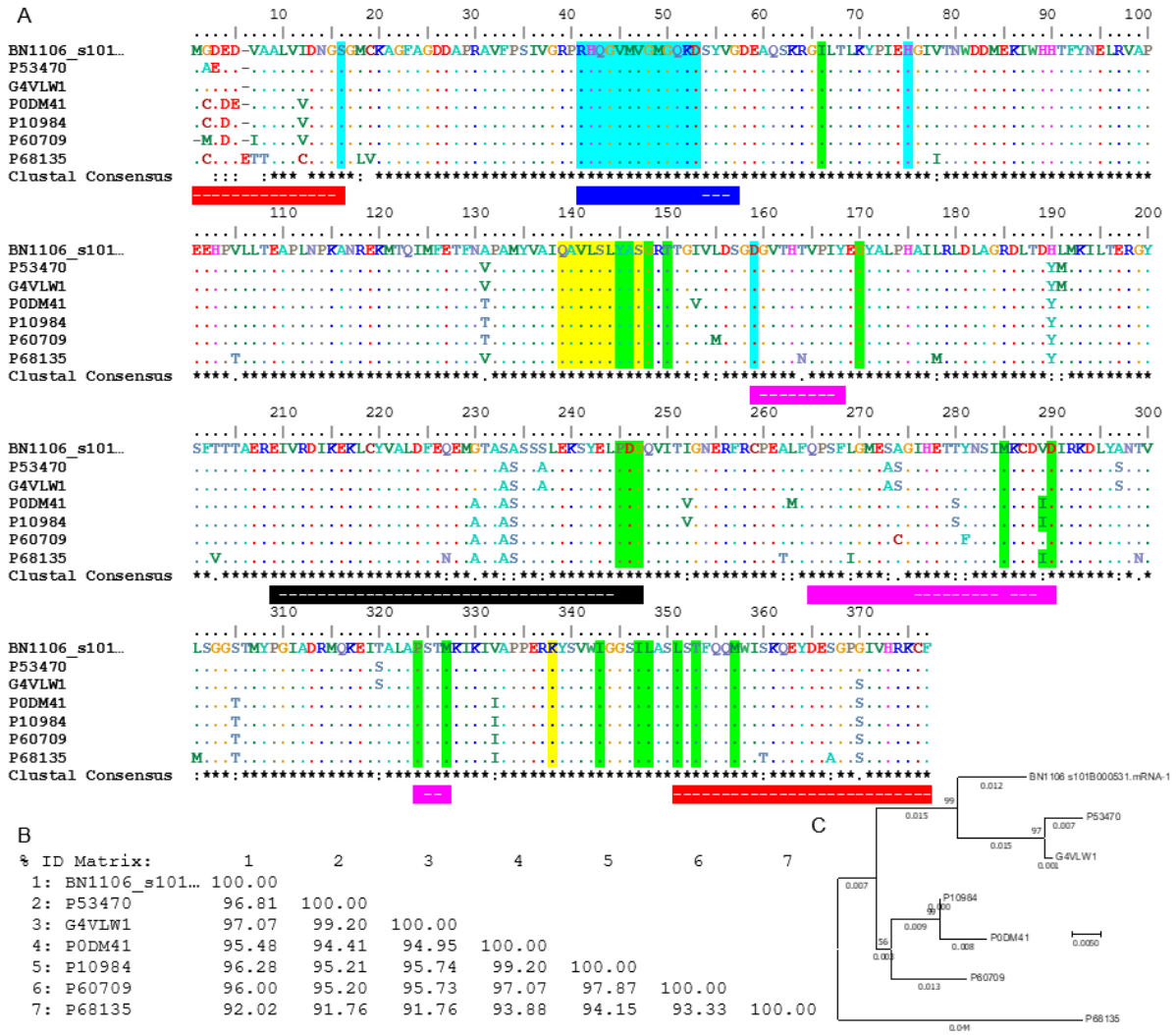

Figure 4.4.1.2.2.1. Phylogenetic analysis of *Fasciola hepatica* (FhACT), model and related parasite ACTs. The selected *F. hepatica* isotype FhACT (BN1106_s101B000531.mRNA-1) was aligned with actin-1, actin-2 and putative actin proteins from *S. mansoni* (SmACT-1: Smp_046600, P53470, www.uniprot.org/uniprot/P53470; *S. mansoni* putative actin: Smp_183710, G4VLW1, www.uniprot.org/uniprot/G4VLW1), *C. elegans* (CeACT-1: T04C12.6, P0DM41, www.uniprot.org/uniprot/P0DM41; CeACT-2: T04C12.5, P10984, www.uniprot.org/uniprot/P10984), *H. sapiens* (HsACT-1: 3LUE, P60709, www.uniprot.org/uniprot/P60709) and *O. cuniculus* (OcACTA1: 1O1F, P68135, www.uniprot.org/uniprot/P68135). (A) The sequence alignment demonstrated very high sequence conservation, with the greatest variation only at the first 6 N-terminal residues. Highlighted residues indicate amino acids of importance, including for actin-associated molecular functions (highlighted in turquoise) and inter-domain (highlighted in yellow) and longitudinal filament (highlighted in green) interactions. Approximate subdomain allocation is indicated (1, red; 2, blue; 3, pink; 4, black) based on residues described in literature (Dominguez and Holmes, 2011), or inferred from 3-D model interpretation shown as "-". (B) Percentage identities indicated highest sequence similarity between ACT isoforms of *S. mansoni* and *C. elegans* (both 99.20%), followed by CeACT2 and HsACT-1 (97.87%), FhACT and SmACT-1, and CeACT-1 and HsACT-1 (both 97.07%). All sequences except OcACTA1 shared above 95.48% sequence similarity with FhACT. (C) The phylogenetic tree reflected these close relationships, highlighting the

phylogenetic distance of OcACTA1. ClustalO and MEGA7 were used to produce the alignment and phylogenetic tree, respectively.

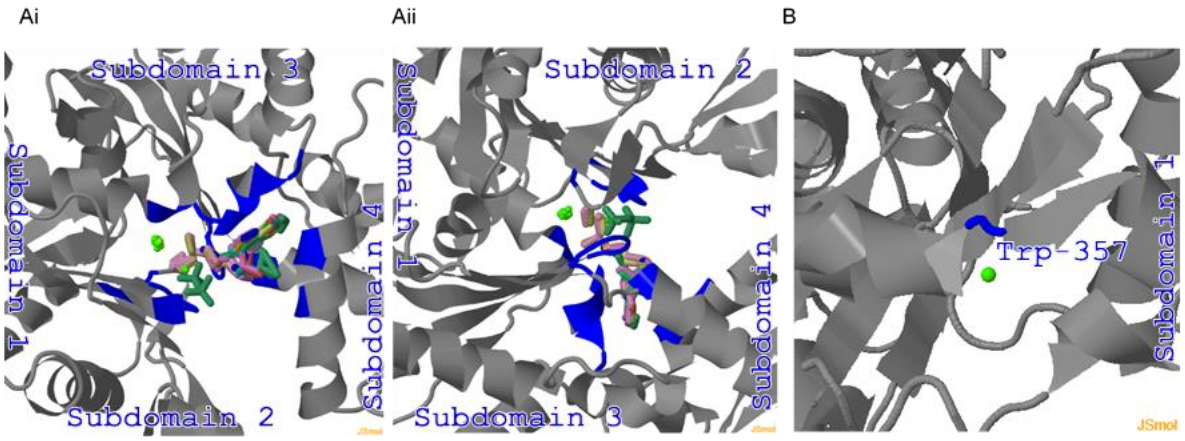

Figure 4.4.1.2.2.2. 3-D predictions of FhACT-ligand binding using 3DLigandSite. The complete FhACT protein expression sequence was used to predict FhACT-ligand interfaces based on sequence similarity to known protein-ligand interactions. Two different residue clusters of ligand binding residues were predicted (A–B), calculated by the 'matching molecular models obtained from theory' approach (MAMMOTH; Ortiz, Strauss and Olmea, 2002). Both metallic (calcium, pale green; magnesium, lime green) and non-metallic (stick models) ligands were predicted at multiple residues, including magnesium (n = 5) (A), calcium (n = 19) (A–B), adenosine-5'-diphosphate (ADP, n = 1) (A) and adenosine-5'-triphosphate (ATP, n = 24) (A) mediated by 21 different residues in the protein between Gly^{14}-Lys^{337} (A); and Trp^{357} (B).

4.4.1.3 Calreticulin (FhCRT)

4.4.1.3.1 FhCRT family association and structural assessments

FhCRT (PRJEB6687, WBPS v10: BN1106_s2673B000071.mRNA-1; scaffold 2673: 17,986–19,605; four exons) was predicted with calreticulin- and calnexin-associated family association using WormBase ParaSite with cross-referencing from InterPro. FhCRT was matched to the calreticulin/calnexin family (IPR001580) by PANTHER (7–387), Pfam (24–331) and PRINTS (99–117, 125–141, 214–227, 241–263, 279–298, 312–332) and to calreticulin family (IPR009196) by PIRSF (1–409). Family-specific domains were further predicted to a concanavalin A-like lectin/glucanase domain (IPR013320) and a calreticulin/calnexin-associated P domain (IPR009033) by Gene3D (N: 13–256; C: 278–299, respectively) and Superfamily (N:17–218; C: 200–314, respectively). C terminal coiled-coils (Ncoils: 352–409) were also predicted. SignalP identified residues 1–44 with signalling association (Y-score), but

a significant cleavage score (C-score) at residue 19 and high signalling score (S-score) 1-21 residues (Figure 4.4.1.3.1).

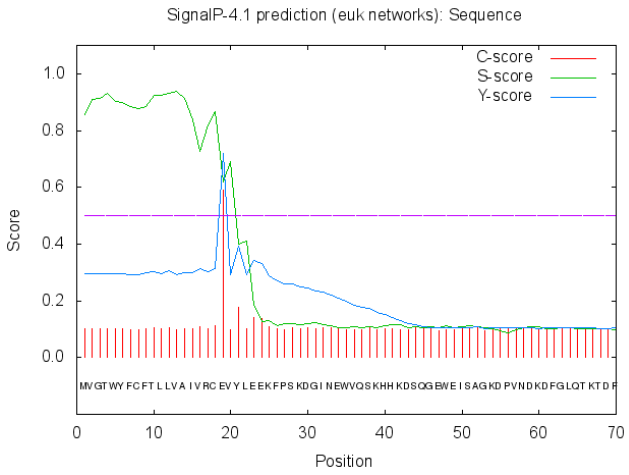

Figure 4.4.1.3.1.1. Protein signalling prediction of FhCRT using SignalP. Residues 1–44 had a signalling peptide score (Y-score), however the only significant scores predicting a cleavage site was at residue 19, with a signalling peptide likely between residues 1–19 in FhCRT.

Further FhCRT calreticulin-related protein functions were identified, including calreticulin/calnexin conserved sites (IPR018123) matched by PROSITE (97–112, 129–137). Calreticulin-associated GO-terms were also identified, including calcium ion (GO:0005509), protein (GO:0005515) and unfolded protein (GO:0051082) binding functions, protein folding (GO:0006457) biological processes, and involvement in the endoplasmic reticulum (GO:0005783) cellular pathway.

The hypothetical 3-D structure of FhCRT was produced using Phyre2 (Figure 4.4.1.3.1.2A) as based on a multi-template analysis against the two highest scoring model templates, which aligned 83% of FhCRT residues (15-366) with 100% confidence (Figure 4.4.1.3.1.2B). These models were the *Canis lupus* calnexin luminal domain (40% ID; 1JHN, PDB: www.rcsb.org/pdb/structure/1JHN) and the *Mus musculus* calreticulin lectin and arm domain (51% ID; 3RG0, PDB: www.rcsb.org/pdb/structure/3RG0). Further matched model templates included the *M. musculus* lectin domain (50% ID; 3O0V, PDB: www.rcsb.org/pdb/structure/3O0V), and the *Entamoeba histolytica* (43% ID; 5HCA, PDB: www.rcsb.org/structure/5HCA) and *Trypanosoma cruzi* (41% ID; 5HCF, PDB: www.rcsb.org/structure/5HCF) calreticulin globular domains, indicating similarity with CRTs of tissue-invading parasites that have identified putative immunomodulatory functions and pathogenesis association (Aguillón *et al.*, 2000, 1995; Ferreira *et al.*, 2005; González *et al.*, 2011; Ribeiro *et al.*, 2009; Vaithilingam *et al.*, 2012; Ximénez *et al.*, 2014).

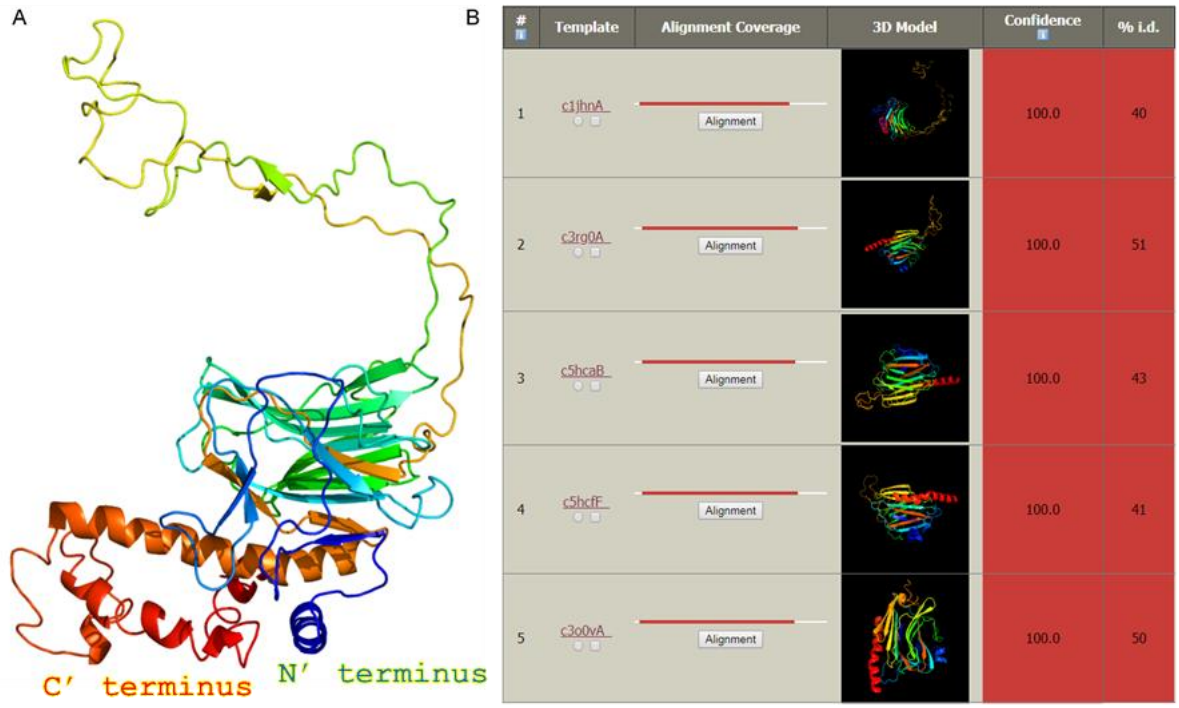

Figure 4.4.1.3.1.2. 3-D prediction and model templates for FhCRT using Phyre2. The 3-D protein structure was predicted for FhCRT (A), showing two arrays of anti-parallel beta-pleated sheets and two long alpha helices forming a putative lectin domain interrupted by a putative arm domain. This prediction was based on FhCRT sequence modelling with the two highest-scoring templates of five high scoring models shown (B), including a calnexin luminal domain from *Canis lupus* (PDB: 1JHN) and a calreticulin from *Mus musculus* for MmCRT lectin domain (PDB: 3RG0).

Based on the 3-D model predictions (FhCRT, Figure 4.4.1.3.1.2A) and X-ray crystallography of the model bearing the closest resemblance (MmCRT, 3RG0 (Pocanschi *et al.*, 2011)), the Phyre2 Investigator further confirmed many structural characteristics were highly conserved. The secondary structure of FhCRT consists of two interfacing arrays of nine- and six-mer anti-parallel beta-pleated sheets, including at N- (lectin N-domain), mid and C- (C-domain) terminal residues, interrupted by a mid-region 104 residue-long C-shaped loop or "arm" (P-domain) containing two short-length anti-parallel beta motifs at the centre (Figure 4.4.1.3.1.2A). Adjacent lectin and arm domains are associated with CRT functionality, forming a carbohydrate binding pocket, which appears to be highly conserved (Guo *et al.*, 2003) and also demonstrable in the predicted 3-D model of FhCRT. At the C-terminal, four sequential alpha-helices of 1, 2.5, 4 and 8 turns are also present (Figure 4.4.1.3.1.2A), and N-terminal residues of FhCRT were the only extracellular portion predicted, consistent with SignalP calculations (Figure 4.4.1.3.1.1) in addition to 15 residues (12–27) of a predicted insoluble

transmembrane helix, and PSORTII also confirmed these findings as well as hypothetical cellular localisations, predicting a cleavage site between residues 18-19 (von Heijne's method) and localisation to the cytoplasm (55.5% probability; Reinhardt's method for cytoplasmic/nuclear discrimination) and extracellular matrix (ECM) (44.4% probability; *k*-Nearest Neighbour prediction, *k* = 9/23).

4.4.1.3.2 FhCRT sequence conservation and functionality

Sequence, structural and functional conservation of FhCRT with other model proteins was investigated through phylogenetic analysis against *Schisotoma mansoni*, *Caenorhabditis elegans*, *Homo sapiens*, *Mus musculus* and *Oryctolagus cuniculus* CRTs (Figure 4.4.1.3.2.1). Data indicated moderate sequence conservation with the highest residue variations at N- and C-terminals between the trio of helminth and mammalian CRTs (Figure 4.4.1.3.2.1A), notwithstanding demonstrable conservation of important CRT-specific structural motifs. Mutagenesis studies of mouse and rabbit CRT have identified further functionally and structurally important residues, including two cysteines in the lectin domain which form a crucial disulfide bond, as well as tyrosine, methionine, aspartate and tryptophan residues involved in CRT-glycan interactions, and protein binding and folding at the ER (Guo *et al.*, 2003; Martin *et al.*, 2006; Kozlov, *et al.*, 2010). These residues are shown (Figure 4.4.1.3.2.1A) and were here found to be conserved in FhCRT alongside all other aligned sequences, supporting their importance in CRT-associated roles for cell homeostasis. The percentage ID matrix and phylogenetic tree also support the overall evolutionary distances between the helminth and mammalian sequence but highlight the closeness of human and rabbit CRT (Figure 4.4.1.3.2.1B–C).

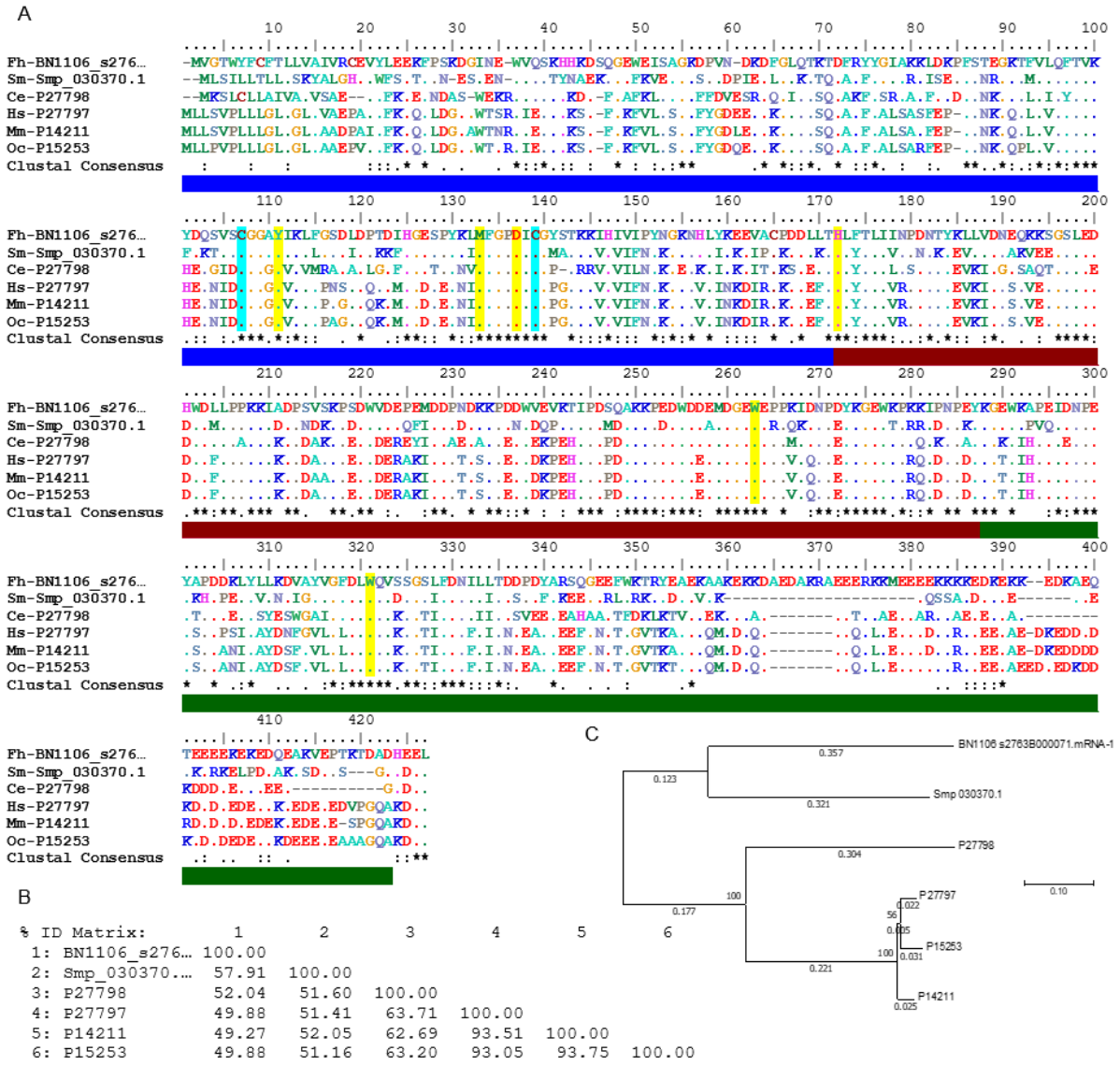

Figure 4.4.1.3.2.1. Phylogenetic analysis of *Fasciola hepatica* (FhCRT), model and related parasite CRTs. The selected *F. hepatica* isotype FhCRT (BN1106_s276B000071.mRNA-1) was aligned with CRT and CNX models, including *S. mansoni* (SmCRT: Sm_030370.1), *C. elegans* (CeCRT-1: Y38A10A.5, P27798, www.uniprot.org/uniprot/P27798), *H. sapiens* (HsCRT globular domain: 3POS, 3POW, P27797, www.uniprot.org/uniprot/P27797), *M. musculus* (MmCRT lectin and arm domains: 3RG0, P14211, www.uniprot.org/uniprot/P14211; MmCRT lectin domain: 3O0V, P14211, www.uniprot.org/uniprot/P14211) and *O. cuniculus* (OcCRT: CALR, P15253, www.uniprot.org/uniprot/P15253). (A) The sequence alignment demonstrated low sequence conservation between all CRTs excluding murine and leporine sequences, with the highest variation within approximately 40 N- and C-terminal residues. Highlighted regions indicate amino acids of functional (highlighted in yellow), and structural and functional (highlighted in turquoise) importance, as well as calreticulin N (1–169 aa), P (170–284 aa) and C (285-400 aa) domains based on literature for HsCRT and MmCRT (Michalak *et al.*, 1999). (B) Percentage identities indicated low sequence similarity, except for murine-leporine (93.05–93.75%), with mammalian ACTs (62.69–63.71%) being followed by FhCRT-SmCRT (57.91%), followed by trematode CRTs with CeCRT (Fh-Ce: 52.04%; Sm-Ce: 51.60%). (C) The phylogenetic tree reflected

the closeness of these relationships, highlighting phylogenetic distances of mammalian and helminth sequences. ClustalO and MEGA7 were used to produce the alignment and phylogenetic tree, respectively.

Table 4.4.1.3.2. Predicted FhCRT ligand binding. FhCRT-ligand interfaces were predicted based on sequence similarity to known protein-ligand interactions using 3DLigandSite. 11 different clusters were based on structural alignments between FhCRT and similar residue-ligand interactions, with significant scores calculated by the MAMMOTH approach (Ortiz, Strauss and Olmea, 2002). Both metallic and non-metallic ligands were predicted at 11 hypothetical clusters of single and/or multiple amino acids, mediated by 17 different residues in the protein (aa 40–308). Abbreviations: BMA, beta-D-mannose; Ca, calcium; GAL, beta-D-galactose; NAG, *N*-acetyl-D-glucosamine; NGA, N-acetyl-D-galactosamine.

MAMMOTH Score (averaged)	Interacting residues	Ligand (n)
13.3	Leu^{307}-Lys^{308}	Ca^{2+} (1)
12.6	Gly^{123}	Ca^{2+} (2)
12.6	Ser^{125}	Ca^{2+} (2)
12.5	Met^{130}, Leu^{155}	BMA (1); GAL (16); NAG (13); NGA (1)
12.5	Leu^{306}-Leu^{307}	Ca^{2+} (1)
12.5	Asn^{328}, Phe^{345}	Ca^{2+} (1)
12.0	Gly^{123}	Ca^{2+} (1)
12.0	Ser^{125}	Ca^{2+} (1)
11.9	Ser^{139}, Lys^{141}, Asp^{164}- Asp^{165}	GAL (1)
11.8	Leu^{306}-Lys^{308}	Ca^{2+} (1)
11.4	His^{40}, Lys^{42}, His^{122}-Ser^{125}	GAL (1)

Conserved active sites and ligand binding activities of FhCRT were investigated using 3DLigandSite based on the final model calculated by Phyre2, with 81% of residues modelled at >90% confidence (Table 4.4.1.3.2; Figure 4.4.1.3.2.2). 17 residues of FhCRT between 40–308 aa were predicted with ligand binding properties, producing significant structural alignment scores (11.4≤13.3 average MAMMOTH score, Table 4.4.1.3.2), and the top three scoring clusters are shown (Figure 4.4.1.3.2.2). Metallic ligands included calcium and non-metallic heterogens included beta-D-mannose (BMA), beta-D-galactose (GAL), N-acetyl-D-glucosamine (NAG) and N-acetyl-D-galactosamine (NGA) monosaccharides. Eight FhCRT-ligand clusters were predicted to bind calcium alone, with one, two or three residues binding to one or two ions, whereby residue number did not reflect the number of ligands bound, suggesting low binding affinity. Interestingly, only one residue (Gly123) was predicted with both metallic and non-metallic ligand-binding properties, which supports the separation of glycan and calcium binding activities (Kozlov, *et al.*, 2010). Three clusters were predicted with non-metallic binding properties to monosaccharides common to glycoproteins, including NAG which is responsible for common O-linked *N*-glycosylation of nucleocytoplasmic glycoproteins (Hart *et al.*, 2007; Zachara *et al.*, 2004). CRTs are known to recognize monoglucosylated

Glc1Man9GlcNAc2 glycan moieties, and these predicted activities are in-keeping with calcium-dependent binding to *N*-oligosaccharide glycosylated proteins that are ER-associated post-translational modifications (Kannicht and Fuchs, 2008; Spiro, 1970; Vassilakos *et al.*, 1998). These putative findings for FhCRT suggest capacity for binding glycan motifs and glycoproteins and protein chaperoning functions.

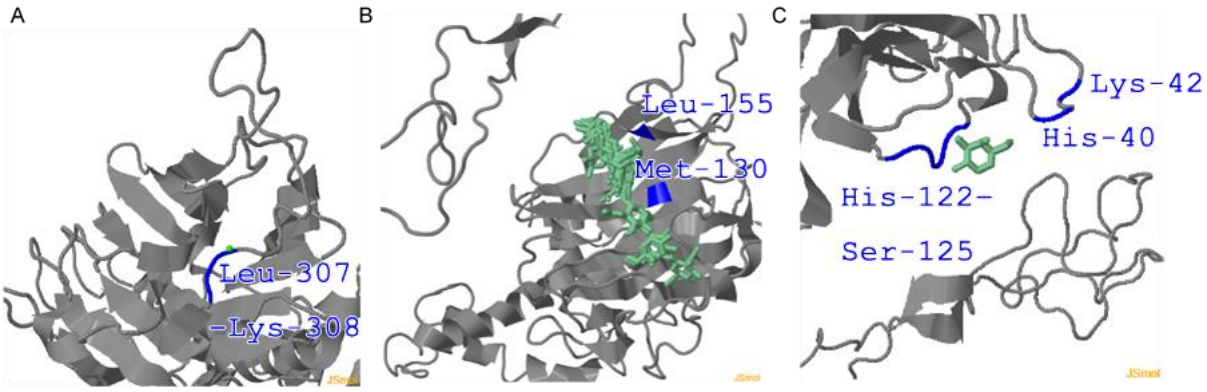

Figure 4.4.1.3.2.2. 3-D predictions of FhCRT-ligand binding using 3DLigandSite. FhCRT-ligand interactions were predicted based on sequence similarity to known protein-ligand interactions. The three highest scoring ligand-binding clusters were calculated by the MAMMOTH approach (Ortiz, Strauss and Olmea, 2002). Three representative clusters with MAMMOTH scores of 13.3 (A), 12.5 (B) and 11.9 (C) of the 11 predicted for FhCRT are shown.

4.4.1.3.3 Truncated calreticulin (FhΔCRT)

The N-terminal signal peptide of FhCRT responsible for the predicted transmembrane region and loss of recombinant target overexpression was removed by truncation as described (4.3.1.1.3; 4.4.2.4). The new truncated FhCRT (FhΔCRT) sequence was confirmed to have no signal peptide using SignalP (data not shown).

4.4.1.4 DJ-1 deglycase (FhDJ-1)

4.4.1.4.1 FhDJ-1 family association and structural assessments

FhDJ-1 (PRJEB6687, WBPS v10: BN1106_s1971B000297.mRNA-1; scaffold: 1971: 311,148–311,699; one exon) was predicted with DJ-1-associated functional and structural domains using WormBase ParaSite with cross-referencing from InterPro. FhDJ-1 was matched to the class I glutamine amidotransferase-like superfamily (IPR029062) by Gene3D (1–183), Superfamily (5–182) and NCBI with a conserved cysteine residue (5–167, 104C), and the

protein/nucleic acid deglycase DJ-1 family (IPR006287) by TIGRFAM (5–178). Further family-specific DJ-1 and Pfpl domains (IPR002818) were matched by Pfam (4–165). PANTHER identified FhDJ-1 to an unnamed protein family (PTHR43444) containing many DJ-1 proteins including model organism orthologues, and with multiple DJ-1-associated GO-terms as follows. FhDJ-1-associated GO-terms included transcription coregulatory molecular function (GO:0003712), biosynthesis (GO:0009058), cellular processing (GO:0009987), nitrogenous compound metabolism (GO:0006807), RNA polymerase II transcription regulation (GO:0006357) and stress response biological pathways (GO:0006950). Prediction within cellular pathways were also predicted, including cytosolic (GO:0005829), mitochondrial (GO:0005739) and nuclear (GO:0005634) localisations.

To investigate any signal peptide, SignalP was used to identify a hypothetical signal sequence and cleavage site (data not shown). Residues 1–37 were predicted with signalling association (Y-score), 19-LYS with a cleavage score (C-score) of >0.3 and the preceding residues 1–18 with small signalling scores (S-score). However, no scores were significant, suggesting FhDJ-1 does not have a transmembrane domain or signalling peptide.

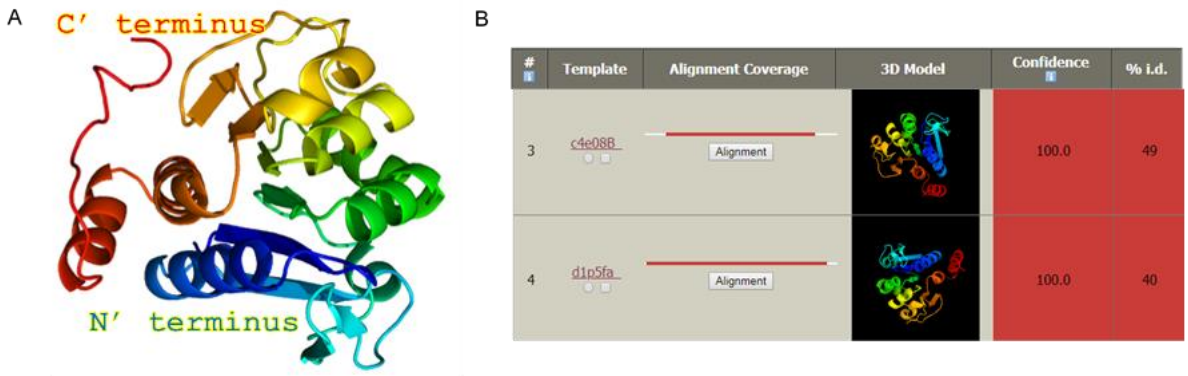

Figure 4.4.1.4.1. 3-D prediction and model templates for FhDJ-1 using Phyre2. The 3-D protein structure was predicted for FhDJ-1, showing an array of beta-pleated sheets sandwiched by three sets of short-length alpha helices (A). This prediction was based on FhDJ-1 sequence modelling with the two highest-scoring templates shown (B), including DJ-1 proteins from *D. melanogaster* (PDB: 4E08) and *Homo sapiens* (PDB: 1P5F).

Structural properties and conserved epitopes were predicted for FhDJ-1 using Phyre2. The hypothetical 3-D structure of FhDJ-1 was produced as based on a multi-template analysis with the two highest scoring model templates for DJ-1, 4E08 (PDB: www.rcsb.org/structure/4E08) and 1P5F (PDB: www.rcsb.org/structure/1P5F; i.e. HsDJ-1/*HsPARK7*), which aligned 94% of FhDJ-1 residues (1–183) with 100% confidence (Figure

4.4.1.4.1). The secondary structure of FhDJ-1 consists of eleven strands in a parallel beta-pleated sheet which are sandwiched by eight short-length alpha-helices (Figure 4.4.1.4.1A), which is the same αβ ratio of HsDJ-1 (Honbou *et al.*, 2003).

The tertiary structure of FhDJ-1 is compact due to the arrangement of alpha helices closely flanking the beta sheets, with the additional C-terminal alpha helix folded towards a substrate cleft between two flanking anti-parallel alpha helices (Figure 4.4.1.4.1A). FhDJ-1 also demonstrates the formation of a Rossmann-like fold due to the alpha-beta-alpha motif arrangement, which is described in monomeric HsDJ-1 (Honbou *et al.*, 2003). The predicted peripheral C- and N-terminal alpha helices and N-terminal beta sheets of FhDJ-1 is also shared with HsDJ-1, which are involved in the natural homodimerization of this protein (Honbou *et al.*, 2003; Tao and Tong, 2003; Wilson *et al.*, 2003), as well as high molecular weight complexes (Baulac *et al.*, 2004), suggesting FhDJ-1 may have the potential to form asymmetric dimeric and further polymeric quaternary structures.

4.4.1.4.2 FhDJ-1 sequence conservation and functionality

To identify DJ-1 sequence conservation, sequences from *Schistosoma mansoni*, *S. japonicum*, *Caenorhabditis elegans*, *Homo sapiens*, and *Drosophila melanogaster* were aligned with FhDJ-1 and a phylogenetic tree was produced (Figure 4.4.1.4.2.1). Data indicated low conservation between all sequences, but HsPARK7 and FhDJ-1 demonstrated the greatest divergence based on protein sequence percentage identities and phylogenetic assessments (Figure 4.4.1.4.2.1B–C). The sequence alignment also indicated FhDJ-1 possessed residues that were otherwise partially conserved between sequences of *Schistosoma spp.* and the other three models (Figure 4.4.1.4.2.1A). Furthermore, greatest diversity between all sequences was demonstrable at the N–mid, mid-sequence and C-terminal regions of these proteins, together suggesting little conservation at non-essential residues that may also be species-specific.

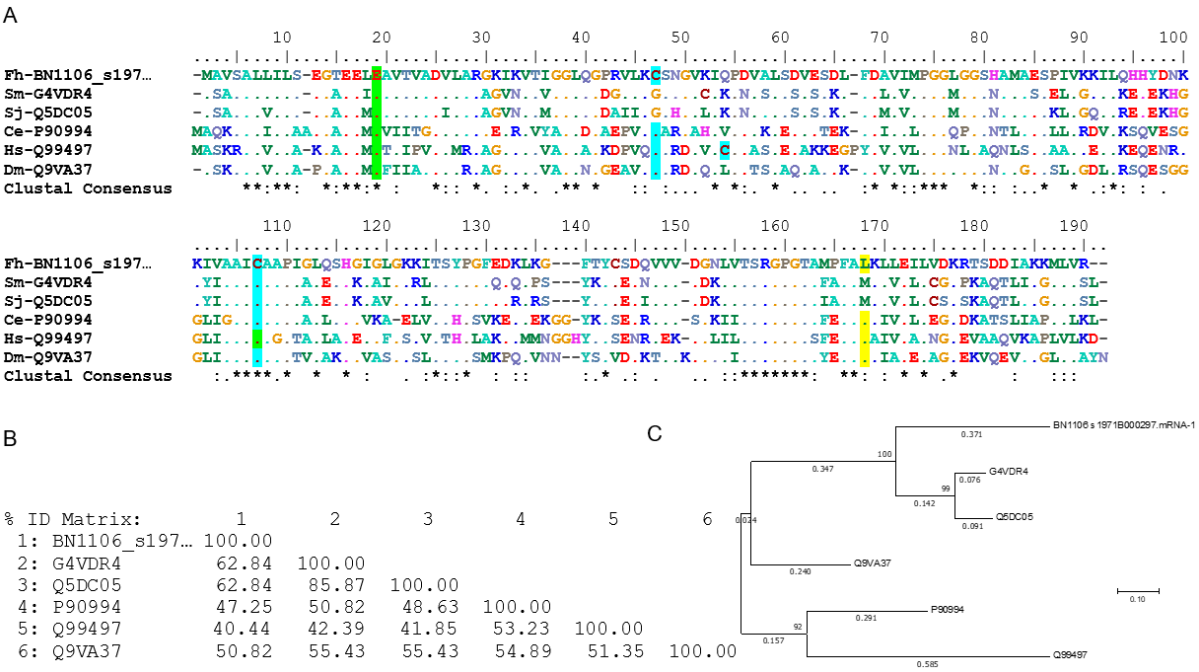

Figure 4.4.1.4.2.1. Phylogenetic analysis of *Fasciola hepatica* (FhDJ-1), model and related parasite DJ-1s. The selected *F. hepatica* isotype FhDJ-1 (BN1106_s1971B000297.mRNA-1) was aligned with DJ-1 and DJ-1-like proteins of *S. mansoni* (Sm family C56 non-peptidase homologue: Smp082030.1, G4VDR4, www.uniprot.org/uniprot/G4VDR4), *S. japonicum* (Sj hypothetical protein: SJCHGC05973, Q5DC05, www.uniprot.org/uniprot/Q5DC05) *C. elegans* (CeDJR-1.1: B0432.2, P90994, www.uniprot.org/uniprot/P90994), *H. sapiens* (HsDJ-1/*HsPARK7*: 1P5F, Q99497, www.uniprot.org/uniprot/Q99497) and *D. melanogaster* (DmDJ-1β: 4E08, Q9VA37, www.uniprot.org/uniprot/Q9VA37). (A) The sequence alignment demonstrated moderate–low sequence conservation, with a small proportion of conserved residues and the highest sequence variation between mid-sequence and C-terminal residues. Highlighted residues indicate amino acids of importance, including for oligomerization (highlighted in yellow), oxidative stress sensing (highlighted in turquoise), and a proposed catalytic triad (highlighted in green) as described HsDJ-1 and involving two residues (Honbou *et al.*, 2003; Tao and Tong, 2003; Wilson *et al.*, 2003). (B) The percentage identity matrix indicated high sequence similarity between *Schistosoma spp.* (85.87%) and all trematode (62.84–85.87%) sequences, whereas low similarity was observed between trematode and non-trematode DJ-1s (40.44–55.43%). (C) The phylogenetic tree reflected these phylogenetic distances, with units of evolutionary distance particularly highlighting the relative closeness of trematode DJ-1s. ClustalO and MEGA7 were used to produce the alignment and phylogenetic tree, respectively.

Several residues of functional and structural importance are shown (Figure 4.4.1.4.2.1A), whereby missense mutations of these amino acids in HsDJ-1/*HsPARK7* can negatively influence biochemical stability and oligomerization, disrupting the normal oxidative stress response (Junn *et al.*, 2009; Park *et al.*, 2005; Taira *et al.*, 2004; Takahashi-

Niki *et al.*, 2004) and contributing to human Parkinsonism (Baulac *et al.*, 2004; Bonifati *et al.*, 2003; Honbou *et al.*, 2003; Olzmann *et al.*, 2004; Wilson *et al.*, 2003). A putative catalytic triad is also shown, based on HsDJ-1 crystallography, whereby two residues of a DJ-1 monomer interact with a Glu residue-contributing protease (Honbou *et al.*, 2003; Tao and Tong, 2003; Wilson *et al.*, 2003). Folding of the DJ-1 polymer is also fitting with the control of enzymatic activities proposed at this catalytic triad, with conformational changes facilitating concealment or exposure of these residues with an inwardly-folded C-terminal helix of HsDJ-1_2 (Honbou *et al.*, 2003). When considering possible residue losses through evolutionary divergence and discrepancies upon realignment here, residues of importance in HsDJ-1 appear to be fully conserved in FhDJ-1 (Figure 4.4.1.4.2.1A), including those that have the potential to cause loss of human enzyme function (Bonifati *et al.*, 2003). No helminth DJ-1s have been characterised despite known glutathione interactions (Lee *et al.*, 2012; Zhou and Freed, 2005), the ligand of the GST protein family that is well-described in *F. hepatica* xenobiotic metabolism (Chemale *et al.*, 2006). Thus, conservation of these critical residues supports the probable stability of FhDJ-1 for oligomerization and functionality under oxidative conditions, in-keeping with previous structural modelling.

Conserved active sites and ligand binding activities of FhDJ-1 were investigated using 3DLigandSite based on the final model calculated by Phyre2, with 94% residues modelled at >90% confidence (Figure 4.4.1.4.2.2). 37 residues between Glu^{11} and Ala^{160} of FhDJ-1 were predicted to have ligand binding properties with significant structural alignment scores (11.2≤20.9 average MAMMOTH score). Heterogens included calcium, magnesium and zinc metal ions, and cobalamin, co-methylcobalamin and flavin mononucleotides, which were identified in five different putative clusters by 47 residues between Leu^{9}-Arg^{183} (Figure 4.4.1.4.2.2). Cluster one predicted the interaction of 37 protein residues (Glu^{11}–Ala^{18}, Thr^{20}–Val^{21}, Lys^{44}–Val^{49}, Ile^{69}–Gly^{76}, Ala^{101}–Ile^{103}, Ala^{105}, Tyr^{124}, Phe^{127}, Lys^{130}, Ser^{150}, Gly^{152}–Pro^{153}, Ala^{156} and Phe^{159}–Ala^{160}) with calcium, magnesium and zinc ions, as well as cobalamin (B12), co-methylcobalamin (COB) and flavin mononucleotide (FMN) ligands (Figure 4.4.1.4.2.2A).

Clusters two, three and four were interactions with metallic heterogens, including calcium and magnesium binding by Gly^{12}–Thr^{13} and Gly^{72} (Figure 4.4.1.4.2.2B), Leu^{9} (Figure 4.4.1.4.2.2C) and Gly^{72}–Leu^{74}, Ser^{77}, Cys^{104}–Ala^{105} (Figure 4.4.1.4.2.2D), respectively. A fifth cluster predicted binding to a flavin mononucleotide by eight residues including Pro153–Gly154, Met157, Ala177, Met180-Arg183 (Figure 4.4.1.4.2.2E). The range of ligands predicted

for FhDJ-1 may reflect the multifunctional roles of DJ-1 nucleotide and protein deglycases associated with the oxidative stress response including autophagy and mitophagy (Björkblom *et al.*, 2014; Meulener *et al.*, 2005; Pantcheva *et al.*, 2014; Taira *et al.*, 2004; Thomas *et al.*, 2011; Zhou and Freed, 2005; Zhu *et al.*, 2016). Zinc (Tashiro *et al.*, 2014), copper (Björkblom *et al.*, 2013; Girotto *et al.*, 2014) and mercury (Björkblom *et al.*, 2013) metal binding activity of DJ-1 has been elucidated as important in contributing to protection against cellular metal-induced cytotoxicity. Direct evidence is yet to confirm the mechanisms of these protective roles by DJ-1, or the binding of other metal ions (Ivanisenko *et al.*, 2004), including calcium or magnesium.

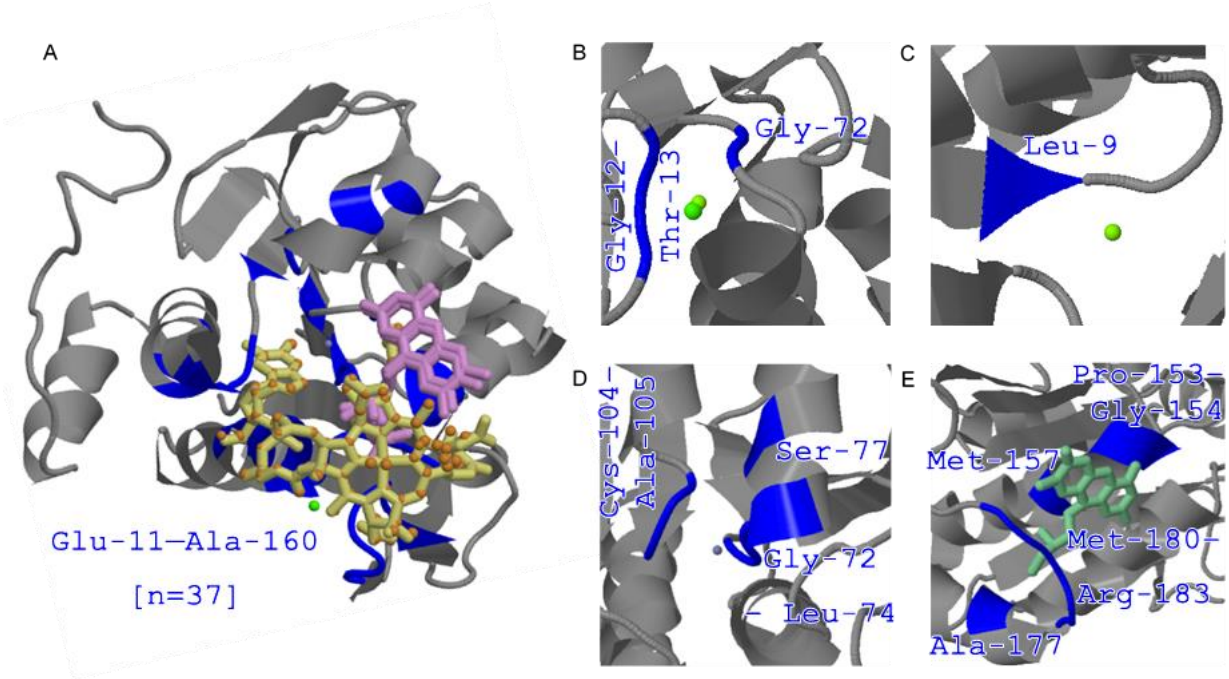

Figure 4.4.1.4.2.2. 3-D predictions of FhDJ-1-ligand binding using 3DLigandSite. The complete FhDJ-1 protein expression sequence was used to predict FhDJ-1-ligand interfaces based on sequence similarity to known protein-ligand interactions. Five different residue clusters of ligand binding residues were predicted (A-E), calculated by the MAMMOTH approach (Ortiz, Strauss and Olmea, 2002). Cluster 1 (A) predicted the involvement of 37 protein residues between Glu^{11} and Ala^{160} binding to six heterogens, including metal calcium (neon green), magnesium (lime green) and zinc (metallic purple) ions and non-metallic cobalamin, co-methylcobalamin and flavin mononucleotide (stick models) ligands. Alternative protein-ligand cluster predictions demonstrated further binding sites for calcium, magnesium and zinc metal ions (B–D) and flavin mononucleotide (E) by FhDJ-1 between residues Pro^{153}–Gly^{154}, Ala^{177} and Met^{180}–Arg^{183}.

4.4.1.5 Enolase (FhENO)

4.4.1.5.1 FhENO family association and structural assessments

FhENO (AAA57450.1: www.ncbi.nlm.nih.gov/protein/AAA57450.1) was matched to BN1106_s3227B000227.mRNA-1 (PRJEB6687, WBPS v10) on the WormBase ParaSite server with >99.5% residue identity (28-403). FhENO (PRJEB6687, WBPS v10, BN1106_s3227B000227.mRNA-1; scaffold: 3227: 262676–267431; four exons) was predicted with enolase-like protein family association using WormBase ParaSite with cross-referencing from InterPro. FhENO was matched to the enolase family (IPR000941) by HAMAP (1–427), PANTHER (1–432), CDD (5–416), TIGRFAM (3–428), PRINTS (35–49, 106–122, 163–176, 317–328, 340–354, 369–386), PIRSF (1–430) and SFLD (3–417). The enolase-like (IPR034390), enolase-like N-terminal (IPR029017) and enolase-like C-terminal (IPR036849) superfamilies were also matched by SFLD (1–423), Gene3D (1–126), and Gene3D (127–431) and Superfamily (142–429), respectively. Specific predictions for enolase-related structural domains were also identified, including an enolase N-terminal domain (IPR020811) by SMART and Pfam (3–133), and an enolase C-terminal TIM barrel domain (IPR020810) by SMART (141–431) and Pfam (142–430). The N- and C-terminal regions are highly conserved between many multifunctional bidomain enzymes in enolase-like superfamilies, with a capping N-terminal domain and TIM-barrel domain being characteristic (Gerlt *et al.*, 2005). FhENO had a further functional prediction within its C-terminal domain for a conserved site (IPR020809) by PROSITE (340–353), which is also a highly conserved region of many enolase-like proteins (Brändén, 1991; Gerlt *et al.*, 2005) and which contains the metal ion-binding site that is an important driver of substrate binding and catalytic events (Brewer, 1981; Schreier and Höcker, 2010).

Cross-referencing between InterPro and PANTHER identified several key enolase-associated GO terms predicted for FhENO as follows. Association with the glycolytic (GO:0006096) biological pathway and the cellular phosphopyruvate hydratase complex (GO:0000015) was predicted, as well as molecular functions including metal binding (GO:0046872), lyase activity (GO:0016829) and phosphopyruvate hydratase activity (GO:0004634). Though no cellular localisation was predicted, enolases are one of the most abundant proteins of the cytosol (Díaz-Ramos *et al.*, 2012), and the multimeric phosphopyruvate hydratase complexes consist of two or eight enolases that are found in the cytosolic portion of cells. Furthermore, enolases have been found in the ECM, including *F.*

hepatica (Bernal *et al.*, 2004; Figueiredo *et al.*, 2015; Ghosh and Jacobs-Lorena, 2011; Liu and Shih, 2007).

Structural properties and conserved epitopes were predicted for FhENO using Phyre2. The hypothetical 3-D structure of FhENO was produced as based on a multi-template analysis using five of the highest scoring model templates, with 1L8P (PDB: www.rcsb.org/structure/1L8P), 3OTR (PDB: www.rcsb.org/structure/3OTR), 2AKM (PDB: www.rcsb.org/structure/2AKM), 2PTW (PDB: www.rcsb.org/structure/2PTW) and 3QTP (PDB: www.rcsb.org/structure/3QTP) having the highest scores and aligning 98% of FhENO residues (1–432) with 100% confidence (Figure 4.4.1.5.1). The secondary and tertiary structures of FhENO demonstrated a bidomain polypeptide structure. The N-terminal region stems from an anti-parallel beta-pleated sheet, three alpha helices, and a further short-length alpha helix that leads into the eight-component ring of beta-pleated sheets in the C-terminal region.

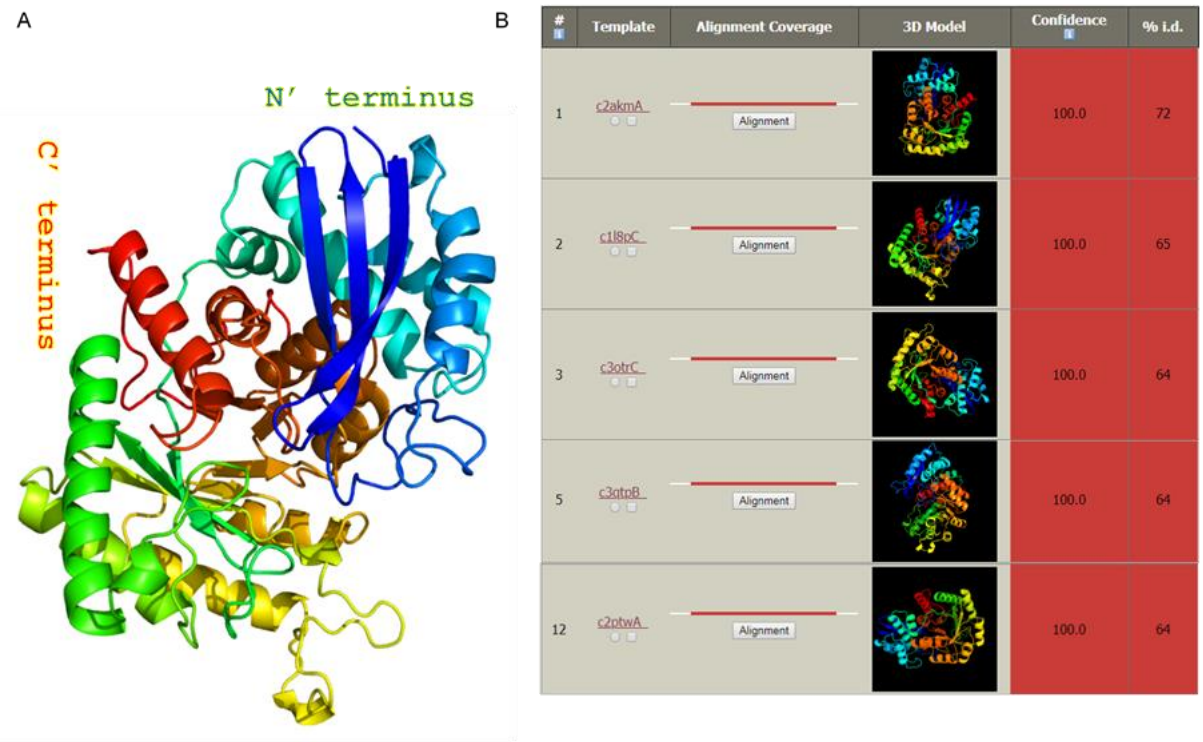

Figure 4.4.1.5.1. 3-D prediction and model templates for FhENO using Phyre2. The 3-D protein structure was predicted for FhENO (A), revealing the N-terminal of an anti-parallel beta-pleated sheet and four alpha helices leading to the C-terminal region of a TIM-barrel like domain of beta-pleated sheets encapsulated by alpha helices. This prediction was based on FhENO sequence modelling with five of the six highest-scoring templates shown (B), including several enolase models (PDB: IL8P, 3OTR, 2AKM, 2PTW, 3QTP).

The FhENO N-terminal configuration of [$\alpha_4\beta_3$] was akin to other alpha-ENOs (Ji *et al.*, 2016), and the C-terminus is formed of a beta-barrel surrounded by a single layer of eight alpha helices, forming a classic $(\alpha\beta)_8$ TIM-barrel structure (Figure 4.4.1.5.1A). However, the C-terminus of others in the ENO superfamily have a highly conserved but modified TIM-barrel consisting of $(\alpha\beta)_7\beta$, which is an unequal balance of beta sheets to alpha helices (Gerlt *et al.*, 2005). Nevertheless, the close alignment of FhENO with the five ENO models (av. 65.8% ID) likely reflects the high structural and functional conservation within this superfamily, and specifically FhENO similarity with ENOs of *Homo sapiens* (2AKM), *Saccharomyces cerevisiae* (1L8P), *Entamoeba histolytica* (3QTP), *Trypanosoma brucei brucei* (2PTW), and *Toxoplasma gondii* (3OTR).

The model enzymes, which includes ENOs from three protozoan parasite species, have all been characterised within the ENZYME commission classification system as enolase (EC 4.2.1.11, ExPASy), with some further assigned as an ENO-1 (alpha: 1L8P, 3QTP, 3OTR) and ENO-2 (gamma: 2AKM). Though TbbENO (2PTW) is not defined, putative sequence alignments with other proteins have suggested closest resemblance of this enzyme with other alpha enolases (data collected from UniProt: www.uniprot.org/uniprot/Q38BV6). Together the findings presented provide evidence to suggest that FhENO is an alpha, ENO-1, isoform, based on structural similarities and through extended and predicted metalloenzyme and glycolytic characteristics (Gerlt *et al.*, 2005; Ji *et al.*, 2016; Livesay and La, 2005; Poyner *et al.*, 2002).

4.4.1.5.2 FhENO sequence conservation and functionality

To identify ENO sequence conservation, ENO-1 and/or ENO-2 sequences from *Schistosoma mansoni*, *Caenorhabditis elegans*, *Homo sapiens*, and *Saccharomyces cerevisiae* were aligned with FhENO and a phylogenetic tree was produced (Figure 4.4.1.5.2.1). Data indicated moderately high sequence conservation between all enolases, with many large sections of residues throughout the protein that were either completely- or partially conserved (Figure 4.4.1.5.2.1A). The greatest residue variation between most sequences was demonstrable at 15 residues at the N–mid region (positions 71-96), 26 residues at the mid–N region (positions 267-289) and eight residues at the C-terminus (positions 422–437).

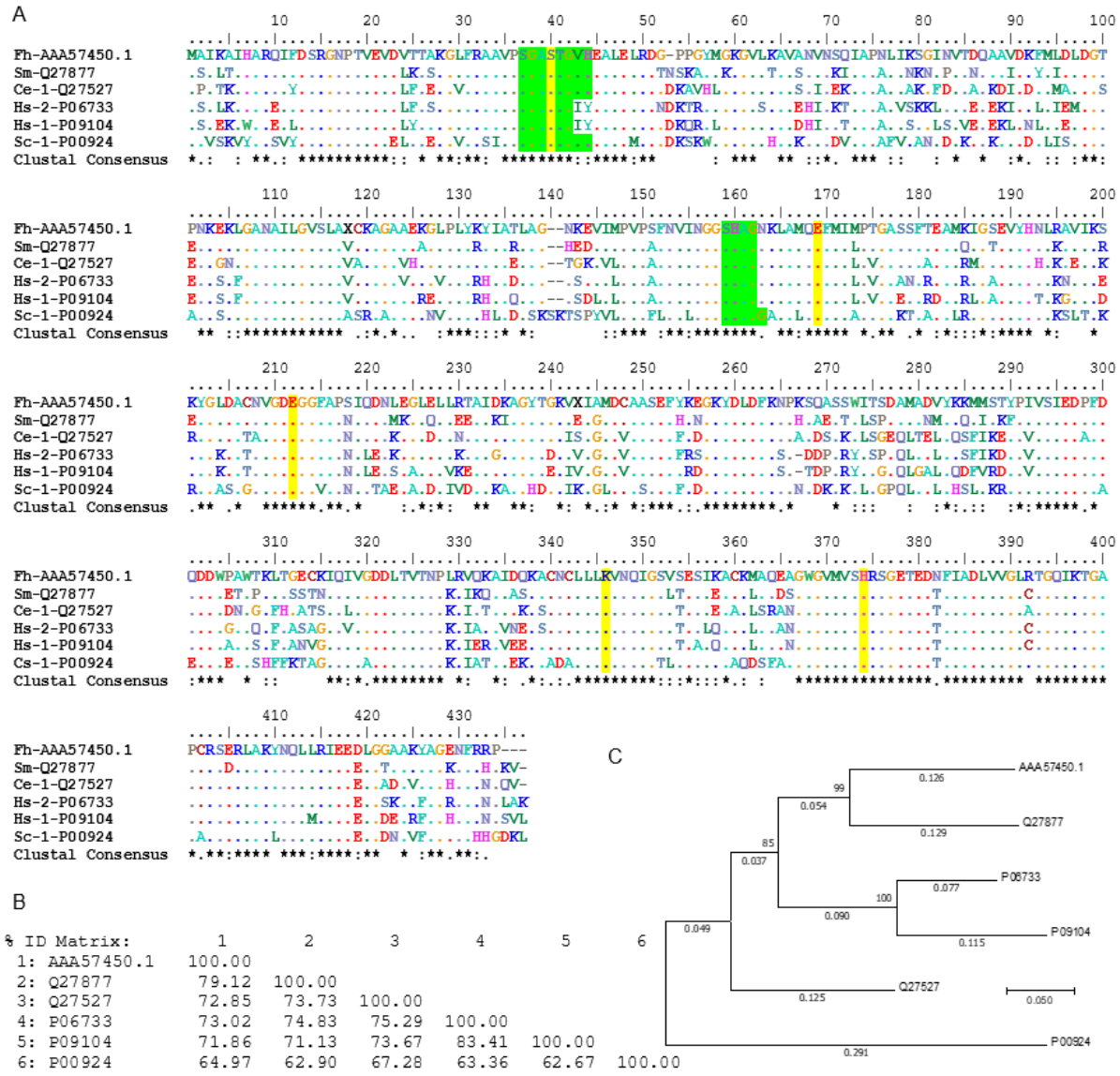

Figure 4.4.1.5.2.1. Phylogenetic analysis of *Fasciola hepatica* (FhENO), model and related parasite ENOs. The selected *F. hepatica* isotype FhENO (AAA57450.1) was aligned with enolase isotypes of *S. mansoni* (SmENO: SM_24110.1, Q27877, www.uniprot.org/uniprot/Q27877), *C. elegans* (CeENO-1: T21B10.2a.3, Q27527, www.uniprot.org/uniprot/Q27527), *H. sapiens* (HsENO-2: 2AKM, P09104, www.uniprot.org/uniprot/P09104; HsENO-1: 3B97, P06733, www.uniprot.org/uniprot/P06733) and *S. cerevisiae* (ScENO-1: 1L8P, P00924, www.uniprot.org/uniprot/P00924). (A) The sequence alignment demonstrated high sequence conservation across multiple regions of the protein sequence, with the highest variation at N–mid (71–96), mid–C (267–289) and C-terminal (422–437) residues. Highlighted residues indicate amino acids of functional importance, including charged residues (highlighted in yellow) and loop-associated residues for substrate interaction (highlighted in green). (B) Percentage identities indicated high sequence similarity between human ENO isotypes (83.41%) and trematode ENOs (79.12%), with moderate similarity between all other sequences (62.67–75.29%). (C) The phylogenetic tree reflected this closeness, highlighting the greatest phylogenetic distance of ScENO from all other sequences. ClustalO and MEGA7 were used to produce the alignment and phylogenetic tree, respectively.

Despite predicted structural similarity between ScENO-1 (PDB: 1L8P, 65% ID, Figure 4.4.1.5.1) and FhENO, this pair demonstrated the most distant phylogenetic relationship compared with the other proteins, whereby CeENO-1, FhENO, HsENO-2, SmENO and HsENO-1 are ordered by decreasing similarity to ScENO-1 (Figure 4.4.1.5.2.1B: 62.67–67.28%; C: 0.465–0.707 units of evolutionary distance). Conversely, when excluding ScENO-1 and not comparing HsENO-1 vs. HsENO-2, sequence identities ranged between 71.13–79.12% (Figure 4.4.1.5.2.1B) and phylogenetically between 0.255–0.367 units of evolutionary distance (Figure 4.4.1.5.2.1B–C), with FhENO most closely related to SmENO followed by HsENO-2, CeENO-1 and Hs-ENO-1.

Several residues of functional importance are also shown (Figure 4.4.1.5.2.1A), including charged amino acids at exposed positions that interact with water and/or metal ions (Brewer *et al.*, 1998, 1997; Poyner *et al.*, 2002, 1996) as well as loops involved in substrate interactions in ScENO (Sangadala *et al.*, 1995). As these residues are all conserved, except for substitutions within the proposed loops of ScENO-1 at G161N which were demonstrable in all proteins and V43I-H44Y in HsENO-1/-2, this supports the probable conservation of these functions, including in FhENO.

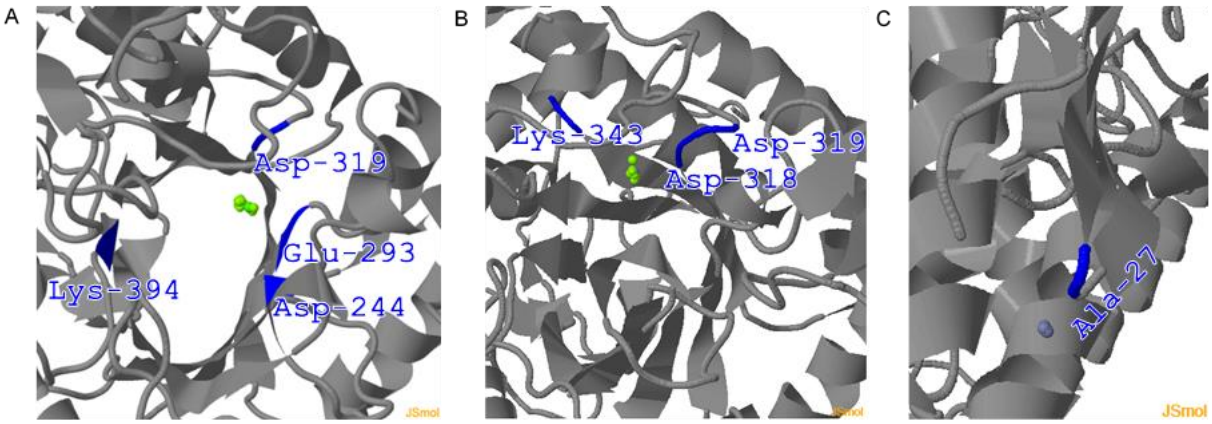

Figure 4.4.1.5.2.2. 3-D predictions of FhENO-ligand binding using 3DLigandSite. The complete FhENO protein expression sequence was used to predict FhENO-ligand interfaces based on sequence similarity to known protein-ligand interactions. Three different residue clusters of ligand binding residues were predicted (A–C), calculated by the MAMMOTH approach (Ortiz, Strauss and Olmea, 2002). All three clusters predicted the involvement of seven protein residues between Ala^{27} and Lys^{394} binding to metallic heterogens, including calcium (neon green), magnesium (lime green) and zinc (metallic purple) ions.

Conserved active sites and ligand binding activities of FhENO were investigated using 3DLigandSite based on the final model calculated by Phyre2, with 98% residues modelled at >90% confidence (Figure 4.4.1.5.2.2). Seven residues between Ala^{27} and Lys^{394} of FhENO were predicted to have ligand binding properties with significant structural alignment scores (47.5≤48.6 average MAMMOTH score). Heterogens included calcium, magnesium and zinc metal ions, which were identified in three different putative clusters (Figure 4.4.1.5.2.2). Cluster one was the only prediction with the binding of all three metallic heterogens, with 25 ligands overall across four residues (Ala^{244}, Glu^{293}, Asp^{318}, Lys^{394}), including 17 magnesium ions, seven zinc ions, and one calcium ion (Figure 4.4.1.5.2.2A). Cluster two involved three residues (Asp^{318}, Asp^{319}, Lys^{343}) and 11 magnesium and five zinc ions (Figure 4.4.1.5.2.2B), and cluster three involved only Ala^{27} with three zinc ions (Figure 4.4.1.5.2.2C). These data for FhENO thereby tie in with the renowned ENO properties and those of other TIM-barrel metalloenzymes as divalent cation-binding proteins (Livesay and La, 2005), important for inducing catalysis and stabilising the enzyme intermediate (Gerlt *et al.*, 2005; Gerlt and Raushel, 2003; Qin *et al.*, 2006; Rakus *et al.*, 2008).

4.4.1.6 Gelsolin (FhGEL)

4.4.1.6.1 FhGEL family association and structural assessments

FhGEL (WBPS v10–14, PRJNA179522: D915_01476; contig 221: 111379–132789; nine exons) was predicted with gelsolin-associated functional and structural domains using WormBase ParaSite with cross-referencing from InterPro. FhGEL was matched to the ADF-H/Gelsolin-like domain superfamily (IPR029006) by Gene3D (33–158, 159–265, 266–364) and the actin depolymerizing protein superfamily (SSF55753: supfam.org/SUPERFAMILY/cgi-bin/scop.cgi?ipid=SSF55753) by Superfamily (47–364). FhGEL was also matched to the Villin/Gelsolin family (IPR007122) by PANTHER (1–361), SMART (48–355), and PRINTS (67–83, 92–110, 179–199, 296–318, 325–344). A further family-specific gelsolin-like domain (IPR007123) was also matched by Pfam (58–138, 180–246).

FhGEL was predicted to possess actin binding (GO:0003779) and actin filament binding (GO:0051015) molecular functions, but no other biological or cellular associations were found from the bioinformatic affiliations described, though many are described for *Homo sapiens* gelsolin (HsGEL: 3FFK, www.rcsb.org/structure/3FFK; 3FFN, www.rcsb.org/structure/3FFN;

P06396, www.uniprot.org/uniprot/P06396). To provide this putative information for FhGEL, PSORTII was used, predicting subcellular compartmental localisation is highly likely to be in the cytoplasm (56.5% probability, *k*-Nearest Neighbour prediction, *k* = 9/23; 89% probability, Reinhardt's method for cytoplasmic/nuclear discrimination) followed by the cytoskeleton (21.7% probability, *k*-Nearest Neighbour prediction, *k* = 9/23), indicating predominant cytoplasmic abundance but having possible involvement with cytoskeletal components.

Structural properties and conserved epitopes were predicted for FhGEL using Phyre2. The hypothetical 3-D structure of FhGEL was produced as based on a multi-template analysis with the six highest scoring protein model templates, 3FFK (PDB: www.rcsb.org/structure/3FFK), 1J72 (PDB: www.rcsb.org/structure/1J72), 1D0N (PDB: www.rcsb.org/structure/1D0N), 3FFN (PDB: www.rcsb.org/structure/3FFN), 1RGI (PDB: www.rcsb.org/structure/1RGI) and 5A1K (PDB: www.rcsb.org/structure/5A1K) which aligned 88% of FhGEL residues (35–331) with 100% confidence (Figure 4.4.1.6.1). The secondary structure of FhGEL consists of two large beta-pleated sheets forming 6- and 8-mer units, and ten alpha-helices of varying length (1–5 turns) (Figure 4.4.1.6.1A).

Nominally and according to the model mammalian plasma GEL, the tertiary structure consists of six 15 kDa tightly-folded homologous domains (S1-6/G1-6) (Way *et al.*, 1990), whereby regional separation has been described as position-dependent, with residues 39–133, 137–247, 271–364, 419–511, 516–618, and 640–731 defining G1–6, respectively (Burtnick *et al.*, 1997; Silacci *et al.*, 2004; Way *et al.*, 1989; Way and Weeds, 1988). As shown in human (PDB: 3FFN, 3FFK) and equine (PDB: 1D0N, 1RGI) plasma GELs (Burtnick *et al.*, 2004, 1997; Nag *et al.*, 2009) and a human adserverin (PDB: 5A1K) model (Chumnarnsilpa *et al.*, 2015), the compact structure undergoes conformational changes following activation by calcium ion binding. However, since full-length mammalian GEL-like proteins are also highly homologous and possess several tandem repeats (Way and Weeds, 1988), this suggests that FhGEL is a gelsolin-like protein fragment or half-gelsolin. This is supported by observations from *in silico* predictions matching FhGEL residues to gelsolin-associated domains, as well as partial protein models (PDB: 3FFK, 1RGI and 5A1K; Figure 4.4.1.6.1B), and mass spectrometric identification of natively-derived gelsolin-like protein (Morphew *et al.*, 2014) and recombinant FhGEL (Figure 4.4.2.7.2.3; Table 4.4.2.7.2). Thus, FhGEL resembles a partial GEL segment including three intact domains, G1–3 or G4–6, which are described as the two major organised regions to have developed following multiplication events of an original (G0)

ancestral gene sequence (Burtnick *et al.*, 1997; Choe *et al.*, 2002; Silacci *et al.*, 2004; Way and Weeds, 1988).

A

B

#	Template	Alignment Coverage	3D Model	Confidence	% i.d.
1	c3ffnA	Alignment		100.0	34
2	c1d0nA	Alignment		100.0	34
3	c1rgiG	Alignment		100.0	34
4	c3ffkD	Alignment		100.0	34
5	c5a1kB	Alignment		100.0	31
6	c1j72A	Alignment		100.0	30

Figure 4.4.1.6.1. 3-D prediction and model templates for FhGEL using Phyre2. The 3-D protein structure was predicted for FhGEL (A), demonstrating two beta-pleated sheets and five short-length alpha helices. This prediction was based on FhGEL sequence modelling with the six highest-scoring templates shown (B), including model gelsolins (PDB: 3FFK, 1D0N, 3FFN, 1RGI) and gelsolin-associated proteins (PDB: 1J72 and 5A1K).

4.4.1.6.2 FhGEL sequence conservation and functionality

To identify FhGEL domains and GEL sequence conservation, sequences from *Schistosoma mansoni*, *Caenorhabditis elegans*, *Homo sapiens* and *Equus callabus* were aligned with FhGEL and a phylogenetic tree was produced (Figure 4.4.1.6.2.1). Data indicated FhGEL resembles G1–3 rather than G4–6 domains, based on sequence matching to the defined categorisation of HsGEL homologous repeats (see colour scheme, Figure 4.4.1.6.2.1A). As such, putative G1–3 domains of FhGEL can be allocated as: 19–114, 119–228, 253–335.

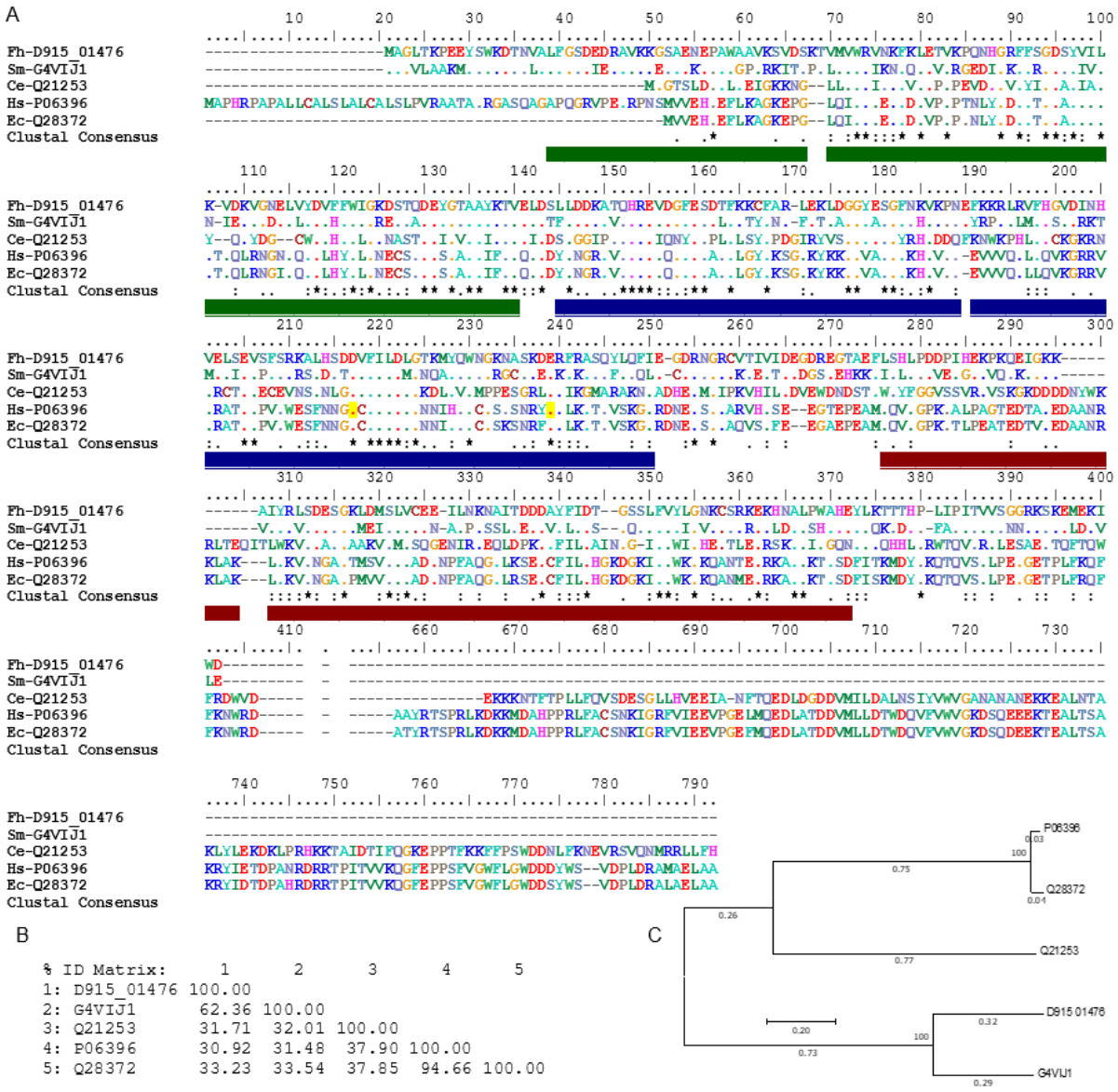

Figure 4.4.1.6.2.1. Phylogenetic analysis of *Fasciola hepatica* (FhGEL), model and related parasite GELs. The selected *F. hepatica* isotype FhGEL (D915_01476) was aligned with gelsolins of *S. mansoni* (SmGEL: XP_002572344/Smp008660, G4VIJ1, www.uniprot.org/uniprot/G4VIJ1), *C. elegans* (CeGEL: Q21253, www.uniprot.org/uniprot/Q21253), *H. sapiens* (HsGEL: 3FFN, 3FFK, P06396, www.uniprot.org/uniprot/P06396), and *E. callabus* (EcGEL: 1D0N, 1RGI, Q28372, www.uniprot.org/uniprot/Q28372). (A) The sequence alignment revealed FhGEL and SmGEL both matched to the N-terminal half of the model gelsolin sequences, indicating their resemblance to G1–3 domains (G1, green; G2, blue; G3, red; G4–6 not shown). Residues of interest are shown based on HsGEL residues associated with Finnish hereditary amyloidosis (when mutated, highlighted in yellow). (B) Percentage identities and (C) the phylogenetic tree following this alignment reflect the highly conserved sequences of the human and equine proteins (94.66%), with moderate similarity between trematode GELs (62.36%), and the greatest evolutionary distance between these two pairs (30.92–33.54%) and CeGEL (31.71–37.90%). ClustalO and MEGA7 were used to produce the alignment and phylogenetic tree, respectively.

Conservation of a widely known functionally important residue was also demonstrated, based on identifications in human familial amyloidosis (Finnish type) (highlighted residues, Figure 4.4.1.6.2.1A). Mutation in HsGEL of an aspartate (D214, domain two, Figure 4.4.1.6.2.1A) has shown to cause loss of function, due to calcium binding at this residue that triggers conformational changes during GEL-ACT interactions (Kazmirski *et al.*, 2002; Levy *et al.*, 1990). Further mutagenesis studies have identified glutamate substitution (E236, domain 2, Figure 4.4.1.6.2.1A) also replicates these results (Huff *et al.*, 2003), supporting the possibility of equal significance if substitutes occur at other calcium-binding sites, especially those related to conformation-regulated activities.

Percentage identities reflected the highest conservation between human and equine GELs (94.66%), and the closest sequence homology of FhGEL was understandably with SmGEL (62.36%) (Figure 4.4.1.6.2.1B), which was confirmed by phylogenetic analysis (Figure 4.4.1.6.2.1C), demonstrating the greatest evolutionary distance between FhGEL and the mammalian models conversely to the closeness of trematode and mammalian GEL pairs.

Conserved active sites and ligand binding activities of FhGEL were investigated using 3DLigandSite based on the final model calculated by Phyre2, with 88% residues modelled at >90% confidence (Figure 4.4.1.6.2.2; Table 4.4.1.6.2). 12 residues between Ala^{12} and Ala^{366} of FhGEL were predicted to have ligand binding properties with significant structural alignment scores (17.1≤37.2 average MAMMOTH score). Heterogens included calcium ion(s) and ATP, which were identified in 10 different putative clusters (Table 4.4.1.6.2), two of which are shown (Figure 4.4.1.6.2.2). One cluster was predicted with an ATP (Figure 4.4.1.6.2.2A) but the majority of clusters (9/10) indicated calcium as the sole ligand irrespective of residue numbers, with five interactions involving one metal ion, and the other four having 15, six, five or four calcium ions per cluster (Table 4.4.1.6.2).

Consequently to its calcium-mediated regulation, calcium binding sites were expected in all present domains (Choe *et al.*, 2002; Nag *et al.*, 2009), and which were predicted in FhGEL by 3D Ligand at two and four residues in the putative G1 and G2 domains, respectively (Table 4.4.1.6.2). These data tie in with the known GEL and ACT-binding protein characteristics, whereby functionality is regulated by calcium abundance, and is often co-regulated with phosphatidylinositol (Janmey and Stossel, 1987). GEL activation mechanisms via calcium binding has been identified to disrupt the compact protein structure through the interruption of G2 and G6 interactions, thereby releasing the C-terminal “latch helix” and allowing each

half-GEL to unravel the sterically hidden active sites for ACTs (Burtnick *et al.*, 1997; Choe *et al.*, 2002; Lin *et al.*, 2000; Nag *et al.*, 2009; Robinson *et al.*, 1999; Silacci *et al.*, 2004). Calcium concentration and binding are thus directly related to GEL activation, with higher ion abundance increasing functionality (Lin *et al.*, 2000; Nag *et al.*, 2009).

Table 4.4.1.6.2. Predicted FhGEL ligand binding using 3DLigandSite. FhGEL-ligand interfaces were predicted based on sequence similarity to known protein-ligand interactions. 10 different clusters were based on structural alignments between FhGEL and similar residue-ligand interactions, with significant scores calculated by the MAMMOTH approach (Ortiz, Strauss and Olmea, 2002). Both metallic and non-metallic ligands were predicted at 10 hypothetical clusters of single and/or multiple amino acids, mediated by 12 different residues in the protein (aa 12–366). Abbreviations: ATP, adenosine triphosphate; Ca, calcium.

MAMMOTH Score (averaged)	Interacting residues	Ligand (n)
37.2	Glu^{217}	Ca^{2+} (1)
21.9	Gly^{74}, Asp^{75}	Ca^{2+} (4)
21.8	Val^{174}	Ca^{2+} (5)
21.1	Asp^{75}, Tyr^{152}	Ca^{2+} (1)
21.1	Val^{174}	Ca^{2+} (1)
21.1	Asp^{75}	Ca^{2+} (1)
19.2	Asp^{117}	Ca^{2+} (1)
19.2	Trp^{12}, Glu^{360}, $Ala^{365-366}$	ATP (1)
17.3	Asp^{117}, Asp^{122}, Leu^{351}	Ca^{2+} (6)
17.1	Asp^{75}	Ca^{2+} (15)

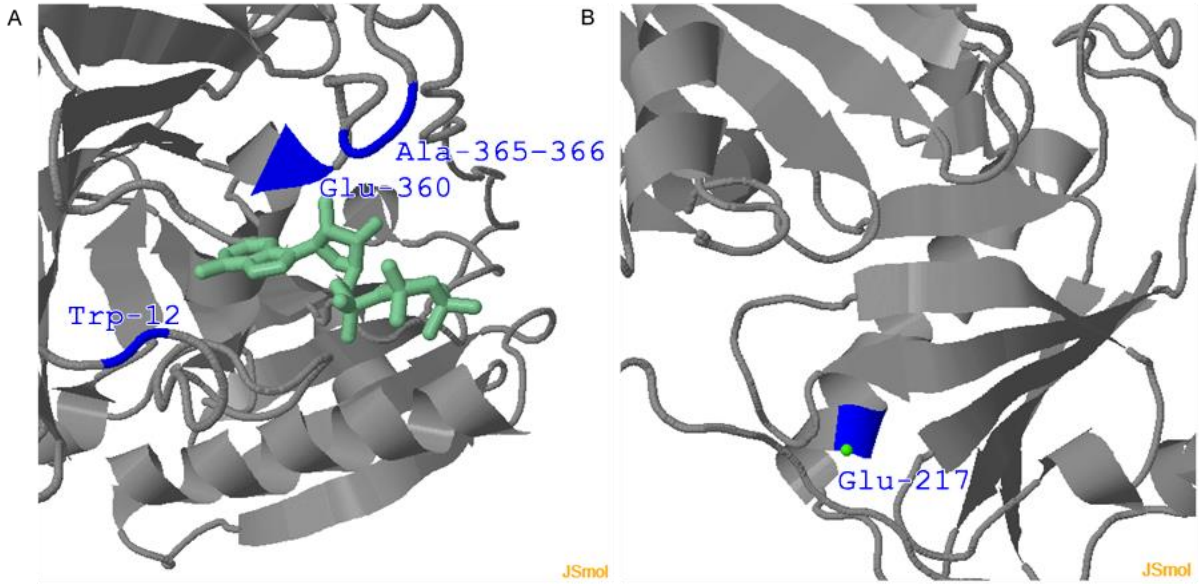

Figure 4.4.1.6.2.2. 3-D predictions of FhGEL-ligand binding using 3DLigandSite. The complete FhGEL protein expression sequence was used to predict FhGEL-ligand interfaces based on sequence similarity to known protein-ligand interactions. Ten different residue clusters of ligand binding residues were predicted, with two shown including an ATP molecule (A) and a calcium metal ion (neon green) (B), calculated by the MAMMOTH approach (Ortiz, Strauss and Olmea, 2002).

ACT-GEL interactions have further identified dual dynamics of cation coordination, whereby type one involves a calcium ion shared between each GEL and ACT counterpart (Choe *et al.*, 2002; Chumnarnsilpa *et al.*, 2015), and type two has GEL-dominated cation possession (Choe *et al.*, 2002; Chumnarnsilpa *et al.*, 2015; McLaughlin *et al.*, 1993; Robinson *et al.*, 1999). This activation is essential for ACT severing and capping functions during cytoskeletal remodelling (Babich and Burkhardt, 2013; Forscher, 1989; Linder and Thors, 1992; Silacci *et al.*, 2004), cytoplasmic stability (Laine *et al.*, 1998; Yin and Stossel, 1979) and scavenging of circulating plasma ACT (Lee and Galbraith, 1992; Lind *et al.*, 1986; Yin *et al.*, 1981). Consequently, mutations in key calcium-binding sites (e.g. G2, Figure 4.4.1.6.2.1A) are linked to partial activation and human disease (Kazmirski *et al.*, 2002; Levy *et al.*, 1990). Interestingly, the G2 D214 residue previously located as a critical calcium-binding site in HsGEL (Figure 4.4.1.6.2.2A) was not predicted to have a significant MAMMOTH score in FhGEL, though three different residues were, including in non-domain regions. Thus, FhGEL likely contains ACT-binding residues and GEL-associated functional capabilities, but based on unmatched calcium ion-binding residue predictions, the putative domain allocation via HsGEL categorisation may not be accurate for less conserved orthologues.

4.4.1.7 Glyceraldehyde-3-phosphate dehydrogenase (FhGAPDH)

4.4.1.7.1 FhGAPDH family association and structural assessments

FhGAPDH (AIE44418: www.ncbi.nlm.nih.gov/protein/AIE44418) was previously successfully cloned by Zinsser *et al.* (2014), and was matched with 100.0% residue identity (1–338) to BN1106_s3550B000215.mRNA-1 (PRJEB6687, WBPS v10; scaffold 3550: 122261–123707; three exons) and D915_10915 (PRJNA179522, WBPS v10–14: contig 3012: 87472–88568; three exons) WormBase ParaSite sequences. FhGAPDH was predicted with GAPDH-associated functional and structural domains using WormBase ParaSite with cross-referencing from InterPro. FhGAPDH was matched to the NAD(P)-binding domain superfamily (IPR036291) by Superfamily (5–174), the glyceraldehyde/erythrose phosphate dehydrogenase family (IPR020831) by PIRSF (2–336), PANTHER (5–336) and PRINTS (112–125, 147–165, 174–190, 231–248, 271–286), and the glyceraldehyde-3-phosphate dehydrogenase type I family (www.ebi.ac.uk/interpro/entry/IPR006424) by TIGRFAM (5–327). Further superfamily identifications were predicted by Gene3D for an NAD(P)-binding Rossmann-like

domain (5–151, 316–329; CATH-Plus: 3.40.50.720) and a dihydrodipicolinate reductase domain 2 (152–315; Cath-Plus: 3.30.360.10) and by Superfamily for a GAPDH-like C-terminal domain (152–315; SSF55347, supfam.org/SUPERFAMILY/cgi-bin/scop.cgi?ipid=SSF55347). Further family-specific domains were also predicted, including a GAPDH NAD(P) binding domain (IPR020828) by SMART (4–153) and Pfam (5–104) and a GAPDH catalytic domain (IPR020829) by Pfam (158–315).

Further functional characteristics were also predicted, including a GAPDH catalytic site (IPR020830) by PROSITE (PS00071: 151–158), as well as many GAPDH-associated GO-terms from direct associations as follows. FhGAPDH was predicted with oxydoreductase activity (GO:0016620; GO:0016491) and frequently associated NADP (GO:0050661) and NAD (GO:0051287) binding, which are directly related to GAPDH type I and NAD(P)-binding activities and protein domains. GAPDH-associated biological processes were also predicted, including a GAPDH metabolic process (GO:0019682), an oxidation-reduction process (GO:0055114), glucose metabolic process (GO:0006006), a glycolytic process (GO:0006096) and a gluconeogenesis process (GO:0006094), which are associated with many glycose metabolic pathways. Further GAPDH-associated GO-terms for molecular functions, biological processes and cellular components were found from the bioinformatic affiliations described (PIRSF000149: Protein Information Resource, pir.georgetown.edu/cgi-bin/ipcSF?id=PIRSF000149). These included the aforementioned GO-terms directly associated with FhGAPDH, but also indicate the abundance of GAPDH-like proteins in most eukaryotic subcellular compartments (Mazzola and Sirover, 2003; Tristan *et al.*, 2011). To confirm this information for FhGAPDH, PSORTII was used, predicting subcellular compartmental localisation is highly likely to be in the cytoplasm (65.2% probability, *k*-Nearest Neighbour prediction, k = 9/23; 94.1% probability, Reinhardt's method for cytoplasmic/nuclear discrimination) followed by nuclear localization (21.7% probability) and mitochondrial (13.0% probability) localizations (*k*-Nearest Neighbour prediction, k = 9/23), indicating predominant cytoplasmic abundance.

Structural properties and conserved epitopes were predicted for FhGAPDH using Phyre2. The hypothetical 3-D structure of FhGAPDH was produced as based on a multi-template analysis with the six highest scoring protein model templates: 3H9E, 1S7C, 3CIE, 3STH, 1IHX and 2B4R (PDB: 3H9E, www.rcsb.org/structure/3H9E; 1S7C, www.rcsb.org/structure/1S7C; 3CIE [1VSV], www.rcsb.org/structure/1VSV; 3STH,

www.rcsb.org/structure/3STH; 1IHX, www.rcsb.org/structure/1IHX; and 2B4R, www.rcsb.org/structure/2B4R) which aligned 88% of FhGAPDH residues (1–328) with 100% confidence (Figure 4.4.1.7.1). The secondary structure of FhGAPDH consists of 11 individual alpha helices of varying lengths (1–4.5 turns) and two beta pleated sheets, including an N-terminal sheet consisting of seven parallel and one anti-parallel short-length strands interrupted by six alpha helices (Figure 4.4.1.7.1A). The region towards the C-terminal also predicted a large beta-sheet, consisting of five long parallel strands as well as three shorter anti-parallel strands, whereby two of these were serial strands interrupted by a small loop of residues (Figure 4.4.1.7.1A).

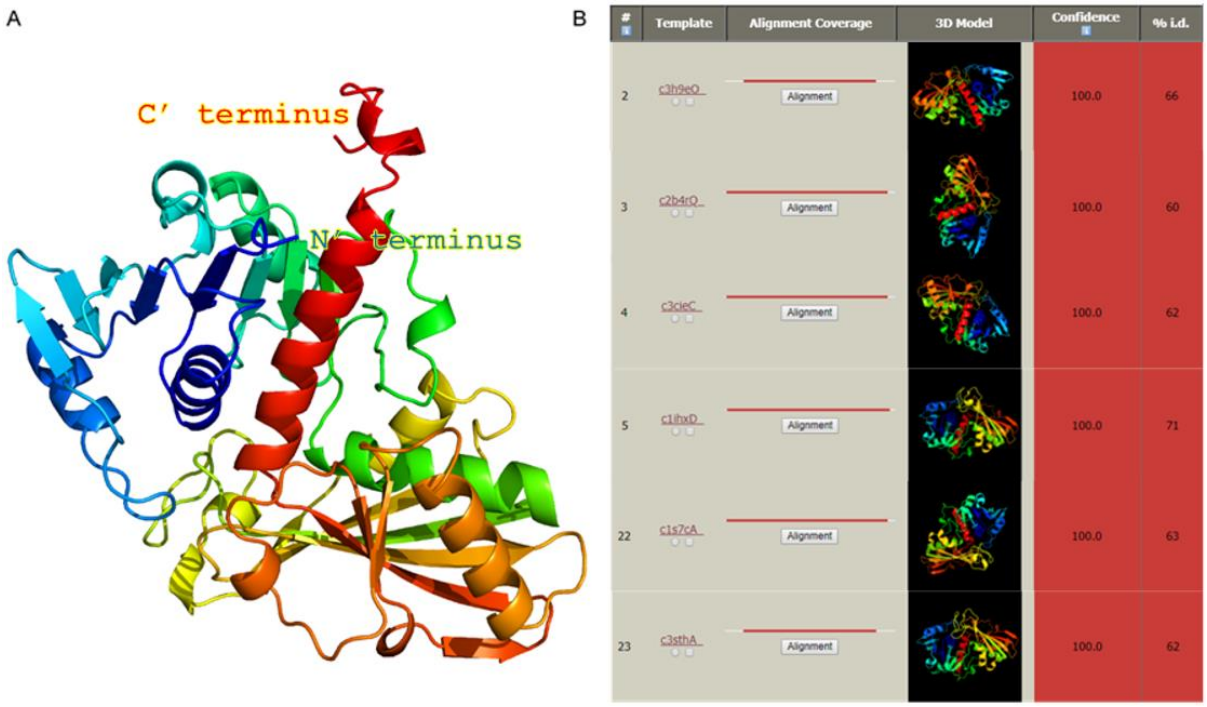

Figure 4.4.1.7.1. 3-D prediction and model templates for FhGAPDH using Phyre2. The 3-D protein structure was predicted for FhGAPDH (A), demonstrating the monomeric structure contains two beta-pleated sheets and 11 alpha helices. This prediction was based on FhGAPDH sequence modelling with the six highest-scoring templates shown (B), including GAPDH structures from a variety of mammalian and parasitic organisms 3H9E, 1S7C, 3CIE (1VSV), 3STH, 1IHX and 2B4R.

The tertiary structure of FhGAPDH shares similarities with other GAPDHs in having two main domains (Figure 4.4.1.7.1; Chaikuad *et al.*, 2011; Jenkins and Tanner, 2006; Zinsser *et al.*, 2014). The N-terminal has a typical Rossmann fold, characterised by an eight-stranded beta-sheet interrupted by alpha helices on both sides. The C-terminal 3-D structure is also

similar to model GAPDH C-domains (Chaikuad *et al.*, 2011), with the typically five-stranded beta-sheet exposed at the protein's periphery and alpha helices formed between beta strands positioned at the inner face. Sequence and structural conservation together indicate FhGAPDH is likely to capable of adopting 3-D and 4-D structures as described in models (e.g. HsGAPDS: Chaikuad *et al.*, 2011), and thus perform proposed GAPDH-associated molecular roles.

4.4.1.7.2 FhGAPDH sequence conservation and functionality

To identify GAPDH sequence conservation, sequences from *Schistosoma mansoni*, *Caenorhabditis elegans*, and *Homo sapiens* (testis- and liver- specific) were aligned to FhGAPDH and a phylogenetic tree was produced (Figure 4.4.1.7.2.1). The greatest sequence variation was at N-terminal and N–mid residues, at which HsGAPDS had a unique N-terminal peptide sequence (positions 1–72) and within which all other sequences contained multiple residue substitutions (positions 127–170), including five additional residues in CeGAPDH (positions 143–147) (Figure 4.4.1.7.2.1A).

Several functionally-important residues were conserved between the GAPDH sequences (Figure 4.4.1.7.2.1A), including the C-domain active site sequence and other residues of functional importance as identified in HsGAPDH/S and OcGAPDH (Chaikuad *et al.*, 2011; Ismail and Park, 2005; Nakajima *et al.*, 2009, 2007). Complete conservation indicated the importance of this sequence, especially at a cysteine residue involved in oligomerization via disulfide bond formation (Nakajima *et al.*, 2009, 2007) and interactions with glyceraldehyde-3-phosphate and NAD, as well as this cysteine and the consecutive histidine contributing to GAPDH catalysis (Chaikuad *et al.*, 2011; Ismail and Park, 2005; Talfournier *et al.*, 1999). Further residues associated with inter-protein and substrate interactions in HsGAPDH, including those contributing to electrostatic availability for oligomerization (Chaikuad *et al.*, 2011; Ismail and Park, 2005), were also highly conserved (Figure 4.4.1.7.2.1A).

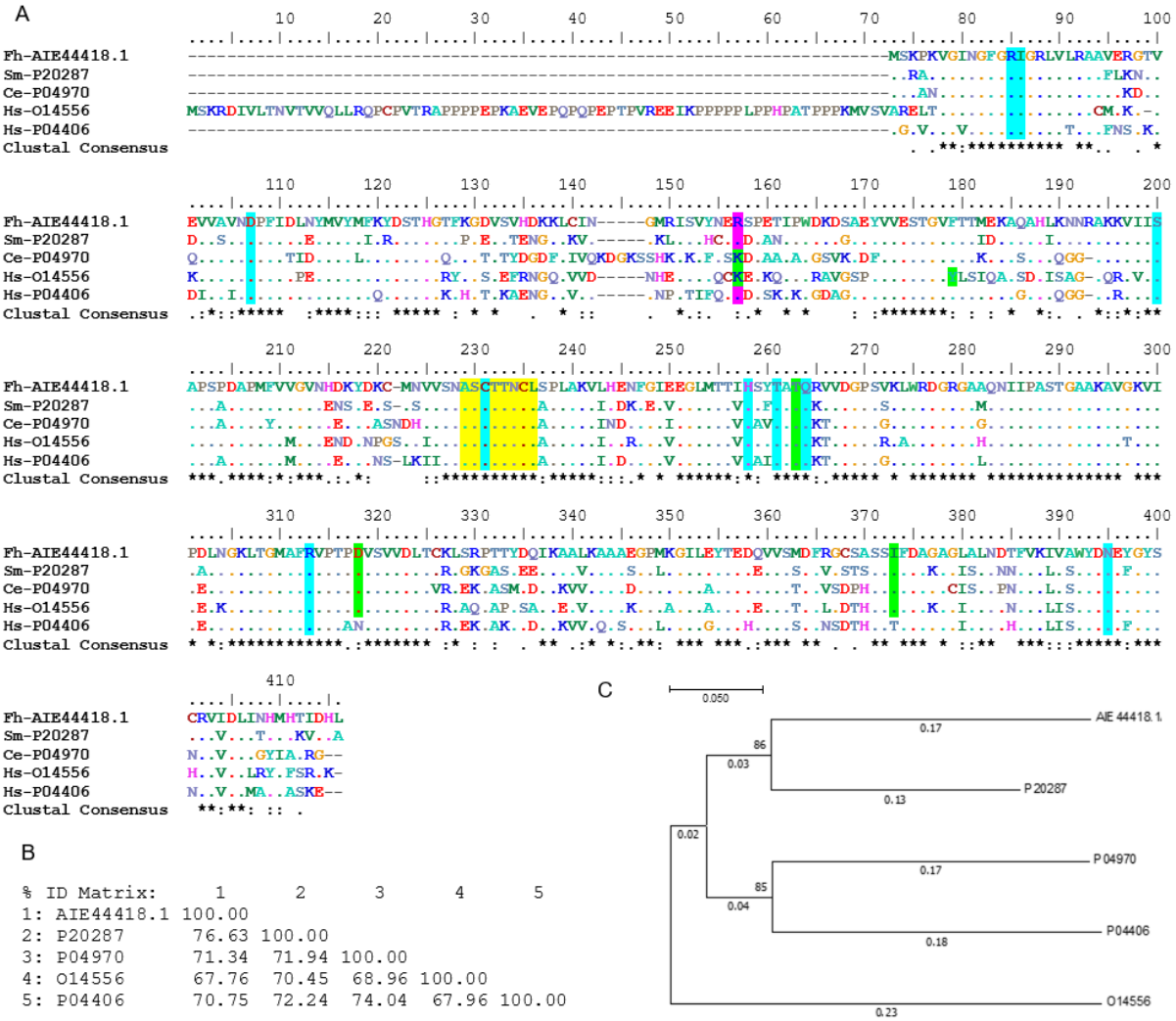

Figure 4.4.1.7.2.1. Phylogenetic analysis of *Fasciola hepatica* (FhGAPDH), model and related parasite GAPDHs.

The selected *F. hepatica* isotype FhGAPDH (AIE4418.1) was aligned with GAPDHs of *S. mansoni* (SmGAPDH: Smp056970.2, P20287, www.uniprot.org/uniprot/P20287), *C. elegans* (CeGAPDH: P20287, www.uniprot.org/uniprot/P20287), and *H. sapiens* (HsGAPDS (testis-specific): 3H9E, O14556, www.uniprot.org/uniprot/O14556; HsGAPDH (liver-specific): 1ZNQ, P04406, www.uniprot.org/uniprot/P04406). (A) The sequence alignment demonstrated 100% sequence conservation at the GAPDH C-domain active site (highlighted in yellow: ASCTTNCL, PS00071, https://prosite.expasy.org/PS00071), and further substrate-binding and structurally-relevant residues, as identified in HsGAPDHS (highlighted in green), HsGAPDH (highlighted in pink) or both (highlighted in turquoise) (Chaikuad *et al.*, 2011; Ismail and Park, 2005; Nakajima *et al.*, 2009, 2007). (B) The percentage identity matrix revealed the highest sequence identity between the trematode species (76.63%), the lowest between *F. hepatica* and *H. sapiens* sequences (67.76–70.75%), and with CeGAPDH sharing the greatest similarity with HsGAPDH (74.04%) over the trematode GAPDHs (71.34–71.94%). (C) The phylogenetic tree reflected this closeness and confirmed the known low HsGAPDH-HsGAPDS conservation. ClustalO and MEGA7 were used to produce the alignment and phylogenetic tree, respectively.

Partially- and non-conserved sequences may influence structural and functional residues observed in HsGAPDH/S models, whereby HsGAPDS-specific Tyr^{173} and Asp^{311} are proposed to improve relative hydrogen bond formation with NAD^+ and negatively influence proximate catalytic residues by changing the pK_a and protonation state, respectively (Chaikuad *et al.*, 2011). Based on the sequence alignment, data indicated the trematode GAPDHs shared the greatest sequence identity (76.63%) but FhGAPDH and HsGAPDS were the most distantly related (67.76%) (Figure 4.4.1.7.2.1B). These findings were mirrored by phylogenetic assessments with 0.3–0.45 units of evolutionary distance between FhGAPDH and SmGAPDH or HsGAPDS, respectively, though a distance of 0.47 units was calculated between HsGAPDS and HsGAPDH (Figure 4.4.1.7.2.1C), highlighting the consequence of non-essential sequence conservation due to spermatogenic specificity (Chaikuad *et al.*, 2011).

Conserved active sites and ligand binding activities of FhGAPDH were investigated using 3DLigandSite based on the final model calculated by Phyre2, with 97% residues modelled at >90% confidence (Figure 4.4.1.7.2.2). 24 residues between Asn^9 and Tyr^{321} were predicted to have ligand binding properties with significant structural alignment scores (40.3 average MAMMOTH score). Heterogens included NBD (N6-benzyl-nicotinamide-adenine-dinucleotide, NBD), NDP (NADPH dihydro-nicotinamide-adenine-dinucleotide phosphate, NDP) and NAD (nicotinamide-adenine-dinucleotide, NAD) dinucleotide cofactors, which were identified in two different putative clusters. One cluster was predicted with one NBD, four NDP and 20 NAD dinucleotides interacting with 24 residues including Asn^9–Ile^{14}, Asn^{34}–Phe^{37}, Glu^{79}–Arg^{80}, Ser^{98}–Gly^{100}, Phe^{102}, Asn^{122}–Ser^{123}, Cys^{153}, Ala^{184}, Asn^{317}–Glu^{318}, and Tyr^{321} (Figure 4.4.1.7.2.2A). Another cluster was predicted with one NBD, two NDP and five NAD dinucleotides interacting with one mid-region residue, Pro^{192} (Figure 4.4.1.7.2.2B).

The N-terminal Rossmann-like fold is typical of GAPDH, and is also an important region of nucleotide and cofactor binding (Baker *et al.*, 2014; Chaikuad *et al.*, 2011; Ismail and Park, 2005). Furthermore, of the residues predicted with substrate-binding properties located in the highly-conserved C-domain active site region 151-ASCTTNC-158 (Prosite: PS00071), Cys^{153} interacted with multiple NAD molecules (Figure 4.4.1.7.2.2A), consistent with other GAPDH enzymes (Chaikuad *et al.*, 2011; Ismail and Park, 2005; Nakajima *et al.*, 2007).

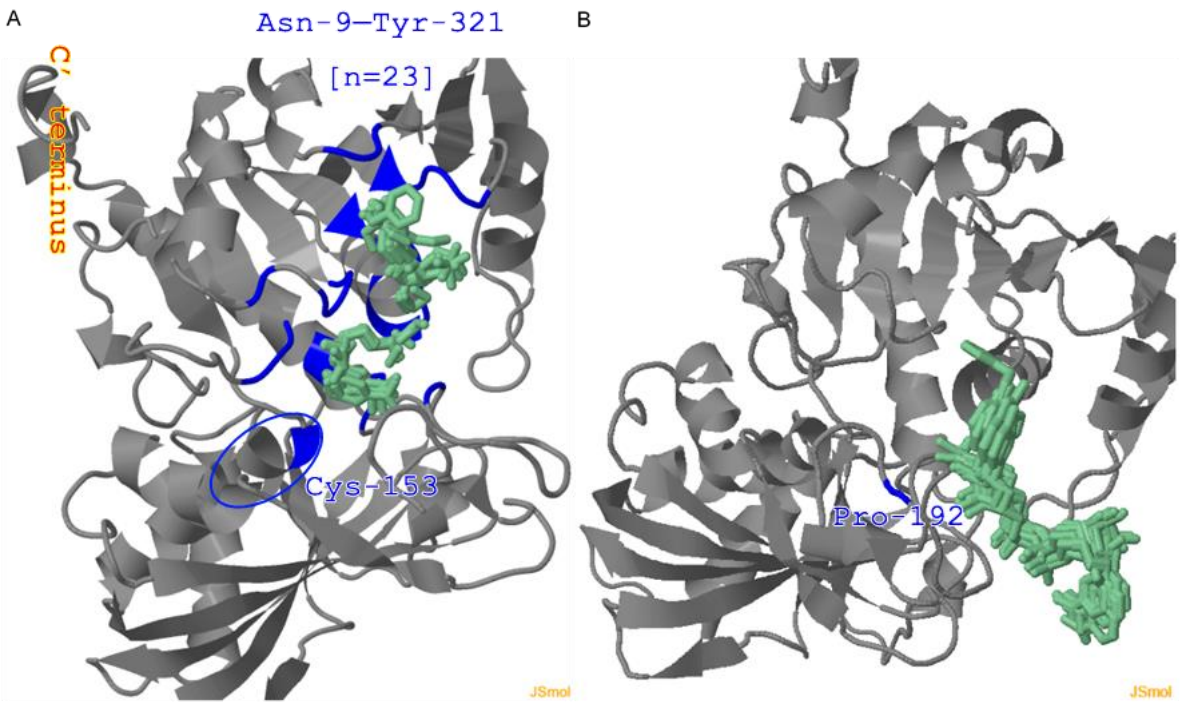

Figure 4.4.1.7.2.2. 3-D predictions of FhGAPDH-ligand binding. The complete FhGAPDH protein expression sequence was used to predict FhGAPDH-ligand interfaces based on sequence similarity to known protein-ligand interactions using 3DLigandSite. Two different clusters of ligand binding residues were predicted (A–B), calculated by the MAMMOTH approach (Ortiz, Strauss and Olmea, 2002). Both clusters predicted the involvement of 24 residues between Asn^{9} and Tyr^{321} binding to non-metallic dinucleotide heterogens, including NBP, NDP and NAD, with 25 ligands bound by 24 residues (Asn^{9}–Tyr^{321}) including Cys-153 in the putative active site (circled: Ala^{152}–Leu^{158}) (A) and eight ligands bound by one residue (Pro^{192}) (B).

4.4.1.8 Triose phosphate isomerase (FhTPI)

4.4.1.8.1 FhTPI family association and structural assessments

The protein sequence for FhTPI (AGJ83762.1: www.ncbi.nlm.nih.gov/protein/AGJ83762.1) that was successfully cloned from *F. hepatica* cDNA (Zinsser *et al.*, 2013b) was matched to BN1106_s3213B000041.mRNA-1 (PRJEB6687, WBPS v10: scaffold 3213: 12,485–22,821, six exons) using the BLAST function on the WormBase ParaSite server with 99.6% residue identity (1–253). FhTPI was predicted with TPI-associated functional and structural domains using WormBase ParaSite with cross-referencing from InterPro. FhTPI was matched to TPI (IPR035990) and aldolase-type TIM barrel (IPR013785) superfamilies by Superfamily (3–250) and Gene3D (1-252), respectively. The protein sequence was also matched to the TPI protein family (IPR000652) by PANTHER (1–251), PROSITE (6–250), CDD (7–249), Pfam (8–248) and TIGRfam (8–243), with further

identification as a member of the TPI bacterial/eukaryotic family (IPR022896) by HAMAP (5–250).

Further functional characteristics were also predicted, including a TPI active site (IPR020861) by PROSITE (PS00171: 167–177), TPI family signature (PS51440) and profile (PS51440) associations, as well as many TPI-associated GO-terms from direct associations as follows. FhTPI was predicted with TPI (GO:0004807), isomerase (GO:0016853) and catalytic (GO:0003824) activities of molecular function. Further associated biological processes were biosynthesis (GO:0009058), catabolism (GO:0009056), cellular processivity (GO:0009987), gluconeogenesis (GO:0006094) and glycolysis (GO:0006096). Cellular localisation was also indicated through GO-terms for both the cytoplasm (GO:0005737) and cytosol (GO:0005829).

Structural properties and conserved epitopes were predicted for FhTPI using Phyre2. The hypothetical 3-D structure of FhTPI was produced as based on a multi-template analysis with the six highest scoring protein model templates: 1SW3, 1MO0, 1R2R, 4OHQ, 5EYW and 3TH6 (PDB: 1SW3, www.rcsb.org/structure/1SW3; 1MO0, www.rcsb.org/structure/1MO0; 1R2R, www.rcsb.org/structure/1R2R; 4OHQ, www.rcsb.org/structure/4OHQ; 5EYW, www.rcsb.org/structure/5EYW; and 3TH6, www.rcsb.org/structure/3TH6), which aligned >97% of FhTPI residues (7–253) with 100% confidence (Figure 4.4.1.8.1). The secondary structure of FhTPI consists of eight parallel beta-pleated sheets (6- and 8-mers) and 14 alpha-helices of varying length (1–5 turns) (Figure 4.4.1.8.1A). TPIs are alternatively abbreviated as TIMs, and responsible for coining the "TIM barrel" fold, upon which a superfamily of proteins and enzymes are now described with the aforementioned structural properties (Borchert *et al.*, 1993a; Brändén, 1991; Livesay and La, 2005; Wierenga, 2001).

The tertiary structure of FhTPI forms a classical canonical beta-barrel, characteristic of TIM barrel proteins, with beta motifs positioned in a ring and eight alpha motifs encircling them and re-joining the C- and N-termini (Figure 4.4.1.8.1A). Eight non-integrated loops between the alternating alpha and beta motifs are deliberately placed for exposure and contain functionally- and structurally-relevant residues (Borchert *et al.*, 1993a; Norledge *et al.*, 2001; Schliebs *et al.*, 1996). TIM barrel proteins form homodimeric quaternary structures *in vivo* and *in vitro* (Borchert *et al.*, 1993a; Norledge *et al.*, 2001). The dimerization of TPIs is mediated by interactions between loops 1 and 4 and 3 of each monomer subunit, involving van der Waal and hydrogen bonds between key residues Lys^{13}, Glu^{97} and Thr^{75}, respectively from each loop (Jogl *et al.*, 2003; Schliebs *et al.*, 1997, 1996). In FhTPI, these residues are

conserved but incremented by one or more positions than described (Figure 4.4.1.8.1A). Furthermore, dimerization is not a prerequisite of functionality (Daar *et al.*, 1986; Ralser *et al.*, 2006), however structural and mutational analyses have shown mutations cause dimer instability, thus demonstrating dimerization conveys improved thermal stability and catalytic potential compared to monomeric forms (Benítez-Cardoza *et al.*, 2001; Celotto *et al.*, 2006; Daar *et al.*, 1986; Ralser *et al.*, 2006; Seigle *et al.*, 2008), including FhTPI (Zinsser *et al.*, 2013b).

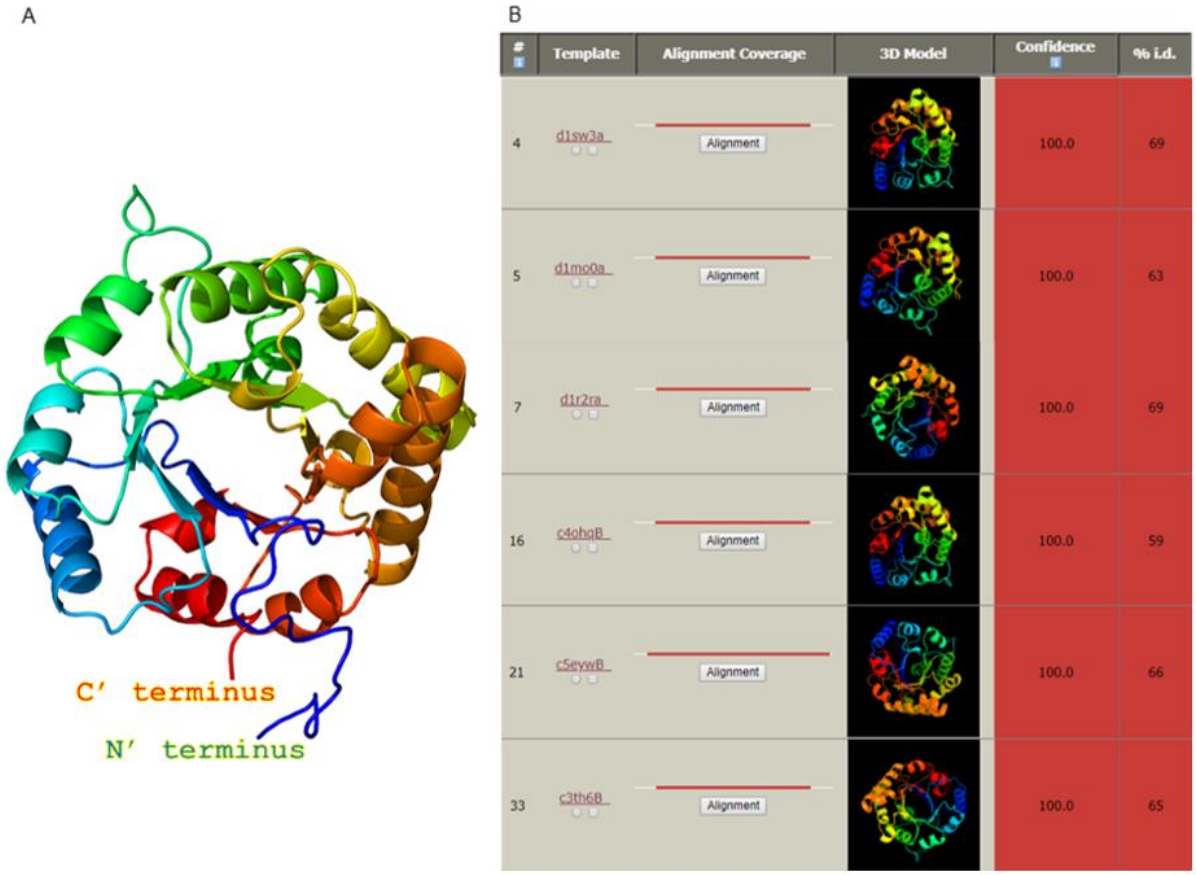

Figure 4.4.1.8.1. 3-D prediction and model templates for FhTPI using Phyre2. The 3-D protein structure was predicted for FhTPI (A), demonstrating the monomeric structure contains eight beta-pleated sheets and 14 alpha helices, forming a beta-barrel structure with the structure folding in a circular arrangement leading to N- and C-terminal proximity and interaction. This prediction was based on FhTPI sequence modelling with the six highest-scoring templates shown (B), including TPI structures from a variety of metazoan and plant model organisms 1SW3, 1MO0, 1R2R, 4OHQ, 5EYW and 3TH6.

4.4.1.8.2 FhTPI sequence conservation and functionality

To identify TPI sequence conservation, sequences from *Schistosoma mansoni*, *Caenorhabditis elegans*, *Homo sapiens* and *Oryctolagus cuniculus* were aligned to FhTPI and a phylogenetic tree was produced (Figure 4.4.1.8.2.1). The sequence alignment indicated partial conservation between all protein sequences (Figure 4.4.1.8.2.1A–B), but interestingly CeTPI was the most divergent sequence, whilst trematode and mammalian sequences branched in closely-related pairs (Figure 4.4.1.8.2.1B–C). Importantly, residues of prospective functionality for dimerization and catalysis, including flanking residues to the PROSITE-predicted active site (FhTPI: 167–177, Glu^{169}), were fully conserved (Figure 4.4.1.8.2.1A).

Conserved active sites and ligand binding activities of FhTPI were investigated using 3DLigandSite based on the final model calculated by Phyre2, with 94% residues modelled at >90% confidence (Figure 4.4.1.8.2.2). Eight residues between Asn^{18} and Leu^{248} were predicted to have ligand binding properties with significant structural alignment scores (17.3–19.5 average MAMMOTH score). Heterogens included 19 magnesium (MG) and five zinc (ZN) metal ions, two sulphur-iron complexes (SF4 and FES) and one S-adenosylmethionine (SAM), which were identified in three different putative clusters (Figure 4.4.1.8.2.2). One cluster was predicted with 19 magnesium and four zinc ions, one SF4 sulphur-iron complex, and one SAM interacting with Asn^{26} located on the first beta strand (Figure 4.4.1.8.2.2A). The second cluster was predicted with one FES sulphur-iron complex interacting with six residues including Phe^{22}, Leu^{55}, Trp^{105}, Ile^{107}, Val^{139} and Leu^{248} on different beta strands inside the beta-barrel structure (Figure 4.4.1.8.2.2B). The third cluster predicted the interaction of a zinc ion with Asn^{18} on loop one, close to the central barrel (Figure 4.4.1.8.2.2C). TPI functionality in the absence of metal ions or cofactors has been described from *in vitro* assessments (Daar *et al.*, 1986), including FhTPI (Zinsser *et al.*, 2013b) and other parasite TPIs (Jiménez *et al.*, 2000; Landa *et al.*, 1997; Zinsser *et al.*, 2013a), suggesting TPI, in at least these organisms, is not dependent on metal ion binding for its glycolytic ligands, dihydroxyacetone phosphate and glyceralde-3-phosphate.

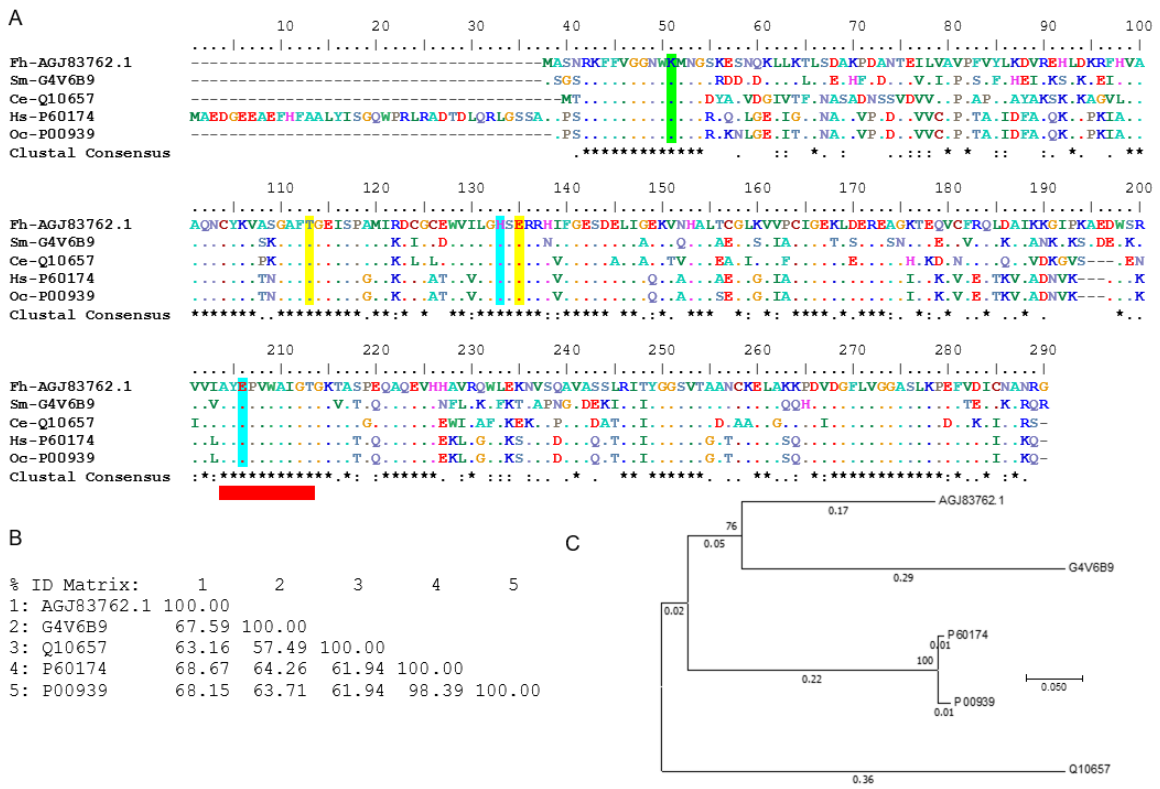

Figure 4.4.1.8.2.1. Phylogenetic analysis of *Fasciola hepatica* (FhTPI), model and related parasite TPIs. The selected *F. hepatica* isotype FhTPI (AGJ83762.1) was aligned with TPIs of *S. mansoni* (Smp003990.1: G4V6B9, www.uniprot.org/uniprot/G4V6B9), *C. elegans* (1MO0, Q10657, www.uniprot.org/uniprot/Q10657), *H. sapiens* (2JK2, P60174, www.uniprot.org/uniprot/P60174) and *O. cuniculus* (1R2R, P00939, www.uniprot.org/uniprot/P00939). (A) The sequence alignment demonstrated low sequence conservation between the protein sequences, with the highest variation at the N–mid-terminal 43 residues. Highlighted residues indicate amino acids of importance for dimerization (highlighted in yellow), catalysis (highlighted in turquoise) or both (highlighted in green), and the highly conserved active site region (PS00171, www.expasy.ch/prosite/PS00171, highlighted in red). (B) The percentage identity matrix further confirmed low sequence similarity, excluding HsTPI-OcTPI (98.39%), with the highest percentage identity between mammalian and liver fluke (68.15–68.67%) sequences, and lowest with CeTPI and all other sequences (57.49–64.16%). (C) The phylogenetic tree reflected this closeness, highlighting the phylogenetic distance of CeTPI from the other sequences. ClustalO and MEGA7 were used to produce the alignment and phylogenetic tree, respectively.

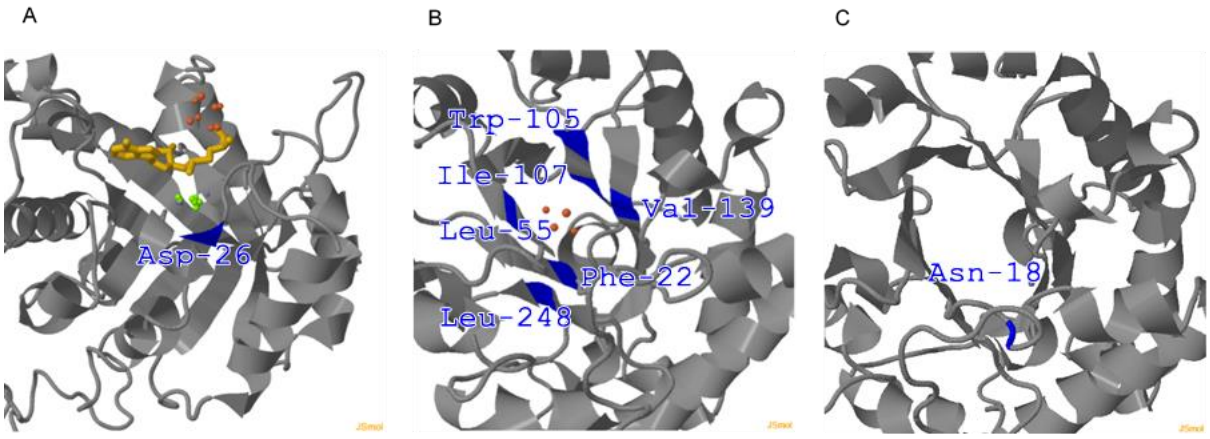

Figure 4.4.1.8.2.2. 3-D predictions of FhTPI-ligand binding using 3DLigandSite. The complete FhTPI protein expression sequence was used to predict FhTPI-ligand interfaces based on sequence similarity to known protein-ligand interactions. Three different residue clusters of ligand binding residues were predicted (A–C), calculated by the MAMMOTH approach (Ortiz, Strauss and Olmea, 2002). All three clusters predicted the involvement of seven protein residues between Asn^{18} and Leu^{248} binding to metallic heterogens including sulphur-iron complexes (SF4 and FES, orange) magnesium (lime green) and zinc (metallic purple) ions, as well as a non-metallic ligand, S-adenosylmethionine (SAM, mustard yellow).

4.4.1.9 Functional consequences of bioinformatic predictions

The hypothesis was that functional characterisation of the seven candidate biomarkers would increase our understanding of their molecular roles, both in general and in the context of the biological response to TCBZ in adult *F. hepatica*, to develop a portfolio for diagnostic development. The key bioinformatic and research literature findings of the molecular characteristics and biochemical activities of the seven candidates were summarised (Table 4.4.1.9).

Extracellular ES patterns leading to exposure at the ECM and host-parasite interface, was different per protein and reflective of their intrinsic molecular functions and localisations. Exposure and detection of each in *F. hepatica* ES products following fluke death was only previously noted for actin (Morphew *et al.*, 2007), whereas live *in vitro* culture has previously identified the presence of enolase (Chemale *et al.*, 2010; Morphew *et al.*, 2007) and GAPDH (Chemale *et al.*, 2010). The observations of extracellular glycolytic enzymes also adds to the growing reports indicating the possibility of hidden, moonlighting, functions of potential pathogenesis facilitation, which is of increasing research interest (Gómez-Arreaza *et al.*, 2014; Ucker *et al.*, 2012). SL [15 $\mu g \cdot mL^{-1}$] and L [50 $\mu g \cdot mL^{-1}$] doses of TCBZ-SO led to the appearance of all biomarkers as previously reported (Morphew *et al.*, 2014) (4.4.1.1), which were only

excreted following anthelmintic exposure. These findings, alongside known biochemical and functional properties, may indicate abnormal extracellular functionalities deliberately initiated to assist xenobiotic metabolism and/or evasion, or as a by-product of drug-induced apoptotic events, in-keeping with the fluke's TCBZ-resistant or -susceptible phenotype, respectively (Chemale *et al.*, 2010; Morphew *et al.*, 2014).

Table 4.4.1.9. Summative molecular, functional and putative characteristics for *Fasciola hepatica* biomarkers of potential diagnosis interest. Bioinformatically-predicted and previously reported observations of molecular features are shown for *F. hepatica* ACT, CRT, DJ-1, ENO, GEL, GAPDH and TPI candidates. Subcellular localisations and functionalities were based on summative cellular-, biological- and molecular-associated GO-terms. Known extracellular secretion patterns, including in *F. hepatica* and other parasites, are also shown.

Biomarker	Accession (WormBase ParaSite[1]; GenBank[2])	Predicted properties					Extracellular extretion/ secretion
		Molecular weight (kDa)	pI	Charge	Subcellular localisation (*highest scoring PSORTII prediction)	Functionality	
Actin	BN1106_s101B000531.mRNA-1[1]	41.646	5.28	-7.0	Cytoskeleton, Adherens junctions, Bicellular tight junctions, Focal adhesions	Cell cycle, Endo/exo-cytosis, Cytoskeletal organisation, Cell migration	Confirmed in *F. hepatica* ES[a**, b**, c*,**,***]
Calreticulin	BN1106_s2673B000071.mRNA-1[1]	48.965	4.42	-32.0	Endoplasmic reticulum, Cytoplasm, ECM	Calcium binding, Protein binding, Protein folding,	Confirmed in *F. hepatica* ES[b***,***] / *T. cruzi*[d]
DJ-1	BN1106_s1971B000297.mRNA-1[1]	19.322	7.80	+3.0	Cytosol, Nucleus, Mitochondrion	Transcription coregulation, Biosynthesis, Metabolism (N), RNA Pol II regulation, Stress response	Confirmed in *F. hepatica* ES[b***]
Enolase	AAA57450.1[2]	46.275	6.28	-2.0	Cytosol	Glycolysis, Gluconeogenesis	Confirmed in *F. hepatica* ES[a*, b*,**,***, c*,**,***] / ECM[e]
Gelsolin	D915_01476[1]	41.496	6.03	-3.0	Cytoplasm* Cytoskeleton	Actin binding	Confirmed in *F. hepatica* ES[b***]
Glyceraldehyde-3-phosphate dehydrogenase	AIE44418.1[2]	36.934	7.10	0.0	Cytoplasm* Nucleus Mitochondrion	Glycolysis	Confirmed in in *F. hepatica* ES[b**, c*,**,***] / Myxobacteria extracellular vesicle cargo[f]
Triose phosphate isomerase	AGJ83762.1[2]	27.783	8.10	+2.0	Cytoplasm, Cytosol	Glycolysis	Confirmed in *F. hepatica* ES[b***]

a Morphew *et al.*, 2007: *in vitro* cultured live flukes* / dead flukes**.
b Morphew *et al.*, 2014: *in vitro* cultured live flukes* / supplemented with TCBZ-SO [15 ug·mL^{-1}]** / [50 ug·mL^{-1}]***.
c Chemale *et al.*, 2010: *in vitro* cultured live flukes* / supplemented with TCBZ-SO [15 ug·mL^{-1}]** / [50 ug·mL^{-1}]***.
d Ferreira *et al.*, 2004a.
e Bernal *et al.*, 2004.
f Evans *et al.*, 2012.

4.4.2 Genetic recombination, expression and purification of *Faciola hepatica* biomarkers

4.4.2.1 Expression vector preparation

pET vectors were digested with NdeI and NotI restriction enzymes as described (4.3.1.2.6.1), removing 74 (pET-23a(+)) (Figure 4.4.2.1A–B) or 73 (pET-28b(+)) (Figure 4.4.2.1C–D) residues of the multiple cloning sites and creating sticky ends for subsequent subcloning.

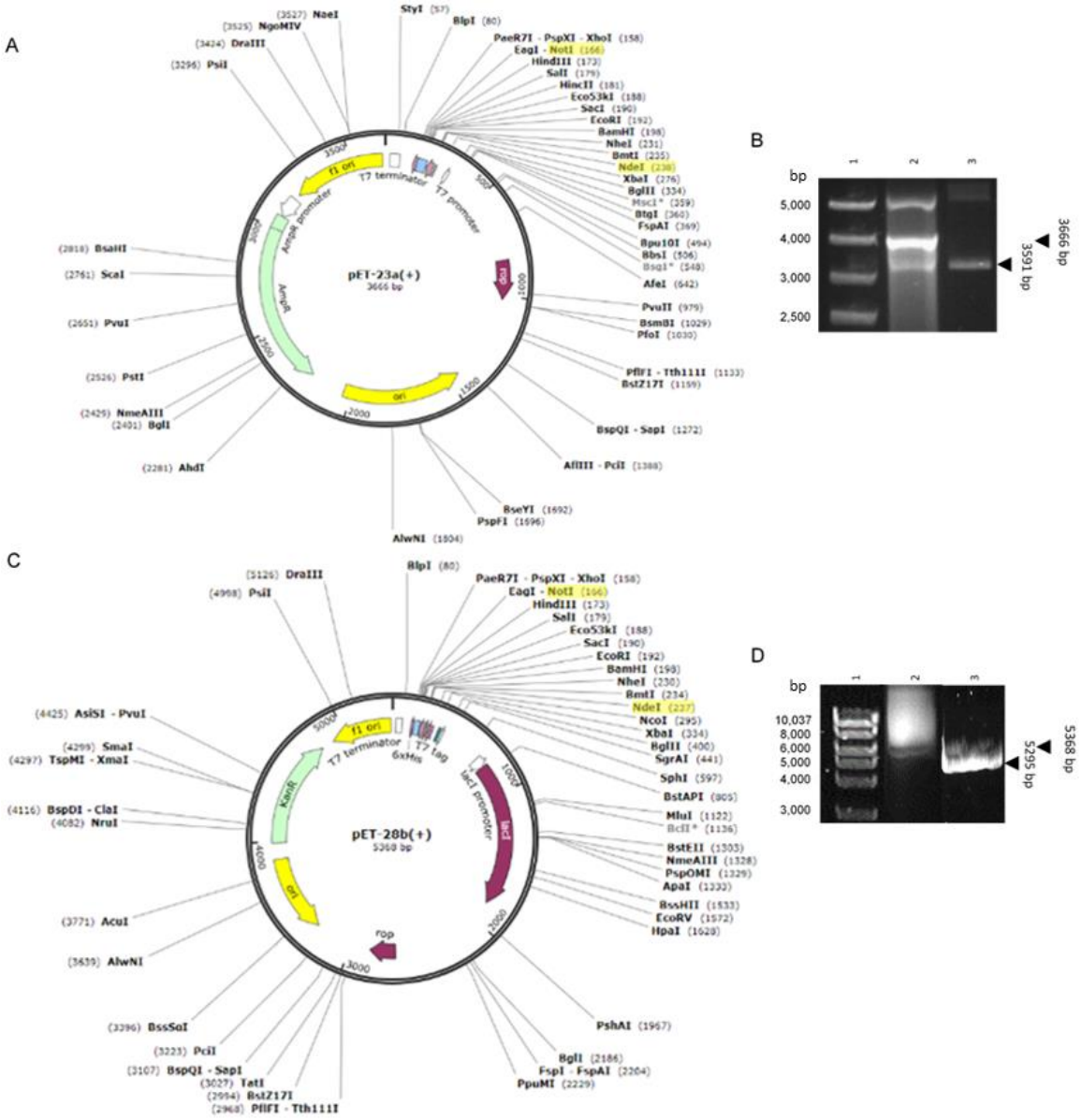

Figure 4.4.2.1. Circular maps and linearisation of pET-23a(+) and pET-28b(+). Circular pET-23a(+) (3666 bp, **A**) and pET-28b(+) (5368 bp, **C**) were NdeI-NotI-linearised to remove 74 and 73 bp of the multiple cloning sites, respectively (pET-23a(+): 3592 bp, **A**; pET-28b(+): 5295 bp, **C**). Restriction endonuclease reactions for vector linearisation were analysed by 1% agarose gel electrophoresis (pET-23a(+), **B**; pET-28b(+), **D**) for direct excision and subsequent ligation of complementary NdeI-NotI-digested insert DNAs.

Abbreviations: (B) Lane 1, Bioline HyperLadder™ 1kb (bp); lane 2, 250 ng undigested circular pET-23a(+) including supercoiled DNAs; lane 3, 250 ng NdeI-NotI-linearised pET-23a(+); (D) Lane 1, Bioline HyperLadder™ 1kb (bp); lane 2, 100 ng undigested circular pET-28b(+); lane 3, 500 ng NdeI-NotI-linearised pET-28b(+).

4.4.2.2 Actin (FhACT)

4.4.2.2.1 Cloning and subcloning

FhACT was PCR-amplified (for primer sequences, see Table 4.3.1.1.3), sequenced (>99.6% ID, Figure 4.4.2.2.1.1A), and electrophoresed (Figure 4.4.2.2.1.1B) for gel excision and direct ligation with pGEM®-T Easy and cloning in α-select *E. coli*.

5' flanking restriction enzyme binding sites were introduced via PCR using *FhACT*-pGEM®-T Easy as the PCR template (for primer sequences, see Table 4.3.1.1.3) and cloned using pGEM®-T Easy as before. NdeI-NotI-digested *FhACT* (Figure 4.4.2.2.1.2A) was then inserted into NdeI-NotI-linearised pET-28b(+) (Figure 4.4.2.1C–D) and confirmed using diagnostic restriction digestion and PCRs (Figure 4.4.2.2.1.2B–C). Positive transformant BL21(DE3)pLysS cell lines were also confirmed via PCR (Figure 4.4.2.2.1.2D) and Sanger Sequencing of *FhACT*-pET-28b(+) was used to identify the correct DNA and protein sequence for expression (>99.5% ID, Figure 4.4.2.2.1.2E).

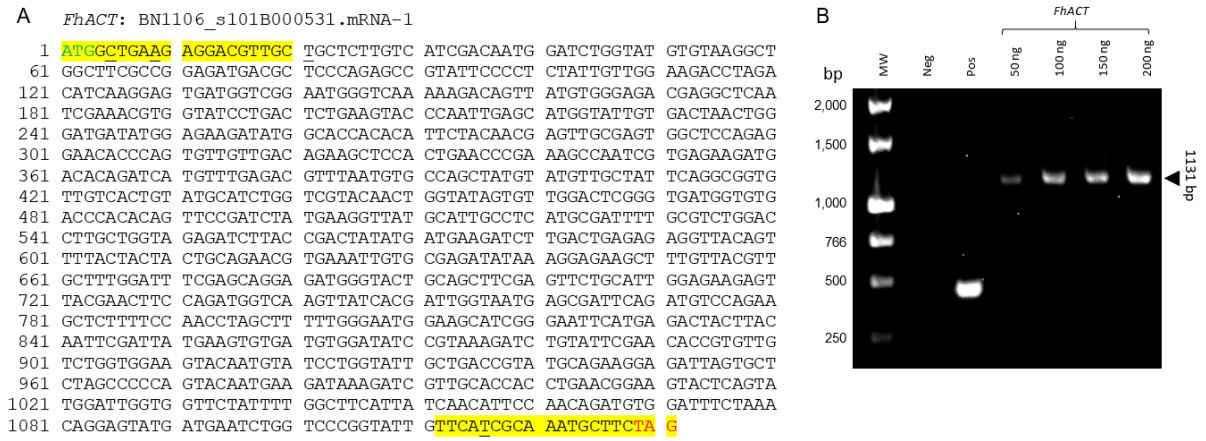

Figure 4.4.2.2.1.1. PCR amplicon target and product for *FhACT*. *FhACT* was targeted for PCR amplification, whereby oligomers were designed to amplify the gene including start and stop codons. Four SNPs were identified by Sanger DNA sequencing (underlined residues) (A) and a single amplicon was demonstrated by 1% agarose gel electrophoresis (B), testing four starting concentrations of *F. hepatica* cDNA.

Abbreviations: MW, NEB Fast DNA Ladder (bp); neg, negative; pos, positive (cDNA: *FhDJ-1*, 552 bp).

Upon *in silico* translation, two amino acid substitutions were identified (G2A, D3E), which PROVEAN identified as synonymous and non-deleterious (Table 4.4.2.2.1), and which is supported by the biochemical properties of these amino acids. The replacement of glycine with alanine is expected to be a synonymous change, as both are very small amino acids, though this leads to the loss of the glycine's unique hydrogen side chain (Betts and Russell, 2007). Furthermore, aspartate substituted by glutamate would cause little downstream consequence, as both are polar, charged, and thus have the potential for ionic bond formation (Betts and Russell, 2007). Thus, FhACT sequence identity differences can be assumed to be of no biochemical consequence.

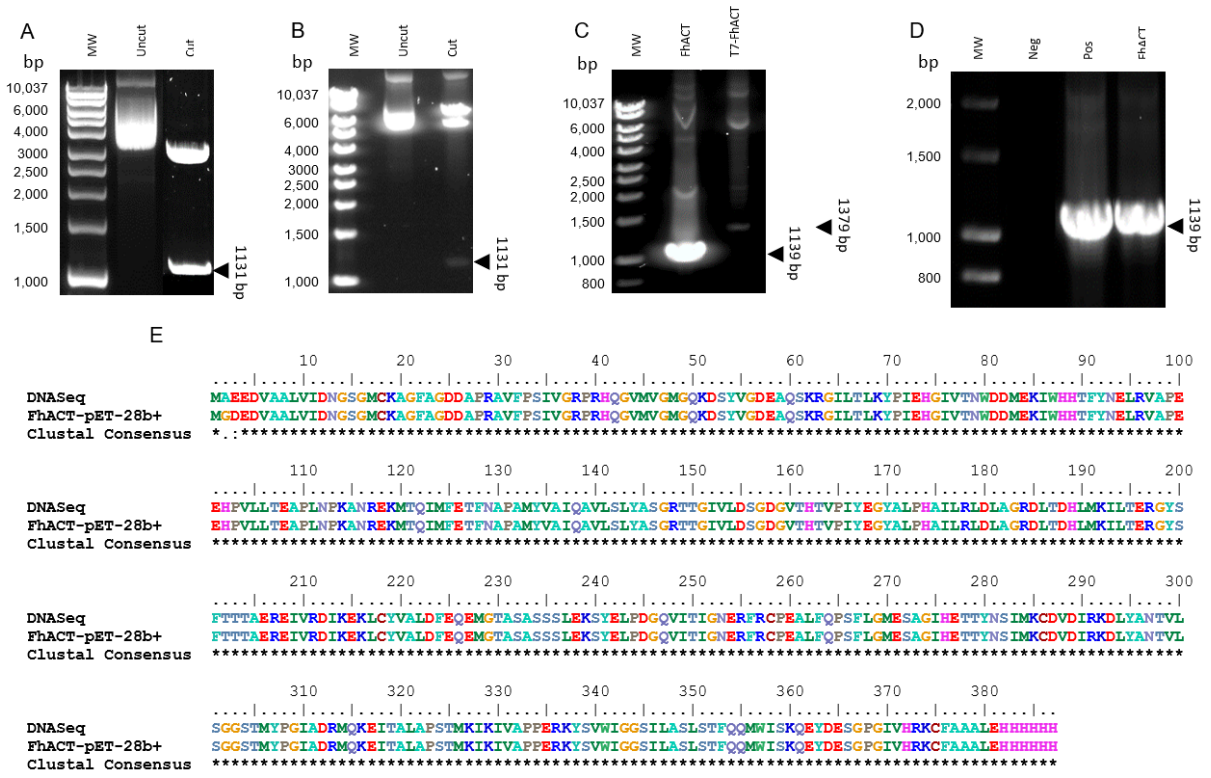

Figure 4.4.2.2.1.2. Subcloning and DNA diagnostics of *FhACT*-pET-28b(+). The subcloning sequence for *FhACT* was isolated from *FhACT*-pGEM®-T Easy via NdeI and NotI double digestion (A) for insertion into NdeI-NotI-linearised pET-28b(+). *FhACT*-pET-28b(+) constructs were tested via diagnostic digestion (NdeI and NotI) (B) and PCRs (C) using *FhACT* subcloning and T7 primers. (D) Positive BL21(DE3)pLysS cell lines were identified via colony PCR using *FhACT* subcloning primers and (E) DNA sequencing identified four SNPs in the *FhACT*-pET-28b(+) expression sequence, leading to two amino acid substitutions upon translation (compiled using BioEdit). Abbreviations: MW, Bioline HyperLadder™ 1kb (bp); neg, negative; pos, positive (cDNA: *FhACT*).

Table 4.4.2.2.1. PROVEAN Prediction for protein sequence analysis of FhACT. Sequence variants (Gly^2-Ala^2, Asp^3-Glu^3) were predicted with scores above the default threshold, which indicate these changes are neutral effects.

Variant	PROVEAN score	Prediction (default threshold ≤ -2.5)
G2A	0.570	Neutral
D3E	-0.335	Neutral

4.4.2.2.2 Expression

Actins (ACTs) have previously been isolated from different expression systems under diverse conditions to obtain the highest target concentration (Cevallos *et al.*, 2011; Tamura *et al.*, 2011, 2006; Valenta *et al.*, 1993; Verkhusha *et al.*, 2003), with the majority of cases purifying a soluble recombinant. rFhACT was predicted to be 43.01 kDa with an isoelectric point of 5.60 and an overall charge of -13.0, and SDS PAGE analysis of soluble expression fractions (Figure 4.4.2.2.2.1) demonstrated optimal target overexpression (~45kDa) in soluble fractions after 0.1 mM IPTG and three hours at 37°C.

IMAC purification was trialled using HIS-Select Nickel (Figure 4.4.2.2.2.2A) and Cobalt (Figure 4.4.2.2.2.2B) resins, but SDS PAGE analysis demonstrated inefficient isolation, suggesting low target concentration or incomplete metal ion-target protein binding. Unexpectedly, despite 0.22 µm filtration the rFhACT soluble lysate rapidly formed of a filamentous, IB-like substance triggered upon sample oscillation at 160 rpm during sample acclimatisation to both ambient and cold temperatures. This assumed filamentous product was solubilised as for IBs (4.3.3.2) and analysed by SDS PAGE, revealing two major proteins close to 50 kDa in molecular mass (Figure 4.4.2.2.2.2C), suggesting possible protein-bound or free actin monomer presence.

In order to identify suspected rFhACT in samples, bands of interest were analysed by LC-MS/MS following in-gel isolation (Table 4.4.2.2.2), including consistent fragments of 48 and 52 kDa (Figures 4.4.2.2.2.1–4.4.2.2.2.2, boxed). Data files were searched against the draft genome for *F. hepatica* (PRJEB6687, WBPS v10) using MASCOT, which did not identify actin or actin-related proteins in the samples ($P < 0.05$), but a ranging number of hits with low scores over the threshold value (MASCOT score range: 31≤65) and false discovery rates were all above 50% (Table 4.4.2.2.2). These findings are suggestive of a mixed protein group at the selected molecular weight bands, which is also likely to be composed of non-recombinant bacterial protein products.

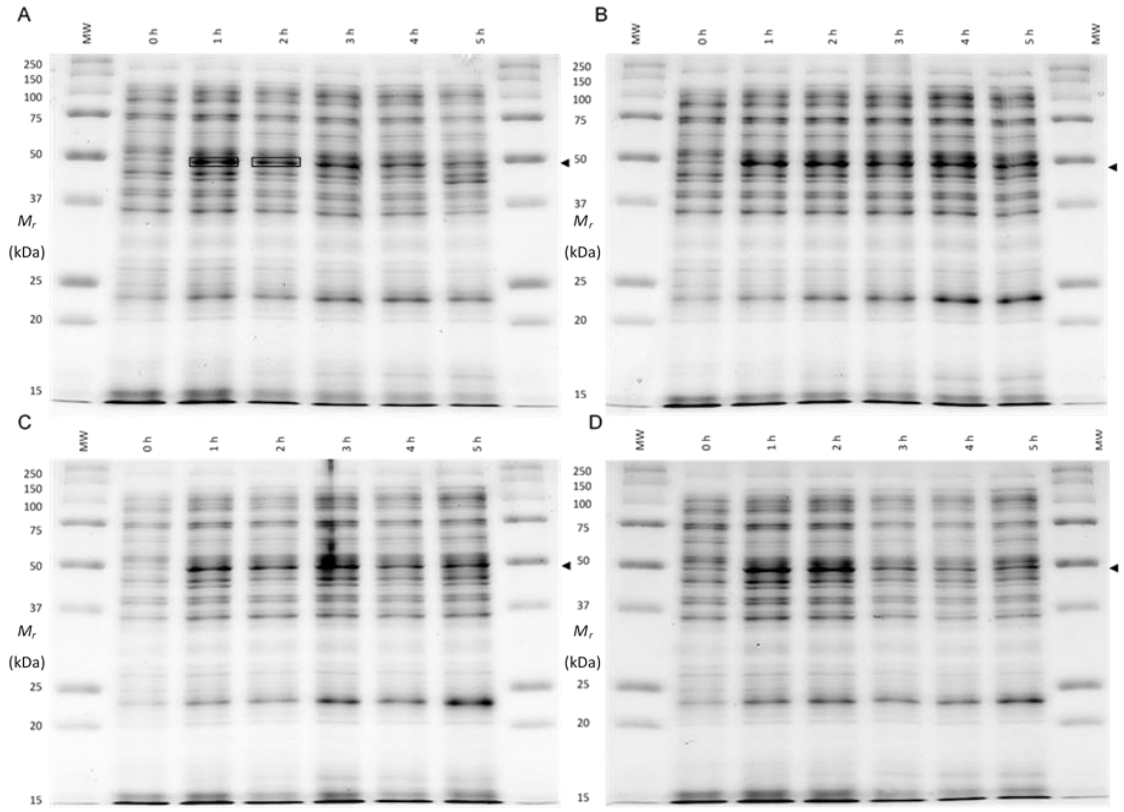

Figure 4.4.2.2.2.1. Pilot expression of rFhACT. 5 µg FhACT-pET-28b(+) BL21(DE3)pLysS recombinant expression lysate was analysed by SDS PAGE following 0.05 mM (A), 0.1 mM (B), 0.5 mM (C) and 1.0 mM (D) IPTG from 0–5 hours post-induction at 37°C.

Abbreviations: MW, Precision Plus Protein™ All Blue Standards (M_r); 0–5 h, hours post-induction.

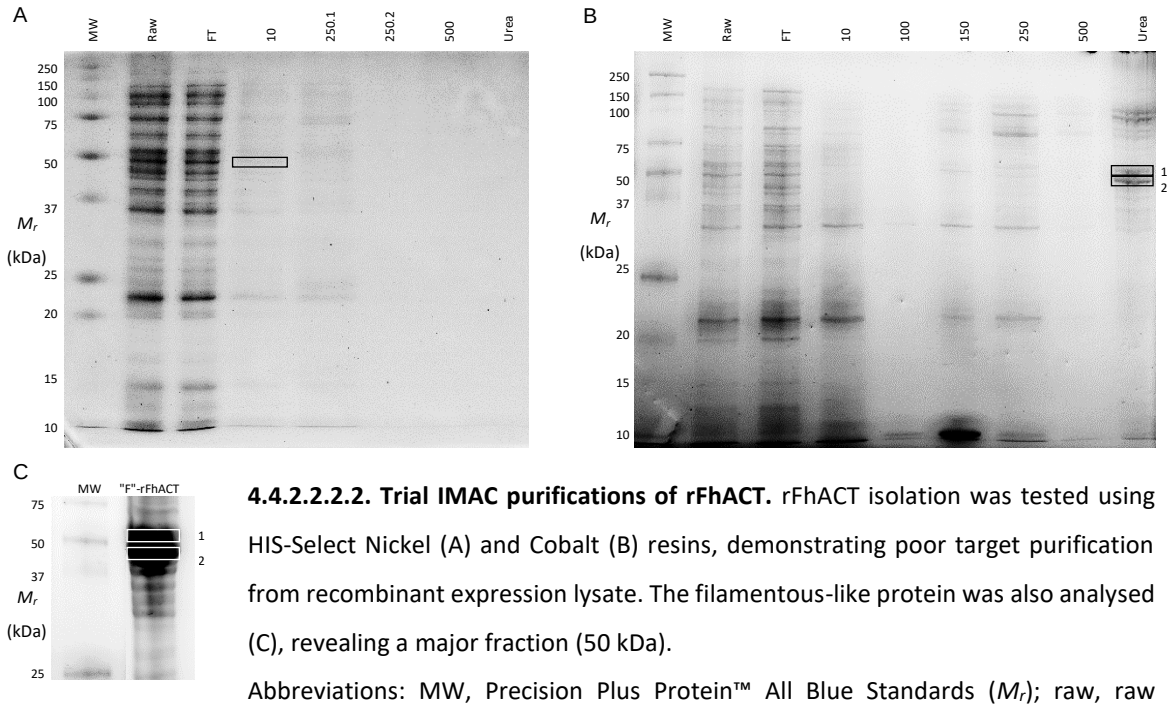

4.4.2.2.2.2. Trial IMAC purifications of rFhACT. rFhACT isolation was tested using HIS-Select Nickel (A) and Cobalt (B) resins, demonstrating poor target purification from recombinant expression lysate. The filamentous-like protein was also analysed (C), revealing a major fraction (50 kDa).

Abbreviations: MW, Precision Plus Protein™ All Blue Standards (M_r); raw, raw bacterial lysate; FT, flow-through; 10-500 [mM], imidazole concentration.

Table 4.4.2.2.2. LC-MS/MS identification of 1-DE-separated rFhACT. rFhACT protein bands/spots of interest were identified by LC-MS/MS against the *F. hepatica* genome (PRJEB6687, WBPS v10) and GenBank (v204), reporting significant hits identified with a score of 31 or greater (P < 0.05).

Figure	Sample	MS/MS ion search					Highest scoring GenBank hit			
		Fh genome hit	MASCOT score	False discovery rate (%)	Peptides matched (non-duplicate)	Sequence coverage (%)	Protein	Organism	Accession	E-value
4.4.2.2.2.1A	1 h	BN1106_s420B000182.mRNA-1	37	96.55	3	4.0	Hypothetical protein T265_06170	*Opisthorchis viverrini*	XP_009169635.1	0.0
		BN1106_s6296B000045.mRNA-1	36		1	7.0	-	-	-	-
		BN1106_s6988B000037.mRNA-1	34		6	6.0	E3 UFM1-protein ligase 1	*Clonorchis sinensis*	GAA47659.1	0.0
		BN1106_s2953B000132.mRNA-1	33		3	2.0	Hypothetical protein T265_11305	*Opisthorchis viverrini*	XP_009176193.1	0.0
		BN1106_s3837B000090.mRNA-1	33		1	1.0	Hypothetical protein T265_15334	*Opisthorchis viverrini*	XP_009175898.1	9E-160
		BN1106_s201B000462.mRNA-1	33		1	5.0	Ras family protein	*Fasciola hepatica*	PIS91693.1	3E-106
		BN1106_s3608B000123.mRNA-1	32		1	2.0	Hypothetical protein D915_01498	*Fasciola hepatica*	PIS90904.1	3E-136
		BN1106_s781B000234.mRNA-1	31		1	9.0	Coiled-coil domain-containing protein 91-like	*Centruroides sculpturatus*	XP_023209433.1	0.21
	2 h	BN1106_s201B000462.mRNA-1	44	123.53	1	5.0	Ras family protein	*Fasciola hepatica*	PIS91693.1	3E-106
		BN1106_s2953B000132.mRNA-1	38		3	3.0	Hypothetical protein T265_11305	*Opisthorchis viverrini*	XP_009176193.1	0.0
		BN1106_s1783B000133.mRNA-1	36		5	2.0	Hypothetical protein D915_11289	*Fasciola hepatica*	PIS81784.1	0.0
		BN1106_s3608B000123.mRNA-1	31		3	7.0	Hypothetical protein D915_01498	*Fasciola hepatica*	PIS90904.1	3E-136
4.4.2.2.2.2A	W	BN1106_s201B000462.mRNA-1	42	150.00	1	5.0	Ras family protein	*Fasciola hepatica*	PIS91693.1	3E-106
4.4.2.2.2.2B	1	BN1106_s1578B000131.mRNA-1	37	66.67	1	4.0	Hypothetical protein D915_09827	*Fasciola hepatica*	PIS83146.1	2E-31
		BN1106_s292B000423.mRNA-1	37		7	7.0	Leucyl-tRNA synthetase	*Clonorchis sinensis*	GAA47219.1	0.0
		BN1106_s6296B000045.mRNA-1	36		1	7.0	-	-	-	-
	2	BN1106_s201B000462.mRNA-1	57	178.57	2	11.0	Ras family protein	*Fasciola hepatica*	PIS91693.1	3E-106
		BN1106_s1303B000673.mRNA-1	40		1	2.0	Hypothetical protein D915_0065	*Fasciola hepatica*	PIS91679.1	0.0
4.4.2.2.2.2C	1	BN1106_s1161B000188.mRNA-1	51	79.59	3	2.0	Hypothetical protein X801_07610	*Opisthorchis viverrini*	OON16577.1	4E-138
		BN1106_s201B000462.mRNA-1	44		3	10.0	Ras family protein	*Fasciola hepatica*	PIS91693.1	3E-106
		BN1106_s1658B000131.mRNA-1	44		9	12.0	Eukaryotic DNA topoisomerase I, DNA binding protein	*Fasciola hepatica*	PIS80443.1	0.0
		BN1106_s503B000223.mRNA-1	39		3	9.0	Adenosine deaminase	*Schistosoma japonicum*	ABB89025.1	8E-98
		BN1106_s4332B000087.mRNA-1	38		5	11.0	ATP synthase F1, alpha subunit	*Opisthorchis viverrini*	OON18049.1	0.0
		BN1106_s81B000700.mRNA-2	37		1	38.0	5-hydroxytryptamine receptor 7	*Clonorchis sinensis*	GAA50114.1	3E-09
		BN1106_s115B000507.mRNA-1	34		3	3.0	Hypothetical protein X801_03687	*Opisthorchis viverrini*	OON20431.1	2E-89
		BN1106_s3945B000134.mRNA-1	33		3	9.0	Dihydroorotate dehydrogenase	*Clonorchis sinensis*	GAA49187.1	1E-104
		BN1106_s3672B000198.mRNA-1	32		7	15.0	Ubiquitinyl hydrolase 1	*Fasciola hepatica*	PIS84765.1	6E-120
		BN1106_s3173B000376.mRNA-1	32		5	8.0	Putative alpha-glucosidase	*Schistosoma mansoni*	XP_018647944.1	0.0
		BN1106_s1735B000362.mRNA-1	32		4	2.0	Transporter, major facilitator family protein	*Fasciola hepatica*	PIS88667.1	0.0
		BN1106_s307B000267.mRNA-1	31		2	5.0		*Opisthorchis viverrini*	XP_009175262.1	2E-169
		BN1106_s2507B000141.mRNA-11	31		1	40.0	Hypothetical protein T265_15195	*Clostridiales bacterium CHKCI006*	WP_089702623.1	8.7

		BN1106_s880B000146.mRNA-1	31		6	8.0	DNA primase Hypothetical protein T265_06677	*Opisthorchis viverrini*	XP_009170266.1	0.0
	2	BN1106_s201B000462.mRNA-1	65	100.00	1	5.0	Ras family protein	*Fasciola hepatica*	PIS91693.1	3E-106
		BN1106_s3608B000123.mRNA-1	46		3	8.0	Hypothetical protein D915_01498	*Fasciola hepatica*	PIS90904.1	3E-136
		BN1106_s3374B000082.mRNA-1	39		10	8.0	Hypothetical protein D915_11690	*Fasciola hepatica*	PIS81408.1	0.0
		BN1106_s3516B000081.mRNA-1	39		10	4.0	Hypothetical protein D915_13627	*Fasciola hepatica*	PIS79583.1	0.0
		BN1106_s2953B000132.mRNA-1	33		4	5.0	Hypothetical protein T265_11305	*Opisthorchis viverrini*	XP_009176193.1	0.0
		BN1106_s2769B000329.mRNA-1	32		18	14.0	Hypothetical protein T265_11878	*Opisthorchis viverrini*	XP_009176947.1	0.0
		BN1106_s2991B000132.mRNA-1	32		4	5.0	Hypothetical protein D915_13412	*Fasciola hepatica*	PIS79791.1	0.0
		BN1106_s2507B000141.mRNA-11	31		1	40.0	DNA primase	*Clostridiales bacterium CHKCI006*	WP_089702623.1	8.7

Two consistent hits were present across 85% and 42% of the samples (Table 4.4.2.2.2), including a *F. hepatica* protein with a predicted Ras-type small GTPase signature (FhRasGAP BN1106_s201B000462.mRNA-1; PIS91693.1: www.ncbi.nlm.nih.gov/protein/PIS91693.1), and an *O. viverrini* protein with a ribonuclease III (*DICER*; RNAseIII) domain and dsRNA binding motif (T265_11305, XP_009176193.1: www.ncbi.nlm.nih.gov/protein/XP_009176193.1). Of these hits, actin association is known for Rho-related GTPases that function in cytoskeletal actin regulation and Ras-type GTPases that are involved in cytoskeletal remodelling (Hall, 1994; Peränen *et al.*, 1996; Wennerberg *et al.*, 2005). To identify the sequence similarity between rFhACT and FhRasGAP or OvT265_11305, protein sequence alignments were conducted and identified 22.67% and 22.19% ID, respectively, indicating possible co-contamination of non-rFhACT proteins.

Based on the findings from these pilot studies for rFhACT, in order to proceed further with this target, overexpression must be optimised for adequate concentrations for further purification and molecular investigation.

4.4.2.3 Calreticulin (FhCRT)

4.4.2.3.1 Cloning and subcloning

FhCRT was PCR-amplified (for primer sequences, see Table 4.3.1.1.3), sequenced (>99.1% ID, Figure 4.4.2.3.1.1A), and electrophoresed (Figure 4.4.2.3.1.1A) for gel excision and direct ligation with pGEM®-T Easy and cloning in α-select *E. coli*.

A

FhCRT: BN1106_s2673B000071.mRNA-1

```
   1 ATGGTTGGTA CGTGGTACTT CTGCTTTACT CTGCTTGTGG CGATTGTTCG TTGTGAAGTT
  61 TACTTGGAAG AAAAATTCCC TAGCAAAGAT GGTATAAATG AATGGGTTCA ATCCAAACAT
 121 CATAAGGATA GTCAAGGCGA ATGGGAGATC TCAGCTGGAA AAGACCCTGT GAATGACAAA
 181 GACTTTGGAT TGCAAACAAA AACAGATTTT CGATACTATG GAATCGCCAA GAAGCTCGAT
 241 AAACCATTTT CTACGGAGGG CAAAACATTT GTTCTTCAGT TTACTGTGAA ATACGATCAA
 301 AGTGTTTCCT GTGGGGGCGC TTACATCAAG CTTTTTGGTT CTGACTTGGA CCCAACGGAC
 361 ATCCATGGTG AATCACCATA TAAACTGATG TTTGGTCCGG ATATTTGCGG GTACAGCACG
 421 AAAAAAATTC ATATAGTCAT ACCGTACAAC GGCAAAAATC ACTTATATAA AGAAGAAGTG
 481 GCTTGTCCTG ATGATTTGCT GACTCACTTG TTCACATTGA TAATCAATCC TGATAATACG
 541 TATAAACTGT TAGTGGACAA TGAACAGAAA AAAAGTGGAT CCCTGGAAGA CCATTGGGAC
 601 CTGTTGCCCC CAAAGAAGAT AGCCGATCCG TCAGTGTCTA AGCCCAGCGA CTGGGTCGAC
 661 GAACCGGAAA TGGACGACCC CAATGACAAA AAGCCTGATG ATTGGGTAGA GGTTAAAACC
 721 ATTCCCGATT CTCAGGCGAA GAAACCAGAA GACTGGGATG ACGAAATGGA CGGTGAATGG
 781 GAGCCACCGA AAATTGATAA TCCGGACTAC AAGGGAGAAT GGAAACCAAA GAAGATTCCC
 841 AACCCAGAAT ACAAAGGAGA GTGGAAAGCT CCCGAGATCG ACAATCCCGA ATACGCACCA
 901 GACGACAAAC TTTATCTGTT GAAGGACGTC GCATACGTCG GGTTTGACTT GTGGCAAGTC
 961 AGCTCGGGCT CGCTTTTCGA CAACATACTC TTGACCAACG ACCCTGATTA CGCCCGTTCT
1021 CAAGGTGAAG AGTTCTGGAA GACACGGTAT GAAGCTGAGA AAGCAGCAAA AGAAAAGAAA
1081 GATGCAGAGG ATGCTAAGAG GGCAGAAGAG GAGCGAAAGA AAATGGAGGA AGAGGAGAAA
1141 AAGAAGAAAG GGGATAAAGA GAAGAAAGAA GATAAAGCAG AACAGACTGA GGAGGAAGAG
1201 AAAGAAAAGG AGGACCAAGA GGCCAAAGTA GAACCGACTA AATCGGATGC CGATCATGAG
1261 GAGTTGTAA
```

B

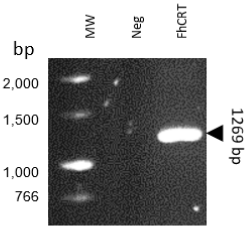

Figure 4.4.2.3.1.1. PCR target and amplicon for *FhCRT*. *FhCRT* was targeted for PCR amplification, whereby oligomers were designed to amplify the gene including start and stop codons. 11 SNPs were identified by Sanger DNA sequencing (underlined residues) (A), and a single amplicon was demonstrated by 1% agarose gel electrophoresis (B).

Abbreviations: MW, NEB Fast DNA Ladder (bp); neg, negative.

5' flanking restriction enzyme binding sites were introduced via PCR using FhCRT-pGEM®-T Easy as the PCR template (for primer sequences, see Table 4.3.1.1.3) and cloned using pGEM®-T Easy as before. NdeI-NotI-digested *FhCRT* was then inserted into NdeI-NotI-linearised pET-23a(+) (Figure 4.4.2.1A–B) and confirmed using diagnostic restriction digestion (Figure 4.4.2.3.1.2A). Positive transformant BL21(DE3) cell lines were also confirmed via PCR (Figure 4.4.2.3.1.2B) and Sanger Sequencing of *FhCRT*-pET-23a(+) was used to identify to identify the correct DNA and protein sequence for expression (>99.3% ID, Figure 4.4.2.3.1.2C).

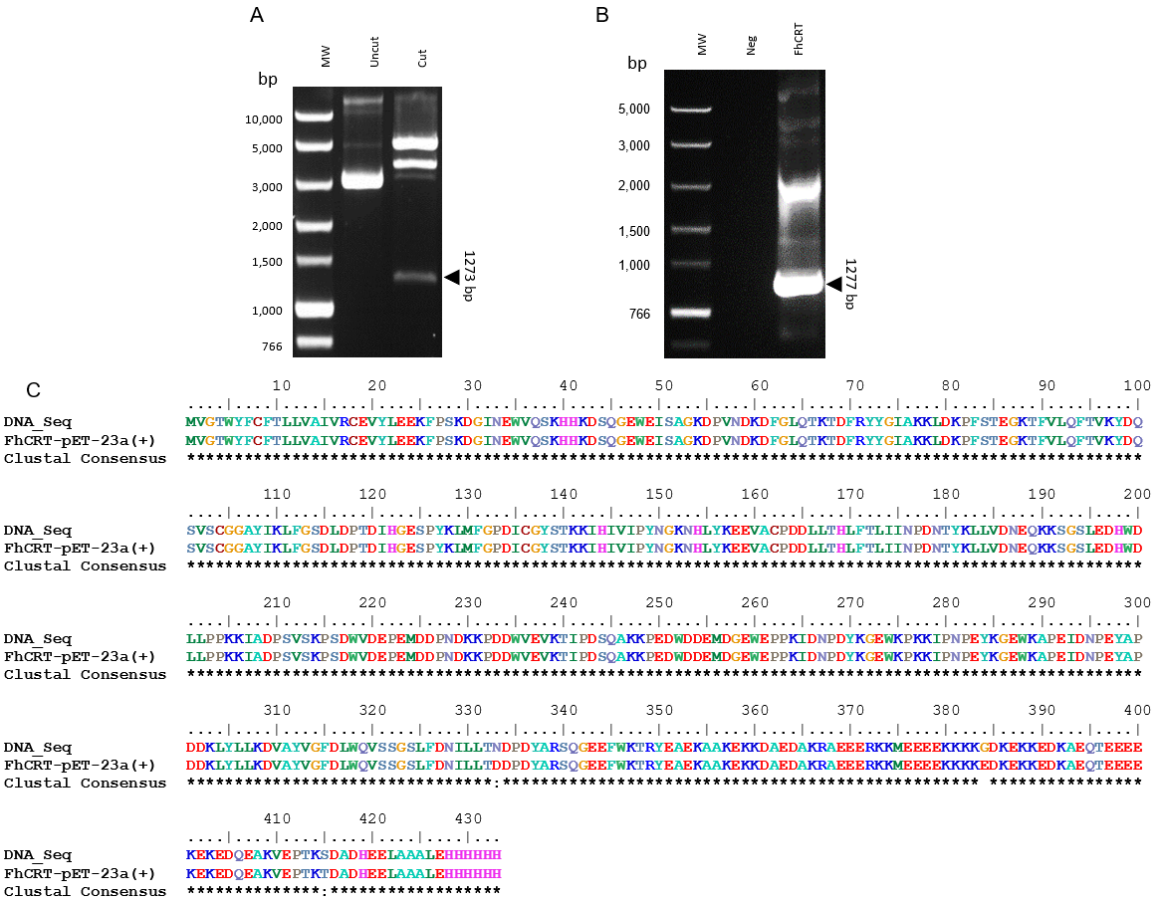

Figure 4.4.2.3.1.2. Subcloning and DNA diagnostics of *FhCRT*-pET-23a(+). The subcloning sequence for *FhCRT* was isolated from *FhCRT*-pGEM®-T Easy via NdeI and NotI double digestion for insertion into NdeI-NotI-linearised pET-23a(+). *FhCRT*-pET-23a(+) constructs were tested via diagnostic digestion (NdeI and NotI) (A). (B) Positive BL21(DE3) cell lines were identified via colony PCR using *FhCRT* subcloning primers and (C) DNA sequencing identified three SNPs in the *FhCRT*-pET-28b(+) expression sequence, leading to three amino acid substitutions upon translation (compiled using BioEdit).

Abbreviations: MW, Bioline HyperLadder™ 1kb (bp); neg, negative.

Upon *in silico* translation, three amino acid substitutions were identified (D333N, E384G, T415S) and PROVEAN identified two as synonymous and non-deleterious and one as non-synonymous and deleterious (Table 4.4.2.3.1). These findings differ from the assumptions that can be made based on the biochemical properties of these amino acids (Betts and Russell, 2007). The non-deleterious effect of Thr^{415} to Ser^{415} is however supported by intrinsic amino acid properties, as these are identical in molecular structure and only differ by a methyl group replacing a hydrogen group (Betts and Russell, 2007). Similar is expected for asparagine-aspartate interchanges, as both have similar molecular weight and functionality in polypeptides, though asparagine causes a loss of a negative charge (Betts and Russell, 2007). The substitution of glutamic acid would conversely be expected to cause a non-

synonymous deleterious effect, being disparate in structure and functionality due to the halved molecular weight and added negative charge that glycine provides (Betts and Russell, 2007). Overall the sequence identity differences of FhCRT at the gene and protein level from the original sequence source may have some consequential structure- or function-related changes of unknown importance. However, as this protein sequence originated from natural cDNA, the possibility of isolated protein residue substitutions having negative impacts on protein function would be a considerable evolutionary disadvantage, and therefore not fully explained or confirmed by *in silico* predictions.

Table 4.4.2.3.1. PROVEAN Prediction for protein sequence analysis of FhCRT. Sequence variants (Asp^{333}–Asn^{333}, Glu^{384}–Gly^{384}, Thr^{415}–Ser^{415}) were predicted with scores above and below the default threshold, which indicate these changes had mixed effects.

Variant	PROVEAN score	Prediction (default threshold ≤ -2.5)
D333N	-3.423	Deleterious
E384G	-1.814	Neutral
T415S	0.379	Neutral

4.4.2.3.2 Expression

Previously, recombinant calreticulins (CRTs) in similar bacterial expression systems have been expressed at low temperatures including 28°C and 32°C (Mendlovic *et al.*, 2004; Rokeach *et al.*, 1991; Wang *et al.*, 2012), and so these conditions were the basis for this pilot expression. rFhCRT was predicted to be 50.24 kDa with an isoelectric point of 4.79 and an overall charge of -37.0, including the signal peptide, and SDS PAGE analysis (Figure 4.4.2.3.2.1) demonstrated target protein overexpression under all conditions in soluble fractions, but particularly after 0.6 mM IPTG and five hours at 28°C.

IMAC purification was trialled using HIS-Select Nickel resin (Figure 4.4.2.3.2.2), but SDS PAGE and western hybridisation with HisProbe™-HRP revealed low target protein abundance and protein elution at low imidazole concentration, respectively.

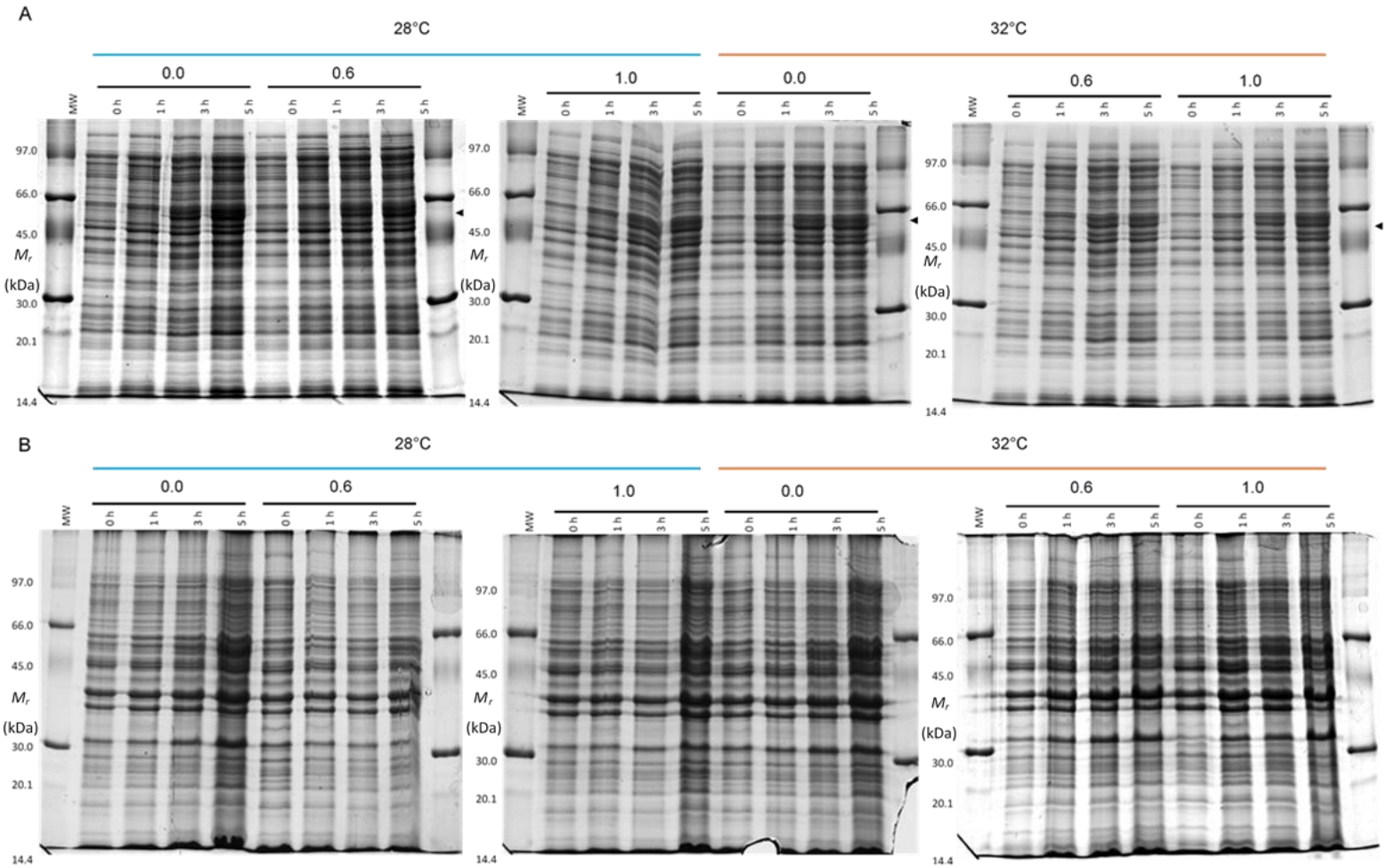

Figure 4.4.2.3.2.1. Pilot expression of rFhCRT. Final concentrations of 0, 0.6 mM and 1.0 mM IPTG and growth temperatures of 28°C and 32°C were trialled for the expression of rFhCRT, and both lysate (A) and IB (B) fractions from 0–5 hours post-induction were analysed.

Abbreviations: MW, Amersham Low Molecular Weight SDS Calibration Kit (M_r); 0–5 h, hours post-induction; IPTG [0.0, 0.6, 1.0 mM]; growth temperature, 28°C and 32°C.

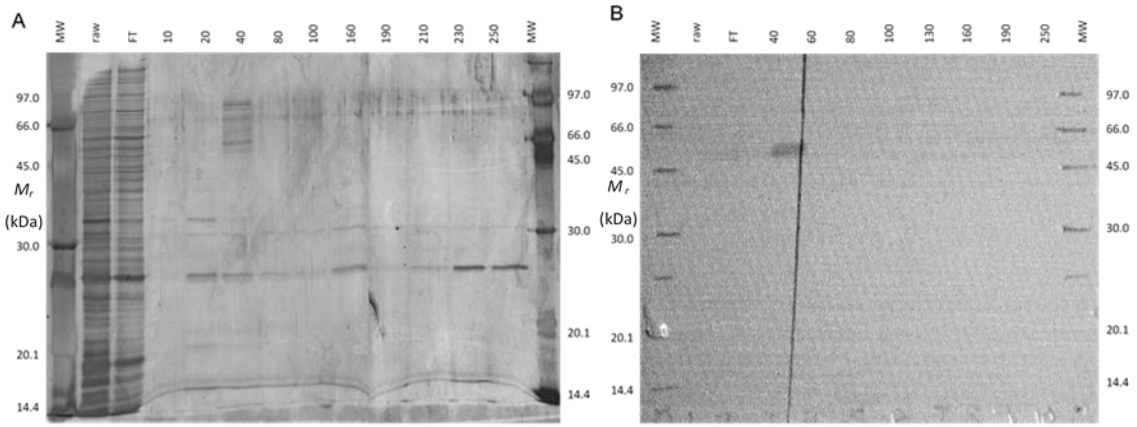

Figure 4.4.2.3.2.2. IMAC purification of rFhCRT. rFhCRT isolation from recombinant expression lysate was tested using HIS-Select Cobalt resin. Fractions were analysed by SDS PAGE (A) demonstrating consistent co-elutents at approximately 27 and 31 kDa, and western blotting with HisProbe™-HRP (B) indicated premature target elution. Abbreviations: MW, Amersham Low Molecular Weight SDS Calibration Kit (M_r); raw, raw bacterial lysate; FT, flow-through; 10–500 [mM], imidazole concentration.

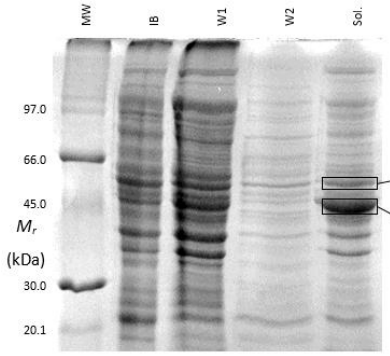

Fh genome hit	MASCOT score (P < 0.05)	Peptides matched (non-duplicate)
BN1106_s201B000462.mRNA-1	78	1
BN1106_s2953B000132.mRNA-1	33	1
BN1106_s1355B000089.mRNA-3	49	1
BN1106_s2004B000173.mRNA-4	34	3

Figure 4.4.2.3.2.3. Trial solubilisation of rFhCRT and LC-MS/MS identification. Fractions from IB protein solubilisation were analysed by 12.5% SDS PAGE, indicating protein composition changes between IB, washes and solubilised fractions. Intense protein bands at approximate molecular weights of interest for FhCRT were investigated by LC-MS/MS and searched against the *Fasciola hepatica* genome (PRJEB6687, WBPS v10) on an in-house MASCOT server (only hits above threshold 31 score shown).
Abbreviations: MW, Amersham Low Molecular Weight SDS Calibration Kit (M_r); IB, inclusion bodies; W, washes; Sol, solubilised IB supernatant.

Since pilot expression conditions were disproportionately conducive towards IB production, this further reduced the soluble fraction proportion containing rFhCRT (following presumed signal peptide cleavage). Thus, further expression trials were conducted at 37°C for five hours and 18°C for 16 hours following IPTG induction, but lysate ratios remained unfavourable and yielded poor target concentration from soluble lysates (data not shown). Thus, to test rFhCRT presence in IBs, samples were denatured as described (4.3.3.2) and

analysed by SDS PAGE and LC-MS/MS (Figure 4.4.2.3.2.3), revealing no CRT-like protein presence and suggesting rFhCRT is not processed into IBs.

To allow for optimal rFhCRT overexpression and purification, subcloning was repeated to remove the signal peptide (4.4.2.4).

4.4.2.4 Truncation of calreticulin (FhΔCRT)

4.4.2.4.1 Subcloning

Following the findings of the previous section (4.4.2.3) and to remove the signal peptide, FhCRT truncation was performed via PCR using *FhCRT*-pGEM®-T Easy as a template (for primer sequences, see Table 4.3.1.1.3), sequenced (Figure 4.4.2.4.1.1A), and electrophoresed (Figure 4.4.2.4.1.1B) for gel excision and direct ligation with pGEM®-T Easy and cloning using α-select *E. coli* as before. NdeI-NotI-digested *FhΔCRT* (Figure 4.4.2.4.1.2A) was then inserted into NdeI-NotI-linearised pET-28b(+) (Figure 4.4.2.1C–D) and confirmed using diagnostic restriction digestion and PCRs (Figure 4.4.2.4.1.2B–C). Positive transformant BL21(DE3)pLysS cell lines were also confirmed via PCR (Figure 4.4.2.4.1.2D) and Sanger Sequencing of *FhΔCRT*-pET-28b(+) was used to identify the correct DNA and protein sequence for expression (>99.2% ID, Figure 4.4.2.4.1.2E).

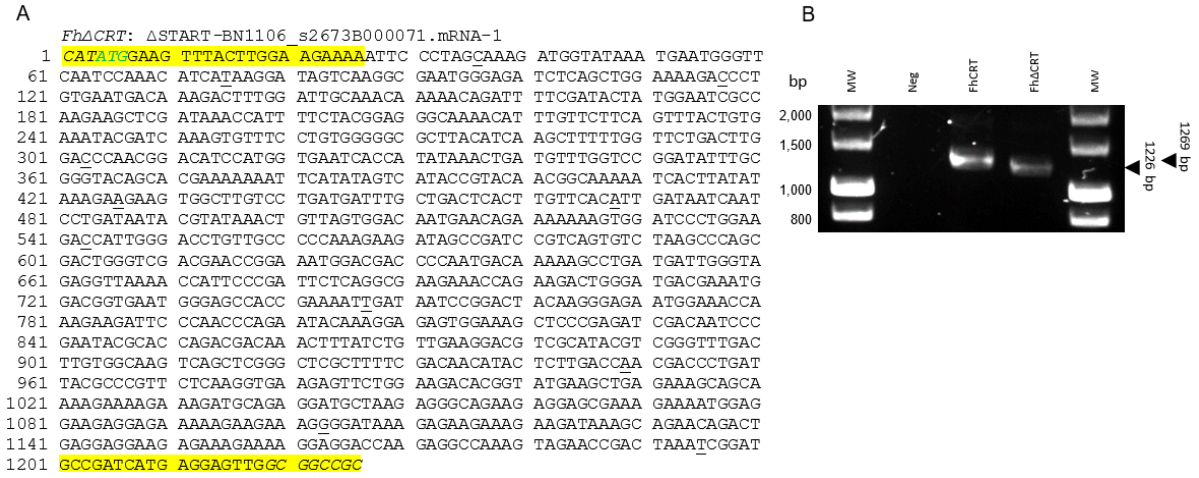

Figure 4.4.2.4.1.1. PCR target and amplicon for truncated *FhΔCRT*. A new 5' oligonucleotide with the NdeI subcloning restriction enzyme site was added via PCR using *FhCRT*-pGEM®-T Easy as a template (A), designed to remove the first 66 base pairs of the *FhCRT* gene sequence (signal peptide-associated amino acids (1–21 aa)) for direct subcloning. A single amplicon of expected molecular weight was demonstrated by 1% agarose gel electrophoresis (B).

Abbreviations: MW, Bioline HyperLadder™ 1kb (bp); neg, negative.

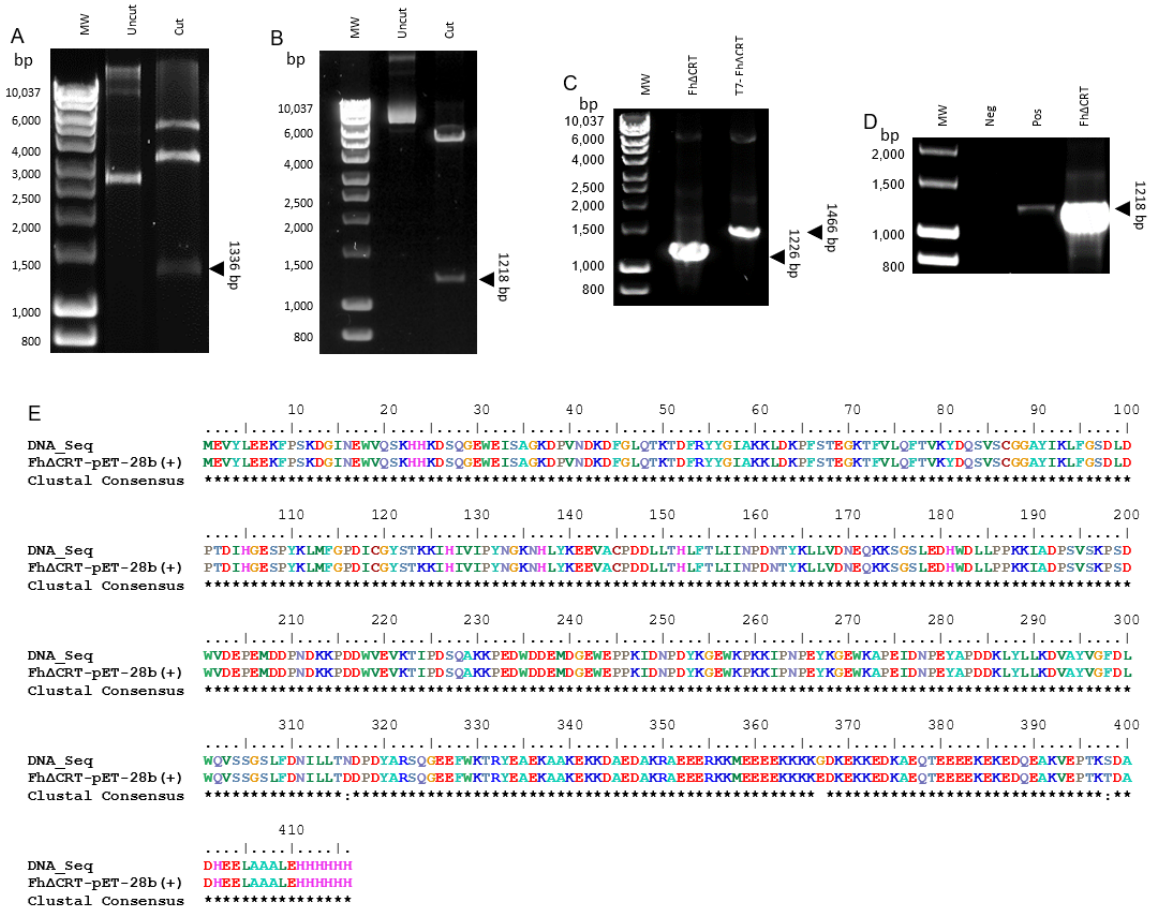

Figure 4.4.2.4.1.2. Subcloning and DNA diagnostics of *FhΔCRT*-pET-28b(+). The subcloning sequence for *FhΔCRT* was isolated from *FhΔCRT*-pGEM®-T Easy via NdeI and NotI double digestion (A) for insertion into NdeI-NotI-linearised pET-28b(+). *FhΔCRT*-pET-28b(+) constructs were tested via diagnostic digestion (NdeI and NotI) (B) and PCRs (C) using *FhΔCRT* subcloning and T7 primers. (D) Positive One Shot® BL21(DE3) Star™ cell lines were identified via colony PCR using *FhΔCRT* subcloning primers and (E) DNA sequencing identified three SNPs in the *FhΔCRT*-pET-28b(+) expression sequence, leading to three amino acid substitutions upon translation (compiled using BioEdit).

Abbreviations: MW, Bioline HyperLadder™ 1kb (bp); neg, negative; pos, positive (cDNA: *FhΔCRT*).

Upon *in silico* translation, three residue substitutions were identified as before (4.4.2.3.1) except in truncation-adjusted positions (D316N, E367G, T398S) but with changed PROVEAN scores (Table 4.4.2.4.1), possibly due to the subtle differences in residue position and *in situ* exposure. However, further predictions with the MutPred2 tool (Li *et al.*, 2009) identified altered molecular mechanisms due to the D316N substitution (P = 0.01≤0.05), affecting a predicted ELM motif for a small ubiquitin-like modifier (SUMO) interaction site that commonly share an aspartate residue (ELME000333, the Eukaryotic Linear Motif resource, Gouw *et al.*, 2018: http://elm.eu.org/elms/LIG_SUMO_SIM_par_1.html). This

leading to a gain of allosteric (0.25 probability) and catalytic (0.13 probability) properties and loss of relative solvent accessibility (0.23 probability) likely reflect the difference in the amino acids' biochemical properties, including charge (D, -1.0 to N, 0.0) and R group (D, hydroxyl to N, amine group; ΔMr: -0.98 $g \cdot mol^{-1}$). Regarding solvent accessibility, interestingly both amino acids are nominally peripherally associated, involved in salt-bridge formation, and similarly involved in functional and binding properties (Betts and Russell, 2007). Thus, these predictions suggest the putative changes could have functional consequences but are difficult to underpin using *in silico* tools.

Table 4.4.2.4.1. PROVEAN Prediction for protein sequence analysis of FhΔCRT. Sequence variants were the same as previously described (Asp^{316}–Asn^{316}, Glu^{367}–Gly^{367}, Thr^{398}–Ser^{398}) were predicted with scores above and below the default threshold, which indicate these changes had mixed effects.

Variant	PROVEAN score	Prediction (default threshold ≤ -2.5)
D316N	-3.381	Deleterious
E367G	-2.100	Neutral
T398S	0.291	Neutral

4.4.2.4.2 Expression

rFhΔCRT was predicted to be 48.27 kDa with an isoelectric point of 4.77 and an overall charge of -38.0, and SDS-PAGE (Figure 4.4.2.4.2.1) demonstrated optimal target protein overexpression (~50 kDa) in soluble fractions after 0.5 mM IPTG and five hours at 37°C. IMAC purification was trialled using HIS-Select Cobalt resin under low pH conditions (pH 6.0), demonstrating contaminant co-elution with rFhΔCRT (Figure 4.4.2.4.2.2A), suggesting suboptimal conditions. All post-IMAC flow-through fractions were therefore pooled for attempted re-purification with HIS-Select Cobalt using solutions buffered to pH 8.0, but sustained co-contaminations (Figure 4.4.2.4.2.2B). Isolated rFhΔCRT protein in the flow-through and wash fractions demonstrated dimorphic CRT isoforms, which has been observed in *Trypanosoma cruzi* calreticulin (Aguillón *et al.*, 2000), and so were analysed by LC-MS/MS, confirming both as *F. hepatica* calreticulin (PRJEB6687, WBPS v10: BN1106_s2673B000071.mRNA-1, Table 4.4.2.4.2). Based on the purity observed, the flow-through fraction was used for further analyses.

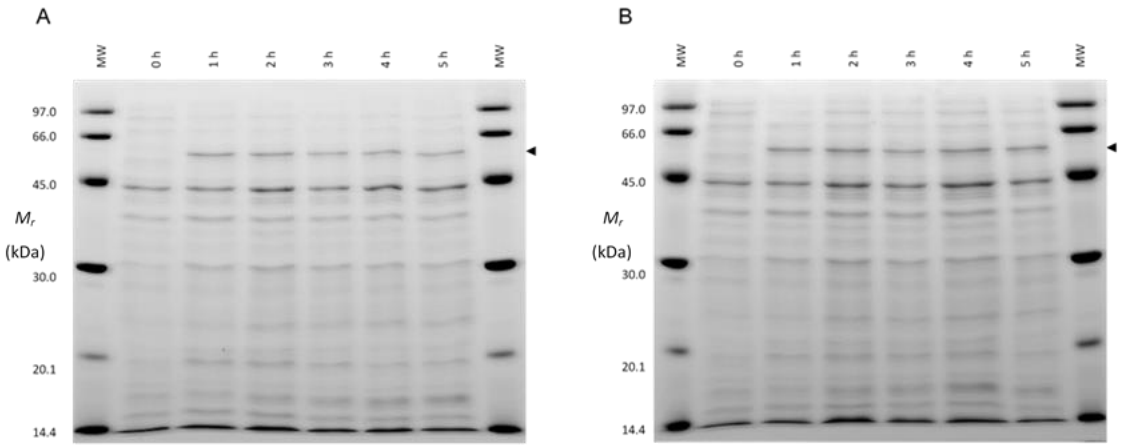

Figure 4.4.2.4.2.1. Pilot expression of rFhΔCRT. 5 µg FhΔCRT-pET-28b(+) BL21(DE3)pLysS recombinant expression lysate containing rFhΔCRT was analysed by SDS PAGE following 0.1 mM (A) and 0.5 mM (B) IPTG from 0–5 hours post-induction at 37°C.

Abbreviations: MW, Amersham Low Molecular Weight SDS Calibration Kit (M_r); 0–5 h, hours post-induction.

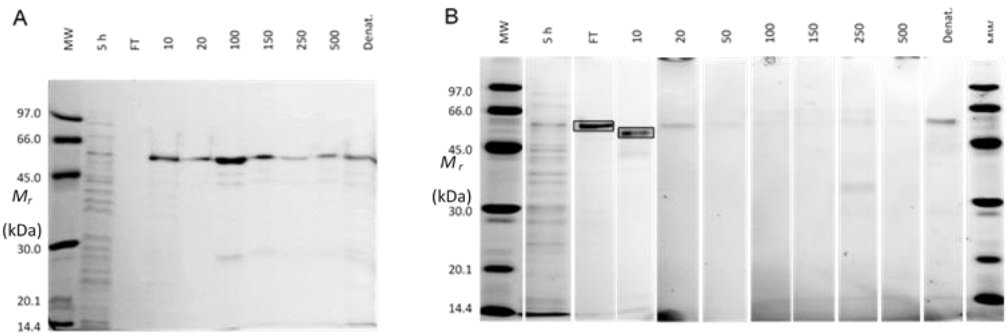

Figure 4.4.2.4.2.2. IMAC purification of rFhΔCRT. rFhΔCRT was isolated from recombinant expression lysate using HIS-Select Cobalt resin over two operations. A trial protocol (pH 6.0) was conducted (A), but due to suboptimal target elution a second trial was subsequently conducted (pH 8) (B) using the pilot purification fractions, leading to high target concentration in flow-through and 10 mM wash fractions identified by LC-MS/MS (Table 4.4.2.4.2).

Abbreviations: MW, Amersham Low Molecular Weight SDS Calibration Kit (M_r); raw, raw bacterial lysate; FT, flow-through; 10–500 [mM], imidazole concentration.

Purified rFhΔCRT was analysed by 1-D and 2-D SDS PAGE (Figure 4.4.2.4.2.3A–B) and resolved at approximately 50 kDa with two putative isomers separating between 5.25 and 5.50 which were analysed by LC-MS/MS (Table 4.4.2.4.2). MASCOT identified both protein isomers as calreticulin (PRJEB6687, WBPS v10: BN1106_s2673B000071.mRNA-1) that scored against the FhCRT GenBank hit (PRJNA179522: WBPS v10–14, GenBank v204; PIS80991.1: www.ncbi.nlm.nih.gov/protein/PIS80991.1; Table 4.4.2.4.2), which is currently the only

annotated sequence for *F. hepatica* calreticulin on this database. A sequence alignment of the cloned sequence and the two available sequences from draft genomes (Figure 4.4.2.4.2.4A) indicated all sequences closely match (85.36–99.01%). The cloned truncated calreticulin differed from BN1106_s2673B000071.mRNA-1 by only three residues, excluding the signal peptide, that were identified by Sanger sequencing previously (Figures 4.4.2.3.1.2 and 4.4.2.4.1.2), but both sequences differed further from PIS80991.1, which had an insertion of 35 residues (132–157) as well as 51 amino acid variants from the other sequences.

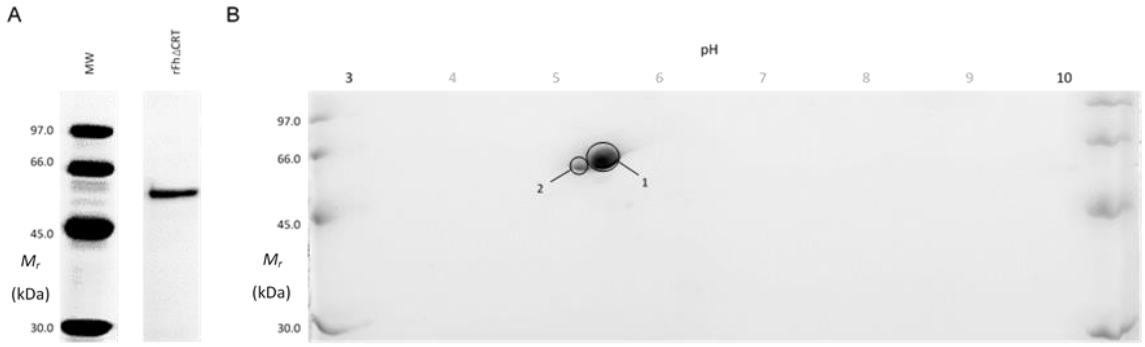

Figure 4.4.2.4.2.3. 1-D and 2-D SDS PAGE separation of purified rFhΔCRT. rFhΔCRT was resolved at approximately 50 kDa by 1-DE (1.5 µg) (A), whereas 2-DE (5 µg) (B) identified isomer separation between 5.25 and 5.50 pH (7 cm IEF 3–10; 12.5% SDS PAGE). LC-MS/MS identified both 2-DE separated isomers as calreticulin (BN1106_s2673B000071.mRNA-1; GenBank: PIS80991.1, Table 4.4.2.4.2).

Abbreviations: MW, Amersham Low Molecular Weight SDS Calibration Kit (M_r).

Table 4.4.2.4.2. LC-MS/MS identification of 1-DE- and 2-DE-separated rFhΔCRT. rFhΔCRT protein bands/spots of interest were identified by LC-MS/MS against the *F. hepatica* genome (PRJEB6687, WBPS v10) and GenBank (v204), reporting significant hits identified with a score of 37 or greater (P < 0.01).

Figure reference	Sample	MS/MS ion search					Highest scoring GenBank hit		
		Fh genome hit	MASCOT score	Peptides matched (non-duplicate)	Sequence coverage (%)	Protein	Organism	Accession	E-value
4.4.2.4.2.2B	1-DE 1	**BN1106_s2673B000071.mRNA-1**	551	51	52.0	**Calreticulin family protein**	***Fasciola hepatica***	**PIS80991.1**	**0.0**
	1-DE 2		586	57	45.0				
4.4.2.4.2.3B	2-DE 1		1842	150	71.0				
	2-DE 2		850	65	68.0				

All peptide residues matched by LC-MS/MS analysis of FhΔCRT are also highlighted (Figure 4.4.2.4.2.4A). Predicted peptide data demonstrated putative post-translational modifications, indicating oxidation at Met^{130}, Met^{224} and Met^{256} residues. Peptide fragmentation data for the highest scoring protein submission (i.e. 2-DE spot 1) were interpreted to investigate the previously-identified aspartate-asparagine (FhΔCRT: D316N) substitution (Figure 4.4.2.4.2.4B). This however could not be conducted for the glycine-glutamate (FhΔCRT: E367G) or threonine-serine (FhΔCRT: T398S) substitutions, as these regions were not identified by LC-MS/MS, likely due to the low concentration of short-length peptides in this region containing a high density of lysine residues at which the trypsin protease cleaves. Fragmentation data for the peptide Asp292-Arg322 (n = 31) indicate the D316N residue was the highest scoring peptide, whereby the majority present (46.77%) had an asparagine residue. These data suggest the cDNA used for this cloning encodes an FhCRT containing this residue substitution (FhCRT: D333N; FhΔCRT: D316N), which is also distinct from previously identified sequences.

Based on the findings from these pilot studies for rFhΔCRT, this recombinant has been optimally overexpressed and purified at adequate concentrations for further investigation of biochemical and diagnostic investigation.

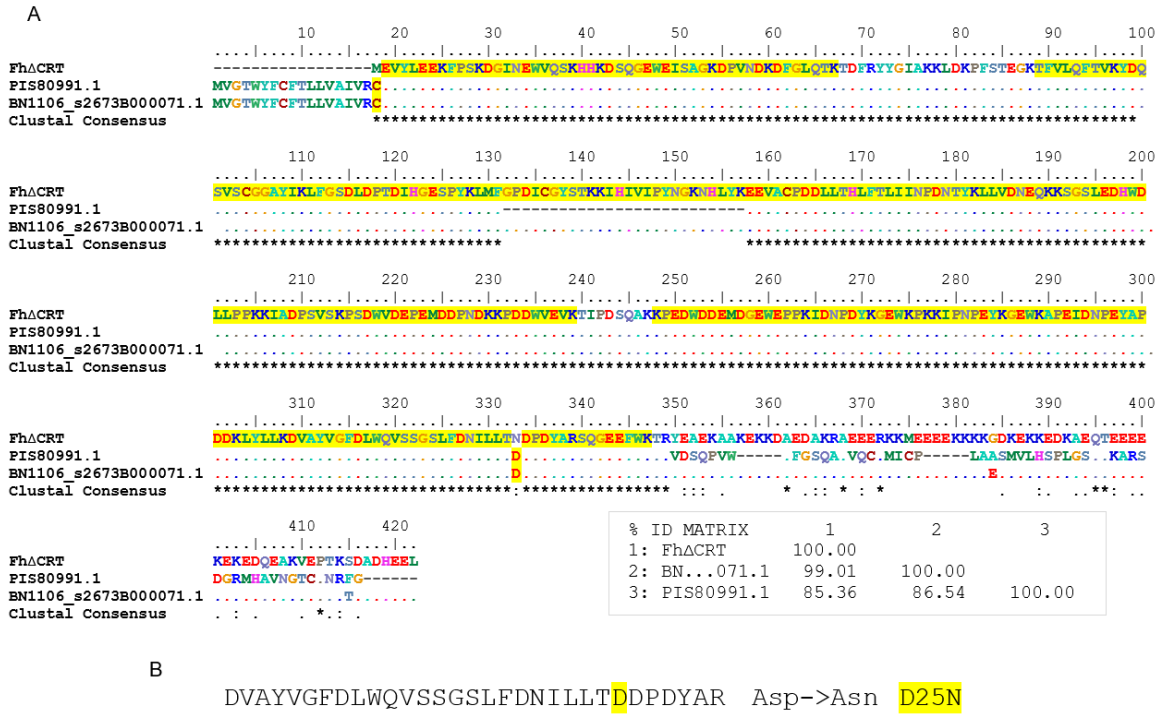

Figure 4.4.2.4.2.4. Comparison of the calreticulin amino acids sequences cloned in this study (FhΔCRT) and two genome sources (dotted lines). (A) Based on DNA sequencing, three amino acids were different in the cloned calreticulin sequence (cDNA: FhΔCRT) from a draft genome expression sequence (PRJEB6687, WBPS v10: BN1106_s2673B000071.mRNA-1) and the GenBank hit identified from LC-MS/MS (PRJNA179522, WBPS v10–14, PIS80991.1: www.ncbi.nlm.nih.gov/protein/PIS80991.1). Highlighted residues represent all peptides matched by LC-MS/MS analysis of rFhΔCRT and the alignment was produced using the ClustalO tool in BioEdit. (B) LC-MS/MS peptide fragmentation data for the FhΔCRT peptide including the SNP at Asn-316 (alignment position: 333) indicated this residue had a high scoring modification with a dominant neutral loss, suggesting an asparagine (N) in place of aspartate (D).

4.4.2.5 DJ-1 deglycase (FhDJ-1)

4.4.2.5.1 Cloning and subcloning

FhDJ-1 was PCR-amplified (for primer sequences, see Table 4.3.1.1.3) sequenced (>99.6% ID, Figure 4.4.2.5.1.1A), and electrophoresed (Figure 4.4.2.5.1.1B) for gel excision and direct ligation with pGEM®-T Easy and cloning in α-select *E. coli*.

5’ flanking restriction enzyme binding sites were introduced via PCR using *FhDJ-1*-pGEM®-T Easy as the PCR template (for primer sequences, see Table 4.3.1.1.3) and cloned using pGEM®-T Easy as before. NdeI-NotI-digested *FhDJ-1* (Figure 4.4.2.5.1.2A) was then inserted into NdeI-NotI-linearised pET-28b(+) (Figure 4.4.2.1C–D) and confirmed using diagnostic restriction digestion and PCRs (Figure 4.4.2.5.1.2C–D). Positive transformant

BL21(DE3)pLysS cell lines were also confirmed via PCR (Figure 4.4.2.5.1.2D) and Sanger Sequencing of *FhDJ-1*-pET-28b(+) was used to identify the correct DNA and protein sequence for expression (>98.9% ID, Figure 4.4.2.5.1.2E).

Figure 4.4.2.5.1.1. PCR target and amplicon for *FhDJ-1*. *FhDJ-1* was targeted for PCR amplification, including start and stop codons. Two SNPs were identified by Sanger DNA sequencing (underlined) (A), and a single amplicon was demonstrated by 1% agarose gel electrophoresis (B).

Abbreviations: MW, Bioline HyperLadder™ 1kb (bp); neg, negative.

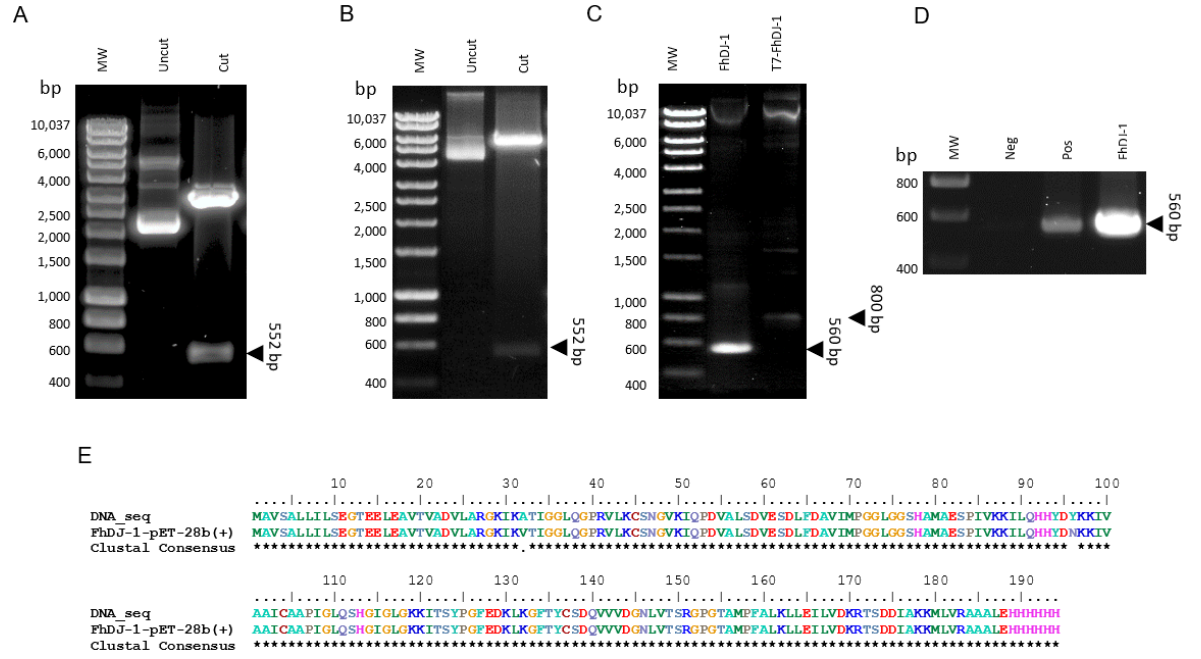

Figure 4.4.2.5.1.2. Subcloning and DNA diagnostics of *FhDJ-1*-pET-28b(+). The subcloning sequence for *FhDJ-1* was isolated from *FhDJ-1*-pGEM®-T Easy via NdeI and NotI double digestion (A) for insertion into NdeI-NotI-linearised pET-28b(+). *FhDJ-1*-pET-28b(+) constructs were tested via diagnostic digestion (NdeI and NotI) (B) and PCRs (C) using *FhDJ-1* subcloning and T7 primers. (D) Positive BL21(DE3)pLysS cell lines were identified via colony PCR using *FhDJ-1* subcloning primers and (E) DNA sequencing identified two SNPs in the *FhDJ-1*-pET-28b(+) expression sequence, leading to two amino acid substitutions upon translation (compiled using BioEdit).

Abbreviations: MW, Bioline HyperLadder™ 1kb (bp); neg, negative; pos, positive (cDNA: *FhDJ-1*).

Upon *in silico* translation, two residue substitutions were identified (V32A, N96Y), which PROVEAN identified as non-synonymous and synonymous, respectively (Table 4.4.2.5.1). This is supported by the biochemical properties of these amino acids, particularly because both substitutes involve significant changes to amino acid moieties. Specifically, alanine's small side chain reduces its polarity compared to valine, and asparagine is non-aromatic conversely to tyrosine, which loses the phenol moiety functionality (Betts and Russell, 2007). It can therefore be inferred from these findings that the residue substitutions could contribute to changes in the structure and/or function of FhDJ-1.

Table 4.4.2.5.1. PROVEAN Prediction for protein sequence analysis of FhDJ-1. Sequence variants (Val^{32}–Ala^{32}, Asn^{96}–Tyr^{96}) were predicted with scores below and above the default threshold, which indicate these changes had mixed but mildly deleterious effects.

Variant	PROVEAN score	Prediction (default threshold ≤ -2.5)
V32A	-3.450	Deleterious
N96Y	-2.367	Neutral

4.4.2.5.2 Expression

Previous studies for the recombinant expression of DJ-1 have used low temperatures, including rDmDJ-1β (PDB: 4E08; Lin, Prahlad and Wilson, 2012) and rHsDJ-1 (PDB: 1P5F; Tao and Tong, 2003) FhDJ-1-associated models (4.4.1.4), and so these conditions were the basis for this pilot expression. Based on previous literature and bioinformatic analyses, DJ-1 dimerisation was also expected (Honbou *et al.*, 2003; Tao and Tong, 2003). rFhDJ-1 was predicted to be 20.60 kDa with an isoelectric point of 7.15 and an overall neutral charge, and SDS-PAGE (Figure 4.4.2.5.2.1) demonstrated potential bands corresponding to the expected molecular weights of monomer (~20 kDa) and dimer (~40 kDa) target protein overexpression in both soluble and insoluble fractions after 0.05, 0.1, 0.5 and 1.0 mM IPTG and 24 hours at 18°C. As for rFhCRT, these primary expression conditions were disproportionately conducive for insoluble IB formation and so a subsequent expression trial would be recommended for upto 5 hours at 37°C as shown for rHsDJ-1 (Zhou *et al.*, 2006).

IMAC purification was trialled using HIS-Select® Nickel (Figure 4.4.2.5.2.2), whereby elution samples indicated several histidine-rich proteins, including targets of approximately 15, 26 and 28 kDa, the last of which continued into subsequent elution fractions. The second 250 mM fraction, although including co-eluting contaminants, was used for further preliminary analysis and molecular characterisation.

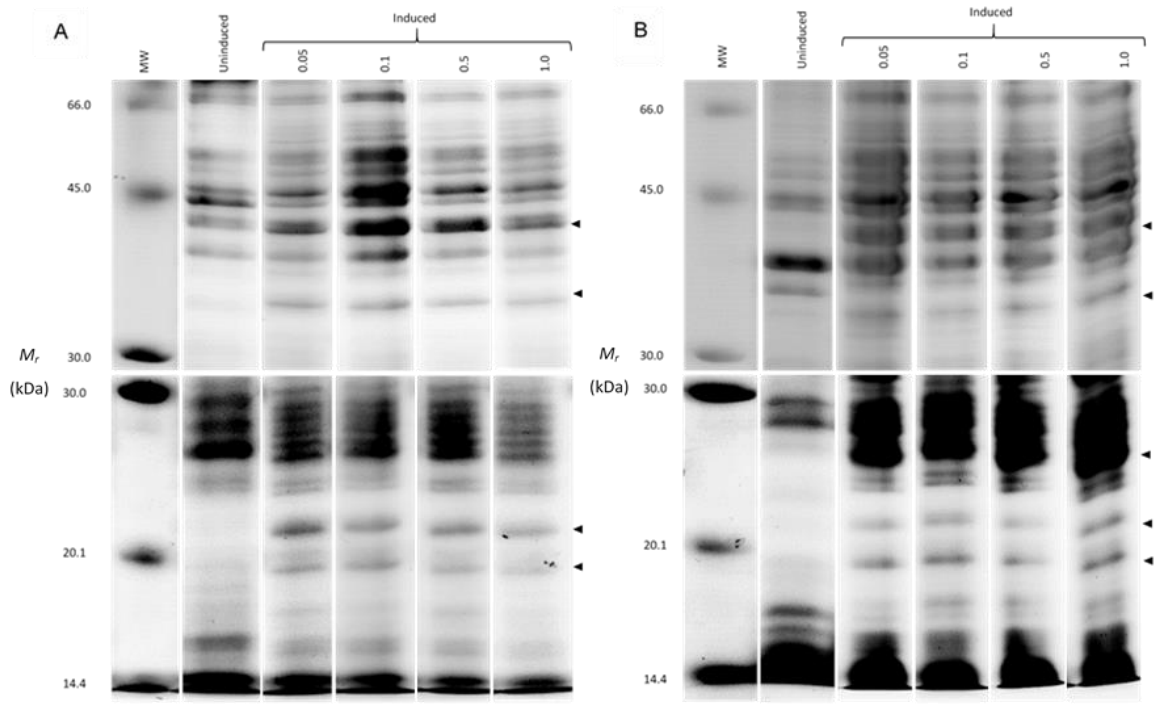

Figure 4.4.2.5.2.1. Pilot expression of rFhDJ-1. 5 µg FhDJ-1-pET-28b(+) BL21(DE3)pLysS recombinant expression lysate (A) and IB (B) fractions following 0.05, 0.1, 0.5 and 1.0 mM IPTG at 0 (uninduced) and 24 (induced) hours post-induction at 18°C were analysed by SDS PAGE. The specific molecular weight ranges between 30.0–66.0 and 14.4–30.0 kDa are shown for expected rFhDJ-1^2 dimers and rFhDJ-1 monomers, respectively.
Abbreviations: MW, Amersham Low Molecular Weight SDS Calibration Kit (M_r); 0.05–1.0, IPTG [mM].

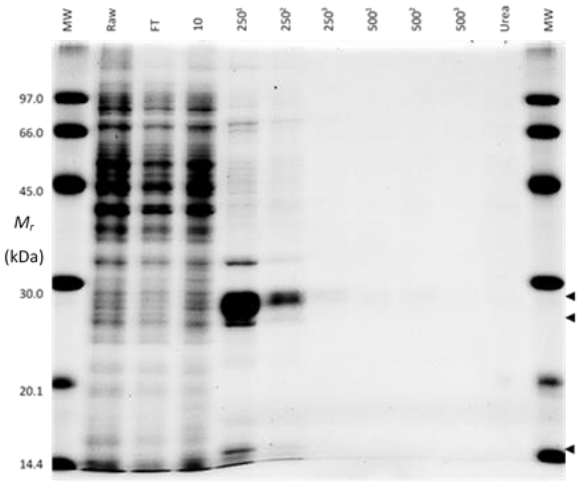

Figure 4.4.2.5.2.2. Trial IMAC purification of rFhDJ-1. rFhDJ-1 purification from recombinant expression lysate was attempted using HIS-Select Nickel resin and analysed by SDS PAGE, indicating a resultant ~25–27 kDa fraction consistent in elutions.
Abbreviations: MW, Amersham Low Molecular Weight SDS Calibration Kit (M_r); raw, raw bacterial lysate; FT, flow-through; 10–500 [mM], imidazole; urea, 8 M wash.

Semi-purified rFhDJ-1 was analysed by 1-D and 2-D SDS PAGE (Figure 4.4.2.5.2.3A–B) and 1-DE indicated three major visible bands at approximately 15, 26 and 28 kDa, where the larger two separated between 4.90 and 6.10 pI and the smallest separated between 8.3 and 8.8 pI based on 2-DE (Figure 4.4.2.5.2.3A–B). LC-MS/MS was used to identify all protein bands/spots (Table 4.4.2.5.2), which together indicated that all proteins were partially

identified as FhDJ-1 (PRJEB6687, WBPS v10: BN1106_s1971B000297.mRNA-1; PRJNA179522, WBPS v10–14, PIS82126.1: www.ncbi.nlm.nih.gov/protein/PIS82126.1; P < 0.025, 10.00-180.00% FDR).

Figure 4.4.2.5.2.3. 1-D and 2-D SDS PAGE separation of purified rFhDJ-1. rFhDJ-1 was analysed by 1-DE (A),

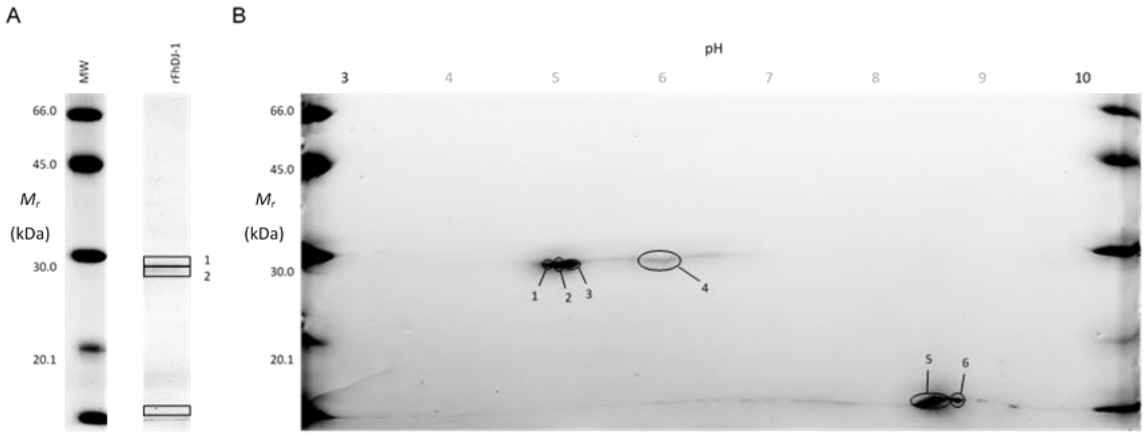

showing three bands of potential interest at approximately 15, 26 and 28 kDa, whereas 2-DE (B) revealed all three proteins separate at two isoelectric point ranges between 4.90 and 6.10, and 8.30 and 8.80 (7 cm IEF 3–10; 12.5% SDS PAGE). LC-MS/MS identified 1-DE and 2-DE separated proteins, including FhDJ-1 (MASCOT Score = 35-86: BN1106_s1971B000297.mRNA-1, PRJEB6687, WBPS v10–14/PRJNA179522, PIS80991.1, GenBank v204). LC-MS/MS results are detailed in Table 4.4.2.5.2.

Abbreviations: MW, Amersham Low Molecular Weight SDS Calibration Kit (M_r).

The 28 kDa fraction across both gel samples were identified as FhDJ-1, whereas identifications of the 26 kDa protein was only from the 1-DE sample and the 15 kDa protein(s) from the 2-DE sample (Table 4.4.2.5.2). Of additional note is that all peptides matched were only from the C-terminal half of the protein sequence (Ile^{121}–Lys^{170}) that is also lysine-rich (Lys, K, contributing 10.8% of residues: 91–183). This biochemical composition may have condemned over-digestion of protein samples by the trypsin protease for this LC-MS/MS preparation, producing fewer measurable peptides owing to the high frequency of this enzyme's target. This C-terminal fragment is also predicted to be 10.10 kDa with a pI of 9.20, which could be suggested as the possible low molecular weight fragment that may be a fragment of FhDJ-1. The low MASCOT scores possibly reflect the low concentrations of FhDJ-1 in the target mixture, but the absence of any N-terminal specific peptide identifications across all samples, regardless of apparent molecular weight, is intriguing, and suggests possible protein modification and/or degradation.

Table 4.4.2.5.2. LC-MS/MS identification of 1-DE- and 2-DE-separated rFhDJ-1. rFhDJ-1 protein bands/spots of interest were identified by LC-MS/MS against the *F. hepatica* genome (PRJEB6687, WBPS v10) and GenBank, reporting significant hits identified with a score of 34 or greater (P < 0.025) for 1-DE samples or 32 or greater (P < 0.05) for 2-DE samples. *Sequence length < 25, searched against *Fasciola hepatica* (taxid: 6192).

Figure	Sample	MS/MS ion search					Highest scoring GenBank hit			
		Fh genome hit	MASCOT score	False discovery rate (%)	Peptides matched (non-duplicate)	Sequence coverage (%)	Protein	Organism	Accession	E-value
4.4.2.5.2.3A	1	**BN1106_s1971B000297.mRNA-1**	**86**	10.00	**8**	**33.0**	**DJ-1 family protein**	***Fasciola hepatica***	**PIS82126.1**	**6E-125**
	2	BN1106_s1635B000167.mRNA-1	45	28.57	1	0.0	Hypothetical protein D915_09188	*Fasciola hepatica*	PIS83734.1	4E-159
		BN1106_s2649B000149.mRNA-1*	40		1	42.0	Hypothetical protein D915_01531	*Fasciola hepatica*	PIS90868.1	0.47
		BN1106_s1971B000297.mRNA-1	**35**		**3**	**12.0**	**DJ-1 family protein**	***Fasciola hepatica***	**PIS82126.1**	**6E-125**
	3	BN1106_s810B000523.mRNA-1	47	180.00	6	0.0	Hypothetical protein T265_11101	*Opisthorchis viverrini*	XP_009175928.1	3E-172
		BN1106_s3433B000184.mRNA-1	39		1	6.0	Hypothetical protein D915_14875	*Fasciola hepatica*	PIS78466.1	4E-69
4.4.2.5.2.3B	1	BN1106_s1635B000167.mRNA-1	40	100.00	1	0.0	Hypothetical protein D915_09188	*Fasciola hepatica*	PIS83734.1	4E-159
		BN1106_s788B000258.mRNA-1	35		4	2.0	KH domain protein	*Fasciola hepatica*	PIS83332.1	0.0
	2	BN1106_s788B000258.mRNA-1	36	125.00	3	1.0	KH domain protein	*Fasciola hepatica*	PIS83332.1	0.0
	3	BN1106_s107B000176.mRNA-1	46	33.33	7	3.0	Centrosomal protein of 290 kDa	*Schistosoma haematobium*	XP_012791862.1	0.0
		BN1106_s788B000258.mRNA-1	43		7	2.0	KH domain protein	*Fasciola hepatica*	PIS83332.1	0.0
		BN1106_s3714B000093.mRNA-10	36		2	52.0	Cytochrome C Oxidase subunit II	*Actinobacteria bacterium*	PZN47944.1	0.24
		BN1106_s1635B000167.mRNA-1	34		1	0.0	Hypothetical protein D915_09188	*Fasciola hepatica*	PIS83734.1	4E-159
	4	BN1106_s3714B000093.mRNA-10	40	114.29	1	52.0	Cytochrome C Oxidase subunit II	*Actinobacteria bacterium*	PZN47944.1	0.24
		BN1106_s1635B000167.mRNA-1	38		2	2.0	Hypothetical protein D915_09188	*Fasciola hepatica*	PIS83734.1	4E-159
		BN1106_s2124B000374.mRNA-1	35		4	1.0	TPR repeat-containing protein C10ORF93	*Clonorchis sinensis*	GAA51949.1	0.0
		BN1106_s1971B000297.mRNA-1	**35**		**3**	**12.0**	**DJ-1 family protein**	***Fasciola hepatica***	**PIS82126.1**	**6E-125**
	5	**BN1106_s1971B000297.mRNA-1**	**70**	28.57	**3**	**15.0**	**DJ-1 family protein**	***Fasciola hepatica***	**PIS82126.1**	**6E-125**
		BN1106_s3433B000184.mRNA-1	36		1	6.0	Hypothetical protein D915_14875	*Fasciola hepatica*	PIS78466.1	4E-69
	6	**BN1106_s1971B000297.mRNA-1**	**75**	28.57	**4**	**16.0**	**DJ-1 family protein**	***Fasciola hepatica***	**PIS82126.1**	**6E-125**
		BN1106_s3433B000184.mRNA-1	34		1	6.0	Hypothetical protein D915_14875	*Fasciola hepatica*	PIS78466.1	4E-69
		BN1106_s3780B000122.mRNA-1	33		2	4.0	Hypothetical protein D915_14358	*Fasciola hepatica*	PIS78914.1	1E-128

Based on these preliminary findings, rFhDJ-1 requires further optimisation to its overexpression and purification, in addition to molecular characterisation to assess possible explanations for the observations in this pilot study.

4.4.2.6 Enolase (FhENO)

4.4.2.6.1 Cloning and subcloning

FhENO was PCR-amplified (for primer sequences, see Table 4.3.1.1.3), sequenced (>99.5% ID, Figure 4.4.2.6.1.1A), and electrophoresed (Figure 4.4.2.6.1.1B) for gel excision and direct ligation with pGEM®-T Easy and cloning in α-select *E. coli*.

5' flanking restriction enzyme binding sites were introduced via PCR using *FhENO*-pGEM®-T Easy as the PCR template (for primer sequences, see Table 4.3.1.1.3) and cloned using pGEM®-T Easy as before. NdeI-NotI-digested *FhENO* (Figure 4.4.2.6.1.2A) was then inserted into NdeI-NotI-linearised pET-28b(+) (Figure 4.4.2.1C–D) and confirmed using diagnostic restriction digestion and PCRs (Figure 4.4.2.6.1.2B–C). Positive transformant BL21(DE3)pLysS cell lines were also confirmed via PCR (Figure 4.4.2.6.1.2D) and Sanger Sequencing of *FhENO*-pET-28b(+) was used to confirm the correct DNA and protein sequence for expression (>99.5% ID, Figure 4.4.2.6.1.2E).

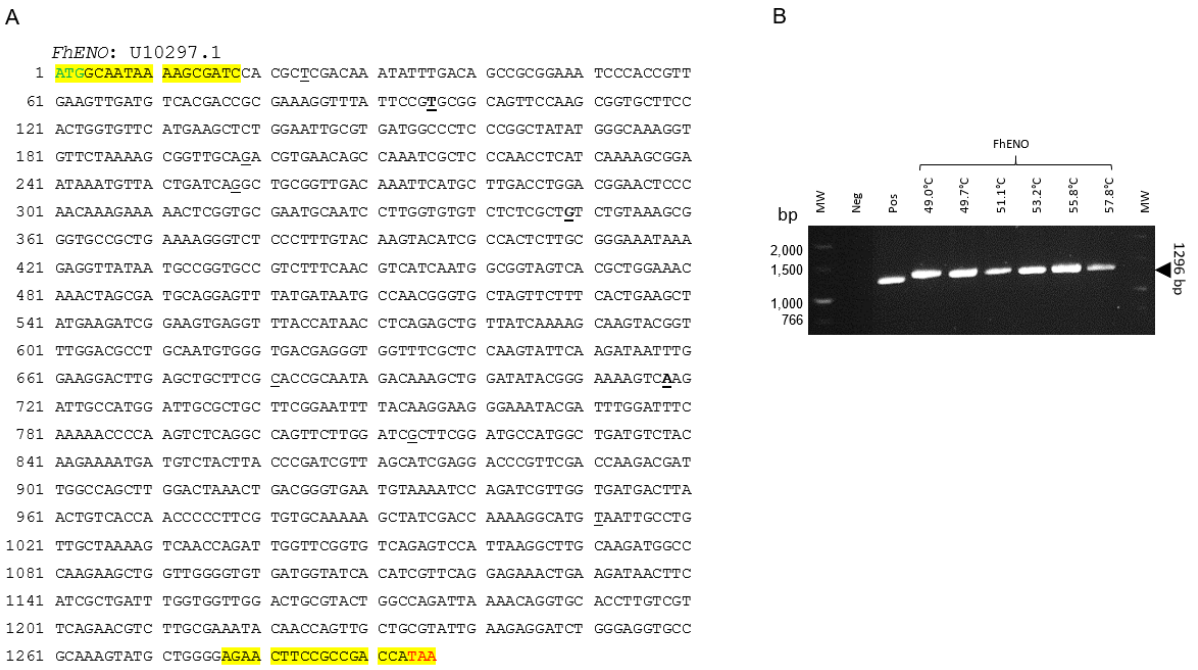

Figure 4.4.2.6.1.1. PCR target and amplicon for *FhENO*. *FhENO* was targeted for PCR amplification, whereby oligomers were designed to amplify the gene including the start and stop codons. Six SNPs were identified by Sanger DNA sequencing (underlined residues), and a further three previously ambiguous nucleotides were confirmed (bolded residues) (A). A single amplicon was demonstrated by 1% agarose gel electrophoresis (B), testing six annealing temperatures for optimal primer binding conditions.

Abbreviations: MW, NEB Fast DNA Ladder (bp); neg, negative; pos, positive (cDNA: *FhCRT*); 49.0–57.8°C, annealing temperature.

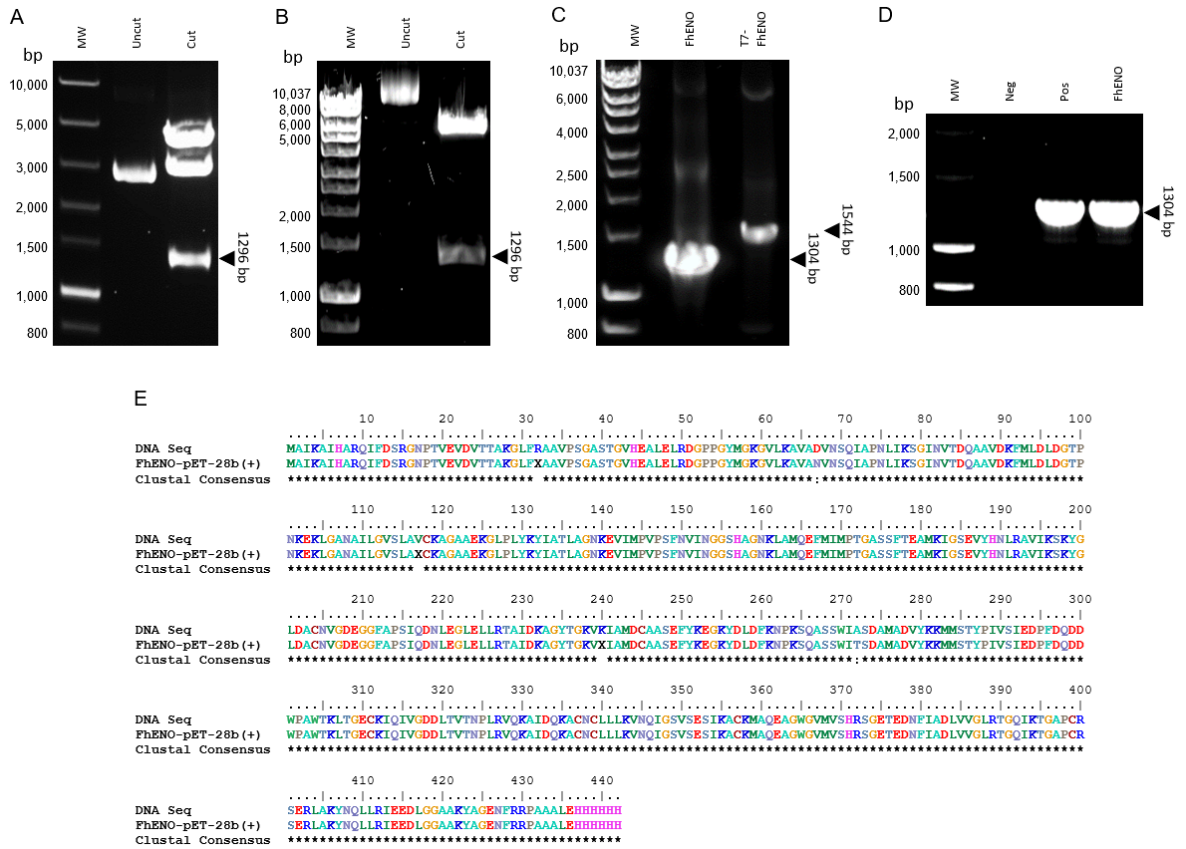

Figure 4.4.2.6.1.2. Subcloning and DNA diagnostics of *FhENO*-pET-28b(+). The subcloning sequence for *FhENO* was isolated from *FhENO*-pGEM®-T Easy via NdeI and NotI double digestion (A) for insertion into NdeI-NotI-linearised pET-28b(+). *FhENO*-pET-28b(+) constructs were tested via diagnostic digestion (NdeI and NotI) (B) and PCRs (C) using *FhENO* subcloning and T7 primers. (D) Positive One Shot® BL21(DE3) Star™ cell lines were identified via colony PCR using *FhENO* subcloning primers and (E) DNA sequencing identified five SNPs in the *FhENO*-pET-28b(+) expression sequence, leading to two amino acid substitutions upon translation, excluding the previously ambiguous residues (AAA57450.1, GenBank v204: X-Arg^{32}, X-Val^{117}, X-Lys^{240}) (compiled using BioEdit). Abbreviations: MW, Bioline HyperLadder™ 1kb (bp); neg, negative; pos, positive (cDNA: *FhENO*).

Upon *in silico* translation, two amino acid substitutions were identified (N67D, T272A) which PROVEAN identified as deleterious and synonymous, respectively (Table 4.4.2.6.1). The replacement of asparagine with aspartate would be expected to be synonymous based on the closely comparable molecular weights and structures (Betts and Russell, 2007), yet could be significant due to the exchange of a carboxamide with a deprotonated α-carboxylic acid group, thus adding in a negative charge at this residue. Conversely to this substitution, an alanine replacement of threonine could be expected to have direct deleterious influence due to the loss of threonine's polarity and involvement in protein post-translational modifications that alanine cannot replace (Betts and Russell, 2007). Thus, it is difficult to draw a single

conclusion from these findings, and there may be little consequence of these residue substitutions in terms of FhENO protein structure and function.

Table 4.4.2.6.1. PROVEAN Prediction for protein sequence analysis of FhENO. Sequence variants (Asn^{67}–Asp^{32}, Thr^{272}–Ala^{272}) were predicted with scores above and below the default threshold, which indicate these changes had mixed effects.

Variant	PROVEAN score	Prediction (default threshold ≤ -2.5)
N67D	-4.204	Deleterious
T272A	-1.885	Neutral

4.4.2.6.2 Expression

Pilot expression conditions were based on previously recombinant ENOs expressed from *Echinococcus granulosus* (Lorenzatto *et al.*, 2012), *Taenia multiceps* (Li *et al.*, 2015), and *Plasmodium falciparum* (Pal-Bhowmick *et al.*, 2004). rFhENO was predicted to be 47.53 kDa with an isoelectric point of 6.43 and an overall charge of -3.0, and SDS PAGE (Figure 4.4.2.6.2.1) demonstrated optimal target protein overexpression (~50 kDa) in soluble fractions after 0.1 mM IPTG and four hours at 37°C.

IMAC purification was trialled using HIS-Select® Nickel (Figure 4.4.2.6.2.2). There was no suggestion of protein binding or elution, however a prominent band in the IMAC flow-through which was also the only band present in any of the elution samples (Figure 4.4.2.6.2.2A–B).

LC-MS/MS of protein bands of interest (boxed, Figure 4.4.2.6.2.2) was conducted to investigate the identity of these proteins. Direct searching against the *F. hepatica* genome (PRJEB6687, WBPS v10) identified no significant hits shared between both samples, with only one hit (Figure 4.4.2.6.2.2, boxed) exceeding significance (BN1106_s1429B000126.mRNA-1, $P < 0.05$, 66.67% FDR) which was scored highest on GenBank (v204, taxid: 6192) as a hypothetical protein D915_10841 (PIS82212.1: www.ncbi.nlm.nih.gov/protein/PIS82212.1, E = 1.1). These findings were also found following direct searching against the GenBank database ($P < 0.001$, 0.00% FDR).

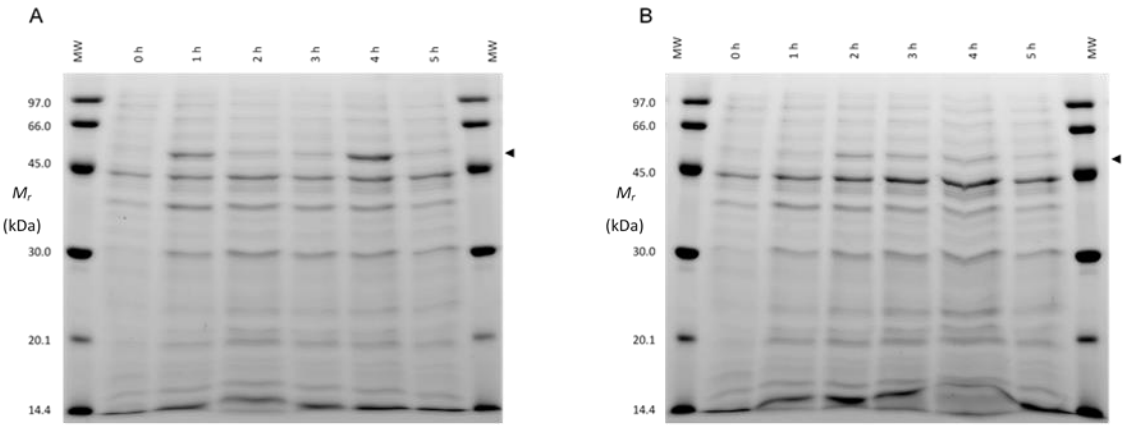

Figure 4.4.2.6.2.1. Pilot recombinant expression of rFhENO. 5 µg FhENO-pET-28b(+) One Shot® BL21(DE3) Star™ recombinant expression lysate was analysed by SDS PAGE following 0.1 mM (A) and 0.5 mM (B) IPTG from 0–5 hours post-induction at 37°C.

Abbreviations: MW, Amersham Low Molecular Weight SDS Calibration Kit (M_r); 0–5 h, hours post-induction.

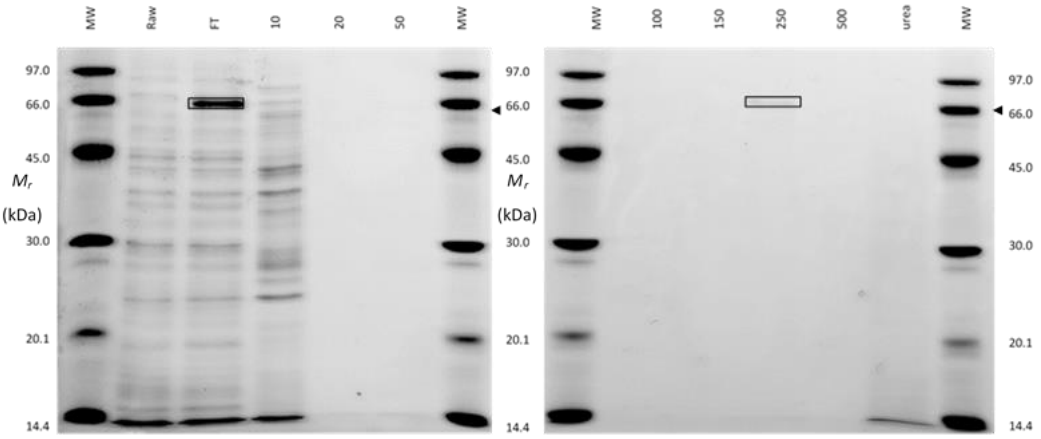

Figure 4.4.2.6.2.2. Trial IMAC purification of rFhENO. rFhENO isolation was tested using HIS-Select Cobalt resin, demonstrating poor target purification from recombinant expression lysate and a protein of interest resolving at approximately 66.0 kDa in both FT and 250 mM imidazole fractions.

Abbreviations: MW, Amersham Low Molecular Weight SDS Calibration Kit (M_r); raw, raw bacterial lysate; FT, flow-through; 10–500 [mM], imidazole; urea, 8 M urea wash.

Based on the findings from these pilot studies for rFhENO, in order to proceed further with this target, overexpression must be optimised for adequate concentrations for further purification and molecular investigation.

4.4.2.7 Gelsolin (FhGEL)

4.4.2.7.1 Cloning and subcloning

FhGEL was PCR-amplified (for primer sequences, see Table 4.3.1.1.3), sequenced (>99.6% ID, Figure 4.4.2.7.1.1A), and electrophoresed (Figure 4.4.2.7.1.1B) for gel excision and direct ligation with pGEM®-T Easy and cloning in α-select *E. coli*.

5' flanking restriction enzyme binding sites were introduced via PCR using *FhGEL*-pGEM®-T Easy as the PCR template (for primer sequences, see Table 4.3.1.1.3) and cloned using pGEM®-T Easy as before. NdeI-NotI-digested *FhGEL* (Figure 4.4.2.7.1.2A) was then inserted into NdeI-NotI-linearised pET-28b(+) (Figure 4.4.2.1C–D) and confirmed using diagnostic restriction digestion and PCRs (Figure 4.4.2.7.1.2B–C). Positive transformant BL21(DE3)pLysS cell lines were also confirmed via PCR (Figure 4.4.2.7.1.2D) and Sanger Sequencing of *FhGEL*-pET-28b(+) was used to confirm the correct DNA and protein sequence for expression (>99.4% ID, Figure 4.4.2.7.1.2E).

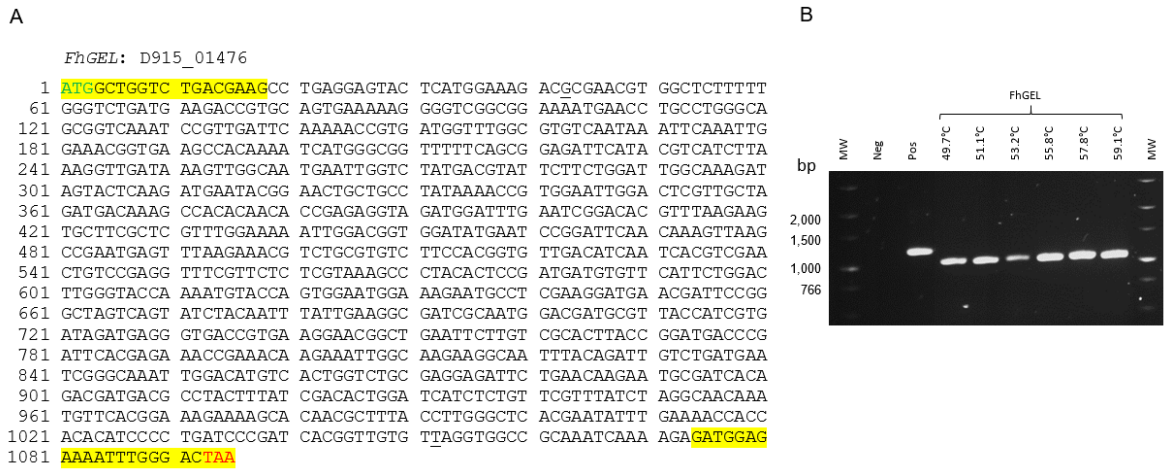

Figure 4.4.2.7.1.1. PCR target and amplicon for *FhGEL*. *FhGEL* was targeted for PCR amplification, whereby oligomers were designed to amplify the gene including start and stop codons. Four SNPs were identified by Sanger DNA sequencing (underlined residues) (A), and a single amplicon was demonstrated by 1% agarose gel electrophoresis (B), testing six annealing temperatures for optimal primer binding conditions.

Abbreviations: MW, NEB Fast DNA Ladder (bp); neg, negative; pos, positive (cDNA: *FhCRT*); 49.7–59.1°C, annealing temperature.

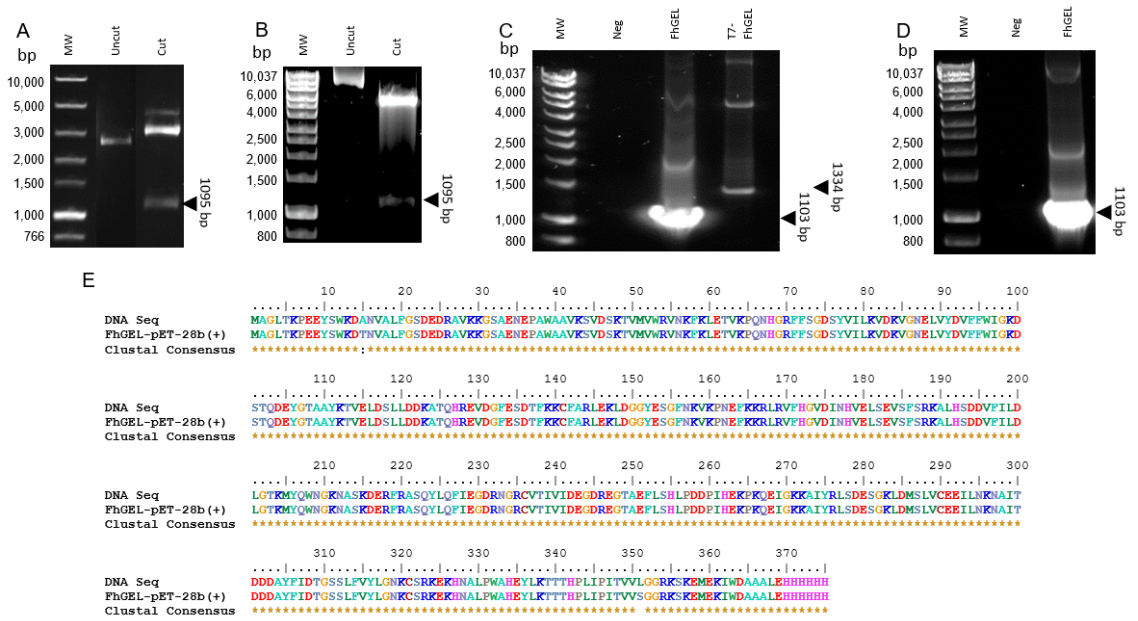

Figure 4.4.2.7.1.2. Subcloning and DNA diagnostics of *FhGEL*-pET-28b(+). The subcloning sequence for *FhGEL* was isolated from *FhGEL*-pGEM®-T Easy via NdeI and NotI double digestion (A) for insertion into NdeI-NotI-linearised pET-28b(+). *FhGEL*-pET-28b(+) constructs were tested via diagnostic digestion (NdeI and NotI) (B) and PCRs (C) using *FhGEL* subcloning and T7 primers. (D) Positive One Shot® BL21(DE3) Star™ cell lines were identified via colony PCR using *FhGEL* subcloning primers and (E) DNA sequencing identified two SNPs in the *FhGEL*-pET-28b(+) expression sequence, leading to two amino acid substitutions upon translation (compiled using BioEdit). Abbreviations: MW, NEB Fast DNA Ladder and Bioline HyperLadder™ 1kb (bp); neg, negative.

Upon *in silico* translation, two amino acid substitutions were identified (T15A, S351L), which PROVEAN identified to be synonymous and non-deleterious, respectively (Table 4.4.2.7.1) and which was supported by the MutPred2 tool (Li *et al.*, 2009). These replacements are similar in that a polar amino acid is substituted by a non-polar one, however threonine-alanine could be described as more synonymous due to their comparable hydrophobicity, molecular weights and structural propensity (Betts and Russell, 2007). However, a serine-leucine substitution is more concerning due to the loss of a small polar residue and addition of a larger, hydrophobic replacement with an aliphatic branch, which may have the potential to influence protein structure or folding (Betts and Russell, 2007). Thus, it is difficult to draw a single conclusion from these findings as to the *in situ* consequence of these residue substitutions for FhGEL protein structure and/or function.

Table 4.4.2.7.1. PROVEAN Prediction for protein sequence analysis of FhGEL. Sequence variants (Thr^{15}–Ala^{15}, Ser^{351}–Lys^{351}) were predicted with scores above the default threshold, which indicate these changes are neutral effects.

Variant	PROVEAN score	Prediction (default threshold ≤ -2.5)
T15A	-1.117	Neutral
S351L	-0.471	Neutral

4.4.2.7.2 Expression

rFhGEL was expressed from BL21(DE3)pLysS cell lines using 0.5-1.0 mM IPTG and soluble fractions were analysed by 12.5% 1-D SDS-PAGE (Figure 4.4.2.7.2.1A–C). The *in silico* polyhistidine-tagged protein was predicted to be 42.77 kDa with an isoelectric point of 5.99 and an overall charge of -9.0.

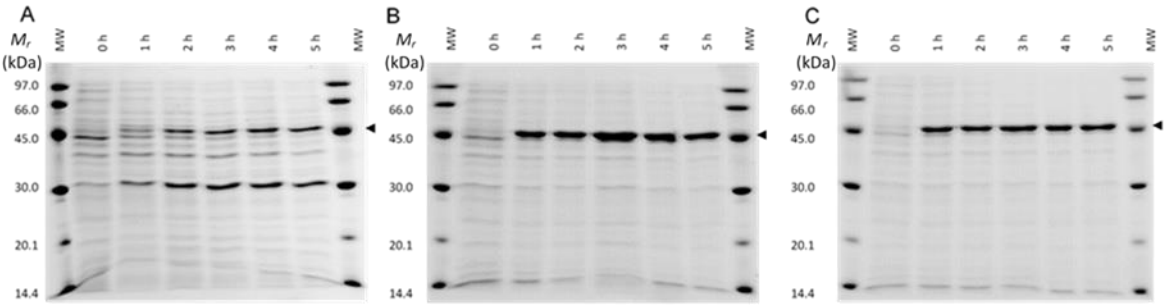

Figure 4.4.2.7.2.1. Pilot recombinant expression of rFhGEL. 5 µg FhGEL-pET-28b(+) One Shot® BL21(DE3) Star™ recombinant expression lysate was analysed by SDS PAGE following 0 mM (A), 0.5 mM (B) and 1.0 mM (C) IPTG from 0–5 hours post-induction at 37°C.

Abbreviations: MW, Amersham Low Molecular Weight SDS Calibration Kit (M_r); 0–5, hours post-induction.

Both partial and whole gelsolin proteins have been recombinantly expressed and synthetically produced for only *H. sapiens* and *M. musculus* models. However, many more studies have been based on native plasma gelsolin due to its native molecular characteristics (Allen, 1997; Lin *et al.*, 2000; Lück *et al.*, 1995; Nag *et al.*, 2009; Pope *et al.*, 1991; Wen *et al.*, 1996), multifaceted nature and *in vivo* applications in pathology (Christofidou-Solomidou *et al.*, 2002; Cunningham *et al.*, 1991; Koya *et al.*, 2000; Rothenbach, 2003; Way *et al.*, 1990; Zhang *et al.*, 2017). Parasite-specific gelsolins also remain uncharacterised, but the severin protein of the gelsolin-like protein superfamily (InterPro: IPR036180) from *Clonorchis sinensis* has been studied (Chen *et al.*, 2013), and the recombinant overexpression conditions for rCsSev as well as the partial rHsGel (Zhang *et al.*, 2017) were the basis of expression conditions for this work. Based on the pilot experiment, the optimal induction of rFhGEL was following

0.5 mM IPTG after growth at 37°C for five hours (Figure 4.4.2.7.2.1B). These conditions were used for all subsequent overexpression for rFhGEL.

rFhGEL was purified using HIS-Select Cobalt (Sigma) and analysed by 12.5% SDS PAGE (Figure 4.4.2.7.2.2), with 50, 250, and 500 mM eluents indicating the greatest purity of the target protein, which were pooled.

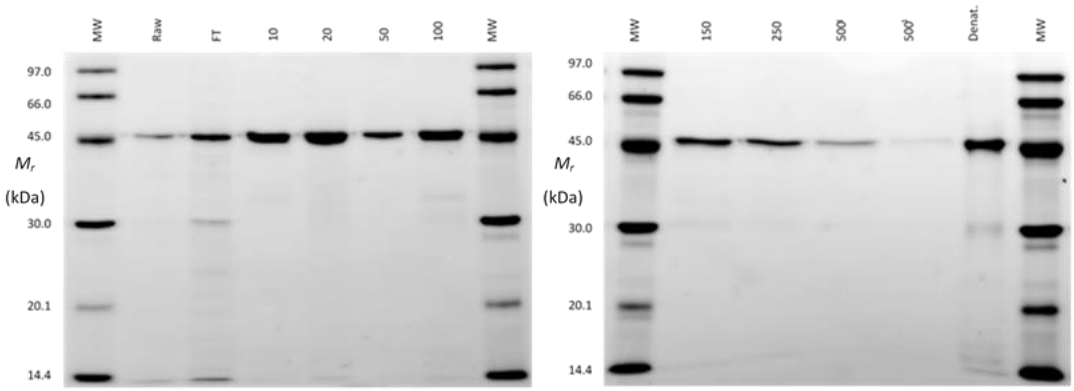

Figure 4.4.2.7.2.2. IMAC purification of recombinant rFhGEL. rFhGEL was isolated from recombinant expression lysate using HIS-Select Cobalt resin, showing efficient isolation of the target protein in imidazole elutions. Abbreviations: MW, Amersham Low Molecular Weight SDS Calibration Kit (M_r); raw, raw bacterial lysate; FT, flow-through; 10–500 [mM], imidazole concentration.

1-D SDS PAGE demonstrated rFhGEL resolves in two bands at approximately 45–47 kDa (Figure 4.4.2.7.2.3A), and isoelectric separation in 2-D SDS PAGE (linear IPG IEF strip, Bio-Rad) indicated with two major isomers of 5.93 at 47.0 kDa and 5.63 at 45.0 kDa (Figure 4.4.2.7.2.3B). LC-MS/MS data were analysed by MASCOT, which identified both protein isomers as gelsolin except matching peptides from two genes when isolated from the 1-DE (PRJEB6687, WBPS v10: BN1106_s2349B000191.mRNA-1) or 2-DE (PRJEB6687, WBPS v10: BN1106_s2349B000188.mRNA-1) SDS PAGE-separated samples (Table 4.4.2.7.2). These hits were matched to two *F. hepatica* gelsolin repeat proteins in GenBank (PRJNA179522, WBPS v10–14/GenBank v204, PIS90920.1: www.ncbi.nlm.nih.gov/protein/PIS90920.1; and PIS80791.1: www.ncbi.nlm.nih.gov/protein/PIS80791.1, respectively), however the majority of other MASCOT hits with significant scores ($P < 0.01$) were interestingly identified as actin (Table 4.4.2.7.2). Based on the MASCOT data for gelsolin hits alongside gel electrophoresis images (Figures 4.4.2.7.2.2–3) the purified protein fraction indicates high purity, however may be dimorphic and comprised of two distinct isomers with varied amino acid sequences.

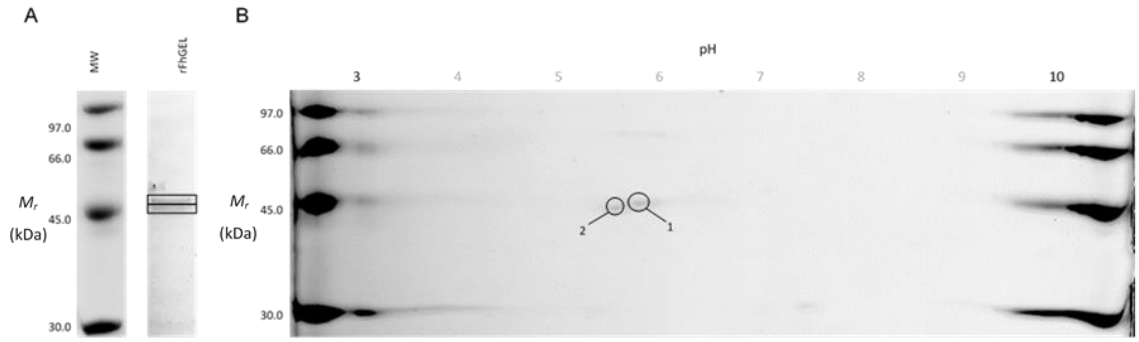

Figure 4.4.2.7.2.3. 1-D and 2-D SDS PAGE separation of purified rFhGEL. 1 µg rFhGEL was resolved in two isoforms between approximately 45–47 kDa by 1-DE (A), which 2-DE (B) revealed to separate at two isoelectric points between 5.5 and 6.0 pH (7 cm IEF 3–10; 12.5% SDS PAGE). LC-MS/MS identified both 1-DE bands and 2-DE separated isomer spots as gelsolin (MASCOT Score = 64–268: BN1106_s2349B000-188/-191.mRNA-1 (WBPS v10); PIS90920.1/PIS80791.1 (www.ncbi.nlm.nih.gov/protein/PIS90920.1 /www.ncbi.nlm.nih.gov/protein/PIS80791.1; PRJNA179522, WBPS v10–14/GenBank v204)). LC-MS/MS results are detailed in Table 4.4.2.7.2.

Abbreviations: MW, Amersham Low Molecular Weight SDS Calibration Kit (M_r).

To investigate the MASCOT findings of two major sequence hits for rFhGEL, a sequence alignment was performed (Figure 4.4.2.7.2.4) to assess differences between the cloned sequence, the original sequence template (D915_01476, PRJNA179522, WBPS v10–14/GenBank v204), the two MASCOT sequences (PRJEB6687, WBPS v10: BN1106_s2349B000191.mRNA-1, BN1106_s2349B000188.mRNA-1) and their highest scoring GenBank hits (PRJNA179522, WBPS v10–14/GenBank v204: PIS90920.1 and PIS80791.1, respectively). These data reflected the matching between PRJEB6687 genome and GenBank hits identified following MASCOT analysis (Table 4.4.2.7.2), though both BN1106_2349B000191.mRNA-1 and PIS80791.1 had additional inserts towards the C-terminal of the sequences compared to their respective match (Figure 4.4.2.7.2.4). The alignment and sequence identity matrix indicated the FhGEL expression sequence bears closest resemblance to PIS90920.1 and secondly to BN1106_s2349B000191.mRNA-1 (92.03–99.45%). Furthermore, the PIS80791.1 and BN1106_s2349B000188.mRNA-1 pair shared 146 non-conserved residues in the other three sequences, suggesting possible divergence events between these sequences.

Table 4.4.2.7.2. LC-MS/MS identification of 1-DE- and 2-DE-separated rFhGEL. rFhGEL protein bands/spots of interest were identified by LC-MS/MS against the *Fasciola hepatica* genome (PRJEB6687) and GenBank, reporting significant hits identified with a score of 38 or greater (P < 0.01).

Figure reference	Sample	MS/MS ion search					Highest scoring GenBank hit			
		Fh genome hit	MASCOT score	False discovery rate (%)	Peptides matched (non-duplicate)	Sequence coverage (%)	Protein	Organism	Accession	E-value
4.4.2.7.2.3A	1-DE 1	**BN1106_s2349B000191.mRNA-1**	**64**	0.00	8	**18.0**	**Gelsolin repeat protein**	***Fasciola. hepatica***	**PIS90920.1**	**0.0**
		BN1106_s420B000182.mRNA-1	42		1	1.0	Hypothetical protein T265_06170	*Opisthorchis viverrini*	XP_009169635.1	0.0
4.4.2.7.2.3A	1-DE 2	**BN1106_s2349B000191.mRNA-1**	**161**	0.00	11	**19.0**	**Gelsolin repeat protein**	***Fasciola. hepatica***	**PIS90920.1**	**0.0**
4.4.2.7.2.3B	2-DE 1	BN1106_s2907B000133.mRNA-1	141	0.00	11	26.0	Hypothetical protein T265_00572 [actin family]	*Opisthorchis viverrini*	XP_009162640.1	0.0
		BN1106_s101B000531.mRNA-1	107		10	28.0	Actin	*Fasciola hepatica*	PIS82094.1	0.0
		BN1106_s1379B000106.mRNA-1	107		10	28.0	Putative actin	*Schistosoma mansoni*	XP_018655546.1	0.0
		BN1106_s1251B000300.mRNA-1	107		10	25.0	Actin	*Fasciola hepatica*	PIS85022.1	0.0
		BN1106_s455B000331.mRNA-1	107		10	25.0	Actin	*Fasciola hepatica*	PIS86458.1	0.0
		BN1106_s1379B000109.mRNA-1	107		10	24.0	Actin	*Fasciola hepatica*	PIS85022.1	0.0
		BN1106_s2349B000188.mRNA-1	**81**		5	**20.0**	**Gelsolin repeat protein**	***Fasciola hepatica***	**PIS80791.1**	**0.0**
4.4.2.7.2.3B	2-DE 2	**BN1106_s2349B000188.mRNA-1**	**268**	0.00	14	**39.0**	**Gelsolin repeat protein**	***Fasciola hepatica***	**PIS80791.1**	**0.0**
		BN1106_s1110B000010.mRNA-1	66		4	16.0	Actin	*Fasciola hepatica*	PIS88900.1	3E-180
		BN1106_s1251B000300.mRNA-1	66		4	11.0	Actin	*Fasciola hepatica*	PIS85022.1	0.0
		BN1106_s455B000331.mRNA-1	66		4	11.0	Actin	*Fasciola hepatica*	PIS86458.1	0.0
		BN1106_s1379B000109.mRNA-1	66		4	10.0	Actin	*Fasciola hepatica*	PIS85022.1	0.0
		BN1106_s101B000531.mRNA-1	66		4	9.0	Actin	*Fasciola hepatica*	PIS82094.1	0.0
		BN1106_s328B000212.mRNA-1	66		4	7.0	Actin-2	*Schistosoma japonicum*	CAX83035.1	1E-149
		BN1106_s2907B000134.mRNA-1	66		4	6.0	Actin	*Larimichthys crocea*	KKF15719.1	0.0
		BN1106_s2907B000132.mRNA-1	66		4	6.0	Predicted actin	*Crassostrea gigas*	XP_011437202.1	0.0
		BN1106_s3541B000067.mRNA-1	66		4	4.0	Actin	*Fasciola hepatica*	PIS81958.1	0.0
		BN1106_s2907B000133.mRNA-1	49		3	7.0	Hypothetical protein T265_00572 [actin family]	*Opisthorchis viverrini*	XP_009162640.1	0.0
		BN1106_s3001B000132.mRNA-1	45		1	6.0	Hypothetical protein D915_06492	*Fasciola hepatica*	PIS86247.1	2E-69
		BN1106_s3001B000132.mRNA-2	45		1	6.0	CUB domain protein	*Fasciola hepatica*	PIS86248.1	6E-93
		BN1106_s3001B000132.mRNA-5	45		1	6.0	Hypothetical protein D915_06492	*Fasciola hepatica*	PIS86247.1	0.041

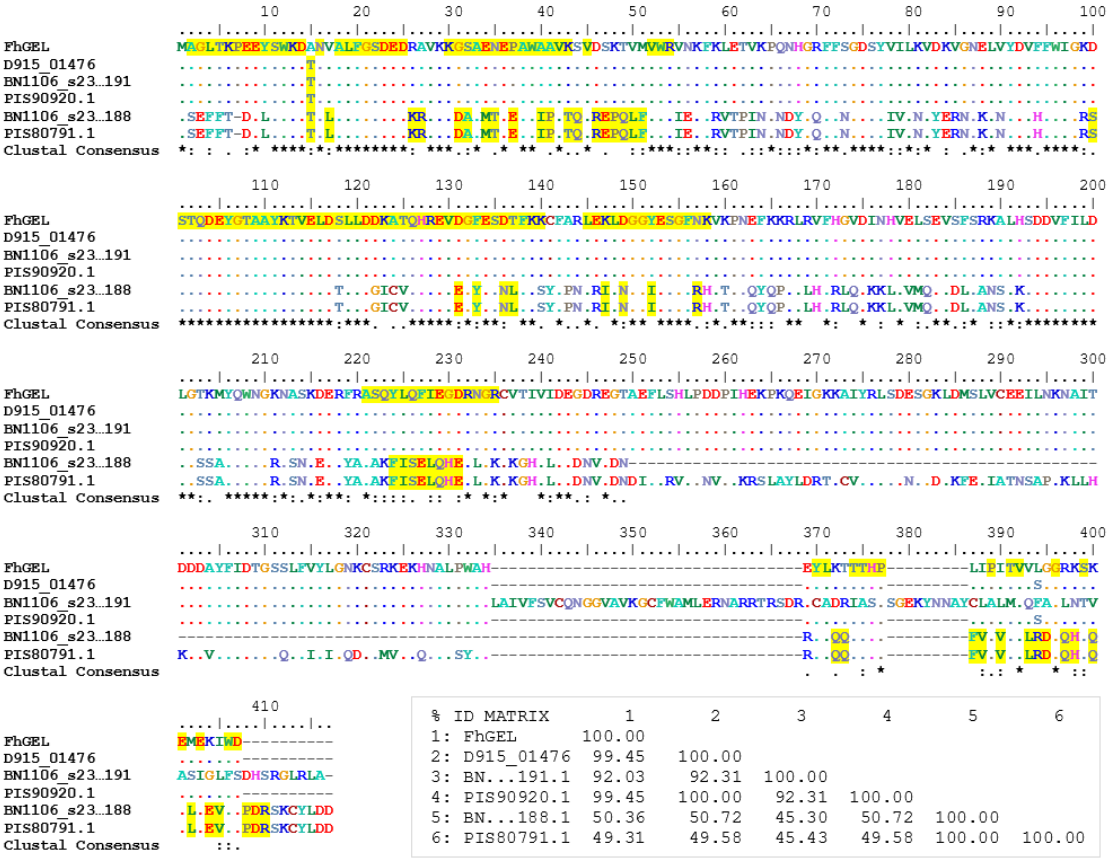

Figure 4.4.2.7.2.4. Comparison of the gelsolin amino acids sequences cloned in this study (FhGEL) with other *Fasciola hepatica* gelsolin-associated proteins (dotted lines). Based on DNA sequencing, two amino acids were different in the cloned gelsolin sequence (cDNA: FhGEL) from draft genomes including the original DNA template (D915_01476, PRJNA179522, WBPS v10–14), two LC-MS/MS hits (BN1106_s2349B000191.mRNA-1; BN1106_s2349B000188.mRNA-1, PRJEB6687, WBPS v10) and their respective GenBank hits (PRJNA179522: PIS90920.1: www.ncbi.nlm.nih.gov/protein/PIS90920.1; PIS80791.1: www.ncbi.nlm.nih.gov/protein/PIS80791.1). Highlighted residues represent all peptides matched by LC-MS/MS analysis of rFhGEL, including peptides from the two disparate LC-MS/MS hits. The alignment was produced using the ClustalO tool in BioEdit.

All peptide residues matched by LC-MS/MS analysis of FhGEL are also highlighted (Figure 4.4.2.7.2.4). Interestingly, several matched peptides overlapped between both sequences. Peptide fragmentation data were interpreted to investigate the previously identified threonine-alanine (FhGEL: T15A) and serine-leucine (FhGEL: S351L) substitutions (Figure 4.4.2.7.2.2E), as these were within the LC-MS/MS-identified regions. These data also demonstrated putative post-translational modifications, indicating oxidation at Met[33] of BN1106_s2349B000188.mRNA-1. Fragmentation data for both Asp14-Arg28 (positions as in Figure 4.4.2.7.2.4, n = 15) and Tyr370–394 (positions as in Figure 4.4.2.7.2.4, n = 25) peptides,

as highlighted, were the highest scoring for each sequence, suggesting no residue substitutions. Furthermore, based on the matches to contradicting peptides throughout both protein sequences, it could be suggested that FhGEL has two isoforms of distinct sequences, one of which may have been predominantly identified during cloning.

Based on the findings from these pilot studies for rFhGEL, this recombinant has been optimally overexpressed and purified at adequate concentrations for further investigation of biochemical and diagnostic investigation.

4.4.2.8 Glyceraldehyde-3-phosphate dehydrogenase (FhGAPDH)

4.4.2.8.1 Cloning and subcloning

FhGAPDH was PCR-amplified (for primer sequences, see Table 4.3.1.1.3), sequenced (>99.5% ID, Figure 4.4.2.8.1.1A), and electrophoresed (Figure 4.4.2.8.1.1B) for gel excision and direct ligation with pGEM®-T Easy and cloning in α-select *E. coli*.

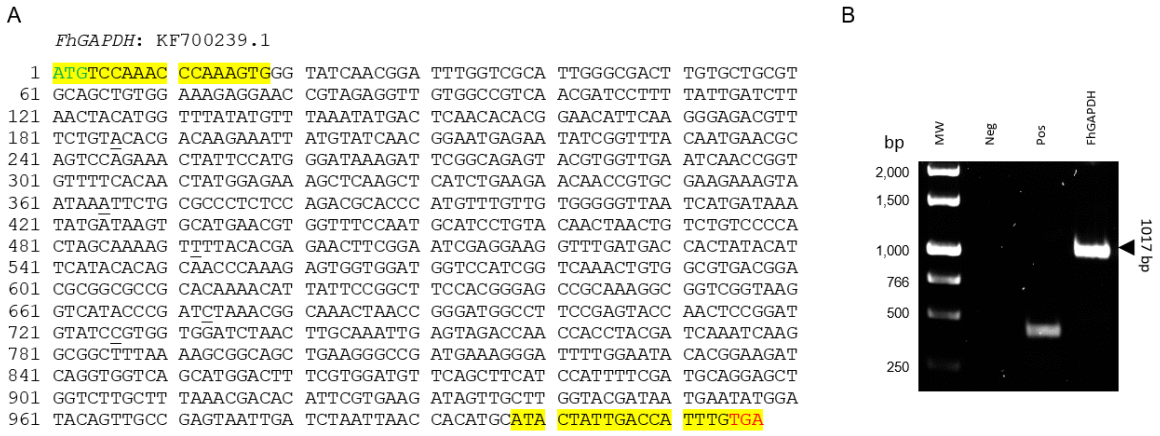

Figure 4.4.2.8.1.1. PCR target and amplicon for *FhGAPDH*. *FhGAPDH* was targeted for PCR amplification, whereby oligomers were designed to amplify the gene including the start and stop codons. Two SNPs were identified by Sanger DNA sequencing (underlined residues) (A), and a single amplicon was demonstrated by 1% agarose gel (B) electrophoresis following nested PCR to account for low product yields following a single round. Abbreviations: MW, NEB Fast DNA Ladder (bp); neg, negative (primers and water); pos, positive (cDNA: *FhDJ-1*, 552 bp).

5' flanking restriction enzyme binding sites were introduced via PCR using *FhGAPDH*-pGEM®-T Easy as the PCR template (for primer sequences, see Table 4.3.1.1.3) and cloned using pGEM®-T Easy as before. NdeI-NotI-digested *FhGAPDH* (Figure 4.4.2.8.1.2A) was then inserted into NdeI-NotI-linearised pET-28b(+) at a ratio of 3:1 (insert:vector) and confirmed

using diagnostic restriction digestion and PCRs (Figure 4.4.2.8.1.2B–C). Positive transformant BL21(DE3)pLysS cell lines were also confirmed via PCR (Figure 4.4.2.8.1.2D) and Sanger Sequencing of *FhGAPDH*-pET-28b(+) was used to identity the correct DNA and protein sequence for expression (99.7% ID, Figure 4.4.2.8.1.2E).

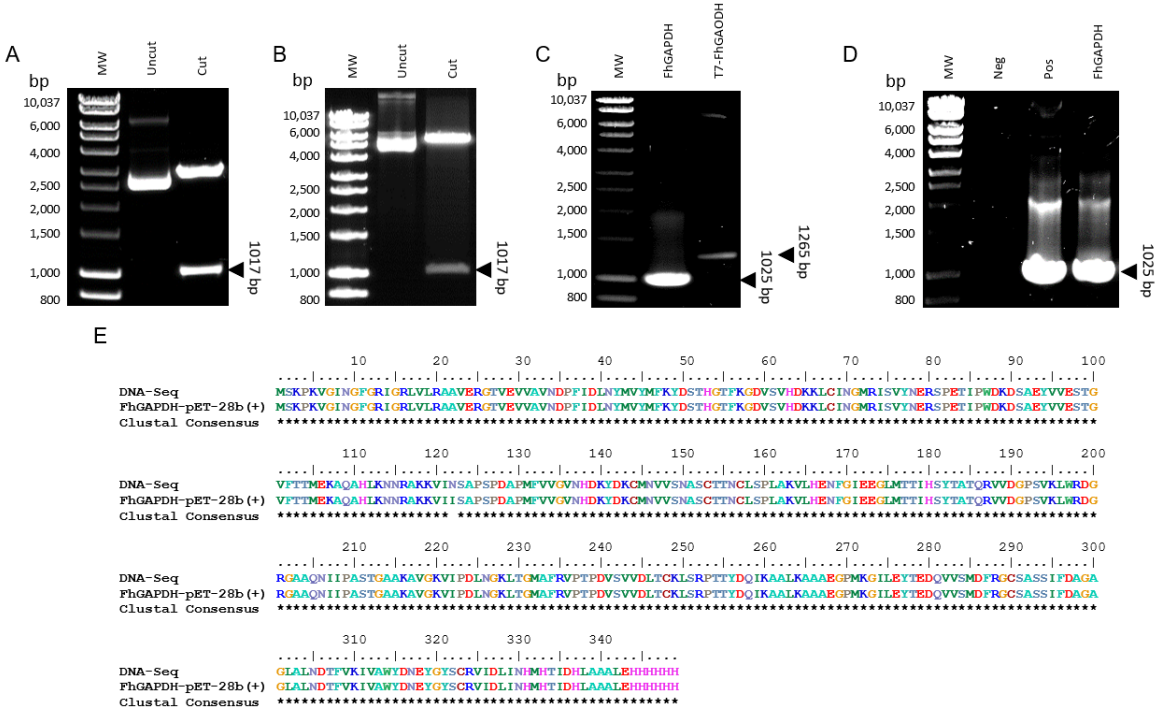

Figure 4.4.2.8.1.2. Subcloning and DNA diagnostics of *FhGAPDH*-pET-28b(+). The subcloning sequence for *FhGAPDH* was isolated from *FhGAPDH*-pGEM®-T Easy via NdeI and NotI double digestion (A) for insertion into NdeI-NotI-linearised pET-28b(+). *FhGAPDH*-pET-28b(+) constructs were tested via diagnostic digestion (NdeI and NotI) (B) and PCRs (C) using *FhGAPDH* subcloning and T7 primers. (D) Positive BL21(DE3)pLysS cell lines were identified via direct colony PCR using *FhGAPDH* subcloning primers and (E) DNA sequencing identified five SNPs in the *FhGAPDH*-pET-28b(+) expression sequence, leading to one amino acid substitutions upon translation (compiled using BioEdit).

Abbreviations: MW, Bioline HyperLadder™ 1kb (bp); neg, negative (primers and water); pos, positive (cDNA: FhGAPDH).

Upon *in silico* translation, an amino acid substitution was identified (I122N), which PROVEAN identified as deleterious, a consequence supported by the amino acids' characteristics (Table 4.4.2.8.1). As isoleucine is a hydrophobic, aliphatic amino acid, it adopts an internal position *in situ*, and thus substitution with a polar and peripheral protein residue, asparagine, may lead to a structural and/or functional difference (Betts and Russell, 2007).

Table 4.4.2.8.1. PROVEAN Prediction for protein sequence analysis of FhGAPDH. A single sequence variant (Asn^{67}–Asp^{32}, Thr^{272}–Ala^{272}) was predicted with scores below the default threshold, which indicate this change had deleterious effects.

Variant	PROVEAN score	Prediction (default threshold ≤ -2.5)
I122N	-5.797	Deleterious

4.4.2.8.2 Expression

rFhGAPDH was expressed from BL21(DE3)pLysS cell lines using 0.05-1.0 mM IPTG and both soluble and insoluble fractions were analysed by 12.5% 1-D SDS-PAGE (Figure 4.4.2.8.2.1A–D). The polyhistidine-tagged protein was predicted to be 38.21 kDa with an isoelectric point of 7.05 and an overall charge of -1.0. Expression conditions were mirrored on a previous study of rFhGAPDH (Zinsser *et al.*, 2014), whereby a low temperature was used to assist protein target sequestration into the bacterial IBs, which has been observed for other recombinantly-expressed GAPDH from a variety of organisms (Barbosa *et al.*, 2006; Hannaert *et al.*, 1995; Liu *et al.*, 2005; Silva *et al.*, 2011), despite this protein's solubility (Gschaedler *et al.*, 1994).

Following induction, cells were incubated at 30°C for five hours and protein extracts were separated for individual analyses by SDS PAGE (Figure 4.4.2.8.2.1Ai–Dii). Target overexpression was most demonstrable at 0.1 and 0.5 mM IPTG, with protein bands of interest resolving between 35–40 kDa in the solubilised IB fraction (Figure 4.4.2.8.2.1). Based on the previous study of rFhGAPDH and other recombinant GAPDH orthologues, subsequent expression was conducted following 0.05/0.1 mM IPTG induction for 24 hours but at a growth temperature of 18°C to increase the time and conducive conditions for IB production.

IBs from rFhGAPDH recombinant expression included a band of interest upon resolution in 12.5% SDS PAGE (~37kDa, Figure 4.4.2.8.2.1A–Dii). LC-MS/MS did not identify FhGAPDH in raw sample bands, but in order to obtain a higher concentration of the target, IBs were prepared for purification under denaturing conditions and on-column refolding as described (4.3.3.2; 4.3.4.3). A pilot experiment was initially attempted using HIS-Select Nickel (Sigma-Aldrich, UK), however concentrations of wash and elution fractions were too low to be calculated, which was reflected by SDS PAGE analysis (data not shown).

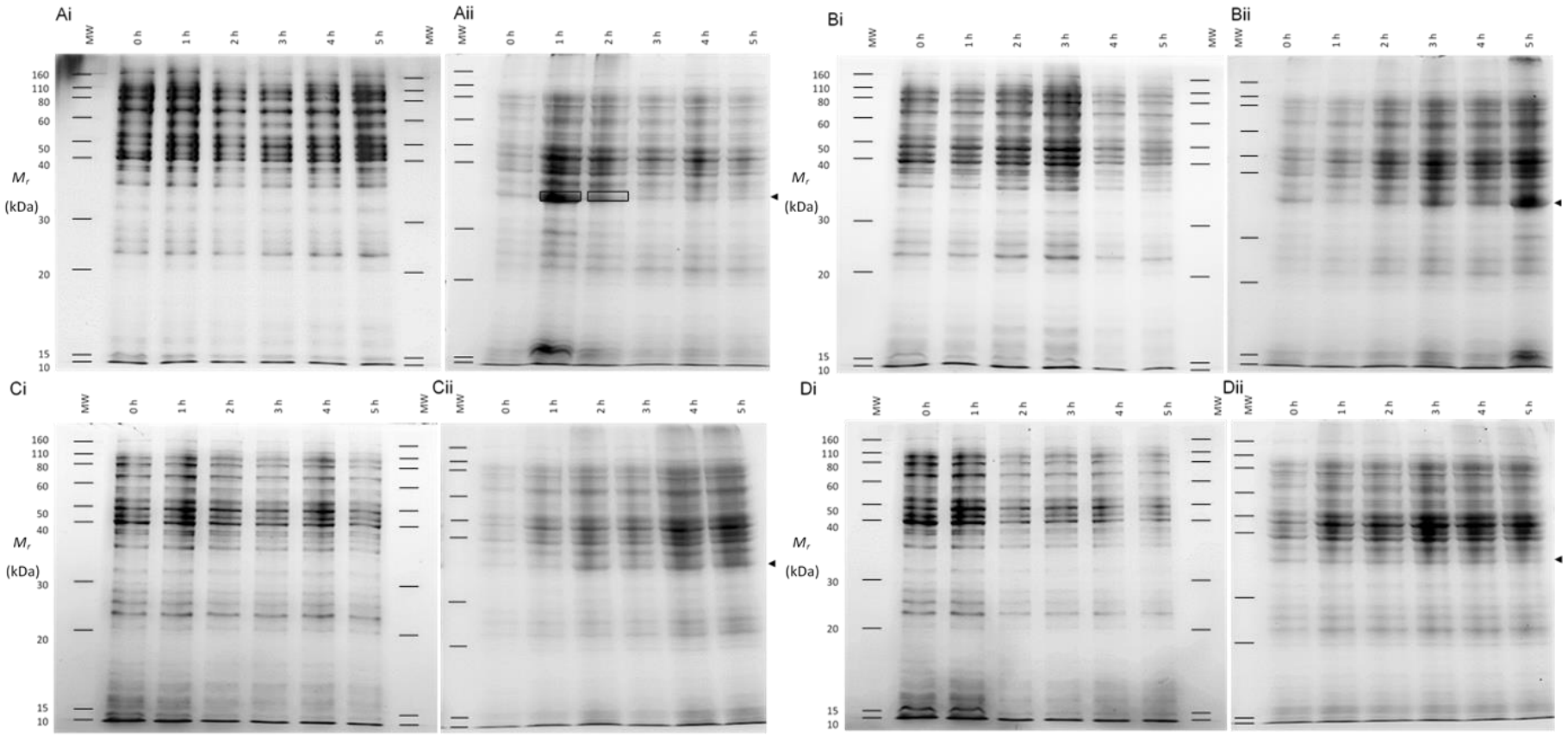

Figure 4.4.2.8.2.1. Pilot recombinant expression of rFhGAPDH. 5 µg FhGAPDH-pET-28b(+) BL21(DE3)pLysS recombinant expression lysate (i) and IB (ii) fractions were analysed by SDS PAGE following 0.05 mM (A), 0.1 mM (B), 0.5 mM (C) and 1.0 mM (D) IPTG from 0–5 hours post-induction at 30°C.

Abbreviations: MW, Novex® Sharp Pre-Stained Protein Standard (M_r); 0–5 h, hours post-induction.

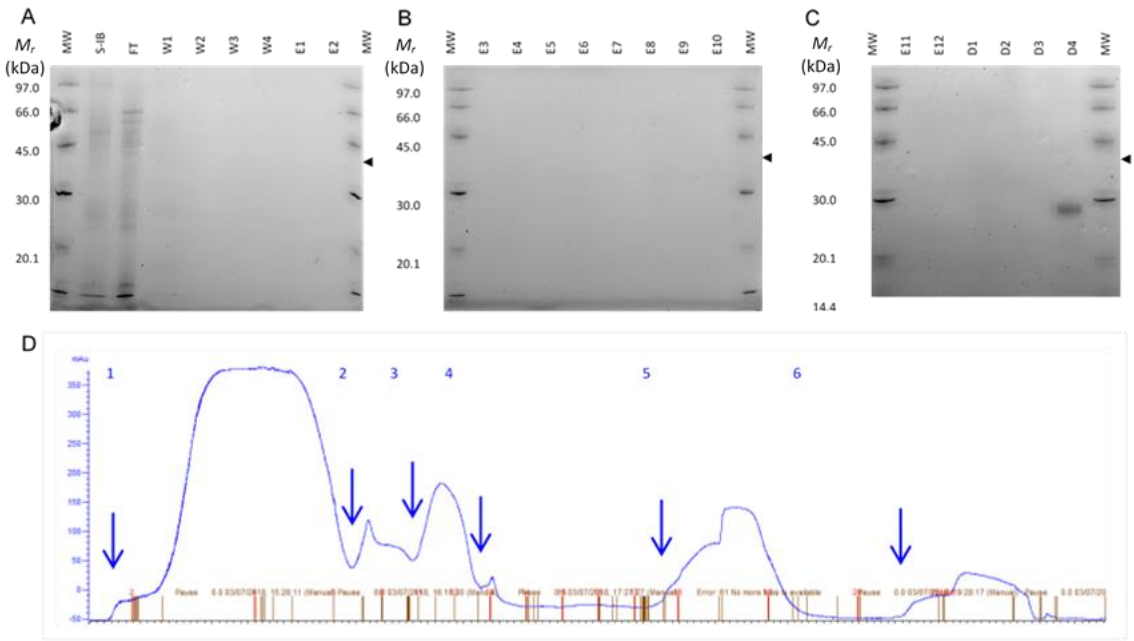

Figure 4.4.2.8.2.2. Trial IMAC purification of rFhGAPDH. rFhGAPDH isolation was tested using Ni-NTA on an ÄKTA Prime system with solubilised IB fractions, including on-column refolding (4.3.4.3). Samples were analysed by SDS PAGE (A–C) and UV readings for protein concentration were analysed using PrimeView™ (v1.00) (D). Abbreviations: MW, Amersham Low Molecular Weight SDS Calibration Kit (M_r); S-IB, solubilised IBs; FT, flow-through; W1-4, washes; E1-12, elutions; D1-4, denaturation washes.

A larger-scale purification was also trialled using Nickel-NTA (ABT, Web Scientific, UK) with an ÄKTA Prime system (GE Healthcare) (Figure 4.4.2.8.2.2D), and rFhGAPDH IB lysate IMAC fractions were analysed using 12.5% SDS PAGE (Figure 4.4.2.8.2.2A–C). As in the trial purification, data indicated low protein concentration in all fractions, including refolding washes (W1–4: 8>0 M urea), imidazole elutions [E1–7: 250 mM; E8–12: 500 mM] and final denaturation washes (Figure 4.4.2.8.2.2D: 1–4; 8 M urea 1 mM DTT) to ensure column-protein release. However, the UV plot indicated protein passage through the HisTrap NiNTA column following injections: 1, protein sample loading; 2, column washed under high denaturant concentration (8M urea); 3, column washed under low denaturant concentration (4 M urea); 4, column washed under non-denaturing conditions; 5, elutions with 250–500 mM imidazole in binding buffer; and 6, column washed in denaturing elution buffer (Figure 4.4.2.8.2.2D). This suggests low levels of rFhGAPDH in the overall protein content and an inability to purify this target with this method.

In order to identify suspected rFhGAPDH in samples, bands of interest were analysed by LC-MS/MS following in-gel isolation (Figure 4.4.2.8.2.1, boxed). Data files were searched

against the draft genome for *F. hepatica* (PRJEB6687) using MASCOT, which did not identify GAPDH proteins in the samples ($P < 0.05$). Three hits were over the threshold score (MASCOT score range: 31≤43) and false discovery rates were above 50% (data not shown), suggesting insignificant FhGAPDH abundance.

Based on the findings from these pilot studies for rFhGAPDH, in order to proceed further with this target, overexpression must be optimised. Specifically, identifying the optimal expression temperature of induced cultures will be valuable to obtain adequate target protein concentrations for subsequent purification and molecular investigation.

4.4.2.9 Triose phosphate isomerase (FhTPI)

The plasmid *FhTPI-pET-46 Ek/LIC* was a gift from Professor David Timson (Brighton University, UK, (Zinsser *et al.*, 2013b)). DNA sequencing was used to confirm 100% sequence identity of the gene sequence to the *in silico* GenBank sequence (v204, KC164346.1; AGJ83762.1: www.ncbi.nlm.nih.gov/protein/AGJ83762.1) and the in-frame expression and N-terminal polyhistidine tag sequences (Figure 4.4.2.9).

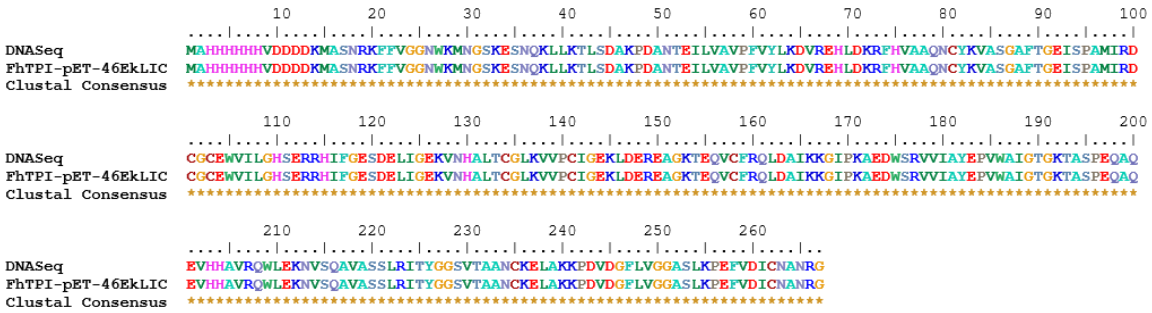

Figure 4.4.2.9. Confirmation of the FhTPI-pET-46Ek/LIC expression sequence. DNA sequencing was used to identify 100% amino acid sequence identity (compiled using BioEdit).

4.4.2.9.1 Expression

rFhTPI was expressed from One Shot® BL21(DE3) Star™ cells using 0.5–2.0 mM IPTG and soluble fractions were analysed by 12.5% 1-D SDS PAGE (Figure 4.4.2.9.1.1A–C). The *in silico* polyhistidine-tagged protein was predicted to be 29.50 kDa with an isoelectric point of 6.89 and an overall charge of -1.0. Induction and overexpression conditions were mirrored on the previous production of rFhTPI (Zinsser *et al.*, 2013b), inducing expression and growing cultures at 37°C for up to three hours. Recombinant protein overexpression in the soluble

lysate was demonstrable at all IPTG concentrations, whereby the protein monomer of approximately 30 kDa and dimer of approximately 60 kDa could be visualised by 1-DE (Figure 4.4.2.9.1.1). For subsequent recombinant overexpression, these conditions were maintained, with 0.5 mM IPTG for induction.

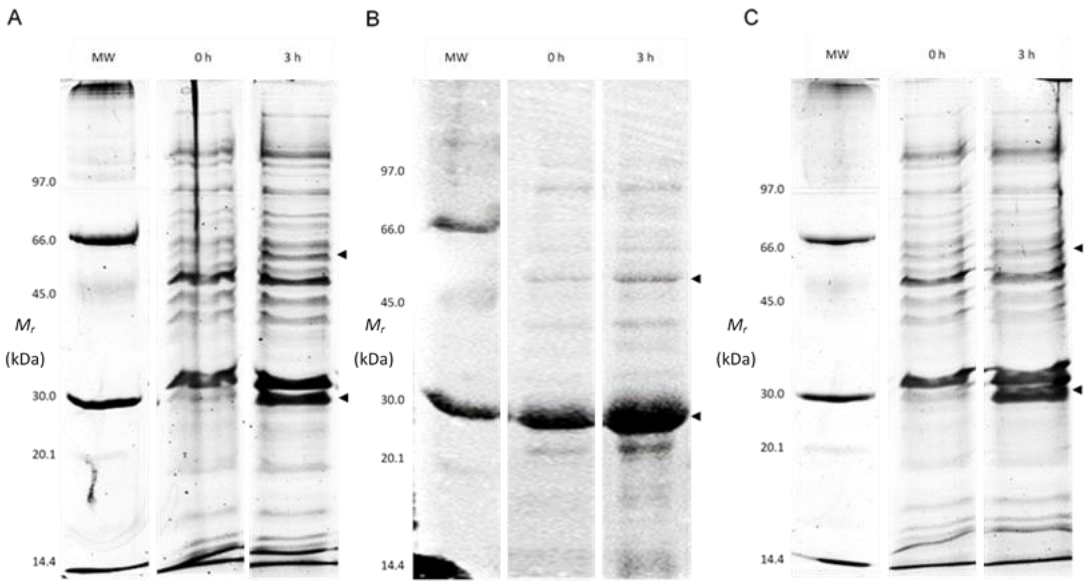

Figure 4.4.2.9.1.1. Pilot recombinant expression of rFhTPI. 5 µg FhTPI-pET-46Ek/LIC One Shot® BL21(DE3) recombinant expression lysate was analysed by SDS PAGE following 0.5 mM (A), 1.0 mM (B) and 2.0 mM (C) IPTG from 0–3 hours post-induction at 37°C**.**

Abbreviations: MW, Amersham Low Molecular Weight SDS Calibration Kit (M_r); 0/3, hours post-induction.

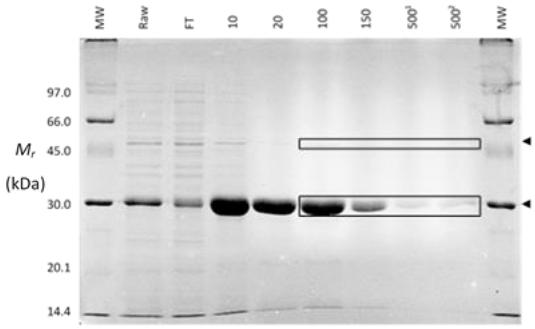

Figure 4.4.2.9.1.2. IMAC purification of rFhTPI. rFhTPI was isolated from recombinant expression lysate using HIS-Select Cobalt, showing efficient isolation of the target protein in imidazole elutions.

Abbreviations: MW, Amersham Low Molecular Weight SDS Calibration Kit (M_r); raw, raw bacterial lysate; FT, flow-through; 10–500 [mM], imidazole concentration.

rFhTPI was purified using HIS-Select Nickel (Sigma) and analysed by 12.5% SDS PAGE (Figure 4.4.2.9.1.2). All elution samples above 100 mM imidazole were analysed by LC-MS/MS following in-gel isolation, whereby the two bands of interest per lane were selected (30, 60 kDa). MASCOT identified all bands as FhTPI (GenBank v204, AGJ83762.1: www.ncbi.nlm.nih.gov/protein/AGJ83762.1) with significant scores ($P < 0.01$) (Table 4.4.2.9.1). Based on these findings, samples between 150-500 mM imidazole, with the

greatest indication of target purity by 1-DE and LC-MS/MS, were pooled and re-analysed by 1-D and 2-D SDS PAGE (Figure 4.4.2.9.1.3) with significant (P < 0.01) MASCOT scores (Table 4.4.2.9.1). 2-DE indicated rFhTPI separates into six isomers with distinct isoelectric points between 7.0–7.6 pI and ranging between 29–31.0 kDa, but no dimers were observed (Figure 4.4.2.9.1.3B).

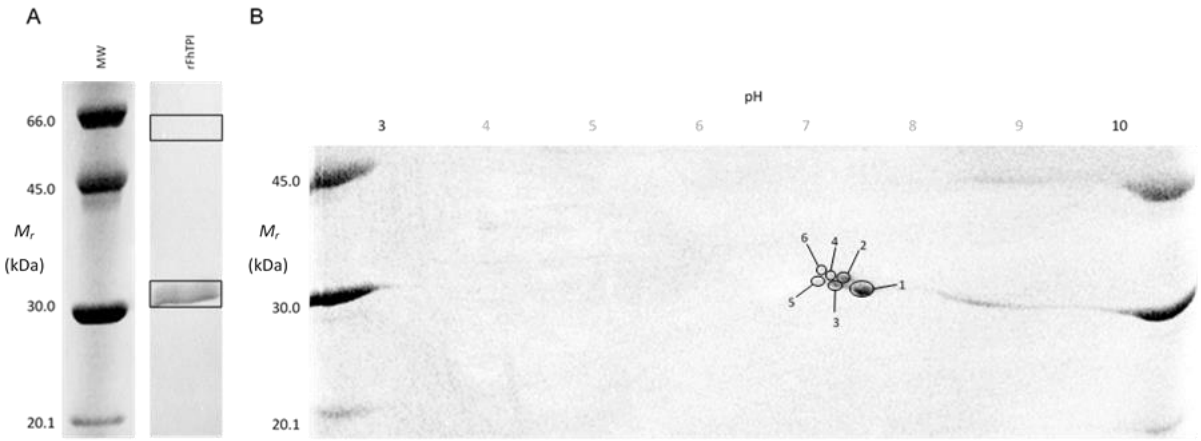

Figure 4.4.2.9.1.3. 1-D and 2-D SDS PAGE of purified rFhTPI. 1 µg rFhTPI was resolved at approximately 31 kDa by 1-DE (A), whereas 2-DE (B) identified six isomers separate within the region of 7.00–7.60 pH (7 cm IEF 3–10; 12.5% SDS PAGE). LC-MS/MS identified all 2-DE separated isomers as triose phosphate isomerase (MASCOT Score = 211–1216: BN1106_s3213B000041.mRNA-1, PRJEB6687, WBPS v10; AGJ83762.1: www.ncbi.nlm.nih.gov/protein/AGJ83762.1, GenBank v204)). LC-MS/MS results of the 2-DE analysis are detailed in Table 4.4.2.9.1.

Abbreviations: MW, Amersham Low Molecular Weight SDS Calibration Kit (M_r).

All peptide residues matched by LC-MS/MS analysis of FhTPI are also highlighted (Figure 4.4.2.9.1.4). Monomer and dimer 1-DE bands and all 2-DE spots were identified by LC-MS/MS with significant (P < 0.01) MASCOT scores matching to FhTPI (PRJEB6687: BN1106_s3213B000041.mRNA-1; GenBank: AGJ83762.1) (Table 4.4.2.9.1), whereby AGJ83762.1 and BN1106_s3213B000041.mRNA-1 share 99.6% sequence similarity due to one residue substitution (T211I) (Figure 4.4.2.9.1.4). Peptide fragmentation data also provided no evidence for amino acid substitutions from the established sequence (AGJ83762.1) but indicated putative post-translational oxidation modifications at Met15 and Met83 residues. Based on the findings from these pilot studies for rFhTPI, this recombinant has been optimally overexpressed and purified at adequate concentrations for further investigation of biochemical and diagnostic investigation.

Figure 4.4.2.9.1.4. Comparison of the triose phosphate isomerase amino acids sequence cloned in this study (FhTPI) and two genome sources (dotted lines). The cloned TPI sequence (excluding the polyhistidine tag) is 100% identical to the GenBank source (AGJ83762.1: www.ncbi.nlm.nih.gov/protein/AGJ83762.1, GenBank v204), but has one residue difference with the *Fasciola hepatica* PRJEB6687 genome sequence (BN1106_s3213B000041.mRNA-1, WBPS v10). All highlighted residues were identified by LC-MS/MS, matching to the GenBank or genome hits, whereby the non-synonymous residue (T211I, position 225) was matched to the expected threonine amino acid as in the sequenced rFhTPI. The alignment was produced using the ClustalO tool in BioEdit.

Table 4.4.2.9.1. LC-MS/MS identification of 1-DE- and 2-DE-separated rFhTPI. rFhTPI protein bands/spots of interest were identified by LC-MS/MS against the *F. hepatica* genome (PRJEB6687, WBPS v10) and GenBank, reporting significant hits identified with a score of 38 or greater (P < 0.01) and average scores of duplicate samples (italicised).

Figure reference	Lane/ spot identity	Band size (approximate, kDa)	MS/MS ion search					Highest scoring GenBank hit			
			Fh genome hit	MASCOT score	False discovery rate (%)	Peptides matched (non-duplicate)	Sequence coverage (%)	Protein	Organism	Accession	E-value
4.4.2.9.1.2	100	30.0	**BN1106_s3213B000041.mRNA-1**	6256	0.27	34	70.0	**Triose phosphate isomerase**	***Fasciola hepatica***	**AGJ83762.1**	**0.0**
		60.0		213	0.00	12	50.0				
	150	30.0		4317	0.00	45	78.0				
		60.0		231	7.69	11	50.0				
	500.1	30.0		2602	0.00	42	76.0				
		60.0		127	0.00	11	50.0				
	500.2	30.0		1077	1.61	29	71.0				
		60.0		70	0.00	9	39.0				
4.4.2.9.1.3A	rFhTPI	30.0		*1626.5±111.5*	*0.00*	*39.5±1.5*	*74.0±1.0*				
		60.0		*68±16*	*0.00*	*7±1*	*27±3*				
4.4.2.9.1.3B	1	30.0		790	0.00	20	66.0				
	2			437	0.00	19	57.0				
	3			405	0.00	19	46.0				
	4			203	0.00	15	50.0				
	5			148	0.00	9	31.0				
	6			151	0.00	8	30.0				

4.5 Discussion

In this thesis, seven *Fasciola hepatica* biomarker candidates previously identified through a novel proteomic approach (Morphew *et al.*, 2014) were selected for systematic bioinformatic assessments (Chapter 5; 4.2.3: objective 1; 4.4.1.2–4.4.1.8) and recombinant expression (Chapter 5; 4.2.3: objective 2; 4.4.2.2–4.4.2.9; summarised in Table 4.3.2.1). Since TCBZ flukicidal mechanisms and resistance are not fully understood (Brennan *et al.*, 2007; Kelley *et al.*, 2016; Stitt *et al.*, 1995), putative roles of each biomarker during these phenotypes is speculative, but improved with predictive tools and bioinformatics (Arnold *et al.*, 2006; Frédéric *et al.*, 2009; Kelley *et al.*, 2015; Li *et al.*, 2009; McArthur and Wright, 2015). To this end, this chapter was able to identify moderate to high sequence and structural conservation in the seven *F. hepatica* biomarker candidates upon comparison with model and related parasite equivalents, in-keeping with the proteins' family and superfamily characteristics following evolutionary divergences. Pathogenic and functionally relevant epitopes and residues were also identified for all protein targets, providing evidence for potential *in situ* roles towards fluke cellular and physiological homeostasis and/or virulence during host infection. Consequently, a provision of background knowledge for these antigens has been collated in this chapter to complement further antigenicity, biochemical, cellular biological and further research topics. As yet, of the biomarker candidates for monitoring TCBZ-SO treatment success, only *F. hepatica* glyceraldehyde-3-phosphate dehydrogenase (FhGAPDH) and triose phosphate isomerase (FhTPI) have been recombinantly expressed for *in vitro* metabolic investigation (Zinsser *et al.*, 2014, 2013b) and only enolase (FhENO) has been natively isolated for the identification of non-glycolytic virulence association (Bernal *et al.*, 2004). Thus, following the successful cloning of *F. hepatica* actin (FhACT), DJ-1 deglycase (FhDJ-1), FhENO and FhGAPDH, and the optimised recombinant protein expression and purification of calreticulin (FhCRT), gelsolin (FhGEL), and FhTPI, this thesis has provided a thorough molecular background and methodology to produce a panel of *F. hepatica* biomarkers for prospective further study and liver fluke diagnostic developments.

In-keeping with the TCBZ survival molecular phenotype (Morphew *et al.*, 2014), CRT, ENO and GAPDH have been widely indicated as virulence factors beyond normal functions by pathogenic organisms and during disease (Barbosa *et al.*, 2006; Bergmann *et al.*, 2004; Díaz-Ramos *et al.*, 2012; Funk *et al.*, 2016; Gómez-Arreaza *et al.*, 2014; Holoshitz *et al.*, 2010;

Jaouannet *et al.*, 2013; Liu and Shih, 2007; Obeid *et al.*, 2007a; Ucker *et al.*, 2012). Equally, biomarkers descriptive of flukicide success appear to reflect fundamental biological roles, including ACT- and GEL-mediated structural stability and cellular proliferation (Dominguez, 2004; Dominguez and Holmes, 2011; Stitt *et al.*, 1992b), DJ-1-mediated protection against oxidative apoptosis (Junn *et al.*, 2009; Taira *et al.*, 2004; Takahashi-Niki *et al.*, 2004), and glycolytic TPI activity (Schliebs *et al.*, 1996; Seigle *et al.*, 2008; Zinsser *et al.*, 2013b).

4.5.1 FhCRT: a putative biomarker of TCBZ-SO survival

CRT has demonstrated diverse roles beyond housekeeping (Dedhar, 1994; Johnson *et al.*, 2001; Michalak *et al.*, 1999), including CRT-drug interactions (Butler *et al.*, 1992; Horibe *et al.*, 2004; Ikehata *et al.*, 2008; Karasawa *et al.*, 2011), immunogenicity (Obeid *et al.*, 2007b, 2007a), and CRT-mediated complement and perforin regulation (Eggleton *et al.*, 1994; Fraser *et al.*, 2000; Kishore *et al.*, 1997). Indeed, several protozoal and haematophagous parasite CRTs also have demonstrable virulence-associated activities, including putative anti-angiogenesis (Cabezón *et al.*, 2008; Molina *et al.*, 2005), immunodominance (Pritchard *et al.*, 1999), immunogenicity (Mutapi *et al.*, 2011) and immune evasion (Ferreira *et al.*, 2004a; Jaworski *et al.*, 1995; Sanchez Ferreira *et al.*, 2002; Suchitra and Joshi, 2005), and complement interaction (Kasper *et al.*, 2001; Kim *et al.*, 2015) and inhibition (Ferreira *et al.*, 2004b, 2004a; Jaworski *et al.*, 1995; Sanchez Ferreira *et al.*, 2002; Schroeder *et al.*, 2009; Weinberger *et al.*, 2017). There is also growing evidence for CRT involvement during cancer, including immune evasion upon CRT downregulation (Peng *et al.*, 2010), as well as drug resistance and metastasis through CRT upregulation, resulting from augmented calcium regulation (Baguley, 2010; Panaretakis *et al.*, 2008) and misfolded protein restoration (Matsukuma *et al.*, 2016; Ri *et al.*, 2010; Zhou *et al.*, 2016). Thus, CRT is considered a resistance biomarker in some cancers (Chou *et al.*, 2015; D'Aguanno *et al.*, 2011; Paulitschke *et al.*, 2013) and so may re-enact this and other virulence roles in trematodes, since CRT upregulation has also been measured post-anthelmintic treatment in both *F. hepatica* (Morphew *et al.*, 2014) and *S. mansoni* (Mutapi *et al.*, 2005). Important to consider however is residual native activities, anchoring its extracellular isolation as an indicator of ER stress (Kopecka *et al.*, 2011; Park *et al.*, 2001) and subsequent cellular protection (Bedard *et al.*, 2004; Pinto *et al.*, 2008). Consequently

therefore, FhCRT may reproduce several of these diverse functionalities and will require consideration for the context of its detection.

4.5.2 FhGEL, FhTPI and related targets: putative biomarkers of TCBZ-SO challenge

As a member of the actin-binding protein superfamily and a key ACT regulator (Dominguez, 2004; Kwiatkowski, 1999; McGough *et al.*, 2003; McLaughlin *et al.*, 1993; Sun *et al.*, 1999; Way *et al.*, 1990), GEL predominantly localises to the cytoplasm (Yin and Stossel, 1979) but can be found circulating as plasma GEL (pGEL) in vertebrates (Yin *et al.*, 1984, 1981). Consequently and following pathology-associated cellular disruption and motility, pGEL can scavenge liberated extracellular ACT (Lee *et al.*, 2009; Lee and Galbraith, 1992; Peddada *et al.*, 2012) and thus acts as a prognostic marker, with increased pGEL in patients' circulation during recovery (DiNubile, 2008; Kim *et al.*, 2004; Kwiatkowski, 1999; Lee *et al.*, 2007; Peddada *et al.*, 2012; Piktel *et al.*, 2018). Due to this association with cellular repair through ACT homeostasis, circulating pGEL has been measured during numerable pathologies including traumas (Bayir *et al.*, 2014; Genre *et al.*, 2014; Guo *et al.*, 2011; Huang *et al.*, 2011; Lee *et al.*, 2006; Mounzer *et al.*, 1999), cancers (He *et al.*, 2014; Kwiatkowski, 1999; Shieh *et al.*, 1999; Winston *et al.*, 2001; Yang *et al.*, 2006, 2004), and infections including eosinophilic fasciolosis (Straub *et al.*, 2011), *Teladorsagia cirumcincta* infection (Goldfinch *et al.*, 2008), and chagasic cardiomyopathy (Wen and Garg, 2012). Furthermore, this has led to the proposition of therapeutic applications as GEL has also been found to promote cell homeostasis and thereby inhibit apoptosis (Antequera *et al.*, 2009; Koya *et al.*, 2000).

As has been described for CRT, the context of GEL recovery and its originator is equally key to determining diagnostic utility, since it has also been found to promote protozoal invasion (Wen and Garg, 2012; Zhou *et al.*, 2011) and even ablation of apoptotic protection by aberrant activities of caspase-3-cleaved GEL subunits (Elmore, 2007; Kothakota *et al.*, 1997; Oikonomou *et al.*, 2009). No helminthic GELs have been investigated until now, though GEL has been identified within ES products of pathogenic juveniles of *F. hepatica*, *Schistosoma bovis*, *Echinococcus granulosus* and *Mesocestoides corti* (Camargo de Lima *et al.*, 2018; De la Torre-Escudero *et al.*, 2011; Hernández-González *et al.*, 2010; Teichmann *et al.*, 2015), adult *F. hepatica* EV membranes (Cwiklinski *et al.*, 2015c; Davis *et al.*, 2019), and adult *F. hepatica* ES and *S. mansoni* tegumental products during anthelmintic challenge (Linder and Thors,

1992; Morphew *et al.*, 2014). Since SmGEL-mediated ACT depolymerisation is triggered at tegumental spines by praziquantel application (Linder and Thors, 1992), this may most closely resemble FhGEL activities following lethal TCBZ-SO challenge in TCBZ-susceptible flukes (Morphew *et al.*, 2014), especially since FhGEL shares 62.36% sequence conservation with SmGEL (Figure 4.4.1.6.2.1). Furthermore, when considering the molecular size of *in vitro*-recovered FhGEL (~43 kDa) resembles pro-apoptotic caspase-3-cleaved GEL (~45 kDa), this additionally supports the hypothesis of FhGEL as an indicator of TCBZ-SO-induced stress via ACT-binding, cellular repair and apoptosis interaction.

The prospect of glycolytic enzyme candidature for molecular diagnosis, treatment and vaccination regimens has set a trend towards their characterisation and testing (Bergquist, 1998; Crowther *et al.*, 2010; Harn *et al.*, 1992, 1985; Harris *et al.*, 2014; J Timson, 2016; Joubert *et al.*, 2001; Kushawaha *et al.*, 2012; Reynolds *et al.*, 1994; Shoemaker *et al.*, 1992; Ucker *et al.*, 2012). TPI is one such contender, since it is a ubiquitous and fundamental cell component, responsible for catalysing the interconversion of dihyroxyacetone phosphate and glyceraldehyde-3-phosphate during glycolysis (Knowles, 1991). As bioinformatic (4.4.1.8) and *in vitro* (4.4.2.9.1) data have also shown for FhTPI, TPI forms a highly stable dimer (TPI_2) (Lambeir *et al.*, 2000; Sun *et al.*, 1993; Waley, 1973; Zinsser *et al.*, 2013b, 2013a) in which it predominantly operates (Waley, 1973; Zabori *et al.*, 1980). There is evidence to suggest that interface mutations not only disrupts this (Borchert *et al.*, 1993b; Daar *et al.*, 1986; Maithal *et al.*, 2002; Ralser *et al.*, 2006) but also contributes to the formation of an inactive, tightly-folded monomer (Morgan *et al.*, 2000; Zabori *et al.*, 1980), suggesting homodimer formation is conducive to functionality, a characteristic which rFhTPI shows high propensity (Zinsser *et al.*, 2013b), including in the absence of appropriate cross-linkers in recombinant expression lysate (Figure 4.4.2.9.1.1).

Incidences of atypical TPI presence, including as a result of drug exposure (Morphew *et al.*, 2014), non-communicable and infectious diseases, has opened a window for determining its putative involvement or biomarker potential during such pathologies and cellular stress. Specifically, cases of neurodegeneration have found increased neuron destruction leads to the aberrant release of glycolytic enzymes (Kolln *et al.*, 2006; Lovato *et al.*, 2008), and subsequently autoantibodies to these proteins (Menon *et al.*, 2011) due to the high glucose metabolism of these cells. Similar dissemination of host TPI in fungi-infected plant tissues has also been observed (González-Fernández and Jorrín-Novo, 2012), but unicellular parasite and

bacterial species present exceptions to this pathology and cell death phenotype, demonstrating surface-expressed TPI can assist in host cell invasion (Fletcher *et al.*, 2001; Furuya and Ikeda, 2011, 2009; Karkowska-Kuleta *et al.*, 2011; Miranda-Ozuna *et al.*, 2016). However, many more reports of invasion by uni- and multi-cellular infectious organisms support virulence functions of ENO and GAPDH, including via host fibronectin and plasminogen binding plasminogen (Barbosa *et al.*, 2006; Bergmann *et al.*, 2004; Bernal *et al.*, 2004; Pancholi and Chhatwal, 2003). In helminths, TPI has been identified in the tegument (Harn *et al.*, 1985) and ES profiles (Hewitson *et al.*, 2008; Moreno and Geary, 2008; Sotillo *et al.*, 2010; Zheng *et al.*, 2011) at several life cycle stages, including *F. hepatica* adult ES (González-Miguel *et al.*, 2019) and tegument (Morphew *et al.*, 2013) proteomes. However, potential roles of TPI in helminth virulence has not yet been determined, though extracellular *Brugia malayi* TPI has been identified as an essential promoter towards *in vitro* microfilariae production (Hewitson *et al.*, 2014). Interestingly, there is evidence for TPI, ENO and GAPDH glycolytic enzyme release during the early stages of apoptotic cell death (Ucker *et al.*, 2012), whereas the change in abundances of these proteins in *F. hepatica* ES products was dependent on *in vitro* anthelmintic dose (Morphew *et al.*, 2014), with TPI being a lethal-associated biomarker and ENO and GAPDH overexpressed under SL (non-lethal) challenge. Thus, with this and the known and expectant virulence associations of these enzymes, FhTPI release is highly suggestive of TCBZ-susceptibility, whereas FhENO and FhGAPDH are likely to represent virulence factors for parasite survival.

4.6 Conclusions

More previously neglected proteins are becoming linked with bespoke roles in disease and pathogenesis through *in vitro* studies and, by extension, sequence matching with bioinformatics (Li *et al.*, 2009; McArthur and Wright, 2015). Thus, bioinformatic analyses are an early step in the functional pipeline for therapy and diagnostics. However, as shown in this chapter, the down-stream production of molecular tools for hypothesis confirmation was highly influenced by bacterial expression dynamics and/or the protein's biochemical properties (Chambers and Swalley, 2009). In particular this was evident for actin (FhACT), DJ-1 deglycase (FhFJ-1), enolase (FhENO) and glyceraldehyde-3-phosphate dehydrogenase (FhGAPDH), the recombinant expression of which was not adequately optimised during this

study, precursory to *in vitro* molecular characterisation. Thus, this chapter has involved extensive bioinformatically analysed seven targets of interest (Chapter 5; 4.2.3: objective 1), which were identified with changed abundance in the excretory/secretory (ES) proteomes of TCBZ-SO-treated verses untreated flukes: FhACT, FhCRT, FhDJ-1, FhENO, FhGEL, FhGADPH, and FhTPI. Furthermore, this chapter has also created blueprints for the production of these seven targets (Chapter 5; 4.2.3: objective 2), with success in the efficient purification of three of these proteins for preliminary study during the scope of this work: FhCRT, FhGEL and FhTPI; and providing antigen material for immediate further study in this thesis (Chapter 6). Additionally, new and in-depth information has been obtained through bioinformatic and *in vitro* proteomics of recombinant candidates, and potential roles of targets have been discussed in the context of drug-terminating or non-terminating fluke phenotypes, providing a basis for further study and research progression.

6 Chapter 6: Determining the diagnostic potential of new *Fasciola hepatica* molecular biomarkers of TCBZ efficacy

6.1 Abstract

Diagnostics play an integral part in liver fluke control strategies, including tactics for monitoring anthelmintic resistance and treatment success. Accordingly, *Fasciola hepatica* cathepsin L (FhCL) proteases remain the leading diagnostic candidate, due to their overabundance in the dynamic juvenile and adult excretory/secretory (ES) proteomes, and their use in parasite detection via blood and faeces. However, multiple molecular candidates of interest have been identified from the work of this thesis and previous underpinning studies, including targets associated with TCBZ efficacy status. Thus, a novel direction to determine drug efficacy and TCBZ-susceptibility profiles is investigated in this chapter.

A panel of molecular tools were used in pilot diagnostic testing, including recombinant *F. hepatica* procathepsin L1 (rFhpCL1), calreticulin (rFhCRT), gelsolin (rFhGEL), and triose phosphate isomerase (rFhTPI) biomarkers and synthetic FhCL1-derived peptides. Additionally, serological samples were prepared for testing, including polyclonal anti-rFhpCL1 antibodies, and sera pooled from three sheep experimentally-infected with TCBZ-susceptible (TCBZ-S) or TCBZ-resistant (TCBZ-R) *F. hepatica* strains. Thus, using a variety of immunologic platforms, including enzyme-linked immunosorbent assay (ELISA), dot blot and western blot approaches, the diagnostic utility of the antigen candidates and polyclonal antibodies was assessed. Resultantly, this identified promising capabilities of anti-FhpCL1 leading to sensitive diagnoses of infection and TCBZ success via faecal antigen capture.

Consequently to the outcomes of this chapter, a strong foundation has been established toward the exploration of new diagnostic targets for liver fluke infection and drug efficacy determination. Through the testing of candidates with putative immunogenic properties or reported TCBZ efficacy association, further progression from this pilot work could also seek to address anthelmintic preservation and develop tools for the profiling of TCBZ-S and TCBZ-R flukes.

6.2 Introduction

6.2.1 Diagnostic test pipeline

Diagnosis is the classification of disease and non-clinical cases based on the identification of pathological symptoms or signs, including those directly or indirectly resultant from the causative agent or pathogen (Altman and Bland, 1994a; Begg, 1987). The accuracy of a

diagnostic test is determined by the correct identification and differentiation between true positive and false negative cases (sensitivity) and true negative and false positive cases (specificity) (Altman and Bland, 1994a; Ferrante di Ruffano *et al.*, 2012; Ransohoff and Feinstein, 1978). These efficacy evaluations can be cause for bias in terms of diagnosis allocation, whereby results on a spectrum of clinical circumstances instead become adopted into a binary system of "rule in or out" positive or negative diagnoses, and thus may falsely overestimate tests' sensitivities and specificities in the study population (Begg, 1987; Lord *et al.*, 2006; Ransohoff and Feinstein, 1978; Whiting *et al.*, 2008). Despite such limitations, primary studies continue to utilise sensitivity and specificity values as the optimal quantitative evaluation of a test's potential to correctly diagnosis positive and negative cases (predictive values), which also takes into account the disease prevalence in the study population (Altman and Bland, 1994b, 1994c; Whiting *et al.*, 2008). Thus, confirmation of these calculations continue to dictate a test's potential therapeutic application(s) in disease control (Ferrante di Ruffano *et al.*, 2012).

6.2.2 Current methods for fasciolosis diagnosis and anthelmintic resistance

The diagnosis of *Fasiola hepatica* infection, like for other parasites, is not often reliant on the outcome of one technique, but is often conducted with complementary parasitological, molecular and/or immunological methods (Charlier *et al.*, 2014b, 2009, 2008; El Bahy *et al.*, 1994; Flanagan *et al.*, 2011b; Mezo *et al.*, 2004; Roeber *et al.*, 2013; Valero *et al.*, 2009). Coprological examination has been the oldest standing method for parasitological identification of helminth infection (Teuscher, 1965). However, the application of coprology via faecal egg counting (FEC) is imperfect for trematode infections at low infection intensities, including fasciolosis, due to the delay of their recovery from 8-13 weeks post-infection (wpi) and the fluctuations of their release and smooth passage into faeces on their way from the host biliary system (Moazeni and Ahmadi, 2016). Thus, in the absence of a gold standard test for fasciolosis, concurrent applications of the available tests are necessary for definitive identification and confirmation of parasite presence, infecting species, activity and drug susceptibility status, wherever each diagnosis might be required (Brockwell *et al.*, 2014, 2013; George *et al.*, 2017; Gordon *et al.*, 2012; Novobilský *et al.*, 2016).

In recent years, assessing the efficacy of anthelmintic treatment has been of equal if not greater concern compared to simply monitoring *F. hepatica* infection levels, and this shift in diagnostic emphasis is driven by increasing global incidences of resistance to TCBZ (Kelley *et al.*, 2016), the only compound targeting pathogenic juvenile fluke, coupled with the continued absence of a commercial vaccine. Thus far, treatment efficacy testing has consisted of the strategic application of parasitological or immunological diagnostics. The aim to confirm resistance quantitatively is accomplished by measuring eggs or coproantigens, i.e. where <95% reductions after anthelmintic treatment indicates resistance (Brockwell *et al.*, 2014; Coles *et al.*, 2006; Daniel *et al.*, 2012; Flanagan *et al.*, 2011b, 2011a; Gordon *et al.*, 2012; Kajugu *et al.*, 2015; Novobilský *et al.*, 2012; Olaechea *et al.*, 2011; Ortiz *et al.*, 2013; Sargison, 2012). Reduction tests (RT) for *F. hepatica* have been standardised for field application (Brockwell *et al.*, 2014; Flanagan *et al.*, 2011a, 2011b; Gordon *et al.*, 2012; Novobilský *et al.*, 2012) and include both the FEC-RT and the coproantigen-RT (C-RT), as directly-detectable indicators of parasite activity and viability post-treatment (PT).

However, in contrast to the ease of application of FEC-RT in supporting the diagnosis of nematode anthelmintic efficacy (Coles *et al.*, 2006, 1992), the application of FEC-RT for fasciolosis flukicide susceptibility is problematic with well-known limitations. The aforementioned irregularity of egg discovery and their interruption is a normal occurrence during infection, which PT can continue and be delayed due to the probable entrapment of eggs in the gall bladder, consequently impeding the true diagnosis of treatment failure and true resistance (Fairweather, 2011b; Sargison, 2012). Measuring the ovicidal activity using an egg hatch assay (EHA) eliminates egg timeline problems and subsequently EHA has been confirmed as a reliable alternative to FEC-RT for resistance identification in experimental isolate and natural infections (Alvarez *et al.*, 2009; Arafa *et al.*, 2015; Canevari *et al.*, 2014; Fairweather *et al.*, 2012; Robles-Pérez *et al.*, 2014). The application of serological diagnoses for measuring treatment efficacy or anthelmintic resistance is limited by immunological memory lingering and silencing the impact of any quantitative changes to antigen abundance PT (Brockwell *et al.*, 2013). Thus, flukicide efficacy testing via RT and EHA satisfy requirements for measuring clinical level resistance in a specialised laboratory but are not suitable for more rapid treatment strategy responses, as would be the paradigm in point-of-care settings (Martínez-Sernández *et al.*, 2011; Ndao, 2009) in avoiding uninformed or inappropriate anthelmintic use (Vercruysse and Claerebout, 2001).

6.2.3 Molecular components of fasciolosis diagnostics

A multitude of tegumental-, leaked cytosolic- and excretory/secretory product (ES)-derived molecular biomarkers of *Fasciola hepatica* have been investigated as potential diagnostic candidates over the last several decades, due to their over-abundance, immunogenicity and/or association with anti-flukicidal metabolism (Dalton *et al.*, 2003; Dalton and Heffernan, 1989; Jefferies *et al.*, 2001; Levieux *et al.*, 1992; McGinty *et al.*, 1993; Morphew *et al.*, 2013, 2014). Prominent among them have been cathepsin L (CL) proteases of the adult ES proteome, which were first identified as an obvious target due to their over-abundance and impacts on host immunity and establishment (Dalton *et al.*, 2003). Thus, exploiting their extracellular abundance for undertaking immunomodulatory and nutritional roles, immunogenic CL proteases from *F. hepatica* have been shown to be key diagnostic candidates, in both laboratory and field studies (Cornelissen *et al.*, 2001, 1999).

Subsequently, the progression of fasciolosis diagnosis has led to repositioning of CL protease peptides as the target for detection by a monoclonal antibody (MM3) for an ELISA test (Mezo *et al.*, 2004), which has become a commercial faecal diagnostic platform for infections of livestock (Brockwell *et al.*, 2013; Gordon *et al.*, 2012; Kajugu *et al.*, 2015; Mezo *et al.*, 2007; Molloy *et al.*, 2005) and humans (Martínez-Sernández *et al.*, 2016, 2011; Ubeira *et al.*, 2009; Valero *et al.*, 2012). However, other ES proteomic changes following TCBZ exposure could offer new molecular candidates for TCBZ resistance tracking as well as descriptive strain-specific biomarkers. Indeed, anthelmintic-induced protein profile differences have been confirmed following TCBZ exposure in *in vitro*-cultured wild type *F. hepatica* (including parasites of an assumed mixture of TCBZ susceptibility status and exposure) (4.4.4; Morphew *et al.*, 2014) and a TCBZ-resistant (TCBZ-R) isolate strain of known TCBZ treatment history (treatment at 12 wpi; summarised in Chapter 4). The influence of TCBZ-associated biomarkers, including seven new recombinant candidates broadened in Chapter 5, on the impact of immunogenicity following potential antigen exposures is also yet to be understood or investigated for *F. hepatica*.

6.2.4 Chapter 6 aims

So far, bar tests based on total *in vitro*-derived ES products (Arjmand *et al.*, 2014; Salimi-Bejestani *et al.*, 2005), the selection and validation of defined diagnostic biomarkers for detecting *Fasciola hepatica* infection has led to the standardisation and wide-spread utilisation of tools based on only the most prominent fluke-derived protein of the host-parasite interactome, i.e. the CL proteases (Cornelissen *et al.*, 2001, 1999; Dalton *et al.*, 2003; Flanagan *et al.*, 2011a; Meshgi *et al.*, 2018; Mezo *et al.*, 2004). However, multiple observations have demonstrated numerous antigen options beyond CL proteases in *F. hepatica*. For example, proteomic changes that are descriptive of fluke viability and drug exposure have been identified in live and dead flukes (3.4.1; 4.4.1; 4.4.2; Morphew *et al.*, 2007) and following TCBZ exposure, observed from wild type fluke with mixed TCBZ-susceptibility and treatment history (4.4.4; Morphew *et al.*, 2014), TCBZ-susceptible (TCBZ-S) fluke isolates (Chemale *et al.*, 2010) and TCBZ-R fluke isolates (4.4.4; Chemale *et al.*, 2010). Thus, in order to investigate novel antigens of diagnostic potential, identified through these experimental observations, the specific objectives of this chapter were:

1) To determine *in vivo* native antigen exposure based on serum recognition of recombinant and synthetic diagnostic candidates during experimental infection with TCBZ-S and TCBZ-R using indirect ELISA;
2) To assess, using a pilot faecal antigen capture ELISA platform, the ability of the anti-procathepsin L polyclonal antibody (anti-rFhΔpCL1 IgG) to detect *F. hepatica* infection and differences between TCBZ-S- or TCBZ-R-specific fluke infections;
3) To test for and identify, if present, antigen and anti-rFhΔpCL1 IgG specificity or cross-reactivity using serum and faecal livestock samples infected with other common UK-endemic parasites.

6.3 Materials and methods

6.3.1 Animal samples

6.3.1.1 *Sample collection and origin*

Faecal and serum samples were provided by Ridgeway Research Ltd UK from sheep experimentally infected with fluke (*Fasciola hepatica*; *Calicophoron daubneyi*) or nematode (*Haemonchus contortus*; *Ostertagia circumcincta*; *Cooperia oncophora*) parasites. All faecal and serum samples were stored at ≤-20°C until required.

6.3.1.2 *Faecal sample preparation*

Crude faeces (freshly collected and subsequently stored at 4°C short-term and -20°C long-term) were homogenised by inversion and vortexing in distilled water (UV-sterilised; 15 MΩ) at a ratio of 1:3 and 1:1 for sheep and cattle, respectively (water:faeces). Resuspended samples were subsequently centrifuged between 1,000-5,000 x *g* for 10 minutes at 4°C as needed in order to pellet large particulates. Supernatants were collected and stored at -20°C until required.

6.3.2 Antigen preparations

6.3.2.1 Fasciola hepatica *excretory/secretory (ES) products*

Fasciola hepatica ES products were prepared as described in the General materials and methods (2.3.2–2.3.3), whereby samples were pooled from six replicates of ten flukes acquired from natural infections at a local slaughterhouse.

6.3.2.2 *Recombinant antigens*

A recombinant *Fasciola hepatica* Leu12Pro mutant procathepsin L (rFhΔpCL1) was kindly gifted by Professor Dalton (Queen's College Belfast, UK) (Roche *et al.*, 1999) and analysed in Chapter 3 (3.4.2.1; 3.4.3.4.1). Recombinantly expressed and IMAC-purified *F. hepatica* calreticulin (rFhΔCRT), gelsolin (rFhGEL) and triose phosphate isomerase (rFhTPI) were produced as described in Chapter 5 (4.4.2.4; 4.4.2.7; 4.4.2.9).

6.3.2.3 *Peptide synthesis*

Three candidate peptide sequences (15-mer) from the signal peptide, inhibitor peptide and protease regions were selected based on sequence conservation, antigenicity (threshold for significant immunogenicity: peptide score > whole protein score), and with guidance from previous immunogenicity evidence, where present (Cornelissen *et al.*, 2001, 1999) (Chapter 3: 3.3.3). Designed peptides were synthesised at >70% purity by Peptide Synthetics (Peptide Protein Research Ltd, UK). Lyophilised peptides were resolubilised with dimethyl sulfoxide (DMSO) (75% v/v) in distilled water (UV-sterilised; 18.2 MΩ) due to the intrinsic insolubility of peptide residues. Resolubilised peptides were stored at -80°C for long-term or -20°C for short-term storage until required.

6.3.3 Antibody preparations

6.3.3.1 *Anti-rFhΔpCL1 purification*

Polyclonal antibodies (PcAb) were raised to rFhΔpCL1 as previously described (2.4.2.1; 3.3.4). IgG PcAbs were individually purified from whole sera isolated pre-exposure and after exposure to rFhΔpCL1 using protein A affinity chromatography (PAAC) as per the manufacturer's guidelines (ABT, Web Scientific). Briefly, 100 µL protein A-coated beads were rinsed and equilibrated with binding buffer (25 mM sodium phosphate, pH 7.0) before applying 400 µL (≥2.5 mg protein by Bradford assay) pre- or post-antigen exposure sera diluted at a ratio of 1:1 in binding buffer for 45-60 minutes. The flow-through was then collected and the resin was washed with 4 mL binding buffer until the run-off A_{280} was the same as the binding buffer, before eluting IgG with elution buffer (glycine 100 mM, pH 3.0) and neutralisation of the sample with the recommended volume of neutralisation buffer (1 M tris, pH 9.0). Samples were kept at -20°C until required.

Purified IgG samples from protein A chromatography were concentrated using Amicon® Ultra 3K Centrifugal Filters (Merck, UK) according to the manufacturer's protocol. Protein A-purified elution samples were filtered at 4°C using centrifugation at 14,000 x *g* for 30 minutes, which was repeated following recovery in 0.05% sodium azide (w/v) in PBS (0.1 M, pH 7.4) in the final volume of approximately 100 µL, which was stored at 4°C (short-term) or -20°C (long-term).

6.3.3.2 *Antibody biotinylation*

Anti-rFhΔpCL1 IgG was labelled with biotin using the Lightning Link® rapid biotinylation kit (Innova Biosciences, UK) according to the manufacturer's instructions. Briefly, 20 µg purified IgG antibody was mixed with LL Rapid Modifier reagent (1 µL per 10 µL antibody solution) and added to the vial containing biotin. The vial was incubated at room temperature (approximately 20°C) for at least 2 hours or overnight (14 hours) before stopping the reaction with LL Rapid Quencher reagent (1 µL per 10 µL antibody solution). Biotinylated antibodies were then stored at 4°C until required.

6.3.4 ELISA procedures

6.3.4.1 *General ELISA protocol*

All ELISA procedures were conducted as follows unless otherwise specified. Antigen (Ag) and antibody coating procedures were conducted by diluting samples at the required concentration in 0.1 M sodium carbonate ($NaHCO_3$-Na_2HCO_3 pH 9.5, coating buffer) onto Immulon 4HBX plates (Thermo Scientific, UK) and incubating overnight at 4°C. Wells were then blocked with 200 µL 2% bovine albumin (SRE00036, Sigma-Aldrich, UK) in PBS (pH 7.4; P4417, Sigma-Aldrich, UK) with 0.05% Tween-20® (2% BSA-PBS-T) for 1 hour at 37°C. For Ag or detection antibody incubations, solutions were prepared using 1% BSA-PBS-T for 100 µL per well, and secondary antibody or additional reagents, e.g. avidin-peroxidase (A3151, Sigma-Aldrich, UK), were prepared using PBS-T for 100 µL/well. All Ag and antibody steps were incubated for 1 hour at 37°C, and avidin peroxidase was incubated for 30 minutes at 37°C. Washing steps were included before and after all steps described, using 200 µL/well PBS-T five times (one minute each) with PBS-T. For reactions using the alkaline phosphatase (AP) system, including AP-conjugated antibodies (A3687, A5187, Sigma-Aldrich, UK), antibodies were diluted to 1:30,000 and 100 µL/well pNPP substrate solution (P7998, Sigma-Aldrich, UK) was incubated at room temperature for up to 30 minutes. AP-PNPP reactions were stopped by the addition of 25 µL/well 3 M (N) NaOH for absorbance (optical density, OD) readings at 405 nm. For reactions using avidin peroxidase, 100 µL/well 1-Step™ Ultra TMB-ELISA (TMB substrate) solution (34028, Thermo Scientific, UK) was incubated in the dark at room temperature for up to 30 minutes and stopped by the addition of 100 µL/well 2 M H_2SO_4 for OD readings at 450 nm.

6.3.4.2 *ES Ag-ELISA for procedure optimisation*

Immulon 4HBX plates were coated overnight with *Fasciola hepatica* ES diluted within the range of 0.05–2 µg·mL^{-1} in coating buffer. After blocking, wells were incubated with experimental infection sera pooled from four uninfected or *F. hepatica*-infected (12 weeks post-infection, wpi) sheep and diluted within the range of 1:250-1:1,000. Antibodies were detected using appropriate secondary antibodies as described (6.3.4.1).

6.3.4.3 *Ag-ELISA for biomarker antigenicity testing: rFhΔpCL1, rFhΔCRT, rFhGEL, rFhTPI*

Recombinant antigens, including rFhΔpCL1, rFhΔCRT, rFhGEL and rFhTPI, were directly coated within the range of 15.625 ng·mL^{-1}–1 µg·mL^{-1}. Control sera pooled from four uninfected or *Fasciola hepatica*-infected (12 weeks post-infection, wpi) sheep were diluted in the first instance to 1:750 to test Ag immunogenicity by the host of an established infection. Experimental sera used for testing were pooled from three pairs of sheep infected with *F. hepatica* of known TCBZ susceptibility (Aberystwyth; Italy; Miskin) or resistance (Kilmarnock; Penrith; Stornoway) (Ridgeway Research Ltd.), between 0-17 wpi (including TCBZ treatment at 12 wpi). Pooled sera were diluted within the range of 1:100–1:750 and incubated for 1–1.5 hours at 37°C as stated per assay.

6.3.4.4 *Sandwich ELISA for antigen capture: anti-rFhΔpCL1 (IgG)*

6.3.4.4.1 Anti-rFhΔpCL1 IgG sandwich ELISA protocol optimisation

In order to calculate the optimal concentrations of sandwich ELISA components, including antigen (rFhΔpCL1), and coating (anti-rFhΔpCL1 IgG) and detection (anti-rFhΔpCL1 IgG-Biotin) antibodies, two preliminary ELISAs were conducted. Initially, the coating antibody and antigen dilutions were tested, with the coating antibody at 5, 10 and 20 µg·mL^{-1}, rFhΔpCL1 Ag within the range of 31.25 ng·mL^{-1}–2 µg·mL^{-1}, 1:10,000 detection antibody, 1:500 avidin-peroxidase and TMB substrate incubation for 7 minutes. A second ELISA was conducted to refine antibody dilutions further, testing by serial dilutions the coating antibody within the range of 78.125 ng·mL^{-1}–5 µg·mL^{-1} and the detection antibody within the range of 1:320,000–1:10,000 with 10 ng·mL^{-1} rFhΔpCL1, 1:10,000 avidin-peroxidase and TMB substrate incubation for 30 minutes before stopping and absorbance measurements.

6.3.4.4.2 Faecal antigen capture

The above method for the anti-rFhΔpCL1 IgG sandwich ELISA was further optimised for faecal antigen capture as follows. Firstly, plates were coated with 100 µL/well of polyclonal anti-rFhΔpCL1 IgG or polyclonal IgG from a non-immunised rabbit diluted to 5 µg·mL^{-1}. Following blocking and wash steps, 100 µL/well of faecal sample pooled from six uninfected sheep (prepared as previously described: 6.3.1.2) and containing rFhΔpCL1 diluted within the range of 31.25 ng·mL^{-1}–1 µg·mL^{-1} were added in duplicate. Six dilutions of biotinylated anti-rFhΔpCL1 IgG (1:4,000, 1:8,000, 1:12,000, 1:15,000, 1:20,000, 1:25,000) were used to determine the optimal detection antibody conditions, followed by 1:10,000 avidin-peroxidase incubation for 30 minutes and TMB substrate incubation for 4.5 minutes before stopping and absorbance measurements. OD measurements were calculated by subtracting OD values of wells coated with non-immunised rabbit IgG from OD values of wells coated with anti-rFhΔpCL1 rabbit IgG.

Based on the optimisation for faecal antigen capture, 1:25,000 was the dilution used for the biotinylated anti-rFhΔpCL1 rabbit IgG detection antibody for experimentally infected sheep faecal samples, and with TMB substrate incubation for 5 minutes before stopping and absorbance measurements.

6.3.4.5 *CL-derived peptide ELISA*

6.3.4.5.1 Peptide antigenicity testing: anti-rFhΔpCL1 IgG sandwich ELISA

The antigenicity of three synthetic peptides derived from the signal, inhibitor and mature regions of FhCL (Chapter 3: 3.4.3) was tested using the aforementioned anti-rFhΔpCL1 IgG sandwich ELISA described (6.3.4.4.1). Peptides were diluted within the range of 312.5 ng·mL^{-1}–10 µg·mL^{-1} following 100 µL/well coating with 5 ug·mL^{-1} anti-rFhΔpCL1 IgG and detection using 1:20,000 anti-rFhΔpCL1 IgG-Biotin, 1:10,000-diluted avidin-peroxidase and TMB substrate incubation for 25 minutes before stopping and absorbance measurements.

6.3.4.5.2 Peptide antigenicity testing: anti-rFhΔpCL1 IgG-Biotin direct ELISA

A direct ELISA approach for testing peptide-anti-rFhΔpCL1 IgG binding was also conducted as follows. Plates were coated with peptides diluted within the range of 625 ng·mL^{-1}–40 µg·mL^{-1} and, following blocking and washing steps, were directly detected with biotinylated anti-rFhΔpCL1 IgG diluted to 1:5,000, 1:10,000-diluted avidin-peroxidase and TMB substrate incubation for 25 minutes before stopping and absorbance measurements.

6.3.4.5.3 Peptide immunogenicity testing: experimental infection sera

The direct peptide ELISA was adapted for use with *Fasciola hepatica*-infected sheep serum as follows. Initially, peptide coating concentrations were tested within the range of 390.625 ng·mL^{-1}–100 µg·mL^{-1} and detected with 1:200-diluted serum from uninfected sheep or sheep infected with *F. hepatica* after 12 wpi. Based on this pilot assay setup, peptides were subsequently coated at 100 µg·mL^{-1} and detected with *F. hepatica*-infected (TCBZ-S or TCBZ-R strain-specific) 1:100-diluted sheep serum taken at 0, 2, 4, 8, 12 and 17 wpi.

6.3.4.6 *Statistical analyses*

For the evaluation of assays with uninfected and infected animal samples, cut-off values were calculated as previously described (Martínez-Sernández *et al.*, 2016) as 1 standard deviation above the mean sample OD value of the negative control (irrelevant antigen/uninfected sample), which were calculated per assay.

6.3.5 SDS PAGE and western hybridisation

0.25–2.0 µg recombinant Ag was prepared for SDS PAGE and western blotting as previously described (General materials and methods: 2.4.1–2.4.2), whereby proteins were probed with serum from experimental infections (6.3.4.3) diluted to 1:1000 and detected with AP-conjugated anti-sheep IgG. Anti-HIS antibody raised in rabbit was used at 1:300–1:1000 as the positive control and detected using AP-conjugated anti-rabbit IgG.

6.3.6 Dot blot

Nitrocellulose membrane (NCM) was washed with distilled water (UV-sterilised; 18.2 MΩ) and equilibrated in Bjerrum buffer, dried then allowed to acclimatise to room temperature. 2–5 µL samples were applied and allowed to absorb onto the membrane. NCM blots with samples applied were allowed to dry at room temperature and thereon treated as in the western blotting procedure (General materials and methods: 2.4.2), including confirmation of antigen binding using Amido Black staining (0.1% (w/v) amido black; 10% (v/v) acetic acid; 25% (v/v) isopropanol).

6.4 Results

6.4.1 Ag-ELISA optimisation

The conditions for optimal serum dilutions for the Ag-ELISA were calculated based on the optimisation assay described above (6.3.4.2) and briefly summarised as follows. Two duplicates were conducted on different occasions, whereby positive (*Fasciola hepatica*-infected sheep) and negative (uninfected sheep) serum IgG levels were detected against *F. hepatica* ES products (0.05–2 $\mu g \cdot mL^{-1}$) and irrelevant Ag (0.05% BSA). All positive sera had average OD scores above the cut-off for this assay (1SD above the 1:250-diluted negative serum), and 1.0 $\mu g \cdot mL^{-1}$ Ag led to the greatest difference in OD above the cut-off and negative sera OD scores (including SDs) (for OD analysis see Supplementary materials: Figure S9). All sera positively correlated with increasing positive control Ag concentration, though quadruplicate data for the positive sera diluted to 1:750 were less variable than the 1:1000 dilution at 1.0 $\mu g \cdot mL^{-1}$ (SD of OD_{av} = 0.03456).

6.4.2 Antigenicity testing of rFhΔpCL1, rFhΔCRT, rFhGEL and rFhTPI

6.4.2.1 *Ag-ELISA optimisation*

For preliminarily assessments of antigen immunogenicity during *Fasciola hepatica* infections, rFhΔpCL1, rFhΔCRT, rFhGEL and rFhTPI recombinant antigens were coated onto 4HBX plates within the range of 15.625 $ng \cdot mL^{-1}$–1 $\mu g \cdot mL^{-1}$ and probed with known negative and positive sera diluted to 1:750 (Figure 6.4.2.1). rFhΔpCL1 demonstrated positive OD scores above 0.25 $\mu g \cdot mL^{-1}$, whereas the other Ags tested demonstrated no OD scores exceeding the cut-off (C-O) for this assay (Figure 6.4.2.1, C-O: 0.123864).

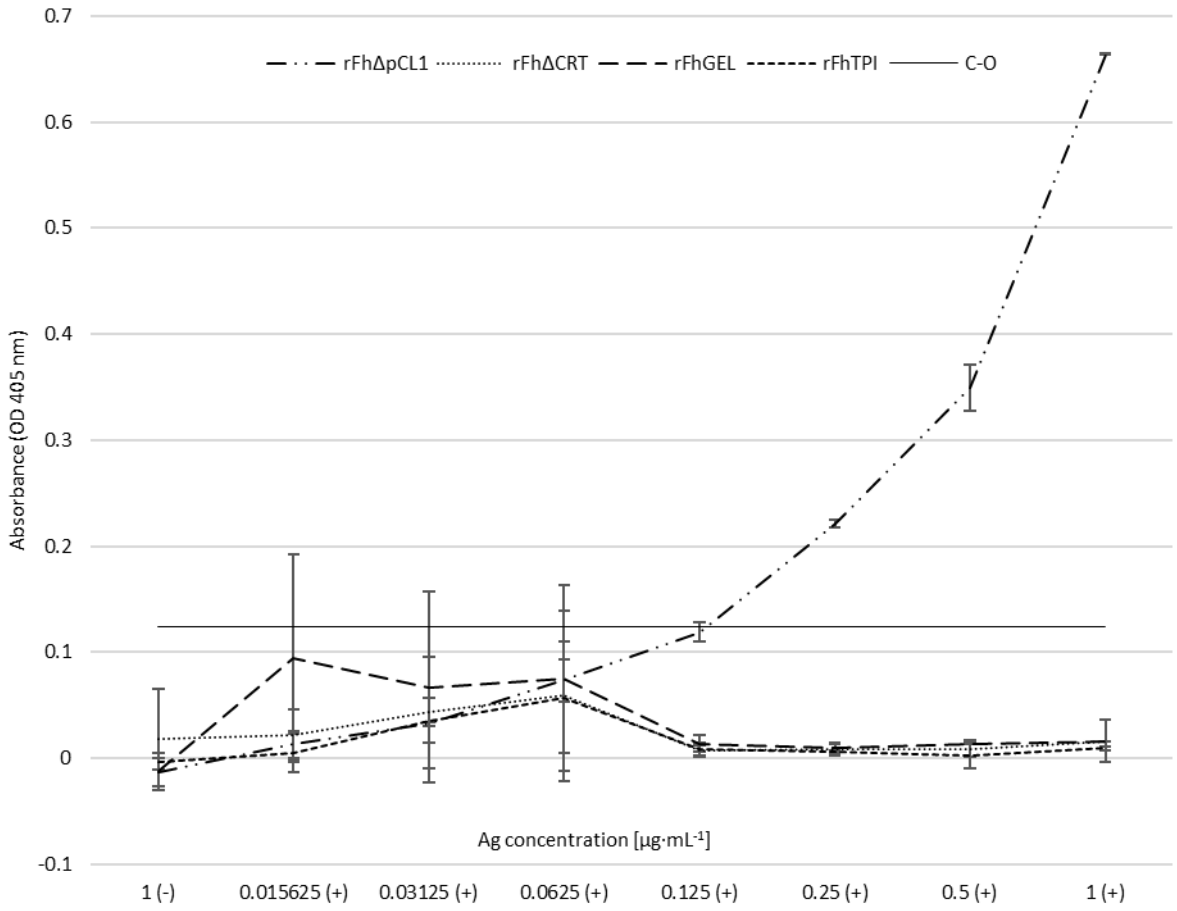

Figure 6.4.2.1. Ag-ELISA for *Fasciola hepatica* infection serum testing against four recombinant *F. hepatica* antigens. Average duplicate OD measures (adjusted by the subtraction of negative BSA control Ag OD) are presented for recombinant Ags, rFhΔpcCL1, rFhΔCRT, rFhGEL and rFhTPI, diluted within the range of 15.625 ng·mL^{-1}–1 µg·mL^{-1}. Ags were probed with positive (+, TCBZ-S *F. hepatica*-infected at 12 wpi) or negative (-, uninfected) sheep serum diluted to 1:750 and detected with anti-sheep IgG secondary antibody and AP detection. Positive OD values were considered when exceeding the cut-off (C-O), shown as one standard deviation above the negative Ag (BSA) OD score (solid line: 0.123864).

6.4.2.2 *Ag-ELISA for the investigation of serum responses to TCBZ-S and TCBZ-R F. hepatica*

ELISAs with experimental sera were subsequently conducted to determine and compare Ag immunogenicity and exposure *in vivo* during *Fasciola hepatica* infection with three TCBZ-S or TCBZ-R *F. hepatica* strains, including before (0–12 wpi) and after (13–17 wpi) clinical TCBZ exposure.

rFhΔpCL1 was coated at 0.5 µg·mL^{-1} and probed with experimental TCBZ-S and TCBZ-R sera diluted to 1:750 (Figure 6.4.2.2.1), demonstrating positive OD scores after 4 and 5 wpi with TCBZ-R and TCBZ-S strains, respectively. Thereon TCBZ-R-specific IgG demonstrated

increasing immunoreactivity to rFhΔpCL1, whereas TCBZ-S-specific IgG OD scores plateaued at 8 wpi, and falling steadily thereon (Figure 6.4.2.2.1).

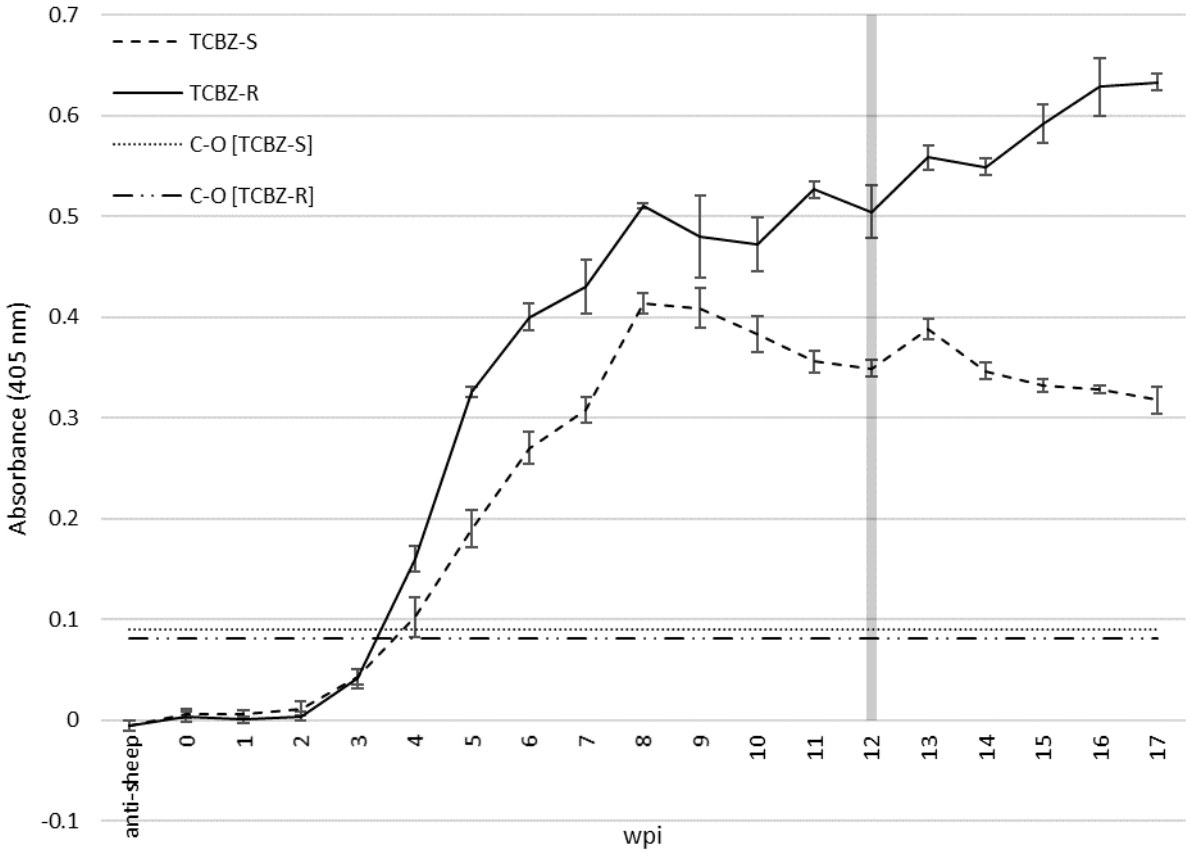

Figure 6.4.2.2.1. rFhΔpCL1 Ag-ELISA for the comparison of serum immunogenicity during infection with TCBZ-S or TCBZ-R *Fasciola hepatica* strains. Average duplicate OD measures from two ELISA plates (adjusted by the subtraction of negative BSA control Ag OD) are presented for rFhΔpCL1 [0.5 μg·mL^{-1}] after detection with representative (n = 3 sheep/parasite strain) serum diluted to 1:750 from 0-17 weeks post infection (wpi) with TCBZ-S (dashed line) or TCBZ-R (solid line), and following clinical administration of TCBZ at 12 wpi. Positive OD values were considered when exceeding the cut-off (C-O), shown as one standard deviation above the negative Ag (BSA) OD score for each sera (dot line, TCBZ-S: 0.0901; dot-dash line, TCBZ-R: 0.0815). Error bars are one standard deviation more and less than average ODs and the shaded line indicates the recommended timepoint at 12 wpi for TCBZ administration in infected animals.

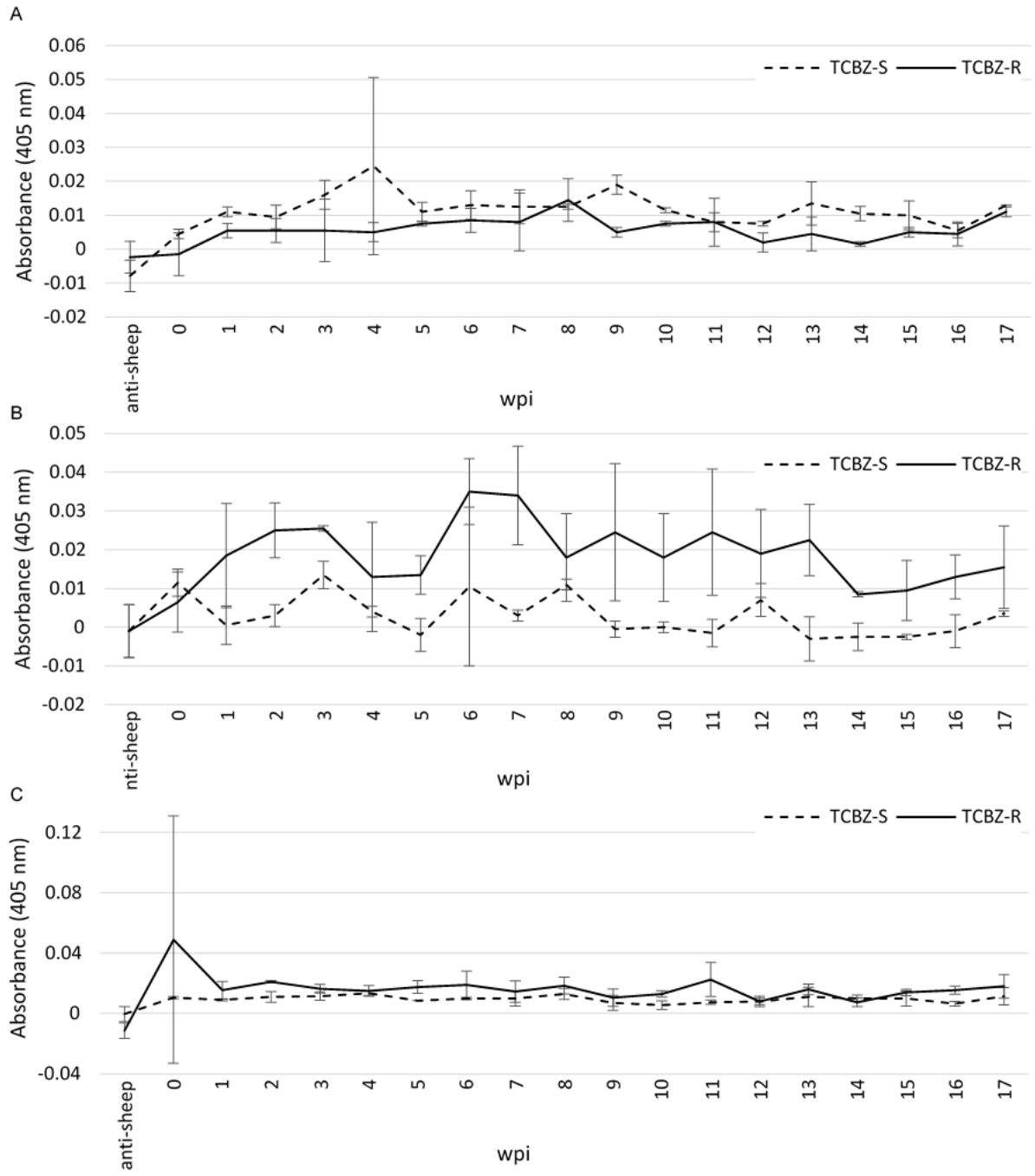

Figure 6.4.2.2.2. Pilot Ag-ELISA for comparative immunogenicity by *Fasciola hepatica*-infected sera. Average duplicate OD measures (adjusted by the subtraction of negative BSA control Ag OD) are presented for (A) rFhΔCRT [0.5 μg·mL^{-1}] (B) rFhGEL [1.0 μg·mL^{-1}] and (C) rFhTPI [0.5 μg·mL^{-1}] after detection with representative (n = 3 sheep/parasite strain) serum from 0-17 weeks post infection (wpi) with TCBZ-S (dashed line) or TCBZ-R (solid line) strains, and following clinical administration of TCBZ at 12 wpi. Sera were diluted to 1:750 and incubated for 1 hour (A) or 1:500 for 1.5 hours (B-C), respectively. Positive OD values were considered when exceeding the cut-off of one standard deviation above the negative Ag (BSA) OD score for each sera (not shown: (A) 0.07941 (TCBZ-S), 0.078828 (TCBZ-R); (B) 0.094414 (TCBZ-S), 0.081414 (TCBZ-R); (C) 0.081621 (TCBZ-S), 0.073621 (TCBZ-R)). Error bars are one standard deviation more and less than average ODs.

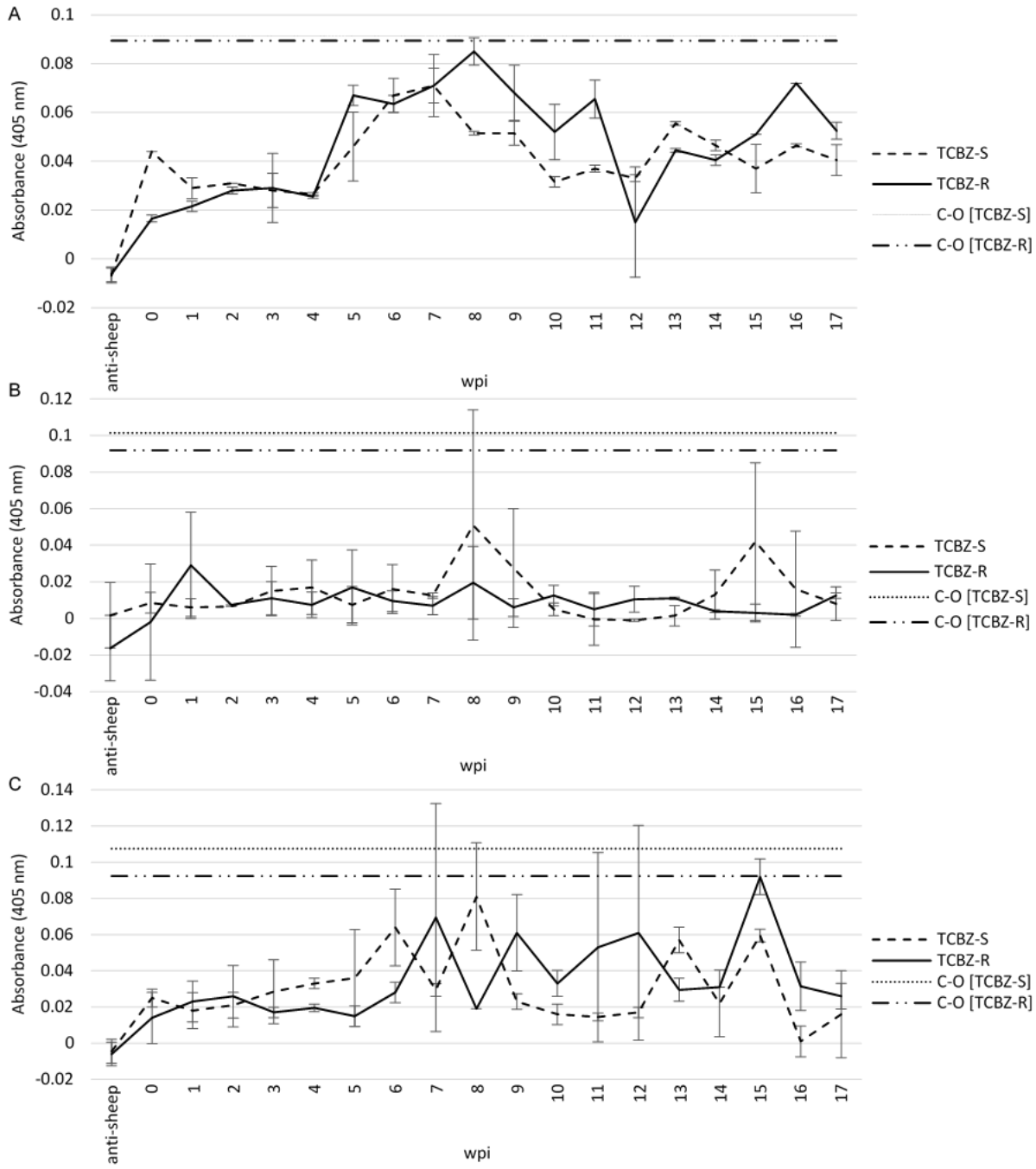

Figure 6.4.2.2.3. Second round of Ag-ELISAs with three recombinant candidates for the comparison of serum immunogenicity during infection with TCBZ-S or TCBZ-R *Fasciola hepatica* strains. Average duplicate OD measures (adjusted by the subtraction of negative BSA control Ag OD) are presented for (A) rFhΔCRT [1.0 µg·mL^{-1}] (B) rFhGEL [2.0 µg·mL^{-1}] and (C) rFhTPI [1.0 µg·mL^{-1}] after detection with representative (n = 3 sheep/parasite strain) serum from 0-17 weeks post infection (wpi) with TCBZ-S (dashed line) or TCBZ-R (solid line) strains, and following clinical administration of TCBZ at 12 wpi. Sera were diluted to 1:250 and incubated for 1.5 hours (A) or 1:200 for 1 hour (B-C), respectively. Positive OD values were considered when exceeding the cut-off (C-O), shown as one standard deviation above the negative Ag (BSA) OD score (dot line (TCBZ-S): (A) 0.091414, (B) 0.101450, (C) 0.107485; dot-dash line (TCBZ-R): (A) 0.089414, (B) 0.091864, (C) 0.092414). Error bars are one standard deviation more and less than average ODs.

Since the preliminary ELISA did not indicate positive OD scores for rFhΔCRT, rFhGEL and rFhTPI, several assay conditions were tested for use with TCBZ-S- and TCBZ-R-specific *F. hepatica* infection sera. Firstly, rFhΔCRT [0.5 ng·mL^{-1}], rFhGEL [1.0 ng·mL^{-1}] and rFhTPI [0.5 ng·mL^{-1}] were coated and probed with serum diluted to 1:750 (rFhΔCRT) for 1 hour or 1:500 (rFhGEL; rFhTPI) for 1.5 hours (Figure 6.4.2.2.2). Since no OD scores exceeded the positive C-O per assay (rFhΔCRT: 0.07941; rFhGEL: 0.094414; rFhTPI: 0.081621), antigen coating concentrations were increased, and serum dilutions were decreased as follows. rFhΔCRT [1.0 ng·mL^{-1}], rFhGEL [2.0 ng·mL^{-1}] and rFhTPI [1.0 ng·mL^{-1}] were coated and probed with serum diluted to 1:250 (rFhΔCRT) for 1.5 hours or 1:200 (rFhGEL; rFhTPI) for 1 hour (Figure 6.4.2.2.3). Assay adjustments led to an increase in overall OD scores for rFhΔCRT and FhTPI, particularly for anti-rFhΔCRT-specific IgG after 5 wpi (Figure 6.4.2.2.3). However, data indicated no positive OD scores above the cut-off for each antigen (rFhΔCRT, 0.091414; rFhGEL, 0.10145; rFhTPI, 0.107485) despite assay modifications.

6.4.2.3 *Western hybridisation trials*

Western hybridisations were utilised as an alternative format to the ELISAs to determine serum immunogenicity to three of the aforementioned candidate antigens by increasing protein availability for antibody binding. Following confirmation of optimal antigen transfers to NCM (Figure 6.4.2.3.1), rFhΔCRT (0.5 µg/lane), rFhGEL (2.0 µg/lane) and rFhTPI (0.25 µg/lane) were probed with experimental TCBZ-S and TCBZ-R sera diluted to 1:1500 (Figure 6.4.2.3.2; for duplicate western hybridisation images see Supplementary materials Figure S10). Blots indicated different immunoreactivity between candidates with the sera tested as follows. TCBZ-R-specific sera demonstrated rFhΔCRT recognition after 6 wpi that appeared to be maintained until 10 wpi (Figure 6.4.2.3.2Aii), conversely to TCBZ-S-specific sera which indicated no antibody-rFhΔCRT binding (Figure 6.4.2.3.2Ai). TCBZ-S-specific sera indicated non-specific immunoreactivity with rFhGEL due to positivity between 0–3 wpi, with more intensity at the dimer-specific bands, and a faintly positive monomer band at 8 wpi (Figure 6.4.2.3.2Bi). Conversely to these findings, TCBZ-R-specific sera indicated immunoreactivity with rFhGEL from 6 wpi, which was maintained until 15 wpi (Figure 6.4.2.3.2Bii). rFhTPI indicated limited immunoreactivity with both sets of sera, with faint positive bands after TCBZ-S-specific sera between 7–8 wpi, and after TCBZ-R-specific sera

from 6 wpi, with positivity which was similarly faint and maintained until approximately 15 wpi. These data together suggest the varied natural abundance and exposure of these Ag candidates during infections, which is further influenced by TCBZ susceptibility status of the infecting *Fasciola hepatica*.

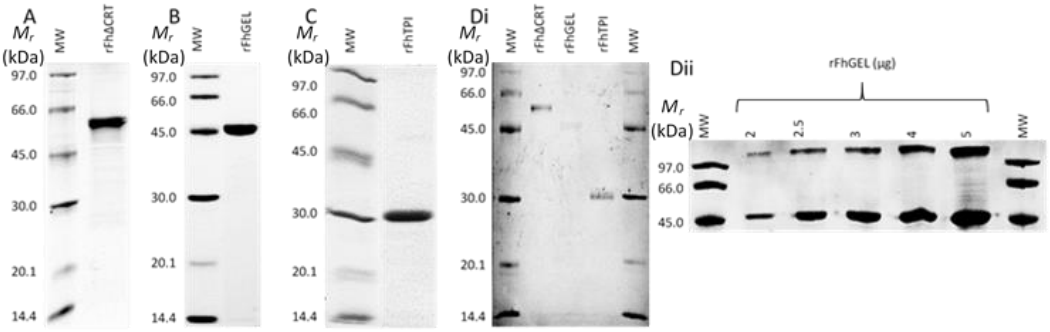

Figure 6.4.2.3.1. SDS PAGE separation of purified recombinant *Fasciola hepatica* diagnostic candidates and confirmation of their transfer to nitrocellulose membrane. (A) 2 µg rFhΔCRT (BN1106_s2673B000071.1) (B) 2 µg rFhGEL (D915_01476) (C) and 1 µg rFhTPI (AGJ83762.1) separated by 12.5% SDS PAGE and Coomassie-stained. (Di) 0.5 µg (rFhΔCRT), 0.5 µg (rFhGEL) and 0.25 µg (rFhTPI) were transferred to nitrocellulose membrane (0.45 µm pores) and stained with Amido Black, but a further range (2-5 µg) of total purified rFhGEL protein were used to determine the optimum concentration for western blotting, due to the formation of a dimer and consequential reduction of monomer protein abundance.

Abbreviations: MW, Amersham Low Molecular Weight SDS Calibration Kit (M_r).

To quantitatively assess the positivity for each band at each time-point (wpi), band intensity data were calculated using ImageQuant TL (GE Life Sciences, UK), which were summarised from duplicate western hybridisations (Table 6.4.2.3). Positivity was first apparent from 1 wpi for rFhΔCRT and rFhGEL^2 against TCBZ-S- and TCBZ-R-infected sera, respectively. Interestingly, all Ag were positive by TCBZ-S and negative by TCBZ-R sera at 12 wpi. rFhGEL demonstrated long-lasting immunoreactivity beginning after 2 wpi in the TCBZ-S sera compared to TCBZ-R serum positivity at only 3 wpi, and compared to rFhGEL^2 that demonstrated partial consensus with rFhGEL positivity in TCBZ-S sera with further positive scores at 1, 5, 10, 11, and 16 wpi. rFhTPI demonstrated the least immunogenicity in TCBZ-S sera at only 11-12 wpi, whereas rFhΔCRT and rFhTPI were only positive for six (3, 6, 7, 14, 15, 17 wpi) and seven (7, 9, 10, 13, 15, 16, 17 wpi) weeks in total in TCBZ-R sera, respectively.

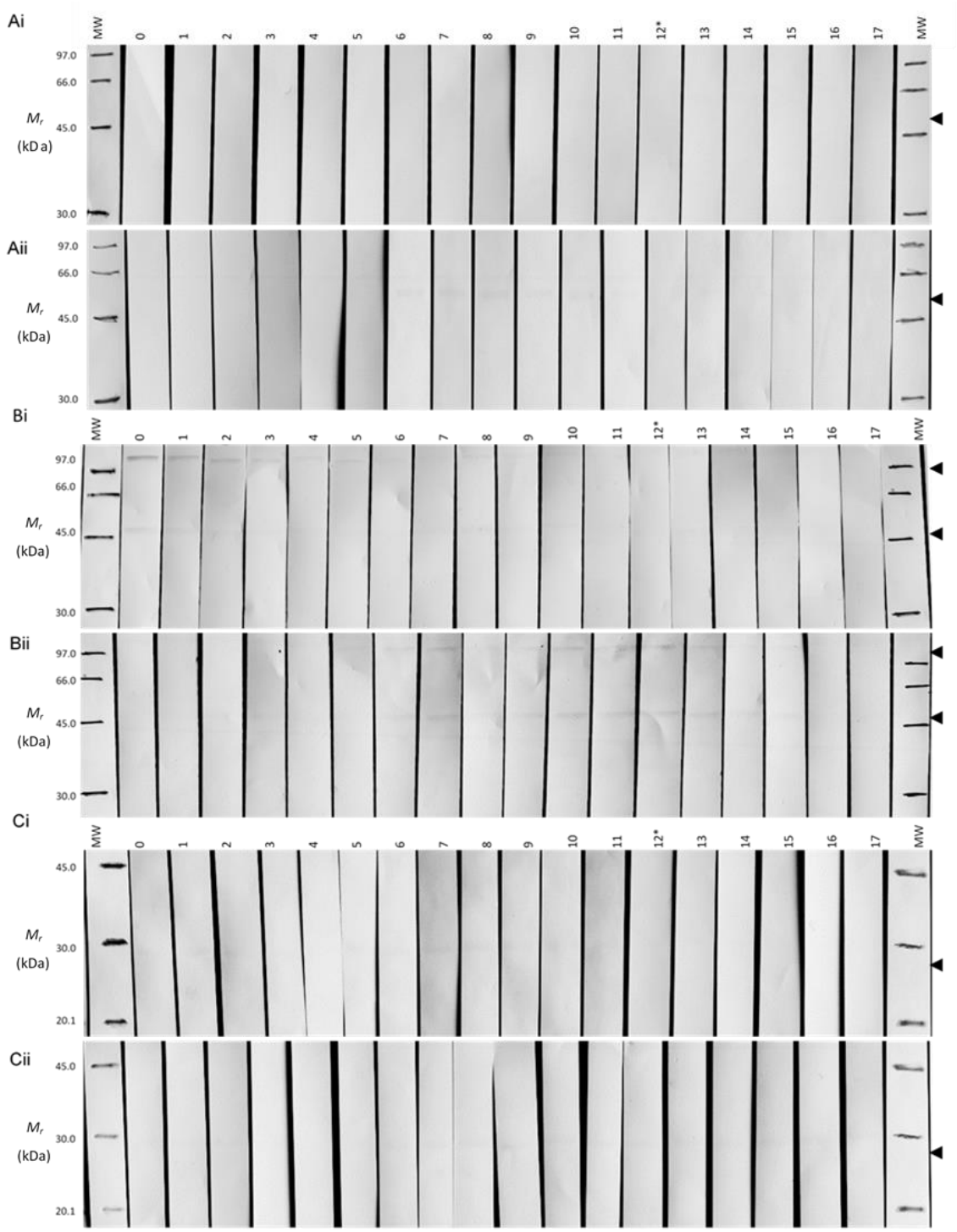

Figure 6.4.2.3.2. Western hybridisation analysis of IgG immunoreactivity against recombinant candidates using experimentally infected sheep with *Fasciola hepatica* drug-susceptible and -resistant isolates. rFhΔCRT (0.25 µg/lane) (A), rFhGEL (2.0 µg/lane) (B) and rFhTPI (0.25 µg/lane) (C) were probed with whole sheep sera diluted to 1:1,500 and pooled from three animals experimentally infected with TCBZ-susceptible (i) or TCBZ-resistant (ii) *F. hepatica* isolates. Lane numbers refer to week post-infection (0–17), with clinical TCBZ dose administration at week 12(*). Images of duplicates of the above western hybridisations are shown in the supplementary materials.

Abbreviations: MW, Amersham Low Molecular Weight SDS Calibration Kit (M_r).

Table 6.4.2.3. Quantitative representation of duplicate western Hybridisations for antigen immunogenicity testing. Data from duplicate western hybridisations were analysed and band areas of interest were interpreted and quantified using ImageQuant TL (GE Life Sciences, UK). Band intensities and serum positivity for each wpi were calculated by subtracting 0 wpi values from each wpi value for each treatment replicate. Data were collated and outcomes were defined, whereby values which were positive in both replicates were considered positive, +; and values which were negative or negative and positive in both replicates were considered negative, -. The asterisk (*) indicates data from one replicate western hybridisation only.

Ag vs. TCBZ-S/TCBZ-R *F. hepatica* (n = 3 parasite strains, n = 3 sheep)			wpi / positivity (-/+)																	
	Biomarker	**Approximate molecular weight (kDa)**	**0**	**1**	**2**	**3**	**4**	**5**	**6**	**7**	**8**	**9**	**10**	**11**	**12**	**13**	**14**	**15**	**16**	**17**
TCBZ-S	**rFhΔCRT**	54.9	-	+	-	-	-	-	-	-	-	+	-	-	+	-	-	+	-	-
	rFhGEL	110.4	-	-	-	-	+	-	-	+	+	-	+	+	+	+	+	+	-	+*
		47.0	-	-	+	-	+	+	+	+	+	+	+	+	+	+	+	+	-	+*
	rFhTPI	29.7	-	-	-	-	-	-	-	-	-	-	-	+	+	-	-	-	-	-
	Biomarker	**Approximate molecular weight (kDa)**	**0**	**1**	**2**	**3**	**4**	**5**	**6**	**7**	**8**	**9**	**10**	**11**	**12**	**13**	**14**	**15**	**16**	**17**
TCBZ-R	**rFhΔCRT**	54.9	-	-	-	+	-	-	-	+	+	-	-	-	-	-	+	+	-	+
	rFhGEL	110.4	-	+	-	+	-	+	-	-	-	-	+	+	-	-	-	-	+	-*
		47.0	-	-	-	+	-	-	-	-	-	-	-	-	-	-	-	-	-	-*
	rFhTPI	29.7	-	-	-	-	-	-	-	+	-	+	+	-	-	+	-	+	+	+

Together, data from western hybridisations indicate the possibility of *in vivo* native FhCRT, FhGEL and FhTPI exposure, with FhCRT and FhGEL immunogenicity indicated from as early as 1-2 wpi until 17 wpi in TCBZ-S *F. hepatica* infections. However, FhCRT and FhTPI exposure appeared limited in both TCBZ-S- and TCBZ-R-specific infections due to the transient natures of positive immunoreactivity for these Ags.

6.4.3 Sandwich ELISA for antigen capture using anti-rFhΔpCL1 (IgG)

6.4.3.1 *Anti-rFhΔpCL1 IgG purification*

In order to prepare polyclonal sera for sandwich and direct ELISA assays, immunologically relevant antibodies (IgG) were purified from pre- and post-immunisation (rFhΔpCL1) rabbit sera using protein A affinity chromatography (PAAC). Whole polyclonal sera (Figure 6.4.3.1: lane 1), PAAC flow-through (Figure 6.4.3.1: lane 2), PAAC elutions before and after additional filtration purification (Figure 6.4.3.1A: lanes 3–4) or PAAC elution fractions

one and two (Figure 6.4.3.1B: lanes 3–4) were analysed by SDS PAGE (i) and western hybridisation (ii). IgG purification was demonstrable in elution fractions, and IgG identification was inferred from the immunoreactivity against goat anti-rabbit IgG (raised against whole molecule) and the established approximate molecular weight of rabbit IgG at 50 kDa and 25 kDa for crystallisable and antigen-binding fragments, respectively.

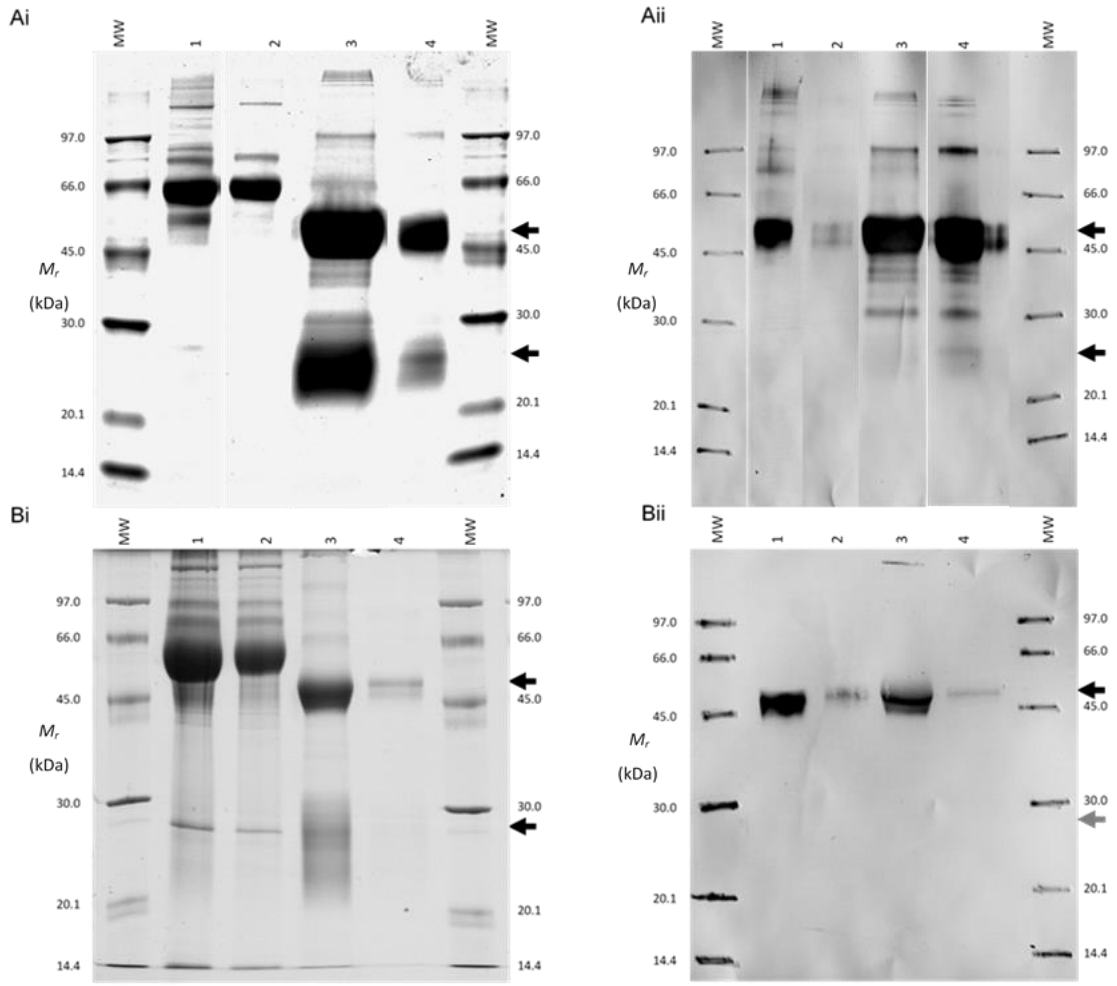

Figure 6.4.3.1. Confirmation of IgG purification from anti-rFhΔpCL1 polyclonal sera. IgG was purified from whole rabbit polyclonal sera following immunisation with rFhΔpCL1 (terminal bleed, A) and pre-immunisation (pre-bleed, B) using Protein A-coated beads (ABT, Web Scientific). (Ai, Bi) SDS PAGE separation and (Aii, Bii) anti-rabbit IgG western hybridisation identified the purification of approximately 25 and 50 kDa bands from whole sera (1 µg, 1), which was lower in abundance in the protein A flow-through (1 µg, 2) and increased in abundance in the elution fractions (A = 2.5 µg, 3-4; B = 1 µg, 3-4). Western hybridisation used 1:30,000-diluted AP-conjugated goat anti-rabbit IgG (raised against whole molecule), the developing time for membranes was shortened from 2.5 minutes for post-immunisation (A) to 1 minute for pre-immunisation (B) samples, reducing to the appearance of immunoreactivity of only monomer crystallisable fragments in the latter (grey arrow). Abbreviations: MW, Amersham Low Molecular Weight SDS Calibration Kit (M_r).

6.4.3.2 *Optimisation of anti-rFhΔpCL1 IgG sandwich ELISA*

The optimal range of Ag, coating IgG and detection IgG concentrations for the anti-rFhΔpCL1 IgG sandwich ELISA was determined as follows using two assays to vary each component. Initially, plates were coated with 5.0–20.0 µg·mL^{-1} polyclonal IgG followed by 31.25 ng·mL^{-1}–2.0 µg·mL^{-1} rFhΔpCL1 Ag and biotinylated anti-rFhΔpCL1 IgG detection antibody diluted to 1:10,000 (Figure 6.4.3.2.1). OD data were calculated by subtracting OD values of irrelevant Ag (BSA) from OD of rFhΔpCL1 samples, which indicated all IgG coating concentrations led to similar positive absorbances (OD >1.50) to the lowest Ag concentration tested. Only two OD values could be identified as outliers, where no antibody coat was applied at Ag concentrations of 62.5 and 125.0 ng·mL^{-1}, suggesting these were minor anomalies (Figure 6.4.3.2.1).

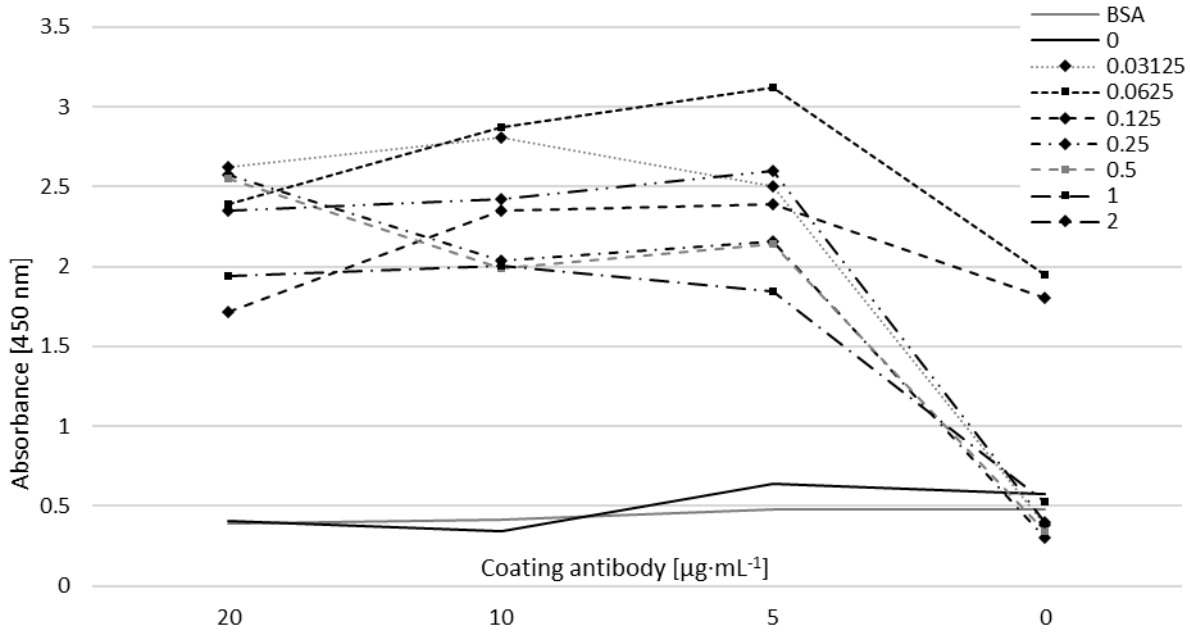

Figure 6.4.3.2.1. Optimisation part one of the anti-rFhΔpCL1 IgG sandwich ELISA. OD measures (450 nm) are shown for the reactivity of 1:10,000-diluted biotinylated anti-rFhΔpCL1 IgG against rFhΔpCL1 diluted within the range of 31.25 ng·mL^{-1}–2.0 µg·mL^{-1} after Ag capture by anti-rFhΔpCL1 IgG coating within the range of 5.0–20.0 µg·mL^{-1}.

Based on the outcome of the initial assay, a second sandwich ELISA was conducted by coating plates with polyclonal IgG 78.125 ng·mL^{-1}–5.0 µg·mL^{-1}, followed by 31.25 ng·mL^{-1} rFhΔpCL1 Ag and probing with biotinylated anti-rFhΔpCL1 IgG detection antibody diluted within the range of 1:10,000–1:320,000 (Figure 6.4.3.2.2). Data demonstrated unprecedented

sensitivity of the biotinylated anti-rFhΔpCL1 IgG against rFhΔpCL1 and anti-rFhΔpCL1 IgG (coating concentration: 5 µg·mL^{-1}) at all dilutions tested, including 1:320,000 (Figure 6.4.3.2.2). Following data collection from subsequent assays, the variation of absorbance observed in these data for the negative control (BSA) were assigned to the deterioration of an avidin-peroxidase working stock solution rather than detection, TMB or stop solutions.

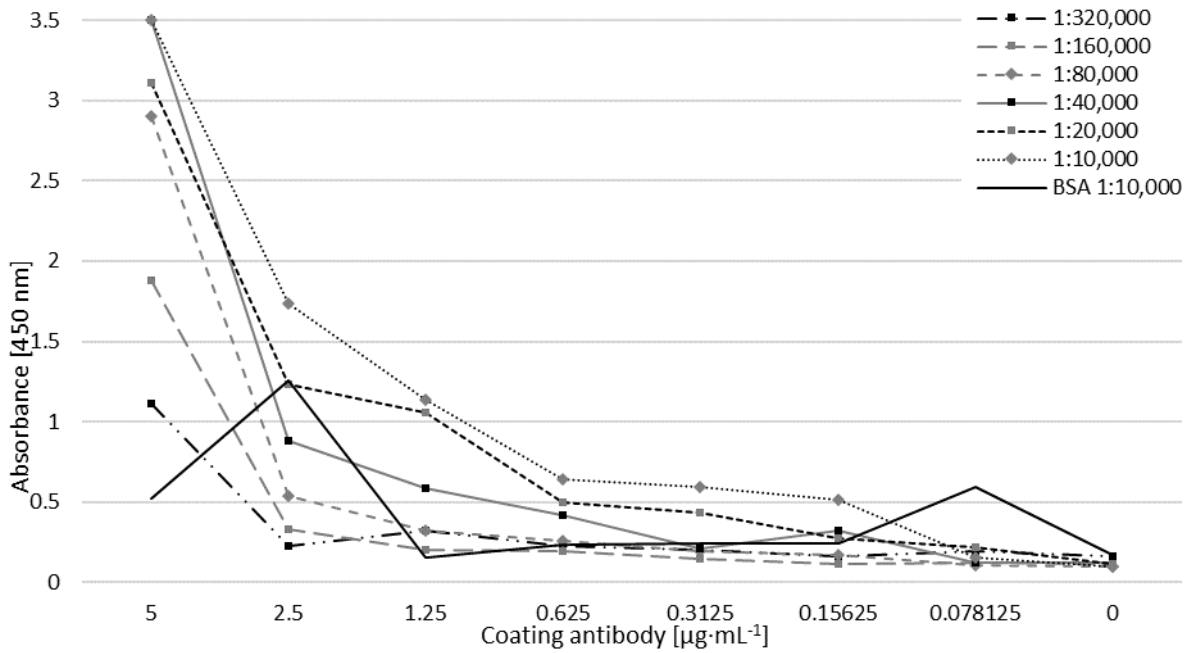

Figure 6.4.3.2.2. Optimisation part two of the anti-rFhΔpCL1 IgG sandwich ELISA. OD measures (450 nm) are shown for the immunoreactivity of biotinylated anti-rFhΔpCL1 IgG against 31.25 ng·mL^{-1} rFhΔpCL1 captured by anti-rFhΔpCL1 IgG diluted within the range of 78.125 ng·mL^{-1}–5.0 µg·mL^{-1}.

6.4.3.3 *Faecal antigen capture with anti-rFhΔpCL1 IgG sandwich ELISA*

6.4.3.3.1 Protocol optimisation

The anti-rFhΔpCL1 IgG sandwich ELISA was optimised for faecal antigen capture using duplicate negative faecal samples (pooled from six uninfected sheep) containing rFhΔpCL1 diluted within the range of 31.25 ng·mL^{-1}–1 µg·mL^{-1} and detected with anti-rFhΔpCL1 IgG diluted to 1:4,000, 1:8,000, 1:12,000, 1:15,000, 1:20,000 or 1:25,000 (Figure 6.4.3.3.1). All Ag and detection antibody dilutions led to similar positive OD scores, indicating the high sensitivity of the biotinylated anti-rFhΔpCL1 IgG to detect the target Ag in faeces.

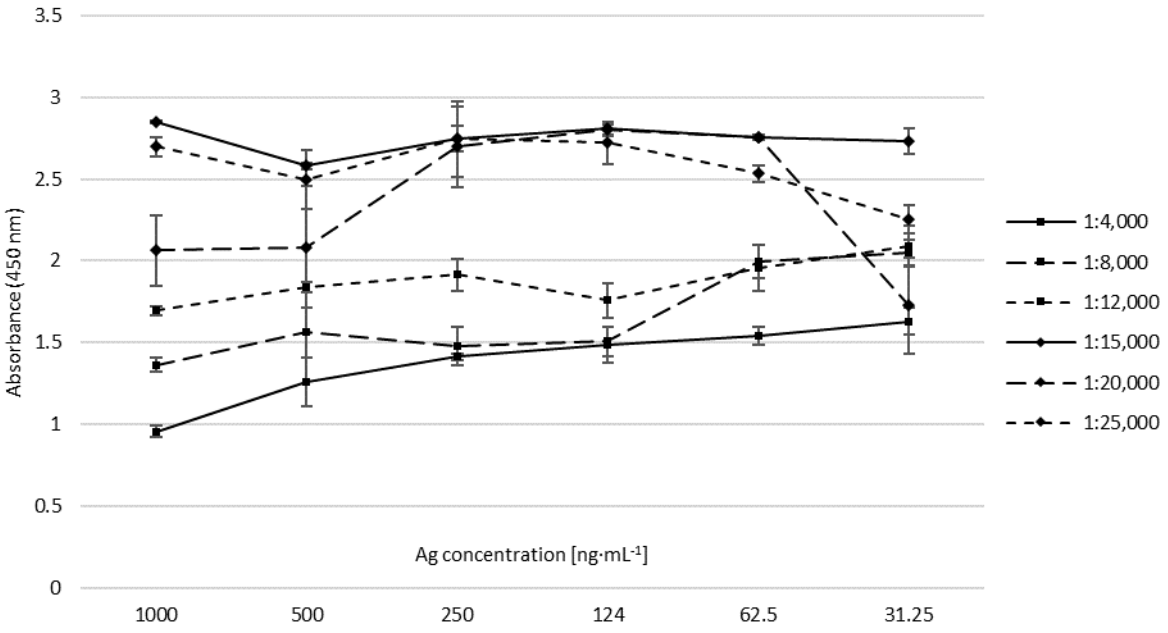

Figure 6.4.3.3.1. Optimisation of anti-rFhΔpCL1 IgG sandwich ELISA for faecal antigen capture. Average duplicate OD measures (adjusted by the subtraction of OD values of non-immunised rabbit IgG coat from positive rabbit anti-rFhΔpCL1 IgG coat) are shown following the dilution of rFhΔpCL1 Ag in uninfected sheep faeces within the range of 31.25 ng·mL^{-1}–1.0 µg·mL^{-1} and detection with biotinylated anti-rFhΔpCL1 IgG diluted to 1:4,000, 1:8,000 and 1:12,000 on one day, and 1:15,000, 1:20,000 and 1:25,000 on a different day. Error bars are one standard deviation more and less than average ODs.

6.4.3.3.2 Faecal antigen capture: experimental *Fasciola hepatica* infections

Based on the optimisation of the anti-rFhΔpCL1 IgG sandwich ELISA for faecal antigen capture, duplicate wells were incubated with faecal samples from *F. hepatica*-infected sheep were detected using biotinylated anti-rFhΔpCL1 IgG diluted to 1:25,000 (Figure 6.4.3.3.2). Samples were pooled between two sheep infected with isolated strains of known TCBZ susceptibility, including TCBZ-S (Aberystwyth, Italian) or TCBZ-R (Kilmarnock, Stornoway) strains, for each week between 0–17 wpi and including TCBZ administration at 12 wpi. OD measurements were averaged between two duplicate measurements conducted on two occasions, calculated by the subtraction of OD values of wells coated with non-immunised rabbit IgG from OD values of wells coated with anti-rFhΔpCL1 rabbit IgG and averaged between ELISA plates. Average ODs demonstrated positive values appearing from 4 wpi in the faeces of sheep infected TCBZ-S, climbing until 12 wpi until TCBZ administration induced a significant drop in OD leading to negative scores by 15 wpi, which was calculated as a 97.36% reduction in OD between 12 and 13 wpi. Conversely, TCBZ-R-infected samples were not

positive until 8 wpi, whereupon OD scores increased sharply until 11 wpi at which point they plateaued with a small increase between 15–16 wpi and decreased slightly at 17 wpi.

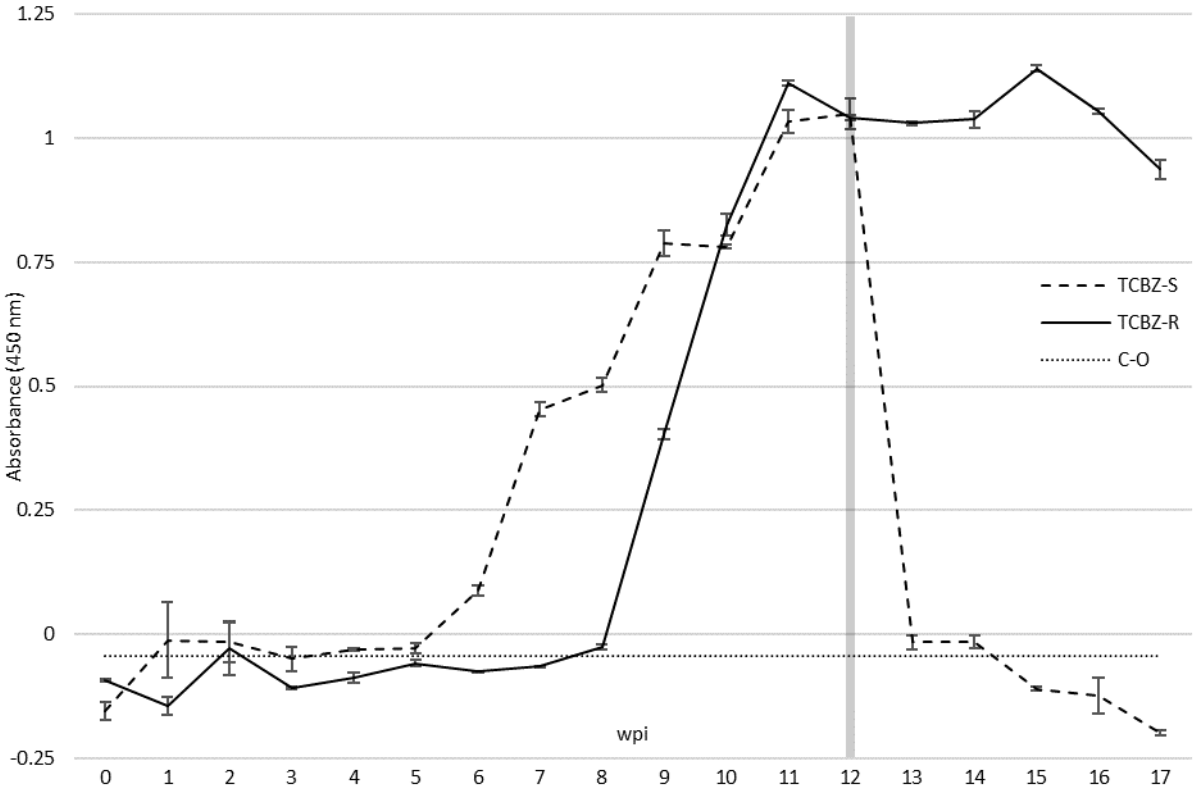

Figure 6.4.3.3.2. Validation of the anti-rFhΔpCL1 IgG sandwich ELISA for faecal antigen capture and identification of treatment success. Average duplicate OD measures from two ELISA plates (adjusted by the subtraction of OD values of non-immunised rabbit IgG coat from rabbit anti-rFhΔpCL1 IgG coat) are shown for sheep faecal samples pooled from two sheep infected with *Fasciola hepatica* of known TCBZ-susceptibility between 0-17 wpi, including TCBZ-S: Aberystwyth or Italian strains, or TCBZ-R: Kilmarnock or Stornoway strains. The calculated cut-off (C-O) for this assay was one SD above the highest average OD value measured for uninfected sheep samples (dot line: -0.04329). Error bars are one standard deviation more and less than average ODs and the shaded line indicates the recommended timepoint at 12 wpi for TCBZ administration in infected animals.

6.4.4 Anti-/rFhΔpCL1 (IgG): specificity testing against UK-endemic livestock rumen fluke and gastrointestinal nematodes

Potential cross-reactivity of serum from animals infected with non-*F. hepatica* helminth parasites were investigated using dot blots for rFhΔCRT, rFhGEL, rFhTPI, rFhΔpCL1 and three synthetic 15-mer peptides designed from FhpCL1 regions (signal peptide, inhibitor peptide, mature protease) (Figure 6.4.4). Serum samples were pooled from two sheep or

cattle infected with UK-endemic livestock helminths, including *Calicophoron daubneyi* (n = 2 sheep, 0 and 16 wpi), *Haemonchus contortus* (n = 2 sheep, 0 and 6 wpi), *Ostertagia circumcincta* (n = 2 sheep, 0 and 6 wpi) and *Cooperia oncophora* (n = 2 cattle, 0 and 3 wpi). Immunoreactivity was demonstrable against rFhGEL and rFhTPI in sheep, including at 0 wpi, though less intense than at 6 wpi. rFhTPI also indicated positive antibody recognition 0 wpi more intensely than at 16 (*C. daubneyi*) or 3 (*C. oncophora*) wpi in cattle, with rFhGEL also positive to a lesser extent at these post-infection dates. rFhΔCRT (positive dot confirmed but faded in image), rFhΔpCL1 and the synthetic peptides did not indicate positivity in the non-fluke infections. These preliminary findings indicate the possibility of cross-reactivity of FhGEL and FhTPI with other parasite and/or host-exposed antigen equivalents, which bears future investigation to ascertain the extent of potential overlapping recognition of these candidates. The utility of the other targets as diagnostic candidates is however supported by these results.

The specificity of anti-rFhΔpCL1 IgG was also tested against faecal samples of livestock hosts infected with either *C. daubneyi* (n = 2 cattle, 12 wpi), *H. contortus* (n = 2 sheep, 6 wpi) or *O. circumcincta* (n = 2 sheep, 6 wpi) using the anti-rFhΔpCL1 IgG sandwich ELISA. Average duplicate OD values were measured from two ELISA plates conducted on separate occasions. High background levels were consistent in all wells coated with irrelevant IgG (pre-immunisation), and so in order to ensure these were not influencing the outcomes, ODs were recalculated by subtracting the lowest OD available for sheep or cattle from test sample ODs from the wells coated with anti-rFhΔpCL1 IgG. Despite adjustments to OD calculations, data indicated no OD values exceeding the cut-off for negative sheep (OD = -0.04329) or cattle (OD = -0.03188) samples so were considered negative (data not shown), suggesting no appearance of cross-reactivity of anti-rFhΔpCL1 IgG with coproantigen secretions recovered from livestock infections with *C. daubneyi*, *H. contortus* or *O. circumcincta*.

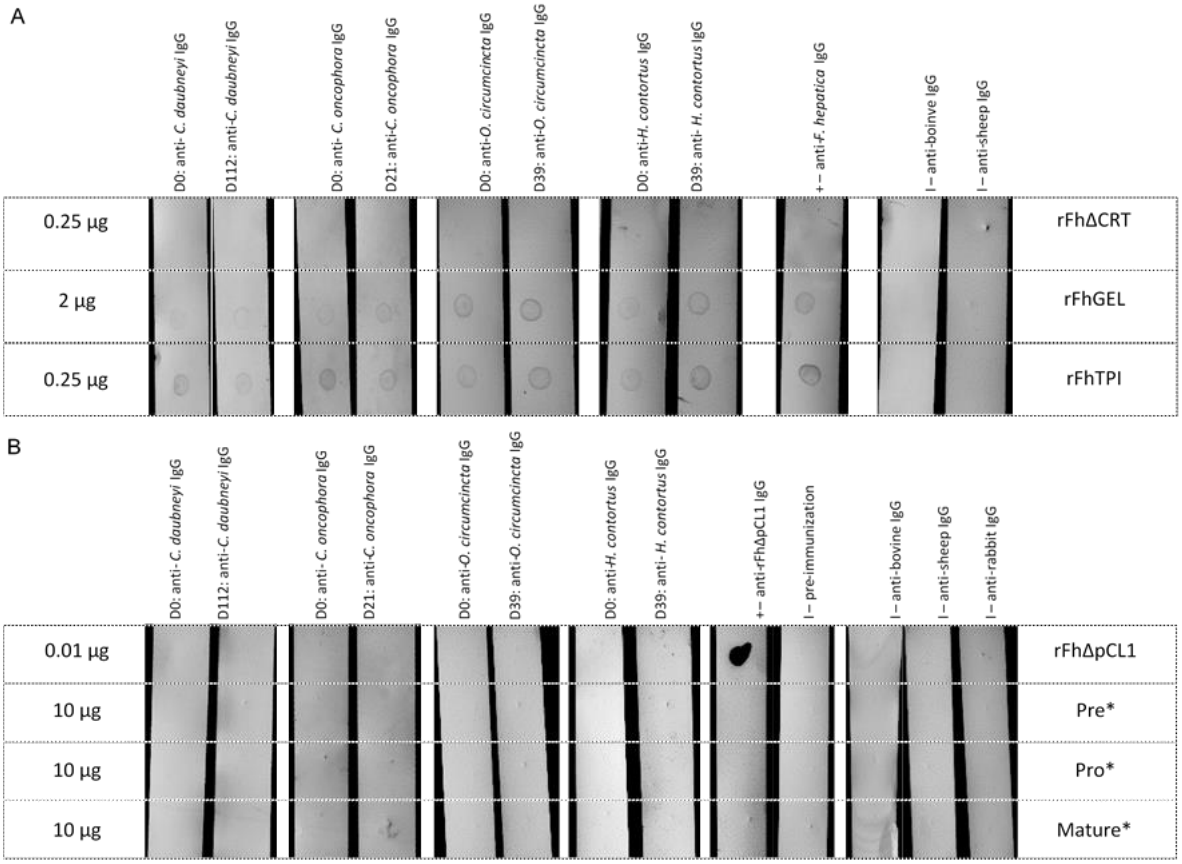

Figure 6.4.4. Dot blot analysis of IgG immunoreactivity of helminth-infected livestock serum against recombinant and synthetic *Fasciola hepatica* antigens. (A) rFhΔCRT (0.25 µg/dot), rFhGEL (2 µg/dot) and rFhTPI (0.25 µg/dot) were probed with whole serum diluted to 1:100. (B) rFhΔpCL1 (0.01 µg/dot) and FhpCL1-based synthetic peptides (10 µg/dot), including (*) pre- (signal peptide), pro- (inhibitor) and mature- (protease) -specific sequences, were probed with whole serum diluted to 1:100 (cattle-specific), 1:700 (sheep-specific), or 1:5,000 (rabbit-specific). IgG binding was detected using anti-cattle or anti-sheep IgG at 1:30,000 and the NBT/BCIP substrate system until precipitant appearance in the positive control. Abbreviations: +, positive control; –, negative control; D, day post-infection.

6.4.5 CL-derived peptide ELISAs

6.4.5.1 *Sandwich CL peptide ELISA with anti-rFhΔpCL1 IgG*

The anti-rFhΔpCL1 IgG sandwich ELISA was used to test the antibody recognition of three synthetic peptides designed for three regions (signal, inhibitor, mature) of a representative preprocathepsin L sequence of *Fasciola hepatica*. Plates were coated with 5 µg·mL^{-1} anti-rFhΔpCL1 IgG and peptides were diluted within the range of 312.5 ng·mL^{-1}–10 µg·mL^{-1} and detected with biotinylated anti-rFhΔpCL1 IgG diluted to 1:10,000 (Figure 6.4.5.1). No ODs were considered positive, indicating either a lack of antibody-peptide recognition or

a possible consumption of the available epitopes by the coated antibodies preventing detection antibody binding.

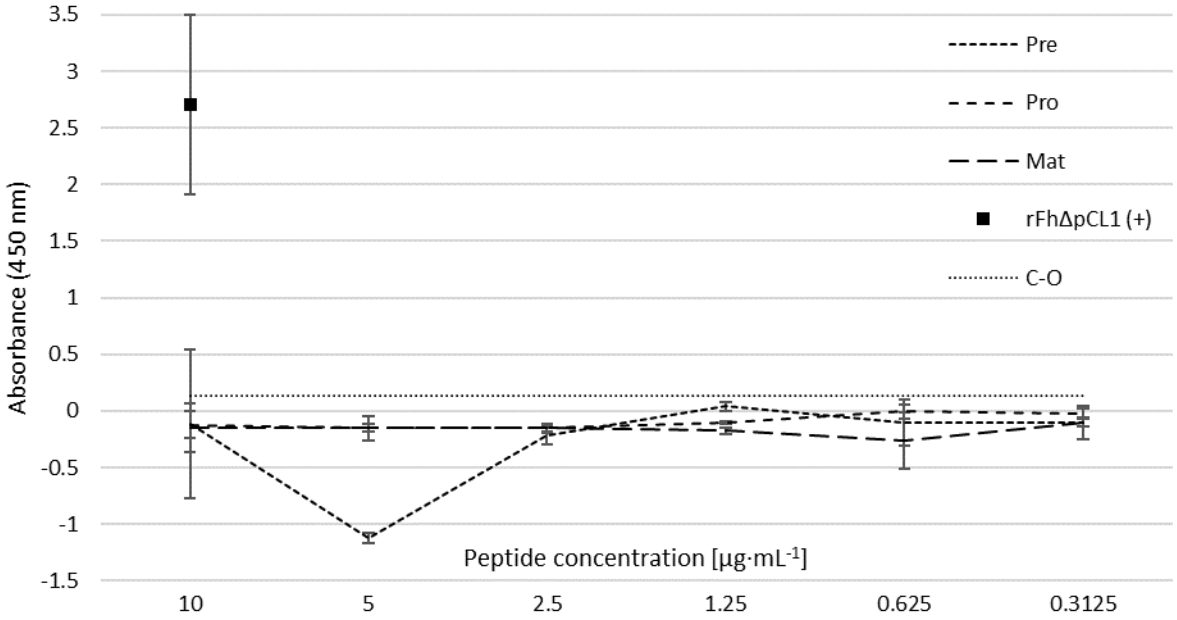

Figure 6.4.5.1. Trial sandwich ELISA for testing polyclonal anti-rFhΔpCL1 IgG recognition of pre- pro- and mature-specific FhpCL1-derived peptides. Average duplicate OD measures from two ELISA plates (adjusted by the subtraction of negative BSA control Ag OD) are shown for peptides diluted within the range of 31.25 ng·mL^{-1}–10 µg·mL^{-1} following capture with 5 µg·mL^{-1} anti-rFhΔpCL1 IgG coat and detection with biotinylated anti-rFhΔpCL1 IgG diluted to 1:10,000. The positive control shown for this assay (+) was rFhΔpCL1 diluted to 10 ng·mL^{-1} and positive OD values were considered when exceeding the cut-off (C-O), shown as one standard deviation above the negative Ag (BSA) OD score (dot line: 0.14027). Error bars are one standard deviation more and less than average ODs.

6.4.5.2 *Direct peptide ELISA using biotinylated anti-rFhΔpCL1 IgG*

In order to further test peptide-anti-rFhΔpCL1 IgG binding and avoid potential competition at epitope binding sites, peptides were directly coated onto plates within the range of 625 ng·mL^{-1}–40 µg·mL^{-1} and detected with biotinylated anti-rFhΔpCL1 IgG diluted to 1:5,000 (Figure 6.4.5.2). Similarly to the sandwich ELISAs, this revealed no positive OD scores, indicating a lack of recognition of anti-rFhΔpCL1 IgG against these synthetic CL-derived peptides.

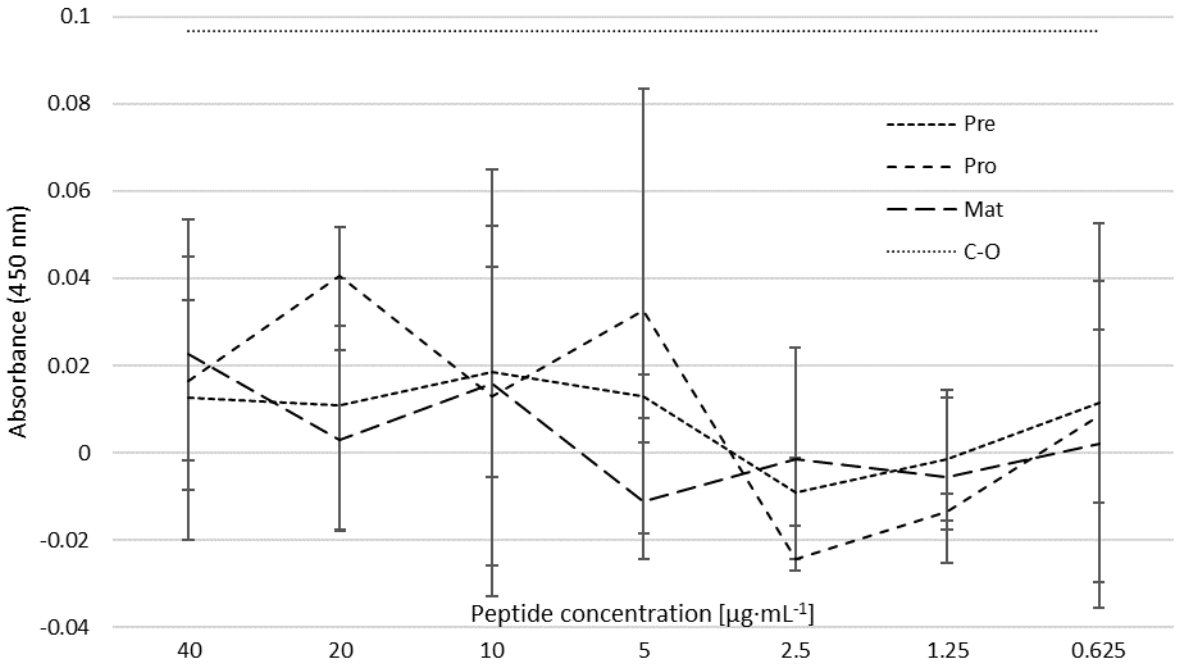

Figure 6.4.5.2. Trial direct ELISA for testing anti-rFhΔpCL1 IgG recognition of pre- pro- and mature-specific FhpCL1-derived peptides. Average duplicate OD measures (adjusted by the subtraction of negative BSA control Ag OD) are shown for peptides diluted within the range of 62.5 ng·mL^{-1}–40 µg·mL^{-1} following detection with biotinylated anti-rFhΔpCL1 IgG diluted to 1:5,000. Positive OD values were considered when exceeding the cut-off (C-O), shown as one standard deviation above the negative Ag (BSA) OD score (dot line: 0.096521). Error bars are one standard deviation more and less than average ODs.

6.4.5.3 *Peptide immunogenicity testing: F. hepatica-infected sheep sera responses*

The exposure and immunogenicity of CL-derived peptide epitopes during natural *Fasciola hepatica* infection was investigated based on the above direct ELISA design using *F. hepatica*-infected sheep serum. To test for optimal coating concentrations, peptides were initially coated within the range of 390.625 ng·mL^{-1}–100 µg·mL^{-1} and detected with 1:200-diluted serum from uninfected sheep or sheep infected with *F. hepatica* at 12 wpi (Figure 6.4.5.3.1). No OD values were considered positive, which was suggestive of a lack of sufficient antibody titre leading to significant Ag-binding or alternatively suggests no recognition of these sera against the CL-derived synthetic peptides.

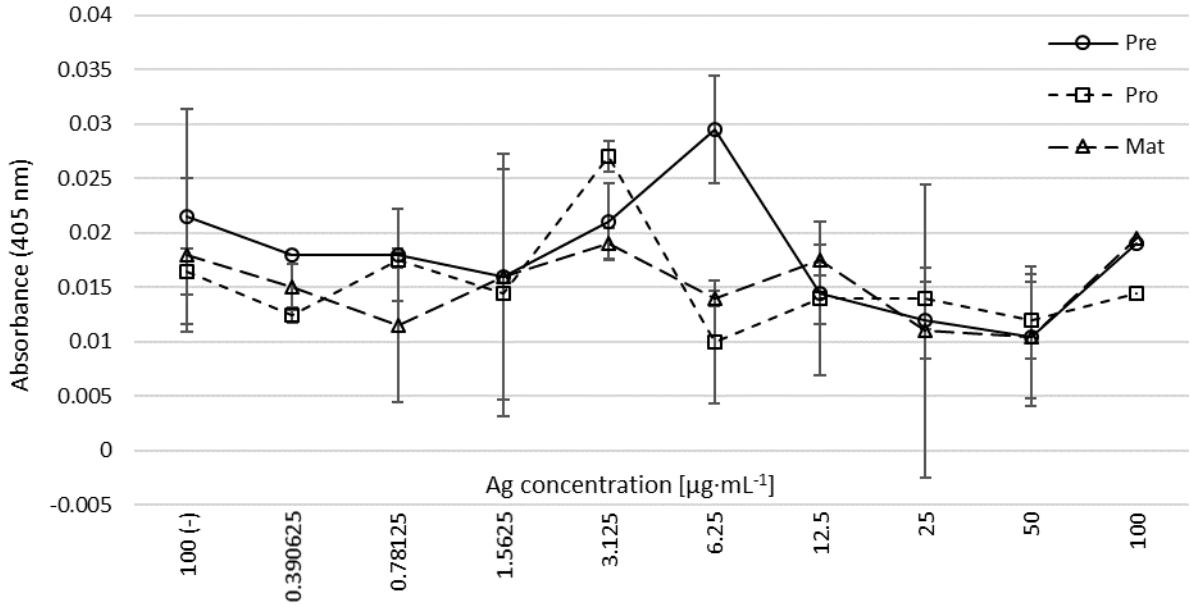

Figure 6.4.5.3.1. ELISA for the investigation of pre- pro- and mature-specific FhpCL1-derived peptide epitope exposure during *Fasciola hepatica* infection. Average duplicate OD measures (adjusted by the subtraction of negative BSA control Ag OD) are shown for peptides diluted within the range of 390.625 ng·mL^{-1}–100 µg·mL^{-1} following detection with *F. hepatica*-infected or non-infected (-) sheep serum diluted to 1:200. Positive OD values were considered when exceeding the cut-off (C-O), calculated as one standard deviation above the negative Ag (BSA) OD score (not shown: 0.072414). Error bars are one standard deviation more and less than average ODs.

To investigate and compare the serum recognition of CL-derived peptides between TCBZ-S and TCBZ-R *F. hepatica* and during the course of infection, the direct peptide ELISA was conducted as in the previous assay except with minor modifications as follows. To allow for maximal binding and detection, if present, peptides were coated at 100 µg·mL^{-1} and detected with 1:100-diluted serum from sheep infected with TCBZ-S (Aberystwyth, Miskin, Italian) or TCBZ-R (Kilmarnock, Penrith, Stornoway) *F. hepatica* strains (Figure 6.4.5.3.2). Sera were collected over the course of infection, including from 0, 2, 4, 8, 12 and 17 wpi, with TCBZ administration at 12 wpi. The mature region-specific peptide indicated positive scores at 12 and 17 wpi with TCBZ-R *F. hepatica*, indicating the exposure of this epitope during TCBZ-R fluke infection in sufficient quantities to be detectable with this assay. No other OD values were considered positive, which together with previous data may suggest that TCBZ-S-specific sera have a lower abundance of anti-CL IgG or alternatively indicates that the pre- and pro-specific epitopes of these synthetic peptides are not reflective of natural preprocathepsin L epitope exposures leading to positive recognition.

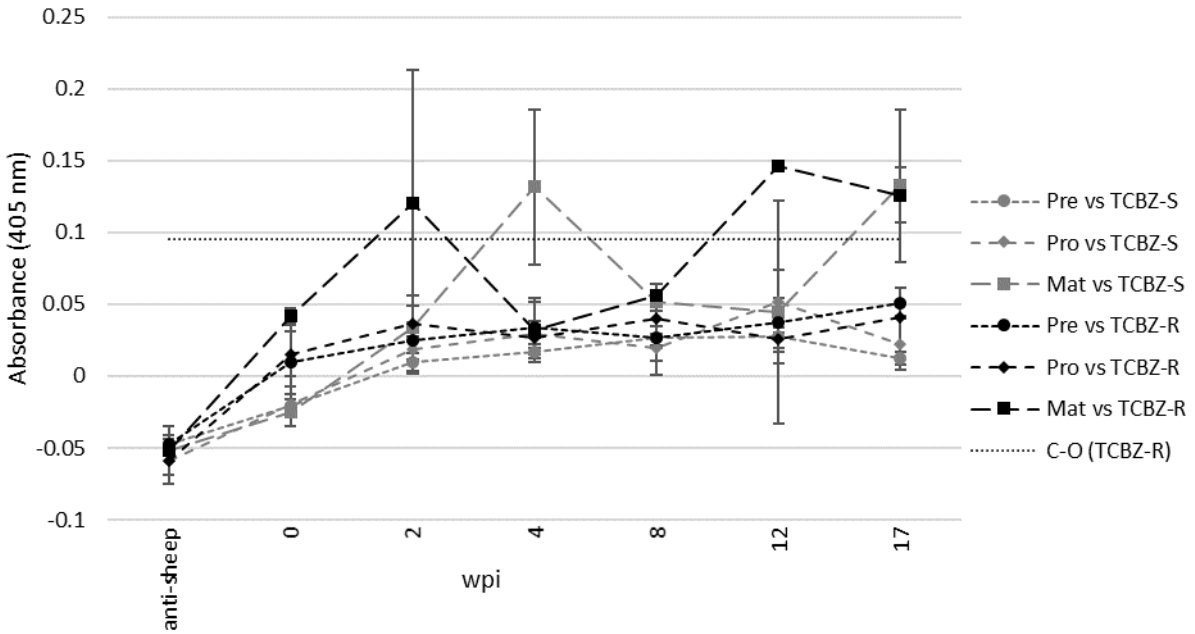

Figure 6.4.5.3.2. ELISA for the investigation and comparison of pre- pro- and mature-specific FhpCL1-derived peptide epitope exposure during infections with TCBZ-S or TCBZ-R *Fasciola hepatica* strains. Average duplicate OD measures (adjusted by the subtraction of negative BSA control Ag OD) are shown for peptides diluted 100 $\mu g \cdot mL^{-1}$ and detected with representative serum (n = 3 sheep/parasite strain) from 0, 2, 4, 8, 12 and 17 wpi with TCBZ-S (dashed line) or TCBZ-R (solid line) *F. hepatica* strains, and following clinical administration of TCBZ at 12 wpi. Sera were diluted to 1:100 and incubated for 1 hour. Positive OD values were considered when exceeding the cut-off (C-O), shown for TCBZ-R sera as one standard deviation above the negative Ag (BSA) OD score (not shown (TCBZ-S): 0.458225; dot line (TCBZ-R): 0.09545). Error bars are one standard deviation more and less than average ODs.

6.5 Discussion

The aim of this chapter was to examine the diagnostic potential of a panel of candidate *Fasciola hepatica* antigens, which were identified through a novel approach incorporating proteomic (4.4.4; Chemale *et al.*, 2010; Morphew *et al.*, 2014) and immunologic (3.4.3) methods. The immunogenicity and natural exposure during *F. hepatica* infection of FhCRT, FhGEL, FhTPI, FhpCL1 (including the preprocathepsin L signal peptide) and a synthetic peptide designed from the FhpCL1 signal peptide had not previously been explored (Chapter 6; 6.2.4: objective 1). Current work has confirmed for the first time the *in vivo* antigenicity and detectability of the zymogen-specific epitopes of FhpCL1, further to *in silico* predictions and *in vitro* work in Chapter 3 (3.4.3). Furthermore, FhpCL1 coproantigen presence in *F. hepatica*-infected host faeces could be verified using newly produced polyclonal IgG antibodies raised to rFhΔpCL1 (Chapter 6; 6.2.4: objective 2) and checked for cross-reactivity with other common UK livestock infections (Chapter 6; 6.2.4: objective 3), confirming the utility of this antigen for the *F. hepatica* infection serodiagnosis and anti-FhpCL1 PcAbs as a new tool for monitoring TCBZ efficacy.

The abundance and consequential host immune exposure to *F. hepatica* antigens during infection is a favourable characteristic of diagnostic candidates, which explains the development of CL proteases from antigens of biological interest into the basis of now commercialised laboratory kits with widespread use (Cornelissen *et al.*, 1999; Dalton *et al.*, 2003; Mezo *et al.*, 2004). However, the changing phenotype of the ES proteome observed from *in vitro* cultures following fluke death or flukicide exposure has since elucidated a range of further potential targets (3.4.1; 4.4.4; Chemale *et al.*, 2010; Morphew *et al.*, 2014, 2007). The lower abundance of such antigens, including FhpCL1 zymogens (3.4.1–3.4.3.4.2), actin, CRT, DJ-1, enolase, GEL, glyceradehyde-3-phosphate dehydrogenase and TPI (4.4.2.2–4.4.2.9; Morphew *et al.*, 2014), may indicate conservative or uncharacterised external roles of these proteins, whilst also offering unexplored immunogenic epitopes (Avilán *et al.*, 2011; Bernal *et al.*, 2004; Chemale *et al.*, 2010; Ghosh and Jacobs-Lorena, 2011; Gómez-Arreaza *et al.*, 2014; Liu and Shih, 2007; Morphew *et al.*, 2014; Ucker *et al.*, 2012).

The natural immunogenicity of the intact rFhΔpCL1 zymogen was shown to be demonstrably extensive (Figure 6.4.2.2.1), whilst the antigenicity of the previously unexplored FhpCL1 signal peptide has also been recognised from coproantigen recovery and

extended to the positive identification of successful TCBZ treatment (Figure 6.4.3.3.2). The thesis was unable to confirm serodiagnosis potential for rFhΔCRT, rFhGEL and rFhTPI AgELISAs in the presence of antigen-specific IgG abundance from *F. hepatica*-infected hosts, including experimental infections with TCBZ-S- or TCBZ-R-specific *F. hepatica* isolates (Figures 6.4.2.2.2-6.4.2.2.3). However, the western hybridisation format for these assays indicated differential antigen-antibody interactions, which presented differential positivity over the course of infection with each representative TCBZ-S and -R parasites (Figure 6.4.2.3.2; Table 6.4.2.3). All immunologic formats for testing the immunogenicity of FhpCL1-based synthetic peptides, including dot blotting (Figure 6.4.4), AgELISAs using direct (Figure 6.4.5.2) and indirect (Figures 6.4.5.3.1–6.4.5.3.2) antibody detection, and via the anti-rFhΔpCL1 IgG sandwich ELISAs (Figure 6.4.3.3.2), failed to confirm recognition of peptide epitopes by *F. hepatica*-infected host or anti-rFhΔpCL1 IgG. The absence of evidence for anti-rFhΔpCL1 IgG-peptide interactions, more so than that for host-infected IgG-peptide binding, suggests the potential loss of native protein epitopes adopted by the peptide sequences *in situ*, particularly the signal and inhibitor peptides towards which the anti-rFhΔpCL1 IgG has shown greatest immunoreactivity (detailed in Chapter 3: 3.4.3.1–3.4.3.2). However, the current findings support the dominance of internal roles for FhCRT, FhGEL and FhTPI compared to Fh(p)CL1, previously presumed from their relatively low abundance in the ES proteome (Morphew *et al.*, 2007, 2014) and based on the unreadable IgG specificity in the current AgELISAs. Consequently to these more limited exposures to the host immune system, antigen-specific serum antibody titres may be too low or undetectable for quantitative serodiagnoses. Moreover, this does not preclude the potential diagnostic value or vaccine candidature of these antigens, since the intrinsic internal localisation and homeostatic functions are an asset for strategies seeking to exploit such properties (Molina-Hernández *et al.*, 2015), such as the *H. contortus* subunit vaccine "Barbervax" utilising native gut-based proteins (Besier *et al.*, 2013; Smith, 2014). Thus, the full diagnostic potential of endogenous FhCRT, FhGEL and FhTPI is yet to be determined, and is deserving of further study with the recombinant tools developed in this thesis.

6.6 Conclusions

This exploration of pre-selected candidates in this thesis is a further step towards the development and understanding of molecular components of the *Fasciola hepatica* proteome and parasite-host interactome, and thus their potential as diagnostic targets. The provision of more descriptive standpoints is a growing necessity during the assessment of *F. hepatica* infection stage, intensity or anthelmintic susceptibility, especially in the face of growing UK endemicity that is becoming exacerbated by increasing incidences of TCBZ resistance (Kelley *et al.*, 2016; Overend and Bowen, 1995) and climate-driven parasite expansion (Fox *et al.*, 2011; Short *et al.*, 2017). The identification and study of key proteomic differences between live and dead, TCBZ-S and TCBZ-R, and untreated and TCBZ-exposed *F. hepatica* have enabled the progression of antigens as targets of preliminary studies conducted here, which has revealed the unexpected potential of FhpCL1 zymogens as immunogenic descriptors of fluke fitness and viability, in a role that has previously remained unexploited. Furthermore, the information gathered for recombinant FhCRT, FhGEL and FhTPI confirm previous findings of the either low native protein abundances and/or relatively low natural immunogenicity and this likely reflected the poor serodiagnosis using recombinant forms. However, the progress here opens a window of possibility for investigating native forms of these candidates, as well as other as-yet uncharacterised endogenous proteins for pilot and eventually penside diagnostics, as well as vaccine approaches.

7 Chapter 7: General Discussion

7 General discussion

This thesis has uncovered new dynamic aspects of the *Fasciola hepatica* excretory/secretory (ES) proteome (Chapter 1; 1.5: objective 2; Chapter 4), whereby changes to the active secretome were shown to be influenced by factors including fluke viability (categorised by live or dead treatment groups) (Figure 4.4.2), parasite strain (defined by natural *in vivo* triclabendazole (TCBZ) susceptibility or resistance) (Figure 4.4.3) and *in vitro* anthelmintic (TCBZ/-sulfoxide (-SO)/-sulfone ($-SO_2$)) exposures (Figures 4.4.4.1–4.4.4.3, Table 4.4.4). Cathepsin proteases have repeatedly emerged as the most consistent and overabundant factors secreted by juvenile and adult parasites during *in vivo* infection, *ex vivo* culture and *in vitro* anthelmintic exposure (Chemale *et al.*, 2010; Hernández-González *et al.*, 2010; Jefferies *et al.*, 2001; Morphew *et al.*, 2007, 2011, 2014; Robinson *et al.*, 2008b, 2009; Stack *et al.*, 2008). As such, cathepsin L proteases (CLs) are the most studied group of *F. hepatica* antigens and remain key candidates of interest (Dalton *et al.*, 2013, 2003; Morphew *et al.*, 2011; Mulcahy and Dalton, 2001; Toet *et al.*, 2014), with a principal focus towards commercial diagnostics (Carnevale *et al.*, 2001; Cornelissen *et al.*, 2001, 1999; Kuerpick *et al.*, 2013; Martínez-Sernández *et al.*, 2011; Mezo *et al.*, 2004; O'Neill *et al.*, 1999; Wilson *et al.*, 1998) and vaccine trial efforts (Dalton *et al.*, 1996; Golden *et al.*, 2010; Piacenza *et al.*, 1999; Wijffels *et al.*, 1994; Zafra *et al.*, 2013a). However, the work conducted in this thesis has realised many more potential diagnostic candidates, vaccine opportunities and drawbacks provided by a dynamic ES proteome (Chapter 1; 1.5: objectives 1, 2 and 4; Chapters 3, 4 and 6). In addition, this thesis has bioinformatically characterised and provided a basis to produce a panel of new liver fluke targets (Chapter 1; 1.5: objective 3; Chapter 5) for future investigations.

7.1 Procathepsin zymogens as diagnostic candidates for *Fasciola hepatica* infection

The thesis presents for the first time procathepsin L (pCL) zymogens as a group of abundant (Chapter 3: Figure 3.4.1, Table 3.4.1) and highly immunogenic biomarkers (Chapter 3: Figures 3.4.3.4.1–3.4.3.4.2, Figure S2), that also differentiate between live and dead adult liver fluke. Using a new indirect ELISA format, investigations further revealed pCL1-specific serum IgG were detectable from *Fasciola hepatica*-infected sheep from 4 weeks post-infection (wpi) for TCBZ-R isolates or 5 wpi for TCBZ-S isolates (Chapter 6: Figure 6.4.2.2.1). In

addition, new pCL-specific anti-recombinant mutant pCL1 (rFhΔpCL1) polyclonal (Pc) antibodies present a prospective tool for *ex vivo* infection detection, including the positive identification of multiple clades of FhpCLs present in adult ES products based on western hybridisations (Chapter 3: Figure 3.4.3.4.2). To this end, anti-rFhΔpCL1 IgG has further demonstrated the potential ability to sensitively detect infection via coproantigen capture from faecal samples of *F. hepatica*-infected sheep from 6 wpi for TCBZ-S isolates or 8 wpi for TCBZ-R isolates using a new preliminary sandwich ELISA format (Chapter 6: Figure 6.4.3.3.2), as well as providing specificity towards *F. hepatica* over other common livestock helminth parasites via dot ELISAs (Chapter 6: Figure 6.4.4). Furthermore, this sandwich ELISA test platform using anti-rFhΔpCL1 Pc IgG could possibly be developed to detect and differentiate between active *F. hepatica* infection, TCBZ failure against TCBZ-R parasites and successful TCBZ treatment. Specifically, a measurable (97.36%) reduction in coproantigen signal was detected after one week post-treatment (PT) in TCBZ-S-infected faecal samples which was followed by a complete reduction (100%) by three weeks PT. Thus, this thesis work has provided a robust starting position for further commercial exploitation of the diagnostic capabilities of FhpCLs and, furthermore, has highlighted for the first time the efficacy of ELISAs using the rFhΔpCL1 antigen and respective anti-rFhΔpCL1 Pc IgG for the detection of livestock *F. hepatica* infection.

7.2 Ultrastructural and proteomic differences of wild type and TCBZ-R *Fasciola hepatica* upon flukicide and anthelmintic challenge

Inspired by previously successful *in vitro* studies coupling histological and proteomic changes following anthelmintic challenge (Chemale *et al.*, 2010; Morphew *et al.*, 2014; Robinson *et al.*, 2002; Stitt *et al.*, 1995), a similar approach was utilised in this thesis. Specifically, the contrast in EV production and tegument infrastructure was determined between live (*in vitro* cultured) and dead (*in vitro* cultured and terminated in ethyl 4-aminobenzoate (1% (w/v) in ethanol) wild type (WT-Fh) adult flukes, and the macroscopic viability and molecular ES profiles were assessed and compared between WT-Fh flukes of mixed TCBZ susceptibility and a TCBZ-R strain (Kilmarnock, K-Fh). As such, this has identified key histological and ES pCL subproteomic changes in the outcome of non-specific flukicide (induced by ethyl 4-aminobenzoate) in adult wild type flukes (mixed TCBZ susceptibility, WT-

Fh) compared to untreated control WT-Fh flukes (Chapter 4: 4.4.1–4.4.2). Additionally, when comparing WT-Fh flukes with K-Fh, a newly isolated TCBZ-R strain, biological and proteomic differences were also observed following TCBZ/-SO/-SO_2 anthelmintic exposure (sub-lethal (SL) dose: [15 µg·mL^{-1}]) (Chapter 4: 4.4.3–4.4.4). Specifically, extracellular vesicle (EV) profiles were demonstrably different between live or dead flukes, including a higher frequency of larger-sized apoptotic body-like vesicles in the latter group. This finding supports previous studies demonstrating disruptions to the tegument syncytial organisation following anthelmintic exposure (Scarcella *et al.*, 2016; Toner *et al.*, 2010b). The comparison of *in vitro* viability scores between WT-Fh and K-Fh flukes demonstrated evidence ($P < 0.00001$) for a difference following anthelmintic challenge (Chapter 4: Figure 4.4.3), suggesting improved fitness of the TCBZ-R K-Fh group. Proteomic assays further delineated ES product changes highlighting differences in the anthelmintic efficacy status of the naturally-acquired flukes compared to a newly confirmed TCBZ-R isolate i.e. discovering CL, enolase (ENO) and gelsolin (GEL) among seven 2DE-separated proteins that were differentially abundant ($P < 0.05$), with actin (ACT) and cathepsin B (CB) among 10 WT-Fh strain-specific TCBZ-response proteins and fatty acid binding proteins 15 (FhFABP I) and 2 (FhFABP II) among 13 K-Fh strain-specific TCBZ-response proteins. These new datasets were both in-keeping (ACT, CL) and novel (ENO, GEL, CB, FABP 5/Fh2) with respect to previous findings for ES changes following TCBZ-SO challenge (Morphew *et al.*, 2014), overall supporting the multifaceted nature and potential utility of these proteins.

7.3 Novel diagnostic candidates of TCBZ response-associated proteomic phenotypes

Previously-identified (Morphew *et al.*, 2014) antigens of diagnostic interest were also assessed by multiple bioinformatics tools in this thesis (Chapter 5: 4.4.1), in order to develop a working understanding of their putative roles in the adult *Fasciola hepatica* TCBZ-SO-associated secretome phenotypes. Thus, multiple sequence similarities of *F. hepatica* ACT, calreticulin (CRT), deglycase DJ-1 (DJ-1), ENO, GEL, glyceraldehyde-3-phosphate dehydrogenase (GAPDH) and triose phosphate isomerase (TPI) proteins were identified within known family and superfamily models and/or parasitic orthologues, assigning structural motifs, functional domains and ligand-binding attributes. Furthermore, annotation permitted the prediction of molecular roles involved in fluke biology (Table 4.4.1.9), from

which activities during *F. hepatica* infection development and treatment can now be considered.

Interestingly, of the TCBZ-SO-associated survival (CRT, ENO, GAPDH) and termination (ACT, DJ-1, GEL, TPI) proteomic phenotypes of *F. hepatica*, there is no commonality between the inherent roles of these biomarkers, except in the case of the three glycolytic enzymes (ENO, GAPDH, TPI). Despite this direct link of the latter candidates, it can be presumed that following TCBZ-SO exposure their glycolytic activities may end, since TCBZ-SO dose-dependent and temporally-specific abundances associate them with TCBZ-SO survival (ENO, GAPDH) or termination (TPI) proteomic signatures (Morphew *et al.*, 2014). However, there have been several isolated observations for all three enzymes that fit virulence- and/or pathogenesis-associated excretion patterns, including via instances of host cell invasion and protein-binding (Avilán *et al.*, 2011; Barbosa *et al.*, 2006; Bergmann *et al.*, 2004; Bernal *et al.*, 2004; Díaz-Ramos *et al.*, 2012; Fletcher *et al.*, 2001; Furuya and Ikeda, 2011, 2009; Gómez-Arreaza *et al.*, 2014; Karkowska-Kuleta *et al.*, 2011; Miranda-Ozuna *et al.*, 2016; Pancholi and Chhatwal, 2003). Conversely to these findings, glycolytic enzyme externalisation has also been observed in apoptotic cell membranes and vesicular exports (Ucker *et al.*, 2012) and GAPDH has been linked to nuclear localisation for DNA repairs during oxidative stress and apoptosis regulation (Dastoor and Dreyer, 2001; Shashidharan *et al.*, 1999), presenting possible perfunctory purposes of extracellular exposure and non-glycolytic functions during cell stress/death. However, prospective pathogenesis-associated TPI functions may not be synonymous for *F. hepatica* since present observations have only been from single-celled bacterial and parasitic organisms, with the exception of *Schistosoma mansoni* (Shoemaker *et al.*, 1992), indicating the importance of the context of antigen discovery.

The TCBZ susceptibility-associated phenotype biomarkers of *F. hepatica* share inter-group characteristics through their localisation to intracellular compartments (ACT, DJ-1, GEL, TPI). Additionally, in line with aforementioned assumed housekeeping and metabolism-associated proteins (Ucker *et al.*, 2012), the release of these factors may be directly associated with fluke death as an artefact or systematic process of apoptosis. However, conflicting observations for FhGEL beyond anthelmintic-specific responses (Linder and Thors, 1992; Markoski *et al.*, 2006; Morphew *et al.*, 2014) find GEL secretion within helminth juvenile ES products (Camargo de Lima *et al.*, 2018; De la Torre-Escudero *et al.*, 2011; Hernández-González *et al.*, 2010; Teichmann *et al.*, 2015) and the host circulation during general illness,

non-communicable diseases and helminthiases (Goldfinch *et al.*, 2008; Kwiatkowski, 1999; Mounzer *et al.*, 1999; Straub *et al.*, 2011; Wen and Garg, 2012). Consequently, it can be inferred that GEL may be involved in internal actin binding, with externalisation upon apoptotic processes, with an extension of functionality to suppress aberrant activities of apoptosis-induced actin circulation.

The bioinformatic data synthesised here have widened the scope for speculation over the prospective functionalities and consequences of antigen exposures, which is complemented in this thesis by wet-laboratory experiments on recombinant protein targets. The developments towards recombinant tools also take us a step forward in the provision of options for the descriptive diagnosis of liver fluke infection, including the possible definition between parasite TCBZ susceptibility status and/or viability.

Final conclusions and recommendations

It has been well established by others within the field that the future applicability and efficacy of anthelmintics are problematic. Emergent findings of parasite persistence PT in natural field-based infections are testament to the challenges of upholding anthelmintics' efficacies for decades at a time. However, outlooks for fasciolosis control strategies are improved by the discovery of more molecular-based profiles coupled to sensitive detection methods. In this capacity, novel directions to identify *Fasiola hepatica* infection and understand parasite fitness could respectively support efforts of monitoring for population mapping and identification of TCBZ treatment efficacy. This thesis has critically examined multiple diagnostic candidates of interest that fit these criteria, leading to the production and pilot testing of several novel molecular tools.

Based on the findings of this thesis, it is recommended that the identification of *F. hepatica* anthelmintic susceptibility needs more in-depth assessment in order to determine the molecular signatures of infecting parasites. Specifically, it has been shown here that several parasite genetic and environmental factors are capable of causing subtle changes to the composition of the *F. hepatica* ES proteome, including fluke fitness, viability (live or dead), TCBZ efficacy status and TCBZ exposure. Therefore, interpretation of antigen-specific diagnoses will require additional understanding to verify the true nature of *in situ* biomarker release. In final conclusion, this thesis has made progress towards the critical analysis, production and putative diagnostic testing of several new biomarkers, which will be of value for future informative approaches for the detection of *F. hepatica* infection, TCBZ exposure and TCBZ efficacy.

Bibliography

Afshan, K., Valero, M.A., Qayyum, M., Peixoto, R. V., Magraner, A., Mas-Coma, S., 2014. Phenotypes of intermediate forms of *Fasciola hepatica* and *F. gigantica* in buffaloes from Central Punjab, Pakistan. J. Helminthol. 88, 417–426. https://doi.org/10.1017/s0022149x13000369

Aguillón, J.C., Bustos, C., Vallejos, P., Hermosilla, T., Morello, A., Repetto, Y., Hellman, U., Orn, A., Ferreira, A., 1995. Purification and preliminary sequencing of Tc45, an immunodominant *Trypanosoma cruzi* antigen: Absence of homology with cruzipain, cruzain, and a 46-kilodalton protein. Am. J. Trop. Med. Hyg. 53, 211–215. https://doi.org/10.4269/ajtmh.1995.53.211

Aguillón, J.C., Ferreira, L., Pérez, C., Colombo, A., Molina, M.C., Wallace, A., Solari, A., Carvallo, P., Galindo, M., Galanti, N., Örn, A., Billetta, R., Ferreira, A., 2000. Tc45, a dimorphic *Trypanosoma cruzi* immunogen with variable chromosomal localization, is calreticulin. Am. J. Trop. Med. Hyg. 63, 306–312.

Ai, L., Dong, S.J., Zhang, W.Y., Elsheikha, H.M., Mahmmod, Y.S., Lin, R.Q., Yuan, Z.G., Shi, Y.L., Huang, W.Y., Zhu, X.Q., 2010a. Specific PCR-based assays for the identification of *Fasciola* species: their development, evaluation and potential usefulness in prevalence surveys. Ann. Trop. Med. Parasitol. 104, 65–72. https://doi.org/10.1179/136485910X12607012373713

Ai, L., Li, C., Elsheikha, H.M., Hong, S.J., Chen, J.X., Chen, S.H., Li, X., Cai, X.Q., Chen, M.X., Zhu, X.Q., 2010b. Rapid identification and differentiation of *Fasciola hepatica* and *Fasciola gigantica* by a loop-mediated isothermal amplification (LAMP) assay. Vet. Parasitol. 174, 228–233. https://doi.org/http://dx.doi.org/10.1016/j.vetpar.2010.09.005

Akers, J.C., Gonda, D., Kim, R., Carter, B.S., Chen, C.C., 2013. Biogenesis of extracellular vesicles (EV): exosomes, microvesicles, retrovirus-like vesicles, and apoptotic bodies. J. Neurooncol. 113, 1–11. https://doi.org/10.1007/s11060-013-1084-8

Aksoy, D.Y., Kerimoglu, U., Oto, S., Erguven, S., Arslan, S., Unal, S., Batman, F., Bayraktar, Y., 2005. Infection with *Fasciola hepatica*. Clin. Microbiol. Infect. 11, 859–861. https://doi.org/10.1111/j.1469-0691.2005.01254.x

Aleixo, M.A., Freitas, D.F., Dutra, L.H., Malone, J., Martins, I.V.F., Molento, M.B., 2015. *Fasciola hepatica*: epidemiology, perspectives in the diagnostic and the use of geoprocessing systems for prevalence studies. Semin. Ciências Agrárias 36. https://doi.org/10.5433/1679-0359.2015v36n3p1451

Allahyari, M., Mohabati, R., Babaie, J., Amiri, S., Siavashani, Z.J., Zare, M., Sadeghiani, G., Golkar, M., 2015. Production of in-vitro refolded and highly antigenic SAG1 for development of a sensitive and specific *Toxoplasma* IgG ELISA. J. Immunol. Methods 416, 157–166. https://doi.org/10.1016/j.jim.2014.11.012

Allen, P.G., 1997. Functional consequences of disulfide bond formation in gelsolin. FEBS Lett. 401, 89–94. https://doi.org/10.1016/S0014-5793(96)01439-1

Almazán, C., Avila, G., Quiroz, H., Ibarra, F., Ochoa, P., 2001. Effect of parasite burden on the detection of *Fasciola hepatica* antigens in sera and feces of experimentally infected sheep. Vet. Parasitol. 97, 101–112. https://doi.org/10.1016/S0304-4017(01)00376-4

Altman, D.G., Bland, J.M., 1994a. Diagnostic tests. 1: Sensitivity and specificity. BMJ 308, 1552. https://doi.org/10.1136/bmj.308.6943.1552

Altman, D.G., Bland, J.M., 1994b. Statistics Notes: Diagnostic tests 2: Predictive values. BMJ 309, 102. https://doi.org/10.1136/bmj.309.6947.102

Altman, D.G., Bland, J.M., 1994c. Statistics Notes: Diagnostic tests 3: Receiver operating characteristic plots. BMJ 309, 188. https://doi.org/10.1136/bmj.309.6948.188

Alvarez-Sanchez, M.A., Mainar-Jaime, R.C., Perez-Garcia, J., Rojo-Vázquez, F.A., 2006. Resistance of *Fasciola hepatica* to triclabendazole and albendazole in sheep in Spain. Vet. Rec. 159, 424–425.

Alvarez, L.I., Moreno, G., Moreno, L., Ceballos, L., Shaw, L., Fairweather, I., Lanusse, C., 2009. Comparative assessment of albendazole and triclabendazole ovicidal activity on *Fasciola hepatica* eggs. Vet. Parasitol. 164, 211–216. https://doi.org/10.1016/j.vetpar.2009.05.014

Antequera, D., Vargas, T., Ugalde, C., Spuch, C., Molina, J.A., Ferrer, I., Bermejo-Pareja, F., Carro, E., 2009. Cytoplasmic gelsolin increases mitochondrial activity and reduces Aβ burden in a mouse model of Alzheimer's disease. Neurobiol. Dis. 36, 42–50. https://doi.org/10.1016/j.nbd.2009.06.018

Arafa, W.M., Shokeir, K.M., Khateib, A.M., 2015. Comparing an in vivo egg reduction test and in vitro egg hatching assay for different anthelmintics against *Fasciola* species, in cattle. Vet. Parasitol. 214, 152–158. https://doi.org/10.1016/j.vetpar.2015.09.023

Araújo, A., Ferreira, L.F., 2000. Paleoparasitology and the Antiquity of Human Host-parasite Relationships. Mem. Inst. Oswaldo Cruz 95, 89–93.

Arjmand, J., Esmaeilnejad, B., Razi Jalali, M.H., Ghorbanpoor, M., Abtahi Froushani, S.M., 2014. Designing and evaluation of Dot-ELISA for diagnosis of *Fasciola* infection in cattle. Vet. Res. Forum 5, 141–4.

Arnold, K., Bordoli, L., Kopp, J., Schwede, T., 2006. The SWISS-MODEL workspace: A web-based environment for protein structure homology modelling. Bioinformatics 22, 195–201. https://doi.org/10.1093/bioinformatics/bti770

Ashrafi, K., Valero, M.A., Panova, M., Periago, M. V., Massoud, J., Mas-Coma, S., 2006. Phenotypic analysis of adults of *Fasciola hepatica*, *Fasciola gigantica* and intermediate forms from the endemic region of Gilan, Iran. Parasitol. Int. 55, 249–260. https://doi.org/10.1016/j.parint.2006.06.003

Ashrafi, K., Valero, M.A., Peixoto, R. V., Artigas, P., Panova, M., Mas-Coma, S., 2015. Distribution of *Fasciola hepatica* and *F. gigantica* in the endemic area of Guilan, Iran: Relationships between zonal overlap and phenotypic traits. Infect. Genet. Evol. 31, 95–109. https://doi.org/10.1016/j.meegid.2015.01.009

Ashton, R.A., Stewart, B.T., Petty, N., Lado, M., Finn, T., Brooker, S., Kolaczinski, J.H., 2011. Accuracy of circulating cathodic antigen tests for rapid mapping of *Schistosoma mansoni* and S*. haematobium* infections in Southern Sudan. Trop. Med. Int. Heal. 16, 1099–1103.

Avilán, L., Gualdrón-López, M., Quiñones, W., González-González, L., Hannaert, V., Michels, P.A.M., Concepción, J.-L., 2011. Enolase: a key player in the metabolism and a probable virulence factor of trypanosomatid parasites-perspectives for its use as a therapeutic target. Enzyme Res. 2011, 1–14. https://doi.org/10.4061/2011/932549

Babich, A., Burkhardt, J.K., 2013. Coordinate control of cytoskeletal remodeling and calcium mobilization during T-cell activation. Immunol. Rev. 256, 80–94. https://doi.org/10.1111/imr.12123

Baguley, B.C., 2010. Multiple drug resistance mechanisms in cancer. Mol. Biotechnol. 46, 308–316. https://doi.org/10.1007/s12033-010-9321-2

Baker, B.Y., Shi, W., Wang, B., Palczewski, K., 2014. High-resolution crystal structures of the photoreceptor glyceraldehyde 3-phosphate dehydrogenase (GAPDH) with three and four-bound NAD molecules. Protein Sci. 23, 1629–1639. https://doi.org/10.1002/pro.2543

Barbosa, M.S., Báo, S.N., Andreotti, P.F., De Faria, F.P., Felipe, M.S.S., Dos Santos Feitosa, L.,

Mendes-Giannini, M.J., De Almeida Soares, C.M., 2006. Glyceraldehyde-3-phosphate dehydrogenase of *Paracoccidioides brasiliensis* is a cell surface protein involved in fungal adhesion to extracellular matrix proteins and interaction with cells. Infect. Immun. 74, 382–389. https://doi.org/10.1128/IAI.74.1.382-389.2006

Barger, I.A., 1999. The role of epidemiological knowledge and grazing management for helminth control in small ruminants. Int. J. Parasitol. 29, 41–47.

Bargues, M.D., Horák, P., Patzner, R.A., Mas-coma, S., 2003. Insights into relationships of Palearctic and Nearctic lymnaeids (Mollusca: Gastropoda) by rDNA ITS-2 sequencing and phylogeny of stagnicoline intermediate host species of Fasciola hepatica. Parasite 10, 243–255. https://doi.org/10.1051/parasite/2003103243

Barnett, C., Hossell, J., Perry, M., Procter, C., Hughes, G., 2006. A handbook of climate trends across Scotland, in: SNIFFER Project CC03, Scotland & Northern Ireland Forum for Environmental Research. p. 66.

Baulac, S., LaVoie, M.J., Strahle, J., Schlossmacher, M.G., Xia, W., 2004. Dimerization of Parkinson's disease-causing DJ-1 and formation of high molecular weight complexes in human brain. Mol. Cell. Neurosci. 27, 236–246. https://doi.org/10.1016/j.mcn.2004.06.014

Bayir, A., Tufecki, N., Vatansev, H., Baran, H., Kara, H., Kayis, S.A., 2014. The Relation between Plasma Gelsolin Levels and Prognosis in Patients with Acute İschemic Stroke upon Admission to Emergency Department. J. Emerg. Med. 46, 283.

Bazsalovicsová, E., Králová-hromadová, I., Jan, Š., Minárik, G., Bokorová, S., Pybus, M., 2015. Genetic interrelationships of North American populations of giant liver fluke *Fascioloides magna*. Parasites and Vectors 8, 288–303. https://doi.org/10.1186/s13071-015-0895-1

Beckham, S.A., Law, R.H.P., Smooker, P.M., Quinsey, N.S., Caffrey, C.R., McKerrow, J.H., Pike, R.N., Spithill, T.W., 2006. Production and processing of a recombinant *Fasciola hepatica* cathepsin B-like enzyme (FhcatB1) reveals potential processing mechanisms in the parasite. Biol. Chem. 387, 1053–1061. https://doi.org/10.1515/BC.2006.130

Beckham, S.A., Piedrafita, D., Phillips, C.I., Samarawickrema, N., Law, R.H.P., Smooker, P.M., Quinsey, N.S., Irving, J.A., Greenwood, D., Verhelst, S.H.L., Bogyo, M., Turk, B., Coetzer, T.H., Wijeyewickrema, L.C., Spithill, T.W., Pike, R.N., 2009. A major cathepsin B protease from the liver fluke *Fasciola hepatica* has atypical active site features and a potential role in the digestive tract of newly excysted juvenile parasites. Int. J. Biochem. Cell Biol. 41, 1601–1612. https://doi.org/10.1016/j.biocel.2009.02.003

Bedard, K., MacDonald, N., Collins, J., Cribb, A., 2004. Cytoprotection Following Endoplasmic Reticulum Stress Protein Induction in Continuous Cell Lines. Basic Clin. Pharmacol. Toxicol. 94, 124–131. https://doi.org/10.1111/j.1742-7843.2004.pto940305.x

Beesley, N.J., Cwiklinski, K., Williams, D.J.L., Hodgkinson, J., 2015. *Fasciola hepatica* from naturally infected sheep and cattle in Great Britain are diploid. Parasitology 142, 1196–1201. https://doi.org/10.1017/S0031182015000499

Beesley, N.J., Williams, D.J.L., Paterson, S., Hodgkinson, J., 2017. *Fasciola hepatica* demonstrates high levels of genetic diversity, a lack of population structure and high gene flow: possible implications for drug resistance. Int. J. Parasitol. 47, 11–20.

Begg, C.B., 1987. Biases in the assessment of diagnostic tests. Stat. Med. 6, 411–423. https://doi.org/10.1002/sim.4780060402

Behm, C.A., Sangster, N.C., 1999. Pathology, pathophysiology and clinical aspects, in: Fasciolosis. CABI Publishing, Wallingford, UK, pp. 185–224.

Bellmann, K., Jäättelä, M., Wissing, D., Burkart, V., Kolb, H., 1996. Heat shock protein hsp70

overexpression confers resistance against nitric oxide. FEBS Lett. 391, 185–188. https://doi.org/10.1016/0014-5793(96)00730-2

Benesh, D.P., Chubb, J.C., Parker, G.A., 2014. The trophic vacuum and the evolution of complex life cycles in trophically transmitted helminths. Proc. R. Soc. B 281, 20131362.

Benítez-Cardoza, C.G., Rojo-Domínguez, A., Hernández-Arana, A., 2001. Temperature-induced denaturation and renaturation of triosephosphate isomerase from *Saccharomyces cerevisiae*: Evidence of dimerization coupled to refolding of the thermally unfolded protein. Biochemistry 40, 9049–9058. https://doi.org/10.1021/bi010528w

Benkert, P., Biasini, M., Schwede, T., 2011. Toward the estimation of the absolute quality of individual protein structure models. Bioinformatics 27, 343–350. https://doi.org/10.1093/bioinformatics/btq662

Bennett, J.L., Köhler, P., 1987. *Fasciola hepatica*: Action in vitro of triclabendazole on immature and adult stages. Exp. Parasitol. 63, 49–57. https://doi.org/10.1016/0014-4894(87)90077-4

Bennett, R., Ijpelaar, J., 2005. Updated Estimates of the Costs Associated with Thirty Four Endemic Livestock Diseases in Great Britain: A Note. J. Agric. Econ. 56, 135–144.

Bennett, R.M., Christiansen, K., Clifton-Hadley, R.S., 1999. Estimating the costs associated with endemic diseases of dairy cattle. J. Dairy Res. 66, 455–459. https://doi.org/10.1017/S0022029999003684

Benson, D.A., Clark, K., Karsch-Mizrachi, I., Lipman, D.J., Ostell, J., Sayers, E.W., 2015. GenBank. Nucleic Acids Res. 43, D30–D35. https://doi.org/10.1093/nar/gku1216

Berasaín, P., Carmona, C., Frangione, B., Dalton, J.P., Goñi, F., 2000. *Fasciola hepatica*: Parasite-secreted proteinases degrade all human IgG subclasses: Determination of the specific cleavage sites and identification of the immunoglobulin fragments produced. Exp. Parasitol. 94, 99–110. https://doi.org/10.1006/expr.1999.4479

Berasaín, P., Goñi, F., McGonigle, S., Dowd, A.J., Dalton, J.P., Frangione, B., Carmona, C., 1997a. Proteinases secreted by *Fasciola hepatica* degrade extracellular matrix and basement membrane components. Parasitology 83, 1–5.

Berasaín, P., Goñi, F., McGonigle, S., Dowd, A.J., Dalton, J.P., Frangione, B., Carmona, C., 1997b. Proteinases Secreted by *Fasciola hepatica* Degrade Extracelullar Matrix and Basement Membrane. Parasitology 83, 1–5.

Berg, C.O., 1973. Biological Control of Snail-Borne diseases: A Review. Exp. Parasitol. 33, 318–330. https://doi.org/10.1016/0014-4894(73)90036-2

Berg, M., Mannaert, A.N., Vanaerschot, M., Der, G.V.A.N., 2013. (Post-) Genomic approaches to tackle drug resistance in *Leishmania*. Parasitology 140, 1492–1505. https://doi.org/10.1017/S0031182013000140

Bergmann, S., Rohde, M., Hammerschmidt, S., 2004. Glyceraldehyde-3-Phosphate Dehydrogenase of *Streptococcus pneumoniae* Is A Surface-Displayed Plasminogen-Binding Protein. Infect. Immun. 72, 2416–2419. https://doi.org/10.1128/IAI.72.4.2416-2419.2004

Bergquist, N.R., 1998. Schistosomiasis Vaccine Development: Progress and Prospects. Mem. Inst. Oswaldo Cruz 93, 95–101. https://doi.org/10.1590/S0074-02761998000700013

Bernal, D., Carpena, I., Espert, A.M., De La Rubia, J.E., Esteban, J.G., Toledo, R., Marcilla, A., 2006. Identification of proteins in excretory/secretory extracts of *Echinostoma friedi* (Trematoda) from chronic and acute infections. Proteomics 6, 2835–2843. https://doi.org/10.1002/pmic.200500571

Bernal, D., De La Rubia, J.E., Carrasco-Abad, A.M., Toledo, R., Mas-Coma, S., Marcilla, A., 2004. Identification of enolase as a plasminogen-binding protein in excretory-secretory products of *Fasciola hepatica*. FEBS Lett. 563, 203–206. https://doi.org/10.1016/S0014-5793(04)00306-0

Besier, B., Lyon, J., Michael, D., Fitzpatrick, J., Michael, G., Smith, D., 2013. Barbervax, a potential commercial vaccine for *Haemonchus contortus*: manufacture and field efficacy trials in Western Australia, in: Proceedings of the WAAVP Congress. WAAVP Congress, pp. 25–29.

Bethony, J.M., Cole, R.N., Guo, X., Kamhawi, S., Lightowlers, M.W., Loukas, A., Petri, W., Reed, S., Valenzuela, J.G., Hotez, P.J., 2011. Vaccines to combat the neglected tropical diseases. Immunol. Rev. 239, 237–270. https://doi.org/10.1111/j.1600-065X.2010.00976.x

Betts, M.J., Russell, R.B., 2007. Amino-Acid Properties and Consequences of Substitutions, in: Bioinformatics for Geneticists: A Bioinformatics Primer for the Analysis of Genetic Data: Second Edition. pp. 311–342. https://doi.org/10.1002/9780470059180.ch13

Björkblom, B., Adilbayeva, A., Maple-Grødem, J., Piston, D., Ökvist, M., Xu, X.M., Brede, C., Larsen, J.P., Møller, S.G., 2013. Parkinson disease protein DJ-1 binds metals and protects against metal-induced cytotoxicity. J. Biol. Chem. 288, 22809–22820. https://doi.org/10.1074/jbc.M113.482091

Björkblom, B., Maple-Grødem, J., Puno, M.R., Odell, M., Larsen, J.P., Møller, S.G., 2014. Reactive Oxygen Species-Mediated DJ-1 Monomerization Modulates Intracellular Trafficking Involving Karyopherin β2. Mol. Cell. Biol. 34, 3024–3040. https://doi.org/10.1128/MCB.00286-14

Bonifati, V., Rizzu, P., van Baren, M.J., Schaap, O., Breedveld, G.J., Krieger, E., Dekker, M.C.J., Squitieri, F., Ibanez, P., Joosse, M., van Dongen, J.W., Vanacore, N., van Swieten, J.C., Brice, A., Meco, G., van Duijn, C.M., Oostra, B.A., Heutink, P., 2003. Mutations in the DJ-1 gene associated with autosomal recessive early-onset parkinsonism. Science (80-.). 299, 256–259. https://doi.org/10.1126/science.1077209

Boray, J.C., 1997. Chemotherapy of infections with Fasciolidae. Immunol. Pathobiol. Control Fasciolosis. New Jersey MSD AGVET Rahw.

Boray, J.C., 1978. The potential impact of exotic *Lymnaea spp*. on fascioliasis in Australasia. Vet. Parasitol. 4, 127–141. https://doi.org/10.1016/0304-4017(78)90004-3

Boray, J.C., 1969. Experimental Fascioliasis in Australia. Adv. Parasitol. Volume 7, 95–210. https://doi.org/http://dx.doi.org/10.1016/S0065-308X(08)60435-2

Boray, J.C., Crowfoot, P.D., Strong, M.B., Allison, J.R., Schellenbaum, M., Von Orelli, M., Sarasin, G., 1983. Treatment of immature and mature *Fasciola hepatica* infections in sheep with triclabendazole. Vet. Rec. 113, 315–317.

Boray, J.C., Enigk, K., 1964. Laboratory studies on the survival and infectivity of Fasciola hepatica- and F. gigantica-metzcei-cariae. Z. Tropenmed. Parasitol. 15, 324–331.

Boray, J.C., Love, S., 2007. Liver fluke disease in sheep and cattle. Dep. Prim. Ind. https://doi.org/ISSN 1832 6668

Borchert, T. V., Abagyan, R.A., Kishan, K.V.R., Zeelen, J.P., Wierenga, R.K., 1993a. The crystal structure of an engineered monomeric triosephosphate isomerase, monoTIM: the correct modelling of an eight-residue loop. Structure 1, 205–213. https://doi.org/10.1016/0969-2126(93)90021-8

Borchert, T. V., Pratt, K., Zeelen, J.P., Callens, M., Noble, M.E.M., Opperdoes, F.R., Michels, P.A.M., Wierenga, R.K., 1993b. Overexpression of trypanosomal triosephosphate isomerase in *Escherichia coli* and characterisation of a dimer-interface mutant. Eur. J.

Biochem. 211, 703–710. https://doi.org/10.1111/j.1432-1033.1993.tb17599.x
Borgsteede, F.H.M., Moll, L., Vellema, P., 2005. Lack of reversion in triclabendazole resistant *Fasciola hepatica*. Vet. Rec. 156, 350–351.
Borgsteede, F.H.M., Taylor, S.M., Gaasenbeek, C.P.H., Couper, A., Cromie, L., 2008. The efficacy of an ivermectin / closantel injection against experimentally induced infections and field infections with gastrointestinal nematodes and liver fluke in cattle. Vet. Parasitol. 155, 235–241. https://doi.org/10.1016/j.vetpar.2008.05.004
Bouchet, F., Guidon, N., Dittmar, K., Harter, S., Ferreira, F., Chaves, S.M., Reinhard, K., Araújo, A., 2003. Parasite remains in archaeological sites. Mem. Inst. Oswaldo Cruz 98, 47–52.
Boyce, W.M., Courtney, C.H., Loggins, P.E., 1987. Resistance to experimental infection with Fasciola hepatica in exotic and domestic breeds of sheep. Int. J. Parasitol. 17, 1233–1237. https://doi.org/10.1016/0020-7519(87)90087-7
Bradford, M.M., 1976. A rapid and sensitive method for the quantitation of microgram quantities of protein using the principle of protein dye binding. Anal. Biochem. 72, 248–254. https://doi.org/10.1016/0003-2697(76)90527-3
Brady, C.P., Dowd, A.J., Tort, J., Roche, L., Condon, B., O'Neill, S.M., Brindley, P.J., Dalton, J.P., 1999. The cathepsin L-like proteinases of liver fluke and blood fluke parasites of the trematode genera *Fasciola* and *Schistosoma*. Biochem. Soc. Trans. 27, 740–745.
Brändén, C.I., 1991. The TIM barrel-the most frequently occurring folding motif in proteins. Curr. Opin. Struct. Biol. 1, 978–983. https://doi.org/10.1016/0959-440X(91)90094-A
Braun, U., Wolfensberger, R., Hertzberg, H., 1995. Diagnosis of liver flukes in cows--a comparison of the findings in the liver, in the feces, and in the bile. Schweiz. Arch. Tierheilkd. 137, 438–444.
Brennan, G.P., Fairweather, I., Trudgett, A., Hoey, E., Mccoy, M., McConville, M., Meaney, M., Robinson, M.W., McFerran, N., Ryan, L., Lanusse, C., Mottier, L., Alvarez, L.I., Solana, H., Virkel, G., Brophy, P.M., 2007. Understanding triclabendazole resistance. Exp. Mol. Pathol. 82, 104–109. https://doi.org/10.1016/j.yexmp.2007.01.009
Breslauer, K.J., Frank, R., Blocker, H., Marky, L.A., 1986. Predicting DNA duplex stability from the base sequence. Proc. Natl. Acad. Sci. U. S. A. 83, 3746–3750. https://doi.org/10.1073/pnas.83.11.3746
Brewer, J.M., 1981. Yeast enolase: Mechanism of activation by metal ion. Crit. Rev. Biochem. Mol. Biol. 11, 209–254. https://doi.org/10.3109/10409238109108702
Brewer, J.M., Glover, C. V., Holland, M.J., Lebioda, L., 1998. Significance of the enzymatic properties of yeast S39A enolase to the catalytic mechanism. Biochim. Biophys. Acta - Protein Struct. Mol. Enzymol. 1383, 351–355. https://doi.org/10.1016/S0167-4838(98)00004-1
Brewer, J.M., Glover, C. V., Holland, M.J., Lebioda, L., 1997. Effect of site-directed mutagenesis of His373 of yeast enolase on some of its physical and enzymatic properties. Biochim. Biophys. Acta - Protein Struct. Mol. Enzymol. 1340, 88–96. https://doi.org/10.1016/S0167-4838(97)00029-0
Brockwell, Y.M., Elliott, T.P., Anderson, G.R., Stanton, R., Spithill, T.W., Sangster, N.C., 2014. Confirmation of *Fasciola hepatica* resistant to triclabendazole in naturally infected Australian beef and dairy cattle. Int. J. Parasitol. Drugs Drug Resist. 4, 48–54. https://doi.org/http://dx.doi.org/10.1016/j.ijpddr.2013.11.005
Brockwell, Y.M., Spithill, T.W., Anderson, G.R., Grillo, V., Sangster, N.C., 2013. Comparative kinetics of serological and coproantigen ELISA and faecal egg count in cattle experimentally infected with *Fasciola hepatica* and following treatment with

triclabendazole. Vet. Parasitol. 196, 417–426. https://doi.org/10.1016/j.vetpar.2013.04.012
Brophy, P.M., Mackintosh, N., Morphew, R.M., 2012. Anthelmintic metabolism in parasitic helminths: proteomic insights. Parasitology 139, 1205–1217. https://doi.org/10.1017/S003118201200087X
Brophy, P.M., Patterson, L.H., Brown, A., Pritchard, D.I., 1995. Glutathione S-transferase (GST) expression in the human hookworm *Necator americanus*: potential roles for excretory-secretory forms of GST. Acta Trop. 59, 259–263. https://doi.org/10.1016/0001-706X(95)00084-R
Burtnick, L.D., Koepf, E.K., Grimes, J., Jones, E.Y., Stuart, D.I., McLaughlin, P.J., Robinson, R.C., 1997. The crystal structure of plasma gelsolin: Implications for actin severing, capping, and nucleation. Cell 90, 661–670. https://doi.org/10.1016/S0092-8674(00)80527-9
Burtnick, L.D., Urosev, D., Irobi, E., Narayan, K., Robinson, R.C., 2004. Structure of the N-terminal half of gelsolin bound to actin: Roles in severing, apoptosis and FAF. EMBO J. 23, 2713–2722. https://doi.org/10.1038/sj.emboj.7600280
Butler, L.E., Thomassen, D., Martin, J.L., Martin, B.M., Kenna, J.G., Pohl, L.R., 1992. The calcium-binding protein calreticulin is covalently modified in rat liver by a reactive metabolite of the inhalation anesthetic halothane. Chem. Res. Toxicol. 5, 406–410.
Cabada, M.M., White, A.C., 2012. New developments in epidemiology, diagnosis, and treatment of fascioliasis. Curr. Opin. Infect. Dis. 25, 518–22.
Cabezón, C., Cabrera, G., Paredes, R., Ferreira, A., Galanti, N., 2008. *Echinococcus granulosus* calreticulin: Molecular characterization and hydatid cyst localization. Mol. Immunol. 45, 1431–1438. https://doi.org/10.1016/j.molimm.2007.08.022
Caffrey, C.R., Goupil, L., Rebello, K.M., Dalton, J.P., Smith, D., 2018. Cysteine proteases as digestive enzymes in parasitic helminths. PLoS Negl. Trop. Dis. 12, e0005840. https://doi.org/10.1371/journal.pntd.0005840
Callahan, H.L., Crouch, R.K., James, E.R., 1988. Helminth anti-oxidant enzymes: a protective mechanism against host oxidants? Parasitol. Today. https://doi.org/10.1016/0169-4758(88)90162-7
Camargo de Lima, J., Monteiro, K.M., Basika Cabrera, T.N., Paludo, G.P., Moura, H., Barr, J.R., Zaha, A., Ferreira, H.B., 2018. Comparative proteomics of the larval and adult stages of the model cestode parasite *Mesocestoides corti*. J. Proteomics 175, 127–135. https://doi.org/10.1016/j.jprot.2017.12.022
Cameron, T.C., Cooke, I., Faou, P., Toet, H., Piedrafita, D., Young, N., Rathinasamy, V., Beddoe, T., Anderson, G.R., Dempster, R., Spithill, T.W., 2017. A novel *ex vivo* immunoproteomic approach characterising *Fasciola hepatica* tegumental antigens identified using immune antibody from resistant sheep. Int. J. Parasitol. 47, 555–567. https://doi.org/10.1016/j.ijpara.2017.02.004
Campbell, S., Landry, M.L., 2013. Rapid Antigen Tests, in: Advanced Techniques in Diagnostic Microbiology. Springer US, Boston, MA, pp. 31–51. https://doi.org/10.1007/978-1-4614-3970-7_3
Cancela, M., Acosta, D., Rinaldi, G., Silva, E., Durán, R., Roche, L., Zaha, A., Carmona, C., Tort, J.F., 2008. A distinctive repertoire of cathepsins is expressed by juvenile invasive *Fasciola hepatica*. Biochimie 90, 1461–1475. https://doi.org/http://dx.doi.org/10.1016/j.biochi.2008.04.020
Cancela, M., Ruétalo, N., Oca, N.D., Silva, E., Smircich, P., Rinaldi, G., Roche, L., Carmona, C., Alvarez-Valín, F., Zaha, A., Tort, J.F., 2010. Survey of transcripts expressed by the invasive

juvenile stage of the liver fluke *Fasciola hepatica*. BMC Genomics 11, 227–241.
Canevari, J., Ceballos, L., Sanabria, R., Romero, J., Olaechea, F., Ortiz, P., Cabrera, M., Gayo, V., Fairweather, I., Lanusse, C., Alvarez, L.I., 2014. Testing albendazole resistance in *Fasciola hepatica*: validation of an egg hatch test with isolates from South America and the United Kingdom. J. Helminthol. 88, 286–292. https://doi.org/10.1017/S0022149X13000163
Carmona, C., Dowd, A.J., Smith, A.M., Dalton, J.P., 1993. Cathepsin L proteinase secreted by Fasciola hepatica in vitro prevents antibody-mediated eosinophil attachment to newly excysted juveniles. Mol. Biochem. Parasitol. 62, 9–17. https://doi.org/http://dx.doi.org/10.1016/0166-6851(93)90172-T
Carnevale, S., Rodrı, I., Guarnera, E.A., Carmona, C., Tanos, T., Angel, S.O., 2001. Immunodiagnosis of fasciolosis using recombinant procathepsin L cystein proteinase. Diagn. Microbiol. Infect. Dis. 41, 43–49.
Caron, Y., Rondelaud, D., Losson, B., 2008. The detection and quantification of a digenean infection in the snail host with special emphasis on *Fasciola sp* . Parasitol. Res. 103, 735–744. https://doi.org/10.1007/s00436-008-1086-1
Castro, G.A., 1996. Chapter 86 Helminths: structure, classification, growth, and development, in: Medical Microbiology 4th Edition. University of Texas Medical Branch at Galveston.
Cawdery, M.J., Stirckland, K.L., Conway, A., Crowe, P.J., 1977. Production effects of liver fluke in cattle. I. The effects of infection on liveweight gain, feed intake and food conversion efficienty in beef cattle. Br. Vet. J. 133, 149–59.
Ceballos, L., Moreno, L., Alvarez, L.I., Shaw, L., Fairweather, I., Lanusse, C., 2010. Unchanged triclabendazole kinetics after co-administration with ivermectin and methimazole: Failure of its therapeutic activity against triclabendazole-resistant liver flukes. BMC Vet. Res. 6, 1–8. https://doi.org/10.1186/1746-6148-6-8
Celotto, A.M., Frank, A.C., Seigle, J.L., Palladino, M.J., 2006. Drosophila model of human inherited triosephosphate isomerase deficiency glycolytic enzymopathy. Genetics 174, 1237–1246. https://doi.org/10.1534/genetics.106.063206
Cervi, L., Rossi, G., Masih, D.T., 1999. Potential role for excretory-secretory forms of glutathione-S-transferase (GST) in *Fasciola hepatica*. Parasitology 119, 627–633. https://doi.org/10.1017/S003118209900517X
Cevallos, A.M., Segura-Kato, Y.X., Merchant-Larios, H., Manning-Cela, R., Alberto Hernández-Osorio, L., Márquez-Dueñas, C., Ambrosio, J.R., Reynoso-Ducoing, O., Hernández, R., 2011. *Trypanosoma cruzi*: Multiple actin isovariants are observed along different developmental stages. Exp. Parasitol. 127, 249–259. https://doi.org/10.1016/j.exppara.2010.08.003
Chaikuad, A., Shafqat, N., Al-Mokhtar, R., Cameron, G., Clarke, A.R., Brady, R.L., Oppermann, U., Frayne, J., Yue, W.W., 2011. Structure and kinetic characterization of human sperm-specific glyceraldehyde-3-phosphate dehydrogenase, GAPDS. Biochem. J. 435, 401–409. https://doi.org/10.1042/BJ20101442
Chambers, S.P., Swalley, S.E., 2009. Designing Experiments for High-Throughput Protein Expression, in: Doyle, S.A. (Ed.), High Throughput Protein Expression and Purification. Humana Press, pp. 19–29. https://doi.org/10.1007/978-1-59745-196-3
Chand, M.A., Herman, J.S., Partridge, D.G., Hewitt, K., Chiodini, P.L., 2009. Imported Human Fascioliasis, United Kingdom. Emerg. Infect. Dis. 15, 1876–1877. https://doi.org/10.3201/eid1511.090511
Chang, A.C.G., Flores, M.J.C., 2015. Morphology and viability of adult *Fasciola gigantica* (giant

liver flukes) from Philippine carabaos (*Bubalus bubalis*) upon in vitro exposure to lead. Asian Pac. J. Trop. Biomed. 5, 493–496. https://doi.org/10.1016/j.apjtb.2015.03.008

Charette, B.D., MacDonald, R.G., Wetzel, S., Berkowitz, D.B., Waldmann, H., 2006. Protein structure similarity clustering: Dynamic treatment of PDB structures facilitates clustering. Angew. Chemie - Int. Ed. 45, 7766–7770. https://doi.org/10.1002/anie.200602125

Charlier, J., De Cat, A., Forbes, A., Vercruysse, J., 2009. Measurement of antibodies to gastrointestinal nematodes and liver fluke in meat juice of beef cattle and associations with carcass parameters. Vet. Parasitol. 166, 235–240. https://doi.org/10.1016/j.vetpar.2009.09.040

Charlier, J., Duchateau, L., Claerebout, E., Williams, D., Vercruysse, J., 2007. Associations between anti-*Fasciola hepatica* antibody levels in bulk-tank milk samples and production parameters in dairy herds. Prev. Vet. Med. 78, 56–66. https://doi.org/10.1016/j.prevetmed.2006.09.010

Charlier, J., Ghebretinsae, A.H., Levecke, B., Ducheyne, E., Claerebout, E., Vercruysse, J., 2016. Climate-driven longitudinal trends in pasture-borne helminth infections of dairy cattle. Int. J. Parasitol. 46, 881–888. https://doi.org/10.1016/j.ijpara.2016.09.001

Charlier, J., Hostens, M., Jacobs, J., van Ranst, B., Duchateau, L., Vercruysse, J., 2012. Integrating fasciolosis control in the dry cow management: The effect of closantel treatment on milk production. PLoS One 7, e43216. https://doi.org/10.1371/journal.pone.0043216

Charlier, J., Meulemeester, L. De, Claerebout, E., 2008. Qualitative and quantitative evaluation of coprological and serological techniques for the diagnosis of fasciolosis in cattle. Vet. J. 153, 44–51. https://doi.org/10.1016/j.vetpar.2008.01.035

Charlier, J., van der Voort, M., Kenyon, F., Skuce, P., Vercruysse, J., 2014a. Chasing helminths and their economic impact on farmed ruminants. Trends Parasitol. 30, 361–367. https://doi.org/10.1016/j.pt.2014.04.009

Charlier, J., Vercruysse, J., Morgan, E., van Dijk, J., Williams, D.J.L., 2014b. Recent advances in the diagnosis, impact on production and prediction of *Fasciola hepatica* in cattle. Parasitology 141, 326–335. https://doi.org/10.1017/S0031182013001662

Chemale, G., Morphew, R.M., Moxon, J. V., Morassuti, A.L., LaCourse, E.J., Barrett, J., Johnston, D.A., Brophy, P.M., 2006. Proteomic analysis of glutathione transferases from the liver fluke parasite, *Fasciola hepatica*. Proteomics 6, 6263–6273. https://doi.org/10.1002/pmic.200600499

Chemale, G., Perally, S., Lacourse, E.J., Prescott, M.C., Jones, L.M., Ward, D., Meaney, M., Hoey, E., Brennan, G.P., Fairweather, I., Trudgett, A., Brophy, P.M., 2010. Comparative proteomic analysis of triclabendazole response in the liver fluke *Fasciola hepatica*. J. Proteome Res. 9, 4940–4951. https://doi.org/10.1021/pr1000785

Chen, X., Li, S., He, L., Wang, X., Liang, P., Chen, W., Bian, M., Ren, M., Lin, J., Liang, C., Xu, J., Wu, Z., Li, X., Huang, Y., Yu, X., 2013. Molecular Characterization of Severin from *Clonorchis sinensis* Excretory/Secretory Products and Its Potential Anti-apoptotic Role in Hepatocarcinoma PLC Cells. PLoS Negl. Trop. Dis. 7, e2606. https://doi.org/10.1371/journal.pntd.0002606

Chiodini, P.L., Moody, A.H., Manser, D.W., 2003. Atlas of Medical Helminthology and Protozoology, Fourth Edition.

Choe, H., Burtnick, L.D., Mejillano, M., Yin, H.L., Robinson, R.C., Choe, S., 2002. The calcium activation of gelsolin: Insights from the 3 Å structure of the G4-G6/actin complex. J. Mol.

Biol. 324, 691–702. https://doi.org/10.1016/S0022-2836(02)01131-2
Choi, Y., 2012. A fast computation of pairwise sequence alignment scores between a protein and a set of single-locus variants of another protein, in: 2012 ACM Conference on Bioinformatics, Computational Biology and Biomedicine, BCB 2012. pp. 414–417. https://doi.org/10.1145/2382936.2382989
Choi, Y., Sims, G.E., Murphy, S., Miller, J.R., Chan, A.P., 2012. Predicting the Functional Effect of Amino Acid Substitutions and Indels. PLoS One 7, e46688. https://doi.org/10.1371/journal.pone.0046688
Chou, H.C., Chen, J.Y., Lin, D.Y., Wen, Y.F., Lin, C.C., Lin, S.H., Lin, C.H., Chung, T.W., Liao, E.C., Chen, Y.J., Wei, Y.S., Tsai, Y.T., Chan, H.L., 2015. Identification of up- and down-regulated proteins in pemetrexed-resistant human lung adenocarcinoma: Flavin reductase and calreticulin play key roles in the development of pemetrexed-associated resistance. J. Proteome Res. 14, 4907–4920. https://doi.org/10.1021/acs.jproteome.5b00794
Christofidou-Solomidou, M., Scherpereel, A., Solomides, C.C., Christie, J.D., Stossel, T.P., Goelz, S., DiNubile, M.J., 2002. Recombinant plasma gelsolin diminishes the acute inflammatory response to hyperoxia in mice. J. Investig. Med. 50, 54–60. https://doi.org/10.2310/6650.2002.33518
Chumnarnsilpa, S., Robinson, R.C., Grimes, J.M., Leyrat, C., 2015. Calcium-controlled conformational choreography in the N-terminal half of adseverin. Nat. Commun. 6, 8254. https://doi.org/10.1038/ncomms9254
Claridge, J., Diggle, P., McCann, C.M., Mulcahy, G., Flynn, R., McNair, J., Strain, S., Welsh, M., Baylis, M., Williams, D.J.L., 2012. *Fasciola hepatica* is associated with the failure to detect bovine tuberculosis in dairy cattle. Nat. Commun. 3, 853. https://doi.org/10.1038/ncomms1840
Claxton, J.R., Sutherst, J., Ortiz, P., Clarkson, M.J., 1999. The effect of cyclic temperatures on the growth of *Fasciola hepatica* and *Lymnaea viatrix*. Vet. J. 157, 166–171. https://doi.org/10.1053/tvjl.1998.0293
Coakley, G., Maizels, R.M., Buck, A.H., 2015. Exosomes and Other Extracellular Vesicles: The New Communicators in Parasite Infections. Trends Parasitol. https://doi.org/10.1016/j.pt.2015.06.009
Coakley, G., McCaskill, J.L., Borger, J.G., Simbari, F., Robertson, E., Millar, M., Harcus, Y., McSorley, H.J., Maizels, R.M., Buck, A.H., 2017. Extracellular Vesicles from a Helminth Parasite Suppress Macrophage Activation and Constitute an Effective Vaccine for Protective Immunity. Cell Rep. 19, 1545–1557. https://doi.org/10.1016/j.celrep.2017.05.001
Coffeng, L.E., Stolk, W.A., Zouré, H.G.M., Veerman, J.L., Agblewonu, K.B., Murdoch, M.E., Noma, M., Fobi, G., Richardus, J.H., Bundy, D.A.P., Habbema, D., De Vlas, S.J., Amazigo, U. V., 2013. African Programme for Onchocerciasis Control 1995-2015: Model-Estimated Health Impact and Cost. PLoS Negl. Trop. Dis. 7, e2032. https://doi.org/10.1371/journal.pntd.0002032
Coles, G.C., Bauer, C., Borgsteede, F.H.M., Geerts, S., Klei, T.R., Taylor, M.A., Waller, P.J., 1992. World Association for the Advancement of Veterinary Parasitology (W.A.A.V.P.) methods for the detection of anthelmintic resistance in nematodes of veterinary importance. Vet. Parasitol. 44, 35–44. https://doi.org/10.1016/0304-4017(92)90141-U
Coles, G.C., Jackson, F., Pomroy, W.E., Prichard, R.K., Von Samson-Himmelstjerna, G., Silvestre, A., Taylor, M.A., Vercruysse, J., 2006. The detection of anthelmintic resistance in nematodes of veterinary importance. Vet. Parasitol.

https://doi.org/10.1016/j.vetpar.2005.11.019
Coles, G.C., Rhodes, A.C., Stafford, K.A., 2000. Activity of closantel against adult resistant *Fasciola hepatica*. Vet. Rec. 146, 504. https://doi.org/10.1136/vr.146.17.504-a
Coles, G.C., Stafford, K.A., 2001. Activity of oxyclozanide, nitroxynil, clorsulon and albendazole against adult triclabendazole-resistant *Fasciola hepatica*. Vet. Rec. 148, 723–724. https://doi.org/10.1136/vr.148.23.723
Collins, P.R., Stack, C.M., O'Neill, S.M., Doyle, S., Ryan, T., Brennan, G.P., Mousley, A., Stewart, M., Maule, A.G., Dalton, J.P., Donnelly, S.M., 2004. Cathepsin L1, the major protease involved in liver fluke (*Fasciola hepatica*) virulence: Propeptide cleavage sites and autoactivation of the zymogen secreted from gastrodermal cells. J. Biol. Chem. 279, 17038–17046. https://doi.org/10.1074/jbc.M308831200
Cooper, J.A., Buhle, E.L., Walker, S.B., Tsong, T.Y., Pollard, T.D., 1983. Kinetic Evidence for a Monomer Activation Step in Actin Polymerization. Biochemistry 22, 2193–2202. https://doi.org/10.1021/bi00278a021
Cordova, M., Jara, J., Del Nery, E., Hirata, I.Y., Araújo, M.S., Carmona, A.K., Juliano, M.A., Juliano, L., 2001. Characterization of two cysteine proteinases secreted by *Fasciola hepatica* and demonstration of their kininogenase activity. Mol. Biochem. Parasitol. 116, 109–115. https://doi.org/10.1016/S0166-6851(01)00309-7
Cornelissen, J.B.W.J., Gaasenbeek, C.P.. H., Boersma, W., Borgsteede, F.H.M., van Milligen, F.J., 1999. Use of a pre-selected epitope of cathepsin-L1 in a highly specific peptide-based immunoassay for the diagnosis of *Fasciola hepatica* infections in cattle. Int. J. Parasitol. 29, 685–696. https://doi.org/10.1016/S0020-7519(99)00017-X
Cornelissen, J.B.W.J., Gaasenbeek, C.P.H., Borgsteede, F.H.M., Holland, W.G., Harmsen, M.M., Boersma, W.J.A., 2001. Early immunodiagnosis of fasciolosis in ruminants using recombinant *Fasciola hepatica* cathepsin L-like protease. Int. J. Parasitol. 31, 728–737. https://doi.org/10.1016/S0020-7519(01)00175-8
Correa, A.C., Escobar, J.S., Durand, P., Renaud, F., David, P., Jarne, P., 2010. Bridging gaps in the molecular phylogeny of the Lymnaeidae (Gastropoda: Pulmonata), vectors of Fascioliasis. BMC Evol. Biol. 10, 381. https://doi.org/10.1186/1471-2148-10-381
Correa, A.C., Escobar, J.S., Noya, O., Velásquez, L.E., González-ramírez, C., 2011. Infection , Genetics and Evolution Morphological and molecular characterization of Neotropic Lymnaeidae (Gastropoda: Lymnaeidae), vectors of fasciolosis. Infect. Genet. Evol. 11, 1978–1988. https://doi.org/10.1016/j.meegid.2011.09.003
Corvo, I., Cancela, M., Cappetta, M., Pi-Denis, N., Tort, J.F., Roche, L., 2009. The major cathepsin L secreted by the invasive juvenile *Fasciola hepatica* prefers proline in the S2 subsite and can cleave collagen. Mol. Biochem. Parasitol. 167, 41–47. https://doi.org/10.1016/j.molbiopara.2009.04.005
Corvo, I., O'Donoghue, A.J., Pastro, L., Pi-Denis, N., Eroy-Reveles, A., Roche, L., McKerrow, J.H., Dalton, J.P., Craik, C.S., Caffrey, C.R., Tort, J.F., 2013. Dissecting the Active Site of the Collagenolytic Cathepsin L3 Protease of the Invasive Stage of *Fasciola hepatica*. PLoS Negl. Trop. Dis. 7, 1–11. https://doi.org/10.1371/journal.pntd.0002269
Coulombe, R., Grochulski, P., Sivaraman, J., Ménard, R., Mort, J.S., Cygler, M., 1996. Structure of human procathepsin L reveals the molecular basis of inhibition by the prosegment. EMBO J. 15, 5492–5503. https://doi.org/066/14
Creaney, J., Wijffels, G.L., Sexton, J.L., Sandeman, R.M., Spithill, T.W., Parsons, J.C., 1995. *Fasciola hepatica*: Localization of Glutathione S-Transferase Isoenzymes in Adult and Juvenile Liver Fluke. Exp. Parasitol. 81, 106–116.

https://doi.org/10.1006/expr.1995.1098
Crofton, H.D., 1971. A Quantitative Approach to Parasitism. Parasitology 62, 179–193. https://doi.org/10.1017/S0031182000071420
Crowther, G.J., Shanmugam, D., Carmona, S.J., Doyle, M.A., Hertz-Fowler, C., Berriman, M., Nwaka, S., Ralph, S.A., Roos, D.S., van Voorhis, W.C., Agüero, F., 2010. Identification of attractive drug targets in neglected- disease pathogens using an *in silico* approach. PLoS Negl. Trop. Dis. 4, e408. https://doi.org/10.1371/journal.pntd.0000804
Cuesta-Astroz, Y., Oliveira, F.S. de, Nahum, L.A., Oliveira, G., 2017. Helminth secretomes reflect different lifestyles and parasitized hosts. Int. J. Parasitol. 47, 529–544. https://doi.org/10.1016/j.ijpara.2017.01.007
Cunningham, C.C., Stossel, T.P., Kwiatkowski, D.J., 1991. Enhanced motility in NIH 3T3 fibroblasts that overexpress gelsolin. Science (80-.). 251, 1233–1236. https://doi.org/10.1126/science.1848726
Cwiklinski, K., Allen, K., LaCourse, E.J., Williams, D.J.L., Paterson, S., Hodgkinson, J.E., 2015a. Characterisation of a novel panel of polymorphic microsatellite loci for the liver fluke, *Fasciola hepatica*, using a next generation sequencing approach. Infect. Genet. Evol. 32, 298–304. https://doi.org/10.1016/j.meegid.2015.03.014
Cwiklinski, K., Dalton, J.P., Dufresne, P.J., La Course, J., Williams, D.J.L., Hodgkinson, J., Paterson, S., 2015b. The *Fasciola hepatica* genome: Gene duplication and polymorphism reveals adaptation to the host environment and the capacity for rapid evolution. Genome Biol. 16, 71–84. https://doi.org/10.1186/s13059-015-0632-2
Cwiklinski, K., De Torre-escudero, E., Trelis, M., Bernal, D., Dufresne, P.J., Brennan, G.P., Neill, S.O., Tort, J., Paterson, S., Marcilla, A., Dalton, J.P., Robinson, M.W., 2015c. The extracellular vesicles of the helminth pathogen, *Fasciola hepatica*: biogenesis pathways and cargo molecules involved in parasite pathogenesis. Mol. Cell. Proteomics 14, 3258–3273. https://doi.org/10.1074/mcp.M115.053934
Cwiklinski, K., Jewhurst, H., McVeigh, P., Barbour, T., Maule, A.G., Tort, J., O'Neill, S.M., Robinson, M.W., Donnelly, S.M., Dalton, J.P., 2018. Infection by the helminth parasite *Fasciola hepatica* requires rapid regulation of metabolic, virulence, and invasive factors to adjust to its mammalian host. Mol. Cell. Proteomics 17, 792–809. https://doi.org/10.1074/mcp.RA117.000445
D'Aguanno, S., D'Alessandro, A., Pieroni, L., Roveri, A., Zaccarin, M., Marzano, V., De Canio, M., Bernardini, S., Federici, G., Urbani, A., 2011. New insights into neuroblastoma cisplatin resistance: A comparative proteomic and meta-mining investigation. J. Proteome Res. 10, 416–428. https://doi.org/10.1021/pr100457n
Daar, I.O., Artymiuk, P.J., Phillips, D.C., Maquat, L.E., 1986. Human triose-phosphate isomerase deficiency: a single amino acid substitution results in a thermolabile enzyme. Proc. Natl. Acad. Sci. U. S. A. 83, 7903–7907. https://doi.org/10.1073/pnas.83.20.7903
Dalton, J.P., Heffernan, M., 1989. Thiol proteases released in vitro by *Fasciola hepatica*. Mol. Biochem. Parasitol. 35, 161–166. https://doi.org/10.1016/0166-6851(89)90118-7
Dalton, J.P., McGonigle, S., Rolph, T.P., Andrews, S.J., 1996. Induction of protective immunity in cattle against infection with *Fasciola hepatica* by vaccination with cathepsin L proteinases and with hemoglobin. Infect. Immun. 64, 5066–5074.
Dalton, J.P., Mulcahy, G., 2001. Parasite vaccines — a reality ? Vet. Parasitol. 98, 149–167.
Dalton, J.P., Neill, S.O., Stack, C., Collins, P.R., Walshe, A., Sekiya, M., Doyle, S., Mulcahy, G., Hoyle, D., Khaznadji, E., Moiré, N., Brennan, G.P., Mousley, A., Kreshchenko, N., Maule, A.G., Donnelly, S.M., 2003. *Fasciola hepatica* cathepsin L-like proteases: biology,

function, and potential in the development of first generation liver fluke vaccines. Int. J. Parasitol. 33, 1173–1181. https://doi.org/10.1016/S0020-7519(03)00171-1

Dalton, J.P., Robinson, M.W., Mulcahy, G., Neill, S.M.O., Donnelly, S.M., 2013. Immunomodulatory molecules of *Fasciola hepatica*: Candidates for both vaccine and immunotherapeutic development. Vet. Parasitol. 195, 272–285. https://doi.org/10.1016/j.vetpar.2013.04.008

Dalton, J.P., Skelly, P., Halton, D.W., 2004. Role of the tegument and gut in nutrient uptake by parasitic platyhelminths. Can. J. Zool. 82, 211–232. https://doi.org/10.1139/z03-213

Daniel, R., van Dijk, J., Jenkins, T., Akca, A., Mearns, R., Williams, D.J.L., 2012. A composite faecal egg count reduction test to detect resistance to triclabendazole in *Fasciola hepatica*. Vet. Rec. 171, 153–158. https://doi.org/10.1136/vr.100588

Dastoor, Z., Dreyer, J.L., 2001. Potential role of nuclear translocation of glyceraldehyde-3-phosphate dehydrogenase in apoptosis and oxidative stress. J. Cell Sci. 114, 1643–1653.

Davis, C.N., Phillips, H., Tomes, J.J., Swain, M.T., Wilkinson, T.J., Brophy, P.M., Morphew, R.M., 2019. The importance of extracellular vesicle purification for downstream analysis: A comparison of differential centrifugation and size exclusion chromatography for helminth pathogens. PLoS Negl. Trop. Dis. 13, e0007191. https://doi.org/10.1371/journal.pntd.0007191

Dawes, B., 1963. The migration of juvenile forms of *Fasciola hepatica L.* through the wall of the intestines in the mouse, with some observations on food and feeding. Parasitology 53, 109–122. https://doi.org/10.1017/S0031182000072589

Dawes, B., 1962a. On the Growth and Maturation of *Fasciola hepatica L.* in the Mouse. J. Helminthol. 36, 11–38. https://doi.org/10.1017/S0022149X00022343

Dawes, B., 1962b. Additional Notes on the Growth of *Fasciola hepatica L*. in the Mouse, with Some Remarks about Recent Researches in Belgium. J. Helminthol. 36, 259–268. https://doi.org/10.1017/S0022149X00023932

Dawes, B., 1961. On the Early Stages of *Fasciola hepatica* Penetrating into the Liver of an Experimental Host, the Mouse: A Histological Picture. J. Helminthol. 35, 41–52. https://doi.org/10.1017/S0022149X00017569

Dawes, B., Hughes, D.L., 1970. Fascioliasis: the Invasive Stages in Mammals, in: Dawes, B.B.T.-A. in P. (Ed.), Advances in Parasitology. Academic Press, pp. 259–274. https://doi.org/https://doi.org/10.1016/S0065-308X(08)60257-2

Dawson, N.L., Lewis, T.E., Das, S., Lees, J.G., Lee, D., Ashford, P., Orengo, C.A., Sillitoe, I., 2017. CATH: An expanded resource to predict protein function through structure and sequence. Nucleic Acids Res. 45, D289–D295. https://doi.org/10.1093/nar/gkw1098

De Bary, A., 1879. Die erscheinung der symbiose: Vortrag gehalten auf der versammlung deutscher naturforscher und aerzte zu cassel. Verlag von Karl J. Trübner, Strassburg.

De la Torre-Escudero, E., Manzano-Román, R., Valero, L., Oleaga, A., Pérez-Sánchez, R., Hernández-González, A., Siles-Lucas, M., 2011. Comparative proteomic analysis of *Fasciola hepatica* juveniles and *Schistosoma bovis* schistosomula. J. Proteomics 74, 1534–1544. https://doi.org/10.1016/j.jprot.2011.05.024

Dedhar, S., 1994. Novel functions for calreticulin: interaction with integrins and modulation of gene expression? Trends Biochem. Sci. 19, 269–271. https://doi.org/10.1016/0968-0004(94)90001-9

Deng, M.H., Zhong, L.Y., Kamolnetr, O., Limpanont, Y., Lv, Z.Y., 2019. Detection of helminths by loop-mediated isothermal amplification assay: A review of updated technology and future outlook. Infect. Dis. Poverty 8, 20. https://doi.org/10.1186/s40249-019-0530-z

Díaz-Ramos, A., Roig-Borrellas, A., García-Melero, A., López-Alemany, R., 2012. α-Enolase, a multifunctional protein: its role on pathophysiological situations. J. Biomed. Biotechnol. 2012, 1–12. https://doi.org/10.1155/2012/156795

DiNubile, M.J., 2008. Plasma gelsolin as a biomarker of inflammation. Arthritis Res. Ther. 10, 124–125. https://doi.org/10.1186/ar2547

Dixit, A.K., Dixit, P., Sharma, R.L., 2008. Immunodiagnostic/protective role of Cathepsin L cysteine proteinases secreted by *Fasciola* species. Vet. Parasitol. 154, 177–184. https://doi.org/http://dx.doi.org/10.1016/j.vetpar.2008.03.017

Dixon, K.E., 1965. The structure and histochemistry of the cyst wall of the metacercaria of *Fasciola hepatica L*. Parasitology 55, 215–226. https://doi.org/10.1017/S0031182000068712

Dominguez, R., 2004. Actin-binding proteins - A unifying hypothesis. Trends Biochem. Sci. 29, 572–578. https://doi.org/10.1016/j.tibs.2004.09.004

Dominguez, R., Holmes, K.C., 2011. Actin structure and function. Annu. Rev. Biophys. 40, 169–86. https://doi.org/10.1146/annurev-biophys-042910-155359

Donnelly, S., O'Neill, S.M., Sekiya, M., Mulcahy, G., Dalton, J.P., 2005. Thioredoxin peroxidase secreted by *Fasciola hepatica* induces the alternative activation of macrophages. Infect. Immun. 73, 166–173. https://doi.org/10.1128/IAI.73.1.166-173.2005

Donnelly, S.M., O'Neill, S.M., Stack, C.M., Robinson, M.W., Turnbull, L., Whitchurch, C., Dalton, J.P., 2010. Helminth cysteine proteases inhibit TRIF-dependent activation of macrophages via degradation of TLR3. J. Biol. Chem. 285, 3383–3392. https://doi.org/10.1074/jbc.M109.060368

Dow, C., Ross, J.G., Todd, J.R., 1968. The histopathology of *Fasciola hepatica* infections in sheep. Parasitology 58, 129–135. https://doi.org/10.1017/S0031182000073480

Dowd, A.J., Dooley, M., Fágáin, C., Dalton, J.P., 2000. Stability studies on the cathepsin L proteinase of the helminth parasite, *Fasciola hepatica*. Enzyme Microb. Technol. 27, 599–604. https://doi.org/10.1016/S0141-0229(00)00259-3

Dowd, A.J., McGonigle, S., Dalton, J.P., 1995. *Fasciola hepatica* Cathepsin L Proteinase Cleaves Fibrinogen and Produces a Novel Type of Fibrin Clot. Eur. J. Biochem. 232, 241–246. https://doi.org/10.1111/j.1432-1033.1995.tb20805.x

Dowd, A.J., Smith, A.M., McGonigle, S., Dalton, J.P., 1994. Purification and characterisation of a second cathepsin L proteinase secreted by the parasitic trematode *Fasciola hepatica*. Eur. J. Biochem. 223, 91–98.

Dowling, D.J., Hamilton, C.M., Donnelly, S.M., La Course, J., Brophy, P.M., Dalton, J.P., O'Neill, S.M., 2010. Major secretory antigens of the Helminth *Fasciola hepatica* activate a suppressive dendritic cell phenotype that attenuates Th17 cells but fails to activate Th2 immune responses. Infect. Immun. 78, 793–801. https://doi.org/10.1128/IAI.00573-09

Dreyfuss, G., Abrous, M., Vignoles, P., Rondelaud, D., 2004. Fasciola hepatica and Paramphistomum daubneyi: Vertical distribution of metacercariae on plants under natural conditions. Parasitol. Res. 94, 70–73. https://doi.org/10.1007/s00436-004-1173-x

Dreyfuss, G., Vignoles, P., Rondelaud, D., 2012. Local adaptation of the trematode *Fasciola hepatica* to the snail *Galba truncatula*. Parasite 19, 271–5. https://doi.org/10.1051/parasite/2012193271

Drozdetskiy, A., Cole, C., Procter, J., Barton, G.J., 2015. JPred4: A protein secondary structure prediction server. Nucleic Acids Res. 43, W389–W394. https://doi.org/10.1093/nar/gkv332

Dutra, L.H., Molento, M.B., Naumann, C.R.C., Biondo, A.W., Fortes, F.S., Savio, D., Malone, J.B., 2010. Mapping risk of bovine fasciolosis in the south of Brazil using geographic information systems. Vet. Parasitol. 169, 76–81. https://doi.org/10.1016/j.vetpar.2009.12.015

Eggleton, P., Lieu, T.S., Zappi, E.G., Sastry, K., Coburn, J., Zaner, K.S., Sontheimer, R.D., Capra, J.D., Ghebrehiwet, B., Tauber, A.I., 1994. Calreticulin is released from activated neutrophils and binds to C1q and mannan-binding protein. Clin. Immunol. Immunopathol. 72, 405–409. https://doi.org/10.1006/clin.1994.1160

El-Bahi, M.M., Malone, J.B., Todd, W.J., Schnorr, K.L., 1992. Detection of stable diagnostic antigen from bile and feces of *Fasciola hepatica* infected cattle. Vet. Parasitol. 45, 157–167. https://doi.org/http://dx.doi.org/10.1016/0304-4017(92)90039-C

El Bahy, M.M., Malone, J.B., Todd, W.J., Schnorr, K.L., 1994. Diagnosis of Fasciola infections by detection of antigens in feces or intestinal content: Patent Number 5,338,660.

El Hage, F., Stroobant, V., Vergnon, I., Baurain, J.-F., Echchakir, H., Lazar, V., Chouaib, S., Coulie, P.G., Mami-Chouaib, F., 2008. Preprocalcitonin signal peptide generates a cytotoxic T lymphocyte-defined tumor epitope processed by a proteasome-independent pathway. Proc. Natl. Acad. Sci. 105, 10119–10124. https://doi.org/10.1073/pnas.0802753105

Elliott, T.P., Spithill, T.W., 2014. The T687G SNP in a P-glycoprotein gene of *Fasciola hepatica* is not associated with resistance to triclabendazole in two resistant Australian populations. Mol. Biochem. Parasitol. 198, 45–47.

Elmore, S., 2007. Apoptosis: A Review of Programmed Cell Death. Toxicol. Pathol. 35, 495–516. https://doi.org/10.1080/01926230701320337

Enigk, K., Hildebrand, J., 1964. Zur lebensdauer der metacercarien von *Fasciola hepatica* im heu. Tierärztliche Rundschau 19, 592–599.

Enigk, K., Hildebrand, J., Zimmer, E., 1964. Zur lebensdauer der infektiösen larven von haustierhelminthen in silage. Dtsch. Tierarztl. Wochenschr. 71, 533–537.

Escamilla, A., Pérez-Caballero, R., Zafra, R., Bautista, M.J., Pacheco, I.L., Ruiz, M.T., Martínez-Cruz, M.S., Martínez-Moreno, A., Molina-Hernández, V., Pérez, J., 2017. Apoptosis of peritoneal leucocytes during early stages of *Fasciola hepatica* infections in sheep. Vet. Parasitol. 238, 49–53. https://doi.org/10.1016/j.vetpar.2017.03.015

Espino, A.M., Finlay, C.M., 1994. Sandwich enzyme-linked immunosorbent assay for detection of excretory secretory antigens in human with fascioliasis. J. Clin. Microbiol. 32, 190–193.

Espino, A.M., Morales, A., Delgado, B., Rivera, F.M., Figueroa, A., Suárez, E., 2010. Partial Immunity to *Fasciola hepatica* in Mice after Vaccination with FhSAP2 Delivered as Recombinant Protein or DNA Construct. Ethn. Dis. 20, 1–12.

Esteban, J.G., Flores, A., Angles, R., Mas-Coma, S., 1999. High endemicity of human fascioliasis between Lake Titicaca and La Paz valley, Bolivia. Trans. R. Soc. Trop. Med. Hyg. 93, 151–156.

Esteban, J.G., Gonzalez, C., Bargues, M.D., Angles, R., Sanchez, C., Naquira, C., Mas-Coma, S., 2002. High fascioliasis infection in children linked to a man-made irrigation zone in Peru. Trop. Med. Int. Heal. 7, 339–348.

Esteves, A., Ehrlich, R., 2006. Invertebrate intracellular fatty acid binding proteins. Comp. Biochem. Physiol. Part C Toxicol. Pharmacol. 142, 262–274. https://doi.org/10.1016/j.cbpc.2005.11.006

Evans, A.G.L., Davey, H.M., Cookson, A., Currinn, H., Cooke-Fox, G., Stanczyk, P.J., Whitworth, D.E., 2012. Predatory activity of *Myxococcus xanthus* outer-membrane vesicles and

properties of their hydrolase cargo. Microbiol. (United Kingdom) 158, 2742–2752. https://doi.org/10.1099/mic.0.060343-0

Ewald, P.W., 1987. Transmission modes and evolution of the parasitism mutualism continuum. Ann. N. Y. Acad. Sci. https://doi.org/10.1007/BF02692179

Fairweather, I., 2011a. Raising the bar on reporting 'triclabendazole resistance.' Vet. Rec. 168, 514–515. https://doi.org/10.1136/vr.d2867

Fairweather, I., 2011b. Reducing the future threat from (liver) fluke: realistic prospect or quixotic fantasy? Vet. Parasitol. 180, 133–143. https://doi.org/10.1016/j.vetpar.2011.05.034

Fairweather, I., 2011c. Liver fluke isolates: a question of provenance. Vet. Parasitol. 176, 1–8. https://doi.org/10.1016/j.vetpar.2010.12.011

Fairweather, I., 2009. Triclabendazole progress report, 2005-2009: an advancement of learning? J. Helminthol. 83, 139–150. https://doi.org/10.1017/S0022149X09321173

Fairweather, I., 2005. Triclabendazole: new skills to unravel an old (ish) enigma. J. Helminthol. 79, 227–234. https://doi.org/10.1079/JOH2005298

Fairweather, I., Boray, J.C., 1999. Fasciolicides: efficacy, actions, resistance and its management. Vet. J. 158, 81–112.

Fairweather, I., Holmes, S.D., Threadgold, L.T., 1984. *Fasciola hepatica*: Motility response to metabolic inhibitors in vitro. Exp. Parasitol. 57, 209–224. https://doi.org/10.1016/0014-4894(85)90082-7

Fairweather, I., McShane, D.D., Shaw, L., Ellison, S.E., O'Hagan, N.T., York, E.A., Trudgett, A., Brennan, G.P., 2012. Development of an egg hatch assay for the diagnosis of triclabendazole resistance in *Fasciola hepatica*: Proof of concept. Vet. Parasitol. 183, 249–259. https://doi.org/10.1016/j.vetpar.2011.07.023

FAO, 1994. Diseases of domestic animals caused by liver flukes: epidemiology, diagnosis and control of *Fasciola*, paramphistome, *Dicroceoelium*, *Eurytrema* and schistosome infections of ruminants in developing countries. Rome.

Farahnak, A., Golmohamdi, T., Eshraghian, M., 2012. In vitro effects of triclabendazole (TCBZ) on the excretory-secretory products (ESP) of Fasciola spp parasites. Acta Med. Iran. 50, 164–168.

Faridi, A., Farhnak, A., Gomohammadi, T., Eshraghian, M., Sharifi, Y., Rad, M., 2014. Triclabendazole (anthelmintic drug) effects on the excretory- secretory proteome of *Fasciola hepatica* in two dimension electrophoresis gel. Iran. J. Parasitol. 9, 202–208.

Felsenstein, J., 1985. Confidence limits on phylogenies: an approach using the bootstrap. Evolution (N. Y). 39, 783–791. https://doi.org/10.2307/2408678

Fernández, V., Estein, S., Ortiz, P., Luchessi, P., Solana, V., Solana, H., 2015. A single amino acid substitution in isozyme GST mu in Triclabendazole resistant *Fasciola hepatica* (Sligo strain) can substantially influence the manifestation of anthelmintic resistance. Exp. Parasitol. 159, 274–279. https://doi.org/10.1016/j.exppara.2015.10.007

Ferrante di Ruffano, L., Hyde, C.J., McCaffery, K.J., Bossuyt, P.M.M., Deeks, J.J., 2012. Assessing the value of diagnostic tests: a framework for designing and evaluating trials. Br. Med. J. 344, 1–9. https://doi.org/10.1017/CBO9781107415324.004

Ferreira, V., Molina, M.C., Schwaeble, W., Lemus, D., Ferreira, A., 2005. Does Trypanosoma cruzi calreticulin modulate the complement system and angiogenesis? Trends Parasitol. https://doi.org/10.1016/j.pt.2005.02.005

Ferreira, V., Molina, M.C., Valck, C., Rojas, Á., Aguilar, L., Ramírez, G., Schwaeble, W., Ferreira, A., 2004a. Role of calreticulin from parasites in its interaction with vertebrate hosts. Mol.

Immunol. 40, 1279–1291. https://doi.org/10.1016/j.molimm.2003.11.018
Ferreira, V., Valck, C., Sanchez, G., Gingras, A., Tzima, S., Molina, M.C., Sim, R., Schwaeble, W., Ferreira, A., 2004b. The classical activation pathway of the human complement system is specifically inhibited by calreticulin from *Trypanosoma cruzi*. J. Immunol. 172, 3042–3050. https://doi.org/10.4049/jimmunol.172.5.3042
Fetterer, R.H., 1986. The effect of albendazole and triclabendazole on colchicine binding in the liver fluke *Fasciola hepatica*. J. Vet. Pharmacol. Ther. 9, 49–54. https://doi.org/10.1111/j.1365-2885.1986.tb00011.x
Fèvre, E.M., Wissmann, B. V., Welburn, S.C., Lutumba, P., 2008. The burden of human African Trypanosomiasis. PLoS Negl. Trop. Dis. 2, e333. https://doi.org/10.1371/journal.pntd.0000333
Figueiredo, B.C., Da'dara, A.A., Oliveira, S.C., Skelly, P.J., 2015. Schistosomes Enhance Plasminogen Activation: The Role of Tegumental Enolase. PLoS Pathog. 11, e1005335. https://doi.org/10.1371/journal.ppat.1005335
Figueroa-Santiago, O., Espino, A.M., 2017. *Fasciola hepatica* ESPs could indistinctly activate or block multiple toll-like receptors in a human monocyte cell line. Ann. Clin. Pathol. 5.
Figueroa-Santiago, O., Espino, A.M., 2014. *Fasciola hepatica* fatty acid binding protein induces the alternative activation of human macrophages. Infect. Immun. 82, 5005–5012. https://doi.org/10.1128/IAI.02541-14
Fitzpatrick, J.L., 2013. Global food security: The impact of veterinary parasites and parasitologists. Vet. Parasitol. 195, 233–248. https://doi.org/10.1016/j.vetpar.2013.04.005
Flanagan, A., Edgar, H.W.J., Forster, F., Gordon, A., Hanna, R.E.B., McCoy, M., Brennan, G.P., Fairweather, I., 2011a. Standardisation of a coproantigen reduction test (CRT) protocol for the diagnosis of resistance to triclabendazole in *Fasciola hepatica*. Vet. Parasitol. 176, 34–42. https://doi.org/10.1016/j.vetpar.2010.10.037
Flanagan, A., Edgar, H.W.J., Gordon, A., Hanna, R.E.B., Brennan, G.P., Fairweather, I., 2011b. Comparison of two assays, a faecal egg count reduction test (FECRT) and a coproantigen reduction test (CRT), for the diagnosis of resistance to triclabendazole in *Fasciola hepatica* in sheep. Vet. Parasitol. 176, 170–176. https://doi.org/10.1016/j.vetpar.2010.10.057
Fletcher, H.L., Hoey, E.M., Orr, N., Trudgett, A., Fairweather, I., Robinson, M.W., 2004. The occurrence and significance of triploidy in the liver fluke, *Fasciola hepatica*. Parasitology 128, 69–72. https://doi.org/10.1017/S003118200300427X
Fletcher, J.M., Nair, S.P., Ward, J.M., Henderson, B., Wilson, M., 2001. Analysis of the effect of changing environmental conditions on the expression patterns of exported surface-associated proteins of the oral pathogen *Actinobacillus actinomycetemcomitans*. Microb. Pathog. 30, 359–368. https://doi.org/10.1006/mpat.2000.0439
Foresight, T.F. of F. and F., Farming, 2011. The Future of Food and Farming : Challenges and choices for global sustainability The Future of Food and Farming : Challenges and choices for.
Foreyt, W.J., 1989. Efficacy of triclabendazole against experimentally induced *Fascioloides magna* infections in sheep. Am. J. Vet. Res. 50, 431–432.
Forscher, P., 1989. Calcium and polyphosphoinositide control of cytoskeletal dynamics. Trends Neurosci. 12, 468–474. https://doi.org/10.1016/0166-2236(89)90098-2
Fox, N.J., White, P.C.L., Mcclean, C.J., Marion, G., Evans, A., Michael, R., 2011. Predicting Impacts of Climate Change on *Fasciola hepatica* Risk. PLoS One 6, 19–21.

https://doi.org/10.1371/journal.pone.0016126
Fraser, S.A., Karimi, R., Michalak, M., Hudig, D., 2000. Perforin Lytic Activity Is Controlled by Calreticulin. J. Immunol. 164, 4150–4155. https://doi.org/10.4049/jimmunol.164.8.4150
Frédéric, M.Y., Lalande, M., Boileau, C., Hamroun, D., Claustres, M., Béroud, C., Collod-Béroud, G., 2009. UMD-predictor, a new prediction tool for nucleotide substitution pathogenicity - Application to four genes: *FBN1*, *FBN2*, *TGFBR1*, and *TGFBR2*. Hum. Mutat. 30, 952–959. https://doi.org/10.1002/humu.20970
Funk, J., Schaarschmidt, B., Slesiona, S., Hallström, T., Horn, U., Brock, M., 2016. The glycolytic enzyme enolase represents a plasminogen-binding protein on the surface of a wide variety of medically important fungal species. Int. J. Med. Microbiol. 306, 59–68. https://doi.org/10.1016/j.ijmm.2015.11.005
Fürst, T., Keiser, J., Utzinger, J., 2012. Global burden of human food-borne trematodiasis : a systematic review and meta-analysis. Lancet Infect. Dis. 12, 210–221. https://doi.org/10.1016/S1473-3099(11)70294-8
Furuya, H., Ikeda, R., 2011. Interaction of triosephosphate isomerase from *Staphylococcus aureus* with plasminogen. Microbiol. Immunol. 55, 855–862. https://doi.org/10.1111/j.1348-0421.2011.00392.x
Furuya, H., Ikeda, R., 2009. Interaction of triosephosphate isomerase from the cell surface of *Staphylococcus aureus* and a-(1A3)-mannooligosaccharides derived from glucuronoxylomannan of *Cryptococcus neoformans*. Microbiology 155, 2707–2713. https://doi.org/10.1099/mic.0.028068-0
Gaasenbeek, C.P.H., Moll, L., Cornelissen, J.B.W.J., Vellema, P., Borgsteede, F.H.M., 2001. An experimental study on triclabendazole resistance of *Fasciola hepatica* in sheep. Vet. Parasitol. 95, 37–43. https://doi.org/doi.org/10.1016/S0304-4017(00)00413-1
Garcia-Campos, A., Ravidà, A., Nguyen, D.L., Cwiklinski, K., Dalton, J.P., Hokke, C.H., O'Neill, S., Mulcahy, G., 2016. Tegument Glycoproteins and Cathepsins of Newly Excysted Juvenile *Fasciola hepatica* Carry Mannosidic and Paucimannosidic N-glycans. PLoS Negl. Trop. Dis. 10. https://doi.org/10.1371/journal.pntd.0004688
Garza-Cuartero, L., Geurden, T., Mahan, S.M., Hardham, J.M., Dalton, J.P., Mulcahy, G., 2018. Antibody recognition of cathepsin L1-derived peptides in *Fasciola hepatica*-infected and/or vaccinated cattle and identification of protective linear B-cell epitopes. Vaccine 36, 958–968. https://doi.org/10.1016/j.vaccine.2018.01.020
Gasteiger, E., Gattiker, A., Hoogland, C., Ivanyi, I., Appel, R.D., Bairoch, A., 2003. ExPASy: The proteomics server for in-depth protein knowledge and analysis. Nucleic Acids Res. 31, 3784–3788. https://doi.org/10.1093/nar/gkg563
Gelly, J.C., Joseph, A.P., Srinivasan, N., De Brevern, A.G., 2011. IPBA: A tool for protein structure comparison using sequence alignment strategies. Nucleic Acids Res. 39, W18–W23. https://doi.org/10.1093/nar/gkr333
Genre, F., López-Mejias, R., Miranda-Filloy, J.A., Ubilla, B., Carnero-López, B., Gómez-Acebo, I., Blanco, R., Ochoa, R., Rueda-Gotor, J., González-Juanatey, C., Llorca, J., González-Gay, M.A., 2014. Gelsolin levels are decreased in ankylosing spondylitis patients undergoing anti-TNF-alpha therapy. Clin. Exp. Rheumatol. 32, 218–224.
George, S.D., Vanhoff, K., Baker, K., Lake, L., Rolfe, P.F., Seewald, W., Emery, D.L., 2017. Application of a coproantigen ELISA as an indicator of efficacy against multiple life stages of *Fasciola hepatica* infections in sheep. Vet. Parasitol. 246, 60–69. https://doi.org/10.1016/j.vetpar.2017.08.028
Gerlt, J.A., Babbitt, P.C., Rayment, I., 2005. Divergent evolution in the enolase superfamily:

The interplay of mechanism and specificity. Arch. Biochem. Biophys. https://doi.org/10.1016/j.abb.2004.07.034
Gerlt, J.A., Raushel, F.M., 2003. Evolution of function in (β/α)8-barrel enzymes. Curr. Opin. Chem. Biol. 7, 252–264. https://doi.org/10.1016/S1367-5931(03)00019-X
Ghosh, A.K., Jacobs-Lorena, M., 2011. Surface-expressed enolases of *Plasmodium* and other pathogens. Mem. Inst. Oswaldo Cruz 106, 85–90.
Gibrat, J.F., Madej, T., Bryant, S.H., 1996. Surprising similarities in structure comparison. Curr. Opin. Struct. Biol. 6, 377–385. https://doi.org/10.1016/S0959-440X(96)80058-3
GIGA Community of Scientists, 2014. The Global Invertebrate Genomics Alliance (GIGA): Developing Community Resources to Study Diverse Invertebrate Genomes. J. Hered. 105, 1–18. https://doi.org/10.1093/jhered/est084
Gilleard, J.S., 2013. *Haemonchus contortus* as a paradigm and model to study anthelmintic drug resistance. Parasitology 240, 1506–1522. https://doi.org/10.1017/S0031182013001145
Gilleard, J.S., Beech, R.N., 2007. Population genetics of anthelmintic resistance in parasitic nematodes. Parasitology 134, 1133–1146. https://doi.org/10.1017/s0031182007000066
Girotto, S., Cendron, L., Bisaglia, M., Tessari, I., Mammi, S., Zanotti, G., Bubacco, L., 2014. DJ-1 Is a copper chaperone acting on SOD1 activation. J. Biol. Chem. 289, 10887–10899. https://doi.org/10.1074/jbc.M113.535112
Gold, D., Goldberg, M., 1976. Effect of light and temperature on hatching in *Fasciola hepatica* (Trematoda: Fasciolidae). Isr. J. Zool. 25, 178–185. https://doi.org/10.1080/00212210.1976.10688436
Golden, O., Flynn, R.J., Read, C., Sekiya, M., Donnelly, S.M., Stack, C., Dalton, J.P., Mulcahy, G., 2010. Protection of cattle against a natural infection of *Fasciola hepatica* by vaccination with recombinant cathepsin L1 (rFhCL1). Vaccine 28, 5551–5557. https://doi.org/10.1016/j.vaccine.2010.06.039
Goldfinch, G.M., Smith, W.D., Imrie, L., McLean, K., Inglis, N.F., Pemberton, A.D., 2008. The proteome of gastric lymph in normal and nematode infected sheep. Proteomics 8, 1909–1918. https://doi.org/10.1002/pmic.200700531
Gómez-Arreaza, A., Acosta, H., Quiñones, W., Concepción, J.L., Michels, P.A.M., Avilán, L., 2014. Extracellular functions of glycolytic enzymes of parasites: Unpredicted use of ancient proteins. Mol. Biochem. Parasitol. 193, 75–81. https://doi.org/10.1016/j.molbiopara.2014.02.005
González-Fernández, R., Jorrín-Novo, J. V., 2012. Contribution of Proteomics to the Study of Plant Pathogenic Fungi. J. Proteome Res. 11, 3–16. https://doi.org/10.1155/2010/932527
González-Miguel, J., Valero, M.A., Reguera-Gomez, M., Mas-Bargues, C., Bargues, M.D., Simón, F., Mas-Coma, S., 2019. Numerous *Fasciola* plasminogen-binding proteins may underlie blood-brain barrier leakage and explain neurological disorder complexity and heterogeneity in the acute and chronic phases of human fascioliasis. Parasitology 146, 284–298. https://doi.org/10.1017/S0031182018001464
González, E., Del Carmen García de Leon, M., Meza, I., Ocadiz-Delgado, R., Gariglio, P., Silva-Olivares, A., Galindo-Gómez, S., Shibayama, M., Morán, P., Valadez, A., Limón, A., Rojas, L., Hernández, E.G., Cerritos, R., Ximenez, C., 2011. *Entamoeba histolytica* calreticulin: an endoplasmic reticulum protein expressed by trophozoites into experimentally induced amoebic liver abscesses. Parasitol. Res. 108, 439–49. https://doi.org/10.1007/s00436-

010-2085-6
Gordon, D.K., Zadoks, R.N., Stevenson, H., Sargison, N.D., Skuce, P.J., 2012. On farm evaluation of the coproantigen ELISA and coproantigen reduction test in Scottish sheep naturally infected with Fasciola hepatica. Vet. Parasitol. 187, 436–444. https://doi.org/10.1016/j.vetpar.2012.02.009
Gough, J., Karplus, K., Hughey, R., Chothia, C., 2001. Assignment of homology to genome sequences using a library of hidden Markov models that represent all proteins of known structure. J. Mol. Biol. 314, 903–919. https://doi.org/10.1006/jmbi.2001.5080
Gouw, M., Michael, S., Sámano-Sánchez, H., Kumar, M., Zeke, A., Lang, B., Bely, B., Chemes, L.B., Davey, N.E., Deng, Z., Diella, F., Gürth, C.M., Huber, A.K., Kleinsorg, S., Schlegel, L.S., Palopoli, N., Roey, K. V., Altenberg, B., Reményi, A., Dinkel, H., Gibson, T.J., 2018. The eukaryotic linear motif resource - 2018 update. Nucleic Acids Res. 46, D428–D434. https://doi.org/10.1093/nar/gkx1077
Graceffa, P., Dominguez, R., 2003. Crystal structure of monomeric actin in the ATP state: Structural basis of nucleotide-dependent actin dynamics. J. Biol. Chem. 278, 34172–34180. https://doi.org/10.1074/jbc.M303689200
Gschaedler, A., Thi Le, N., Boudrant, J., 1994. Glucose and acetate influences on the behavior of the recombinant strain *Escherichia coli* HB 101 (GAPDH). J. Ind. Microbiol. 13, 225–232. https://doi.org/10.1007/BF01569753
Guex, N., Peitsch, M.C., Schwede, T., 2009. Automated comparative protein structure modeling with SWISS-MODEL and Swiss-PdbViewer: A historical perspective. Electrophoresis 30, S162–S173. https://doi.org/10.1002/elps.200900140
Gunn, A., Pitt, S.J., 2012a. Helminth Parasites, in: Parasitology. John Wiley & Sons, Ltd, pp. 86–136. https://doi.org/10.1002/9781119968986.ch3
Gunn, A., Pitt, S.J., 2012b. Parasite Transmission, in: Parasitology. John Wiley & Sons, Ltd, pp. 180–211. https://doi.org/10.1002/9781119968986.ch5
Guo, L., Groenendyk, J., Papp, S., Dabrowska, M., Knoblach, B., Kay, C., Parker, J.M.R., Opas, M., Michalak, M., 2003. Identification of an N-domain Histidine Essential for Chaperone Function in Calreticulin. J. Biol. Chem. 278, 50645–50653. https://doi.org/10.1074/jbc.M309497200
Guo, X.C., Luo, B.Y., Li, X.F., Yang, D.G., Zheng, X.N., Zhang, K., 2011. Plasma gelsolin levels and 1-year mortality after first-ever ischemic stroke. J. Crit. Care 26, 608–612. https://doi.org/10.1016/j.jcrc.2011.02.007
Gutiérrez, A., Pointier, J.P., Fraga, J., Jobet, E., Modat, S., Pérez, R.T., Yong, M., Sanchez, J., Loker, E.S., Théron, A., 2003. Fasciola hepatica: Identification of molecular markers for resistant and susceptible *Pseudosuccinea columella* snail hosts. Exp. Parasitol. 105, 211–218. https://doi.org/10.1016/j.exppara.2003.12.006
Haçariz, O., Akgün, M., Kavak, P., Yüksel, B., Sağiroğlu, M.Ş., 2015. Comparative transcriptome profiling approach to glean virulence and immunomodulation-related genes of *Fasciola hepatica*. BMC Genomics 16. https://doi.org/10.1186/s12864-015-1539-8
Halferty, L., Brennan, G.P., Hanna, R.E.B., Edgar, H.W., Meaney, M.M., Mcconville, M., Trudgett, A., Hoey, L., Fairweather, I., 2008. Tegumental surface changes in juvenile *Fasciola hepatica* in response to treatment in vivo with triclabendazole. Vet. Parasitol. 155, 49–58. https://doi.org/10.1016/j.vetpar.2008.04.011
Halferty, L., Brennan, G.P., Trudgett, A., Hoey, L., Fairweather, I., 2009. Relative activity of triclabendazole metabolites against the liver fluke, *Fasciola hepatica*. Vet. Parasitol. 159, 126–138. https://doi.org/10.1016/j.vetpar.2008.10.007

Hall, A., 1994. Small GTP-binding proteins and the regulation of the actin cytoskeleton. Annu. Rev. Cell Biol. 10, 31–54. https://doi.org/10.1146/annurev.cb.10.110194.000335

Hall, T.A., 1999. BioEdit: a user-friendly biological sequence alignment editor and analysis program for Windows 95/98/NT. Nucleic Acids Symp. Ser. https://doi.org/citeulike-article-id:691774

Halton, D.W., 1967. Observations on the nutrition of digenetic trematodes. Parasitology 57, 639. https://doi.org/10.1017/S003118200007311X

Halton, W., 1997. Nutritional Adaptations to Parasitism Platyhelminthes. Int. J. Parasitol. 27, 696–704.

Hamilton, C.M., Dowling, D.J., Loscher, C.E., Morphew, R.M., Brophy, P.M., O'Neill, S.M., 2009. The *Fasciola hepatica* tegumental antigen suppresses dendritic cell maturation and function. Infect. Immun. 77, 2488–2498. https://doi.org/10.1128/IAI.00919-08

Hanna, R., 2015. *Fasciola hepatica*: Histology of the Reproductive Organs and Differential Effects of Triclabendazole on Drug-Sensitive and Drug-Resistant Fluke Isolates and on Flukes from Selected. Pathogens 4, 431–456. https://doi.org/10.3390/pathogens4030431

Hanna, R.E.B., 1980. *Fasciola hepatica*: An immunofluorescent study of antigenic changes in the tegument during development in the rat and the sheep. Exp. Parasitol. 50, 155–170. https://doi.org/http://dx.doi.org/10.1016/0014-4894(80)90017-X

Hanna, R.E.B., Edgar, H.W., Mcconnell, S., Toner, E., Mcconville, M., Brennan, G.P., Devine, C., Flanagan, A., Halferty, L., Meaney, M., Shaw, L., Moffett, D., Mccoy, M., Fairweather, I., 2010. *Fasciola hepatica*: Histological changes in the reproductive structures of triclabendazole (TCBZ) -sensitive and TCBZ-resistant flukes after treatment *in vivo* with TCBZ and the related benzimidazole derivative , Compound Alpha. Vet. Parasitol. 168, 240–254. https://doi.org/10.1016/j.vetpar.2009.11.014

Hanna, R.E.B., Forster, F.I., Brennan, G.P., Fairweather, I., 2013. *Fasciola hepatica*: Histological demonstration of apoptosis in the reproductive organs of flukes of triclabendazole-sensitive and triclabendazole-resistant isolates, and in field-derived flukes from triclabendazole-treated hosts, using in situ hybridisatio. Vet. Parasitol. 191, 240–251. https://doi.org/10.1016/j.vetpar.2012.09.014

Hanna, R.E.B., McMahon, C., Ellison, S., Edgar, H.W., Kajugu, P.-E., Gordon, A., Irwin, D., Barley, J.P., Malone, F.E., Brennan, G.P., Fairweather, I., 2015. *Fasciola hepatica* : A comparative survey of adult fluke resistance to triclabendazole, nitroxynil and closantel on selected upland and lowland sheep farms in Northern Ireland using faecal egg counting, coproantigen ELISA testing. Vet. Parasitol. 207, 34–43. https://doi.org/10.1016/j.vetpar.2014.11.016

Hanna, R.E.B., Scarcella, S., Solana, H., McConnell, S., Fairweather, I., 2012. Early onset of changes to the reproductive system of *Fasciola hepatica* following *in vivo* treatment with triclabendazole. Vet. Parasitol. 184, 341–347. https://doi.org/10.1016/j.vetpar.2011.08.023

Hannaert, V., Opperdoes, F.R., Michels, P.A.M., 1995. Glycosomal Glyceraldehyde-3-Phosphate Dehydrogenase of *Trypanosoma brucei* and *Trypanosoma cruzi* - Expression in *Escherichia coli*, Purification, and Characterization of the Enzymes. Protein Expr. Purif. 6, 244–250. https://doi.org/DOI 10.1006/prep.1995.1031

Harmsen, M.M., Cornelissen, J.B.W.J., Buijs, H.E.C.M., Boersma, W.J.A., Jeurissen, S.H.M., van Milligen, F.J., 2004. Identification of a novel *Fasciola hepatica* cathepsin L protease containing protective epitopes within the propeptide. Int. J. Parasitol. 34, 675–682.

Harn, D.A., Gu, W., Oligino, L.D., Mitsuyama, M., Gebremichael, A., Richter, D., 1992. A protective monoclonal antibody specifically recognizes and alters the catalytic activity of schistosome triose-phosphate isomerase. J. Immunol. 148, 562–567.

Harn, D.A., Mitsuyama, M., Huguenel, E.D., Oligino, L., David, J.R., 1985. Identification by monoclonal antibody of a major (28 kDa) surface membrane antigen of *Schistosoma mansoni*. Mol. Biochem. Parasitol. 16, 345–354. https://doi.org/10.1016/0166-6851(85)90075-1

Harris, M.T., Mitchell, W.G., Morris, J.C., 2014. Targeting Protozoan Parasite Metabolism: Glycolytic Enzymes in the Therapeutic Crosshairs. Curr. Med. Chem. 21, 1668–1678. https://doi.org/10.2174/09298673113206660286

Hart, G.W., Housley, M.P., Slawson, C., 2007. Cycling of O-linked beta-N-acetylglucosamine on nucleocytoplasmic proteins. Nature 446, 1017–1022. https://doi.org/10.1038/nature05815

He, X., Wang, Y., Zhang, W., Li, H., Luo, R., Zhou, Y., Li, C., Liao, M., Huang, H., Lv, X., Xie, Z., He, M., 2014. Screening differential expression of serum proteins in AFP-negative HBV-related hepatocellular carcinoma using iTRAQ -MALDI-MS/MS. Neoplasma 61, 17–26. https://doi.org/10.4149/neo_2014_001

Hein, W.R., Harrison, G.B.L., 2005. Vaccines against veterinary helminths. Vet. Parasitol. 132, 217–222. https://doi.org/10.1016/j.vetpar.2005.07.006

Hendrickx, G., Biesemans, J., De Deken, R., 2004. The use of GIS in Veterinary Parasitology., in: GIS and Spatial Analysis in Veterinary Science. pp. 145–176.

Hennessy, D.R., Lacey, E., Steel, J.W., Prichard, R.K., 1987. The kinetics of triclabendazole disposition in sheep. J. Vet. Pharmacol. Ther. 10, 64–72. https://doi.org/10.1111/j.1365-2885.1987.tb00078.x

Herd, R.P., Chappel, R.J., Biddell, D., 1975. Immunization of dogs against *Echinococcus granulosus* using worm secretory antigens. Int. J. Parasitol. 5, 395–399. https://doi.org/10.1016/0020-7519(75)90004-1

Hernández-González, A., Valero, M.L.L., Pino, M.S. del, Oleaga, A., Siles-Lucas, M., 2010. Proteomic analysis of in vitro newly excysted juveniles from *Fasciola hepatica*. Mol. Biochem. Parasitol. 172, 121–128. https://doi.org/10.1016/j.molbiopara.2010.04.003

Hewitson, J.P., Harcus, Y.M., Curwen, R.S., Dowle, A.A., Atmadja, A.K., Ashton, P.D., Wilson, A., Maizels, R.M., 2008. The secretome of the filarial parasite, *Brugia malayi*: Proteomic profile of adult excretory-secretory products. Mol. Biochem. Parasitol. 160, 8–21. https://doi.org/10.1016/j.molbiopara.2008.02.007

Hewitson, J.P., Rückerl, D., Harcus, Y., Murray, J., Webb, L.M., Babayan, S.A., Allen, J.E., Kurniawan, A., Maizels, R.M., 2014. The Secreted Triose Phosphate Isomerase of *Brugia malayi* Is Required to Sustain Microfilaria Production *In Vivo*. PLoS Pathog. 10, e1003930.

Higón, M., Monteagudo, C., Fried, B., Esteban, J.G., Toledo, R., Marcilla, A., 2008. Molecular cloning and characterization of *Echinostoma caproni* heat shock protein-70 and differential expression in the parasite derived from low- and high-compatible hosts. Parasitology 135, 1469–1477. https://doi.org/10.1017/S0031182008004927

Hillyer, G. V, 2005. Fasciola antigens as vaccines against fascioliasis and schistosomiasis. J. Helminthol. 79, 241–247. https://doi.org/10.1079/JOH2005304

Hodasi, M., 1972. The output of cercariae of *Fasciola hepatica* by *Lymnaea truncatula* and the distribution of metacercariae on grass. Parasitology 64, 53–60. https://doi.org/10.1017/S0031182000044644

Hodgkinson, J., Cwiklinski, K., Beesley, N.J., Paterson, S., Williams, D.J.L., 2013. Identification

of putative markers of triclabendazole resistance by a genome-wide analysis of genetically recombinant *Fasciola hepatica*. Parasitology 140, 1523–1533. https://doi.org/10.1017/S0031182013000528

Holoshitz, J., De Almeida, D.E., Ling, S., 2010. A role for calreticulin in the pathogenesis of rheumatoid arthritis. Ann. N. Y. Acad. Sci. 1209, 91–98. https://doi.org/10.1111/j.1749-6632.2010.05745.x

Hombach, J., Pircher, H., Tonegawa, S., Zinkernagel, R.M., 1995. Strictly transporter of antigen presentation (TAP)-dependent presentation of an immunodominant cytotoxic T lymphocyte epitope in the signal sequence of a virus protein. J. Exp. Med. 182, 1615–9. https://doi.org/10.1084/jem.182.5.1615

Honbou, K., Suzuki, N.N., Horiuchi, M., Niki, T., Taira, T., Ariga, H., Inagaki, F., 2003. The crystal structure of DJ-1, a protein related to male fertility and Parkinson's disease. J. Biol. Chem. 278, 31380–31384. https://doi.org/10.1074/jbc.M305878200

Horibe, T., Matsui, H., Tanaka, M., Nagai, H., Yamaguchi, Y., Kato, K., Kikuchi, M., 2004. Gentamicin binds to the lectin site of calreticulin and inhibits its chaperone activity. Biochem. Biophys. Res. Commun. 323, 281–287. https://doi.org/10.1016/j.bbrc.2004.08.099

Hotez, P.J., Brindley, P.J., Bethony, J.M., King, C.H., Pearce, E.J., Jacobson, J., 2008. Review series Helminth infections: the great neglected tropical diseases. J. Clin. Invest. 118, 1311–1321. https://doi.org/10.1172/JCI34261.tion

Hourdin, P., Rondelaud, D., Cabaret, J., 1992. Effect of concurrent infection with *Muellerius capillaris* on the development of redial generations of *Fasciola hepatica* in *Lymnaea truncatula*. J. Helminthol. 66, 108–117. https://doi.org/10.1017/S0022149X00012670

Howell, A., Baylis, M., Smith, R., Pinchbeck, G., Williams, D.J.L., 2015. Epidemiology and impact of *Fasciola hepatica* exposure in high-yielding dairy herds. Prev. Vet. Med. 121, 41–48. https://doi.org/10.1016/j.prevetmed.2015.05.013

Huang, L.F., Yao, Y.M., Li, J.F., Dong, N., Liu, C., Yu, Y., He, L.X., Sheng, Z.Y., 2011. Reduction of plasma gelsolin levels correlates with development of multiple organ dysfunction syndrome and fatal outcome in burn patients. PLoS One 6, e25748. https://doi.org/10.1371/journal.pone.0025748

Huff, M.E., Page, L.J., Balch, W.E., Kelly, J.W., 2003. Gelsolin domain 2 Ca2+affinity determines susceptibility to furin proteolysis and familial amyloidosis of Finnish type. J. Mol. Biol. 334, 119–127. https://doi.org/10.1016/j.jmb.2003.09.029

Hussein, A.-N., Hassan, I.M., Khalifa, R.M.A., 2010. Description of eggs and larval stages of Fasciola, light scanning electron microscopic studies. Res. J. Parasitol. 5, 1–12.

Hussein, A.N.A., Khalifa, R.M.A., 2010. Phenotypic description and prevalence of *Fasciola* species in Qena Governorate, Egypt with special reference to a new strain of *Fasciola hepatica*. J. King Saud Univ. - Sci. 22, 1–8. https://doi.org/10.1016/j.jksus.2009.12.001

Huyse, T., Poulin, R., Théron, A., 2005. Speciation in parasites : a population genetics approach. Trends Parasitol. 21, 469–475. https://doi.org/10.1016/j.pt.2005.08.009

Ikehata, K., Duzhak, T.G., Galeva, N.A., Ji, T., Koen, Y.M., Hanzlik, R.P., 2008. Protein targets of reactive metabolites of thiobenzamide in rat liver *in vivo*. Chem. Res. Toxicol. 21, 1432–1442. https://doi.org/10.1021/tx800093k

Intapan, P.M., Sadee, P., Wongkham, C., Maleewong, W., 2004. Development of rapid agglutination test using *Fasciola gigantica* specific antigen for serodiagnosis of human fascioliasis. Southeast Asian J. Trop. Med. Public Health 35, 313–317.

Intapan, P.M., Tantrawatpan, C., Maleewong, W., Wongkham, S., Wongkham, C., Nakashima,

K., 2005. Potent epitopes derived from *Fasciola gigantica* cathepsin L1 in peptide-based immunoassay for the serodiagnosis of human fascioliasis. Diagn. Microbiol. Infect. Dis. 53, 125–129. https://doi.org/10.1016/j.diagmicrobio.2005.05.010

Irwin, J.A., Morrissey, P.E.W., Ryan, J.P., Walshe, A., O'Neill, S.M., Carrington, S.D., Matthews, E., Fitzpatrick, E., Mulcahy, G., Corfield, A.P., Dalton, J.P., 2004. Glycosidase activity in the excretory-secretory products of the liver fluke, *Fasciola hepatica*. Parasitology 129, 465–472. https://doi.org/10.1017/S0031182004005803

Ismail, S.A., Park, H.W., 2005. Structural analysis of human liver glyceraldehyde-3-phosphate dehydrogenase. Acta Crystallogr. Sect. D Biol. Crystallogr. 61, 1508–1513. https://doi.org/10.1107/S0907444905026740

Ivanisenko, V.A., Pintus, S.S., Grigorovich, D.A., Kolchanov, N.A., 2004. PDBSiteScan: A program for searching for active, binding and posttranslational modification sites in the 3D structures of proteins. Nucleic Acids Res. 32, W549–W554. https://doi.org/10.1093/nar/gkh439

J Timson, D., 2016. Metabolic enzymes of helminth parasites: potential as drug targets. Curr. Protein Pept. Sci. 17, 280–295.

James, C.E., Hudson, A.L., Davey, M.W., 2009. Drug resistance mechanisms in helminths: is it survival of the fittest? Trends Parasitol. 25, 328–335. https://doi.org/10.1016/j.pt.2009.04.004

Janmey, P.A., Stossel, T.P., 1987. Modulation of gelsolin function by phosphatidylinositol 4,5-Bisphosphate. Nature 325, 362–364. https://doi.org/10.1038/325362a0

Jaouannet, M., Magliano, M., Arguel, M.J., Gourgues, M., Evangelisti, E., Abad, P., Rosso, M.N., 2013. The Root-Knot Nematode Calreticulin Mi-CRT Is a Key Effector in Plant Defense Suppression. Mol. Plant-Microbe Interact. 26, 97–105. https://doi.org/10.1094/MPMI-05-12-0130-R

Jaworski, D.C., Simmen, F.A., Lamoreaux, W., Coons, L.B., Muller, M.T., Needham, G.R., 1995. A secreted calreticulin protein in ixodid tick (*Amblyomma americanum*) saliva. J. Insect Physiol. 41, 369–375. https://doi.org/10.1016/0022-1910(94)00107-R

Jayaraj, R., Piedrafita, D., Dynon, K., Grams, R., Spithill, T.W., Smooker, P.M., 2009. Vaccination against fasciolosis by a multivalent vaccine of stage-specific antigens. Vet. Parasitol. 160, 230–236. https://doi.org/10.1016/j.vetpar.2008.10.099

Jefferies, J.R., Campbell, A.M., van Rossum, A.J., Barrett, J., Brophy, P.M., 2001. Proteomic analysis of *Fasciola hepatica* excretory-secretory products. Proteomics 1, 1128–1132. https://doi.org/10.1002/1615-9861(200109)1:9<1128::AID-PROT1128>3.0.CO;2-0

Jenkins, J.L., Tanner, J.J., 2006. High-resolution structure of human D-glyceraldehyde-3-phosphate dehydrogenase. Acta Crystallogr. Sect. D Biol. Crystallogr. 62, 290–301. https://doi.org/10.1107/S0907444905042289

Jepps, M.W., 1933. Miracidia of the liver fluke for laboratory work. Nature 132, 171.

Jerala, R., Zerovnik, E., Kidric, J., Turk, V., 2002. pH-induced Conformational Transitions of the Propeptide of Human Cathepsin L. J. Biol. Chem. 273, 11498–11504. https://doi.org/10.1074/jbc.273.19.11498

Ji, H., Wang, J., Guo, J., Li, Y., Lian, S., Guo, W., Yang, H., Kong, F., Zhen, L., Guo, L., Liu, Y., 2016. Progress in the biological function of alpha-enolase. Anim. Nutr. 2, 12–17. https://doi.org/10.1016/j.aninu.2016.02.005

Jiménez, L., Vibanco-Pérez, N., Navarro, L., Landa, A., 2000. Cloning, expression and characterisation of a recombinant triosephosphate isomerase from *Taenia solium*. Int. J. Parasitol. 30, 1007–1012. https://doi.org/10.1016/S0020-7519(00)00089-8

Jogl, G., Rozovsky, S., McDermott, A.E., Tong, L., 2003. Optimal alignment for enzymatic proton transfer: Structure of the Michaelis complex of triosephosphate isomerase at 1.2-A resolution. Proc. Natl. Acad. Sci. 100, 50–55. https://doi.org/10.1073/pnas.0233793100

John, B.C., Davies, D.R., Williams, D.J.L., Hodgkinson, J.E., 2019. A review of our current understanding of parasite survival in silage and stored forages, with a focus on *Fasciola hepatica* metacercariae. Grass Forage Sci. 74, 211–217. https://doi.org/10.1111/gfs.12429

Johns, D.R., Dickeson, S.J., 1979. Efficacy of albendazole against *Fasciola hepatica* in sheep. Aust. Vet. J. 55, 431–432. https://doi.org/10.1111/j.1751-0813.1979.tb05599.x

Johnson, S., Michalak, M., Opas, M., Eggleton, P., 2001. The ins and outs of calreticulin: From the ER lumen to the extracellular space. Trends Cell Biol. 11, 122–129. https://doi.org/10.1016/S0962-8924(01)01926-2

Jones, B.A., Grace, D., Kock, R., Alonso, S., Rushton, J., Said, M.Y., 2013. Zoonosis emergence linked to agricultural intensification and environmental change. PNAS 110, 8399–8404. https://doi.org/10.1073/pnas.1208059110

Jones, P., Binns, D., Chang, H.Y., Fraser, M., Li, W., McAnulla, C., McWilliam, H., Maslen, J., Mitchell, A., Nuka, G., Pesseat, S., Quinn, A.F., Sangrador-Vegas, A., Scheremetjew, M., Yong, S.Y., Lopez, R., Hunter, S., 2014. InterProScan 5: Genome-scale protein function classification. Bioinformatics 30, 1236–1240. https://doi.org/10.1093/bioinformatics/btu031

Jones, R.A., Williams, H.W., Dalesman, S., Brophy, P.M., 2015. Confirmation of *Galba truncatula* as an intermediate host snail for *Calicophoron daubneyi* in Great Britain, with evidence of alternative snail species hosting *Fasciola hepatica*. Parasites and Vectors 8, 656–659. https://doi.org/10.1186/s13071-015-1271-x

Joubert, F., Neitz, A.W.H., Louw, A.I., 2001. Structure-based inhibitor screening: A family of sulfonated dye inhibitors for malaria parasite triosephosphate isomerase. Proteins Struct. Funct. Genet. 45, 136–143. https://doi.org/10.1002/prot.1133

Junn, E., Jang, W.H., Zhao, X., Jeong, B.S., Mouradian, M.M., 2009. Mitochondrial localization of DJ-1 leads to enhanced neuroprotection. J. Neurosci. Res. 87, 123–129. https://doi.org/10.1002/jnr.21831

Kajugu, P.-E., Hanna, R.E.B., Edgar, H.W., McMahon, C., Cooper, M., Gordon, A., Barley, J.P., Malone, F.E., Brennan, G.P., Fairweather, I., 2015. *Fasciola hepatica*: Specificity of a coproantigen ELISA test for diagnosis of fasciolosis in faecal samples from cattle and sheep concurrently infected with gastrointestinal nematodes, coccidians and/or rumen flukes (paramphistomes), under field conditions. Vet. Parasitol. 212, 181–187. https://doi.org/10.1016/j.vetpar.2015.07.018

Kamaludeen, J., Graham-Brown, J., Stephens, N., Miller, J., Howell, A., Beesley, N.J., Hodgkinson, J., Learmount, J., Williams, D., 2019. Lack of efficacy of triclabendazole against *Fasciola hepatica* is present on sheep farms in three regions of England, and Wales. Vet. Rec. 184, vetrec-2018. https://doi.org/10.1136/vr.105209

Kannicht, C., Fuchs, B., 2008. Post-translational Modifications of proteins, in: Molecular Biomethods Handbook: Second Edition. pp. 427–449. https://doi.org/10.1007/978-1-60327-375-6_28

Kaplan, R.M., 2001. *Fasciola hepatica*: a review of the economic impact in cattle and considerations for control. Vet. Ther. 2, 40–50.

Karasawa, T., Wang, Q., David, L.L., Steyger, P.S., 2011. Calreticulin binds to gentamicin and

reduces drug-induced ototoxicity. Toxicol. Sci. 124, 378–387. https://doi.org/10.1093/toxsci/kfr196

Karkowska-Kuleta, J., Kedracka-Krok, S., Rapala-Kozik, M., Kamysz, W., Bielinska, S., Karafova, A., Kozik, A., 2011. Molecular determinants of the interaction between human high molecular weight kininogen and *Candida albicans* cell wall: Identification of kininogen-binding proteins on fungal cell wall and mapping the cell wall-binding regions on kininogen molecule. Peptides 32, 2488–2496.

Kasper, G., Brown, A., Eberl, M., Vallar, L., Kieffer, N., Berry, C., Girdwood, K., Eggleton, P., Quinnell, R., Pritchard, D.I., 2001. A calreticulin-like molecule from the human hookworm *Necator americanus* interacts with C1q and the cytoplasmic signalling domains of some integrins. Parasite Immunol. 23, 141–152. https://doi.org/10.1046/j.1365-3024.2001.00366.x

Kazmirski, S.L., Isaacson, R.L., An, C., Buckle, A., Johnson, C.M., Daggett, V., Fersht, A.R., 2002. Loss of a metal-binding site in gelsolin leads to familial amyloidosis-Finnish type. Nat. Struct. Biol. 9, 112–116. https://doi.org/10.1038/nsb745

Keiser, J., 2009. Food-Borne Trematodiases. Clin. Microbiol. Rev. 22, 466–483. https://doi.org/10.1128/CMR.00012-09

Keiser, J., Utzinger, J., 2005. Emerging Foodborne Trematodiasis. Emerg. Infect. Dis. 11, 1507–1514.

Kelley, J.M., Elliott, T.P., Beddoe, T., Anderson, G.R., Skuce, P., Spithill, T.W., 2016. Current Threat of Triclabendazole Resistance in *Fasciola hepatica*. Trends Parasitol. 32, 458–469. https://doi.org/http://dx.doi.org/10.1016/j.pt.2016.03.002

Kelley, L.A., Mezulis, S., Yates, C.M., Wass, M.N., Sternberg, M.J., 2015. The Phyre2 web portal for protein modeling, prediction and analysis. Nat. Protoc. 10, 845. https://doi.org/10.1038/nprot.2009.2

Kendall, S.B., 1970. Relationships between the Species of *Fasciola* and their Molluscan Hosts. Adv. Parasitol. 8, 251–258. https://doi.org/https://doi.org/10.1016/S0065-308X(08)60256-0

Kendall, S.B., 1949. Nutritional Factors affecting the Rate of Development of *Fasciola hepatica* in Limnaea truncatula. J. Helminthol. 23, 179–190. https://doi.org/10.1017/S0022149X00032491

Kendall, S.B., McCullough, F.S., 1951. The Emergence of the Cercariae of *Fasciola hepatica* from the Snail *Limnaea truncatula*. J. Helminthol. 25, 77–92. https://doi.org/DOI: 10.1017/S0022149X0001899X

Kendall, S.B., Ollerenshaw, C.B., 1963. The effect of nutrition on the growth of *Fasciola hepatica* in its snail host, in: Proceedings of the Nutrition Society. pp. 41–46.

Kenyon, F., Greer, A.W., Coles, G.C., Cringoli, G., Papadopoulos, E., Cabaret, J., Berrag, B., Varady, M., van Wyk, J.A., Thomas, E., Vercruysse, J., Jackson, F., 2009a. The role of targeted selective treatments in the development of refugia-based approaches to the control of gastrointestinal nematodes of small ruminants. Vet. Parasitol. 164, 3–11. https://doi.org/10.1016/j.vetpar.2009.04.015

Kenyon, F., Sargison, N.D., Skuce, P.J., Jackson, F., 2009b. Sheep helminth parasitic disease in south eastern Scotland arising as a possible consequence of climate change. Vet. Parasitol. 163, 293–297. https://doi.org/10.1016/j.vetpar.2009.03.027

Kim, H.L., Seligson, D., Liu, X., Janzen, N., Bui, M.H.T., Yu, H., Shi, T., Figlin, R.A., Horvath, S., Belldegrun, A.S., 2004. Using protein expressions to predict survival in clear cell renal carcinoma. Clin. Cancer Res. 10, 5464–5471. https://doi.org/10.1158/1078-0432.CCR-

04-0488
Kim, T.K., Ibelli, A.M.G., Mulenga, A., 2015. *Amblyomma americanum* tick calreticulin binds C1q but does not inhibit activation of the classical complement cascade. Ticks Tick. Borne. Dis. 6, 91–101. https://doi.org/10.1016/j.ttbdis.2014.10.002
King, C.H., 2010. Parasites and poverty: The case of schistosomiasis. Acta Trop. 113, 95–104. https://doi.org/10.1016/j.actatropica.2009.11.012
Kishore, U., Sontheimer, R.D., Sastry, K.N., Zaner, K.S., Zappi, E.G., Hughes, G.R., Khamashta, M.A., Strong, P., Reid, K.B., Eggleton, P., 1997. Release of calreticulin from neutrophils may alter C1q-mediated immune functions. Biochem. J. 322, 543–550. https://doi.org/10.1042/bj3220543
Kistner, T.P., Koller, L.D., 1975. Experimentally induced *Fasciola hepatica* infections in black-tailed deer. J. Wildl. Dis. 11, 214–20. https://doi.org/10.7589/0090-3558-11.2.214
Knowles, J.R., 1991. Enzyme catalysis: Not different, just better. Nature 350, 121–124. https://doi.org/10.1038/350121a0
Knox, D.P., Redmond, D.L., Skuce, P.J., Newlands, G.F.J., 2001. The contribution of molecular biology to the development of vaccines against nematode and trematode parasites of domestic ruminants. Vet. Parasitol. https://doi.org/10.1016/S0304-4017(01)00558-1
Kofta, W., Mieszczanek, J., Plucienniczak, G., Wędrychowicz, H., 2000. Successful DNA immunisation of rats against fasciolosis. Vaccine 18, 2985–2990. https://doi.org/10.1016/S0264-410X(00)00095-5
Kohagne, L.T., 2013. Zoonotic Diseases Emergence: A Challenge for Biodiversity Preservation in the Congo Basin, in: Advances in Environmental Research. pp. 65–110.
Kolaskar, A.S., Tongaonkar, P.C., 1990. A semi-empirical method for prediction of antigenic determinants on protein antigens. FEBS Lett. 276, 172–4.
Kolln, J., Ren, H.-M., Da, R.-R., Zhang, Y., Spillner, E., Olek, M., Hermanowicz, N., Hilgenberg, L.G., Smith, M.A., van den Noort, S., Qin, Y., 2006. Triosephosphate Isomerase- and Glyceraldehyde-3-Phosphate Dehydrogenase-Reactive Autoantibodies in the Cerebrospinal Fluid of Patients with Multiple Sclerosis. J. Immunol. 177, 5652–5658. https://doi.org/10.4049/jimmunol.177.8.5652
Kopecka, J., Campia, I., Brusa, D., Doublier, S., Matera, L., Ghigo, D., Bosia, A., Riganti, C., 2011. Nitric oxide and P-glycoprotein modulate the phagocytosis of colon cancer cells. J. Cell. Mol. Med. 15, 1492–1504. https://doi.org/10.1111/j.1582-4934.2010.01137.x
Kõressaar, T., Lepamets, M., Kaplinski, L., Raime, K., Andreson, R., Remm, M., 2018. Primer3-masker: Integrating masking of template sequence with primer design software. Bioinformatics 34, 1937–1938. https://doi.org/10.1093/bioinformatics/bty036
Koressaar, T., Remm, M., 2007. Enhancements and modifications of primer design program Primer3. Bioinformatics 23, 1289–1291. https://doi.org/10.1093/bioinformatics/btm091
Kothakota, S., Azuma, T., Reinhard, C., Klippel, A., Tang, J., Chu, K., McGarry, T.J., Kirschner, M.W., Koths, K., Kwiatkowski, D.J., Williams, L.T., 1997. Caspase-3-generated fragment of gelsolin: Effector of morphological change in apoptosis. Science (80-.). 278, 294–298. https://doi.org/10.1126/science.278.5336.294
Kotze, A.C., Hunt, P.W., Skuce, P., Von Samson-himmelstjerna, G., Martin, R.J., Sager, H., Krücken, J., Hodgkinson, J., Lespine, A., Jex, A.R., Gilleard, J.S., Beech, R.N., Wolstenholme, A.J., Demeler, J., Robertson, A.P., Charvet, C.L., Neveu, C., Kaminsky, R., Rufener, L., Alberich, M., Menez, C., Prichard, R.K., 2014. Recent advances in candidate-gene and whole-genome approaches to the discovery of anthelmintic resistance markers

and the description of drug/receptor interactions. Int. J. Parasitol. Drugs Drug Resist. 4, 164–184. https://doi.org/10.1016/j.ijpddr.2014.07.007

Kovjazin, R., Volovitz, I., Daon, Y., Vider-Shalit, T., Azran, R., Tsaban, L., Carmon, L., Louzoun, Y., 2011. Signal peptides and trans-membrane regions are broadly immunogenic and have high CD8+ T cell epitope densities: Implications for vaccine development. Mol. Immunol. 48, 1009–1018. https://doi.org/10.1016/j.molimm.2011.01.006

Koya, R.C., Fujita, H., Shimizu, S., Ohtsu, M., Takimoto, M., Tsujimoto, Y., Kuzumaki, N., 2000. Gelsolin inhibits apoptosis by blocking mitochondrial membrane potential loss and cytochrome c release. J. Biol. Chem. 275, 15343–15349. https://doi.org/10.1074/jbc.275.20.15343

Kozlov, G., Pocanschi, C.L., Rosenauer, A., Bastos-Aristizabal, S., Gorelik, A., Williams, D.B., Gehring, K., 2010. Structural basis of carbohydrate recognition by calreticulin. J. Biol. Chem. 285, 38612–38620. https://doi.org/10.1074/jbc.M110.168294

Krull, W.H., 1934. Notes on the hatchability and infectivity of refrigerated eggs of *Fasciola hepatica*, in: Proceedings of the Iowa Academy of Science. pp. 309–311.

Kudryashov, D.S., Grintsevich, E.E., Rubenstein, P.A., Reisler, E., 2010. A nucleotide state-sensing region on actin. J. Biol. Chem. 285, 25591–25601. https://doi.org/10.1074/jbc.M110.123869

Kuerpick, B., Schnieder, T., Strube, C., 2013. Evaluation of a recombinant cathepsin L1 ELISA and comparison with the Pourquier and ES ELISA for the detection of antibodies against *Fasciola hepatica*. Vet. Parasitol. 193, 206–213. https://doi.org/10.1016/j.vetpar.2012.11.021

Kuerpick, B., Schnieder, T., Strube, C., 2012. Seasonal pattern of fasciola hepatica antibodies in dairy herds in Northern Germany. Parasitol. Res. 111, 1085–1092. https://doi.org/10.1007/s00436-012-2935-5

Kumar, S., Stecher, G., Tamura, K., 2016. MEGA7: Molecular Evolutionary Genetics Analysis Version 7.0 for Bigger Datasets. Mol. Biol. Evol. 33, 1870–1874. https://doi.org/10.1093/molbev/msw054

Kushawaha, P.K., Gupta, R., Tripathi, C.D.P., Khare, P., Jaiswal, A.K., Sundar, S., Dube, A., 2012. Leishmania donovani Triose Phosphate Isomerase: A Potential Vaccine Target against Visceral Leishmaniasis. PLoS One 7, e45766. https://doi.org/10.1371/journal.pone.0045766

Kwa, M.S.G., Veenstra, J.G., Roos, M.H., 1994. Benzimidazole resistance in *Haemonchus contortus* is correlated with a conserved mutation at amino acid 200 in β-tubulin isotype 1. Mol. Biochem. Parasitol. 63, 299–303. https://doi.org/10.1016/0166-6851(94)90066-3

Kwiatkowski, D.J., 1999. Functions of gelsolin: motility, signalling, apoptosis, cancer. Curr. Opin. Cell Biol. 11, 103–108.

Lacey, E., 1988. The role of the cytoskeletal protein, tubulin, in the mode of action and mechanism of drug resistance to benzimidazoles. Int. J. Parasitol. 18, 885–936.

LaCourse, E.J., Perally, S., Morphew, R.M., Moxon, J. V., Prescott, M., Dowling, D.J., O'Neill, S.M., Kipar, A., Hetzel, U., Hoey, E., Zafra, R., Buffoni, L., Arévalo, J., Brophy, P.M., 2012. The Sigma class glutathione transferase from the liver fluke *Fasciola hepatica*. PLoS Negl. Trop. Dis. 6, e1666. https://doi.org/10.1371/journal.pntd.0001666

Lagrange, E., Gutmann, A., 1961. Experimental Infection of Mice by *Fasciola hepatica*. Riv. Parassitol. 22, 93–101.

Laine, R.O., Phaneuf, K.L., Cunningham, C.C., Kwiatkowski, D., Azuma, T., Southwick, F.S.,

1998. Gelsolin, a protein that caps the barbed ends and severs actin filaments, enhances the actin-based motility of *Listeria monocytogenes* in host cells. Infect. Immun. 66, 3775–3782.

Lambeir, A.M., Backmann, J., Ruiz-Sanz, J., Filimonov, V., Nielsen, J.E., Kursula, I., Norledge, B. V., Wierenga, R.K., 2000. The ionization of a buried glutamic acid is thermodynamically linked to the stability of *Leishmania mexicana* triose phosphate isomerase. Eur. J. Biochem. 267, 2516–2524. https://doi.org/10.1046/j.1432-1327.2000.01254.x

Landa, A., Rojo-Domínguez, A., Jiménez, L., Fernández-Velasco, D.A., 1997. Sequencing, expression and properties of triosephosphate isomerase from *Entamoeba histolytica*. Eur. J. Biochem. 247, 348–355. https://doi.org/10.1111/j.1432-1033.1997.00348.x

Law, R.H.P., Smooker, P.M., Irving, J.A., Piedrafita, D., Ponting, R., Kennedy, N.J., Whisstock, J.C., Pike, R.N., Spithill, T.W., 2003. Cloning and expression of the major secreted cathepsin B-like protein from juvenile *Fasciola hepatica* and analysis of immunogenicity following liver fluke infection. Infect. Immun. 71, 6921–32. https://doi.org/10.1128/IAI.71.12.6921-6932.2003

Le Jambre, L.F., 2006. Eradication of targeted species of internal parasites. Vet. Parasitol. 139, 360–370.

Lee, B.Y., Bacon, K.M., Bottazzi, M.E., Hotez, P.J., 2013. Global economic burden of Chagas disease: A computational simulation model. Lancet Infect. Dis. 13, 342–348. https://doi.org/10.1016/S1473-3099(13)70002-1

Lee, C.G., Cho, S.H., Lee, C.Y., 1995. Metacercarial production of *Lymnaea viridis* experimentally infected with *Fasciola hepatica*. Vet. Parasitol. 58, 313–318. https://doi.org/10.1016/0304-4017(94)00725-R

Lee, J.Y., Song, J., Kwon, K., Jang, S., Kim, C., Baek, K., Kim, J., Park, C., 2012. Human DJ-1 and its homologs are novel glyoxalases. Hum. Mol. Genet. 21, 3215–3225. https://doi.org/10.1093/hmg/dds155

Lee, P.-S., Sampath, K., Karumanchi, S.A., Tamez, H., Bhan, I., Isakova, T., Gutierrez, O.M., Wolf, M., Chang, Y., Stossel, T.P., Thadhani, R., 2009. Plasma Gelsolin and Circulating Actin Correlate with Hemodialysis Mortality. J. Am. Soc. Nephrol. 20, 1140–1148. https://doi.org/10.3233/WOR-141845

Lee, P.S., Drager, L.R., Stossel, T.P., Moore, F.D., Rogers, S.O., 2006. Relationship of plasma gelsolin levels to outcomes in critically III surgical patients. Ann. Surg. 243, 399–403. https://doi.org/10.1097/01.sla.0000201798.77133.55

Lee, P.S., Waxman, A.B., Cotich, K.L., Chung, S.W., Perrella, M.A., Stossel, T.P., 2007. Plasma gelsolin is a marker and therapeutic agent in animal sepsis. Crit. Care Med. 35, 849–855. https://doi.org/10.1097/01.CCM.0000253815.26311.24

Lee, W.M., Galbraith, R.M., 1992. The Extracellular Actin-Scavenger System and Actin Toxicity. N. Engl. J. Med. 326, 1335–1341. https://doi.org/10.1056/NEJM199205143262006

Leung, T.L.F., Poulin, R., 2008. Parasitism, commensalism, and mutualism: Exploring the many shades of symbioses. Vie Milieu 58, 107–115.

Levieux, D., Levieux, A., Mage, C., Garel, J.P., 1992. Immunological detection of chemotherapeutic success in bovine fasciolosis using the specific antigen f2. Vet. Parasitol. 45, 81–88. https://doi.org/10.1016/0304-4017(92)90029-9

Levy, E., Haltia, M., Fernandez-Madrid, I., Koivunen, O., Ghiso, J., Prelli, F., Frangione, B., 1990. Mutation in gelsolin gene in Finnish hereditary amyloidosis. J. Exp. Med. Med. 172, 1865–1867. https://doi.org/10.1084/jem.172.6.1865

Li, B., Krishnan, V.G., Mort, M.E., Xin, F., Kamati, K.K., Cooper, D.N., Mooney, S.D., Radivojac,

P., 2009. Automated inference of molecular mechanisms of disease from amino acid substitutions. Bioinformatics 25, 2744–2750. https://doi.org/10.1093/bioinformatics/btp528

Li, W.H.H., Qu, Z.G.G., Zhang, N.Z.Z., Yue, L., Jia, W.Z.Z., Luo, J.X.X., Yin, H., Fu, B.Q.Q., 2015. Molecular characterization of enolase gene from *Taenia multiceps*. Res. Vet. Sci. 102, 53–58. https://doi.org/10.1016/j.rvsc.2015.06.013

Lightowlers, M.W., Colebrook, A.L., Gauci, C.G., Gauci, S.M., Kyngdon, C.T., Monkhouse, J.L., Vallejo Rodriquez, C., Read, A.J., Rolfe, R.A., Sato, C., 2003. Vaccination against cestode parasites: Anti-helminth vaccines that work and why. Vet. Parasitol. 115, 83–123. https://doi.org/10.1016/S0304-4017(03)00202-4

Lightowlers, M.W., Flisser, A., Gauci, C.G., Heath, D.D., Jensen, O., Rolfe, R., 2000. Vaccination against cysticercosis and hydatid disease. Parasitol. Today 16, 191–196. https://doi.org/10.1016/S0169-4758(99)01633-6

Lin, J., Prahlad, J., Wilson, M.A., 2012. Conservation of oxidative protein stabilization in an insect homologue of parkinsonism-associated protein DJ-1. Biochemistry 51, 3799–3807. https://doi.org/10.1021/bi3003296

Lin, K.M., Mejillano, M., Yin, H.L., 2000. Ca2+ regulation of gelsolin by its C-terminal tail. J. Biol. Chem. 275, 27746–27752. https://doi.org/10.1074/jbc.M003732200

Lind, S.E., Smith, D.B., Janmey, P.A., Stossel, T.P., 1986. Role of plasma gelsolin and the vitamin D-binding protein in clearing actin from the circulation. J. Clin. Invest. 78, 736–742. https://doi.org/10.1172/JCI112634

Linder, E., Thors, C., 1992. *Schistosoma mansoni*: praziquantel-induced tegumental lesion exposes actin of surface spines and allows binding of actin depolymerizing factor, gelsolin. Parasitology 105, 71–79.

Lindsay, W.M., Mc Donnell, R.J., Williams, C.D., Knutson, L., Gormally, M.J., 2009. Biology of the snail-killing fly *Ilione albiseta* (Scopoli, 1763) (Diptera: Sciomyzidae). Stud. dipterologica 16, 245–307.

Line, K., Isupov, M.N., LaCourse, E.J., Cutress, D.J., Morphew, R.M., Brophy, P.M., Littlechild, J.A., 2019. X-ray structure of *Fasciola hepatica* Sigma class glutathione transferase 1 reveals a disulfide bond to support stability in gastro-intestinal environment. Sci. Rep. 9, 1–9. https://doi.org/10.1038/s41598-018-37531-5

Liu, K.-J., Shih, N.-Y., 2007. The Role of Enolase in Tissue Invasion and Metastasis of Pathogens and Tumor Cells. J. Cancer Mol. 3, 45–48.

Liu, Y., Oshima, S.I., Kurohara, K., Ohnishi, K., Kawai, K., 2005. Vaccine efficacy of recombinant GAPDH of *Edwardsiella tarda* against Edwardsiellosis. Microbiol. Immunol. 49, 605–612. https://doi.org/10.1111/j.1348-0421.2005.tb03652.x

Livesay, D.R., La, D., 2005. The evolutionary origins and catalytic importance of conserved electrostatic networks within TIM-barrel proteins. Protein Sci. 14, 1158–70. https://doi.org/10.1110/ps.041221105

Lord, S.J., Irwig, L., Simes, R.J., 2006. When is measuring sensitivity and specificity sufficient to evaluate a diagnostic test, and when do we need randomized trials? Ann. Intern. Med. 144, 850–855. https://doi.org/10.7326/0003-4819-144-11-200606060-00011

Lorenzatto, K.R., Monteiro, K.M., Paredes, R., Paludo, G.P., Da Fonsêca, M.M., Galanti, N., Zaha, A., Ferreira, H.B., 2012. Fructose-bisphosphate aldolase and enolase from *Echinococcus granulosus*: Genes, expression patterns and protein interactions of two potential moonlighting proteins. Gene 506, 76–84. https://doi.org/10.1016/j.gene.2012.06.046

Lotfy, W.M., Brant, S. V., DeJong, R.J., Thanh, H.L., Demiaszkiewicz, A., Rajapakse, R.P.V.J., Perera, V.B.V.P., Laursen, J.R., Loker, E.S., 2008. Evolutionary origins, diversification, and biogeography of liver flukes (Digenea, Fasciolidae). Am. J. Trop. Med. Hyg. 79, 248–255.

Lovato, L., Cianti, R., Gini, B., Marconi, S., Bianchi, L., Armini, A., Anghileri, E., Locatelli, F., Paoletti, F., Franciotta, D., Bini, L., Bonetti, B., 2008. Transketolase and 2',3'-Cyclic-nucleotide 3'-Phosphodiesterase Type I Isoforms Are Specifically Recognized by IgG Autoantibodies in Multiple Sclerosis Patients. Mol. Cell. Proteomics 7, 2337–2349. https://doi.org/10.1074/mcp.M700277-MCP200

Lowther, J., Robinson, M.W., Donnelly, S.M., Xu, W., Stack, C.M., Matthews, J.M., Dalton, J.P., 2009. The importance of pH in regulating the function of the *Fasciola hepatica* cathepsin L1 cysteine protease. PLoS Negl. Trop. Dis. 3, 1–11. https://doi.org/10.1371/journal.pntd.0000369

Loyacano, A.F., Williams, J.C., Gurie, J., DeRosa, A.A., 2002. Effect of gastrointestinal nematode and liver fluke infections on weight gain and reproductive performance of beef heifers. Vet. Parasitol. 107, 227–234. https://doi.org/10.1016/S0304-4017(02)00130-9

Lück, A., D'Haese, J., Hinssen, H., 1995. A gelsolin-related protein from lobster muscle: cloning, sequence analysis and expression. Biochem. J. 305, 767–775.

MacGillivray, F., De Waal, T., Maguire, D., Taylor, M.A., Boughtflower, V., Daniel, R., Jenkins, T., Rice, B., Forbes, A.B., 2013. An abattoir survey to determine the population profile in the autumn of *Fasciola hepatica* in condemned bovine livers from Ireland and the United Kingdom. Int. J. Appl. Res. Vet. Med. 11, 1–6.

MacKintosh, N., 2011. Tools for Monitoring Drug Resistant *Fasciola hepatica* in Cattle and Sheep. Aberystwyth University.

Madeira, F., Park, Y. mi, Lee, J., Buso, N., Gur, T., Madhusoodanan, N., Basutkar, P., Tivey, A.R.N., Potter, S.C., Finn, R.D., Lopez, R., 2019. The EMBL-EBI search and sequence analysis tools APIs in 2019. Nucleic Acids Res. 47, W636–W641. https://doi.org/10.1093/nar/gkz268

Maithal, K., Ravindra, G., Balaram, H., Balaram, P., 2002. Inhibition of *Plasmodium falciparum* triose-phosphate isomerase by chemical modification of an interface cysteine: Electrospray ionization mass spectrometric analysis of differential cysteine reactivities. J. Biol. Chem. 277, 25106–25114. https://doi.org/10.1074/jbc.M202419200

Malcicka, M., 2015. Life history and biology of *Fascioloides magna* (Trematoda) and its native and exotic hosts. Ecol. Evol. 5, 1381–1397. https://doi.org/10.1002/ece3.1414

Maqbool, I., Wani, Z.A., Shahardar, R.A., Allaie, I.M., Shah, M.M., 2016. Integrated parasite management with special reference to gastro-intestinal nematodes. J. Parasit. Dis. 41, 1–8. https://doi.org/10.1007/s12639-016-0765-6

Marcilla, A., De La Rubia, J.E., Sotillo, J., Bernal, D., Carmona, C., Villavicencio, Z., Acosta, D., Tort, J., Bornay, F.J., Esteban, J.G., Toledo, R., 2008. Leucine aminopeptidase is an immunodominant antigen of *Fasciola hepatica* excretory and secretory products in human infections. Clin. Vaccine Immunol. 15, 95–100. https://doi.org/10.1128/CVI.00338-07

Marcilla, A., Trelis, M., Cortés, A., Sotillo, J., Cantalapiedra, F., Minguez, M.T., Valero, M.L., Sánchez del Pino, M.M., Muñoz-Antoli, C., Toledo, R., Bernal, D., 2012. Extracellular Vesicles from Parasitic Helminths Contain Specific Excretory/Secretory Proteins and Are Internalized in Intestinal Host Cells. PLoS One 7, e45974. https://doi.org/10.1371/journal.pone.0045974

Marek, J., 1927. Neuere beiträge zur kenntnis der leberegelkrankheit mit besonderer berücksichtigung der infektionsweise, der entwicklung der distomen und der therapie. Dtsch. Tierarztl. Wochenschr. 32, 513–519.

Markoski, M.M., Trindade, E.S., Cabrera, G., Laschuk, A., Galanti, N., Zaha, A., Nader, H.B., Ferreira, H.B., 2006. Praziquantel and albendazole damaging action on in vitro developing *Mesocestoides corti* (Platyhelminthes: Cestoda). Parasitol. Int. 55, 51–61. https://doi.org/10.1016/j.parint.2005.09.005

Martin, B.D., Schwab, E., 2012. Current Usage of Symbiosis and Associated Terminology. Int. J. Biol. 5. https://doi.org/10.5539/ijb.v5n1p32

Martin, V., Groenendyk, J., Steiner, S.S., Guo, L., Dabrowska, M., Parker, J.M.R., Müller-Esterl, W., Opas, M., Michalak, M., 2006. Identification by mutational analysis of amino acid residues essential in the chaperone function of calreticulin. J. Biol. Chem. 281, 2338–2346. https://doi.org/10.1074/jbc.M508302200

Martínez-Pérez, J.M., Robles-Pérez, D., Rojo-Vázquez, F.A., Martínez-Valladares, M., 2012. Comparison of three different techniques to diagnose *Fasciola hepatica* infection in experimentally and naturally infected sheep. Vet. Parasitol. 190, 80–86. https://doi.org/10.1016/j.vetpar.2012.06.002

Martínez-Sernández, V., Muiño, L., Perteguer, M.J., Gárate, T., Mezo, M., González-Warleta, M., Muro, A., Correia da Costa, J.M., Romarís, F., Ubeira, F.M., 2011. Development and evaluation of a new lateral flow immunoassay for serodiagnosis of human fasciolosis. PLoS Negl. Trop. Dis. 5. https://doi.org/10.1371/journal.pntd.0001376

Martínez-Sernández, V., Orbegozo-Medina, R.A., Gonzalez-Warleta, M., Mezo, M., Ubeira, F.M., 2016. Rapid Enhanced MM3-COPRO ELISA for Detection of *Fasciola* Coproantigens. PLoS Negl. Trop. Dis. 10, e0004872. https://doi.org/10.1371/journal.pntd.0004872

Martínez-Valladares, M., Cordero-pérez, C., Rojo-Vázquez, F.A., 2014. Efficacy of an anthelmintic combination in sheep infected with *Fasciola hepatica* resistant to albendazole and clorsulon. Exp. Parasitol. 136, 59–62. https://doi.org/10.1016/j.exppara.2013.10.010

Martins dos Santos, T.R., 2012. Genetic characterization of Portuguese *Fasciola hepatica* isolates. Universidade Nova de Lisboa.

Martoglio, B., Dobberstein, B., 1998. Signal sequences: More than just greasy peptides. Trends Cell Biol. 8, 410–415. https://doi.org/10.1016/S0962-8924(98)01360-9

Mas-Coma, S., 2005. Epidemiology of fascioliasis in human endemic areas. J. Helminthol. 79, 207–216. https://doi.org/10.1079/JOH2005296

Mas-Coma, S., Bargues, M.D., 1997. Human liver flukes: a review. Res. Rev. Parasitol. 57, 145–218.

Mas-Coma, S., Bargues, M.D., Valero, M.A., 2018. Human fascioliasis infection sources, their diversity, incidence factors, analytical methods and prevention measures. Parasitology 145, 1665–1699. https://doi.org/10.1017/S0031182018000914

Mas-Coma, S., Bargues, M.D., Valero, M.A., 2005. Fascioliasis and other plant-borne trematode zoonoses. Int. J. Parasitol. 35, 1255–1278. https://doi.org/10.1016/j.ijpara.2005.07.010

Mas-Coma, S., Esteban, J.G., Bargues, M.D., 1999. Epidemiology of human fascioliasis: a review and proposed new classification.

Mas-Coma, S., Funatsu, I.R., Bargues, M.D., 2001. *Fasciola hepatica* and lymnaeid snails occurring at very high altitude in South America. Parasitology 123, 115–127. https://doi.org/10.1017/s0031182001008034

Mas-Coma, S., Valero, M.A., Bargues, M.D., 2009. Climate change effects on trematodiases, with emphasis on zoonotic fascioliasis and schistosomiasis. Vet. Parasitol. 163, 264–280. https://doi.org/10.1016/j.vetpar.2009.03.024

Matouskova, P., Vokr, I., Lamka, J., Matous, P., Skálová, L., 2016. The Role of Xenobiotic-Metabolizing Enzymes in Anthelmintic Deactivation and Resistance in Helminths. Trends Parasitol. 32, 481–491. https://doi.org/10.1016/j.pt.2016.02.004

Matsukuma, S., Yoshimura, K., Ueno, T., Oga, A., Inoue, M., Watanabe, Y., Kuramasu, A., Fuse, M., Tsunedomi, R., Nagaoka, S., Eguchi, H., Matsui, H., Shindo, Y., Maeda, N., Tokuhisa, Y., Kawano, R., Furuya-Kondo, T., Itoh, H., Yoshino, S., Hazama, S., Oka, M., Nagano, H., 2016. Calreticulin is highly expressed in pancreatic cancer stem-like cells. Cancer Sci. 107, 1599–1609. https://doi.org/10.1111/cas.13061

Mazzola, J.L., Sirover, M.A., 2003. Subcellular localization of human glyceraldehyde-3-phosphate dehydrogenase is independent of its glycolytic function. Biochim. Biophys. Acta - Gen. Subj. 1622, 50–56. https://doi.org/10.1016/S0304-4165(03)00117-X

Mc Donnell, R.J., Paine, T.D., Mulkeen, C.J., Gormally, M.J., 2014. Effects of temperature and prey availability on the malacophagous larval stage of *Sepedon spinipes* (Scopoli) (Diptera: Sciomyzidae): Potential biocontrol for gastropod vectors of parasitic diseases. Biol. Control 70, 42–47. https://doi.org/10.1016/j.biocontrol.2013.12.001

McArthur, A.G., Wright, G.D., 2015. Bioinformatics of antimicrobial resistance in the age of molecular epidemiology. Curr. Opin. Microbiol. 27, 45–50. https://doi.org/10.1016/j.mib.2015.07.004

McCann, C.M., Baylis, M., Williams, D.J.L., 2010. The development of linear regression models using environmental variables to explain the spatial distribution of *Fasciola hepatica* infection in dairy herds in England and Wales. Int. J. Parasitol. 40, 1021–1028. https://doi.org/10.1016/j.ijpara.2010.02.009

McConville, M., Brennan, G.P., McCoy, M., Castillo, R., Hernandez-Campos, A., Ibarra, F., Fairweather, I., 2006. Immature triclabendazole-resistant *Fasciola hepatica*: Tegumental responses to *in vitro* treatment with the sulphoxide metabolite of the experimental fasciolicide compound alpha. Parasitol. Res. 100, 365–377. https://doi.org/10.1007/s00436-006-0270-4

McCusker, P., McVeigh, P., Rathinasamy, V., Toet, H., McCammick, E., O'Connor, A., Marks, N.J., Mousley, A., Brennan, G.P., Halton, D.W., Spithill, T.W., Maule, A.G., 2016. Stimulating Neoblast-Like Cell Proliferation in Juvenile *Fasciola hepatica* Supports Growth and Progression towards the Adult Phenotype In Vitro. PLoS Negl. Trop. Dis. 10. https://doi.org/10.1371/journal.pntd.0004994

McGinty, A., Halton, D.W., Moore, M., Walker, B., 1993. Characterization of the cysteine proteinases of the common liver fluke *Fasciola hepatica* using novel, active-site directed affinity labels. Parasitology 106, 487–493. https://doi.org/10.1017/S0031182000076782

McGonigle, L., Mousley, A., Marks, N.J., Brennan, G.P., Dalton, J.P., Spithill, T.W., Day, T.A., Maule, A.G., 2008. The silencing of cysteine proteases in *Fasciola hepatica* newly excysted juveniles using RNA interference reduces gut penetration. Int. J. Parasitol. 38, 149–155. https://doi.org/10.1016/j.ijpara.2007.10.007

McGonigle, S., Dalton, J.P., James, E.R., 1998. Peroxidoxins: A new antioxidant family. Parasitol. Today. https://doi.org/10.1016/S0169-4758(97)01211-8

McGough, A.M., Staiger, C.J., Min, J., Simonetti, K.D., 2003. The gelsolin family of actin regulatory proteins: modular structures, versatile functions. FEBS Lett. 552, 75–81. https://doi.org/10.1016/S0014-5793(03)00932-3

McGrath, M.E., 1999. The Lysosomal Cysteine Proteases. Annu. Rev. Biophys. Biomol. Struct. 28, 181–204. https://doi.org/10.1146/annurev.biophys.28.1.181

McIlroy, S.G., Goodall, E.A., Stewart, D.A., Taylor, S.M., McCracken, R.M., 1990. A computerised system for the accurate forecasting of the annual prevalence of fasciolosis. Prev. Vet. Med. 9, 27–35.

McKellar, Q.A., Scott, E.W., 1990. The benzimidazole anthelmintic agents-a review. J. Vet. Pharmacol. Ther. 13, 223–247. https://doi.org/10.1111/j.1365-2885.1990.tb00773.x

McLaughlin, P.J., Gooch, J.T., Mannherz, H.G., Weeds, A.G., 1993. Structure of gelsolin segment 1-actin complex and the mechanism of filament severing. Nature 3634, 685–692. https://doi.org/10.1038/364685a0

McVeigh, P., Maule, A.G., Dalton, J.P., Robinson, M.W., 2012. Fasciola hepatica virulence-associated cysteine peptidases: a systems biology perspective. Microbes Infect. 14, 301–10. https://doi.org/10.1016/j.micinf.2011.11.012

Mebius, M.M., Op Heij, J.M.J., Tielens, A.G.M., Se Groot, P.G., Urbanus, R.T., van Hellemond, J.J., 2018. Fibrinogen and fibrin are novel substrates for *Fasciola hepatica* cathepsin L peptidases. Mol. Biochem. Parasitol. 221, 10–13. https://doi.org/10.1016/j.molbiopara.2018.02.001

Medina, F.R., Ritchie, L.S., 1980. Molluscicidal activity of the Puerto Rican Weed, Solatium nodiflorum, against snail hosts of *Fasciola hepatica*. Econ. Bot. 34, 368–375. https://doi.org/10.1007/BF02858313

Medina, F.R., Woodbury, R., 1979. Terrestrial plants molluscicidal to Lymnaeid hosts of *Fasciola hepatica* in Puerto Rico. J. Agric. Univ. Puerto Rico 63, 366–376.

Meemon, K., Sobhon, P., 2015. Juvenile-specific cathepsin proteases in Fasciola spp.: their characteristics and vaccine efficacies. Parasitol. Res. https://doi.org/10.1007/s00436-015-4589-6

Meléndez, P.A., Capriles, V.A., 2002. Molluscicidal activity of plants from Puerto Rico. Ann. Trop. Med. Parasitol. 96, 209–218. https://doi.org/10.1179/000349802125000600

Ménard, R., Carmona, E., Takebe, S., Dufour, É., Plouffe, C., Mason, P., Mort, J.S., 1998. Autocatalytic processing of recombinant human procathepsin L: Contribution of both intermolecular and unimolecular events in the processing of procathepsin L *in vitro*. J. Biol. Chem. 273, 4478–4484. https://doi.org/10.1074/jbc.273.8.4478

Mendes, R.E., Pérez-Écija, R.A., Zafra, R., Buffoni, L., Martínez-Moreno, Á., Dalton, J.P., Mulcahy, G., Pérez, J., 2010. Evaluation of hepatic changes and local and systemic immune responses in goats immunized with recombinant Peroxiredoxin (Prx) and challenged with *Fasciola hepatica*. Vaccine 28, 2832–2840. https://doi.org/10.1016/j.vaccine.2010.01.055

Mendlovic, F., Ostoa-Saloma, P., Solís, C.F., Martínez-Ocaña, J., Flisser, A., Laclette, J.P., 2004. Cloning, characterization, and functional expression of *Taenia solium* calreticulin. J. Parasitol. 90, 891–3. https://doi.org/10.1645/GE-3325RN

Menon, K.N., Steer, D.L., Short, M., Petratos, S., Smith, I., Bernard, C.C.A., 2011. A novel unbiased proteomic approach to detect the reactivity of cerebrospinal fluid in neurological diseases. Mol. Cell. Proteomics 10, M110.000042. https://doi.org/10.1074/mcp.M110.000042

Meshgi, B., Jalousian, F., Fathi, S., Jahani, Z., 2018. Design and synthesis of a new peptide derived from *Fasciola gigantica* cathepsin L1 with potential application in serodiagnosis of fascioliasis. Exp. Parasitol. 189, 76–86. https://doi.org/10.1016/j.exppara.2018.04.013

Meulener, M., Whitworth, A.J., Armstrong-Gold, C.E., Rizzu, P., Heutink, P., Wes, P.D., Pallanck, L.J., Bonini, N.M., 2005. *Drosophila* DJ-1 mutants are selectively sensitive to environmental toxins associated with Parkinson's disease. Curr. Biol. 15, 1572–1577. https://doi.org/10.1016/j.cub.2005.07.064

Mezo, M., González-Warleta, M., Carro, C., Ubeira, F.M., 2004. An ultrasensitive capture ELISA for detection of *Fasciola hepatica* coproantigens in sheep and cattle using a new monoclonal antibody (MM3). J. Parasitol. 90, 845–852. https://doi.org/10.1645/GE-192R

Mezo, M., González-Warleta, M., Castro-Hermida, J.A., Muiño, L., Ubeira, F.M., 2011. Association between anti-*Fasciola hepatica* antibody levels in milk and production losses in dairy cows. Vet. Parasitol. 180, 237–242. https://doi.org/10.1016/j.vetpar.2011.03.009

Mezo, M., González-Warleta, M., Ubeira, F.M., 2007. The use of MM3 monoclonal antibodies for the early immunodiagnosis of ovine fascioliasis. J. Parasitol. 93, 65–72.

Michalak, M., Corbett, E.F., Mesaeli, N., Nakamura, K., Opas, M., 1999. Calreticulin: one protein, one gene, many functions. Biochem. J. 344 Pt 2, 281–92.

Miranda-Ozuna, J.F.T., Hernández-García, M.S., Brieba, L.G., Benítez-Cardoza, C.G., Ortega-López, J., González-Robles, A., Arroyo, R., 2016. The glycolytic enzyme triosephosphate isomerase of *Trichomonas vaginalis* is a surface-associated protein induced by glucose that functions as a laminin- and fibronectin-binding protein. Infect. Immun. 84, 2878–2794. https://doi.org/10.1128/IAI.00538-16

Mitchell, G., 2002. Update on fasciolosis in cattle and sheep. In Pract. 24, 378–385.

Mitchell, G.B., Maris, L., Bonniwell, M.A., 1998. Triclabendazole-resistant liver fluke in Scottish sheep. Vet. Rec.

Mitchell, S., Hunt, K., Wood, R., McLean, B., 2006. Anthelmintic resistance in sheep flocks in Wales. Vet. Rec. 156, 860. https://doi.org/10.1136/vr.159.25.860-a

Moazeni, M., Ahmadi, A., 2016. Controversial aspects of the life cycle of *Fasciola hepatica*. Exp. Parasitol. 169, 81–89. https://doi.org/https://doi.org/10.1016/j.exppara.2016.07.010

Molina-Hernández, V., Mulcahy, G., Pérez, J., Martínez-Moreno, Á., Donnelly, S., Neill, S.M.O., Dalton, J.P., Cwiklinski, K., 2015. *Fasciola hepatica* vaccine: We may not be there yet but we're on the right road. Vet. Parasitol. 208, 101–111. https://doi.org/10.1016/j.vetpar.2015.01.004

Molina, M.C., Ferreira, V., Valck, C., Aguilar, L., Orellana, J., Rojas, A., Ramirez, G., Billetta, R., Schwaeble, W., Lemus, D., Ferreira, A., 2005. An *in vivo* role for *Trypanosoma cruzi* calreticulin in antiangiogenesis. Mol. Biochem. Parasitol. 140, 133–140. https://doi.org/10.1016/j.molbiopara.2004.12.014

Moll, L., Gaasenbeek, C.P.H., Vellema, P., Borgsteede, F.H.M., 2000. Resistance of *Fasciola hepatica* against triclabendazole in cattle and sheep in The Netherlands. Vet. Parasitol. 91, 153–158.

Molloy, J.B., Anderson, G.R., Fletcher, T.I., Landmann, J., Knight, B.C., 2005. Evaluation of a commercially available enzyme-linked immunosorbent assay for detecting antibodies to *Fasciola hepatica* and *Fasciola gigantica* in cattle, sheep and buffaloes in Australia. Vet. Parasitol. 130, 207–212. https://doi.org/10.1016/j.vetpar.2005.02.010

Montaner, S., Galiano, A., Trelis, M., Martin-Jaular, L., Del Portillo, H.A., Bernal, D., Marcilla, A., 2014. The role of extracellular vesicles in modulating the host immune response during parasitic infections. Front. Immunol. 5, 433.

https://doi.org/10.3389/fimmu.2014.00433
Mooney, L., Good, B., Hanrahan, J.P., Mulcahy, G., Waal, T. De, 2009. The comparative efficacy of four anthelmintics against a natural acquired *Fasciola hepatica* infection in hill sheep flock in the west of Ireland. Vet. Parasitol. 164, 201–205. https://doi.org/10.1016/j.vetpar.2009.05.017
Morand, S., Krasnov, B.R., Poulin, R., Degen, A.A., 2006. Micromammals and macroparasites: Who is who and how do they interact?, in: Micromammals and Macroparasites: From Evolutionary Ecology to Management. pp. 3–9. https://doi.org/10.1007/978-4-431-36025-4_1
Moreau, E., Chauvin, A., 2010. Immunity against helminths: interactions with the host and the intercurrent infections. J. Biomed. Biotechnol. 2010, 428593. https://doi.org/10.1155/2010/428593
Moreno, L., Ceballos, L., Fairweather, I., Lanusse, C., Alvarez, L.I., 2014. Time-course and accumulation of triclabendazole and its metabolites in bile, liver tissues and flukes collected from treated sheep. Exp. Parasitol. 136, 14–19. https://doi.org/10.1016/j.exppara.2013.10.014
Moreno, Y., Geary, T.G., 2008. Stage- and gender-specific proteomic analysis of *Brugia malayi* excreto-secretory products. PLoS Negl. Trop. Dis. 2, e326. https://doi.org/10.1371/journal.pntd.0000326
Morgan, C.J., Wilkins, D.K., Smith, L.J., Kawata, Y., Dobson, C.M., 2000. A compact monomeric intermediate identified by NMR in the denaturation of dimeric triose phosphate isomerase. J. Mol. Biol. 300, 11–16. https://doi.org/10.1016/j.matdes.2004.02.002
Morgan, E., Charlier, J., Hendrickx, G., Biggeri, A., Catalan, D., von Samson-himmelstjerna, G., Demeler, J., Müller, E., van Dijk, J., Kenyon, F., Skuce, P.J., Höglund, J., O'Kiely, P., van Ranst, B., De Waal, T., Rinaldi, L., Cringoli, G., Hertzberg, H., Torgerson, P., Wolstenholme, A.J., Vercruysse, J., 2013. Global Change and Helminth Infections in Grazing Ruminants in Europe: Impacts, Trends and Sustainable Solutions. Agriculture 3, 484–502. https://doi.org/10.3390/agriculture3030484
Mori, Y., Notomi, T., 2009. Loop-mediated isothermal amplification (LAMP): a rapid, accurate, and cost-effective diagnostic method for infectious diseases. J. Infect. Chemother. 15, 62–69. https://doi.org/10.1007/s10156-009-0669-9
Morley, N.J., Lewis, J.W., 2015. Thermodynamics of trematode infectivity. Parasitology 142, 585–597. https://doi.org/10.1017/S0031182014001632
Morphew, R.M., Hamilton, C.M., Wright, H.A., Dowling, D.J., Neill, S.M.O., 2013. Identification of the major proteins of an immune modulating fraction from adult *Fasciola hepatica* released by Nonidet P40. Vet. Parasitol. 191, 379–385. https://doi.org/10.1016/j.vetpar.2012.08.029.Identification
Morphew, R.M., Mackintosh, N., Hart, E.H., Prescott, M.C., Lacourse, E.J., Brophy, P.M., 2014. In vitro biomarker discovery in the parasitic flatworm *Fasciola hepatica* for monitoring chemotherapeutic treatment. EuPA Open Proteomics 3, 85–99. https://doi.org/10.1016/j.euprot.2014.02.013
Morphew, R.M., Wilkinson, T.J., Mackintosh, N., Jahndel, V., Paterson, S., McVeigh, P., Abbas Abidi, S.M., Saifullah, K., Raman, M., Ravikumar, G., 2016. Exploring and Expanding the Fatty-Acid-Binding Protein Superfamily in *Fasciola* Species. J. Proteome Res. 15, 3308–3321.
Morphew, R.M., Wright, H.A., LaCourse, E.J., Porter, J., Barrett, J., Debra, J., Brophy, P.M., 2011. Towards Delineating Functions within the *Fasciola* Secreted Cathepsin L Protease

Family by Integrating *In Vivo* Based Sub-Proteomics and Phylogenetics. PLoS Negl. Trop. Dis. 5, e937. https://doi.org/10.1371/journal.pntd.0000937

Morphew, R.M., Wright, H.A., LaCourse, E.J., Woods, D.J., Brophy, P.M., 2007. Comparative Proteomics of Excretory-Secretory Proteins Released by the Liver Fluke *Fasciola hepatica* in Sheep Host Bile and during in Vitro Culture *ex Host*. Mol. Cell. Proteomics 6, 963–972. https://doi.org/10.1074/mcp.M600375-MCP200

Morrison, C.A., Colin, T., Sexton, J.L., Bowen, F., Wicker, J., Friedel, T., Spithill, T.W., 1996. Protection of cattle against *Fasciola hepatica* infection by vaccination with glutathione S-transferase. Vaccine 14, 1603–1612. https://doi.org/10.1016/S0264-410X(96)00147-8

Mottier, L., Alvarez, L.I., Ceballos, L., Lanusse, C., 2006a. Drug transport mechanisms in helminth parasites: Passive diffusion of benzimidazole anthelmintics. Exp. Parasitol. 113, 49–57. https://doi.org/10.1016/j.exppara.2005.12.004

Mottier, L., Alvarez, L.I., Fairweather, I., Lanusse, C., 2006b. Resistance-induced changes in triclabendazole transport in *Fasciola hepatica*: ivermectin reversal effect. J. Parasitol. 92, 1355–1360. https://doi.org/10.1645/GE-922R.1

Mottier, L., Moreno, L., Alvarez, L.I., Virkel, G., Lanusse, C., 2004a. Measurement of triclabendazole and its metabolites in liver flukes: Method development and full validation. J. Pharm. Biomed. Anal. 35, 991–999. https://doi.org/10.1016/j.jpba.2004.02.038

Mottier, L., Virkel, G., Solana, H., Alvarez, L.I., Salles, J., Lanusse, C., 2004b. Triclabendazole biotransformation and comparative diffusion of the parent drug and its oxidized metabolites into *Fasciola hepatica*. Xenobiotica 34, 1043–1057. https://doi.org/10.1080/00498250400015285

Mounzer, K.C., Moncure, M., Smith, Y.R., DiNubile, M.J., 1999. Relationship of admission plasma gelsolin levels to clinical outcomes in patients after major trauma. Am. J. Respir. Crit. Care Med. 160, 1673–1681. https://doi.org/10.1164/ajrccm.160.5.9807137

Mugambi, R.M., Agola, E.L., Mwangi, I.N., Kinyua, J., Shiraho, E.A., Mkoji, G.M., 2015. Development and evaluation of a Loop Mediated Isothermal Amplification (LAMP) technique for the detection of hookworm (*Necator americanus*) infection in fecal samples. Parasites and Vectors 8, 574. https://doi.org/10.1186/s13071-015-1183-9

Muiño, L., Perteguer, M.J., Gárate, T., Martínez-Sernández, V., Beltrán, A., Romarís, F., Mezo, M., González-Warleta, M., Ubeira, F.M., 2011. Molecular and immunological characterization of *Fasciola* antigens recognized by the MM3 monoclonal antibody. Mol. Biochem. Parasitol. 179, 80–90. https://doi.org/10.1016/j.molbiopara.2011.06.003

Mulcahy, G., Dalton, J.P., 2001. Cathepsin L proteinases as vaccines against infection with *Fasciola hepatica* (liver fluke) in ruminants. Res. Vet. Sci. 70, 83–86. https://doi.org/10.1053/rvsc.2000.0425

Mulcahy, G., Neill, S.O., Fanning, J., Mccarthy, E., Sekiya, M., 2005. Tissue migration by parasitic helminths – an immunoevasive strategy ? Trends Parasitol. 21, 273–277. https://doi.org/10.1016/j.pt.2005.04.003

Mundia, M.M., Demers, R.W., Chow, M.L., Perieteanu, A.A., Dawson, J.F., 2012. Subdomain location of mutations in cardiac actin correlate with type of functional change. PLoS One 7, e36821. https://doi.org/10.1371/journal.pone.0036821

Mutapi, F., Bourke, C., Harcus, Y., Midzi, N., Mduluza, T., Turner, C.M., Burchmore, R., Maizels, R.M., 2011. Differential recognition patterns of *Schistosoma haematobium* adult worm antigens by the human antibodies IgA, IgE, IgG1 and IgG4. Parasite Immunol. 33, 181–192. https://doi.org/10.1111/j.1365-3024.2010.01270.x

Mutapi, F., Burchmore, R., Mduluza, T., Foucher, A., Harcus, Y., Nicoll, G., Midzi, N., Turner, C.M., Maizels, R.M., 2005. Praziquantel Treatment of Individuals Exposed to *Schistosoma haematobium* Enhances Serological Recognition of Defined Parasite Antigens. J. Infect. Dis. 192, 1108–1118. https://doi.org/doi:10.1086/432553

Nabity, S.A., Ribeiro, G.S., Aquino, C.L., Takahashi, D., Damião, A.O., Gonçalves, A.H.O., Miranda-Filho, D.B., Greenwald, R., Esfandiari, J., Lyashchenko, K.P., 2012. Accuracy of a dual path platform (DPP) assay for the rapid point-of-care diagnosis of human leptospirosis. PLoS Negl. Trop. Dis. 6, e1878.

Nag, S., Ma, Q., Wang, H., Chumnarnsilpa, S., Lee, W.L., Larsson, M., Kannan, B., Hernandez-Valladares, M., Burtnick, L.D., Robinson, R.C., 2009. Ca2+ binding by domain 2 plays a critical role in the activation and stabilization of gelsolin. Proc. Natl. Acad. Sci. U. S. A. 106, 13713–13718. https://doi.org/10.1073/pnas.0812374106

Nahum, L.A., Mourão, M.M., Oliveira, G., 2012. New frontiers in *schistosoma* genomics and transcriptomics. J. Parasitol. Res.

Nakajima, H., Amano, W., Fujita, A., Fukuhara, A., Azuma, Y.T., Hata, F., Inui, T., Takeuchi, T., 2007. The active site cysteine of the proapoptotic protein glyceraldehyde-3- phosphate dehydrogenase is essential in oxidative stress-induced aggregation and cell death. J. Biol. Chem. 282, 26562–26574. https://doi.org/10.1074/jbc.M704199200

Nakajima, H., Amano, W., Kubo, T., Fukuhara, A., Ihara, H., Azuma, Y.T., Tajima, H., Inui, T., Sawa, A., Takeuchi, T., 2009. Glyceraldehyde-3-phosphate dehydrogenase aggregate formation participates in oxidative stress-induced cell death. J. Biol. Chem. 248, 34331–34341. https://doi.org/10.1074/jbc.M109.027698

Ndao, M., 2009. Diagnosis of Parasitic Diseases: Old and New Approaches. Interdiscip. Perspect. Infect. Dis. Article ID 278246. https://doi.org/10.1155/2009/278246

Nice, N.G., Wilson, R.A., 1974. A study of the effect of temperature on the growth of *Fasciola hepatica* in *Lymnaea truncatula*. Parasitology 68, 47–56. https://doi.org/10.1017/S0031182000045364

Nielsen, H., 2017. Predicting secretory proteins with signaIP, in: Methods in Molecular Biology Vol. 1611. pp. 59–73. https://doi.org/10.1007/978-1-4939-7015-5_6

Norbury, L.J., Beckham, S.A., Pike, R.N., Grams, R., Spithill, T.W., Fecondo, J. V., Smooker, P.M., 2011. Adult and juvenile *Fasciola* cathepsin L proteases: Different enzymes for different roles. Biochimie 93, 604–611. https://doi.org/10.1016/j.biochi.2010.12.004

Norledge, B. V., Lambeir, A.M., Abagyan, R.A., Rottmann, A., Fernandez, A.M., Filimonov, M., Vladimir, V., Peter, G., Wierenga, R.K., 2001. Modeling, mutagenesis, and structural studies on the fully conserved phosphate-binding loop (loop 8)of triosephosphate isomerase: Toward a new substrate specificity. Proteins Struct. Funct. Genet. 42, 383–389. https://doi.org/10.1002/1097-0134(20010215)42:3<383::AID-PROT80>3.0.CO;2-G

Novobilský, A., Amaya Solis, N., Skarin, M., Höglund, J., 2016. Assessment of flukicide efficacy against *Fasciola hepatica* in sheep in Sweden in the absence of a standardised test. Int. J. Parasitol. Drugs Drug Resist. 6, 141–147. https://doi.org/10.1016/j.ijpddr.2016.06.004

Novobilský, A., Averpil, H.B., Höglund, J., 2012. The field evaluation of albendazole and triclabendazole efficacy against *Fasciola hepatica* by coproantigen ELISA in naturally infected sheep. Vet. Parasitol. 190, 272–276. https://doi.org/10.1016/j.vetpar.2012.06.022

Novobilský, A., Engström, A., Sollenberg, S., Gustafsson, K., Morrison, D.A., Höglund, J., 2014. Transmission patterns of *Fasciola hepatica* to ruminants in Sweden. Vet. Parasitol. 203, 276–286. https://doi.org/10.1016/j.vetpar.2014.04.015

Novobilský, A., Höglund, J., 2015. First report of closantel treatment failure against *Fasciola hepatica* in cattle. Int. J. Parasitol. Drugs Drug Resist. 5, 172–177. https://doi.org/10.1016/j.ijpddr.2015.07.003

Novobilský, A., Kašný, M., Beran, L., Rondelaud, D., Höglund, J., 2013. *Lymnaea palustris* and *Lymnaea fuscus* are potential but uncommon intermediate hosts of *Fasciola hepatica* in Sweden. Parasites and Vectors 6, 251. https://doi.org/10.1186/1756-3305-6-251

Nyindo, M., Lukambagire, A., 2015. Fascioliasis : An Ongoing Zoonotic Trematode Infection. Biomed Res. Int. 2015.

O'Neill, S.M., Parkinson, M., Dowd, A.J., Strauss, W., Angles, R., Dalton, J.P., 1999. Short report: Immunodiagnosis of human fascioliasis using recombinant *Fasciola hepatica* cathepsin L1 cysteine proteinase. Am. J. Trop. Med. Hyg. 60, 749–751.

Obeid, M., Tesniere, A., Ghiringhelli, F., Fimia, G.M., Apetoh, L., Perfettini, J.L., Castedo, M., Mignot, G., Panaretakis, T., Casares, N., Métivier, D., Larochette, N., Van Endert, P., Ciccosanti, F., Piacentini, M., Zitvogel, L., Kroemer, G., 2007a. Calreticulin exposure dictates the immunogenicity of cancer cell death. Nat. Med. 13, 54–61. https://doi.org/10.1038/nm1523

Obeid, M., Tesniere, A., Panaretakis, T., Tufi, R., Joza, N., Van Endert, P., Ghiringhelli, F., Apetoh, L., Chaput, N., Flament, C., Ullrich, E., De Botton, S., Zitvogel, L., Kroemer, G., 2007b. Ecto-calreticulin in immunogenic chemotherapy. Immunol. Rev. 220, 22–34. https://doi.org/10.1111/j.1600-065X.2007.00567.x

Oikonomou, N., Thanasopoulou, A., Tzouvelekis, A., Harokopos, V., Paparountas, T., Nikitopoulou, I., Witke, W., Karameris, A., Kotanidou, A., Bouros, D., Aidinis, V., 2009. Gelsolin expression is necessary for the development of modelled pulmonary inflammation and fibrosis. Thorax 64, 467–475. https://doi.org/10.1136/thx.2008.107946

Olaechea, F., Lovera, V., Larroza, M., Raffo, F., Cabrera, R., 2011. Resistance of *Fasciola hepatica* against triclabendazole in cattle in Patagonia (Argentina). Vet. Parasitol. 178, 364–366. https://doi.org/http://dx.doi.org/10.1016/j.vetpar.2010.12.047

Ollerenshaw, C.B., 1971. Some observations on the epidemiology and control of fascioliasis in Wales. Int. Liverfluke Colloq. Wageningen, Oct. 2-6. 1967.

Ollerenshaw, C.B., 1966. The approach to forecasting the incidence of fascioliasis over England and Wales 1958–1962. Agric. Meteorol. 3, 35–53. https://doi.org/10.1016/0002-1571(66)90004-5

Ollerenshaw, C.B., 1959. The ecology of the liver fluke (*Fasciola hepatica*). Vet. Rec. 71, 957–963.

Ollerenshaw, C.B., Rowlands, W.T., 1959. A method of forecasting the incidence of fascioliasis in Anglesey. Vet. Rec. 71, 591–598.

Olzmann, J.A., Brown, K., Wilkinson, K.D., Rees, H.D., Huai, Q., Ke, H., Levey, A.I., Li, L., Chin, L.S., 2004. Familial Parkinson's Disease-associated L166P Mutation Disrupts DJ-1 Protein Folding and Function. J. Biol. Chem. 279, 8506–8515. https://doi.org/10.1074/jbc.M311017200

Ortiz, A.R., Strauss, C.E.M., Olmea, O., 2002. MAMMOTH (matching molecular models obtained from theory): an automated method for model comparison. Protein Sci. a Publ. Protein Soc. 11, 2606–2621. https://doi.org/10.1110/ps.0215902

Ortiz, P., Scarcella, S., Cerna, C., Rosales, C., Cabrera, M., Guzmán, M., Lamenza, P., Solana, H., 2013. Resistance of *Fasciola hepatica* against Triclabendazole in cattle in Cajamarca (Peru): A clinical trial and an *in vivo* efficacy test in sheep. Vet. Parasitol. 195, 118–121.

https://doi.org/http://dx.doi.org/10.1016/j.vetpar.2013.01.001
Ortiz, P., Terrones, S., Cabrera, M., Hoban, C., Ceballos, L., Moreno, L., Canton, C., Donadeu, M., Lanusse, C., Alvarez, L.I., 2014. Oxfendazole flukicidal activity in pigs. Acta Trop. 136, 10–13. https://doi.org/10.1016/j.actatropica.2014.03.024
Ottesen, E.A., 2000. The Global Programme to Eliminate Lymphatic Filariasis. Trop. Med. Int. Heal. 5. https://doi.org/10.1046/j.1365-3156.2000.00620.x
Overend, D.J., Bowen, F.L., 1995. Resistance of *Fasciola hepatica* to triclabendazole. Aust. Vet. J. 72, 275–276. https://doi.org/10.1111/j.1751-0813.1995.tb03546.x
Owji, H., Nezafat, N., Negahdaripour, M., Hajiebrahimi, A., Ghasemi, Y., 2018. A comprehensive review of signal peptides: Structure, roles, and applications. Eur. J. Cell Biol. 97, 422–441. https://doi.org/10.1016/j.ejcb.2018.06.003
Pagni, M., Ioannidis, V., Cerutti, L., Zahn-Zabal, M., Jongeneel, C.V., Hau, J., Martin, O., Kuznetsov, D., Falquet, L., 2007. MyHits: Improvements to an interactive resource for analyzing protein sequences. Nucleic Acids Res. 35, W433–W437. https://doi.org/10.1093/nar/gkm352
Pal-Bhowmick, I., Sadagopan, K., Vora, H.K., Sehgal, A., Sharma, S., Jarori, G.K., 2004. Cloning, over-expression, purification and characterization of *Plasmodium falciparum* enolase. Eur. J. Biochem. 271, 4845–4854. https://doi.org/10.1111/j.1432-1033.2004.04450.x
Palmer, D.G., Lyon, J., Palmer, M.A., Forshaw, D., 2014. Evaluation of a copro-antigen ELISA to detect *Fasciola hepatica* infection in sheep, cattle and horses. Aust. Vet. J. 92, 357–361. https://doi.org/10.1111/avj.12224
Panaretakis, T., Joza, N., Modjtahedi, N., Tesniere, A., Vitale, I., Durchschlag, M., Fimia, G.M., Kepp, O., Piacentini, M., Froehlich, K.U., van Endert, P., Zitvogel, L., Madeo, F., Kroemer, G., 2008. The co-translocation of ERp57 and calreticulin determines the immunogenicity of cell death. Cell Death Differ. 15, 1499–1509. https://doi.org/10.1038/cdd.2008.67
Pancholi, V., Chhatwal, G.S., 2003. Housekeeping enzymes as virulence factors for pathogens. Int. J. Med. Microbiol. 293, 391–401. https://doi.org/10.1078/1438-4221-00283
Pankao, V., Sirisriro, A., Grams, R., Vichasri-Grams, S., Meepool, A., Kangwanrangsan, N., Wanichanon, C., Ardseungneon, P., Viyanant, V., Upatham, E.S., Sobhon, P., 2006. Classification of the parenchymal cells in *Fasciola gigantica* based on ultrastructure and their expression of fatty acid binding proteins (FABPs). Vet. Parasitol. 142, 281–292. https://doi.org/10.1016/j.vetpar.2006.07.009
Pantcheva, P., Elias, M., Duncan, K., Borlongan, C. V., Tajiri, N., Kaneko, Y., 2014. The role of DJ-1 in the oxidative stress cell death cascade after stroke. Neural Regen. Res. 9, 1430. https://doi.org/10.4103/1673-5374.139458
Papandreou, M.-E.E., Tavernarakis, N., 2017. Autophagy and the endo/exosomal pathways in health and disease. Biotechnol. J. 12, 1600175. https://doi.org/10.1002/biot.201600175
Park, B.J., Lee, D.G., Yu, J.R., Jung, S.K., Choi, K., Lee, J., Lee, J., Kim, Y.S., Lee, J.I., Kwon, J.Y., Lee, J., Singson, A., Song, W.K., Eom, S.H., Park, C.S., Kim, D.H., Bandyopadhyay, J., Ahnn, J., 2001. Calreticulin, a calcium-binding molecular chaperone, is required for stress response and fertility in *Caenorhabditis elegans*. Mol. Biol. Cell 12, 2835–2845. https://doi.org/10.1091/mbc.12.9.2835
Park, J., Sung, Y.K., Cha, G.H., Sung, B.L., Kim, S., Chung, J., 2005. *Drosophila* DJ-1 mutants show oxidative stress-sensitive locomotive dysfunction. Gene 361, 133–139. https://doi.org/10.1016/j.gene.2005.06.040
Pathak, K.M.L., Gaur, S.N.S., 1990. Immunization of pigs with culture antigens of *Taenia solium*. Vet. Parasitol. 34, 353–356. https://doi.org/10.1016/0304-4017(90)90081-L

Paulitschke, V., Haudek-Prinz, V., Griss, J., Berger, W., Mohr, T., Pehamberger, H., Kunstfeld, R., Gerner, C., 2013. Functional classification of cellular proteome profiles support the identification of drug resistance signatures in melanoma cells. J. Proteome Res. 12, 3264–3276. https://doi.org/10.1021/pr400124w

Paz-Silva, A., Sánchez-Andrade, R., Suárez, J.L., Pedreira, J., Arias, M., López, C., Panadero, R., Díaz, P., Díez-Baños, P., Morrondo, P., 2003. Prevalence of natural ovine fasciolosis shown by demonstrating the presence of serum circulating antigens. Parasitol. Res. 91, 328–331. https://doi.org/10.1007/s00436-003-0961-z

Peddada, N., Sagar, A., Ashish, Garg, R., 2012. Plasma gelsolin: A general prognostic marker of health. Med. Hypotheses 78, 203–210. https://doi.org/10.1016/j.mehy.2011.10.024

Peng, R.Q., Chen, Y.B., Ding, Y., Zhang, R., Zhang, X., Yu, X.J., Zhou, Z.W., Zeng, Y.X., Zhang, X.S., 2010. Expression of calreticulin is associated with infiltration of T-cells in stage III B colon cancer. World J. Gastroenterol. 16, 2428–2434. https://doi.org/10.3748/wjg.v16.i19.2428

Peränen, J., Auvinen, P., Virta, H., Wepf, R., Simons, K., 1996. Rab8 promotes polarized membrane transport through reorganization of actin and microtubules in fibroblasts. J. Cell Biol. 135, 153–167. https://doi.org/10.1083/jcb.135.1.153

Periago, M. V., Valero, M.A., El Sayed, M., Ashrafi, K., El Wakeel, A., Mohamed, M.Y., Desquesnes, M., Curtale, F., Mas-Coma, S., 2008. First phenotypic description of *Fasciola hepatica*/*Fasciola gigantica* intermediate forms from the human endemic area of the Nile Delta, Egypt. Infect. Genet. Evol. 8, 51–58. https://doi.org/10.1016/j.meegid.2007.10.001

Periago, M. V., Valero, M.A., Panova, M., Mas-Coma, S., 2006. Phenotypic comparison of allopatric populations of *Fasciola hepatica* and *Fasciola gigantica* from European and African bovines using a computer image analysis system (CIAS). Parasitol. Res. 99, 368–378. https://doi.org/10.1007/s00436-006-0174-3

Perlman, D., Halvorson, H.O., 1983. A putative signal peptidase recognition site and sequence in eukaryotic and prokaryotic signal peptides. J. Mol. Biol. 167, 391–409. https://doi.org/10.1016/S0022-2836(83)80341-6

Perry, B.D., Randolph, T.F., 1999. Improving the assessment of the economic impact of parasitic diseases and of their control in production animals. Vet. Parasitol. 83, 145–168. https://doi.org/10.1016/S0304-4017(99)00040-0

Piacenza, L., Acosta, D., Basmadjian, I., Dalton, J.P., Carmona, C., 1999. Vaccination with cathepsin L proteinases and with leucine aminopeptidase induces high levels of protection against fascioliasis in sheep. Infect. Immun. 67, 1954–1961.

Pike, A.W., Erasmus, D.A., 1967. The formation, structure and histochemistry of the metacercarial cyst of three species of digenetic trematodes. Parasitology 57, 683–694. https://doi.org/10.1017/S0031182000073157

Piktel, E., Levental, I., Durnaś, B., Janmey, P.A., Bucki, R., 2018. Plasma gelsolin: Indicator of inflammation and its potential as a diagnostic tool and therapeutic target. Int. J. Mol. Sci. 19, 2516. https://doi.org/10.3390/ijms19092516

Pinto, J.P., Ramos, P., De Almeida, S.F., Oliveira, S., Breda, L., Michalak, M., Porto, G., Rivella, S., De Sousa, M., 2008. Protective role of calreticulin in HFE hemochromatosis. Free Radic. Biol. Med. 44, 99–108. https://doi.org/10.1016/j.freeradbiomed.2007.09.014

Pocanschi, C.L., Kozlov, G., Brockmeier, U., Brockmeier, A., Williams, D.B., Gehring, K., 2011. Structural and functional relationships between the lectin and arm domains of calreticulin. J. Biol. Chem. 286, 27266–27277. https://doi.org/10.1074/jbc.M111.258467

Pollard, T.D., 2016. Actin and actin-binding proteins. Cold Spring Harb. Perspect. Biol. 8. https://doi.org/10.1101/cshperspect.a018226

Ponting, C.P., Marshall, J.M., Cederholm-Williams, S.A., 1992. Plasminogen: a structural review. Blood Coagul. Fibrinolysis an Int. J. Haemost. Thromb. 3, 605–14.

Pope, B., Way, M., Weeds, A.G., 1991. Two of the three actin-binding domains of gelsolin bind to the same subdomain of actin: Implications for capping and severing mechanisms. FEBS Lett. 280, 70–74. https://doi.org/10.1016/0014-5793(91)80206-I

Poulin, R., 2011. The many roads to parasitism. A tale of convergence. Adv. Parasitol. 74, 1–40. https://doi.org/10.1016/B978-0-12-385897-9.00001-X

Poulin, R., Randhawa, H.S., 2015. Evolution of parasitism along convergent lines : from ecology to genomics. Parasitology 142, 6–15. https://doi.org/10.1017/S0031182013001674

Poyner, R.R., Larsen, T.M., Wong, S.W., Reed, G.H., 2002. Functional and structural changes due to a serine to alanine mutation in the active-site flap of enolase. Arch. Biochem. Biophys. 401, 155–163. https://doi.org/10.1016/S0003-9861(02)00024-3

Poyner, R.R., Laughlin, L.T., Sowa, G.A., Reed, G.H., 1996. Toward identification of acid/base catalysts in the active site of enolase: Comparison of the properties of K345A, E168Q, and E211Q variants. Biochemistry 35, 1692–1699. https://doi.org/10.1021/bi952186y

Pritchard, D.I., Brown, A., Kasper, G., Mcelroy, P., Loukas, A., Hewitt, C., Berry, C., Füllkrug, R., Beck, E., 1999. A hookworm allergen which strongly resembles calreticulin. Parasite Immunol. 21, 439–450. https://doi.org/10.1046/j.1365-3024.1999.00238.x

Pritchard, G.C., Forbes, A.B., Williams, D.J.L., Salimi-Bejestani, M.R., Daniel, R.G., 2005. Emergence of fasciolosis in cattle in East Anglia. Vet. Rec. 157, 578–582. https://doi.org/10.1136/vr.157.19.578

Qin, J., Chai, G., Brewer, J.M., Lovelace, L.L., Lebioda, L., 2006. Fluoride inhibition of enolase: Crystal structure and thermodynamics. Biochemistry 45, 793–800. https://doi.org/10.1021/bi051558s

Raadsma, H.W., Kingsford, N.M., Suharyanta, Spithill, T.W., Piedrafita, D., 2007. Host responses during experimental infection with *Fasciola gigantica* or *Fasciola hepatica* in Merino sheep. I. Comparative immunological and plasma biochemical changes during early infection. Vet. Parasitol. 143, 275–286. https://doi.org/10.1016/j.vetpar.2006.09.008

Rajcevic, M., 1929. Length of Life of Cercaria of Liver Fluke in Dried Hay. Dtsch. Tierarztl. Wochenschr. 37.

Rakus, J.F., Fedorov, A.A., Fedorov, E. V., Glasner, M.E., Hubbard, B.K., Delli, J.D., Babbitt, P.C., Almo, S.C., Gerlt, J.A., 2008. Evolution of enzymatic activities in the enolase superfamily: L-rhamnonate dehydratase. Biochemistry 47, 9944–8854. https://doi.org/10.1021/bi800914r

Ralser, M., Heeren, G., Breitenbach, M., Lehrach, H., Krobitsch, S., 2006. Triose phosphate isomerase deficiency is caused by altered dimerization-not catalytic inactivity-of the mutant enzymes. PLoS One 1, e30. https://doi.org/10.1371/journal.pone.0000030

Ransohoff, D.F., Feinstein, A.R., 1978. Problems of Spectrum and Bias in Evaluating the Efficacy of Diagnostic Tests. N. Engl. J. Med. 299, 926–930. https://doi.org/10.1056/NEJM197810262991705

Raposo, G., Stoorvogel, W., 2013. Extracellular vesicles: exosomes, microvesicles, and friends. J. Cell Biol. 200, 373–83. https://doi.org/10.1083/jcb.201211138

Rapsch, C., Dahinden, T., Heinzmann, D., Torgerson, P.R., Braun, U., Deplazes, P., Hurni, L.,

Bär, H., Knubben-Schweizer, G., 2008. An interactive map to assess the potential spread of *Lymnaea truncatula* and the free-living stages of *Fasciola hepatica* in Switzerland. Vet. Parasitol. 154, 242–249. https://doi.org/10.1016/j.vetpar.2008.03.030

Reichel, M.P., Vanhoff, K., Baxter, B., 2005. Performance characteristics of an enzyme-linked immunosorbent assay performed in milk for the detection of liver fluke (*Fasciola hepatica*) infection in cattle. Vet. Parasitol. 129, 61–66. https://doi.org/10.1016/j.vetpar.2004.12.013

Relf, V., Good, B., Hanrahan, J.P., McCarthy, E., Forbes, A.B., deWaal, T., 2011. Temporal studies on *Fasciola hepatica* in *Galba truncatula* in the west of Ireland. Vet. Parasitol. 175, 287–292. https://doi.org/10.1016/j.vetpar.2010.10.010

Reszka, N., Cornelissen, J.B.W.J., Harmsen, M.M., Bieńkowska-Szewczyk, K., De Bree, J., Boersma, W.J., Rijsewijk, F.A.M., 2005. *Fasciola hepatica* procathepsin L3 protein expressed by a baculovirus recombinant can partly protect rats against fasciolosis. Vaccine 23, 2987–2993. https://doi.org/10.1016/j.vaccine.2004.12.007

Reynolds, S.R., Dahl, C.E., Harn, D.A., 1994. T and B epitope determination and analysis of multiple antigenic peptides for the *Schistosoma mansoni* experimental vaccine triose-phosphate isomerase. J. Immunol. 152, 193–200.

Ri, M., Iida, S., Nakashima, T., Miyazaki, H., Mori, F., Ito, A., Inagaki, A., Kusumoto, S., Ishida, T., Komatsu, H., Shiotsu, Y., Ueda, R., 2010. Bortezomib-resistant myeloma cell lines: A role for mutated PSMB5 in preventing the accumulation of unfolded proteins and fatal ER stress. Leukemia 24, 1506–1512. https://doi.org/10.1038/leu.2010.137

Ribeiro, C.H., López, N.C., Ramírez, G.A., Valck, C.E., Molina, M.C., Aguilar, L., Rodríguez, M., Maldonado, I., Martínez, R., González, C., Troncoso, R., Lavandero, S., Gingras, A.R., Schwaeble, W., Ferreira, A., 2009. *Trypanosoma cruzi* calreticulin: A possible role in Chagas' disease autoimmunity. Mol. Immunol. 46, 1092–1099. https://doi.org/10.1016/j.molimm.2008.10.034

Rickard, M.D., Williams, J.F., 1982. Hydatidosis/Cysticercosis: Immune Mechanisms and Immunization Against Infection. Adv. Parasitol. 21, 229–296. https://doi.org/10.1016/S0065-308X(08)60277-8

Rim, H.-J., Farag, H.F., Sornmani, S., Cross, J.H., 1994. Food-borne trematodes: Ignored or emerging? Parasitol. Today 10, 207–209. https://doi.org/http://dx.doi.org/10.1016/0169-4758(94)90111-2

Roberts, D.B., Copeman, J.A., 2006. Distribution of metacercariae of *Fasciola gigantica* on rice straw. Trop. Anim. Health Prod. 38, 117–119. https://doi.org/10.1007/s11250-006-4312-9

Roberts, J.A., Suhardono, 1996. Approaches to the control of fasciolosis in ruminants. Int. J. Parasitol. 26, 971–981. https://doi.org/10.1016/S0020-7519(96)80074-9

Roberts, L.S., 2000. The crowding effect revisited. J. Parasitol. 86, 209–211.

Roberts, T., Murrell, K.D., Marks, S., 1994. Economic losses caused by foodborne parasitic diseases. Parasitol. Today 10, 419–423. https://doi.org/10.1016/0169-4758(94)90171-6

Robinson, M.W., Corvo, I., Jones, P.M., George, A.M., Padula, M.P., To, J., Cancela, M., Rinaldi, G., Tort, J.F., Roche, L., Dalton, J.P., 2011. Collagenolytic activities of the major secreted cathepsin L peptidases involved in the virulence of the helminth pathogen, *Fasciola hepatica*. PLoS Negl. Trop. Dis. 5.

Robinson, M.W., Dalton, J.P., 2009. Zoonotic helminth infections with particular emphasis on fasciolosis and other trematodiases. Philos. Trans. R. Soc. B 364, 2763–2776. https://doi.org/10.1098/rstb.2009.0089

Robinson, M.W., Dalton, J.P., Donnelly, S.M., 2008a. Helminth pathogen cathepsin proteases: it's a family affair. Trends Biochem. Sci. 33, 601–608. https://doi.org/10.1016/j.tibs.2008.09.001

Robinson, M.W., Menon, R., Donnelly, S.M., Dalton, J.P., Ranganathan, S., 2009. An Integrated Transcriptomics and Proteomics Analysis of the Secretome of the Helminth Pathogen *Fasciola hepatica*: proteins associated with invasion and infection of the mammalian hos. Mol. Cell. Proteomics 8, 1891–1907. https://doi.org/10.1074/mcp.M900045-MCP200

Robinson, M.W., Tort, J.F., Lowther, J., Donnelly, S.M., Wong, E., Xu, W., Stack, C.M., Padula, M., Herbert, B., Dalton, J.P., 2008b. Proteomics and phylogenetic analysis of the cathepsin L protease family of the helminth pathogen *Fasciola hepatica*: expansion of a repertoire of virulence-associated factors. Mol. Cell. Proteomics 7, 1111–1123. https://doi.org/10.1074/mcp.M700560-MCP200

Robinson, M.W., Trudgett, A., Hoey, E.M., Fairweather, I., 2002. Triclabendazole-resistant *Fasciola hepatica*: beta-tubulin and response to in vitro treatment with triclabendazole. Parasitology 124, 325–38. https://doi.org/10.1017/S003118200100124X

Robinson, R.C., Mejillano, M., Le, V.P., Burtnick, L.D., Yin, H.L., Choe, S., 1999. Domain movement in gelsolin: A calcium-activated switch. Science (80-.). 286, 1939–1942. https://doi.org/10.1126/science.286.5446.1939

Robles-Pérez, D., García-García, P., Martínez-Pérez, J.M., Rojo-Vázquez, F.A., Martínez-Valladares, M., 2015. Analysis of genetic variability of *Fasciola hepatica* populations from different geographical locations by ISSR-PCR. Parasitology 142, 527–533. https://doi.org/10.1017/S003118201400153X

Robles-Pérez, D., Martínez-Pérez, J.M., Rojo-Vázquez, F.A., 2013. The diagnosis of fasciolosis in feces of sheep by means of a PCR and its application in the detection of anthelmintic resistance in sheep flocks naturally infected. Vet. Parasitol. 197, 277–282. https://doi.org/10.1016/j.vetpar.2013.05.006

Robles-Pérez, D., Martínez-Pérez, J.M., Rojo-Vázquez, F.A., Martínez-Valladares, M., 2014. Development of an egg hatch assay for the detection of anthelmintic resistance to albendazole in *Fasciola hepatica* isolated from sheep. Vet. Parasitol. 203, 217–221. https://doi.org/10.1016/j.vetpar.2013.11.020

Roche, L., Tort, J., Dalton, J.P., 1999. The propeptide of *Fasciola hepatica* cathepsin L is a potent and selective inhibitor of the mature enzyme. Mol. Biochem. Parasitol. 98, 271–277. https://doi.org/10.1016/S0166-6851(98)00164-9

Rodríguez-Pérez, J., Hillyer, G. V., 1995. Detection of excretory-secretory circulating antigens in sheep infected with *Fasciola hepatica* and with *Schistosoma mansoni* and *F. hepatica*. Vet. Parasitol. 56, 57–66. https://doi.org/10.1016/0304-4017(94)00666-Z

Rodríguez, E., Noya, V., Cervi, L., Chiribao, M.L., 2015. Glycans from *Fasciola hepatica* Modulate the Host Immune Response and TLR-Induced Maturation of Dendritic Cells. PLoS Negl. Trop. Dis. 9, 1–26. https://doi.org/10.1371/journal.pntd.0004234

Roeber, F., Jex, A.R., Gasser, R.B., 2013. Advances in the diagnosis of key gastrointestinal nematode infections of livestock, with an emphasis on small ruminants. Biotechnol. Adv. 31, 1135–1152. https://doi.org/10.1016/j.biotechadv.2013.01.008

Rokeach, L.A., Haselby, J.A., Hoch, S.O., 1991. High-level bacterial expression, purification and characterization of human calreticulin. Protein Engl. 4, 981–987.

Rokni, M.B., Mirhendi, H., Mizani, A., Mohebali, M., Sharbatkhori, M., Kia, E.B., Abdoli, H., Izadi, S., 2010. Identification and differentiation of *Fasciola hepatica* and *Fasciola gigantica* using a simple PCR-restriction enzyme method. Exp. Parasitol. 124, 209–213.

https://doi.org/10.1016/j.exppara.2009.09.015
Rondelaud, D., 1994. *Fasciola hepatica*: The Infection Rate and the Development of Redial Generations in *Lymnaea Truncatula* Exposed to Miracidia after Experimental Desiccation and Activation in Water. J. Helminthol. 68, 63–66. https://doi.org/10.1017/S0022149X00013493
Rondelaud, D., Belfaiza, M., Vignoles, P., Moncef, M., Dreyfuss, G., 2009. Redial generations of *Fasciola hepatica*: A review. J. Helminthol. 83, 245–254. https://doi.org/10.1017/S0022149X09222528
Rondelaud, D., Teukeng, F.F.D., Vignoles, P., Dreyfuss, G., 2015. Lymnaea glabra: Progressive increase in susceptibility to *Fasciola hepatica* through successive generations of experimentally infected snails. J. Helminthol. 89, 398–403. https://doi.org/10.1017/S0022149X14000169
Rondelaud, D., Titi, A., Vignoles, P., Mekroud, A., Dreyfuss, G., 2014. Adaptation of *Lymnaea fuscus* and *Radix balthica* to *Fasciola hepatica* through the experimental infection of several successive snail generations. Parasites and Vectors 7, 296. https://doi.org/10.1186/1756-3305-7-296
Rondelaud, D., Titi, A., Vignoles, P., Mekroud, A., Dreyfuss, G., 2013. Consequence of temperature changes on cercarial shedding from *Galba truncatula* infected with *Fasciola hepatica* or *Paramphistomum daubneyi*. Parasite 20, 10. https://doi.org/10.1051/parasite/2013009
Rondelaud, D., Vignoles, P., Dreyfuss, G., 2002. The presence of predators modifies the larval development of Fasciola hepatica in surviving *Lymnaea truncatula*. J. Helminthol. 76, 175–178. https://doi.org/10.1079/joh2001103
Ross, I.C., McKay, A.C., 1929. The bionomics of Fasciola hepatica in New South Wales and of the intermediate host, *Limnea brazieri*. Bull. Counc. Sci. Ind. Res. 43, 62.
Ross, J.G., 1970. The economics of *Fasciola hepatica* infections in cattle. Br. Vet. J. 126, xiii–xv.
Rothenbach, P.A., 2003. Recombinant plasma gelsolin infusion attenuates burn-induced pulmonary microvascular dysfunction. J. Appl. Physiol. 96, 25–31. https://doi.org/10.1152/japplphysiol.01074.2002
Rozman, J., Stojan, J., Kuhelj, R., Turk, V., Turk, B., 1999. Autocatalytic processing of recombinant human procathepsin B is a bimolecular process. FEBS Lett. 459, 358–362. https://doi.org/10.1016/S0014-5793(99)01302-2
Ryan, L.A., Hoey, E., Trudgett, A., Fairweather, I., Fuchs, M., Robinson, M.W., Chambers, E., Timson, D.J., Ryan, E., Feltwell, T., Ivens, A., Bentley, G., Johnston, D., 2008. *Fasciola hepatica* expresses multiple α- and β-tubulin isotypes. Mol. Biochem. Parasitol. 159, 73–78. https://doi.org/10.1016/j.molbiopara.2008.02.001
Sachs, J., Malaney, P., 2002. The economic and social burden of malaria. Nature 415, 680–685. https://doi.org/10.1038/415680a
Saitou, N., Nei, M., 1987. The neighbour-joining method: a new method for reconstructing phylogenetic trees. Mol. Biol. Evol. 10, 471–483. https://doi.org/10.1093/oxfordjournals.molbev.a040454
Salazar-Calderon, M., Martin-Alonso, J.M., Ruiz de Eguino, A.D., Casais, R., Marin, M.S., Parra, F., 2000. *Fasciola hepatica*: heterologous expression and functional characterization of a thioredoxin peroxidase. Exp. Parasitol. 95, 63–70. https://doi.org/10.1006/expr.2000.4495
Salimi-Bejestani, M.R., McGarry, J.W., Felstead, S., Ortiz, P., Akca, A., Williams, D.J.L., 2005.

Development of an antibody-detection ELISA for *Fasciola hepatica* and its evaluation against a commercially available test. Res. Vet. Sci. 78, 177–181. https://doi.org/10.1016/j.rvsc.2004.08.005

Sanabria, R., Ceballos, L., Moreno, L., Romero, J., Lanusse, C., Alvarez, L.I., 2013. Identification of a field isolate of *Fasciola hepatica* resistant to albendazole and susceptible to triclabendazole. Vet. Parasitol. 193, 105–110. https://doi.org/http://dx.doi.org/10.1016/j.vetpar.2012.11.033

Sanabria, R., Mouzet, R., Courtioux, B., Vignoles, P., Rondelaud, D., Dreyfuss, G., Cabaret, J., Romero, J., 2012. Intermediate snail hosts of French *Fasciola hepatica*: *Lymnaea neotropica* and *Lymnaea viatrix* are better hosts than local *Galba truncatula*. Parasitol. Res. 111, 2011–2016. https://doi.org/10.1007/s00436-012-3049-9

Sanchez-Vazquez, M.J., Lewis, F.I., 2013. Investigating the impact of fasciolosis on cattle carcase performance. Vet. Parasitol. 193, 307–311. https://doi.org/10.1016/j.vetpar.2012.11.030

Sanchez Ferreira, C.A., Da Silva Vaz, I., Da Silva, S.S., Haag, K.L., Valenzuela, J.G., Masuda, A., 2002. Cloning and partial characterization of a *Boophilus microplus* (Acari: Ixodidae) calreticulin. Exp. Parasitol. 101, 25–34. https://doi.org/10.1016/S0014-4894(02)00032-2

Sangadala, V.S., Glover, C. V., Robson, R.L., Holland, M.J., Lebioda, L., Brewer, J.M., 1995. Preparation by site-directed mutagenesis and characterization of the E211Q mutant of yeast enolase 1. Biochim. Biophys. Acta (BBA)/Protein Struct. Mol. 1251, 23–31. https://doi.org/10.1016/0167-4838(95)00049-Z

Santra, P.K., Prasad, A., Ghosh, S., 1999. Efficacy of triclabendazole against experimental fasciolosis in lambs. J. Vet. Parasitol. 13, 111–122.

Sanyal, P.K., Gupta, S.C., 1996. Efficacy and pharmacokinetics of triclabendazole in buffalo with induced fasciolosis. Vet. Parasitol. 63, 75–82.

Sargison, N., 2012. Diagnosis of triclabendazole resistance in *Fasciola hepatica*. Vet. Rec. 171, 151–152. https://doi.org/10.1136/vr.e5357

Savage, J., Meaney, M., Brennan, G.P., Hoey, E., Trudgett, A., Fairweather, I., 2014. Disruption of vitellogenesis and spermatogenesis by triclabendazole (TCBZ) in a TCBZ-resistant isolate of *Fasciola hepatica* following incubation *in vitro* with a P-glycoprotein inhibitor. Parasitology 141, 1064–1079. https://doi.org/10.1017/S0031182014000377

Scarcella, S., Hanna, R.E.B., Brennan, G.P., Solana, H., Fairweather, I., 2016. *Fasciola hepatica*: Histological changes in the somatic and reproductive tissues of liver fluke following closantel treatment of experimentally-infected sheep. Vet. Parasitol. 215, 38–47. https://doi.org/10.1016/j.vetpar.2015.10.029

Schliebs, W., Thanki, N., Eritja, R., Wierenga, R., 1996. Active site properties of monomeric triosephosphate isomerase (monoTIM) as deduced from mutational and structural studies. Protein Sci. 5, 229–239. https://doi.org/10.1002/pro.5560050206

Schliebs, W., Thanki, N., Jaenicke, R., Wierenga, R.K., 1997. A double mutation at the tip of the dimer interface loop of triosephosphate isomerase generates active monomers with reduced stability. Biochemistry 36, 9655–9662. https://doi.org/10.1021/bi963086a

Schreier, B., Höcker, B., 2010. Engineering the enolase magnesium II binding site: Implications for its evolution. Biochemistry 49, 7582–7589. https://doi.org/10.1021/bi100954f

Schroeder, H., Skelly, P.J., Zipfel, P.F., Losson, B., Vanderplasschen, A., 2009. Subversion of complement by hematophagous parasites. Dev. Comp. Immunol. 33, 5–13. https://doi.org/10.1016/j.dci.2008.07.010

Schweizer, G., Braun, U., Deplazes, P., Torgerson, P.R., 2005. Estimating the financial losses due to bovine fasciolosis in Switzerland. Vet. Rec. 157, 188–193.

Seigle, J.L., Celotto, A.M., Palladino, M.J., 2008. Degradation of functional triose phosphate isomerase protein underlies sugarkill pathology. Genetics 179, 885–862. https://doi.org/10.1534/genetics.108.087551

Sekiya, M., Mulcahy, G., Irwin, J.A., Stack, C.M., Donnelly, S.M., Xu, W., Collins, P.R., Dalton, J.P., 2006. Biochemical characterisation of the recombinant peroxiredoxin (FhePrx) of the liver fluke, *Fasciola hepatica*. FEBS Lett. 580, 5016–5022. https://doi.org/10.1016/j.febslet.2006.08.019

Selemetas, N., Phelan, P., Kiely, P.O., Waal, T. De, 2015. Cluster analysis of fasciolosis in dairy cow herds in Munster province of Ireland and detection of major climatic and environmental predictors of the exposure risk. Geospat. Health 9, 271–279.

Selemetas, N., Waal, T. De, 2015. Detection of major climatic and environmental predictors of liver fluke exposure risk in Ireland using spatial cluster analysis. Vet. Parasitol. 209, 242–253. https://doi.org/10.1016/j.vetpar.2015.02.029

Sexton, J.L., Milner, A.R., Panaccio, M., Waddington, J., Wijffels, G.L., Chandler, D., Thompson, C., Wilson, L.R., Spithill, T.W., Mitchell, G.F., 1990. Glutathione S-transferase. Novel vaccine against *Fasciola hepatica* infection in sheep. J. Immunol. 145, 3905–10.

Shaheen, H.I., Kamal, K.A., Farid, Z., Mansour, N., Boctor, F.N., Woody, J.N., 1989. Dot-Enzyme-Linked Immunosorbent Assay (Dot-ELISA) for the rapid diagnosis of human fascioliasis. J. Parasitol. 75, 549–552.

Shahzad, W., Mehmood, K., Munir, R., Aslam, W., Ijaz, M., Ahmad, R., Khan, M.S., Sabir, A.J., 2012. Prevalence and molecular diagnosis of *Fasciola hepatica* in sheep and goats in different districts of Punjab, Pakistan. Pak. Vet. J. 32, 535–538.

Shareef, P.A.A., Brennan, G.P., McVeigh, P., Khan, M.A.H., Morphew, R.M., Mousley, A., Marks, N.J., Saifullah, M.K., Brophy, P.M., Maule, A.G., Abidi, S.M.A., 2014. Time-dependent tegumental surface changes in juvenile *Fasciola gigantica* in response to triclabendazole treatment in goat. Acta Trop. 136, 108–117. https://doi.org/10.1016/j.actatropica.2014.04.011

Shashidharan, P., Chalmers-Redman, R.M.E., Carlile, G.W., Rodic, V., Gurvich, N., Yuen, T., Tatton, W.G., Sealfon, S.C., 1999. Nuclear translocation of GAPDH-GFP fusion protein during apoptosis. Neuroreport 10, 1149–1153. https://doi.org/10.1097/00001756-199904060-00045

Shaw, J.N., Simms, B.T., 1930. Studies in Fascioliasis in Oregon Sheep and Goats. Station Bulletin 266. Agricultural Experiment Station Oregon State Agricultural College.

Sheterline, P., Clayton, J., Sparrow, J.C., 1999. Actin. OUP Oxford.

Shieh, D.B., Godleski, J., Herndon, J.E., Azuma, T., Mercer, H., Sugarbaker, D.J., Kwiatkowski, D.J., 1999. Cell motility as a prognostic factor in stage I nonsmall cell lung carcinoma: The role of gelsolin expression. Cancer 85, 45–57. https://doi.org/10.1002/(SICI)1097-0142(19990101)85:1<47::AID-CNCR7>3.0.CO;2-L

Shoemaker, C., Gross, A., Gebremichael, A., Harn, D., 1992. cDNA cloning and functional expression of the *Schistosoma mansoni* protective antigen triose-phosphate isomerase. Proc. Natl. Acad. Sci. 89, 1842–1846. https://doi.org/10.1073/pnas.89.5.1842

Short, E., Caminade, C., Thomas, B., 2017. Climate Change Contribution to the Emergence or Reemergence of Parasitic Diseases. Infect. Dis. Res. Treat. 10, 1–7.

Sigrist, C.J.A., De Castro, E., Cerutti, L., Cuche, B.A., Hulo, N., Bridge, A., Bougueleret, L., Xenarios, I., 2013. New and continuing developments at PROSITE. Nucleic Acids Res. 41,

D344-347. https://doi.org/10.1093/nar/gks1067
Silacci, P., Mazzolai, L., Gauci, C., Stergiopulos, N., Yin, H.L., Hayoz, D., 2004. Gelsolin superfamily proteins: Key regulators of cellular functions. Cell. Mol. Life Sci. 61, 2614–2623. https://doi.org/10.1007/s00018-004-4225-6
Silva, A., Almeida, B., Sampaio-Marques, B., Reis, M.I.R., Ohlmeier, S., Rodrigues, F., Vale, A. do, Ludovico, P., 2011. Glyceraldehyde-3-phosphate dehydrogenase (GAPDH) is a specific substrate of yeast metacaspase. Biochim. Biophys. Acta - Mol. Cell Res. 1813, 2044–2049. https://doi.org/10.1016/j.bbamcr.2011.09.010
Silva, N.M., Gazzinelli, R.T., Silva, D.A.O., Ferro, E.A. V, Kasper, L.H., Mineo, J.R., 1998. Expression of *Toxoplasma gondii*-specific heat shock protein 70 during *in vivo* conversion of bradyzoites to tachyzoites. Infect. Immun. 66, 3959–3963.
Silva, P.E.A., Freitas, C., Vieira, L., Beltrão, M., 2016. Assessing the risk of bovine fasciolosis using linear regression analysis for the state of Rio Grande do Sul, Brazil. Vet. Parasitol. 217, 7–13. https://doi.org/10.1016/j.vetpar.2015.12.021
Silvestre, A., Humbert, J.F., 2002. Diversity of benzimidazole-resistance alleles in populations of small ruminant parasites. Int. J. Parasitol. 32, 921–928. https://doi.org/10.1016/S0020-7519(02)00032-2
Skuce, P.J., Zadoks, R.N., 2013. Liver fluke – A growing threat to UK livestock production. Cattle Pract. 21, 138–149.
Smeal, M.G., Hall, C.A., 1983. The activity of triclabendazole against immature and adult *Fasciola hepatica* infections in sheep. Aust. Vet. J. 60, 329–331. https://doi.org/10.1111/j.1751-0813.1983.tb02833.x
Smith, A.M., Dowd, A.J., Heffernan, M., Robertson, C.D., Dalton, J.P., 1993a. *Fasciola hepatica*: A secreted cathepsin L-like proteinase cleaves host immunoglobulin. Int. J. Parasitol. 23, 977–983. https://doi.org/http://dx.doi.org/10.1016/0020-7519(93)90117-H
Smith, A.M., Dowd, A.J., McGonigle, S., Keegan, P.S., Brennan, G., Trudgett, A., Dalton, J.P., 1993b. Purification of a cathepsin L-like proteinase secreted by adult *Fasciola hepatica*. Mol. Biochem. Parasitol. 62, 1–8. https://doi.org/10.1016/0166-6851(93)90171-S
Smith, D., 2014. Barbervax: the first commercially available subunit vaccine for a nematode parasite, Moredun Research Institute, Edinburgh.
Smith, G., Wilson, R.A., 1980. Seasonal Variations in the Microclimate of *Lymnaea truncatula* Habitats. J. Appl. Ecol. 17, 329–342.
Smith, R.E., Spithill, T.W., Pike, R.N., Meeusen, E.N.T., Piedrafita, D., 2008. *Fasciola hepatica* and *Fasciola gigantica*: Cloning and characterisation of 70 kDa heat-shock proteins reveals variation in HSP70 gene expression between parasite species recovered from sheep. Exp. Parasitol. 118, 536–542. https://doi.org/10.1016/j.exppara.2007.11.012
Smith, W.D., Zarlenga, D.S., 2006. Developments and hurdles in generating vaccines for controlling helminth parasites of grazing ruminants. Vet. Parasitol. 139, 347–359. https://doi.org/10.1016/j.vetpar.2006.04.024
Smooker, P.M., Kennedy, N.J., Steeper, K.R., Christopoulos, H., Spithill, T.W., 2001. *Fasciola*: kinetics and quality of humoral responses to fatty acid binding protein and cathepsin l following delivery as DNA vaccines in mice. Exp. Parasitol. 97, 154–160. https://doi.org/10.1006/expr.2001.4601
Smooker, P.M., Steeper, K.R., Drew, D.R., Strugnell, R.A., Spithill, T.W., 1999. Humoral responses in mice following vaccination with DNA encoding glutathione S-transferase of *Fasciola hepatica*: Effects of mode of vaccination and the cellular compartment of antigen expression. Parasite Immunol. 21, 357–364. https://doi.org/10.1046/j.1365-

3024.1999.00235.x
Sojikul, P., Buehner, N., Mason, H.S., 2003. A plant signal peptide-hepatitis B surface antigen fusion protein with enhanced stability and immunogenicity expressed in plant cells. Proc. Natl. Acad. Sci. 100, 2209–2214. https://doi.org/10.1073/pnas.0438037100
Solana, M. V., Domínguez, M.F., Scarcella, S., Radio, S., Smircich, P., Fernández, S., Solana, H., Tort, J.F., 2018. Different SNPs in *Fasciola hepatica* P-glycoprotein from diverse Latin American populations are not associated with Triclabendazole resistance. Mol. Biochem. Parasitol. 224, 57–60. https://doi.org/10.1016/j.molbiopara.2018.07.005
Song, Y., Luo, Q., Long, H., Hu, Z., Que, T., Zhang, X., Li, Z., Wang, G., Yi, L., Liu, Z., Fang, W., Qi, S., 2014. Alpha-enolase as a potential cancer prognostic marker promotes cell growth, migration, and invasion in glioma. Mol. Cancer 13, 1. https://doi.org/DOI: 10.1186/1476-4598-13-65
Sorrell, I., White, A., Pedersen, A.B., Hails, R.S., Boots, M., 2009. The evolution of covert , silent infection as a parasite strategy. Proc. R. Soc. B 276, 2217–2226. https://doi.org/10.1098/rspb.2008.1915
Sotillo, J., Valero, M.L., Sánchez Del Pino, M.M., Fried, B., Esteban, J.G., Marcilla, A., Toledo, R., 2010. Excretory/secretory proteome of the adult stage of *Echinostoma caproni*. Parasitol. Res. 107, 691–697. https://doi.org/10.1007/s00436-010-1923-x
Spiess, C., Beil, A., Ehrmann, M., 1999. A temperature-dependent switch from chaperone to protease in a widely conserved heat shock protein. Cell 97, 339–347. https://doi.org/10.1016/S0092-8674(00)80743-6
Spiro, R.G., 1970. Glycoproteins. Annu. Rev. Biochem. 39, 599–638.
Srivastava, P., 2002. Roles of heat-shock proteins in innate and adaptive immunity. Nat. Rev. Immunol. https://doi.org/10.1038/nri749
Stack, C.M., Caffrey, C.R., Donnelly, S.M., Seshaadri, A., Lowther, J., Tort, J.F., Collins, P.R., Robinson, M.W., Xu, W., McKerrow, J.H., Craik, C.S., Geiger, S.R., Marion, R., Brinen, L.S., Dalton, J.P., 2008. Structural and functional relationships in the virulence-associated cathepsin L proteases of the parasitic liver fluke, *Fasciola hepatica*. J. Biol. Chem. 283, 9896–9908.
Stack, C.M., Donnelly, S.M., Lowther, J., Xu, W., Collins, P.R., Brinen, L.S., Dalton, J.P., 2007. The Major Secreted Cathepsin L1 Protease of the Liver Fluke, *Fasciola hepatica*. J. Biol. Chem. 282, 16532–16543. https://doi.org/10.1074/jbc.M611501200
Stitt, A.W., Fairweather, I., 1996. *Fasciola hepatica*: Disruption of the vitelline cells *in vitro* by the sulphoxide metabolite of triclabendazole. Parasitol. Res. 82, 333–339. https://doi.org/10.1007/s004360050122
Stitt, A.W., Fairweather, I., 1993a. *Fasciola hepatica*: The effect of the microtubule inhibitors colchicine and tubulozole-C on the ultrastructure of the adult fluke. Parasitology 107, 297–309. https://doi.org/10.1017/S0031182000079270
Stitt, A.W., Fairweather, I., 1993b. *Fasciola hepatica*: Tegumental surface changes in adult and juvenile flukes following treatment *in vitro* with the sulphoxide metabolite of triclabendazole (Fasinex). Parasitol. Res. 79, 529–536. https://doi.org/10.1007/BF00932235
Stitt, A.W., Fairweather, I., 1992. Spermatogenesis in *Fasciola hepatica*: An ultrastructural comparison of the effects of the anthelmintic, triclabendazole (“fasinex”) and the microtubule inhibitor, tubulozole. Invertebr. Reprod. Dev. 22, 139–150. https://doi.org/10.1080/07924259.1992.9672266
Stitt, A.W., Fairweather, I., Johnston, C.F., 1991. *Fasciola hepatica*: Disruption of

spermatogenesis by the microfilament inhibitor cytochalasin B. Parasitol. Res. 77, 123–128. https://doi.org/10.1007/BF00935425

Stitt, A.W., Fairweather, I., Mackender, R.O., 1995. The effect of triclabendazole ("Fasinex") on protein synthesis by the liver fluke, *Fasciola hepatica*. Int. J. Parasitol. 25, 421–429. https://doi.org/10.1016/0020-7519(94)00140-J

Stitt, A.W., Fairweather, I., Trudgett, A.G., Johnston, C.F., 1992a. *Fasciola hepatica*: localization and partial characterization of tubulin. Parasitol. Res. 78, 103–107. https://doi.org/10.1007/BF00931649

Stitt, A.W., Fairweather, I., Trudgett, A.G., Johnston, C.F., Anderson, S.M.L., 1992b. Localisation of actin in the liver fluke, *Fasciola hepatica*. Parasitol. Res. 78, 96–102. https://doi.org/10.1007/BF00931648

Straub, C., Burnham, J.P., White, A.C., Pazdrak, K., Sanchez, C., Watanabe, L.C., Kurosky, A., Montes, M., 2011. Altered eosinophil proteome in a patient with hypereosinophilia from acute fascioliasis. Clin. Vaccine Immunol. 18, 1999–2002. https://doi.org/10.1128/CVI.05373-11

Suchitra, S., Joshi, P., 2005. Characterization of *Haemonchus contortus* calreticulin suggests its role in feeding and immune evasion by the parasite. Biochim. Biophys. Acta 1722, 293–303. https://doi.org/10.1016/j.bbagen.2004.12.020

Sun, A.Q., Yuksel, K.U., Gracy, R.W., 1993. Limited proteolysis of triose-phosphate isomerase and characterization of the catalytically active peptide complex. J. Biol. Chem. 268, 26872–26878.

Sun, H.Q., Yamamoto, M., Mejillano, M., Yin, H.L., 1999. Gelsolin, a multifunctional actin regulatory protein. J. Biol. Chem. https://doi.org/10.1074/jbc.274.47.33179

Sunita, K., Kumar, P., Singh, V.K., Singh, D.K., 2013. *In vitro* phytotherapy of vector snails by binary combinations of larvicidal active components in effective control of fascioliasis. Rev. Inst. Med. Trop. Sao Paulo 55, 303–308. https://doi.org/10.1590/s0036-46652013000500002

Sunita, K., Singh, D.K., 2011. Fascioliasis control: *In vivo* and *in vitro* phytotherapy of vector snail to kill *Fasciola* larva. J. Parasitol. Res. 2011, 1–7. https://doi.org/10.1155/2011/240807

Swai, E.S., Ulicky, E., 2009. An evaluation of the economic losses resulting from condemnation of cattle livers and loss of carcass weight due to Fasciolosis: A case study from Hai town abattoir, Kilimanjaro region, Tanzania. Livest. Res. Rural Dev. 21.

Swan, G.E., 1999. The pharmacology of halogenated salicylanilides and their anthelmintic use. J. S. Afr. Vet. Assoc. 70, 61–70.

Taira, T., Saito, Y., Niki, T., Iguchi-Ariga, S.M.M., Takahashi, K., Ariga, H., 2004. DJ-1 has a role in antioxidative stress to prevent cell death. EMBO Rep. 5, 213–218. https://doi.org/10.1038/sj.embor.7400074

Takahashi-Niki, K., Niki, T., Taira, T., Iguchi-Ariga, S.M.M., Ariga, H., 2004. Reduced anti-oxidative stress activities of DJ-1 mutants found in Parkinson's disease patients. Biochem. Biophys. Res. Commun. 320, 389–397. https://doi.org/10.1016/j.bbrc.2004.05.187

Talfournier, F., Colloc'h, N., Mornon, J.P., Branlant, G., 1999. Functional characterization of the phosphorylating D-glyceraldehyde 3- phosphate dehydrogenase from the archaeon *Methanothermus fervidus* by comparative molecular modelling and site-directed mutagenesis. Eur. J. Biochem. 252, 447–457. https://doi.org/10.1046/j.1432-1327.1999.00681.x

Tamura, M., Ito, K., Kunihiro, S., Yamasaki, C., Haragauchi, M., 2011. Production of human β-actin and a mutant using a bacterial expression system with a cold shock vector. Protein Expr. Purif. 78, 1–5. https://doi.org/10.1016/j.pep.2010.09.007

Tamura, M., Itoh, K., Akita, H., Takano, K., Oku, S., 2006. Identification of an actin-binding site in p47phox an organizer protein of NADPH oxidase. FEBS Lett. 580, 261–267. https://doi.org/10.1016/j.febslet.2005.11.080

Tao, X., Tong, L., 2003. Crystal structure of human DJ-1, a protein associated with early onset Parkinson's disease. J. Biol. Chem. 278, 31372–31379. https://doi.org/10.1074/jbc.M304221200

Tashiro, S., Caaveiro, J.M.M., Wu, C.-X., Hoang, Q.Q., Tsumoto, K., 2014. Thermodynamic and Structural Characterization of the Specific Binding of Zn(II) to Human Protein DJ-1. Biochemistry 53, 2218–2220. https://doi.org/10.1021/bi500294h

Taylor, M.A., 2012. Emerging parasitic diseases of sheep. Vet. Parasitol. 189, 2–7. https://doi.org/10.1016/j.vetpar.2012.03.027

Taylor, M.G., 1980. Vaccination against trematodes., in: Symposium of the British Society for Parasitology. Blackwell Scientific Publications., pp. 115–140.

Teichmann, A., Vargas, D.M., Monteiro, K.M., Meneghetti, B. V., Dutra, C.S., Paredes, R., Galanti, N., Zaha, A., Ferreira, H.B., 2015. Characterization of 14-3-3 isoforms expressed in the *Echinococcus granulosus* pathogenic larval stage. J. Proteome Res. 14, 1700–1715. https://doi.org/10.1021/pr5010136

Teuscher, E., 1965. A new single method of examining faeces for the diagnosis of helminth diseases of ruminants. Zentralblatt für Veterinärmedizin R. B 12, 241–249. https://doi.org/10.1111/j.1439-0450.1965.tb01388.x

Thaa, B., Sinhadri, B.C., Tielesch, C., Krause, E., Veit, M., 2013. Signal Peptide Cleavage from GP5 of PRRSV: A Minor Fraction of Molecules Retains the Decoy Epitope, a Presumed Molecular Cause for Viral Persistence. PLoS One 8, e65548. https://doi.org/10.1371/journal.pone.0065548

Thomas, A.P., 1883. Memoirs: the life history of the liver-fluke (*Fasciola hepatica*). J. Cell Sci. 2, 99–133.

Thomas, K.J., McCoy, M.K., Blackinton, J., Beilina, A., van der Brug, M., Sandebring, A., Miller, D., Maric, D., Cedazo-Minguez, A., Cookson, M.R., 2011. DJ-1 acts in parallel to the PINK1/parkin pathway to control mitochondrial function and autophagy. Hum. Mol. Genet. 20, 40–50. https://doi.org/10.1093/hmg/ddq430

Toet, H., Piedrafita, D.M., Spithill, T.W., 2014. Liver fluke vaccines in ruminants: Strategies, progress and future opportunities. Int. J. Parasitol.

Tolan, R.W., 2011. Fascioliasis Due to *Fasciola hepatica* and *Fasciola gigantica* Infection: An Update on This "Neglected" Neglected Tropical Disease. Lab. Med. 42, 107–116.

Toner, E., Brennan, G.P., Hanna, R.E.B., Edgar, H.W., Fairweather, I., 2011a. Disruption of egg formation by *Fasciola hepatica* following treatment in vivo with triclabendazole in the sheep host. Vet. Parasitol. 177, 79–89.

Toner, E., Brennan, G.P., Hanna, R.E.B., Edgar, H.W., Fairweather, I., 2010a. Tegumental surface changes in adult *Fasciola hepatica* in response to treatment *in vivo* with triclabendazole in the sheep host. Vet. Parasitol. 172, 238–248. https://doi.org/10.1016/j.vetpar.2010.05.012

Toner, E., Brennan, G.P., Hanna, R.E.B., Edgar, H.W., Fairweather, I., 2010b. Time-dependent changes to the tegumental system and gastrodermis of adult *Fasciola hepatica* following treatment *in vivo* with triclabendazole in the sheep host. Vet. Parasitol. 174, 218–227.

https://doi.org/10.1016/j.vetpar.2010.09.008
Toner, E., Brennan, G.P., Hanna, R.E.B., Edgar, H.W.J., Fairweather, I., 2011b. *Fasciola hepatica*: Time-dependent disruption of spermatogenesis following *in vivo* treatment with triclabendazole. Parasitol. Res. 109, 1035–1043. https://doi.org/DOI 10.1007/s00436-011-2341-4
Toner, E., Brennan, G.P., McConvery, F., Meaney, M., Fairweather, I., 2010c. A transmission electron microscope study on the route of entry of triclabendazole into the liver fluke, *Fasciola hepatica*. Parasitology 137, 855–870. https://doi.org/10.1017/S0031182009991247
Toner, E., McConvery, F., Brennan, G.P., Meaney, M., 2009. A scanning electron microscope study on the route of entry of triclabendazole into the liver fluke, *Fasciola hepatica*. Parasitology 136, 523–535. https://doi.org/doi:10.1017/S0031182009005642
Torgerson, P., Claxton, J., 1999. Epidemiology and control, in: Fascioliasis. Fasciolosis, pp. 113–149.
Torgerson, P.R., Devleesschauwer, B., Praet, N., Speybroeck, N., Willingham, A.L., Kasuga, F., Rokni, M.B., Zhou, X.N., Fèvre, E.M., Sripa, B., Gargouri, N., Fürst, T., Budke, C.M., Carabin, H., Kirk, M.D., Angulo, F.J., Havelaar, A., De Silva, N., 2015. World Health Organization Estimates of the Global and Regional Disease Burden of 11 Foodborne Parasitic Diseases, 2010: A Data Synthesis. PLoS Med. 12, e1001920. https://doi.org/10.1371/journal.pmed.1001920
Tort, J., Brindley, P.J., Knox, D., Wolfe, K.H., Dalton, J.P., 1999. Proteinases and associated genes of parasitic helminths. Adv. Parasitol. Volume 43, 161–266. https://doi.org/http://dx.doi.org/10.1016/S0065-308X(08)60243-2
Tristan, C., Shahani, N., Sedlak, T.W., Sawa, A., 2011. The diverse functions of GAPDH: Views from different subcellular compartments. Cell. Signal. 23, 317–323. https://doi.org/10.1016/j.cellsig.2010.08.003
Tsang, V.C., Brand, J.A., Boyer, A.E., 1989. An Enzyme-Linked Immunoelectrotransfer Blot Assay and Glycoprotein Antigens for Diagnosing Human Cysticercosis (*Taenia solium*). J. Infect. Dis. 159, 50–59.
Turk, V., Stoka, V., Vasiljeva, O., Renko, M., Sun, T., Turk, B., Turk, D., 2012. Cysteine cathepsins: From structure, function and regulation to new frontiers. Biochim. Biophys. Acta - Proteins Proteomics 1824, 68–88. https://doi.org/10.1016/j.bbapap.2011.10.002
Turk, V., Turk, B., Turk, D., 2001. Lysosomal cysteine proteases: facts and opportunities. EMBO J. 20, 4629–4633. https://doi.org/10.5177/ntvt2010.02.08143
Twu, O., Johnson, P.J., 2014. Parasite Extracellular Vesicles: Mediators of Intercellular Communication. PLoS Pathog. 10. https://doi.org/10.1371/journal.ppat.1004289
Ubeda, J.-M., Légaré, D., Raymond, F., Ouameur, A., Boisvert, S., Rigault, P., Corbeil, J., Tremblay, M.J., Olivier, M., Papadopoulou, B., Ouellette, M., 2008. Modulation of gene expression in drug resistant *Leishmania* is associated with gene amplification, gene deletion and chromosome aneuploidy. Genome Biol. 9, R115. https://doi.org/10.1186/gb-2008-9-7-r115
Ubeira, F.M., Muiño, L., Valero, M.A., Periago, M. V., Pérez-Crespo, I., Mezo, M., González-Warleta, M., Romarís, F., Paniagua, E., Cortizo, S., Llovo, J., Más-Coma, S., 2009. MM3-ELISA Detection of *Fasciola hepatica* Coproantigens in Preserved Human Stool Samples. Am. J. Trop. Med. Hyg. 81, 156–162.
Ucker, D.S., Jain, M.R., Pattabiraman, G., Palasiewicz, K., Birge, R.B., Li, H., 2012. Externalized glycolytic enzymes are novel, conserved, and early biomarkers of apoptosis. J. Biol.

Chem. 287, 10325–10343. https://doi.org/10.1074/jbc.M111.314971
Untergasser, A., Cutcutache, I., Koressaar, T., Ye, J., Faircloth, B.C., Remm, M., Rozen, S.G., 2012. Primer3-new capabilities and interfaces. Nucleic Acids Res. 40, e115. https://doi.org/10.1093/nar/gks596
Vaithilingam, A., Teixeira, J.E., Miller, P.J., Heron, B.T., Huston, C.D., 2012. *Entamoeba histolytica* cell surface calreticulin binds human C1q and functions in amebic phagocytosis of host cells. Infect. Immun. 80, 2008–2018. https://doi.org/10.1128/IAI.06287-11
Valenta, R., Ferreira, F., Grote, M., Swoboda, I., Vrtala, S., Duchene, M., Deviller, P., Meagher, R.B., McKinney, E., Heberle-Bors, E., Kraft, D., Scheiner, O., 1993. Identification of profilin as an actin-binding protein in higher plants. J. Biol. Chem. 268, 22777–22781.
Valero, A., Espinoza, R., Herrera, P., Terashima, A., Valero, M.A., Periago, M. V., Pé Rez-Crespo, I., Angles, R., Villegas, F., Aguirre, C., Strauss, W., Espinoza, J.R., Herrera, P., Terashima, A., Tamayo, H., Engels, D., Gabrielli, A.F., Mas-Coma, S., Keiser, J., 2012. Field Evaluation of a Coproantigen Detection Test for Fascioliasis Diagnosis and Surveillance in Human Hyperendemic Areas of Andean Countries. PLoS Negl. Trop. Dis. 6. https://doi.org/10.1371/journal.pntd.0001812
Valero, M.A., Bargues, M.D., Calderón, L., Artigas, P., Mas-Coma, S., 2018. First phenotypic and genotypic description of *Fasciola hepatica* infecting highland cattle in the state of Mexico, Mexico. Infect. Genet. Evol. 8, 51–58. https://doi.org/10.1016/j.meegid.2018.06.032
Valero, M.A., Mas-Coma, S., 2000. Comparative infectivity of *Fasciola hepatica* metacercariae from isolates of the main and secondary reservoir animal host species in the Bolivian Altiplano high human endemic region. Folia Parasitol. (Praha). 47, 17–22. https://doi.org/10.14411/fp.2000.004
Valero, M.A., Perez-Crespo, I., Periago, M. V., Khoubbane, M., Mas-Coma, S., 2009. Fluke egg characteristics for the diagnosis of human and animal fascioliasis by *Fasciola hepatica* and *F. gigantica*. Acta Trop. 111, 150–159. https://doi.org/10.1016/j.actatropica.2009.04.005
Valero, M.A., Renzi, M.D.E., Panova, M., 2006. Crowding effect on adult growth, pre-patent period and egg shedding of *Fasciola hepatica*. Parasitology 133, 453–463. https://doi.org/10.1017/S003118200600059X
van Dijk, J., Sargison, N.D., Kenyon, F., Skuce, P.J., 2010. Climate change and infectious disease : helminthological challenges to farmed ruminants in temperate regions. Animal 4, 377–392. https://doi.org/10.1017/S1751731109990991
van Niel, G., D'Angelo, G., Raposo, G., 2018. Shedding light on the cell biology of extracellular vesicles. Nat. Rev. Mol. Cell Biol. 19, 213–228. https://doi.org/10.1038/nrm.2017.125
van Regenmortel, M.H. V., Muller, S., 1998. D-peptides as immunogens and diagnostic reagents. Curr. Opin. Biotechnol. 9, 377–382. https://doi.org/10.1016/S0958-1669(98)80011-6
Vassilakos, A., Michalak, M., Lehrman, M.A., Williams, D.B., 1998. Oligosaccharide binding characteristics of the molecular chaperones calnexin and calreticulin. Biochemistry 37, 3480–3490. https://doi.org/10.1021/bi972465g
Vercruysse, J., Claerebout, E., 2001. Treatment vs non-treatment of helminth infections in cattle: defining the threshold. Vet. Parasitol. 98, 195–214.
Vercruysse, J., Holdsworth, P., Letonja, T., Barth, D., Conder, G., Hamamoto, K., Okano, K., 2001. International harmonisation of anthelmintic efficacy guidelines. Vet. Parasitol. 96,

171–193.
Verkhusha, V. V., Shavlovsky, M.M., Nevzglyadova, O. V., Gaivoronsky, A.A., Artemov, A. V., Stepanenko, O. V., Kuznetsova, I.M., Turoverov, K.K., 2003. Expression of recombinant GFP-actin fusion protein in the methylotrophic yeast *Pichia pastoris*. FEMS Yeast Res. 3, 105–111. https://doi.org/10.1016/S1567-1356(02)00160-5
Vernet, T., Berti, P.J., De Montigny, C., Musil, R., Tessier, D.C., Menard, R., Magny, M.C., Storer, A.C., Thomas, D.Y., 1995. Processing of the papain precursor. The ionization state of a conserved amino acid motif within the pro region participates in the regulation of intramolecular processing. J. Biol. Chem. 270, 10838–10846. https://doi.org/10.1074/jbc.270.18.10838
Vilas, R., Vázquez-Prieto, S., Paniagua, E., 2012. Contrasting patterns of population genetic structure of *Fasciola hepatica* from cattle and sheep: implications for the evolution of anthelmintic resistance. Infect. Genet. Evol. J. Mol. Epidemiol. Evol. Genet. Infect. Dis. 12, 45–52. https://doi.org/10.1016/j.meegid.2011.10.010
Vukman, K. V., Adams, P.N., Dowling, D., Metz, M., Maurer, M., O'Neill, S.M., 2013. The effects of *Fasciola hepatica* tegumental antigens on mast cell function. Int. J. Parasitol. 43, 531–539. https://doi.org/10.1016/j.ijpara.2013.01.011
Waley, S.G., 1973. Refolding of triose phosphate isomerase. Biochem. J. 135, 165–172. https://doi.org/10.1042/bj1350165
Walker, S.M., Hoey, E., Fletcher, H., Brennan, G.P., Fairweather, I., Trudgett, A., 2006. Stage-specific differences in fecundity over the life-cycle of two characterized isolates of the liver fluke, *Fasciola hepatica*. Parasitology 133, 209–216. https://doi.org/10.1017/S003118200600014X
Walker, S.M., Johnston, C., Hoey, E.M., Fairweather, I., Borgsteede, F., Gaasenbeek, C., Prodöhl, P.A., Trudgett, A., 2011. Population dynamics of the liver fluke, *Fasciola hepatica*: The effect of time and spatial separation on the genetic diversity of fluke populations in the Netherlands. Parasitology 138, 215–223. https://doi.org/10.1017/S0031182010001149
Walker, S.M., Prodöhl, P.A., Fletcher, H.L., Hanna, R.E.B., Kantzoura, V., Hoey, E.M., Trudgett, A., 2007. Evidence for multiple mitochondrial lineages of *Fasciola hepatica* (liver fluke) within infrapopulations from cattle and sheep. Parasitol. Res. 101, 117–125. https://doi.org/10.1007/s00436-006-0440-4
Waller, P.J., 1999. International approaches to the concept of integrated control of nematode parasites of livestock. Int. J. Parasitol. 29, 155–164. https://doi.org/http://dx.doi.org/10.1016/S0020-7519(98)00178-7
Walsh, T.R., Ainsworth, S., Armstong, S., Walker, A., Hodgkinson, S.H.J., Williams, D., 2018. Development of a Pen-side Diagnostic Test for Liver Fluke Infections in Cattle and Sheep. University of Liverpool.
Walton, C.L., 1918. Liver Rot of Sheep, and Bionomics of *Limnaea truncatula* in the Aberystwyth Area. Parasitology 10, 232–266. https://doi.org/DOI: 10.1017/S0031182000003814
Wang, L., Fang, Q., Zhu, J., Wang, F., Rean Akhtar, Z., Ye, G., 2012. Molecular cloning and functional study of calreticulin from a lepidopteran pest, *Pieris rapae*. Dev. Comp. Immunol. 38, 55–65. https://doi.org/10.1016/j.dci.2012.03.019
Wang, Y., Geer, L.Y., Chappey, C., Kans, J.A., Bryant, S.H., 2000. Cn3D: Sequence and structure views for Entrez. Trends Biochem. Sci. 25, 300–302. https://doi.org/10.1016/S0968-0004(00)01561-9

Wass, M.N., Kelley, L.A., Sternberg, M.J.E., 2010. 3DLigandSite: Predicting ligand-binding sites using similar structures. Nucleic Acids Res. 38, W469–W473. https://doi.org/10.1093/nar/gkq406

Way, M., Gooch, J., Pope, B., Weeds, A.G., 1989. Expression of human plasma gelsolin in *Escherichia coli* and dissection of actin binding sites by segmental deletion mutagenesis. J. Cell Biol. 109, 593–605. https://doi.org/10.1083/jcb.109.2.593

Way, M., Pope, B., Gooch, J., Hawkins, M., Weeds, A.G., 1990. Identification of a region in segment 1 of gelsolin critical for actin binding. EMBO J. 9, 4103–4109.

Way, M., Weeds, A., 1988. Nucleotide sequence of pig plasma gelsolin: Comparison of protein sequence with human gelsolin and other actin-severing proteins shows strong homologies and evidence for large internal repeats. J. Mol. Biol. 203, 1127–1133. https://doi.org/10.1016/0022-2836(88)90132-5

Weinberger, K., Collazo, N., Aguillón, J.C., Molina, M.C., Rosas, C., Penã, J., Pizarro, J., Maldonado, I., Cattan, P.E., Apt, W., Ferreira, A., 2017. *Triatoma infestans* Calreticulin: Gene cloning and expression of a main domain that interacts with the host complement system. Am. J. Trop. Med. Hyg. 96, 295–303. https://doi.org/10.4269/ajtmh.16-0642

Wen, D., Corina, K., Pingchang Chow, E., Miller, S., Janmey, P.A., Blake Pepinsky, R., 1996. The plasma and cytoplasmic forms of human gelsolin differ in disulfide structure. Biochemistry 35, 9700–9709. https://doi.org/10.1021/bi960920n

Wen, J.J., Garg, N.J., 2012. Proteome expression and carbonylation changes during *Trypanosoma cruzi* infection and Chagas disease in rats. Mol Cell Proteomics 11, M111-010918. https://doi.org/10.1074/mcp.M111.010918

Wennerberg, K., Rossman, K.L., Der, C.J., 2005. The Ras superfamily at a glance. J. Cell Sci. 118, 843–846. https://doi.org/doi: 10.1242/jcs.01660

Whiting, P.F., Sterne, J.A.C., Westwood, M.E., Bachmann, L.M., Harbord, R., Egger, M., Deeks, J.J., 2008. Graphical presentation of diagnostic information. BMC Med. Res. Methodol. 8, 20. https://doi.org/10.1186/1471-2288-8-20

Wierenga, R.K., 2001. The TIM-barrel fold: A versatile framework for efficient enzymes. FEBS Lett. 492, 193–198. https://doi.org/10.1016/S0014-5793(01)02236-0

Wijffels, G.L., Salvatore, L., Dosen, M., Waddington, J., Wilson, L.R., Thompson, C., Campbell, N., Sexton, J., Wicker, J., Bowen, F., Friedel, T., Spithill, T.W., 1994. Vaccination of Sheep with Purified Cysteine Proteinases of *Fasciola hepatica* Decreases Worm Fecundity, Experimental Parasitology. https://doi.org/10.1006/expr.1994.1014

Wikerhauser, T., 1960. A rapid method for determining the viability of *Fasciola hepatica* metacercariae. Am. J. Vet. Res. 21, 895–897.

Wikerhauser, T., Brglez, J., 1961. O vitalnosti metacerkarija *F. hepatica* iz salaze. Vet. Arh. 31, 315–318.

Wilkinson, R., Law, C.J., Hoey, E.M., Fairweather, I., Brennan, G.P., Trudgett, A., 2012. An amino acid substitution in *Fasciola hepatica* P-glycoprotein from triclabendazole-resistant and triclabendazole-susceptible populations. Mol. Biochem. Parasitol. 186, 69–72. https://doi.org/10.1016/j.molbiopara.2012.08.008

Wilson, L.R., Good, R.T., Panaccio, M., Wijffels, G.L., Sandeman, R.M., Spithill, T.W., 1998. *Fasciola hepatica*: Characterization and Cloning of the Major Cathepsin B Protease Secreted by Newly Excysted Juvenile Liver Fluke. Exp. Parasitol. 88, 85–94. https://doi.org/http://dx.doi.org/10.1006/expr.1998.4234

Wilson, M.A., Collins, J.L., Hod, Y., Ringe, D., Petsko, G.A., 2003. The 1.1-A resolution crystal structure of DJ-1, the protein mutated in autosomal recessive early onset Parkinson's

disease. Proc. Natl. Acad. Sci. 100, 9256–9261. https://doi.org/10.1073/pnas.1133288100

Wilson, R.A., Draskau, T., 1976. The stimulation of daughter redia production during the larval development of *Fasciola hepatica*. Parasitology 72, 245–257. https://doi.org/10.1017/S0031182000049465

Wilson, R.A., Pullin, P., Denison, J., 1971. An investigation of the mechanism of infection by digenetic trematodes: the penetration of the miracidium of *Fasciola hepatica* into its snail host *Lymnaea truncatula*. Parasitology 63, 491–506.

Wilson, R.A., Wright, J.M., De Castro-Borges, W., Parker-Manuel, S.J., Dowle, A.A., Ashton, P.D., Young, N.D., Gasser, R.B., Spithill, T.W., 2011. Exploring the Fasciola hepatica tegument proteome. Int. J. Parasitol. 41, 1347–59. https://doi.org/10.1016/j.ijpara.2011.08.003

Winston, J.S., Asch, H.L., Zhang, P.J., Edge, S.B., Hyland, A., Asch, B.B., 2001. Downregulation of gelsolin correlates with the progression to breast carcinoma. Breast Cancer Res. Treat. 65, 11–21. https://doi.org/10.1023/A:1006446108411

Wolstenholme, A.J., Fairweather, I., Prichard, R., Samson-himmelstjerna, G. Von, Sangster, N.C., 2006. Drug resistance in veterinary helminths. Trends Parasitol. 20, 469–476. https://doi.org/10.1016/j.pt.2004.07.010

World Health Organization, 1995. WHO, Technical Report Series.

Ximénez, C., González, E., Nieves, M.E., Silva-Olivares, A., Shibayama, M., Galindo-Gómez, S., Escobar-Herrera, J., García De León, M.D.C., Morán, P., Valadez, A., Rojas, L., Hernández, E.G., Partida, O., Cerritos, R., 2014. *Entamoeba histolytica* and *E*. *dispar* calreticulin: Inhibition of classical complement pathway and differences in the level of expression in amoebic liver abscess. Biomed Res. Int. 2014, 127453. https://doi.org/10.1155/2014/127453

Xu, M., Molento, M., Blackhall, W., Ribeiro, P., Beech, R.N., Prichard, R., 1998. Ivermectin resistance in nematodes may be caused by alteration of P-glycoprotein homolog. Mol. Biochem. Parasitol. 91, 327–335. https://doi.org/10.1016/S0166-6851(97)00215-6

Yang, J., Ramnath, N., Moysich, K.B., Asch, H.L., Swede, H., Alrawi, S.J., Huberman, J., Geradts, J., Brooks, J.S.J., Tan, D., 2006. Prognostic significance of MCM2, Ki-67 and gelsolin in non-small cell lung cancer. BMC Cancer 6, 203. https://doi.org/10.1186/1471-2407-6-203

Yang, J., Tan, D., Asch, H.L., Swede, H., Bepler, G., Geradts, J., Moysich, K.B., 2004. Prognostic significance of gelsolin expression level and variability in non-small cell lung cancer. Lung Cancer 46, 29–42. https://doi.org/10.1016/j.lungcan.2004.03.022

Yin, H.L., Albrecht, J.H., Fattoum, A., 1981. Identification of gelsolin, a Ca2+-dependent regulatory protein of actin gel-sol transformation, and its intracellular distribution in a variety of cells and tissues. J. Cell Biol. 91, 901–906. https://doi.org/10.1083/jcb.91.3.901

Yin, H.L., Kwiatokowski, D.J., Mole, J.E., Cole, F.S., 1984. Structure and biosynthesis of cytoplasmic and secreted variants of gelsolin. J. Biol. Chem. 259, 5271–5276.

Yin, H.L., Stossel, T.P., 1979. Control of cytoplasmic actin gel-sol transformation by gelsolin, a calcium-dependent regulatory protein. Nature 281, 583–586. https://doi.org/10.1038/281583a0

Young, N.D., Jex, A.R., Young, N.D., Hall, R.S., Jex, A.R., Cantacessi, C., Gasser, R.B., 2010. Elucidating the transcriptome of *Fasciola hepatica* - A key to fundamental and biotechnological discoveries for a neglected parasite. Biotechnol. Adv. 28, 222–231.

https://doi.org/10.1016/j.biotechadv.2009.12.003
Zabori, S., Rudolph, R., Jaenicke, R., 1980. Folding and Association of Triose Phosphate Isomerase from Rabbit Muscle. Zeitschrift für Naturforsch. C 35, 999–1004. https://doi.org/10.1515/znc-1980-11-1224
Zachara, N.E., Cheung, W.D., Hart, G.W., 2004. Nucleocytoplasmic glycosylation, O-linked beta-N-acetylglucosamine. Curr. Org. Chem. 8, 369–383. https://doi.org/10.2174/1385272043485873
Zafra, R., Pérez-Écija, R.A., Buffoni, L., Moreno, P., Bautista, M.J., Martínez-Moreno, A., Mulcahy, G., Dalton, J.P., Pérez, J., 2013a. Early and Late Peritoneal and Hepatic Changes in Goats Immunized with Recombinant Cathepsin L1 and Infected with *Fasciola hepatica*. J. Comp. Pathol. 148, 373–384. https://doi.org/10.1016/j.jcpa.2012.08.007
Zafra, R., Pérez-écija, R.A., Buffoni, L., Pacheco, I.L., Martínez-Moreno, A., LaCourse, E.J., Perally, S., Brophy, P.M., Pérez, J., 2013b. Early hepatic and peritoneal changes and immune response in goats vaccinated with a recombinant glutathione transferase sigma class and challenged with *Fasciola hepatica*. Res. Vet. Sci. 94, 602–609.
Zafra, R., Pérez, J., Buffoni, L., Martínez-Moreno, F.J., Acosta, I., Mozos, E., Martínez-Moreno, A., 2013c. Peripheral blood lymphocyte subsets in *Fasciola hepatica* infected and immunised goats. Vet. Immunol. Immunopathol. 155, 135–138. https://doi.org/10.1016/j.vetimm.2013.06.006
Zhang, Q., Lu, W., Ji, L., Hua, Z.C., 2017. Expression, purification, and characterization of recombinant 8 kDa gelsolin fragment. Protein Expr. Purif. 135, 33–36. https://doi.org/10.1016/j.pep.2017.04.016
Zheng, M., Hu, K., Liu, W., Hu, X., Hu, F., Huang, L., Wang, P., Hu, Y., Huang, Y., Li, W., Liang, C., Yin, X., He, Q., Yu, X., 2011. Proteomic analysis of excretory secretory products from *Clonorchis sinensis* adult worms: Molecular characterization and serological reactivity of a excretory-secretory antigen-fructose-1,6-bisphosphatase. Parasitol. Res. 109, 737–744. https://doi.org/10.1007/s00436-011-2316-5
Zhou, D.H., Yuan, Z.G., Zhao, F.R., Li, H.L., Zhou, Y., Lin, R.Q., Zou, F.C., Song, H.Q., Xu, M.J., Zhu, X.Q., 2011. Modulation of mouse macrophage proteome induced by *Toxoplasma gondii* tachyzoites *in vivo*. Parasitol. Res. 109, 1637–1646. https://doi.org/10.1007/s00436-011-2435-z
Zhou, W., Freed, C.R., 2005. DJ-1 up-regulates glutathione synthesis during oxidative stress and inhibits A53T α-synuclein toxicity. J. Biol. Chem. 280, 43150–43158. https://doi.org/10.1074/jbc.M507124200
Zhou, W., Zhu, M., Wilson, M.A., Petsko, G.A., Fink, A.L., 2006. The oxidation state of DJ-1 regulates its chaperone activity toward α-synuclein. J. Mol. Biol. 356, 1036–1048. https://doi.org/10.1016/j.jmb.2005.12.030
Zhou, X., Yao, K., Zhang, L., Zhang, Y., Han, Y., Liu, H.L., Liu, X.W., Su, G., Yuan, W.Z., Wei, X.D., Guan, Q.L., Zhu, B.D., 2016. Identification of Differentiation-Related Proteins in Gastric Adenocarcinoma Tissues by Proteomics. Technol. Cancer Res. Treat. 15, 697–706. https://doi.org/10.1177/1533034615595792
Zhu, L., Mou, C., Yang, X., Lin, J., Yang, Q., 2016. Mitophagy in TGEV infection counteracts oxidative stress and apoptosis. Oncotarget 7, 27122. https://doi.org/10.18632/oncotarget.8345
Zinsser, V.L., Farnell, E., Dunne, D.W., Timson, D.J., 2013a. Triose phosphate isomerase from the blood fluke *Schistosoma mansoni*: Biochemical characterisation of a potential drug and vaccine target. FEBS Lett. 587, 3422–3427.

https://doi.org/10.1016/j.febslet.2013.09.022
Zinsser, V.L., Hoey, E.M., Trudgett, A., Timson, D.J., 2014. Biochemical characterisation of glyceraldehyde 3-phosphate dehydrogenase (GAPDH) from the liver fluke, *Fasciola hepatica*. Biochim. Biophys. Acta - Proteins Proteomics 1844, 744–749. https://doi.org/10.1016/j.bbapap.2014.02.008
Zinsser, V.L., Hoey, E.M., Trudgett, A., Timson, D.J., 2013b. Biochemical characterisation of triose phosphate isomerase from the liver fluke *Fasciola hepatica*. Biochimie 95, 2182–2189. https://doi.org/10.1016/J.BIOCHI.2013.08.014
Zuckerkandl, E., Pauling, L., 1965. Evolutionary divergence and convergence in proteins, in: Evolving Genes and Proteins. pp. 97–166. https://doi.org/10.1209/epl/i1998-00224-x

Supplementary materials

Chapter 3 supplementary materials

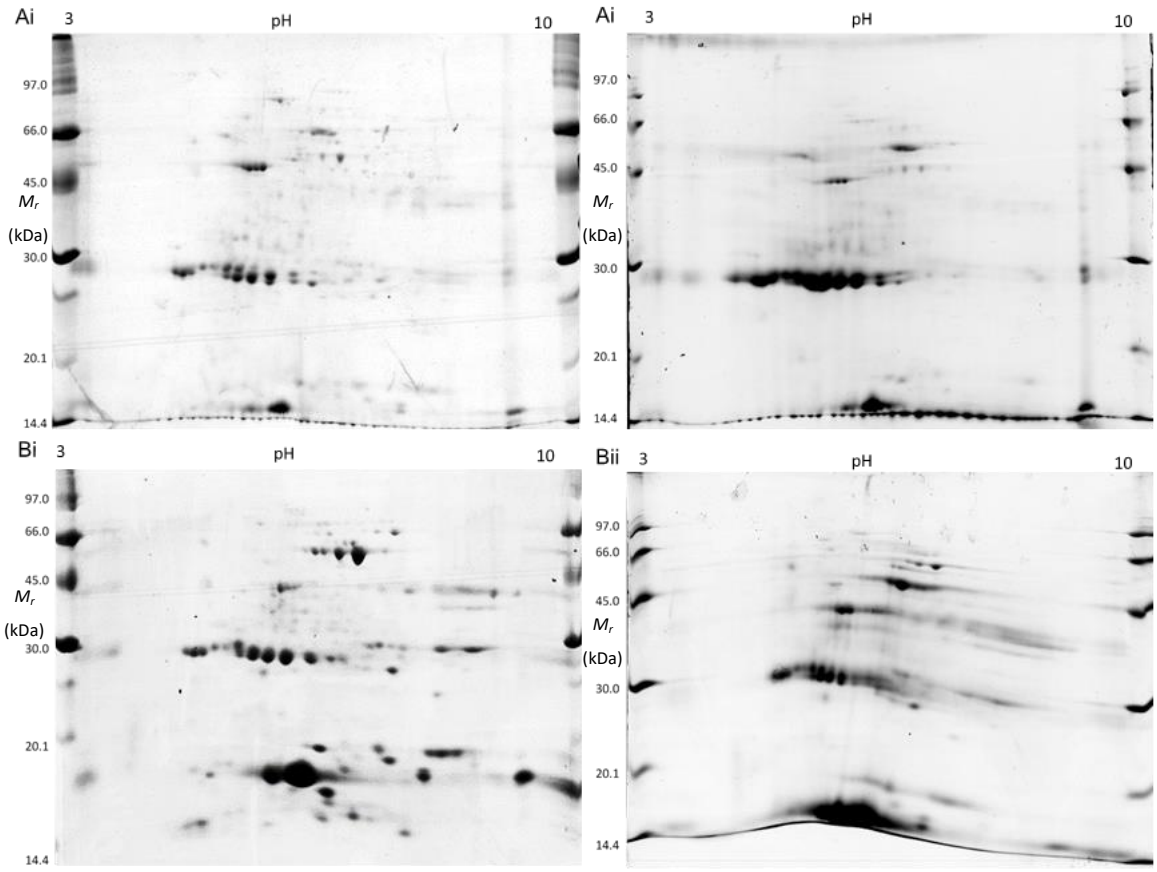

Figure S1. 2-D SDS PAGE of whole excretory/secretory (ES) proteomic profiles of alive and dead *in vitro* cultured *Fasciola hepatica*. Replicate ES protein extracted from pooled (A) live and (B) dead (ethyl 4-aminobenzoate-treated) *in vitro* cultures were analysed by 2-D SDS PAGE and subsequently selected for duplicate analyses by LC-MS/MS.

Abbreviations: MW, Amersham Low Molecular Weight SDS Calibration Kit (M_r).

Table S1. LC-MS/MS identification of 1-DE-separated recombinant *Fasciola hepatica* procathepsin L proteins. LC-MS/MS identification of rFhΔpCL1, rFhpCL1^{WT}, and rFhpCL1 were analysed by duplicate 12.5% SDS PAGE and bands of interest were selected for investigation using LC-MS/MS. All protein hits listed were identified against the GenBank database using an in-house MASCOT (Matrix Science) server, including reliable error tolerance and reporting significant hits consistent between duplicates with an average score of 67 or greater ($P < 0.05$). Top hits are **bolded** (summarised in shortened version of this table: Table 3.4.2) and further hits are shown where matching with peptide samesets, subsets and intersections, whereby the numbers of peptides matched were calculated from those of the original hits. The asterisk (*) indicates a protein hit identified across both replicates for rFhpCL1 sample 5, but absent from all other samples including the negative controls, where 144 peptide samesets, subsets and intersections were associated but excluded from this summary (data not shown).

rFhpCL1	Approximate molecular weight (sample number)	GenBank hit	MASCOT score (Av)	Peptides matched (non-duplicate)	Sequence coverage (%)	Protein	Organism	Accession	E-value
rFhΔpCL1	37	**gi|163310848**	**1677.0±1078.0**	**71.5±37.5**	**73.0±10.0**	**Chain A, Crystal Structure Of Procathepsin L1**	***F. hepatica***	**2O6X_A**	**0.0**
		gi|116488416	1582.0±1076.0	71.5±37.5	62.0±9.0	Secreted cathepsin L 1	*F. hepatica*	AAB41670.2	0.0
		gi|31558997	1419.0±1059.0	71.5±37.5	40.0±5.0	Cathepsin L	*F. hepatica*	AAP49831.1	0.0
		gi|377823949	1309.0±899.0	71.5±37.5	34.0±0.0	Cathepsin L1	*F. gigantica*	AFB77219.1	0.0
		gi|20136379	1233.5±862.5	71.5±37.5	44.5±2.5	Cathepsin L, partial	*F. hepatica*	AAM11647.1	0.0
		gi|157862759	1056.5±898.5	71.5±37.5	23.0±3.0	Cathepsin L, partial	*F. gigantica*	ABV90502.1	0.0
		gi|74765984	864.5±453.5	71.5±37.5	44.0±6.0	Cathepsin L-like proteinase	*F. hepatica*	Q24940.1	0.0
		gi|7271889	805.5±490.5	71.5±37.5	30.5±3.5	Cathepsin L	*F. gigantica*	AAF44675.1	0.0
		gi|4574304	801.0±491.0	71.5±37.5	30.5±3.5	Cathepsin	*F. gigantica*	AAD23996.1	0.0
		gi|379991182	618.5±300.5	71.5±37.5	35.0±4.0	Cathepsin protein CatL1-MM3p, partial	*F. hepatica*	CCA61803.1	0.0
		gi|13774082	612.0±297.0	71.5±37.5	34.5±2.5	Cathepsin L-like	*F. hepatica*	AAK38169.1	0.0
		gi|41152538	612.0±297.0	71.5±37.5	37.0±5.0	Cathepsin L protein	*F. hepatica*	AAR99518.1	0.0
		gi|21263041	612.0±297.0	71.5±37.5	27.0±0.0	Cathepsin L2	*F. gigantica*	AAM44832.1	0.0
		gi|211909242	501.5±290.5	71.5±37.5	24.5±3.5	Cathepsin L1D	*F. hepatica*	ACJ12894.1	0.0
		gi|10798511	497.5±294.5	71.5±37.5	23.5±1.5	Cathepsin L1	*F. hepatica*	CAC12806.1	0.0
		gi|211909240	497.5±294.5	71.5±37.5	24.5±3.5	Cathepsin L1D	*F. hepatica*	ACJ12893.1	0.0
		gi|545734	493.0±192.0	71.5±37.5	21.0±5.0	Cysteine protease	*Fasciola sp.*	AAB30089.1	0.0
		gi|310751866	**441.5±281.5**	**30.5±17.5**	**39.0±8.0**	**Cathepsin L-like proteinase**	***F. hepatica***	**ADP09371.1**	**0.0**
		gi|7271895	383.5±187.5	71.5±37.5	20.0±9.0	Cathepsin L, partial	*F. gigantica*	AAF44678.1	1E-164
		gi|7271891	364.0±295.0	71.5±37.5	16.5±1.5	Cathepsin L	*F. gigantica*	AAF44676.1	0.0
		gi|107921814	355.5±298.5	71.5±37.5	10.5±0.5	Cathepsin L4	*F. hepatica*	ABF85682.1	2E-172
		gi|195729975	355.5±298.5	71.5±37.5	8.5±1.5	Cathepsin L1	*F. magna*	ACG50798.1	0.0
		gi|167427529	355.5±298.5	71.5±37.5	7.5±0.5	Cathepsin L4, partial	*F. hepatica*	ABZ80401.1	0.0
		gi|38045864	355.5±298.5	71.5±37.5	7.0±0.0	Cathepsin L	*F. gigantica*	AAR08900.1	0.0
		gi|146147376	302.0±1.0	71.5±37.5	25.5±5.5	Cathepsin	*F. gigantica*	ABQ01982.1	0.0
		gi|50403821	301.5±2.5	71.5±37.5	24.5±4.5	Cathepsin L1 proteinase	*F. hepatica*	AAT76664.1	0.0
		gi|41152540	297.5±1.5	71.5±37.5	38.0±5.0	Cathepsin L protein	*F. hepatica*	AAR99519.1	9E-180
		gi|108735840	193.0±2.0	71.5±37.5	22.0±0.0	Cathepsin L2	*F. hepatica*	ABG00259.1	7E-167
		gi|19909509	154.0±1.0	71.5±37.5	21.5±4.5	Cathepsin L	*F. gigantica*	BAB86959.1	0.0

		gi|452266	154.0±1.0	71.5±37.5	23.0±11.0	Cathepsin L-like protease	*F. hepatica*	CAA80450.1	8E-124
		gi|8547325	90.5±21.5	19.5±14.5	8.0±6.0	Cathepsin L	*F. hepatica*	AAF76330.1	0.0
rFhpCL1^{WT}	37	**gi|116488416**	**132.5±56.5**	**17.0±4.0**	**38.5±1.5**	**Secreted cathepsin L 1**	***F. hepatica***	**AAB41670.2**	**0.0**
		gi|163310848	132.5±56.5	17.0±4.0	40.5±1.5	Chain A, Crystal Structure Of Procathepsin L1	*F. hepatica*	2O6X_A	0.0
		gi|74765984	130.5±54.5	17.0±4.0	33.0±4.0	Cathepsin L-like proteinase	*F. hepatica*	Q24940.1	0.0
		gi|4574304	107.0±42.0	17.0±4.0	20.0±0.0	Cathepsin	*F. gigantica*	AAD23996.1	0.0
		gi|545734	107.0±42.0	17.0±4.0	21.5±1.5	Cysteine protease	*Fasciola sp.*	AAB30089.1	0.0
		gi|7271889	107.0±42.0	17.0±4.0	21.5±1.5	Cathepsin L	*F. gigantica*	AAF44675.1	0.0
		gi|31558997	102.0±26.0	17.0±4.0	23.5±1.5	Cathepsin L	*F. hepatica*	AAP49831.1	0.0
		gi|7271895	96.5±35.5	17.0±4.0	19.0 ±2.0	Cathepsin L, partial	*F. gigantica*	AAF44678.1	1E-164
		gi|379991182	83.0±39.0	17.0±4.0	22.5±3.5	Cathepsin protein CatL1-MM3p, partial	*F. hepatica*	CCA61803.1	0.0
		gi|20136379	79.0±22.0	17.0±4.0	22.0±4.0	Cathepsin L, partial	*F. hepatica*	AAM11647.1	0.0
		gi|13774082	77.0±33.0	17.0±4.0	22.0±4.0	Cathepsin L-like	*F. hepatica*	AAK38169.1	0.0
		gi|41152538	77.0±33.0	17.0±4.0	20.5±3.5	Cathepsin L protein	*F. hepatica*	AAR99518.1	0.0
		gi|41152540	77.0±33.0	17.0±4.0	26.5±3.5	Cathepsin L protein	*F. hepatica*	AAR99519.1	9E-180
		gi|50403821	77.0±33.0	17.0±4.0	19.5±2.5	Cathepsin L1 proteinase	*F. hepatica*	AAT76664.1	0.0
		gi|21263041	77.0±33.0	17.0±4.0	15.0±1.0	Cathepsin L2	*F. gigantica*	AAM44832.1	0.0
		gi|146147376	77.0±33.0	17.0±4.0	15.0±1.0	Cathepsin	*F. gigantica*	ABQ01982.1	0.0
		gi|377823949	77.0±33.0	17.0±4.0	15.0±1.0	Cathepsin L1	*F. gigantica*	AFB77219.1	0.0
rFhpCL1^{WT}	35	**gi|116488416**	**117.0±51.0**	**13.5±3.5**	**41.0±4.0**	**Secreted cathepsin L 1**	***F. hepatica***	**AAB41670.2**	**0.0**
		gi|163310848	117.0±51.0	13.5±3.5	43.0±4.0	Chain A, Crystal Structure Of Procathepsin L1	*F. hepatica*	2O6X_A	0.0
		gi|74765984	116.5±51.5	13.5±3.5	35.5±6.5	Cathepsin L-like proteinase	*F. hepatica*	Q24940.1	0.0
		gi|4574304	104.0±45.0	13.5±3.5	21.5±3.5	Cathepsin	*F. gigantica*	AAD23996.1	0.0
		gi|545734	104.0±45.0	13.5±3.5	21.5±1.5	Cysteine protease	*Fasciola sp.*	AAB30089.1	0.0
		gi|7271889	104.0±45.0	13.5±3.5	24.0±4.0	Cathepsin L	*F. gigantica*	AAF44675.1	0.0
		gi|31558997	94.5±29.5	13.5±3.5	26.0±4.0	Cathepsin L	*F. hepatica*	AAP49831.1	0.0
		gi|20136379	86.0±33.0	13.5±3.5	24.5±6.5	Cathepsin L, partial	*F. hepatica*	AAM11647.1	0.0
		gi|7271895	79.0±20.0	13.5±3.5	21.0±3.0	Cathepsin L, partial	*F. gigantica*	AAF44678.1	1E-164
rFhpCL1	37 (1)	**gi|379991182**	**87.0±13.0**	**10.5±3.5**	**30.0±4.0**	**Cathepsin protein CatL1-MM3p, partial**	***F. hepatica***	**CCA61803.1**	**0.0**
		gi|74765984	87.0±13.0	10.5±3.5	27.0±4.0	Cathepsin L-like proteinase	*F. hepatica*	Q24940.1	0.0
		gi|116488416	87.0±13.0	10.5±3.5	24.0±4.0	Cathepsin L-like	*F. hepatica*	AAK38169.1	0.0
		gi|163310848	87.0±13.0	10.5±3.5	22.5±3.5	Chain A, Crystal Structure Of Procathepsin L1	*F. hepatica*	2O6X_A	0.0
		gi|13774082	86.5±12.5	10.5±3.5	22.5±3.5	Secreted cathepsin L 1	*F. hepatica*	AAB41670.2	0.0
		gi|41152538	86.5±12.5	10.5±3.5	22.5±3.5	Cathepsin L protein	*F. hepatica*	AAR99518.1	0.0
		gi|7271889	86.5±12.5	10.5±3.5	18.0±4.0	Cathepsin L	*F. gigantica*	AAF44675.1	0.0
		gi|21263041	86.5±12.5	10.5±3.5	18.0±4.0	Cathepsin L2	*F. gigantica*	AAM44832.1	0.0
		gi|377823949	86.5±12.5	10.5±3.5	18.0±4.0	Cathepsin L1	*F. gigantica*	AFB77219.1	0.0
		gi|4574304	86.5±12.5	10.5±3.5	15.0±4.0	Cathepsin	*F. gigantica*	AAD23996.1	0.0
		gi|10798511	85.5±13.5	10.5±3.5	14.0±4.0	Cathepsin L1	*F. hepatica*	CAC12806.1	0.0
		gi|211909240	85.5±13.5	10.5±3.5	9.0±4.0	Cathepsin L1D	*F. hepatica*	ACJ12893.1	0.0
		gi|211909242	85.5±13.5	10.5±3.5	9.0±4.0	Cathepsin L1D	*F. hepatica*	ACJ12894.1	0.0
		gi|146147376	70.5±3.5	10.5±3.5	14.0±0.0	Cathepsin	*F. gigantica*	ABQ01982.1	0.0
		gi|41152540	70.5±3.5	10.5±3.5	22.0±0.0	Cathepsin L protein	*F. hepatica*	AAR99519.1	9E-180
		gi|50403821	70.5±3.5	10.5±3.5	16.0±0.0	Cathepsin L1 proteinase	*F. hepatica*	AAT76664.1	0.0
		gi|545734	70.5±3.5	10.5±3.5	18.0±4.0	Cysteine protease	*Fasciola sp.*	AAB30089.1	0.0

		gi|20136379	68.0±15.0	10.5±3.5	26.5±4.5	Cathepsin L, partial	*F. hepatica*	AAM11647.1	0.0
		gi|31558997	67.0±14.0	10.5±3.5	12.0±4.0	Cathepsin L	*F. hepatica*	AAP49831.1	0.0
rFhpCL1	32 (2)	**gi|379991182**	**101.0±29.0**	**14.0±4.0**	**36.5±7.5**	**Cathepsin protein CatL1-MM3p, partial**	***F. hepatica***	**CCA61803.1**	**0.0**
		gi|74765984	101.0±29.0	14.0±4.0	33.5±7.5	Cathepsin L-like proteinase	*F. hepatica F. hepatica*	Q24940.1	0.0
		gi|116488416	97.0±32.0	14.0±4.0	28.5±7.5	Secreted cathepsin L 1		AAB41670.2	0.0
		gi|163310848	97.0±32.0	14.0±4.0	26.0±4.0	Chain A, Crystal Structure Of Procathepsin L1	*F. hepatica*	2O6X_A	0.0
		gi|41152540	95.5±23.5	14.0±4.0	30.0±5.0	Cathepsin L protein	*F. hepatica*	AAR99519.1	9E-180
		gi|50403821	95.5±23.5	14.0±4.0	19.0±0.0	Cathepsin L1 proteinase	*F. hepatica*	AAT76664.1	0.0
		gi|41152538	95.0±23.0	14.0±4.0	28.5±7.5	Cathepsin L protein	*F. hepatica*	AAR99518.1	0.0
		gi|13774082	95.0±23.0	14.0±4.0	30.0±8.0	Cathepsin L-like	*F. hepatica*	AAK38169.1	0.0
		gi|4574304	91.5±26.5	14.0±4.0	21.0±7.0	Cathepsin	*F. gigantica*	AAD23996.1	0.0
		gi|545734	91.0±26.0	14.0±4.0	19.5±3.5	Cysteine protease	*Fasciola sp.*	AAB30089.1	0.0
		gi|7271889	91.0±26.0	14.0±4.0	23.5±7.5	Cathepsin L	*F. gigantica*	AAF44675.1	0.0
		gi|21263041	91.0±26.0	14.0±4.0	23.5±7.5	Cathepsin L2	*F. gigantica*	AAM44832.1	0.0
		gi|146147376	91.0±26.0	14.0±4.0	19.5±3.5	Cathepsin	*F. gigantica*	ABQ01982.1	0.0
		gi|377823949	91.0±26.0	14.0±4.0	23.5±7.5	Cathepsin L1	*F. gigantica*	AFB77219.1	0.0
		gi|108735840	81.0±31.0	14.0±4.0	7.0±0.0	Cathepsin L2	*F. hepatica*	ABG00259.1	7E-167
		gi|211909240	81.0±31.0	14.0±4.0	14.5±7.5	Cathepsin L1D	*F. hepatica*	ACJ12893.1	0.0
		gi|211909242	81.0±31.0	14.0±4.0	14.5±7.5	Cathepsin L1D	*F. hepatica*	ACJ12894.1	0.0
		gi|10798511	80.0±25.0	14.0±4.0	20.5±7.5	Cathepsin L1	*F. hepatica*	CAC12806.1	0.0
		gi|310751866	79.5±25.5	14.0±4.0	27.0±7.0	Cathepsin L-like proteinase	*F. hepatica*	ADP09371.1	0.0
		gi|7271895	77.0±27.0	14.0±4.0	16.5±5.5	Cathepsin L, partial	*F. gigantica*	AAF44678.1	1E-164
		gi|20136379	70.5±6.5	14.0±4.0	32.5±7.5	Cathepsin L, partial	*F. hepatica*	AAM11647.1	0.0
rFhpCL1	24 (3)	**gi|379991182**	**479.0±21.0**	**40.5±0.5**	**62.5±0.5**	**Cathepsin protein CatL1-MM3p, partial**	***F. hepatica***	**CCA61803.1**	**0.0**
		gi|74765984	462.0±10.0	40.5±0.5	58.5±1.5	Cathepsin L-like proteinase	*F. hepatica*	Q24940.1	0.0
		gi|13774082	457.5±7.5	40.5±0.5	52.5±0.5	Cathepsin L-like	*F. hepatica*	AAK38169.1	0.0
		gi|41152538	457.5±7.5	40.5±0.5	53.5±0.5	Cathepsin L protein	*F. hepatica*	AAR99518.1	0.0
		gi|116488416	435.0±9.0	40.5±0.5	43.0±1.0	Secreted cathepsin L 1	*F. hepatica*	AAB41670.2	0.0
		gi|21263041	430.5±6.5	40.5±0.5	40.5±0.5	Cathepsin L2	*F. gigantica*	AAM44832.1	0.0
		gi|7271889	430.5±6.5	40.5±0.5	41.0±1.0	Cathepsin L	*F. gigantica*	AAF44675.1	0.0
		gi|377823949	430.5±6.5	40.5±0.5	40.5±0.5	Cathepsin L1	*F. gigantica*	AFB77219.1	0.0
		gi|4574304	430.5±6.5	40.5±0.5	51.5±1.5	Cathepsin	*F. gigantica*	AAD23996.1	0.0
		gi|163310848	426.0±5.0	40.5±0.5	40.5±3.5	Chain A, Crystal Structure Of Procathepsin L1	*F. hepatica*	2O6X_A	0.0
		gi|41152540	401.5±0.5	40.5±0.5	63.0±1.0	Cathepsin L protein	*F. hepatica*	AAR99519.1	9E-180
		gi|50403821	391.0±2.0	40.5±0.5	25.0±0.0	Cathepsin L1 proteinase	*F. hepatica*	AAT76664.1	0.0
		gi|10798511	378.0±2.0	34.0±16.0	39.5±0.5	Cathepsin L1	*F. hepatica*	CAC12806.1	0.0
		gi|146147376	376.0±0.0	40.5±0.5	27.0±1.0	Cathepsin	*F. gigantica*	ABQ01982.1	0.0
		gi|545734	376.0±0.0	40.5±0.5	33.5±1.5	Cysteine protease	*Fasciola sp.*	AAB30089.1	0.0
		gi|211909240	353.5±3.5	40.5±0.5	33.0±0.0	Cathepsin L1D	*F. hepatica*	ACJ12893.1	0.0
		gi|211909242	353.5±3.5	40.5±0.5	33.0±0.0	Cathepsin L1D	*F. hepatica*	ACJ12894.1	0.0
		gi|7271895	300.5±9.5	40.5±0.5	47.5±0.5	Cathepsin L, partial	*F. gigantica*	AAF44678.1	1E-164
		gi|**310751866**	**245.0±20.0**	**24.0±1.0**	**42.5±0.5**	**Cathepsin L-like proteinase**	***F. hepatica***	**ADP09371.1**	**0.0**
		gi|20136379	241.5±37.5	40.5±0.5	52.5±0.5	Cathepsin L, partial	*F. hepatica*	AAM11647.1	0.0
		gi|108735840	292.5±14.5	40.5±0.5	7.5±0.5	Cathepsin L2	*F. hepatica*	ABG00259.1	7E-167
		gi|31558997	189.5±19.5	40.5±0.5	43.0±1.0	Cathepsin L	*F. hepatica*	AAP49831.1	0.0
		gi|452266	149.0±12.0	40.5±0.5	25.5±4.5	Cathepsin L-like protease	*F. hepatica*	CAA80450.1	8E-124

		gi|19909509	129.5±14.5	29.5±10.5	31.0±1.0	Cathepsin L	*F. gigantica*	BAB86959.1	0.0
		gi|157862759	108.0±12.0	40.5±0.5	46.5±0.5	Cathepsin L, partial	*F. gigantica*	ABV90502.1	0.0
		gi|7271891	100.5±9.5	40.5±0.5	10.0±0.0	Cathepsin L	*F. gigantica*	AAF44676.1	0.0
		gi|107921814	98.5±7.5	40.5±0.5	10.0±0.0	Cathepsin L4	*F. hepatica*	ABF85682.1	2E-172
		gi|167427529	98.5±7.5	40.5±0.5	7.0±0.0	Cathepsin L4, partial	*F. hepatica*	ABZ80401.1	0.0
		gi|195729975	98.5±7.5	40.5±0.5	7.0±0.0	Cathepsin L1	*F. magna*	ACG50798.1	0.0
		gi|38045864	98.5±7.5	40.5±0.5	7.0±0.0	Cathepsin L	*F. gigantica*	AAR08900.1	0.0
rFhpCL1	22 (4)	**gi|379991182**	**148.0±24.0**	**18.5±4.5**	**45.0±1.0**	**Cathepsin protein CatL1-MM3p, partial**	***F. hepatica***	**CCA61803.1**	**0.0**
		gi|163310848	147.5±24.5	18.5±4.5	31.0±1.0	Chain A, Crystal Structure Of Procathepsin L1	*F. hepatica*	2O6X_A	0.0
		gi|74765984	146.5±25.5	18.5±4.5	42.0±1.0	Cathepsin L-like proteinase	*F. hepatica*	Q24940.1	0.0
		gi|116488416	146.5±25.5	18.5±4.5	37.0±1.0	Secreted cathepsin L 1	*F. hepatica*	AAB41670.2	0.0
		gi|7271889	122.5±27.5	18.5±4.5	31.0±0.0	Cathepsin L	*F. gigantica*	AAF44675.1	0.0
		gi|21263041	122.5±27.5	18.5±4.5	31.0±0.0	Cathepsin L2	*F. gigantica*	AAM44832.1	0.0
		gi|377823949	122.5±27.5	18.5±4.5	31.0±0.0	Cathepsin L1	*F. gigantica*	AFB77219.1	0.0
		gi|4574304	122.5±27.5	18.5±4.5	28.0±0.0	Cathepsin	*F. gigantica*	AAD23996.1	0.0
		gi|13774082	122.5±27.5	18.5±4.5	38.0±0.0	Cathepsin L-like	*F. hepatica*	AAK38169.1	0.0
		gi|41152538	122.5±27.5	18.5±4.5	37.0±1.0	Cathepsin L protein	*F. hepatica*	AAR99518.1	0.0
		gi|310751866	119.0±18.0	15.0±1.0	35.5±1.5	Cathepsin L-like proteinase	*F. hepatica*	ADP09371.1	0.0
		gi|50403821	114.5±16.5	18.5±4.5	19.0±0.0	Cathepsin L1 proteinase	*F. hepatica*	AAT76664.1	0.0
		gi|146147376	113.0±18.0	18.5±4.5	25.5±2.5	Cathepsin	*F. gigantica*	ABQ01982.1	0.0
		gi|545734	113.0±18.0	18.5±4.5	24.0±0.0	Cysteine protease	*Fasciola sp.*	AAB30089.1	0.0
		gi|41152540	113.0±18.0	18.5±4.5	35.0±0.0	Cathepsin L protein	*F. hepatica*	AAR99519.1	9E-180
		gi|211909240	105.0±14.0	18.5±4.5	22.0±0.0	Cathepsin L1D	*F. hepatica*	ACJ12893.1	0.0
		gi|211909242	105.0±14.0	18.5±4.5	22.0±0.0	Cathepsin L1D	*F. hepatica*	ACJ12894.1	0.0
		gi|10798511	104.0±15.0	18.5±4.5	28.0±0.0	Cathepsin L1	*F. hepatica*	CAC12806.1	0.0
		gi|108735840	102.5±0.5	18.5±4.5	7.0±0.0	Cathepsin L2	*F. hepatica*	ABG00259.1	7E-167
		gi|20136379	101.0±18.0	18.5±4.5	41.5±1.5	Cathepsin L, partial	*F. hepatica*	AAM11647.1	0.0
		gi|7271895	97.0±6.0	18.5±4.5	22.0±0.0	Cathepsin L, partial	*F. gigantica*	AAF44678.1	1E-164
		gi|31558997	72.0±24.0	18.5±4.5	27.0±1.0	Cathepsin L	*F. hepatica*	AAP49831.1	0.0
rFhpCL1	18 (5)	**gi|379991182**	**270.5±32.5**	**20.5±1.5**	**44.0±0.0**	**Cathepsin protein CatL1-MM3p, partial**	***F. hepatica***	**CCA61803.1**	**0.0**
		gi|74765984	257.0±31.0	20.5±1.5	41.0±0.0	Cathepsin L-like proteinase	*F. hepatica*	Q24940.1	0.0
		gi|13774082	245.5±34.5	20.5±1.5	40.5±0.5	Cathepsin L-like	*F. hepatica*	AAK38169.1	0.0
		gi|41152538	245.5±34.5	20.5±1.5	36.0±0.0	Cathepsin L protein	*F. hepatica*	AAR99518.1	0.0
		gi|20136379	243.5±25.5	20.5±1.5	40.5±0.5	Cathepsin L, partial	*F. hepatica*	AAM11647.1	0.0
		gi|116488416	234.0±30.0	20.5±1.5	36.0±0.0	Secreted cathepsin L 1	*F. hepatica*	AAB41670.2	0.0
		gi|21263041	222.5±33.5	20.5±1.5	34.0±0.0	Cathepsin L2	*F. gigantica*	AAM44832.1	0.0
		gi|7271889	222.5±33.5	20.5±1.5	34.0±0.0	Cathepsin L	*F. gigantica*	AAF44675.1	0.0
		gi|377823949	222.5±33.5	20.5±1.5	34.0±0.0	Cathepsin L1	*F. gigantica*	AFB77219.1	0.0
		gi|4574304	222.5±33.5	20.5±1.5	34.0±0.0	Cathepsin	*F. gigantica*	AAD23996.1	0.0
		gi|163310848	217.0±36.0	20.5±1.5	33.0±0.0	Chain A, Crystal Structure Of Procathepsin L1	*F. hepatica*	2O6X_A	0.0
		gi|41152540	201.0±17.0	20.5±1.5	39.0±0.0	Cathepsin L protein	*F. hepatica*	AAR99519.1	9E-180
		gi|31558997	194.5±27.5	20.5±1.5	26.0±0.0	Cathepsin L	*F. hepatica*	AAP49831.1	0.0
		gi|50403821	184.0±33.0	20.5±1.5	19.0±0.0	Cathepsin L1 proteinase	*F. hepatica*	AAT76664.1	0.0
		gi|146147376	178.0±26.0	20.5±1.5	26.0±0.0	Cathepsin	*F. gigantica*	ABQ01982.1	0.0
		gi|545734	178.0±26.0	20.5±1.5	26.0±0.0	Cysteine protease	*Fasciola sp.*	AAB30089.1	0.0
		gi|310751866	160.0±9.0	18.0±1.0	34.5±0.5	Cathepsin L-like proteinase	*F. hepatica*	ADP09371.1	0.0

		gi|10798511	156.5±6.5	20.5±1.5	28.5±0.5	Cathepsin L1	*F. hepatica*	CAC12806.1	0.0
		gi|452266	154.0±27.0	20.5±1.5	25.5±4.5	Cathepsin L-like protease	*F. hepatica*	CAA80450.1	8E-124
		gi|19909509	149.0±20.0	20.5±1.5	24.0±0.0	Cathepsin L	*F. gigantica*	BAB86959.1	0.0
		gi|211909240	134.5±5.5	20.5±1.5	25.0±0.0	Cathepsin L1D	*F. hepatica*	ACJ12893.1	0.0
		gi|211909242	134.5±5.5	20.5±1.5	25.0±0.0	Cathepsin L1D	*F. hepatica*	ACJ12894.1	0.0
		gi|157862759	105.5±0.5	20.5±1.5	20.0±0.0	Cathepsin L, partial	*F. gigantica*	ABV90502.1	0.0
		*gi|127525	94.0±12.0	3.5±0.5	33.0±0.0	Major outer membrane lipoprotein	*S. marcescens*	P02938.1	4E-46
		gi|7271895	93.0±2.0	20.5±1.5	26.0±0.0	Cathepsin L, partial	*F. gigantica*	AAF44678.1	1E-164
		gi|7271891	89.0±7.0	20.5±1.5	10.0±0.0	Cathepsin L	*F. gigantica*	AAF44676.1	0.0
		gi|107921814	89.0±7.0	20.5±1.5	10.5±0.5	Cathepsin L4	*F. hepatica*	ABF85682.1	2E-172
		gi|167427529	89.0±7.0	20.5±1.5	7.5±0.5	Cathepsin L4, partial	*F. hepatica*	ABZ80401.1	0.0
		gi|195729975	89.0±7.0	20.5±1.5	7.0±0.0	Cathepsin L1	*F. magna*	ACG50798.1	0.0
		gi|38045864	89.0±7.0	20.5±1.5	7.0±0.0	Cathepsin L	*F. gigantica*	AAR08900.1	0.0
		gi|108735840	83.5±5.5	20.5±1.5	7.0±0.0	Cathepsin L2	*F. hepatica*	ABG00259.1	7E-167
rFhpCL1	≤14 (6)	**gi|379991182**	**462.0±16.0**	**40.5±3.5**	**51.0±0.0**	**Cathepsin protein CatL1-MM3p, partial**	***F. hepatica***	**CCA61803.1**	**0.0**
		gi|74765984	436.5±17.5	40.5±3.5	48.0±0.0	Cathepsin L-like proteinase	*F. hepatica*	Q24940.1	0.0
		gi|116488416	432.5±14.5	40.5±3.5	43.0±0.0	Secreted cathepsin L 1	*F. hepatica*	AAB41670.2	0.0
		gi|163310848	427.5±9.5	40.5±3.5	38.0±0.0	Chain A, Crystal Structure Of Procathepsin L1	*F. hepatica*	2O6X_A	0.0
		gi|13774082	422.5±14.5	40.5±3.5	38.5±0.5	Cathepsin L-like	*F. hepatica*	AAK38169.1	0.0
		gi|41152538	422.5±14.5	40.5±3.5	43.0±0.0	Cathepsin L protein	*F. hepatica*	AAR99518.1	0.0
		gi|21263041	418.0±12.0	40.5±3.5	37.0±1.0	Cathepsin L2	*F. gigantica*	AAM44832.1	0.0
		gi|4574304	418.0±12.0	40.5±3.5	37.0±1.0	Cathepsin	*F. gigantica*	AAD23996.1	0.0
		gi|7271889	418.0±12.0	40.5±3.5	37.0±1.0	Cathepsin L	*F. gigantica*	AAF44675.1	0.0
		gi|377823949	418.0±12.0	40.5±3.5	37.0±1.0	Cathepsin L1	*F. gigantica*	AFB77219.1	0.0
		gi|10798511	366.0±27.0	40.5±3.5	29.0±0.0	Cathepsin L1	*F. hepatica*	CAC12806.1	0.0
		gi|41152540	363.0±29.0	40.5±3.5	42.5±1.5	Cathepsin L protein	*F. hepatica*	AAR99519.1	9E-180
		gi|211909240	362.5±24.5	40.5±3.5	28.0±1.0	Cathepsin L1D	*F. hepatica*	ACJ12893.1	0.0
		gi|211909242	362.5±24.5	40.5±3.5	28.0±1.0	Cathepsin L1D	*F. hepatica*	ACJ12894.1	0.0
		gi|146147376	359.5±33.5	40.5±3.5	23.5±0.5	Cathepsin	*F. gigantica*	ABQ01982.1	0.0
		gi|545734	359.5±33.5	40.5±3.5	29.0±1.0	Cysteine protease	*Fasciola sp.*	AAB30089.1	0.0
		gi|50403821	358.5±33.5	40.5±3.5	24.0±1.0	Cathepsin L1 proteinase	*F. hepatica*	AAT76664.1	0.0
		gi|108735840	300.5±22.5	40.5±3.5	7.5±0.5	Cathepsin L2	*F. hepatica*	ABG00259.1	7E-167
		gi|7271895	304.5±18.5	40.5±3.5	30.5±1.5	Cathepsin L, partial	*F. gigantica*	AAF44678.1	1E-164
		gi|20136379	215.5±39.5	40.5±3.5	42.0±1.0	Cathepsin L, partial	*F. hepatica*	AAM11647.1	0.0
		gi|310751866	**203.0±35.0**	**27.0±0.0**	**42.0±0.0**	**Cathepsin L-like proteinase**	***F. hepatica***	**ADP09371.1**	**0.0**
		gi|31558997	166.5±38.5	40.5±3.5	32.5±0.5	Cathepsin L	*F. hepatica*	AAP49831.1	0.0
		gi|19909509	**123.5±18.5**	**16.0±2.0**	**28.0±0.0**	**Cathepsin L**	***F. gigantica***	**BAB86959.1**	**0.0**
		gi|157862759	109.5±51.5	40.5±3.5	33.0±1.0	Cathepsin L, partial	*F. gigantica*	ABV90502.1	0.0
		gi|452266	106.0±10.0	40.5±3.5	21.0±0.0	Cathepsin L-like protease	*F. hepatica*	CAA80450.1	8E-124
		gi|107921814	105.0±24.0	40.5±3.5	11.0±0.0	Cathepsin L4	*F. hepatica*	ABF85682.1	2E-172
		gi|7271891	105.0±47.0	40.5±3.5	10.0±0.0	Cathepsin L	*F. gigantica*	AAF44676.1	0.0
		gi|167427529	105.0±47.0	40.5±3.5	8.0±0.0	Cathepsin L4, partial	*F. hepatica*	ABZ80401.1	0.0
		gi|195729975	105.0±47.0	40.5±3.5	7.0±0.0	Cathepsin L1	*F. magna*	ACG50798.1	0.0
		gi|38045864	105.0±47.0	40.5±3.5	7.0±0.0	Cathepsin L	*F. gigantica*	AAR08900.1	0.0

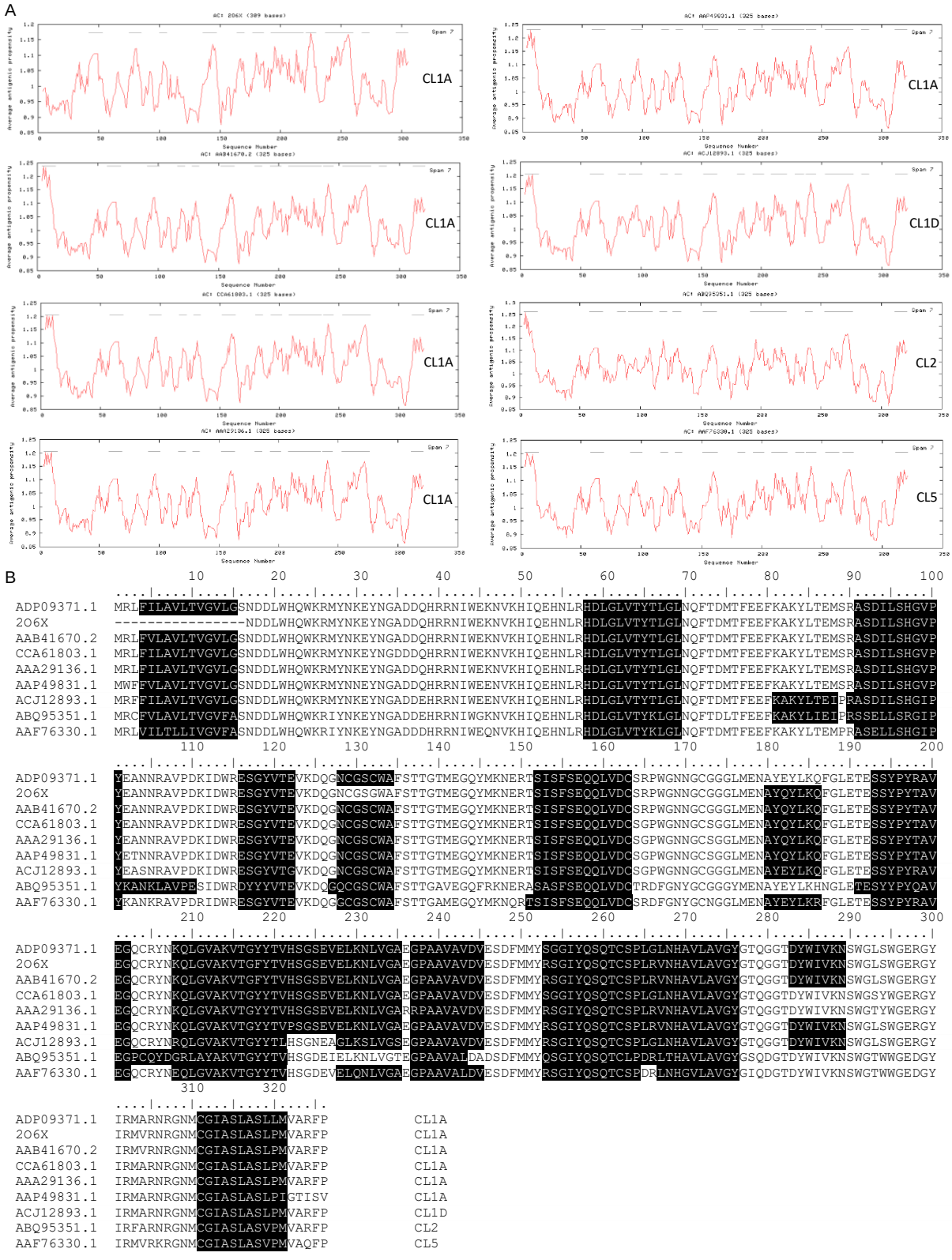

Figure S2. Antigenicity profile predictions for *Fasciola hepatica* procathepsin L proteins. CL sequences of interest identified from recombinant and native studies described were analysed for putative B cell epitopes (A), showing antigenic peptides of interest which scored above each protein's overall average antigenicity score. (B) Antigenic determinants of each sequence are highlighted, with broadly similar peptides across all CL protein sequences analysed and minor deviations at antigenic residue substitutions.

Table S2. Residue conservation scores based on multiple sequence alignments of procathepsin L candidate peptides. Sequences for candidate peptides (6–20, signal–inhibitor; 26–40, inhibitor; 115–129, mature protease) from nine procathepsin Ls were aligned and residue conservation was analysed using the Scorecons Server (Thornton Group, European Bioinformatics Institute: www.ebi.ac.uk/thornton-srv/databases/cgi-bin/valdar/scorecons_server.pl). Ten residues were identical within the signal–inhibitor- and mature protease-derived peptides, and 11 were identical within the inhibitor-derived peptide (residue conservation score: 1.000). Average residue conservation scores were 0.889, 0.934 and 0.878 for signal–inhibitor-, inhibitor- and mature protease-derived peptides, respectively, leading to low diversity scores of 39.90% (*excluding 2O6X_A for residues 6-16), 35.10% (26–40) and 43.30% (115–129).

Peptide position	Sequence source (GenBank v204) (ADP09371.1, 2O6X_A, AAB41670.2, CCA61803.1, AAA29136.1, AAP49831.1, ACJ12893.1, ABQ95351.1, AAF76330.1)	Residue conservation score (0–1)	Overall diversity score (0–100%)
Signal–inhibitor 6–20↓	L-LLLLLLL	1.000*	39.90*
	A-AAATAAA	0.692*	
	V-VVVLVVV	0.692*	
	L-LLLLLLL	1.000*	
	T-TTTITTT	0.653*	
	V-VVVVVVV	1.000*	
	G-GGGGGGG	1.000*	
	V-VVVVVVV	1.000*	
	L-LLLFLFL	0.669*	
	G-GGGAGAG	0.628*	
	S-SSSSSSS	1.000*	
	NNNNNNNNN	1.000	
	DDDDDDDDD	1.000	
	DDDDDDDDD	1.000	
	LLLLLLLLL	1.000	
Inhibitor 26–40↓	RRRRRRRRR	1.000	35.10
	MMMMMMMII	0.772	
	YYYYYYYYY	1.000	
	NNNNNNNNN	1.000	
	KKKKKNKKK	0.831	
	EEEEEEEEE	1.000	
	YYYYYYYYY	1.000	
	NNNNNNNNN	1.000	
	GGGGGGGGG	1.000	
	AAADAAAAA	0.774	
	DDDDDDDDD	1.000	
	DDDDDDDDD	1.000	
	QQQQQQQED	0.637	
	HHHHHHHHH	1.000	
	RRRRRRRRR	1.000	
Mature Protease 115–129↓	RRRRRRRRR	1.000	43.30
	EEEEEEEDE	0.774	
	SSSSSSSYS	0.585	
	GGGGGGGYG	0.472	
	YYYYYYYYY	1.000	
	VVVVVVVVV	1.000	
	TTTTTTTTT	1.000	
	EEEEEEGEE	0.833	
	VVVVVVVVV	1.000	
	KKKKKKKKK	1.000	
	DDDDDDDDD	1.000	
	QQQQQQQQQ	1.000	
	GGGGGGGGG	1.000	
	NNNNNNNQG	0.507	
	CCCCCCCCC	1.000	

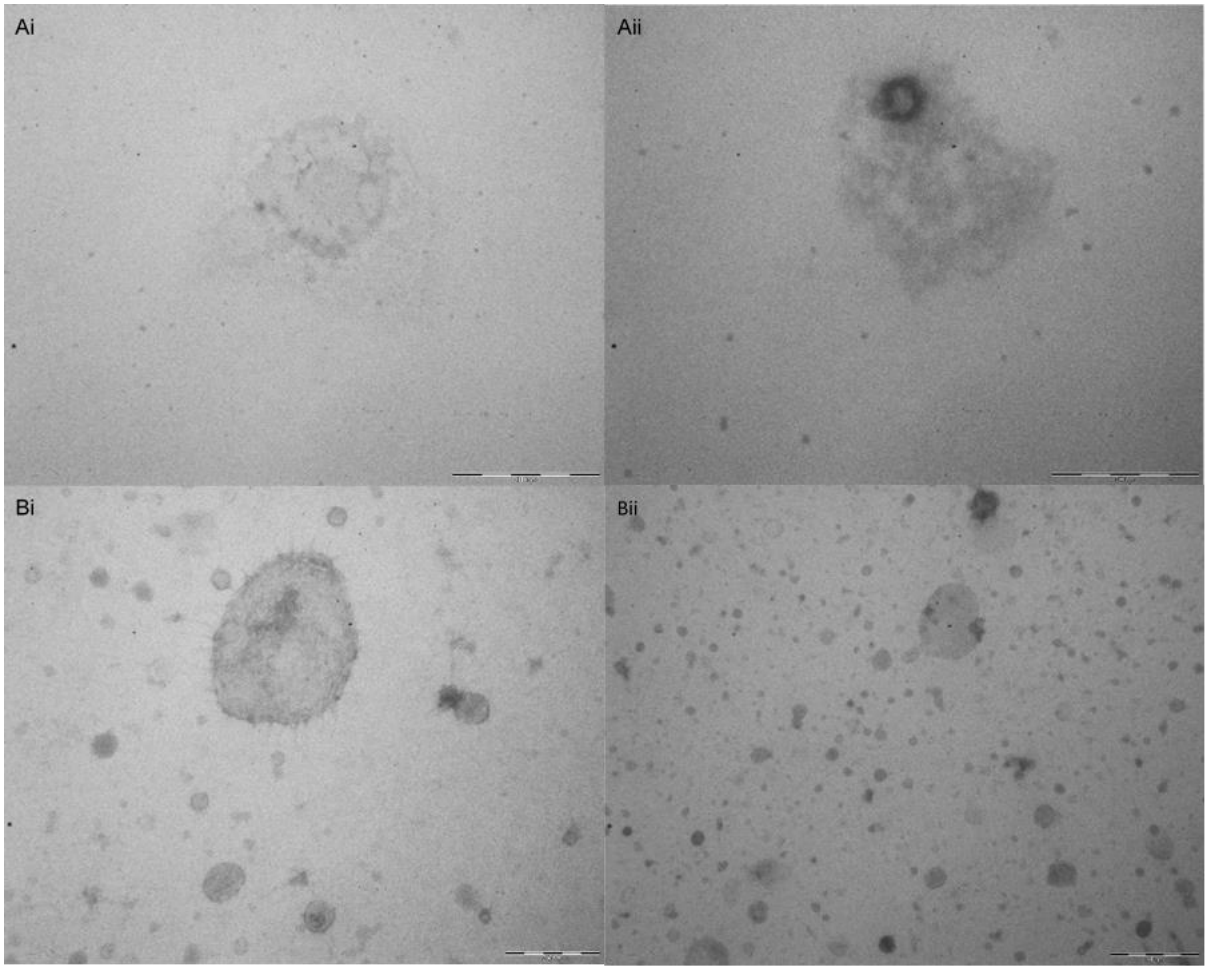

Figure S3. Transmission electron microscopy (TEM) visualisation of SEC-derived extracellular vesicles (EVs) from excretory/secretory (ES) products of *Fasciola hepatica* after *in vitro* culture (live fluke group). EVs derived from 10 adult *F. hepatica* ES products were analysed by TEM following *in vitro* culture. qEV original fractionation of large-sized (EV_1) EVs (Ai-ii) and small-sized (EV_2) EVs (Bi-ii) was confirmed.

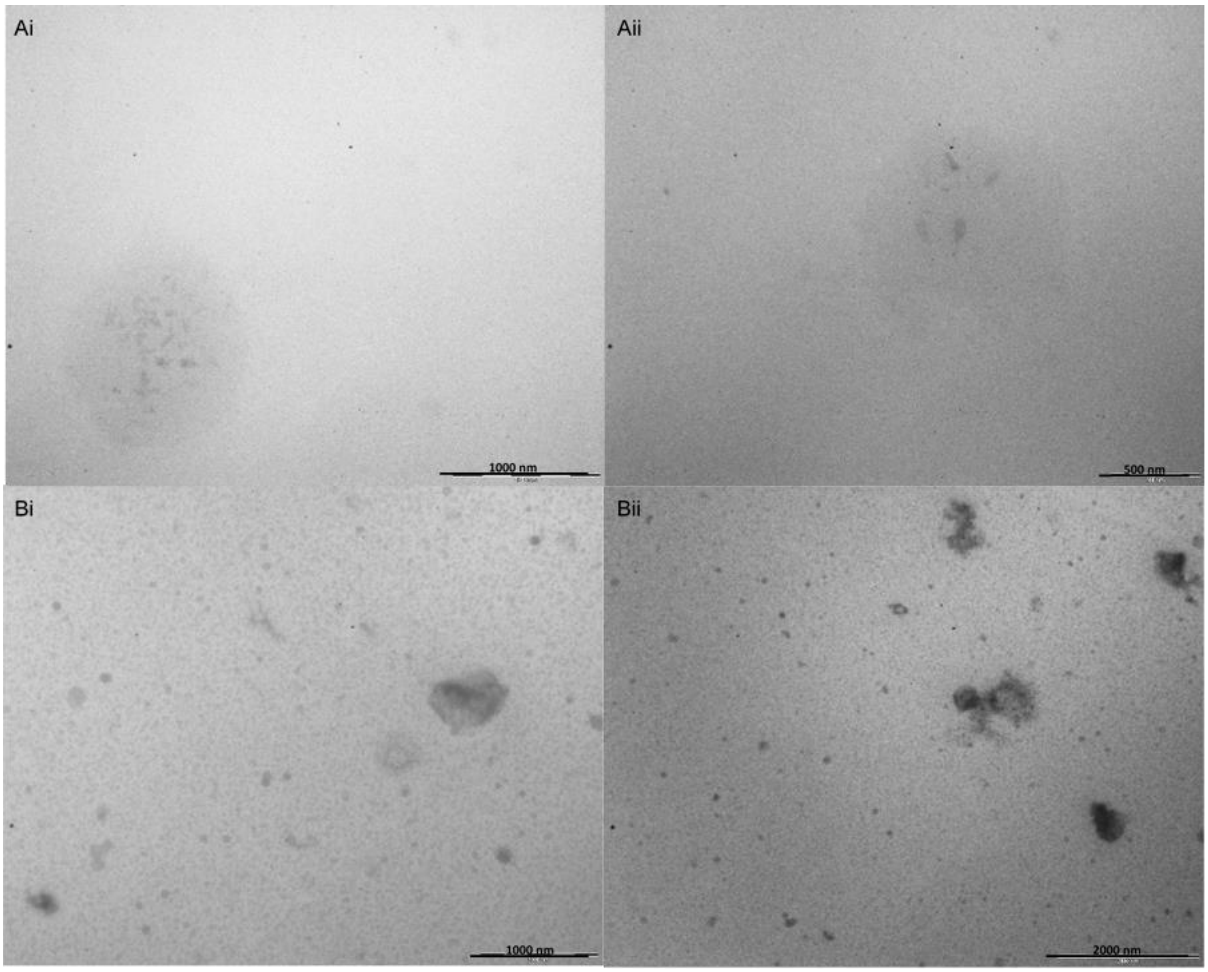

Figure S4. Transmission electron microscopy (TEM) visualisation of SEC-derived extracellular vesicles (EVs) from excretory/secretory (ES) products of *Fasciola hepatica* after ethyl 4-aminobenzoate exposure (dead fluke group). EVs derived from 10 adult *F. hepatica* from natural infections were analysed by TEM following exposure to ethyl 4-aminobenzoate. qEV original fractionation of large-sized (EV_1) EVs (Ai-ii) and small-sized (EV_2) EVs (Bi-ii) was confirmed.

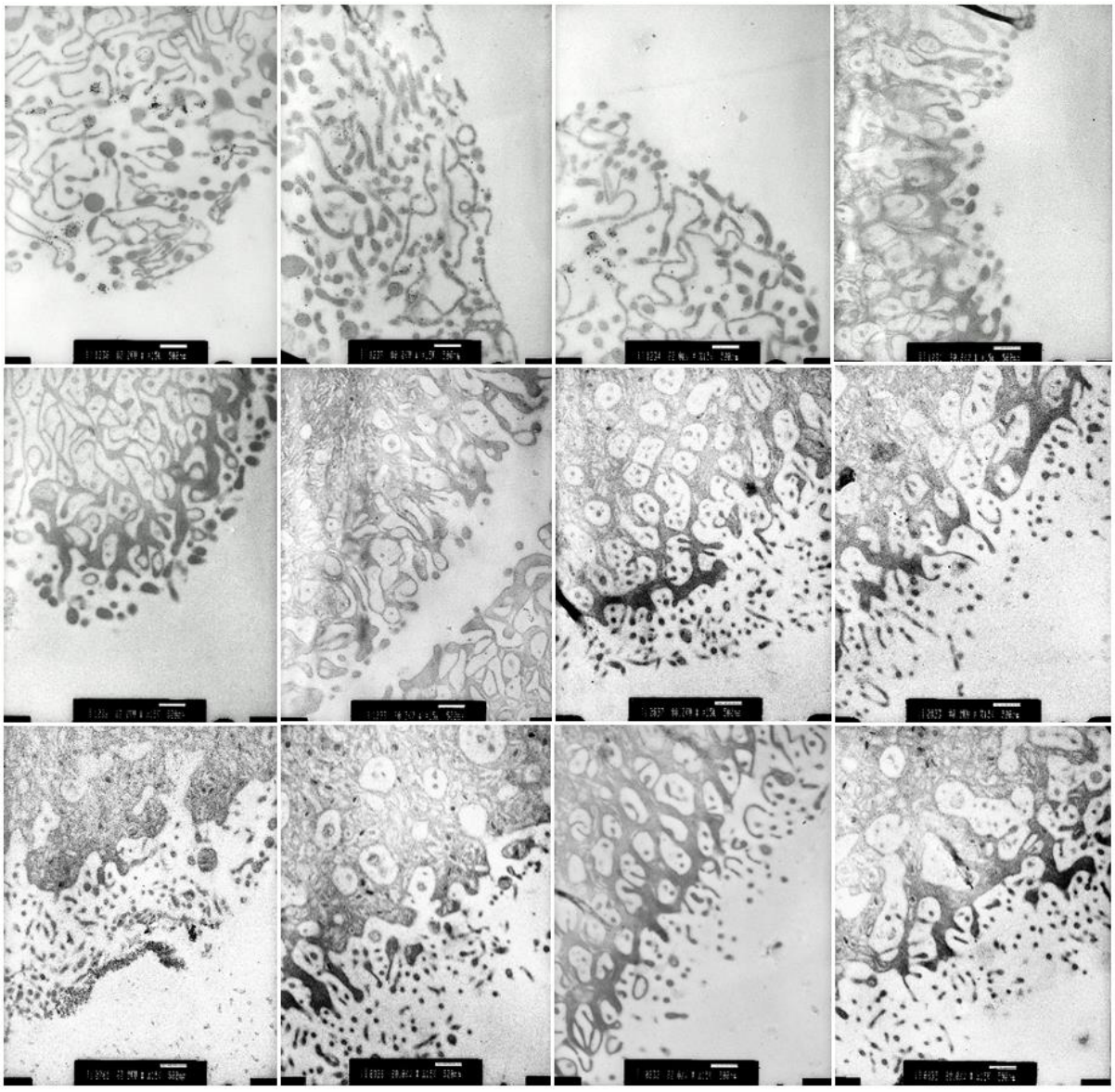

Figure S5. Transmission electron microscopy (TEM) visualisation of *Fasciola hepatica* tegument after *in vitro* culture (untreated control group). Five size-matched adult *F. hepatica* from natural infections were analysed by TEM following *in vitro* culture. Scale bar: 500 nm.

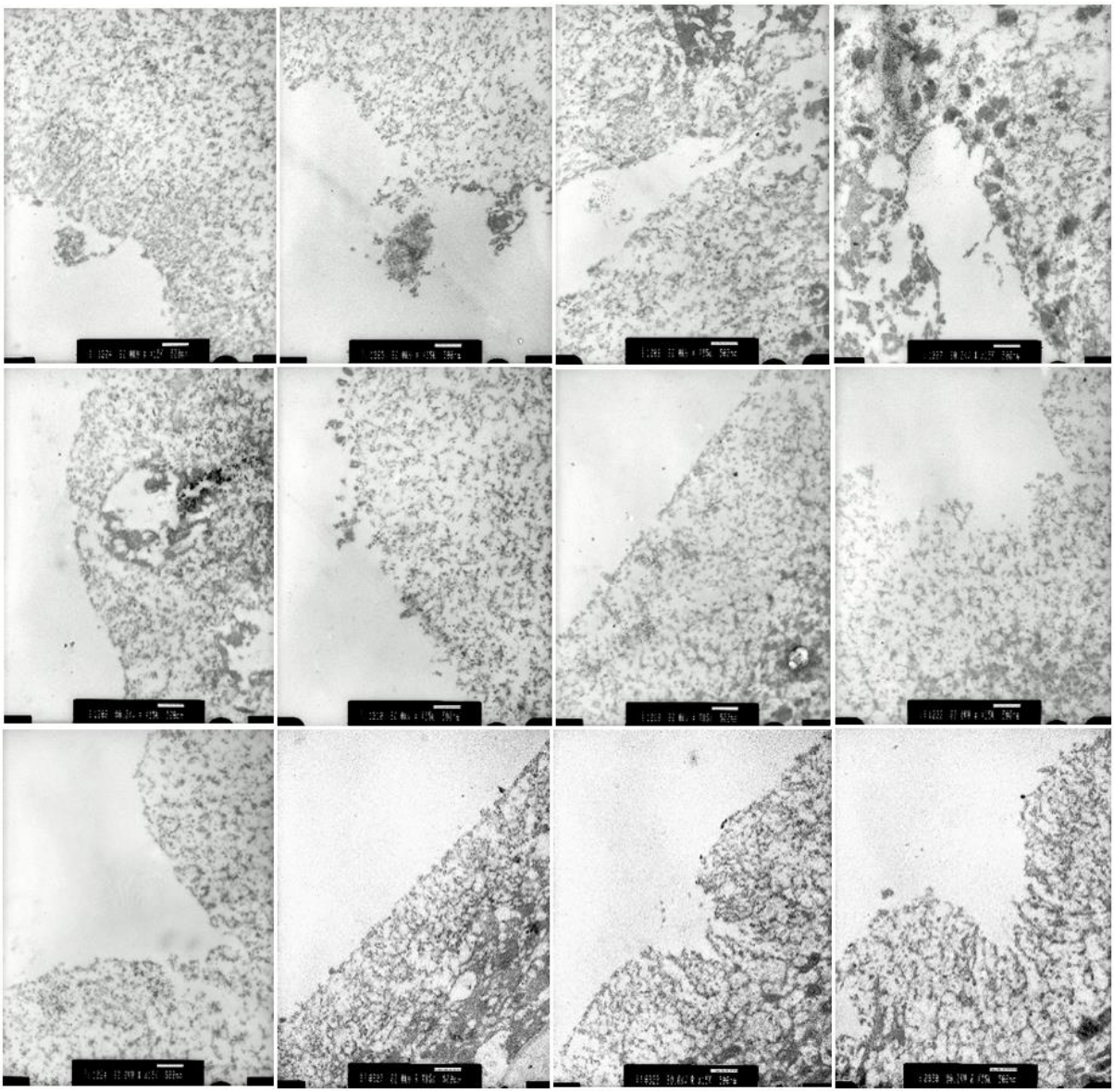

Figure S6. Transmission electron microscopy (TEM) visualisation of *Fasciola hepatica* tegument after *in vitro* culture (ethyl 4-aminobenzoate-treated group). Five size-matched adult *F. hepatica* from natural infections were analysed by TEM following *in vitro* culture and exposure (<1 minute) to ethyl 4-aminobenzoate. Scale bar: 500 nm.

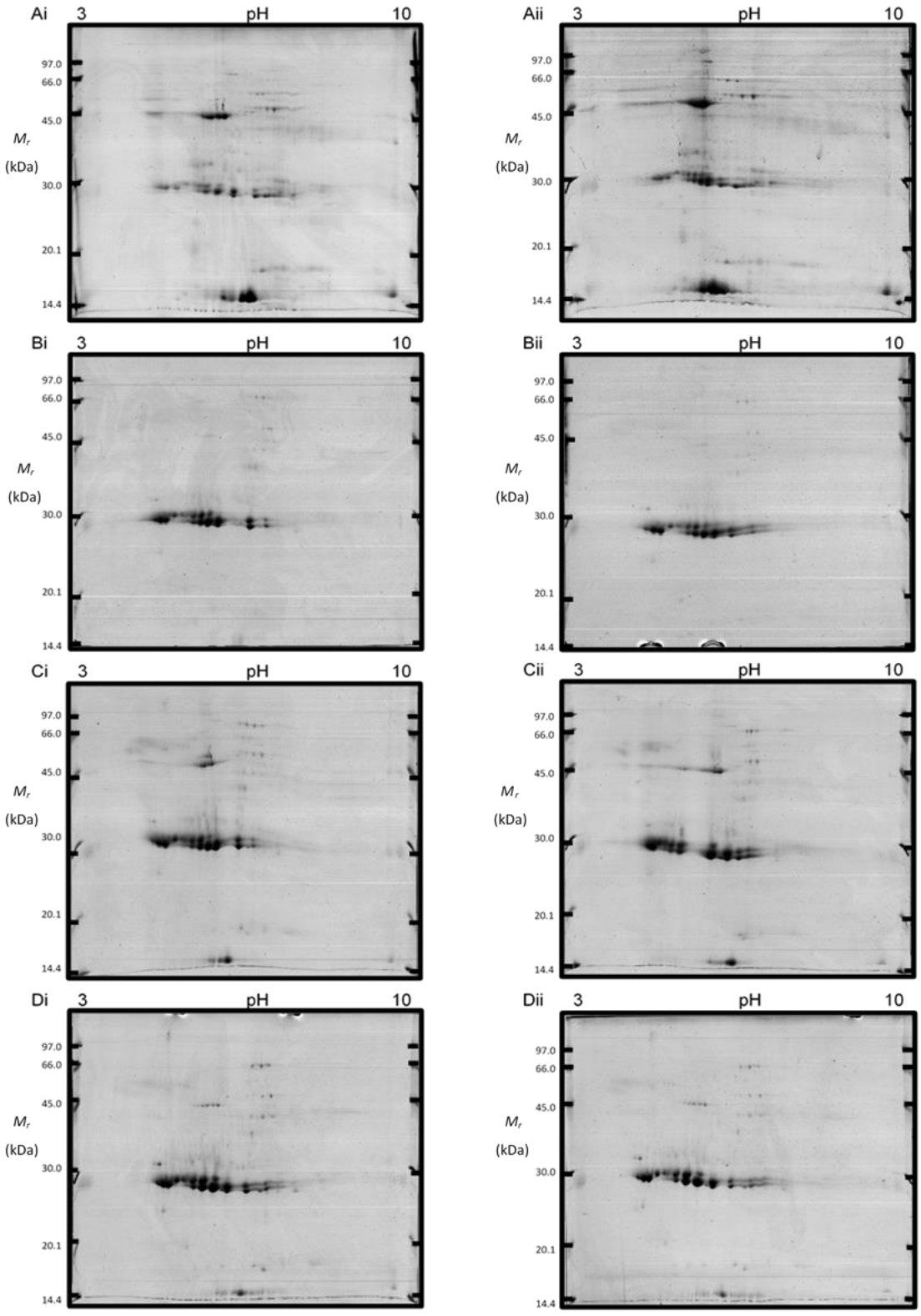

Figure S7. 2-D SDS PAGE of whole extracellular vesicle (EV)-depleted excretory/secretory proteomic profiles of drug-treated (sub-lethal dose [15 µg·mL^{-1}]: TCBZ, TCBZ-SO, TCBZ-SO$_2$) wild type *Fasciola hepatica* (WT-Fh, mixed TCBZ susceptibility). All protein material (≤100 µg, EV-depleted by SEC) acquired from 90 flukes per treatment were analysed by duplicate 2-D SDS PAGE: (A) DMSO, (B) TCBZ, (C) TCBZ-SO and (D) TCBZ-SO$_2$.

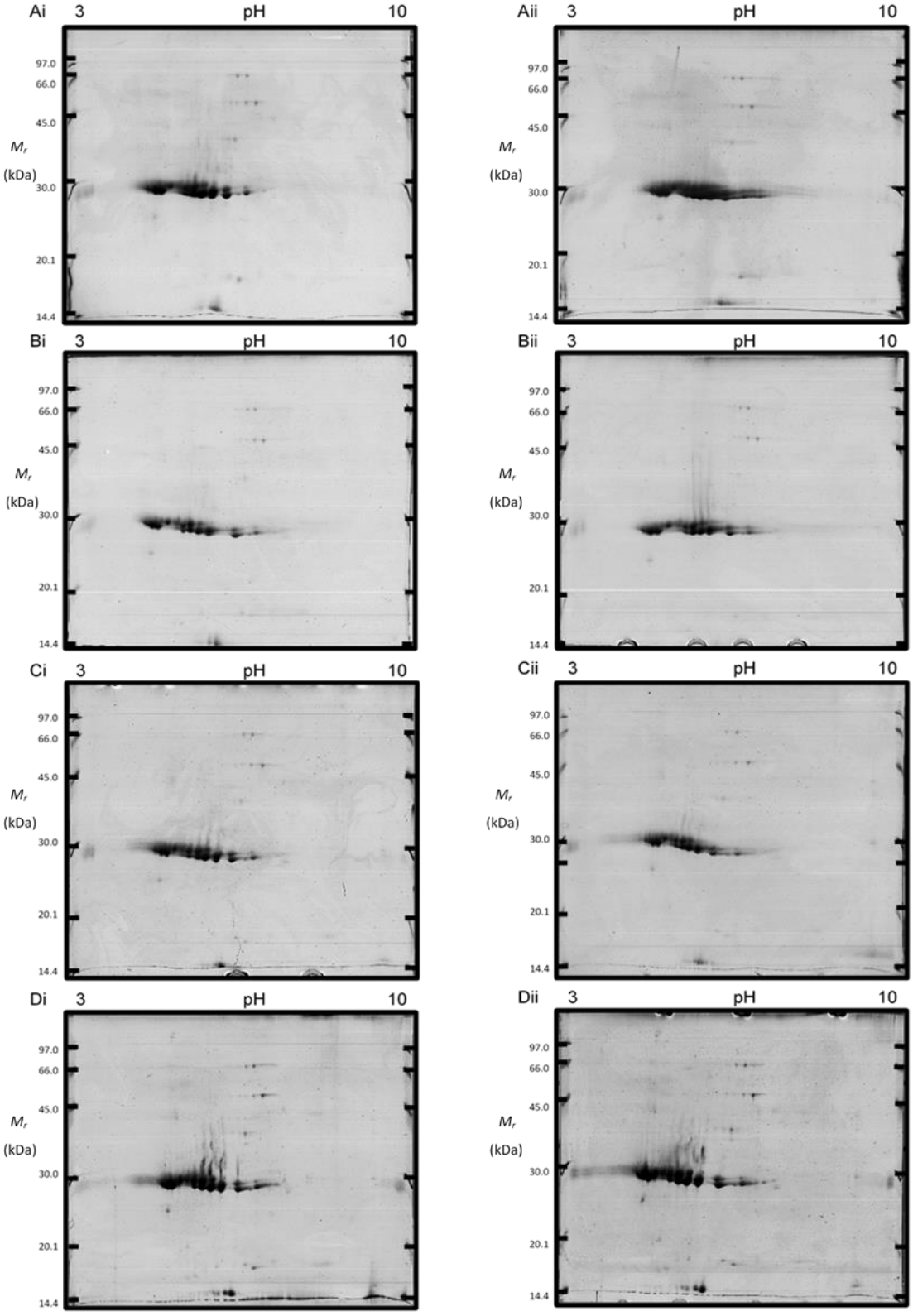

Figure S8. 2-D SDS PAGE of whole extracellular vesicle (EV)-depleted excretory/secretory proteomic profiles of drug-treated (sub-lethal dose [15 µg·mL^{-1}]: TCBZ, TCBZ-SO, TCBZ-SO$_2$) Kilmarnock *Fasciola hepatica* (K-Fh, TCBZ-resistant). All protein material (≤100 µg, EV-depleted by SEC) acquired from 90 flukes per treatment were analysed by duplicate 2-D SDS PAGE: (A) DMSO, (B) TCBZ, (C) TCBZ-SO and (D) TCBZ-SO$_2$.

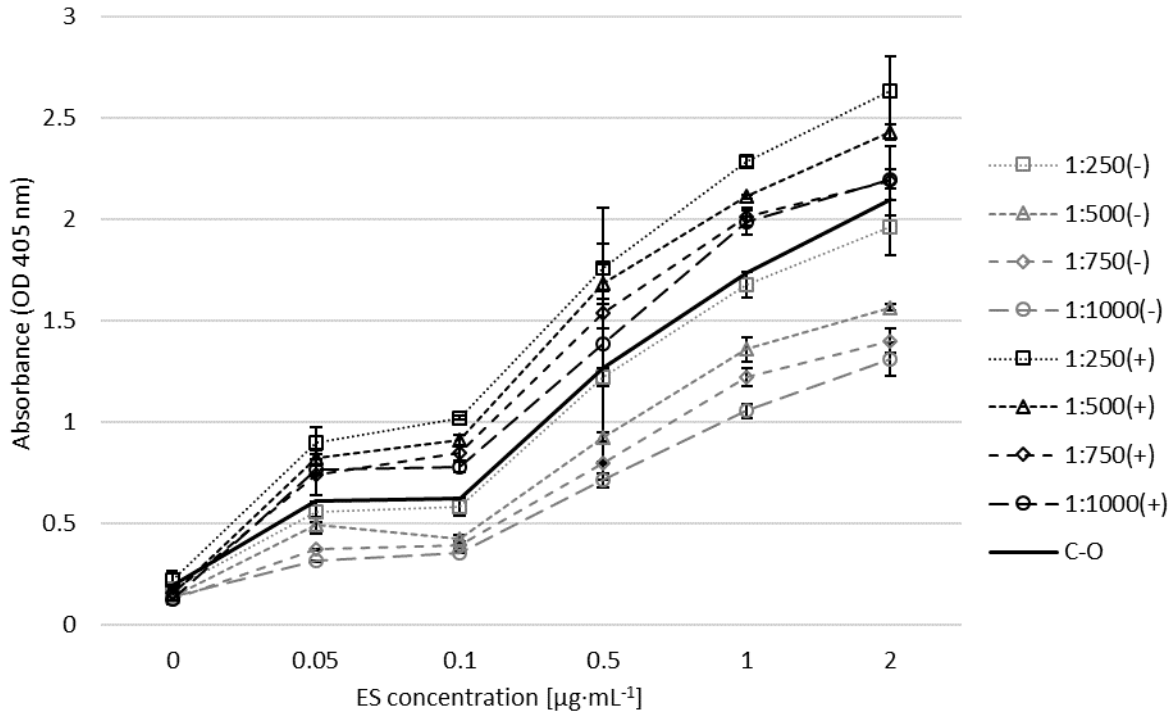

Figure S9. Representative Ag-ELISA absorbances (OD 405 nm) of non-infected and positive ovine infection sera against *F. hepatica* ES products for the determination of optimal ES AgELISA conditions. Average OD measures are shown for two duplicate tests conducted on different days and adjusted by the subtraction of negative BSA control Ag OD per serum dilution. Whole ES products within the range of 0.05–2 µg·mL^{-1} were probed with pooled negative (-) and positive (+) sera (1:250–1:1000). Positive OD values were considered when exceeding the cut-off (C-O), shown as one standard deviation above the highest OD value observed at each Ag concentration using negative serum (solid line (1:250): 0.19701–2.09909).

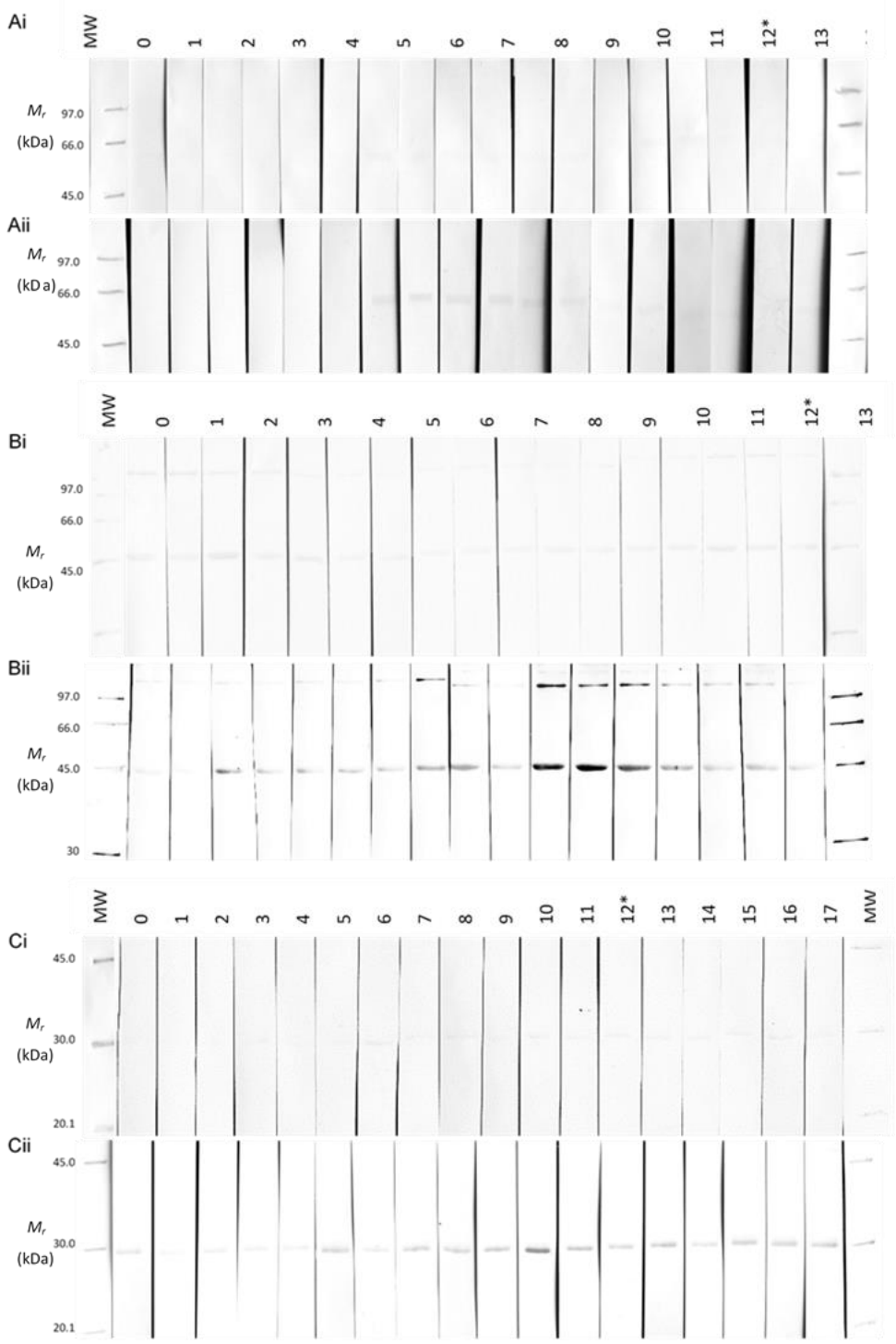

Figure S10. Replicate western hybridisation analysis of IgG immunoreactivity against recombinant candidates using experimentally infected sheep with *Fasciola hepatica* drug-susceptible and -resistant isolates. rFhΔCRT (0.5 µg/well) (A), rFhGEL (0.5 µg/well) (B) and rFhTPI (0.25 µg/well) (C) were probed with whole sheep sera diluted to 1:1,500 and pooled from three animals experimentally infected with TCBZ-susceptible (i) or TCBZ-resistant (ii) *F. hepatica* isolates. Lane numbers refer to week post-infection (0–17), with clinical TCBZ dose administration at week 12(*). Due to the immunoreactivity at 0 wpi (B–C), conditions for antibody detection were adjusted to reduce non-specific antibody binding for the replicate western hybridisation (Figure 6.4.2.3.2).